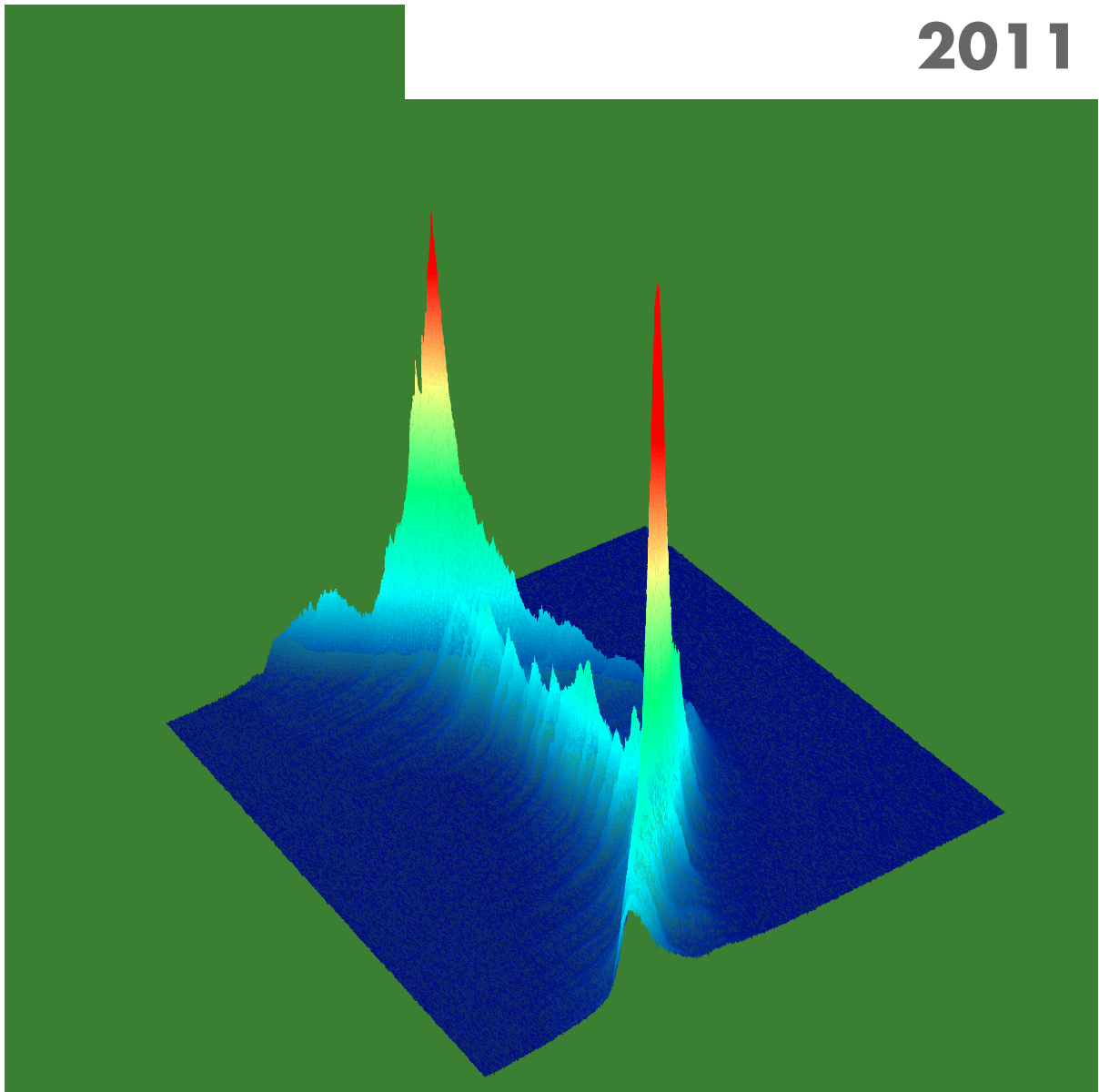


UNIVERSITÄT LEIPZIG

REPORT
Institute für Physik
The Physics Institutes

2011



The Physics Institutes of Universität Leipzig, Report 2011
M. Grundmann (Ed.)

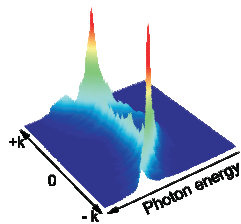
Technical Editor: Anja Heck

This work is subject to copyright. All rights are reserved.
© Universität Leipzig 2012

Printed in Germany

online available at
http://www.uni-leipzig.de/~exph2/report_2011.pdf

Front cover



The front-cover image shows the photoluminescence intensity from an exciton-polariton system in a ZnO-based microcavity as a function of energy and in-plane momentum (k) at 10K. The two pronounced peaks at finite $\pm k$ correspond to the laser emission from a radially propagating Bose-Einstein condensate of exciton-polaritons, accelerated by the repulsive, pump-laser profile induced potential.

Back covers

Announcement, recent publication

**Institut für Experimentelle Physik I
Institut für Experimentelle Physik II
Institut für Theoretische Physik**

**Fakultät für
Physik und Geowissenschaften**

Universität Leipzig

**Institute for Experimental Physics I
Institute for Experimental Physics II
Institute for Theoretical Physics**

Faculty of Physics and Earth Sciences

Universität Leipzig

Report 2011

Addresses

Institute for Experimental Physics I

Linnéstraße 5

D-04103 Leipzig, Germany

Phone: +49 341 97-32551

Fax: +49 341 97-32599

WWW: <http://www.uni-leipzig.de/~physik/exp1.html>

Mailing

address: Postfach 100 920, D-04009 Leipzig, Germany

Institute for Experimental Physics II

Linnéstraße 5

D-04103 Leipzig, Germany

Phone: +49 341 97-32650

Fax: +49 341 97-32668

WWW: <http://www.uni-leipzig.de/~physik/exp2.html>

Mailing

address: Postfach 100 920, D-04009 Leipzig, Germany

Institute for Theoretical Physics

Vor dem Hospitaltore 1

D-04103 Leipzig, Germany

Phone: +49 341 97-32420

Fax: +49 341 97-32548

WWW: <http://www.uni-leipzig.de/~physik/thph.html>

Mailing

address: Postfach 100 920, D-04009 Leipzig, Germany

Preface

Welcome to the 2011 Report of the Physics Institutes of the Universität Leipzig presenting to you an overview of our research in numerous projects. We have enjoyed research and interaction with colleagues and partners worldwide. We are grateful to our guests for enriching our academic year with their contributions in the colloquium and within the work groups. 2011 has seen the BuildMoNa Symposium on ‘Hot Nanoparticles and Nanostructures’, bringing together theoretical and experimental experts on the rapidly emerging and highly interdisciplinary field of laser-heated nanoparticles and nanostructures at the intersection of nanophotonics and nanoscale non-equilibrium stochastic thermodynamics.

The newly established Collaborative Research Center SFB/TRR 102 *Polymers under Multiple Constraints: Restricted and Controlled Molecular Order and Mobility*, a collaboration with colleagues in Halle, has started its work in July 2011. The Collaborative Research Center SFB 762 *Functionality of Oxide Interfaces* was successfully defended with our colleagues in Halle/Saale and has by now started its second funding period 2012–2015. The binational Graduate School *Statistical Physics of Complex Systems* with Nancy Université, France, supported by the Deutsch-Französische Hochschule (DFH-UFA) started into its second funding period in January 2011. The Sächsische Forschergruppe FOR 877 *From Local Constraints to Macroscopic Transport*, a joint initiative with colleagues from Dresden and Chemnitz, has started the second granting period in July 2011.

A new Institute Partnership with the Institute for Condensed Matter Physics of the National Academy of Sciences of Ukraine in Lviv, funded by the Alexander von Humboldt Foundation has been approved in 2011 and commenced work in April 2012.

Most of our activities are only possible due to the generous support from various funding agencies for which we are very grateful and which is individually acknowledged in the brief reports.

Leipzig,
May 2012

M. Grundmann
J.A. Käs
W. Janke
Directors

Contents

1	Structure and Staff of the Institutes	21
1.1	Institute for Experimental Physics I	21
1.1.1	Office of the Director	21
1.1.2	Molecular Nano-Photonics, Molekulare Nanophotonik [MON]	21
1.1.3	Molecular Physics, Molekülphysik [MOP]	22
1.1.4	Physics of Interfaces, Grenzflächenphysik [GFP]	23
1.1.5	Soft Matter Physics, Physik der weichen Materie [PWM]	24
1.2	Institute for Experimental Physics II	25
1.2.1	Office of the Director	25
1.2.2	Magnetic Resonance of Complex Quantum Solids, Magnetische Resonanz Komplexer Quantenfestkörper [MQF]	25
1.2.3	Nuclear Solid State Physics, Nukleare Festkörperphysik [NFP]	26
1.2.4	Semiconductor Physics, Halbleiterphysik [HLP]	27
1.2.5	Solid State Optics and Acoustics, Festkörperoptik und -akustik [FKO]	29
1.2.6	Superconductivity and Magnetism, Supraleitung und Magnetismus [SUM]	29
1.3	Institute for Theoretical Physics	30
1.3.1	Office of the Director	30
1.3.2	Computational Quantum Field Theory, Computerorientierte Quantenfeldtheorie [CQT]	30
1.3.3	Molecular Dynamics / Computer Simulation, Moleküldynamik / Computersimulation [MDC]	31
1.3.4	Quantum Field Theory and Gravity, Quantenfeldtheorie und Gravitation [QFG]	32
1.3.5	Statistical Physics, Statistische Physik [STP]	33
1.3.6	Theory of Condensed Matter, Theorie der kondensierten Materie [TKM]	33
1.3.7	Theory of Elementary Particles, Theorie der Elementarteilchen [TET]	34

I	Institute for Experimental Physics I	35
2	Molecular Nano-Photonics	37
2.1	Introduction	37
2.2	Steering Self-Propelled Thermophoretic Particles	38
2.3	Photothermal Microscopy: Detection of a Nanolens	39
2.4	Twin-Focus Photothermal Correlation Spectroscopy	41
2.5	Back Focal Plane Imaging of the Emission from Photonic Crystals	42
2.6	Local Phase Transitions in Liquid Crystals	43
2.7	Surface Charges on CdSe/ZnS Semiconductor Quantum Dots in Apolar Solvents	45
2.8	Funding	46
2.9	Organizational Duties	46
2.10	External Cooperations	47
2.11	Publications	47
2.12	Graduations	49
2.13	Guests	50
3	Molecular Physics	53
3.1	Introduction	53
3.2	Glassy dynamics of isolated polymer coils	53
3.3	Nanometric sample capacitors	54
3.4	Glassy dynamics of polybutadiene in uniaxial nano-porous membranes	56
3.5	Segmental and chain dynamics in thin layers of cis-polyisoprene	57
3.6	Dynamics of cis-polyisoprene in 1D and 2D geometrical confinement	58
3.7	Molecular dynamics of glass forming-liquids confined in two dimensional constraints of uni-directional nanopores	59
3.8	Rotational and translational diffusion in glass-forming N,N-Diethyl-3-methylbenzamide (DEET)	61
3.9	Brownian dynamics determine universality of charge transport in ionic liquids	62
3.10	Glassy dynamics of imidazole-based liquids confined in nanoporous silica	63
3.11	Molecular dynamics and morphology in confined 4-heptan-4'-isothiocyanatobiphenyl liquid crystals	64
3.12	Infrared Transition Moment Orientation Analysis (IR-TMOA) as applied to semicrystalline polyolefins	65
3.13	The Infrared signature of glassy dynamics	66
3.14	Structural levels of organization in spider silk - a combined mechanical and IR-spectroscopic study	67
3.15	Dynamic force spectroscopy on the binding of the monoclonal antibody HPT-101 to tau peptides	68
3.16	Optical tweezers setup with optical height detection and active height regulation under white light illumination	70
3.17	Optical Tweezers to study DNA/PrP-Interaction on a Single Molecule Level	72

3.18	Friction within Single Pairs of DNA-Grafted Colloids as studied by Optical Tweezers	72
3.19	Dynamic force spectroscopy on fluorescence-labeled tau-peptides and monoclonal antibodies measured by Optical Tweezers	73
3.20	Drag reduction by DNA-grafting for single microspheres in a dilute λ -DNA solution	73
3.21	A novel video-based microsphere localization algorithm for low contrast silica particles under white light illumination	74
3.22	Electrophoretic mobility of ds-DNA-grafted single colloids as studied by optical tweezers	75
3.23	Funding	76
3.24	Organizational Duties	77
3.25	External Cooperations	77
3.26	Publications	77
3.27	Graduations	78
3.28	Guests	79
4	Physics of Interfaces	85
4.1	Introduction	85
4.2	Diffusion of Fluids During Melting in Mesopores	85
4.3	Probing Fluid Distribution in Porous Materials	86
4.4	NMR Diffusion Studies Using Super-High Gradient Pulses	87
4.5	Magnetic Resonance Measurements of Iron Turn-Over Processes in Natural Sands	89
4.6	X Observe NMR Probe Design for Diffusion Studies with Li^+ and Cs^+ Cations and CO_2 in Porous Systems	90
4.7	Intra-Crystalline Diffusion Study of Light Hydrocarbons in Zeolite ZSM-58	91
4.8	Hindering Effects in Diffusion of CO_2/CH_4 Mixtures in ZIF-8 Crystals	92
4.9	Funding	92
4.10	Organizational Duties	94
4.11	External Cooperations	95
4.12	Publications	97
4.13	Graduations	102
4.14	Guests	102
5	Soft Matter Physics	103
5.1	Introduction	103
5.2	Counterion-induced formation of regular actin bundle networks	103
5.3	Calcium imaging in the Optical Stretcher	105
5.4	The mechanics of cellular compartmentalization as a model for tumor spreading	106
5.5	Stochastic actin dynamics in lamellipodia reveal parameter space for cell type classification	107
5.6	Actin and microtubule networks contribute differently to cell response for small and large strain	108

5.7	Directed persistent motion maintains sheet integrity during multi-cellular spreading and migration	110
5.8	Nonlinear pattern formation in biomimetic lipid membranes	111
5.9	Structural Investigation on the Absorption of the MARCKS Peptide on Anionic Lipid Monolayers - Effects Beyond Electrostatic	112
5.10	Actin Filament Elasticity and Retrograde Flow Shape the Force-Velocity Relation of Motile Cells	113
5.11	Funding	114
5.12	Organizational Duties	115
5.13	External Cooperations	116
5.14	Publications	117
5.15	Graduations	119
5.16	Guests	121
II Institute for Experimental Physics II		123
6	Magnetic Resonance of Complex Quantum Solids	125
6.1	Introduction	125
6.2	High-pressure spin shifts in the pseudogap regime of superconducting $\text{YBa}_2\text{Cu}_4\text{O}_8$ as revealed by ^{17}O NMR	125
6.3	NMR signal averaging in 62T pulsed fields	126
6.4	An Electron Spin Resonance Study of Nitroxide Radical Adsorption at Cupric Ions in the Metal-Organic Framework Compound $\text{Cu}_3(\text{Btc})_2$	126
6.5	Effects of varying water adsorption on a $\text{Cu}_3(\text{BTC})_2$ metal-organic framework (MOF) as studied by ^1H and ^{13}C solid-state NMR spectroscopy	128
6.6	Single Crystal to Single Crystal Topochemical Photoreactions: Measuring the Degree of Disorder in the [2 + 2] Photodimerization of <i>trans</i> -Cinnamic Acid Using Single-Crystal ^{13}C NMR Spectroscopy	128
6.7	Optimized NMR spectroscopic strategy to characterize water dynamics in soil samples	129
6.8	Paramagnetic resonance study of nickel ions in hexagonal barium titanate	129
6.9	Funding	130
6.10	Organizational Duties	131
6.11	External Cooperations	131
6.12	Publications	132
6.13	Graduations	136
6.14	Guests	137
7	Nuclear Solid State Physics	139
7.1	Introduction	139
7.2	Alignment tolerances and octupole aberration corrections in an ion nanoprobe	140
7.3	Optimizing the Rutherford backscattering spectrometry setup at the LIPSION nanoprobe	141

7.4	Quantitative microscopy of a macrodimensional specimen: high definition PIXE	142
7.5	3D analysis of an induced murine atherosclerotic lesion by PIXE stacking	144
7.6	Iron and myelin in the human brain: Distribution and T_1 -contrast in gray matter	146
7.7	Calibration and improvement of the single cell analysis setup at LIPSION	148
7.8	Study of nanoparticle uptake and quantification in lung cells by ion beam microscopy	149
7.9	Investigation of intracellular multilayer decomposition of layer-by-layer self-assembled particles by PIXE	151
7.10	Methodical developments for quantitative high resolution ion beam analysis on lateral highly inhomogeneous meteorite samples	152
7.11	3D imaging of cells using limited-angle STIM and PIXE tomography . .	153
7.12	Greyscale Proton Beam writing in p-type GaAs	153
7.13	Development of a fully digital user-friendly TDPAC-spectrometer . . .	155
7.14	FPGA implementation of digital constant fraction algorithm with fractional delay for optimal time resolution	157
7.15	Perturbed Angular Correlation of the stretched cascade in the decay of ^{180m}Hf using a digital spectrometer	157
7.16	Funding	157
7.17	Organizational Duties	158
7.18	External Cooperations	158
7.19	Publications	160
7.20	Graduations	163
8	Semiconductor Physics	165
8.1	Introduction	165
8.2	Structural and electrical properties of CoFe_2O_4 and NiFe_2O_4 thin films grown by pulsed-laser deposition	166
8.3	ZnO-based n -channel junction field-effect transistor with room-temperature fabricated amorphous p -type ZnCo_2O_4 gate	168
8.4	Double-sided (Mg,Zn)O narrow bandwidth metal-semiconductor-metal photodetectors	170
8.5	Tungsten trioxide as high- κ gate dielectric for highly transparent and temperature-stable zinc-oxide-based thin-film transistors	172
8.6	ZnO-based active multielectrode arrays for cells on chip measurements	174
8.7	Temperature-dependent investigations of high quality PdO_x/ZnO Schottky contacts on ZnO thin films	176
8.8	On the T2 deep-level in zinc oxide thin films	177
8.9	Defect-studies on nickel-doped ZnO thin films	179
8.10	Defect studies on 1.6 MeV proton-bombarded ZnO thin-films	181
8.11	Extraction of the effective Richardson constant from Pd/ZnO Schottky contacts on ZnO thin film	183
8.12	Exciton-Polaritons in ZnO-based microcavities – macroscopic quantum states and pseudo-spin polarization	184
	8.12.1 Propagating Bose-Einstein condensates	185
	8.12.2 Pseudo-spin polarization	185

8.13	Whispering gallery modes in irregular and inhomogeneous hexagonal resonators	189
8.13.1	The elongated hexagon: one- and two-dimensional cavity modes in ZnO microwires	190
8.13.2	The inhomogeneous hexagon: microwire quantum well heterostructures	191
8.14	Visible emission from ZnCdO/ZnO multiple quantum well structures .	193
8.15	Radiative decay times in ZnO/(Mg,Zn)O quantum wells with and without the quantum-confined Stark effect	195
8.16	Tunneling dynamics of excitons in random semiconductor alloys	196
8.17	Overestimation of the Stokes shift due to self absorption in MgZnO . .	197
8.18	Persistent layer by layer growth in Pulse Laser Homoepitaxy of (0001) ZnO thin films	198
8.19	Model for 1LO Raman scattering mechanisms in wurtzite crystals excited above the band gap	199
8.20	Magneto-optical ellipsometry	202
8.21	Plasmons on structured substrates	204
8.22	Funding	206
8.23	Organizational Duties	207
8.24	External Cooperations	208
8.25	Publications	209
8.26	Graduations	217
8.27	Guests	218
9	Superconductivity and Magnetism	219
9.1	Introduction	219
9.2	A spin-calorics device based on $\text{La}_{0.7}\text{Sr}_{0.3}\text{MnO}_3/\text{SrRuO}_3$ superlattices . .	219
9.3	Exchange coupling and exchange bias in $\text{La}_{0.7}\text{Sr}_{0.3}\text{MnO}_3\text{-SrRuO}_3$ superlattices	219
9.4	Hall effect of orthorhombic and tetragonal SrRuO_3 layers	220
9.5	Angular dependence of the magnetoelectric effect in orthorhombic HoMnO_3 films	221
9.6	Enhancement of the ferromagnetic order of graphite after sulphuric acid treatment	223
9.7	Andreev Reflection and Granular Superconductivity Features Observed in Mesoscopic Samples Using Amorphous Tungsten Carbide Superconductors	223
9.8	Spin transport in a thin graphite flake	223
9.9	Funding	224
9.10	Organizational Duties	224
9.11	External Cooperations	225
9.12	Publications	226
9.13	Guests	228

III Institute for Theoretical Physics	231
10 Computational Quantum Field Theory	233
10.1 Introduction	233
10.2 How Grafting of a Single Polymer Influences its Statistical Properties near an Attractive Substrate	235
10.3 Thermodynamics of Polymer Adsorption to a Flexible Membrane . . .	236
10.4 Polymer Adsorption to a Fractal Substrate	238
10.5 Polymer Chain Inside an Attractive Sphere Potential	240
10.6 Thermodynamics of a Model Protein in Spherical Confinement	241
10.7 Shapes of Θ -Polymers in Crowded Media under Stretching Force	243
10.8 Scale-Free Enumeration of Self-Avoiding Walks on Critical Percolation Clusters	245
10.9 Two-Dimensional Pinned Flexible Polymers in Hard-Disk Disorder . .	246
10.10 Development of a Framework Allowing fast Programming of Monte Carlo Simulation of Polymers	247
10.11 Stochastic Description of a Binary Frustrated Unit	249
10.12 Mass Condensation in Stochastic Transport Models	250
10.13 Mixed Heisenberg Spin Chains: Theory and Quantum Monte Carlo Simulations	252
10.14 Directional Ordering in the Three-Dimensional Compass Model	253
10.15 Multicanonical Analysis of the Gonihedric Ising Model and its Dual . .	255
10.16 GPU Computing: Parallel Tempering Simulations of Polymer Statistics	257
10.17 Funding	258
10.18 Organizational Duties	259
10.19 External Cooperations	260
10.20 Publications	262
10.21 Graduations	267
10.22 Guests	267
11 Molecular Dynamics / Computer Simulation	271
11.1 Introduction	271
11.2 Analytical Treatment and Computer Simulations of the influence of the crystal surface on the exchange of guest molecules between zeolite nanocrystals and the surrounding gas phase	272
11.3 Diffusion and Rotation of Water in the Zeolite Chabazite	272
11.4 Influence of the shape of the potential landscape on diffusion	273
11.5 Lattice Flexibility and Diffusion of Guest Molecules in the Metal Organic Framework Zntbip	273
11.6 Simulation and Experiments of Membrane Diffusion of guest molecules in the Metal Organic Framework ZIF-8	274
11.7 Funding	276
11.8 Organizational Duties	276
11.9 External Cooperations	276

11.10	Publications	277
11.11	Graduations	278
11.12	Guests	278
12	Quantum Field Theory and Gravity	279
12.1	Temperature Dependence of the Casimir Force	279
12.2	Higher order correlation corrections to color ferromagnetic vacuum state at finite temperature	279
12.3	Structure of the gauge orbit space and study of gauge theoretical models	280
12.4	Quantum field theory on non-commutative geometries, quantum field theory and cosmology, generally covariant quantum field theory	281
12.5	Funding	281
12.6	Organizational Duties	282
12.7	External Cooperations	283
12.8	Publications	284
12.9	Guests	284
13	Statistical Physics	287
13.1	Introduction	287
13.2	Topological superconductivity in the doped Kitaev-Heisenberg model .	288
13.3	Robust one-dimensional wires in lattice mismatched bilayer graphene .	289
13.4	Gapless Excitations in Strongly Fluctuating Superconducting Wires . .	291
13.5	Signatures of non-Abelian statistics in non-linear coulomb blockaded transport	292
13.6	Neutral mode heat transport and fractional quantum Hall shot noise . .	294
13.7	Theory of the Fabry-Perot quantum Hall interferometer	296
13.8	Charge fractionalization on quantum Hall edges	298
13.9	Photonic Josephson effect, phase transitions, and chaos in optomechanical systems	299
13.10	Funding	300
13.11	Organizational Duties	300
13.12	External Cooperations	300
13.13	Publications	301
13.14	Guests	303
14	Theory of Condensed Matter	305
14.1	Introduction	305
14.2	Stochastic Phenomena in Systems with Many Degrees of Freedom	306
14.3	Randomly Evolving Idiotypic Networks	307
14.4	T Cell Regulation, Differentiation, and Plasticity	308
14.5	Generalized Stokes–Einstein relation for hot Brownian motion	310
14.6	Inelastic mechanics of biopolymer networks and cells	310
14.7	Tube-width fluctuations in entangled stiff polymers	311
14.8	WLC monomer dynamics	312
14.9	Wind driven sand transport. A two-species continuum model of aeolian sand transport.	313

14.10	Time-symmetric quantum mechanics	314
14.11	Funding	315
14.12	Organizational Duties	316
14.13	External Cooperations	316
14.14	Publications	317
14.15	Graduations	320
14.16	Guests	321
15	Theory of Elementary Particles	323
15.1	Introduction	323
15.2	Propagators and Wilson loops in numerical stochastic perturbation theory	323
15.3	Symmetries and integrability in gauge field theories	325
15.4	Funding	326
15.5	Organizational Duties	326
15.6	External Cooperations	326
15.7	Publications	327
15.8	Graduations	327
	Author Index	329

1

Structure and Staff of the Institutes

1.1 Institute for Experimental Physics I

1.1.1 Office of the Director

Prof. Dr. Josef A. Käs (director)

Prof. Dr. Frank Cichos (vice director)

1.1.2 Molecular Nano-Photonics, Molekulare Nanophotonik [MON]

Prof. Dr. Frank Cichos

Technical staff

Christine Adolph

Dipl.-Phys. Uwe Weber

PhD candidates

Nicole Amecke

Andreas Bregulla

Romy Schachoff

Markus Selmke

Nils Neubauer

Rebecca Wagner

Marco Braun

Subhasis Adhikari

Martin Pampa

Students

Vladimir Bubar

David Plotzki

Thomas Heyn

Lars Herklotz
André Heber
Jonas Buchmann
Sascha Loebel
Nikolai Kortenbruck

1.1.3 Molecular Physics, Molekülphysik [MOP]

Prof. Dr. F. Kremer

Secretary

Karin Girke

Technical staff

Harmut Domröse
Dipl.-Phys. Cordula Bärbel Krause
Dipl.-Ing. Jörg Reinmuth
Dipl.-Phys. Wiktor Skokow

Academic staff

Dr. Mahdy Elmahdy
Dr. Christof Gutsche
Dr. Ciprian Ghiorghita Iacob
Dr. Malgozarta Jasiurkowska

PhD candidates

Dipl.-Phys. Markus Anton
Wycliffe Kiprop Kipnusu, M.Sc.
Dipl.-Phys. Wilhelm Kossack
Emmanuel Urandu Mapesa, M.Sc.
Ilya Semenov, M.Sc.
Dipl.-Phys. Tim Stangner
Dipl.-Phys. Martin Treß
Dipl.-Phys. Olaf Überschär
Dipl.-Phys. Carolon Wagner

Students

Patrick Beer
Markus Fuchs
Ludwig Popp
Lisa Schade
Benjamin Suttner

1.1.4 Physics of Interfaces, Grenzflächenphysik [GFP]

PD Dr. Frank Stallmach

Technical staff

Lutz Moschkowitz
Stefan Schlayer

Academic staff

Dr. Christian Chmelik
Dr. Laurent Gueudré
Prof. Dr. Grit Kalies
Prof. Dr. Jörg Kärger (em.)
PD Dr. Frank Stallmach
Dr. Rustem Valiullin

PhD candidates

Dipl.-Phys. Steffen Beckert
Dipl.-Phys. Tomas Binder
Dipl.-Phys. Marcel Gratz
Dipl.-Phys. Florian Hibbe
Dipl.-Phys. Carsten Horch
Dipl.-Math. Daria Kondrashova
Dipl.-Phys. Dirk Mehlhorn
Dipl.-Phys. Mikulas Peksa
Dipl.-Phys. Anne-Kristin Pusch
Dipl.-Phys. Christian Reichenbach
Dipl.-Phys. Alexander Shakhov
Dipl.-Phys. Tobias Titze
Dipl.-Phys. Markus Wehring
Dipl.-Phys. Philipp Zeigermann

Students

Alexander Lauerer
Anne Maiwald
Friederike Pielenz
Tino Viertel
Tobias Splith

1.1.5 Soft Matter Physics, Physik der weichen Materie [PWM]

Prof. Dr. Josef A. Käs

Secretary

Claudia Brück

Technical staff

Dr. Undine Dietrich
Dipl.-Phys. Bernd Kohlstrunk
Ing. Elke Westphal

Academic staff

Dr. Mareike Zink
Dr. Claus Fütterer

PhD candidates

Silke Agte, M.Sc.
Dipl.-Phys. Claudia Brunner
Paul Heine, M.Sc.
Dipl.-Phys. Tina Händler
Anatol Fritsch, M.Sc.
Thomas Fuhs, M.Sc.
Markus Gyger, M.Sc.
Dipl.-Phys. Florian Huber
Dipl.-Phys. Tobias Kießling
Dipl.-Phys. Melanie Knorr
Dipl.-Phys. Karla Müller
Kenechukwu David Nnetu, M.Sc.
Dipl.-Phys. Steve Pawlizak
Dipl.-Phys. Philipp Rauch
Susanne Rönicke, M.Sc.
Dipl.-Phys. Sebastian Schmidt
Dipl.-Phys. Jörg Schnauß
Dipl.-Phys. Carsten Schuldt
Dipl.-Phys. Roland Stange
Dipl.-Phys. Dan Strehle
Dipl.-Phys. Franziska Wetzel
Dipl.-Phys. Lydia Woiterski

Students

Katharina Ander
Uta Allenstein
Tim Hohmann
Thomas Els
Sabrina Friebe
Martin Glaser
Tom Golde
Steffen Grosser
Michael Krahe
Sebastian Koth
Hans Kubitschke
Tom Kunschmann
Sascha Loebe
Erik Morawetz
Peter Palm
Marcus Purfürst
Wolfram Pönisch
Stefanie Puder
Angelika Rauch
Daniel Rose
Eva Rose
Lydia Reuter
Enrico Warmt
Luisa Zobelt

1.2 Institute for Experimental Physics II**1.2.1 Office of the Director**

Prof. Dr. Marius Grundmann (director)
Prof. Dr. Pablo Esquinazi (vice director)

**1.2.2 Magnetic Resonance of Complex Quantum Solids,
Magnetische Resonanz Komplexer Quantenfestkörper [MQF]**

Prof. Dr. Jürgen Haase

Secretary

Sophie Jung

Technical staff

Dipl.-Phys. Gert Klotzsche
Dipl.-Ing. Kathrin Koch
Christian Gahse

Academic staff

Dr. Marko Bertmer
apl. Prof. Dr. Andreas Pöppl
Dr. Damian Rybicki

PhD candidates

Dipl.-Phys. Ingo Hilschenz
Dipl.-Phys. Benno Meier
Dipl.-Phys. Thomas Meißner
Dipl.-Phys. Gregor Thörmer
Dipl.-Phys. Alexander Jäger
Dipl.-Chem. Bettina Jee
Farhana Gul-E-Noor, M.Sc.
Anusree Viswanath Kuttathayil, M.Sc.
Michael Jurkutat, M.Sc.
Dimo Ivanov, M.Sc.
Nataliya Georgieva, M.Sc.
Dipl.-Phys. Jonas Kohlrantz
Dipl.-Phys. Sebastian Sambale
Dipl.-Phys. Matthias Mendt

Students

Steven Reichardt
Marc Lux
Emmanouil Veroutis
Thomas Meier
Robin Gühne
Christian Scheidler
Andy Thäder

**1.2.3 Nuclear Solid State Physics,
Nukleare Festkörperphysik [NFP]**

Prof. Dr. Tilman Butz (retired in March 2011)
Dr. Daniel Spemann (since April 2011)

Technical staff

Carsten Pahnke
Dipl.-Ing. Joachim Starke

Academic staff

Dr. Frank Menzel
Dr. Daniel Spemann
Dr. Jürgen Vogt

PhD candidates

Dipl.-Phys. Tobias Andrea
M.Sc. Nirav Barapatre
Dipl.-Phys. René Feder
Dipl.-Inf. B.Sc. Markus Jäger
Dipl.-Phys. Steffen Jankuhn
Dipl.-Phys. Wolfgang Larisch
Dipl.-Phys. Martin Rothermel

Students

David Diering
Nico Klingner
Jan Lehnert
Annemarie Sickert
Julia Trützscher
Ralf Wunderlich

**1.2.4 Semiconductor Physics,
Halbleiterphysik [HLP]**

Prof. Dr. Marius Grundmann

Secretary

Anja Heck

SANDiE Network Office/BuildMoNa Office

Dr. Alexander Weber (Officer)
Birgit Wendisch (Secretary)

Technical staff

Dipl.-Phys. Gabriele Benndorf
Monika Hahn
Dipl.-Ing. Holger Hochmuth
Dipl.-Phys. Jörg Lenzner
Gabriele Ramm
Roswitha Riedel

Academic staff

Dr. Heiko Frenzel
Prof. Dr. Michael Lorenz
PD Dr. Reiner Pickenhain
Prof. Dr. Bernd Rheinländer (retired)
Dr. Rüdiger Schmidt-Grund
Dr. Chris Sturm
Dr. Alexander Weber
Dr. Holger von Wenckstern

PhD candidates

Dipl.-Phys. Tammo Böntgen
Michael Bonholzer, M.Sc.
Dipl.-Phys. Kerstin Brachwitz
Dipl.-Phys. Christof Peter Dietrich
Dipl.-Phys. Helena Franke
Dipl.-Phys. Fabian Klüpfel
Dipl.-Phys. Christian Kranert
Dipl.-Phys. Alexander Lajn
Dipl.-Phys. Martin Lange
Dipl.-Phys. Michael Lorenz
Dipl.-Phys. Alexander Müller
Dipl.-Phys. Stefan Müller
Dipl.-Phys. Friedrich Leonhard Schein
Dipl.-Phys. Florian Schmidt
Dipl.-Phys. Matthias Schmidt
Dipl.-Phys. Marko Stölzel
Martin Thunert, M.Sc.
Dipl.-Phys. Zhang Zhipeng
Dipl.-Phys. Jan Zippel

Students

Tobias Diez
Christian Heinrichs
Marcus Jenderka

Tobias Herzig
Robert Karsthof
Oliver Kramer
Tobias Lühmann
Tom Michalsky
Anna Reinhardt
Peter Schlupp
Daniel Splith
Peter Schwinkendorf
Markus Winter

1.2.5 Solid State Optics and Acoustics, Festkörperoptik und -akustik [FKO]

Prof. Dr. Wolfgang Grill

Secretary

Annette Käthner

Technical staff

PTA Hans-Joachim vom Hofe
Dipl.-Ing. (FH) Ulrike Teschner

Academic staff

Dr. Mieczyslaw Pluta

PhD candidates

Amro Abdelrahman, M.Sc.
Esam Eldin Ahmed Mohamed, M.Sc.
Dipl.-Phys. Erik von der Burg
Dipl.-Phys. Moritz von Buttlar
Albert Kamanyi, M.Sc.
Zakir Hossain Muhammad, M.Sc.

1.2.6 Superconductivity and Magnetism, Supraleitung und Magnetismus [SUM]

Prof. Dr. Pablo Esquinazi

Secretary

Sandy Ehlers

Technical staff

Dr. Winfried Böhlmann
Klaus Grünwald
Dipl.-Krist. Annette Setzer

Academic staff

Dr. José Barzola-Quiquia
Dr. Prasanta Kumar Muduli
PD Dr. Michael Ziese

PhD candidates

Ana Ballestar
Francis Bern
Srujana Dusari
Muhammad Khalid
Tuhin Maity

Students

Julia Tesch
Mahsa Zoraghi
Ecaterina Bodnariuc
Justus Krüger
Thomas Scheike
Tobias Lehmann

1.3 Institute for Theoretical Physics

1.3.1 Office of the Director

Prof. Dr. Wolfhard Janke

Secretary

1.3.2 Computational Quantum Field Theory, Computerorientierte Quantenfeldtheorie [CQT]

Prof. Dr. Wolfhard Janke

Technical staff

–

Academic staff

Dr. Stefan Schnabel
Prof. Dr. Handan Arkin-Olgar

PhD candidates

Dipl.-Phys. Mathias Aust
Dipl.-Phys. Rainer Bischof
Dipl.-Phys. Mario Collura (jointly with Nancy Université)
Dipl.-Phys. Niklas Fricke
Dipl.-Phys. Martin Marenz
Dipl.-Phys. Monika Möddel
Dipl.-Phys. Hannes Nagel
Dipl.-Phys. Andreas Nußbaumer
Dipl.-Phys. Jeremi Ochab (jointly with Jagiellonian University Krakow)
Dipl.-Phys. Sebastian Schöbl
Dipl.-Phys. Micha Wiedenmann
M.Sc. Johannes Zierenberg

Students

Eugen Ehrenpreis
Johannes Bock
Max Gerlach
Momchil Ivanov
Marco Müller
Thomas Peschel
Felix Schramm
Arnd Tretbar
Christoph Vogelsberg
Andreas Wagner
Robert Wiesen
Pan Zhichao

**1.3.3 Molecular Dynamics / Computer Simulation,
Moleküldynamik / Computersimulation [MDC]**

PD Dr. S. Fritzsche

Academic staff

PD Dr. S. Fritzsche

PhD candidates

MSc. P. Pilvar
Msc. U. Arsawang

Msc. R. Channajaree
Msc. K. Seehamart

Students

BSc. P. Schierz
BSc. M. Stiller
Bsc. S. Reimann

1.3.4 Quantum Field Theory and Gravity, Quantenfeldtheorie und Gravitation [QFG]

Prof. Dr. Gerd Rudolph (Speaker)
Prof. Dr. Rainer Verch

Academic staff

Priv.-Doz. Dr. Michael Bordag
Dr. José M. Muñoz-Castañeda
Dr. Matthias Schmidt

Retired

Prof. em. Bodo Geyer
Prof. em. Armin Uhlmann

PhD candidates

Zhirayr Avetisyan, M.Sc.
Dipl.-Phys. Marcus Borrís
Dipl.-Phys. Benjamin Eltzner
Erik Fuchs, M.Sc.
Dipl.-Phys. Thomas Ludwig
Dipl.-Phys. Jan Zschoche

Students

Leander Fiedler
Michael Gransee
Mathias Hänsel
Alexander Knospe
Falk Lindner
Adam Reichold
Martin Teuchler

1.3.5 Statistical Physics, Statistische Physik [STP]

Prof. Dr. Bernd Rosenow

Academic staff

Dr. Mats Horsdal

Dr. Timo Hyart

Dr. Tony Wright

PhD candidates

Dipl. Phys. Alexander Janot

Mirco Milletari, M.Sc.

Martin Treffkorn, M.Sc.

Dipl. Phys. Björn Zocher

Students

Lukas Kimme

Heinrich-Gregor Zirnstein

1.3.6 Theory of Condensed Matter, Theorie der kondensierten Materie [TKM]

Prof. Dr. Ulrich Behn (Speaker)

Prof. Dr. Klaus Kroy

Prof. Dr. Dieter Ihle (retired)

Prof. Dr. Adolf Kühnel (retired)

Academic staff

Dr. Dipanjan Chakraborty

Dr. Lars Wolff

PhD candidates

Dipl.-Phys. Jakob Tómas Bullerjahn

Dipl.-Phys. Jens Glaser

Dipl.-Phys. Andrea Kramer

Dipl.-Phys. Marc Lämmel

Dipl.-Phys. Daniel Rings

Dipl.-Phys. Holger Schmidtchen

Dipl.-Phys. Sebastian Sturm

Students

Marc Höll
Andreas Kühn
Norma Kühn
Damaris Kröber
Rüdiger Kürsten
Heinz Sachsenweger
Robert Schulz
Sven Willner

**1.3.7 Theory of Elementary Particles,
Theorie der Elementarteilchen [TET]**

Prof. Dr. Klaus Sibold

Academic staff

PD Dr. Roland Kirchner
PD Dr. Arwed Schiller
Dr. Meinulf Göckeler
Dr. Li Yiao

PhD candidates

Christoph Dehne
Alexander Ivanov

Students

Tobias Reichenbach
Robert Feldmann

I

Institute for Experimental Physics I

2

Molecular Nano-Photonics

2.1 Introduction

The challenge of experimental physics on the nanoscale is to access local phenomena, that occur for example at interfaces, at specific molecular sites or at certain places within nano-structured materials. These local phenomena may control molecular dynamics, drive self-organization, cause charge separation or alter light propagation. Their importance extends to almost every field involved in future nanotechnology. The research of the molecular nano-photonics group thus aims at the development and application of optical techniques to access nanoscale (dynamical) processes in various fields such as chemical physics, biology or semiconductor physics. The understanding of these dynamical processes shall ultimately lead to a control over single molecules and other nano-objects by applying heat, flow, shear forces, electric fields or current.

The main experimental tool within our research is optical single molecule detection by ultra-sensitive microscopic techniques including time-resolved confocal microscopy, wide-field fluorescence or photothermal microscopy. Single molecules or semiconductor quantum dots provide the ideal local probes to access nanoscale physical properties inside materials while keeping the information on the heterogeneity of the system. Using these techniques recent projects focused on the

- Photothermal detection of single gold nanoparticles and nanorods
- Thermally propelled particles and micromachines
- Nanometric phase transitions in liquid crystalline systems
- Electrochemical manipulation of the emission of colloidal semiconductor nanocrystals
- Angle resolved spectroscopy of photonic crystals

During the year 2011 the Molecular Nanophotonics Group has achieved the following important scientific goals

- The group has developed a quantitative theoretical framework for single particle light scattering in microscopy.

- The group has developed the foundation for absorption-cross section measurements on single molecules and nanoparticles.
- The group has developed and realized concepts for the thermally induced propulsion of particles at the micro and nanoscale.

In the year 2011, the group has contributed significantly to the extension application of the DFG research unit 877 "From Local Constraints to Macroscopic Transport". We have organized several scientific symposia among them a well recognized Minisymposium on "Hot Nanoparticle and Nanostructure" as well as a WE Heraeus Seminar 877 on "Single Molecule Detection". Collaborations with the group of Prof. Dr. Klaus Kroy (University Leipzig), Prof. Dr. Michael Mertig (TU Dresden) and Prof. Dr. Haw Yang (Princeton University) have been very fruitful. Collaborative measurements with the groups of Prof. Friedrich Kremer and Prof. Markus Grundmann have been carried out.

Frank Cichos

2.2 Steering Self-Propelled Thermophoretic Particles

A. Bregulla, V. Bubar, F. Cichos,

Temperature gradients along the surface of micro- and nanoparticles in solution cause interfacial liquid flow, which lead to phoretic motion of particles. This temperature gradient can be created either externally by a heat source or by the particle itself. The latter case has been explored in this project by coating polystyrene particles partly with a thin gold layer (so called Janus particles). This thin gold layer can be heated optically via its plasmon resonance. It has been shown in previous experiments by the group, that this temperature gradient leads to a self-propelled motion of the particles with a velocity of several micrometer per second. The particle moves with the uncoated side forward but its motion is randomized by rotational diffusion. In collaboration with the group of Prof. Haw Yang at Princeton University we have demonstrated, that a simple optical feedback mechanism can be applied to use the rotational diffusion to trap or steer the particles in solution without optical gradient forces. This feedback mechanism is termed photon nudging and analyzes the orientation and position of a Janus particle in real time. If the particle direction is pointing towards a target, a laser is switched on to drive the self-propelled motion towards the target. Thus the rotational diffusion is used to stochastically drive the particle. Thus trapping and steering has been achieved (see Figure 2.1). The localization accuracy achieved is about $0.4 \mu\text{m}$ and is expected to scale with the particle radius. Thus it shall be possible to achieve even better localization accuracies for smaller particles. This is a considerable advantage as compared to optical tweezers, since they require extremely high trapping intensities for small particles. In summary, this switchable self-propelled motion of Janus particles delivers new ways to control particle motion by feedback mechanisms. Thus new studies of the interaction and dynamics of swarming particles will become possible.

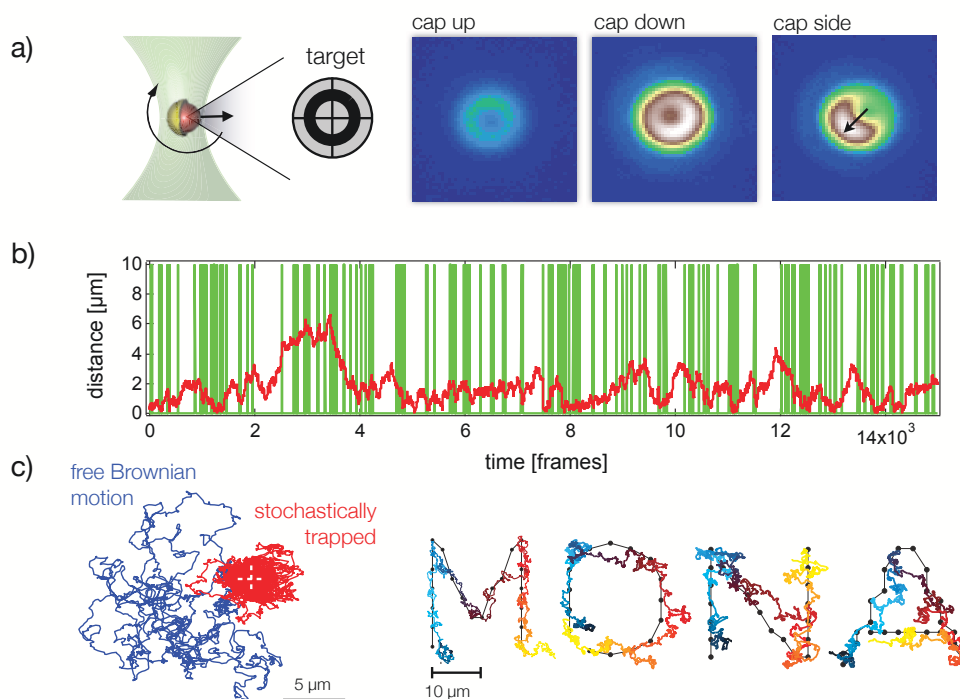


Figure 2.1: *a)* Principle of the Janus particle steering. The orientational images (top right) are used to analyze the particle orientation. If the particle orientation points towards the target, the gold cap of the particle is heated to cause a directed motion. *b)* Distance trajectory of a particle from a selected target and heating periods (green lines) during which the particle is nudged towards the target. *c) left:* Comparison of a freely diffusing and a photon nudged particle trajectory over the same period of time. *c) right:* Steered particle with a series of targets (black points).

2.3 Photothermal Microscopy: Detection of a Nanolens

M. Selmke, M. Braun, F. Cichos,

The generation of heat on the nanoscale is becoming an important tool for the optical detection and spectroscopy of nanoscale absorbers. It has been recently integrated into optical microscopy setups and its sensitivity has been pushed down to the limit of single molecules. Photothermal detection employs the heat released by an absorbing particle or molecule to generate a small refractive index change in the local environment which is finally detected by a second probe laser. While the general principle behind photothermal detection is known, there has been no detailed understanding of the signal generation mechanism for individual absorbers. Within this project, we have carried out for the first time a detailed experimental and theoretical analysis of photothermal signal generation on single absorbing metal nanoparticles. A LORENTZ-MIE light scattering framework has been developed to calculate the scattering of continuous

spherical refractive index profiles in strongly focused laser beams. The results of this complex theory in conjunction with the experimental results demonstrate, that the heat induced refractive index profile around the heated nanoparticle acts like a diverging lens to the probe laser. According to our results, the spatial distribution of the signal

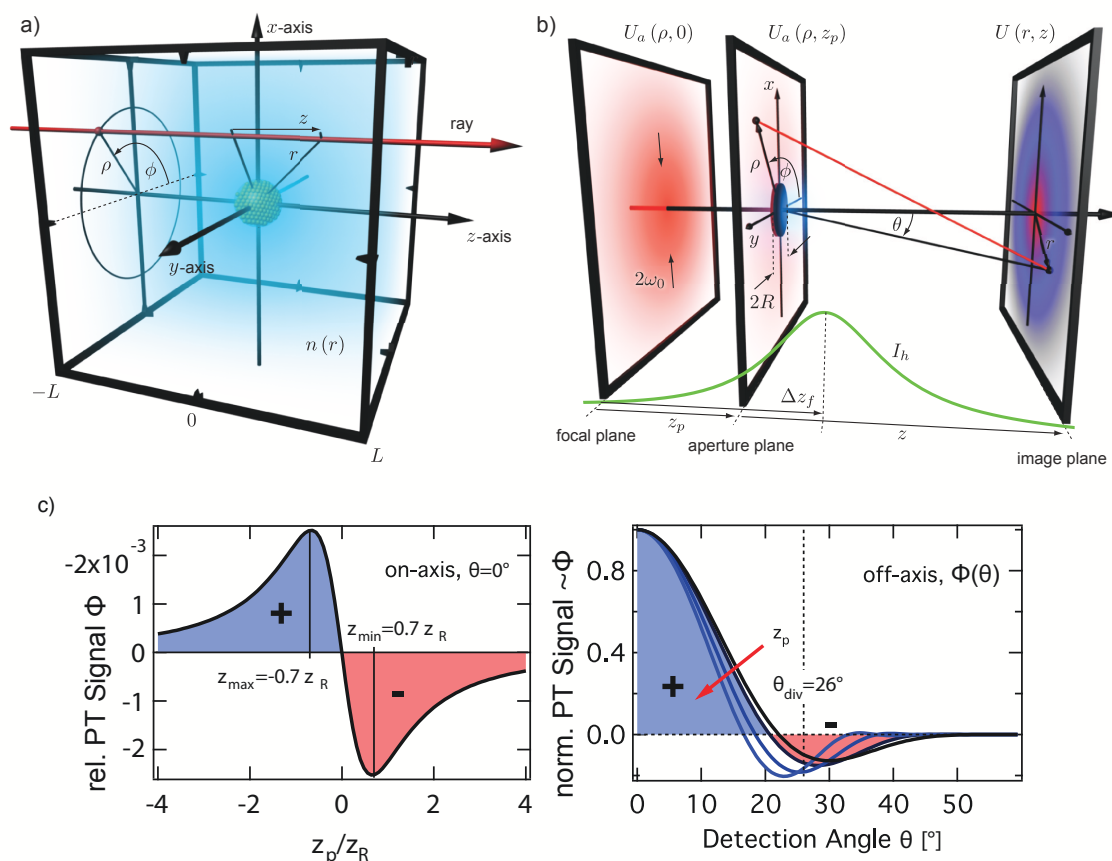


Figure 2.2: *a)* Geometry for the computation of the phase advance of the photothermal lens in a diffraction model. *b)* Geometry for the diffraction integral. The shading in the image-plane corresponds to the difference in intensities between the diffraction of a cold and a hot nanoparticle, which corresponds to the photothermal signal. *c) left:* z_p -Scan of the rel. photothermal signal for on-axis detection. The chosen laser-offset between heating and probe laser results in a symmetric shape. *c) right:* Angular pattern of the photothermal signal demonstrating that an optimal numerical aperture of the detection exists.

can be considerably influenced by the relative position of the excitation and probe laser focus, which leads to new applications (see i.e. Twin-Phocs section). While the LORENTZ-MIE theory is rather complex, the main result of a lensing action has triggered the development of a simpler diffraction theory in which the refractive index profile causes a phase advance of an incident electromagnetic wave. This approach is capturing all experimentally observed features as well and allows a simple quantitative analysis of experimental results.

The achieved detailed understanding of the signal generation mechanism will push the sensitivity of photothermal microscopy to a new level and provide new methods for dynamic studies of single molecules and nanoparticles in solution.

2.4 Twin-Focus Photothermal Correlation Spectroscopy

M. Braun, M. Selmke, R. Schachoff, D. Rings*, K. Kroy†, F. Cichos

*Institute of Theoretical Physics

†Institute of Theoretical Physics

Our analysis of the signal generation mechanism of photothermal microscopy has revealed, that the detection volume of this method is split into two disjunct volume parts where the photothermal signal is positive or negative, respectively. This twin focal volume is the direct consequence of the lensing action of the refractive index profile around the nanoparticle. Its main feature is a sharp boundary between the positive and negative signal part. This can be advantageously used in a photothermal correlation spectroscopy scheme, which provides great potential for applications in biophysics similar to the well known fluorescence correlation spectroscopy (FCS). The Twin-Focus

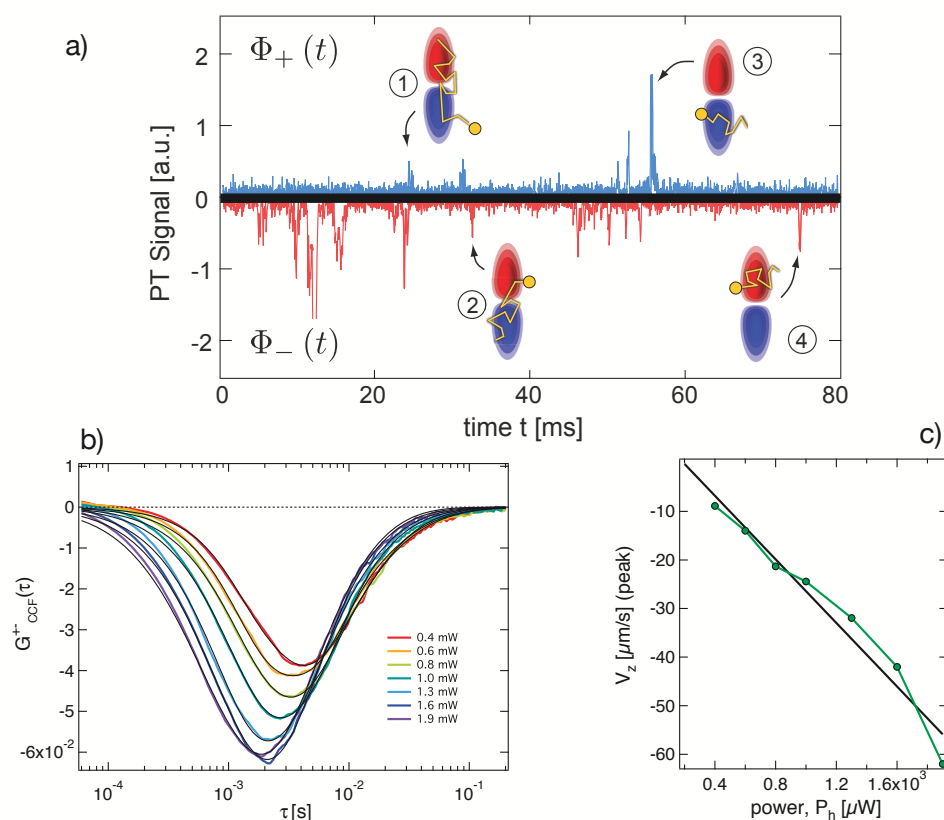


Figure 2.3: *a)* Phase-sensitive photothermal signal of gold nanoparticle ($R = 30 \text{ nm}$) diffusing through the twin-focal volume. The marked events in the time series correspond to the 4 event types, that can be analyzed by TwinPhoCS. *b)* Cross-correlation functions for the diffusion of $R = 30 \text{ nm}$ gold nanoparticles for different heating laser powers. *c)* Determined axial particle velocity due to the radiation pressure of the heating laser.

Photothermal Correlation Spectroscopy (TwinPhoCS) detects the concentration fluctuations of small absorbing entities (such as gold nanoparticles) in solution. Due to the split focal volume, fluctuations in both focal volume parts as well as cross-correlations

between the fluctuations in both focal volumes can be sensed (see Figure 2.3 a)). Calculating the auto-correlations or cross-correlations of the individual signal one finds the characteristic timescale of the fluctuations. Especially the cross-correlation delivers information on the anisotropy of gold nanoparticle motion in solution due to radiation pressure. The radiation pressure results in a particle flow along the optical axis, which we have measured as a function of the incident heating laser power. We detect nanoparticle velocities of a few ten micrometers per millisecond (see Figure 2.3 c)), which is far below any velocity fluorescence correlation spectroscopy is able to detect reliably. Further the twin-focus allows the detection of spatial inhomogeneities of the particle dynamics, since it intrinsically delivers two focal volumes, where the particle dynamics can be analyzed separately. The method is therefore of great advantage in inhomogeneous media such as cellular environments.

A patent application for this method has been submitted to the European Patent Office.

2.5 Back Focal Plane Imaging of the Emission from Photonic Crystals

R. Wagner, L. Heerklotz, N. Kortenbruck F. Cichos

Photonic Crystals (PCs) are materials, where the dielectric constant varies periodically on a length scale of the wavelength of visible light to cause a photonic band structure. The most prominent feature of this band structure are the strong Bragg reflections in spectral and angular regions, where light propagation is not allowed. The strength and the spectral shape of these so-called stop bands for example strongly depend on the structure of the photonic crystal including defects such as stacking faults or cracks. Due to this interrelation between structure and optical properties, tools for the characterization of the optical properties of photonic crystals are of great importance. Here we have studied the angular resolved light propagation in 3-dimensional colloidal photonic crystals. We have developed a method, which allows a fast microscopic evaluation angular and spectrally resolved light propagation. This method employs either fluorescent beads incorporated into the photonic crystal or the auto-fluorescence of the crystal material itself. The emission is excited in the focus of a confocal microscopy setup and collected by a microscope objective lens. This lens images all light incident under a certain angle into a single point in its back-focal plane (see Figure 2.4 a)). The back focal plane therefore contains an angular resolved emission pattern. This angular emission pattern is imaged onto the entrance slit of a spectrograph, which selects a single line from the back focal plane image. This line is spectrally dispersed to provide 100 emission spectra from the photonic crystal at different emission angles. By shifting the slit across the back focal plane image, we obtain a full set of angle resolved emission spectra for about 72 % of the half solid angle. This method is extremely fast as compared to conventional angle resolved emission spectroscopy and allows a microscopic study of the photonic crystals band structure. An even faster version of the method uses a band-pass filter to select a narrow spectral range from the light in the back-focal plane. The back-focal plane can then be directly imaged onto a CCD to obtain information on the band structure of the photonic crystal (see Figure 2.4 b)).

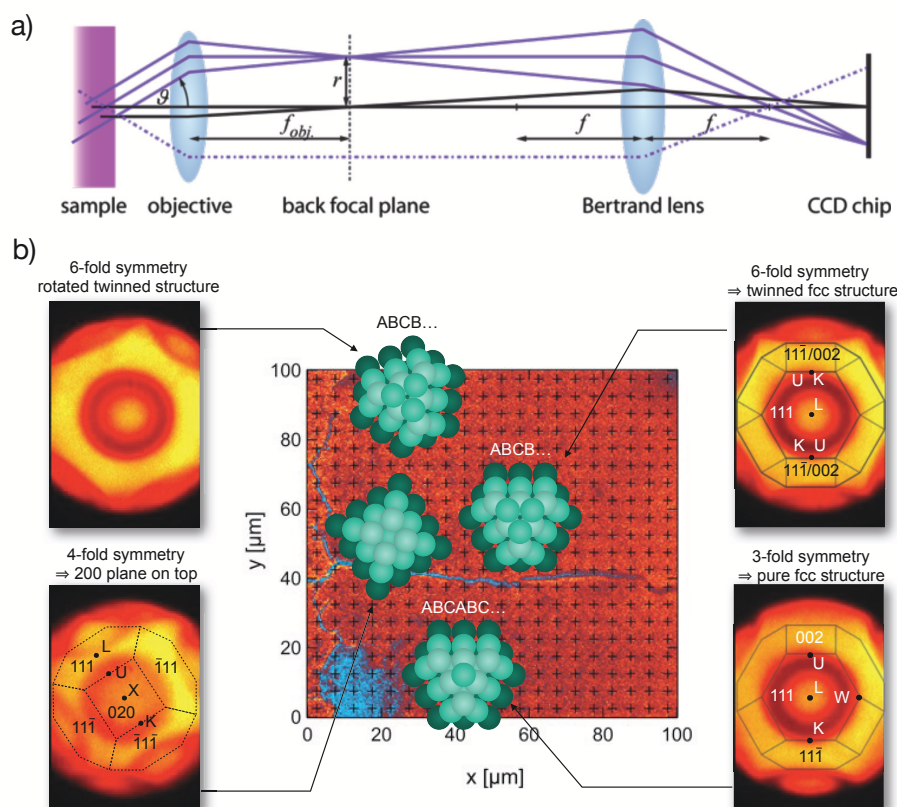


Figure 2.4: *a)* Scheme of the back focal plane imaging setup. The angle resolved emission intensity is obtained in the back focal plane of the objective lens. The back-focal plane is imaged with a Bertrand lens to a CCD chip. *b)* Angle resolved emission patterns (565 nm emission wavelength) collected at different positions of a colloidal photonic crystal. The emission patterns directly reflect the Bragg reflections of the denoted lattice planes and reveal structural defects, stacking faults and crystal orientations.

2.6 Local Phase Transitions in Liquid Crystals

A. Heber, S. Loebel, M. Braun, M. Selmke, M. Pumpa, F. Cichos

We employ the phase transition of liquid crystals from an ordered nematic or smectic phase to an disordered isotropic phase to enhance the photothermal signal from small absorbing gold nanoparticles. As described earlier (see), the photothermal signal is based on a refractive index change induced by a local temperature rise. This temperature rise is the result of nonradiative processes in the absorber which cause the release of heat to the local environment. While the temperature rise around such an absorber can be adjusted by changing the amount of absorbed optical power, the refractive index change with temperature is largely limited by the material and in general on the order of $10^{-4} K^{-1}$. Liquid crystal show a much higher change of the refractive index especially at the phase transition between the ordered and the disordered phase, where the refractive index change can be 3 orders of magnitude larger than in common materials. Here we have studied the photothermal signal generated by a single gold nanoparticle in the

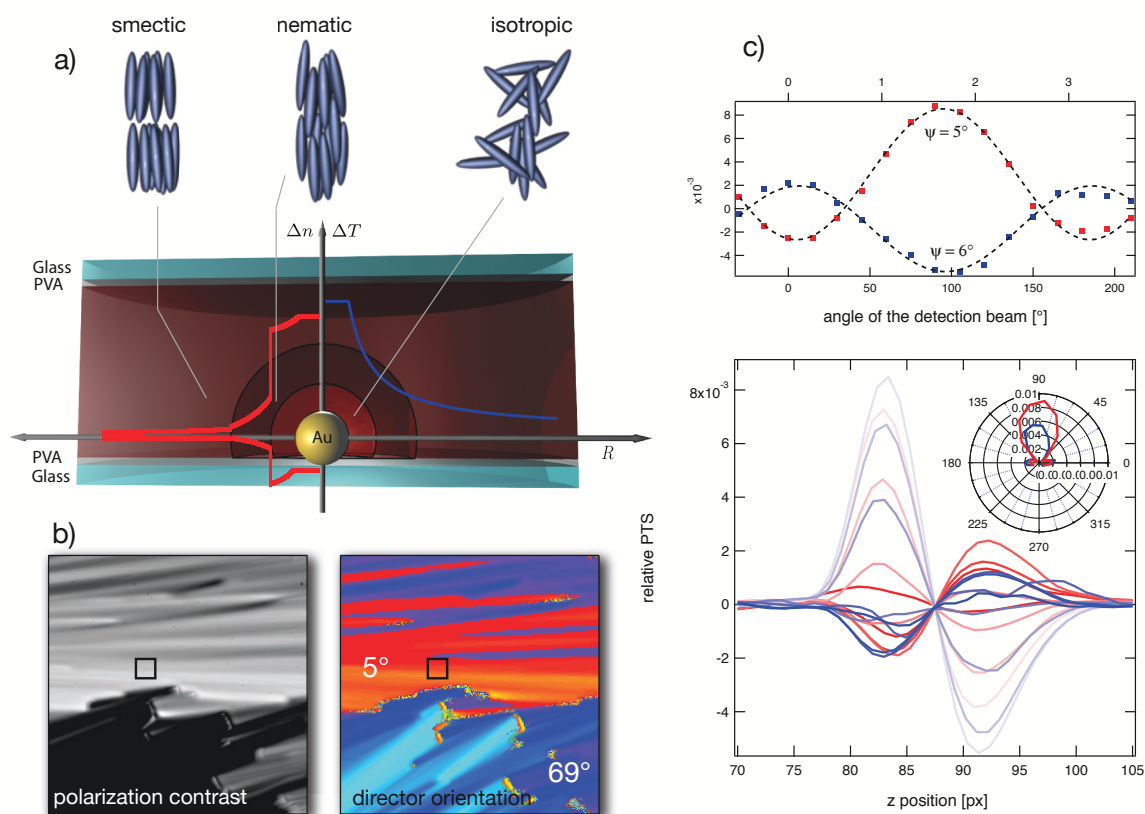


Figure 2.5: *a)* Sketch of the expected phase state of the liquid crystal 8CB around a heated gold nanoparticle. Shells of an isotropic, nematic and smectic phase are formed. *b)* Transmission through the 8CB liquid crystal cell in crossed polarizer configuration showing the different orientations of the liquid crystal director in the smectic phase. The black square marks the area in which the photothermal measurements on a single $R = 30 \text{ nm}$ gold nanoparticle have been carried out. *c) top:* Polarization dependence of the photothermal signal at different defocusing of the particle (red: 83 px, blue: 92 px in the axial scans shown below) *c) bottom:* Axial dependence of the photothermal signal at variable polarization. The inset shows a polar plot of the two maxima/minima at variable polarization angle.

liquid crystal 8CB as a function of the incident polarization. The results show, that a 10-fold signal enhancement of the photothermal signal can be obtained depending on the incident polarization (see Figure 2.5). This signal enhancement can be further increased by heating the liquid crystal closer to its nematic-isotropic phase transition. Moreover placing an analyzer in the detection path provides control of the incident electric field polarization which provides the means of new optical manipulations with heated nanoparticles in liquid crystals.

2.7 Surface Charges on CdSe/ZnS Semiconductor Quantum Dots in Apolar Solvents

N. Amecke, D. Plotzki, F. Cichos

CdSe/ZnS semiconductor quantum dots (QDs) are very efficient, photostable, wave-length tunable sources of light in the visible range. They show interrupted emission (blinking) with spectral diffusion and fluctuating lifetime. Those interruptions and shifts are generally assumed to originate from charges tunneling in and out of the crystal core or simply residing and diffusing in its close vicinity. They can lead to non-radiative exciton decay channels (Auger processes) and transition energy shifts (Stark effect). Such effects are distance dependent and strongest for charges directly in the core, being able to quench the fluorescence close to [?] or below the detection limit. However, direct correlation of charged QDs and their emission still needs to be demonstrated. This

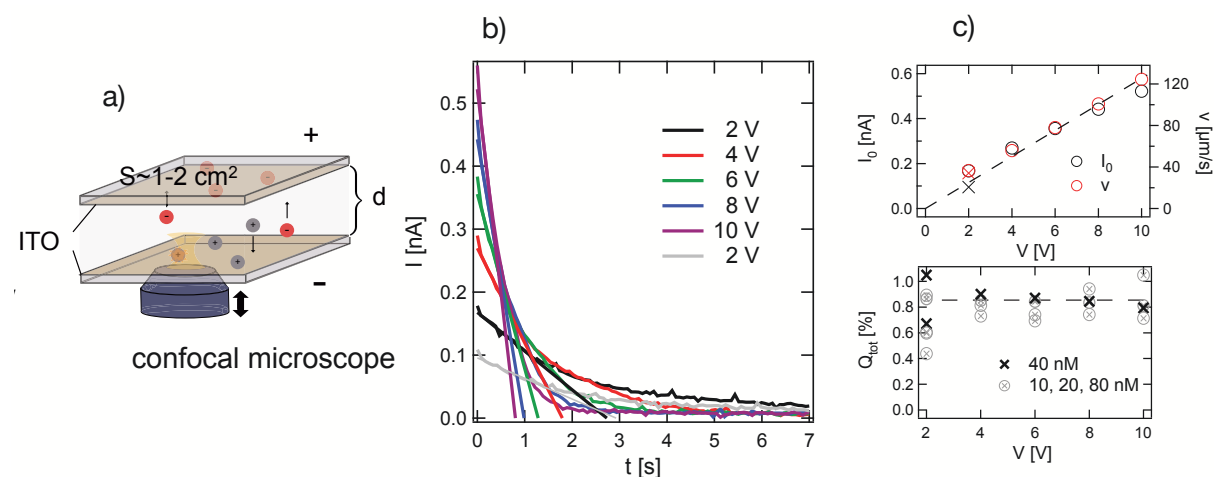


Figure 2.6: *a)* Sketch of the measurement cell with two ITO electrodes. *b)* Transient current of charges in a cell filled with CdSe/ZnS quantum dots dissolved in dodecane. The current occurs in the cell after a voltage pulse. The linear part at the beginning is characteristic for a polarization current. *c) top:* The instantaneous polarization current I_0 as a function of voltage and the corresponding quantum dot velocities at variable voltage. *c) bottom:* Fraction of positively charged CdSe/ZnS quantum dots in dodecane as a function of the applied voltage. The constant charge fraction of roughly 1 % is due to thermal charging presumably of surface states.

research project is devoted to the study of quantum dots in electric fields in non-polar solvents to monitor and influence their charge state. For this purpose we have constructed an electrochemical cell for the manipulation of quantum dots in solution and simultaneous fluorescence microscopy. With intensity profiles, velocities and electrical current we can follow the QD motion and charge concentrations in solution. We find that the majority of fluorescent QDs in toluene move in the direction of negative potential when a homogeneous electric field is applied. Their remaining high fluorescence intensity and lifetime suggest a positive charge on the surface. In contrast, in dodecane, the same QDs show no charge except for a low percentage that can be explained by thermal charging (see Figure 2.6). Comparison of emission lifetime and intensity in dodecane and toluene show that a positive surface charge itself does not considerably

alter a QDs fluorescence. These findings are unexpected and pose new questions on the importance of surface charges in the blinking process.

2.8 Funding

Light Emission of Single Emitters in 3-dimensional Photonic Crystals

Frank Cichos

CI 33/5-2

Ortsaufgelöste Detektion von Struktur und Dynamik in nematischen Phasen biaxialer Moleküle

Frank Cichos

CI 33/6-1

FG 877: Constrained Single Molecule Dynamics in Glassy Polymer Systems

Frank Cichos

CI 33/7-1

FG 877: Hot Brownian Motion

Frank Cichos

CI 33/7-2

FG 877: Static and dynamic properties of DNA-based polymer structures under constraints and confinement

Frank Cichos

CI 33/11-2

FG 877: From Local Constraints to Macroscopic Transport

Frank Cichos

CI 33/12 -1

BuildMONA, ESF-NFG: Funktionale multiskalige Strukturen

SFB TRR102, Interaction of Single Polymer Chains in a Thermophoretic Trap

2.9 Organizational Duties

Frank Cichos

- Speaker of the DFG Research Unit 877 "From Local Constraint to Macroscopic Transport"
- Head of the Eignungsfeststellungskommission Fakultät für Physik und Geowissenschaften
- Vice head Promotionsausschuss
- Member of the Prüfungsausschuss
- Organizer of the Physik-Kolloquium der Fakultät für Physik und Geowissenschaften
- Referee: Phys. Rev. B, Phys. Rev. Lett., Nature, Chem. Phys. Lett., Appl. Phys. Lett., ACS Petroleum Research Fund

2.10 External Cooperations

Academic

- TU Dresden
Prof. Dr. Michael Mertig
- TU Dresden
Dr. Ralf Seidel
- TU Chemnitz
Prof. Dr. Christian von Borczyskowski
- TU Chemnitz
Dr. Harald Graaf
- Universität Mainz
Prof. Dr. T. Basché
- Princeton University
Prof. Dr. H. Yang
- MPI Kohleforschung Mühlheim
Dr. Frank Marlow

2.11 Publications

Journals

N. Amecke, F. Cichos, J. Lumin. 131, 375-378, 2011. Intermediate Intensity Levels During the Emission Intermittency of Single CdSe/ZnS Quantum Dots

S. Adhikari, F. Cichos, M. Selmke, PCCP 13, 1849-1856, 2011, Temperature Dependent Single Molecule Rotational Dynamics in PMA

D. Rings, M. Selmke, F. Cichos, K. Kroy, Soft Matter 7, 3441-3451, 2011, Theory of Hot Brownian Motion

M. Selmke, M. Braun, F. Cichos, arXiv:1105.3815v1, 2011, Photothermal Single Particle Microscopy: Detection of a Nanolens

M. Selmke, M. Braun, F. Cichos, arXiv:1109.2772v1, 2011, Nanolens Diffraction around a Single Heated Nanoparticle

D. Chakraborty, M. V. Gnann, D. Rings, J. Glaser, F. Otto, F. Cichos, K. Kroy, Eur. Phys. Lett. 96, 60009, 2011, Generalized Einstein Relation for Hot Brownian Motion

T. Blaudeck, E. I. Zenkevich, M. Abdel-Mottaleb, K. Szwaykowska, D. Kowerko, F. Cichos, C. von Borczyskowski, ChemPhysChem, DOI:10.1002/cphc.20110071, 2011, Formation Principles and Ligand Dynamics of Nanoassemblies of CdSe Quantum Dots and Functionalised Dye Molecules

Talks

Frank Cichos: From Hot Brownian Motion to Self-Propelled Particles, Diffusion Fundamentals IV Troy/USA, 21.8.-24.8. 2011

Frank Cichos: Licht, Kamera, Action - Moderne Optik, Absolvententreffen der Fakultät f'ur Physik und Geowissenschaften, Universität Leipzig, 10.9.2011

Frank Cichos: Hot Brownian Motion and beyond, Physikalisches Kolloquium, Universität Bayreuth, 29.11.2011

Frank Cichos: Single Molecules and Particles: Reporters and Generators of Local Perturbations, WEH 488 Seminar Chemnitz, 12.7.2011

M. Braun, M. Selmke, F. Cichos: Signal Generation in Photothermal Microscopy: Detection of a Nanolens, Focus on Microscopy 2011, Konstanz, Germany, 17.-20. April 2011

M. Selmke, M. Braun, F. Cichos: Quantitative Photothermal Microscopy, Focus on Microscopy 2011, Konstanz, Germany, 17.-20. April 2011

R. Wagner, L. Heerklotz, F. Cichos: Angle-Resolved Fluorescence Spectroscopy in Photonic Crystals, 75. DPG Spring Meeting, Dresden, Germany, 13.-18. March 2011

R. Wagner, L. Heerklotz, F. Cichos: Back Focal Plane Imaging of Photonic Crystals, Institut für Angewandte Physik, Universität Hamburg, 06. September 2011

M. Braun, M. Selmke, F. Cichos: Twin-Focus Photothermal Correlation Spectroscopy, 488. WE Heraeus Seminar, Single Molecule Spectroscopy: Current Status and Perspectives, Chemnitz, 15.-20. Juli 2011

S. Adhikari, M. Selmke, F. Cichos: Temperature dependent single molecule rotational dynamics in PMA, 75. DPG Spring Meeting, Dresden, Germany, 13.-18. March 2011

Posters

A. Heber, N. Amecke, F. Cichos: The accurate estimation of power law exponents in terms of binned data, 75. DPG Spring Meeting, Dresden, Germany, 13.-18. March 2011

A. Bregulla, M. Selmke, R. Seidel, M. Mertig, K. Kroy, F. Cichos: Gold Capped Microparticles as Self-Propelled Switchable Swimmers, 75. DPG Spring Meeting, Dresden, Germany, 13.-18. March 2011

A. Bregulla, D. Charkborty, D. Rings, K. Kroy, H. Yang, F. Cichos: Surface Interaction of self-propelled thermophoretic Janus-Particles, HotNano Symposium, Leipzig, Germany, 10.-11. October 2011

L. Heerklotz, R. Wagner, and F. Cichos: New features about angle-resolved fluorescence microscopy in Photonic Crystals, 75. DPG Spring Meeting, Dresden, Germany, 13.-18. March 2011

R. Wagner, L. Heerklotz, N. Kortenbruck and F. Cichos: Angle Resolved Fluorescence Spectroscopy of Single Emitters in Photonic Crystals, 488. WE. Heraeus Seminar: Single Molecule Spectroscopy: Current Status and Perspectives, Chemnitz, Germany, 12.-15. July, 2011

N. Amecke, F. Cichos: Optical Detection of a Surface Charge on CdSe/ZnS Quantum Dots in Apolar Solvents, 488. WE Heraeus Seminar, Chemnitz, Germany, 12. -15. July 2011

N. Amecke, F. Cichos: Detection of a surface charge on fluorescent CdSe/ZnS quantum dots in toluene, 75. Spring Meeting, Dresden, Germany, 13. -18. March 2011

M. Braun, M. Selmke, F. Cichos: Photothermal Detection: New Experimental Perspectives from a Quantitative Theory, 75. DPG Spring Meeting, Dresden, Germany, 13.-18. March 2011

M. Braun, M. Selmke, F. Cichos: Photothermal Microscopy: New Experimental Perspectives from a Quantitative Theory, Focus on Microscopy 2011, Konstanz, Germany, 17.-20. April 2011

M. Braun, M. Selmke, F. Cichos: Photothermal detection of gold nanoparticles embedded in a liquid crystal, Hot Nanoparticles and Nanostructures, 1st Scientific Symposium, Leipzig, 10.-11. October 2011

R. Schachoff, M. Selmke, M. Braun, F. Cichos: Twin-focus Photothermal Correlation Spectroscopy, Hot Nanoparticles and Nanostructures, Leipzig, Germany, 10.-11. October 2011

M. Pumpa, F. Cichos: Single Molecule Diffusion in Liquid Crystals, 4. Diffusion Fundamentals, Troy, NY, USA, 21.-24. August 2011

M. Pumpa, F. Cichos: Single Molecule Studies in Liquid Crystals, 75. DPG Spring Meeting, Dresden, Germany, 13.-18. March 2011

2.12 Graduations

Diploma

- Andreas Bregulla
Self propelled thermophoretic motion of a gold capped polystyrene sphere
December 2010

Bachelor

- Sascha Loebel
Detektion einzelner Partikel in Flüssigkristallen
November 2011
- Nikolai Kortenbruck
Konoskopie an fluoreszenzdotierten photonischen Kristallen
Dezember 2011

2.13 Guests

- Haw Yang
Princeton University, USA
9.-11. October 2011
- Alois Würger
Université Bordeaux I, France
9.-11. October 2011
- Masaki Sano
University of Tokyo
9.-11. October 2011
- Michel Orrit
University of Leiden
9.-11. October 2011
- Ralph Vogelgesang
MPI Solid State Research Stuttgart
9.-11. October 2011
- Roberto Piazza
TU Chemnitz
17.-18. May 2011
- Ramin Golestanian
University of Oxford
9.-11. October 2011
- Dieter Braun
LMU Munich
9.-11. October 2011
- Peter Reimann
Universität Bielefeld
9.-11. October 2011
- Gregory Hartland
University of Notre Dame, USA
9.-11. October 2011
- Jean-Louis Barrat
Université Joseph Fourier Grenoble, France
9.-11. October 2011
- Brahim Lounis
Université Bordeaux I, France
9.-11. October 2011
- Claire Cobley
Universität Heidelberg
9.-11. October 2011

- Ross Brown
Université Pau, France
12.-15. July 2011
- Patrice Bordat
Université Pau, France
12.-15. July 2011

3

Molecular Physics

3.1 Introduction

Research requires persistency: After efforts starting in 2008 the universities of Halle and Leipzig successfully applied for a Collaborative Research Center (Transregio) on "Polymers under multiple constraints: restricted and controlled molecular order and mobility". The decisive meeting with the reviewer panel of the DFG took place in April 2011, the letter of approval of the president of the German Science Foundation arrived in June and at the beginning of July the center started to work. Our group is engaged with two projects dealing with "Structural levels of organisation in spider silk - a combined mechanical and IR spectroscopic study" (B5) and "Broadband Dielectric Spectroscopy to study the molecular dynamics in nanometer thin layers of Block copolymers" (B8). The novel SFB is an extraordinary encouragement for the polymer community in the region of the Universities in Halle and in Leipzig. - Fully unexpectedly I was awarded with the Wolfgang-Ostwald-Prize of the German Colloid Society for the year 2011. This reflects nicely that the activities of our group in colloid science, especially the experiments with single colloids, are highly acknowledged.

January 2012

Prof. Dr. Friedrich Kremer

3.2 Glassy dynamics of isolated polymer coils

M. Treß, E.U. Mapesa, F. Kremer

For the first time, the glassy dynamics of randomly distributed, isolated poly(2-vinylpyridine) (P2VP) polymer coils is studied by means of Broadband Dielectric Spectroscopy (BDS). This is achieved by recently developed nano-structured electrode arrangements where isolated polymer coils are deposited onto ultra-flat, highly conductive silicon electrodes. Atomic Force Microscopy scans (see Fig. 3.1a) to c)) of the identical sample before and after the BDS measurement prove that the volume of the coils matches, within a factor of 10 (reflecting the broad molecular weight distribution), with the expected volume of a single chain (considering bulk density and the respective molecular weight) as depicted in Fig. 3.1d). The observed dynamics compares well

with that of bulk (presented in Fig. 3.2a) but is slowed down by up to a factor of about 10 (demonstrated in Fig. 3.2b)). This is attributed to attractive interactions of the P2VP segments with the supporting silica surface - effects which were not observed before in our investigations on polymer layers down to thicknesses of 5 nm [1, 2].

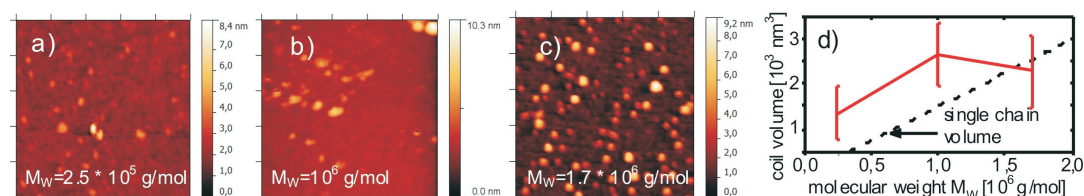


Figure 3.1: a) to c) AFM pictures ($1 \times 1 \mu\text{m}^2$) of isolated P2VP polymer coils of different molecular weight as indicated: d) average coil volume (deduced by AFM) plotted vs molecular weight, the dashed line indicates the volume of a single chain as expected under bulk conditions.

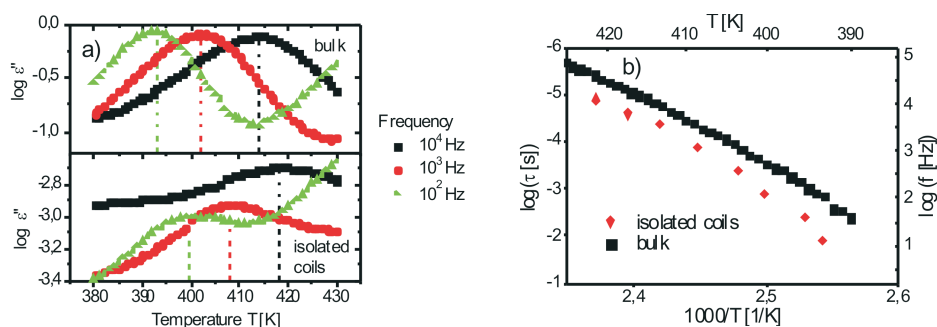


Figure 3.2: a) Dielectric loss ϵ'' versus Temperature of bulk and isolated polymer coils of P2VP measured at different frequencies as indicated: b) activation plot of the data shown in a).

- [1] M. Tress, M. Erber, E. U. Mapesa, H. Huth, J. Müller, A. Serghei, C. Schick, K.-J. Eichhorn, B. Voit and F. Kremer, *F. Macromol.* **43**, 9937 (2010)
- [2] E. U. Mapesa, M. Erber, M. Tress, K.-J. Eichhorn, A. Serghei, B. Voit and F. Kremer, *Eur. Phys. J. Spec. Top.* **173**, 189 (2010)

3.3 Nanometric sample capacitors

M. Treß, E.U. Mapesa, F. Kremer

Recently, a sample arrangement for applying Broadband Dielectric Spectroscopy (BDS) to nanometric samples was realized [1] by the application of ultra-flat highly conductive silicon wafers featured with insulating silica nanostructures which act as spacers. Technically speaking, a flat wafer (without nano-structures) is covered with sample material and is then covered by the counter electrode which carries the nanostructures to keep it in defined separation and avoid an electrical short circuit (schemed in Fig. 3.3a). Initially, this technique was conducted with randomly distributed silica colloidal particles [2], resulting in electrode separations of about a micrometer leading to

capacitor volumes of tens of nanoliters. The introduction of nano-structures as spacers [2] (Fig. 3.3b) displays an array of such structures) and permanent improvement of the insulation quality of the nano-structures as well as the supporting electrode yielded sample capacitors of less than 100 nm in thickness and a probe volume of one nanoliter. Fig. 3.3c) shows an image of a nano-structure as high as 60 nm obtained by atomic force microscopy (AFM). Due to the high electrical insulation of the silica nano-structures, extremely low values of the dielectric loss ϵ'' can be detected in these nanometric probe volumes. Fig. 3.4 exemplifies this for an empty sample cell built from 60-nm-high nano-structures where in the frequency range from 1 Hz to 10 kHz a dielectric loss of less than 10^{-3} is achieved. This enables us to measure dielectric properties of extremely small amounts of material in these sample capacitors reaching volumes as small as one picoliter [3, 4]. Further, the surface of the substrate can be modified [5].

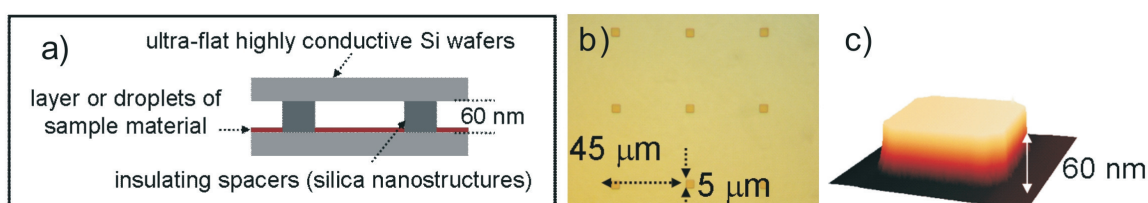


Figure 3.3: a) Scheme of the sample capacitor; b) and c) images of the regular nano-structure array and a single nano-structure obtained by optical microscopy and AFM, respectively.

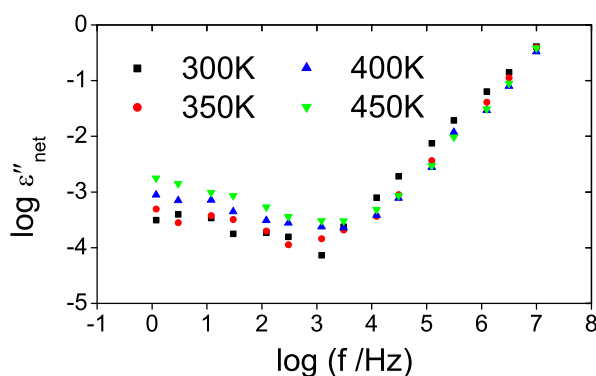


Figure 3.4: Spectra of the dielectric loss of an empty capacitor built from nano-structured electrodes of 60 nm thickness recorded at different temperatures as indicated.

- [1] A. Serghei and F. Kremer, *Rev. Sci. Inst.* **79**, 026101 (2008)
- [2] A. Serghei and F. Kremer, *Rev. Sci. Inst.* **77**, 116108 (2006)
- [3] M. Tress, M. Erber, E. U. Mapesa, H. Huth, J. Müller, A. Serghei, C. Schick, K.-J. Eichhorn, B. Voit and F. Kremer, *F. Macromol.* **43**, 9937 (2010)
- [4] E. U. Mapesa, M. Erber, M. Tress, K.-J. Eichhorn, A. Serghei, B. Voit and F. Kremer, *Eur. Phys. J. Spec. Top.* **173**, 189 (2010)

- [5] M. Erber, M. Tress, E. U. Mapesa, A. Serghei, K.-J. Eichhorn, B. Voit and F. Kremer, *F. Macromol.* **43**, 7729 (2010)

3.4 Glassy dynamics of polybutadiene in uniaxial nanoporous membranes

M. Treß, E.U. Mapesa, F. Kremer

The molecular dynamics of polybutadiene (PB) is measured in the confinement of nano-porous membranes of anodized aluminium oxide (AAO) by means of Broadband Dielectric Spectroscopy (BDS). This investigation is part of a project in the framework of DFG priority program 1369 which combines the expertise of several groups. In the collaborating chemistry institute of the University of Osnabrück an anodization setup, particularly developed for this purpose, is used to create uni-axial channels of nanometric diameter in an aluminium template which is thermally oxidized thereafter (see Fig. 3.5).

The segmental motion (glassy dynamics) of PB is studied in the confinement of these pores in diameters down to 20 nm. Our measurements reveal that under these conditions the glassy dynamics is not shifted compared to the bulk (Fig. 3.6). This result coincides with the findings of other project participants who investigate the same samples by means of nuclear magnetic resonance [2] or perform computer simulations on these systems [3].

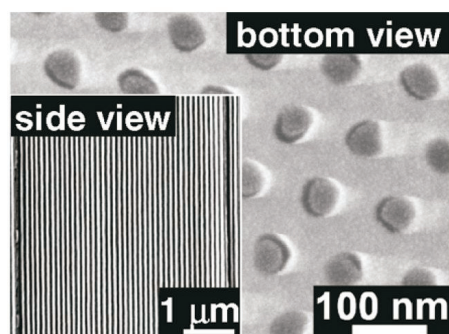


Figure 3.5: Scanning electron micrographs of AAO. Bottom of a 100 μm thick self-ordered AAO membrane (60 nm pore diameter) after infiltration with PB. Inset: cross section of a self-ordered AAO membrane prior to infiltration. Image and caption (modified) taken from [1]

- [1] S. Ok, M. Steinhart, A. Erbescu, C. Franz, F. Vaca Chávez and K. Saalwächter, *Macromol.* **43**, 4429 (2010)
[2] M. Hofmann, A. Herrmann, S. Ok, C. Franz, D. Kruk, K. Saalwächter, M. Steinhart and E. A. Röessler, E. A., *Macromol.* **44**, 4017 (2011)
[3] L. Yelash, P. Virnau, K. Binder and W. Paul, *Phys. Rev. E* **82**, 050801 (2010)

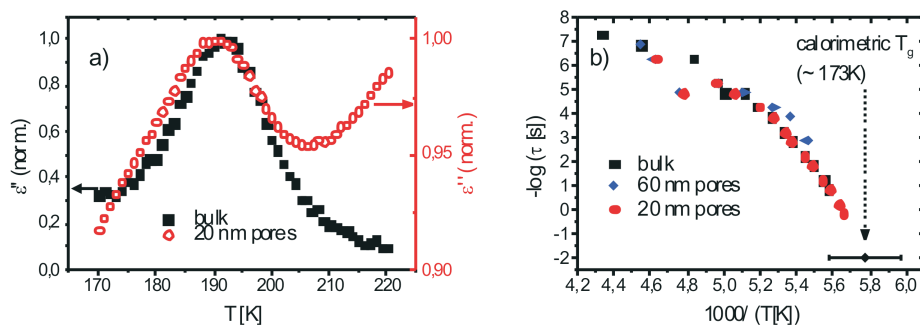


Figure 3.6: a) Dielectric loss ϵ'' versus Temperature of PB in nano-porous AAO membranes (pore diameter as indicated) and bulk recorded at a frequency of 1.2 kHz. b) Activation plot of the α -relaxation of PB in nano-porous AAO membranes (pore diameter as indicated) and bulk.

3.5 Segmental and chain dynamics in thin layers of cis-polyisoprene

E.U. Mapesa, M. Trefß, F. Kremer

Using a novel capacitor assembly - where silica nanostructures serve as spacers between highly-doped silicon electrodes [1] - thin layers of cis-polyisoprene (44.5, 53 and 75 kg/mol) were studied by means of Broadband Dielectric Spectroscopy (BDS). cis-polyisoprene has a non-zero component of its dipole moment aligned along the main chain thus enabling the investigation, by BDS, of the fluctuation of its end-to-end vector. Effectively then, two distinct relaxation modes taking place at two different length scales can be studied: the segmental motion which involves structures of about one nanometer in size (2 to 3 monomer units) and the normal mode which represents the dynamics of the whole macromolecule [1]. Thin layers were prepared by spincoating polyisoprene/chloroform solutions at 3000 rpm for 20 s, and their thicknesses systematically varied by changing the concentration of the solutions. The topography of the spin-cast samples was checked by AFM before and after dielectric measurement to exclude possible dewetting effects on the measured dynamics. Down to 7 nm, it is observed (Fig. 3.7) that: (i) the segmental mode as a local relaxation process is independent of layer thickness; and (ii) the normal mode becomes faster with decreasing layer thickness, in dependence on molecular weight. The former result - consistent with our previous findings [3] - underscores the fact that the dynamic glass transition is invariant, at least in the studied thickness range, while the latter points to a possible alteration of the chain conformation when the polymer is confined in thin films.

- [1] A. Serghei and F. Kremer, *Rev. Sci. Instrum.* **79**, 026101 (2008)
- [2] I. Bahar, B. Erman, F. Kremer, E.W. Fischer, *Macromolecules* **25**, 816 (1992)
- [3] E.U. Mapesa, M. Erber, M. Tress, K.J. Eichhorn, A. Serghei, B. Voit and F. Kremer, *Eur. Phys. J.-ST.* **189** **173**, (2010)

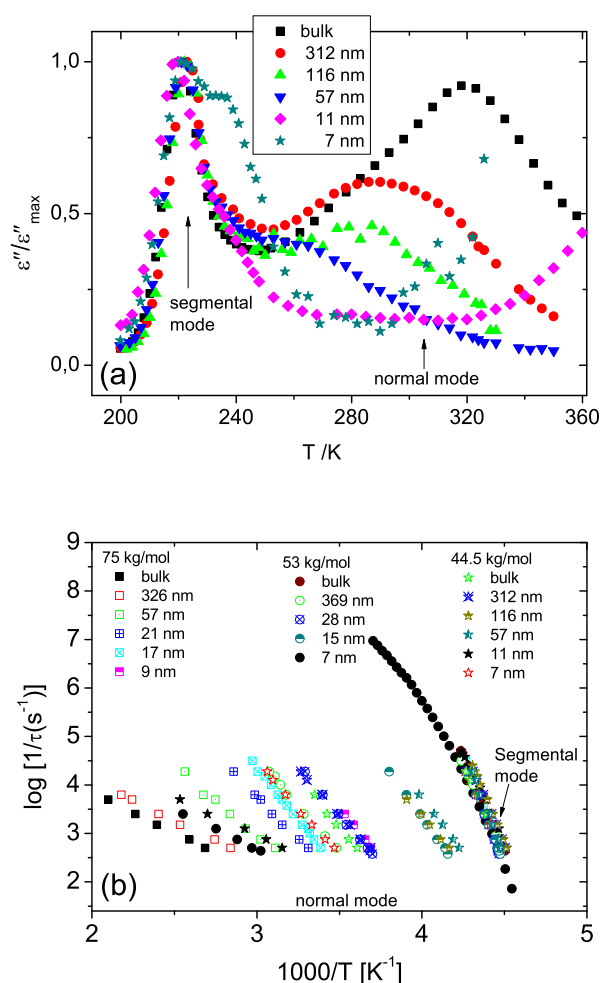


Figure 3.7: (a) Dielectric loss (normalized w.r.t the maximum value of the segmental mode) plotted versus temperature for polyisoprene (44.5 kg/mol) layers, (b) relaxation rate $1/\tau_{max}$ as a function of inverse temperature for polyisoprene (Mw: 44.5, 53 and 75 kg/mol) in thin layers (as indicated).

3.6 Dynamics of cis-polyisoprene in 1D and 2D geometrical confinement

E.U. Mapesa, W. Kipnusu, M. Treß, F. Kremer

A fundamental question must be addressed: how does the dimensionality of geometric confinement affect the dynamics of the constrained material? For the same material, 1-D and 2-D confinements can be attained by preparing thin films and by filling in nanopores, respectively. Cis-polyisoprene, being a Type A [1] polymer, is the apt candidate for this study because both the local and global dynamics of the chain can be accessed by Broadband Dielectric Spectroscopy. In a current study, thin films of polyisoprene (53 kDa) are measured in a nano-structured electrode arrangement that employs highly insulating silica structures as spacers (Fig. 3.8a, b). The same polymer is also filled - under conditions of high vacuum - into porous media of anodized aluminium

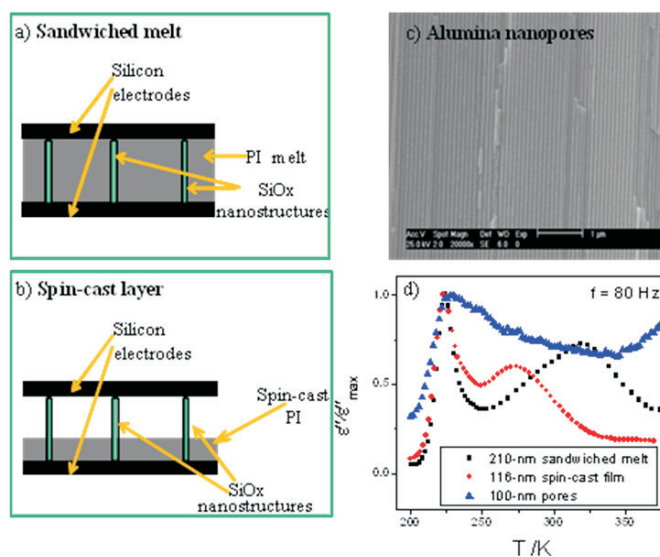


Figure 3.8: Schematic representation of how the polyisoprene melt (a) and thin films (b) are assembled using silica nanostructures for dielectric measurements; a Scanning Electrode Microscope image of an AAO membrane showing uni-axial pores, 100 nm in diameter (c); Normalized dielectric loss (at 80 Hz) as a function of temperature for polyisoprene (53 kDa) measured in different configurations as indicated.

oxide (AAO) (Fig. 3.8c) for dielectric studies. Preliminary results (Fig. 3.8d) show that, compared to bulk (the 210-nm sandwiched melt), (i) the temperature position of the segmental mode is independent of the dimensionality of confinement, (ii) a spin-cast thin film exhibits a faster normal mode, while (iii) the normal mode of the molecules confined in porous media is drastically suppressed. The optimization of the pore-filling procedure as well as a reduction of the pore diameter are the subjects of an on-going effort.

[1] W.H. Stockmayer, *Pure Appl. Chem.* **15**, 539 (1967)

3.7 Molecular dynamics of glass forming-liquids confined in two dimensional constraints of uni-directional nanopores

W.K. Kipnusu, C. Iacob, J.R. Sangoro, F. Kremer

Broadband Dielectric Spectroscopy (BDS) and Pulsed Field Gradient Nuclear Magnetic Resonance (PFG NMR) spectroscopy, are combined to study the molecular dynamics of low molecular weight glass forming liquids (e.g. alkylcitrate) in the bulk state and when confined in unidirectional nanopores (diameter: 4, 8, and 10.4 nm, length: 50 μ m) prepared by electrochemical etching of highly doped p-type < 100 > silicon and subsequent oxidation. By converting diffusion coefficients obtained from PFG-NMR to relaxation rates via Einstein-Smoluchowski relation and merging with the BDS data, the temperature dependence of structural -relaxation is traced by more than 12 orders

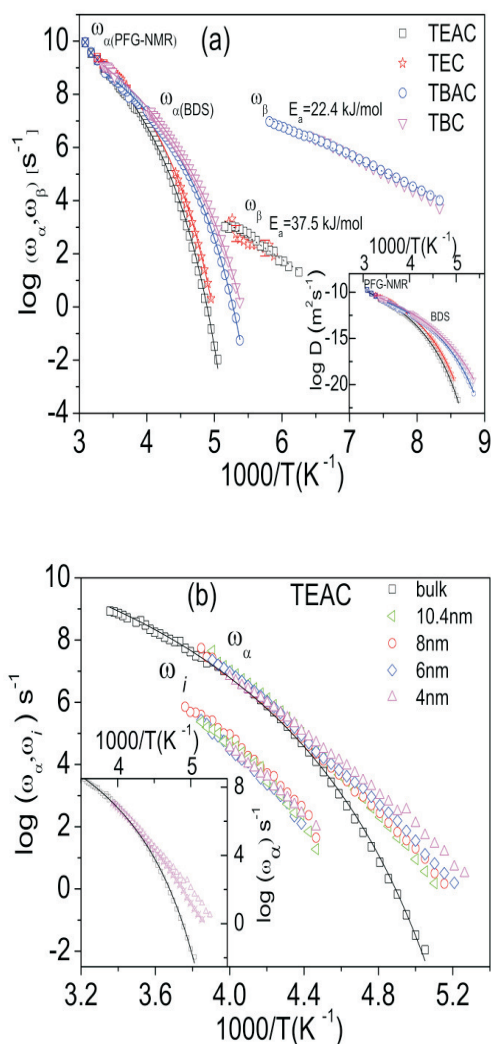


Figure 3.9: (a) Thermal activation plot of the structural (α) and the secondary (β) relaxation processes for Triethylacetyl citrate (TEAC), Triethyl citrate (TEC), Tributylacetyl citrate (TBAC), and Tributyl citrate (TBC). Structural relaxation at higher temperatures (crossed symbols) is obtained from PFG-NMR measurements. Solid lines are fits by the VFT equation while dotted lines are Arrhenius fits. Inset: Diffusion coefficients from both PFG-NMR and BDS measurements. (b) Structural relaxation versus inverse temperature for bulk and confined TEAC molecules. Inset: Comparison of α -relaxation in silanized and unsilanized (crossed symbols) 4nm pores.

of magnitude (fig. 3.9a). Under confinement, an additional process (slower than the α -process) assigned to relaxation of interfacial layers is observed for the alkyl citrates studied. Exact thickness of these layers can be obtained by analysis of dielectric strength of the bulk and confined molecules. Silanization of the pores removes the interfacial layer process and lowers the structural α -relaxation (inset: fig. 3.9b) which, is however enhanced by more than 2 orders of magnitude (at lower temperatures) for molecules constrained in coated 4 nm pores in comparison to the bulk. This is attributed to changes in molecular packing due to geometrical constraints.

[1] M. Arndt, et. al., Physical review. E **54**, 5377 (1996)

[2] F. Kremer, *Broadband Dielectric Spectroscopy*, Springer, Berlin, 2003.

[3] R. Prisk, and P. E. Sokol, *J. Chem. Phys.* **134**, 114506 (2011)

3.8 Rotational and translational diffusion in glass-forming N,N,-Diethyl-3-methylbenzamide (DEET)

J.R. Sangoro, C. Iacob, W.K. Kipnusu, F. Kremer

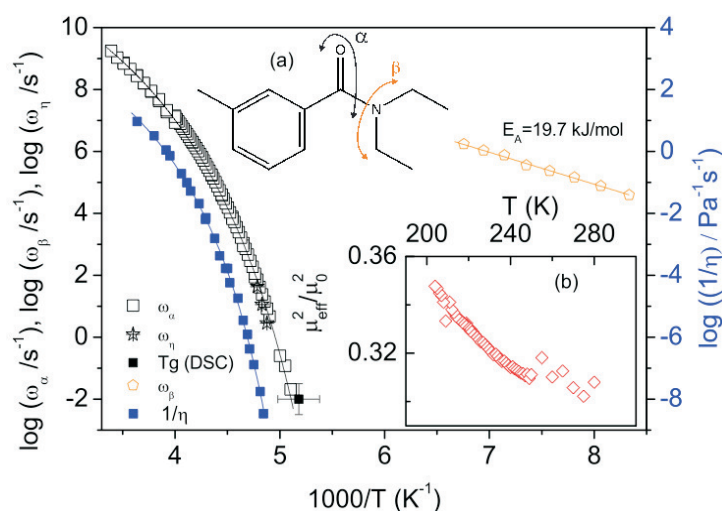


Figure 3.10: : Activation plot of the structural α -relaxation rates as measured by broadband dielectric spectroscopy (ω_α) and dynamic mechanical spectroscopy (ω_η) as well as the secondary dipolar relaxation rates (ω_β). Fluidity ($1/\eta$) as a function of inverse temperature is shown as well. The solid lines are fits by the empirical Vogel-Fulcher-Tammann equation. The calorimetric glass transition temperature determined by differential scanning calorimetry (DSC) (time-scale of 100 seconds assumed) is also indicated. Inset: (a) Chemical structure of N,N-Diethyl-3-methylbenzamide. The possible molecular motions corresponding to the α - and β - relaxations are indicated. (b) The temperature dependence of the Kirkwood/Fröhlich correlation factor

Rotational and translational diffusion in N,N,-Diethyl-3-Methylbenzamide (DEET) are investigated in wide frequency and temperature ranges by a combination of broadband dielectric spectroscopy (BDS), pulsed field gradient nuclear magnetic resonance (PFG NMR), dynamic mechanical spectroscopy (DMS) and calorimetry (Fig. 3.10). It is proven that the (dynamic) glass transition (as measured by BDS, DMS and calorimetry) and charge transport (as measured by PFG NMR and BDS) follow quantitatively the Einstein and Einstein-Smoluchowski relations. The effective number densities of molecules participating in rotational and translational diffusion are found to coincide within the limits of experimental accuracy [1].

[1] J.R. Sangoro et al., *Soft Matter* **7**, 10565 (2011)

3.9 Brownian dynamics determine universality of charge transport in ionic liquids

J.R. Sangoro, C. Iacob, F. Kremer

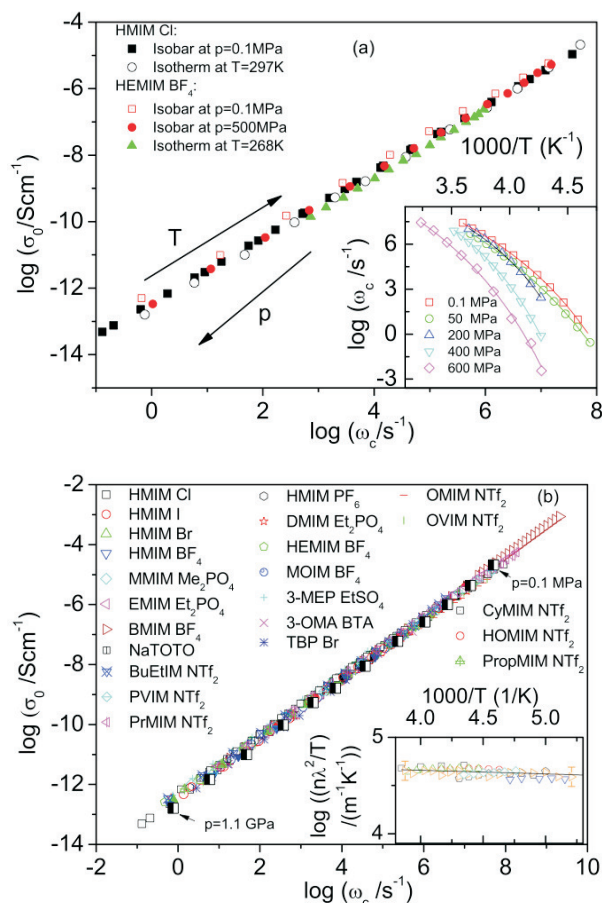


Figure 3.11: dc conductivity, σ_0 , versus the characteristic rate, ω_c , for: (a) two ionic liquids obtained from isobaric and isothermal dielectric measurements. Inset: The temperature dependence of ω_c at different pressures as indicated. (b) various ionic liquids at 0.1 MPa and [HMIM][Cl] at different pressures (denoted by filled symbols, may not be completely visible due to overlap with other data sets: (black squares): 50 MPa, (red circles): 200 MPa, (green triangles): 400 MPa, (blue inverted triangles): 600 MPa). Additionally, values obtained from dielectric measurements at different pressures between 0.1 MPa and 1.1 GPa at 297 K for [HMIM][Cl] are included. Inset: the term $n\lambda^2/T$ versus inverse temperature for arbitrarily selected ionic liquids (the symbols are consistent with the main figure). For [HMIM][Cl], the isobaric data obtained at 600 MPa for the different temperatures is plotted.

Broadband Dielectric Spectroscopy is employed to investigate charge transport in a variety of glass-forming ionic liquids over wide frequency, temperature and pressure ranges (Fig. 3.11). The dielectric spectra are dominated - on the low frequency side - by electrode polarization effects, while, for higher frequencies, charge transport in a disordered matrix is the underlying physical mechanism. Using Einstein, Einstein-Smoluchowski, Maxwell and Langevin equations, the universality of charge transport

in ionic liquids is traced back to the dominant role of Brownian dynamics in these systems. It would be interesting to check the extent to which the current description could be applicable to other classes of amorphous ion-conducting materials.

[1] J.R. Sangoro et al., under preparation

[2] J.R. Sangoro and F. Kremer, *Acc. Chem. Res.* (2012). DOI:10.1021/ ar2001809

3.10 Glassy dynamics of imidazole-based liquids confined in nanoporous silica

C. Iacob, J.R. Sangoro, F. Kremer,

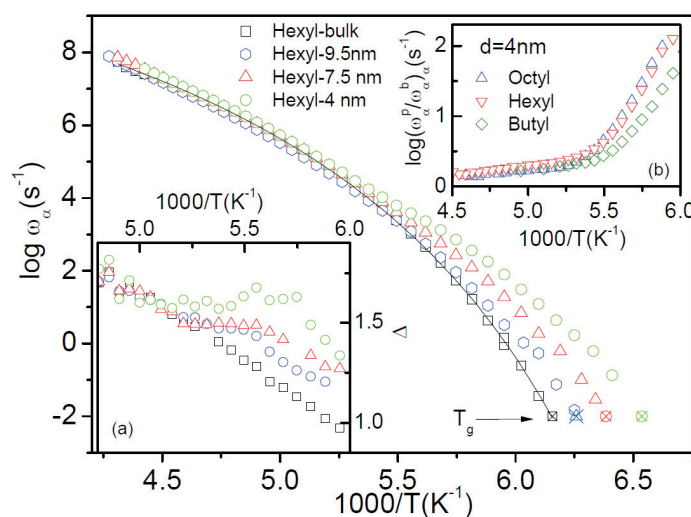


Figure 3.12: The mean structural α -relaxation rates, ω_α for bulk and confined 1-Hexylimidazole versus inverse temperature. The solid line is a fit using the Vogel-Fulcher-Tammann (VFT) equation applied to the bulk ω_α . The fit parameters are: $\omega_\alpha = 1.38 \times 10^{12} \text{ s}^{-1}$, $D=7.97$, and $T_0=131 \text{ K}$. Insets: (a) difference quotients versus $1/T$ for the bulk 1-Hexylimidazole (square symbols) and confined in porous silica with mean diameters of 9.5 nm, 7.5 and 4 nm as determined experimentally, (b) the ratio between α -relaxation rates for bulk and under nano-confinement for imidazole in 4 nm pores versus inverse temperature. T_g represents the glass transition temperature for bulk 1-Hexylimidazole obtained from calorimetric measurements (DSC). For the different nanopores, the T_g is taken as the temperature at which ω_α is 10^{-2} s .

Broadband Dielectric Spectroscopy (BDS) is employed to study glassy dynamics in homologous series of imidazole-based liquids confined in unidirectional silica nanopores with mean diameters of 4, 7.5 and 9.5 nm. The dielectric spectra are interpreted in terms of dipolar relaxation and a conductivity contribution. In pores of mean diameter 4 nm, the structural α -relaxation rates are faster than the corresponding bulk values by two orders of magnitude (Fig. 3.12). Experimentally determined difference quotients of α -relaxation rates show unusual temperature dependence attributed to a subtle competition between surface and confinement effects [1–3].

- [1] Iacob, C., et al. *Soft Matter* **8**, 289 (2011).
 [2] Iacob, C., et al. *Phys. Chem. Chem. Phys.* **12**, 13798 (2010).
 [3] Iacob, C., et al. *J. Chem. Phys.* **129** (23), 234511 (2008).

3.11 Molecular dynamics and morphology in confined 4-heptan-4'-isothiocyanatobiphenyl liquid crystals

M. Jasiurkowska, W. Kossack, R. Ene, C. Iacob, W. Kipnusu, P. Papadopoulos*, J. Rume-Sangoro, F. Kremer

*Max-Planck-Institute for Polymer Research, Postfach 3148, D-55021 Mainz, Germany

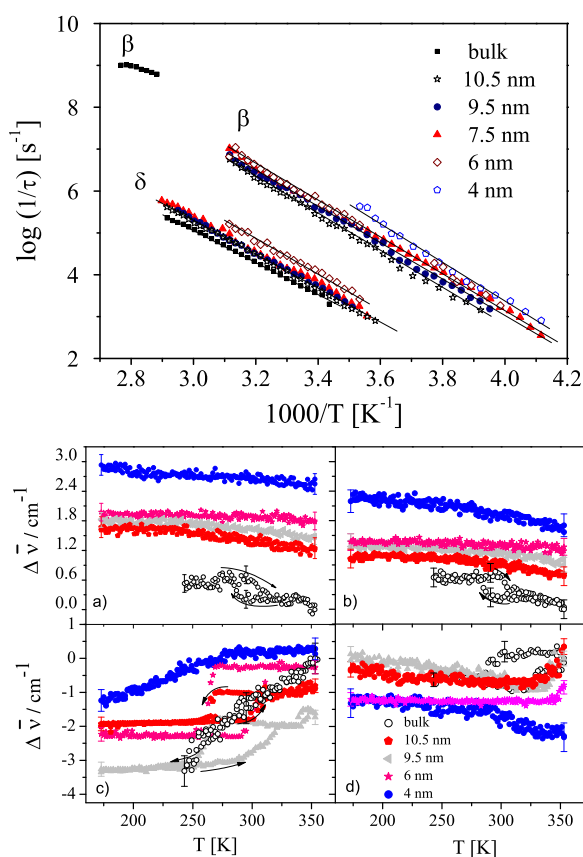


Figure 3.13: (A) Activation plot of 7BT upon cooling in bulk and confined in pores of mean diameters 4 nm, 6 nm, 7.5 nm, 9.5 nm and 10.5 nm. (B) Shift of the alkyl chain absorption band at a) 1400 cm⁻¹, b) 1403 cm⁻¹ and the phenyl absorption band at c) 1602 cm⁻¹ d) 1610 cm⁻¹ compared to the bulk sample in the isotropic phase at 353 K. The error bars denotes the average fitting uncertainty.

Molecular dynamics and orientational order of 4-heptan-4'-isothiocyanato-biphenyl (7BT) [1] in nanopores of mean diameters from 4 nm to 10.5 nm are studied by a combination of Broadband Dielectric and Fourier-Transform Infrared Spectroscopy. A novel approach: Transition Moment Orientational Analysis [2] is employed to explore the

orientational order of molecules in pores. Based on results of both BDS and FTIR methods, we propose a microscopic picture of the morphology of molecules in nanopores of different sizes [3]. It was found that the stiff molecular units are perpendicular to the pore walls in 10.5 nm diameter pores whereas in smaller nanopores (4 nm and 6 nm) they show a preferential alignment along the pore axis.

- [1] M. Jasiurkowska, P.M. Zieliński, M. Massalska-Arodź, Y. Yamamura, K. Saito, J. Phys. Chem. B **115**, 12327 (2011)
- [2] W. Kossack, P. Papadopoulos, P. Heinze, H. Finkelmann and F. Kremer, *Macromolecules* **43**, 7532 (2010)
- [3] M. Jasiurkowska, W. Kossack, R. Ene, C. Iacob, W. Kipnusu, P. Papadopoulos, J. Rume Sangoro, M. Massalska-Arodź, F. Kremer, submitted to *Soft Matter*

3.12 Infrared Transition Moment Orientation Analysis (IR-TMOA) as applied to semicrystalline polyolefins

W. Kossack, P. Papadopoulos*, M. Parkinson†, F. Prades‡, F. Kremer

*Max-Planck-Institute for Polymer Research, Postfach 3148, D-55021 Mainz, Germany

†Borealis Polyolefine GmbH, St.-Peter-Strasse 25, AT-4021 Linz, Austria

‡Borealis Polyolefine GmbH, St.-Peter-Strasse 25, AT-4021 Linz, Austria

Transition Moment Orientation Analysis, recently developed in our group, is employed to determine the three dimensional orientation and order of the different molecular moieties in semi-crystalline polyolefins [1]. Based on IR transmission spectra for varying polarisation and inclination (Fig. 3.14), the ensemble averaged square of the transition moments corresponding to specific vibrations is deduced. By that, the full order parameter tensor and its orientation with respect to the sample coordinate system is obtained [1, 2]. Polyethylene and Polypropylene films are widely used materials of high technological importance, because of their remarkable property variability resulting from the films micro structure. Usually produced by blown film processes these materials undergo stress-induced crystallization and molecular orientation depending on process parameters like die gap, blow-up ratio, frost line height, etc. To improve the physical and mechanical properties it is inevitable to understand the relation between these parameters and the micro structure of amorphous and crystalline phases within the sample [1].

- [1] W. Kossack et al., *Polymer* **52**, 6061 (2011).
- [2] W. Kossack et al., *Macromolecules* **43**, 7532 (2010).

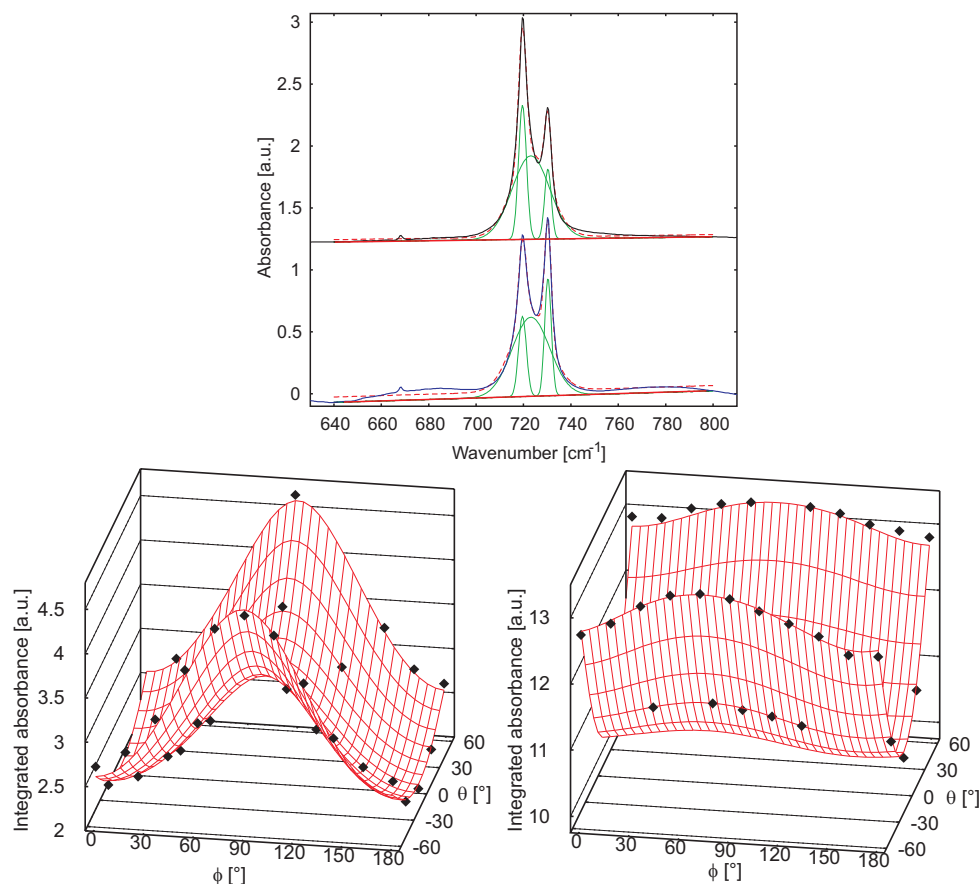


Figure 3.14: In (a) the CH_2 rocking band (721 cm^{-1}) is shown for an inclination angle of 60° in "s" (blue) and "p" polarization (black). For semi-crystalline samples this band splits up into three (shown as thin green lines), where the broad unchanged component corresponds to the amorphous state. The baseline used for correction (straight red line) and the fitted bands (dashed red line) are shown as well. Subplot (b) displays the dependence of the integrated absorbance (peak area, black dots) on inclination (θ) and polarization (ϕ) of the incoming light for the crystalline phases CH_2 rocking vibration with its transition moment parallel to the a axis of the lamellar crystallites. (b) shows the dependence for the amorphous phase. The red grid lines in (b) and (c) depict the fit.

3.13 The Infrared signature of glassy dynamics

W. Kossack, P. Papadopoulos*, F. Kremer

*Max-Planck-Institute for Polymer Research, Postfach 3148, D-55021 Mainz, Germany

Glassy dynamics reflects a continuous slowing down of molecular fluctuations in a glass forming system. It is characterized by a temperature dependence according to the empirical Vogel-Fulcher-Tammann (VFT) law and scales with the calorimetric glass transition temperature (T_G), typically taking place at a relaxation rate of 0.01 Hz. Combining methods measuring intermolecular interactions (Broadband Dielectric Spectroscopy, Calorimetry, Dilatometry) with IR spectroscopy sensing intramolecular vibrations of the specific signature of a glass forming system is unraveled by analyzing the temperature dependent spectral features of IR-absorption bands corresponding to the different

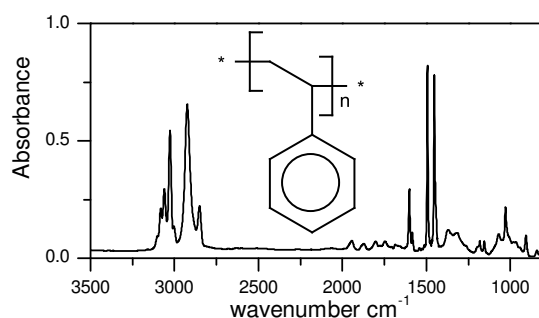


Figure 3.15: IR spectrum of Polystyrene at 300K, The inset shows the chemical structure of the monomer.

molecular moieties. First results for polystyrene are shown (Fig. 3.15).

3.14 Structural levels of organization in spider silk - a combined mechanical and IR-spectroscopic study

M. Anton, W. Kossack, R. Ene, P. Papadopoulos*, C. Gutsche, F. Kremer

*Max-Planck-Institute for Polymer Research, Postfach 3148, D-55021 Mainz, Germany

The unique mechanical properties of spider silk are based on a refined architecture at a molecular and mesoscopic scale. Nanocrystals are interconnected with prestrained amorphous regions causing an internal pressure, which is counterbalanced by the fiber's elastic matrix and outer skin. By that, external stress is directly transferred to a molecular level and can be determined by a shift of an IR absorption band (964 cm^{-1}) being specific for the Alanine-rich nanocrystals [1, 2]. The intention of the project is to unravel the interplay between external and internal constraints by analyzing the pressure and temperature dependence of specific IR absorption bands in response to hydrostatic pressure provided by a diamond anvil cell. For calibration a pressure-dependent spectral shift of the R1 and R2-fluorescence lines of chrome doped Al_2O_3 [3] is used (Fig. 3.17) which is inserted in the cell. Preliminary measurements in collaboration with Prof. Dr. Christine Kuntscher from the university of Augsburg led to promising results. The pressure-dependent frequency shift of the Alanine specific absorption band follows (Fig. 3.17) a linear dependence and exhibits the same slope as known from uni-axial stress-dependent measurements [1].

[1] P. Papadopoulos et al., *Colloid. Polym. Sci.* **287**, 231 (2009)

[2] P. Papadopoulos et al., *Macromol. Rapid Commun.* **30**, 851 (2009)

[3] K. Syassen, *High Press. Res.* **28**, 75 (2008)

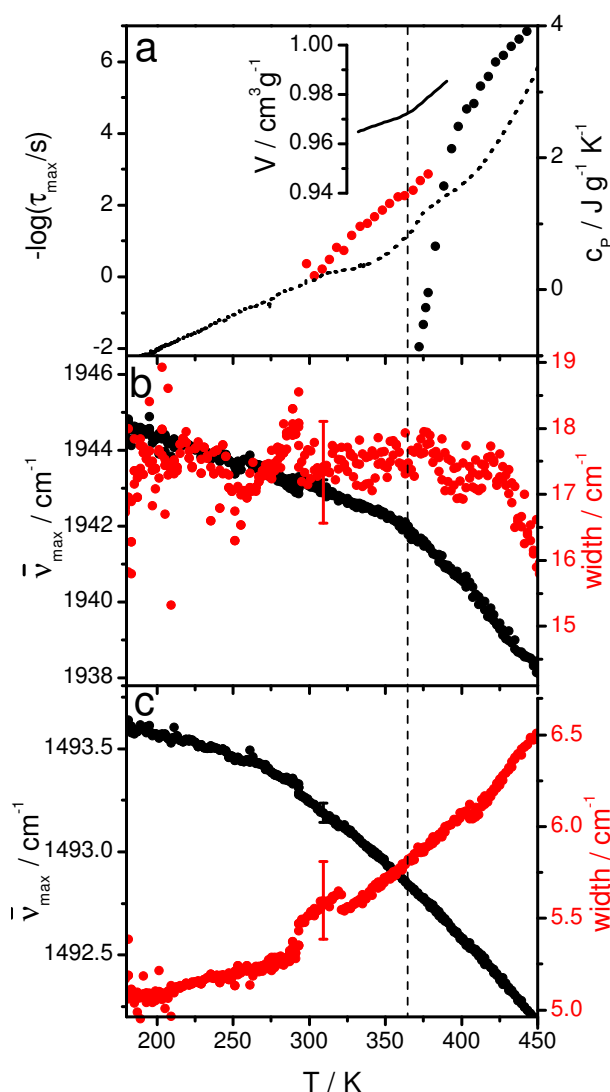


Figure 3.16: Characteristic features in the dynamic glass transition of Polystyrene; (a) relaxation rates of the α - and β -relaxation (black and red dots) measured by broadband dielectric spectroscopy and heat capacity at constant pressure c_p (from DSC, dotted line) versus temperature. The inset shows the specific volume as measured by dilatometry. All quantities (except the β -relaxation) exhibit a clear change at T_G . Spectral position (black) and width (red) of specific absorption bands for (b) the combined in- and off-plane ring vibration; and (c) the in-plane ring stretching vibration versus temperature. Apparently both modes exhibit strongly different dependencies; while for the former the slope changes the latter is uninfluenced at T_G (dashed line).

3.15 Dynamic force spectroscopy on the binding of the monoclonal antibody HPT-101 to tau peptides

C. Wagner, D. Singer*, T. Stangner, O. Ueberschär, C. Gutsche, R. Hoffmann*, F. Kremer

*BBZ, Fakultät für Chemie und Mineralogie, Universität Leipzig, Deutscher Platz 5, 04103 Leipzig

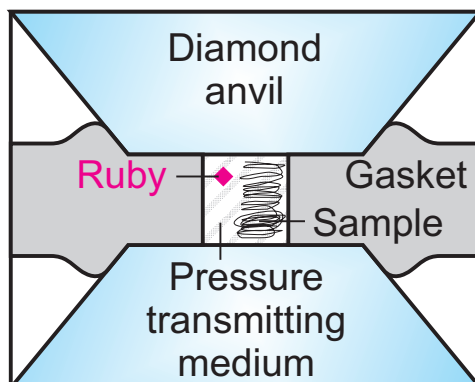


Figure 3.17: Basic construction of a diamond anvil cell. Sample and ruby embedded in a pressure transmitting medium and surrounded by a gasket undergo hydrostatic pressure.

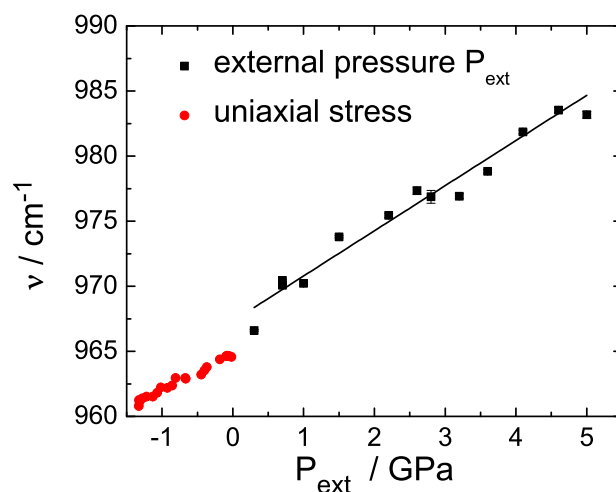


Figure 3.18: Spectral position of the Alanine-specific absorption band versus (external) hydrostatic or uniaxial stress-in

Optical tweezers-assisted dynamic force spectroscopy (DFS) is employed to investigate specific receptor/ligand bindings on the level of single binding events [1]. Here, the specific binding of the anti-human tau monoclonal antibody (mAb), HPT-101, to synthetic tau-peptides with 2 potential phosphorylation sites is analyzed (Fig. 3.19a). According to Enzyme-linked Immunosorbent Assay (ELISA) measurements, the antibody binds only specifically to the double-phosphorylated tau-peptide. It is shown by DFS that HPT-101 binds also to each sort of the mono-phosphorylated peptides, but with a shorter lifetime (Fig. 3.19a). By analyzing the measured rupture-force distributions characteristic parameters like the lifetime of the bond without force τ_0 , the characteristic length x_{ts} and the free energy of activation ΔG are determined for all interactions. Thereby it can be investigated how the attachments with the mono-phosphorylated peptides add up in the case of the double-phosphorylated peptide in order to form the strong specific binding.

[1] C. Wagner et al., *Soft Matter* 7 (9), 4370 (2011)

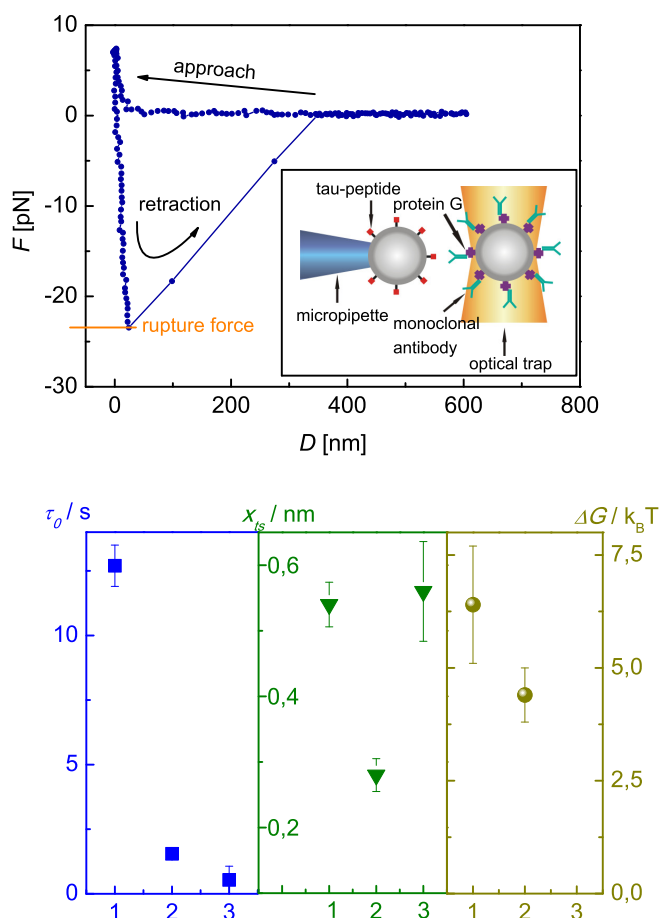


Figure 3.19: a) A typical force-distance dependence is shown. The beads are brought in contact and pulled apart with a preset velocity. Due to an individual binding between the tau-peptide and the mAb the particle in the optical trap is shifted out of the equilibrium position. Inset: The experimental configuration. b) The characteristic parameters lifetime of the bond without force τ_0 , characteristic length x_{ts} and free energy of activation ΔG are shown for the interactions of HPT-101 to (1) the double-phosphorylated peptide, (2) the peptide phosphorylated at Thr231 and (3) the peptide phosphorylated at Ser235.

3.16 Optical tweezers setup with optical height detection and active height regulation under white light illumination

C. Wagner, T. Stangner, C. Gutsche, O. Ueberschär, F. Kremer

An optical tweezers setup with optical detection in three dimensions and active height regulation has been developed [1]. The presented novel method to determine the relative height of a microparticle from its microscopic image is based on the analysis of the integrated light intensity of the main maximum of the diffraction pattern ($S(z)$). After the determination of a master curve as reference (Fig. 3.20a), the height can be detected

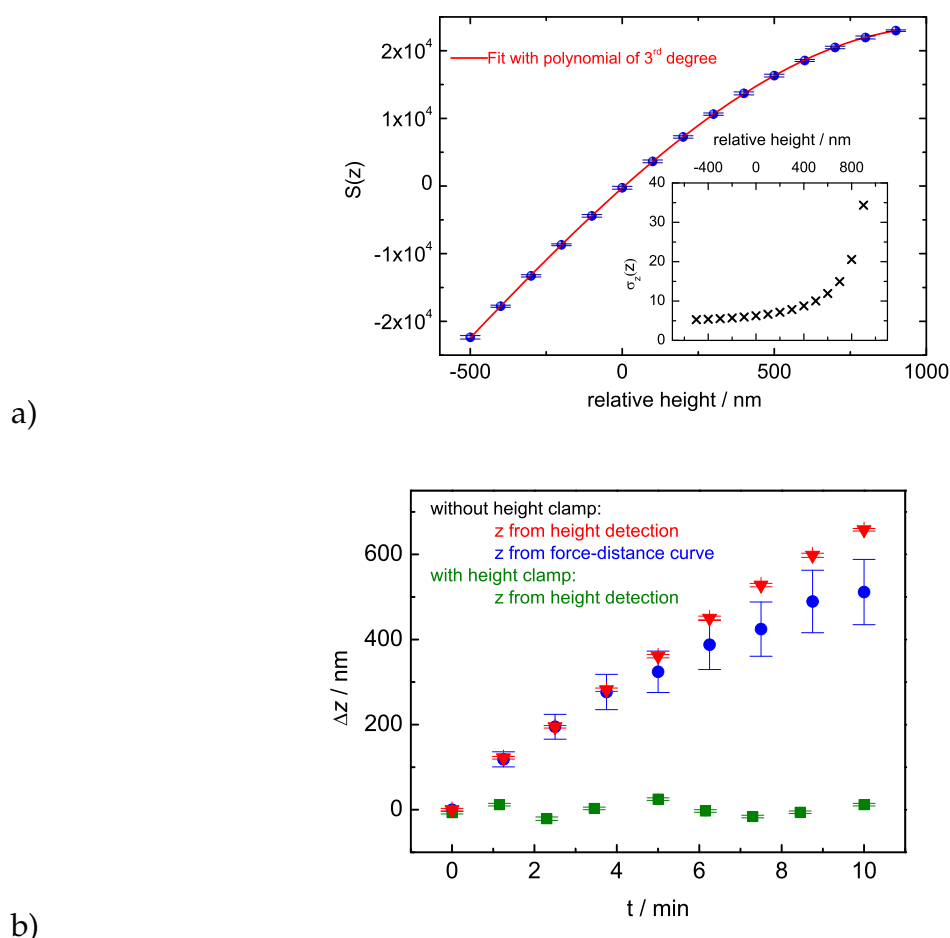


Figure 3.20: (a): The values of $S(z)$ are shown in dependence on the shift in z -direction with respect to a reference height ($z=0$). The height of the particle is changed in steps of 100 nm by use of the piezo stage. Each data point represents the average over 20 images at a constant height. The error bars are defined by the standard deviation. For the whole range of 1400 nm a monotonically increasing dependence of $S(z)$ on the height is found. It can be fitted to a polynomial of degree 3, constituting a master curve. The height of a colloid is then determined by calculating $S(z)$ for the actual image and finding the root of the master curve. Inset: The standard deviation of the height obtained from single images is shown. It is calculated for each height from the standard deviation of $S(z)$. An optimum standard deviation in z of 5 nm is obtained. (b) The height values in different time intervals of 1.25 min are shown for the measurements with and without height clamp. The green squares are the mean values of Δz obtained by the height detection in an experiment with active drift compensation. The height difference as determined by the height detection in the experiment without height clamp is depicted by red triangles. The error bars constitute in both cases the standard deviation over 50 images. The blue circles correspond to the height difference of the particles in the experiment without height clamp as calculated from the force-distance curves by geometrical considerations. The error bars are determined by the limitations of the position detection in the xy -plane together with the error of the fit. For a drift of less than 500 nm ($t < 6.5$ min), the results for Δz obtained by the geometrical calculation coincide with those of the height detection within the experimental uncertainty.

with an accuracy of up to 2 nm. The method is applicable under microscopic white light illumination and is simple to implement. As an example of measurements where active

height regulation is indispensable, force-distance curves are discussed. Furthermore, the colloid height is calculated geometrically. In the range where the geometrical estimation provides reliable results, the values are found to be in quantitative agreement with the suggested algorithm (Fig. 3.20b).

[1] C. Wagner et al., *Journal of Optics* **13**, 115302 (2011)

3.17 Optical Tweezers to study DNA/PrP-Interaction on a Single Molecule Level

C. Wagner, O. Otto*, R. Bujdoso[†], U.F. Keyser*, F. Kremer

*Cavendish Laboratory, University of Cambridge, Cambridge, UK

[†]Department of Veterinary Medicine, University of Cambridge Cambridge, UK

TPrP (Prion Protein) plays a crucial role in neurodegenerative diseases called transmissible spongiform encephalopathies (TSE). The prion diseases affect the structure of the brain or other neural tissue by causing a "spongy" architecture. Up to now these diseases are untreatable and fatal. The infective PrP^{Sc} is the misfolded form of PrP^C, which is ubiquitous in cell membranes. For a long time, the generally accepted hypothesis for the initiation of the transformation was the "protein only-hypothesis" saying that contact with PrP^{Sc} reforms PrP^C. However, new results suggest that also a contact with DNA or RNA is necessary for the misfolding [1, 2]. The interaction of recombinant ovine PrP^C with a single DNA strand is investigated by nanocapillaries and optical tweezers. A change in current is observed suggesting an interaction of DNA and PrP (Fig. 3.21a,b). In order to characterize this interaction, an optical tweezers setup with force clamp is employed. At a force of 2 pN no reduction of the DNA length is observed implying that PrP does not condensate the DNA (Fig. 3.21c).

[1] A. Grossman, *Neurochemical Research* **28**, (6) 955(2003)

[2] N.R. Deleault et al., *Nature* **425**, 717 (2003)

3.18 Friction within Single Pairs of DNA-Grafted Colloids as studied by Optical Tweezers

M.M. Elmahdy, O. Ueberschär, C. Wagner, T. Stangner, C. Gutsche, F. Kremer

Optical Tweezers are employed to study the transition from sliding to stick-slip friction between two DNA grafted (grafting density ~ 1250 molecules per particle, number of base pairs per grafted chain ~ 4000) colloids [1, 2], which are moved (in y-direction, Fig. 1a) in respect to each other with a relative velocity ranging between 50 nm/s up to 3 $\mu\text{m/s}$. For that one colloid is fixed to a micropipet while the other is held in an optical trap hence enabling one to determine and to separate the forces of interaction in the direction parallel (y-direction) and perpendicular (x-direction) to

the motion. A transition from sliding (Fig. 3.22b/c) to stick-slip friction (Fig. 3.22d/e) is found. It depends on the salt (NaCl) concentration in the surrounding medium (Fig. 3.22f) and is shown to be controlled by two factors, (i) interaction volume and (ii) interaction time.

[1] K. Kegler, M. Salomo and F. Kremer *Phys. Rev. Lett.* **23**, 058304 (2007)

[2] C. Gutsche et al. *J. Phys.: Condens. Matter* **23**, 184114 (2011)

3.19 Dynamic force spectroscopy on fluorescence-labeled tau-peptides and monoclonal antibodies measured by Optical Tweezers

T. Stangner, C. Wagner, D. Singer*, C. Gutsche, O. Ueberschär, R. Hoffmann*, F. Kremer

*BBZ, Fakultät für Chemie und Mineralogie, Universität Leipzig, Deutscher Platz 5, 04103 Leipzig

Optical tweezers are experimental tools with extraordinary resolution in positioning (± 1 nm) a micron-sized colloid and in the measurement of forces (± 0.5 pN) acting on it - without any mechanical contact. The combination of optical tweezers and dynamic force spectroscopy is a promising approach to gain deep insight into biological systems on the level of single receptor-ligand-interactions. Here we report about the specific binding of an anti-human tau-monoclonal antibody (mAb), HPT-104, interacting with a synthetic fluorescence-labeled tau-peptide, containing a phosphorylation at Thr231. The fluorescent tagged tau-peptides, anchored on Melanmin-resin beads, are presorted with the fluorescence activated cell sorting (FACS) method (Fig. 3.23a, b)) in order to achieve homogenous and reproducible surface coverage. By that the results can be more easily compared with other experiments, using different antibodies and/or phosphorylation pattern. Specific binding events between peptide and mAbs, obtained by dynamic force spectroscopy, are described according to the Dudko-Hummer-Szabo-model [1] (Fig. 3.23c)). Fitting parameters are bond lifetime (τ_0), binding length (x_{ts}) and depth of the binding potential ΔG . A comparison between labeled and non-labeled tau-peptides [2] and their interactions with mAbs shows that, due to the presence of the fluorescence dye (Fluorescein), the bond lifetime and binding length is reduced.

[1] O. Dudko, G. Hummer, A. Szabo; *PNAS* **105**, 5755 (2008)

[2] C. Wagner, D. Singer, T. Stangner, O. Ueberschär, C. Gutsche, R. Hoffmann, F. Kremer; *Soft Matter* **7**, 4370 (2011)

3.20 Drag reduction by DNA-grafting for single microspheres in a dilute λ -DNA solution

O. Ueberschär, C. Wagner, T. Stangner, K. Kühne*, C. Gutsche, F. Kremer

*Molekulare Onkologie, Universitätsfrauenklinik Leipzig, Arbeitsgruppe Prof. Kurt Engeland, Semmelweisstraße 14, 04103 Leipzig, Germany

The fluid resistance of single micrometre-sized blank and DNA-grafted polystyrene microspheres under shear flow is compared in purified water and dilute λ -DNA solutions by means of optical tweezers experiments with a high spatial (± 4 nm) and temporal (± 0.2 ms) resolution. The measurement results show that the drag experienced by a colloid in a dilute λ -DNA solution (molecular weight of 48502 bp per molecule, radius of gyration of $0.5 \mu\text{m}$) is significantly decreased if the microsphere bears a grafted DNA brush. This newly discovered drag reduction effect is studied for different parameters, comprising the molecular weight of the grafted DNA molecules (250 bp, 1000 bp and 4000 bp), the concentration of the λ -DNA solution (11, 17 and $23 \mu\text{g/ml}^{-1}$, all being significantly smaller than the critical entanglement concentration c^*), the microsphere core diameter ($2 \mu\text{m}$, $3 \mu\text{m}$ and $6 \mu\text{m}$) as well as the flow speed of the medium (10 to $50 \mu\text{m/s}$). The maximum extent of the drag reduction is found to amount to $(60 \pm 20)\%$ compared to the λ -DNA-induced contribution on the drag acting for blank colloids. We propose a theoretical explanation of this effect based on the combination of the drift diffusion model of Rauscher and co-workers [2] and the stagnation length theory of polymer brushes, as it was established by Kim, Lobaskin et al. [3]. In particular, the solution of the Stokes equation (i.e., the Navier-Stokes equation for creeping flow) for the studied system yields a numerical prediction that is found to be in full accord with our experimental results within experimental uncertainty.

- [1] O. Ueberschär, C. Wagner, T. Stangner, K. Kühne, C. Gutsche, F. Kremer, *Polymer* **52**, 4021 (2011)
- [2] M. Rauscher, *J. Phys.: Condens. Matter* **22**, 364109 (2010)
- [3] Y. W. Kim, V. Lobaskin, C. Gutsche, F. Kremer, P. Pincus, R. R. Netz, *Macromolecules* **42**, (10) 3650 (2008)

3.21 A novel video-based microsphere localization algorithm for low contrast silica particles under white light illumination

O. Ueberschär, C. Wagner, T. Stangner, C. Gutsche, F. Kremer,

On the basis of a brief review of four common image recognition algorithms for microspheres made of polystyrene or melamine resin, we present a new microsphere localization method for low-contrast silica beads under white light illumination. We compare both the polystyrene and silica procedures with respect to accuracy and precision by means of an optical tweezers setup providing CMOS video microscopy capability. By that we demonstrate that our new silica algorithm achieves a relative position uncertainty of less than ± 1 nm for micron-sized microspheres, significantly exceeding the precision of the other silica approaches studied. Second, we present an advancement of our single microsphere tracking method to scenarios where two polystyrene, melamine resin or silica microspheres are in close-to-contact proximity. While the majority of the

analysis algorithms studied generate artefacts due to interference effects under these conditions, we show that our new approach yields accurate and precise results. In summary, we recommend using our new algorithms with preference when tracking silica microspheres in video microscopy, as it is often required in optical tweezers experiments.

- [1] O. Ueberschär, C. Wagner, T. Stangner, C. Gutsche, F. Kremer, *Optics and Lasers in Engineering* **50**, 423 (2012)

3.22 Electrophoretic mobility of ds-DNA-grafted single colloids as studied by optical tweezers

I. Semenov, C. Gutsche, M.M. Elmahdy, O. Ueberschär, F. Kremer

The electrophoretic mobility of single colloids grafted with double stranded (ds) DNA is studied by Single Colloid Electrophoresis [1, 2]. For that Optical Tweezers (OT) are employed to measure separately the complex electrophoretic mobility of a single colloid and the complex electroosmotic response of the surrounding medium. Parameters to be varied are the concentration (10^{-5} - 1 mol/l) and valency (KCl, CaCl₂, LaCl₃) of the ions in the surrounding aqueous medium, as well as the contour length (250, 1000 and 4000 base pairs) of the grafted chains in the latter case. For the ds-DNA-grafted colloids a pronounced decrease of the electrophoretic mobility is observed in comparison to blank particles and with increasing DNA molecular weight, under identical conditions (Fig. 3.26(left)). The findings are discussed in terms of the Standard Electrokinetic Model [3]. The electrophoretic mobility of a ds-DNA-grafted single colloid at high ionic strength can be understood quantitatively within the limits of the linearized Poisson-Boltzmann equation, i.e. using the so-called Smoluchowski formula:

$$\mu_e = -\frac{eZ_{eff}^{total}}{4\pi\eta\alpha_{eff}(1+\kappa\alpha)}$$

where the effective hydrodynamic radius $\alpha_{eff} = R_{bare} + \Delta R$ of a single ds-DNA-grafted particle in varying ionic strength of the surrounding medium is determined by means of Brownian motion analysis and OT accomplished with fast position detection [4]. The effective charge Z_{eff}^{bare} is obtained from the measurements of the interaction forces between two identical ds-DNA-grafted colloids in electrolyte solutions of different concentrations assuming that the zeta potential of the blank particle is to be defined at the slipping plane of the whole DNA brush, as it show on Fig. 3.26(right).

$$Z_{eff}^{total} = (Z_{eff}^{bare} - \eta) \exp(-\chi\Delta R) + Z_{eff}^{DNA Layer}$$

- [1] I. Semenov et al., *Journal of Physics: Condensed Matter* **22**, 494109 (2010).
 [2] I. Semenov et al., *Journal of Colloid and Interface Science* **337**, 260 (2009).
 [3] R. W. O'Brien, and L. R. White, *J. Chem. Soc., Faraday Transactions 2: Molecular and Chemical Physics* **74**,1607 (1978).
 [4] O. Ueberschär et al., *Polymer* **52**, 1829 (2011).

3.23 Funding

FOR 877: " From local constraints to macroscopic transport" TP 7 "Electric field driven motion of single polyelectrolyte grafted colloids" TP3 "Dynamics of DNA under tension and confinement"

Prof. Dr. F. Kremer and Prof. Dr. K. Kroy

KR 1138/21-1 (2007-2011)

FOR 877: " From local constraints to macroscopic transport" TP 7 "Electric field driven motion of single polyelectrolyte grafted colloids"

Prof. Dr. F. Kremer

KR 1138/21-2 (2011-2014)

SPP 1191 "Ionic Liquids" TP "Charge transport and glassy dynamics in ionic liquids"

Prof. Dr. F. Kremer

KR 1138/18-3 (2010-2012)

SPP 1369 "Polymer-Solid Contacts: Interfaces and Interphases" TP "Interfacial dynamics of polymers in interaction with solid substrates"

Prof. Dr. F. Kremer

KR 1138/23-1 (2008-2011), KR 1138/23-2 (2011-2014)

Graduate School "Leipzig School of Natural Sciences -Building with Molecules and Nano-objects" BuildMoNa, TP 15 "Dynamics of DNA under tension and in confinement"

Prof. Dr. F. Kremer

GSC 185/1 (2008-2012)

Prof. Dr. F. Kremer is Principal Investigator and Lecturer in the International Research Training Group "Diffusion in Porous Materials" headed by Prof. Dr. R. Gläser and Prof. Dr. F. Kapteijn.

IRTG "Diffusion in Porous Materials" TP "Molecular Dynamics in Intentionally Tailored Nanopores"

Prof. Dr. F. Kremer

GRK 1056/02 (2009-2013)

Prof. Dr. F. Kremer is Principal Investigator and Lecturer in the International Research Training Group "Diffusion in Porous Materials" headed by Prof. Dr. R. Gläser and Prof. Dr. F. Kapteijn.

SFB/TRR 102 " Polymers under multiple constraints: restricted and controlled molecular order and mobility" TP B05 "Structural levels of organisation in spider-silk - a combined mechanical and IR-spectroscopic study" (2011-2015) TP B08 "Broadband Dielectric Spectroscopy to study the molecular dynamics in nanometer thin layers of block copolymers" (2011-2015)

Prof. Dr. F. Kremer

Prof. Dr. F. Kremer is deputy chairman of the SFB-TRR 102 on "Polymers under multiple constraints: restricted and controlled molecular order and mobility" of the Universities of Halle and Leipzig.

3.24 Organizational Duties

Hartmut Domröse

- electronic technician

Karin Girke

- secretary

Dipl.-Phys. Cordula Bärbel Krause

- secretary

Dipl.-Ing. Jörg Reinmuth

- technician

Dipl.-Phys. Wiktor Skokow

- technician

3.25 External Cooperations

Industry

- Novocontrol, Hundsangen, Germany
- BOREALIS Polyolefine GmbH, Linz, Austria
- Comtech GmbH, München, Germany
- inotec FEG mbH, Markkleeberg, Germany

3.26 Publications

Journals

Wagner, C., C. Olbrich, H. Brutzer, M. Salomo, U. Kleinekathöfer, U.F. Keyser, F. Kremer "DNA condensation by TmHU studied by optical tweezers, AFM and molecular dynamics simulations" *Journal of Biological Physics* **37**, 117-131 (2011). DOI: 10.1007/s10867-010-9203-7

Gutsche, C., M.M. Elmahdy, K. Kegler, I. Semenov, T. Stangner, O. Otto, O. Ueberschär, U.F. Keyser, M. Krüger, M. Rauscher, R. Weber, J. Harting, Y.W. Kim, V. Lobaskin, R.R. Netz and F. Kremer "Micro-rheology on (polymer-grafted) colloids using Optical Tweezers" *J. of Phys. Condensed Mater* **23**, 184114-184131 (2011) DOI:10.1088/0953-8984/23/18/184114

Sangoro, J. R., Iacob, C., Naumov, S., Hunger, J., Rexhausen, H., Valiullin, R., Strehmel, V., Buchner, R., Kärger, J., and Kremer, F. "Duffusion in ionic liquids: the interplay between molecular structure and dynamics". *Soft Matter* **7**, 1678-1681 (2011) DOI:10.1039/C0SM01404D

Ueberschär, O., C. Wagner, T. Stangner, C. Gutsche, F. Kremer "The effective hydrodynamic radius of single DNA-grafted colloids as measured by fast Brownian motion analysis" *Polymer* **52**, 1829-1836 (2011) DOI:10.1016/j.polymer.2011.02.001

Sangoro, J.R., C. Iacob, R. Valiullin, C. Friedrich, J. Kärger, F. Kremer "Rotational and translational diffusion in glass-forming N,N,-diethyl-3-methylbenzamide (DEET)". *Soft Matter*, **7**, (22) 10565-10568 (2011) DOI: 10.1039/C1SM06377D

Spiess, K., R. Ene, C. Keenan, J. Senker, F. Kremer, T. Scheibel "Impact of initial solvent on thermal stability and mechanical properties of recombinant spider silk films" *J. Mater. Chem.*, **21**, 13594-13604 (2011) DOI: 10.1039/c1jm11700a

Wagner, C., D. Singer, O. Ueberschär, T. Stangner, C. Gutsche, R. Hoffmann, F. Kremer "Dynamic force spectroscopy on the binding of monoclonal antibodies and tau peptides" *Soft Matter* **7**, 4370-4378 (2011) DOI: 10.1039/c0sm01414a

Ueberschär, O., C. Wagner, T. Stangner, K. Kühne, C. Gutsche, F. Kremer "Drag reduction by DNA-grafting for single microspheres in a dilute -DNA solution" *Polymer* **52**, 4021-4032 (2011) DOI: 10.1016/j.polymer.2011.06.057

Hagenau, A., P. Papadopoulos, F. Kremer, T. Scheibel, "Mussel collagen molecules with silk-like domains as load-bearing elements in distal byssal threads" *J. Structural Biology* **175** (3) 339-347 (2011) DOI: 10.1016/j.jsb.2011.05.016

Wagner, C., T. Stangner, C. Gutsche, O. Ueberschär, F. Kremer "Optical tweezers setup with optical height detection and active height regulation under white light illumination" *Journal of Optics* **13**, 115302 (2011) DOI: 10.1088/2040-8978/13/11/115302

Kossack, W., P. Papadopoulos, M. Parkinson, F. Prades, F. Kremer "IR Transition moment orientational analysis on semi-crystalline polyethylene films" *Polymer* **52**, 6061-6065 (2011) DOI: 10.1016/j.polymer.2011.10.051

Books

Serghei, A., J.R. Sangoro, F. Kremer "Broadband Dielectric Spectroscopy on electrode polarization and its scaling" Chapter 15 of the book "Electrical Phenomena at Interfaces and Biointerfaces: Fundamentals in Nano- Bio- and Environmental Sciences" Ed. Hiroyuki Ohshima, accepted by John Wiley&Sons, Inc. New York, (2011)

3.27 Graduations

Doctorate

- Dipl.-Chem. Roxana Ene
Structural levels of organization in spider silk as studied by time-resolved polarized FTIR spectroscopy

Diploma

- Tim Stangner
Wechselwirkungen zwischen Polymer-gepfropften Kolloiden
- Tilmann Schubert
Charakteristische Eigenschaften von molekularen Fluiden und Polymeren am dynamischen Glasübergang

Bachelor

- Hannes Krauß
FT IR-Messungen zur Temperaturabhängigkeit der Absorption von organischen Glasbildnern
- Benjamin Schott
Untersuchung photophysikalischer Eigenschaften des Photosensibilisators THPTS

3.28 Guests

- Dr. El-Habib Belarbi
Khalidoun University, Tiaret, Algeria
- M.Sc. Ignacio Martin-Fabiani Carrato
C.S.I.C., Madrid, Spain
- Dr. Christina Krywka
Uni Kiel, Germany

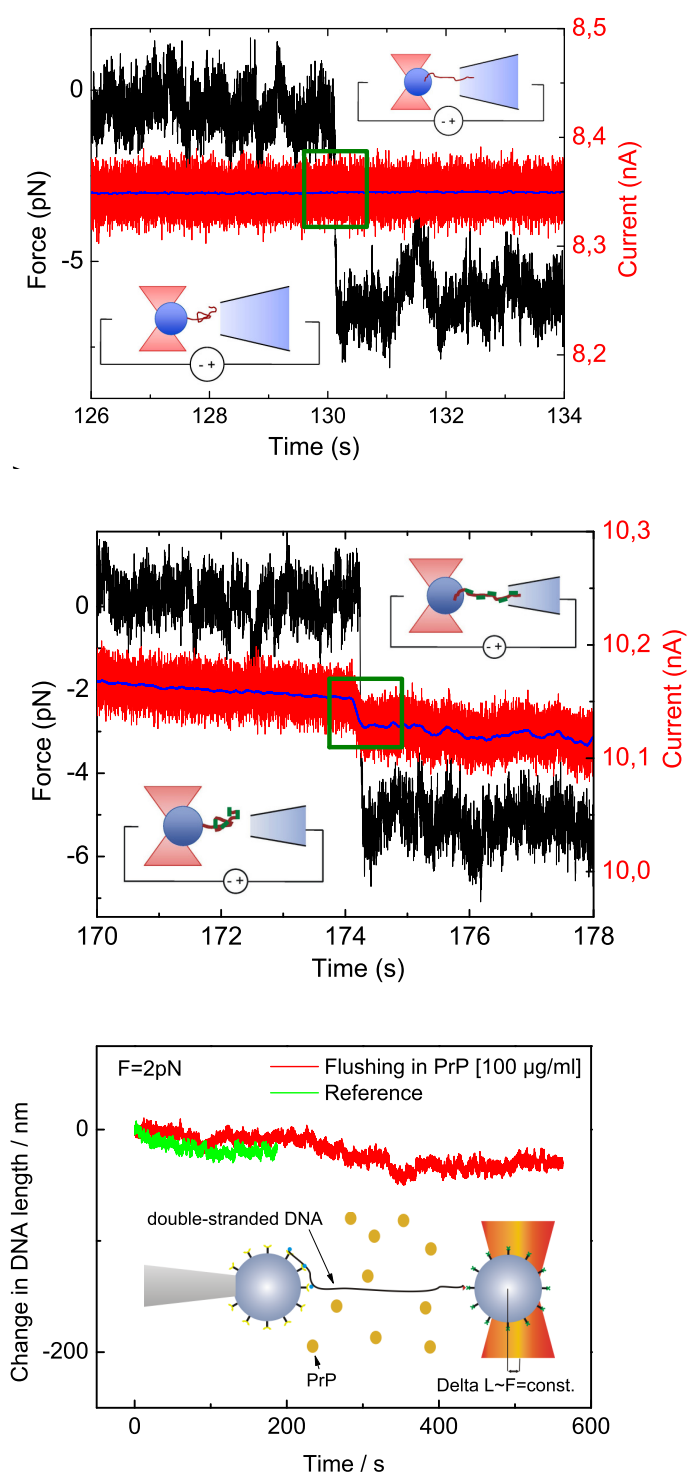


Figure 3.21: a) Insertion of bare DNA in capillary (Diameter ~ 500 nm) at a voltage of 200 mV. No jump in current can be observed. b) Insertion of PrP/DNA-complex in capillary at a Voltage of 200 mV. A jump in current of ~ 0.05 nA is observed. c) The sketch shows the experimental setup: double-stranded DNA is spanned between two colloids while one of them is held in the optical trap. A feedback-loop ensures that the force is constant at 2 pN. The red line shows the change in DNA length while flushing in PrP. No change is observed. As a reference (green line), PBS buffer is flushed in under similar conditions.

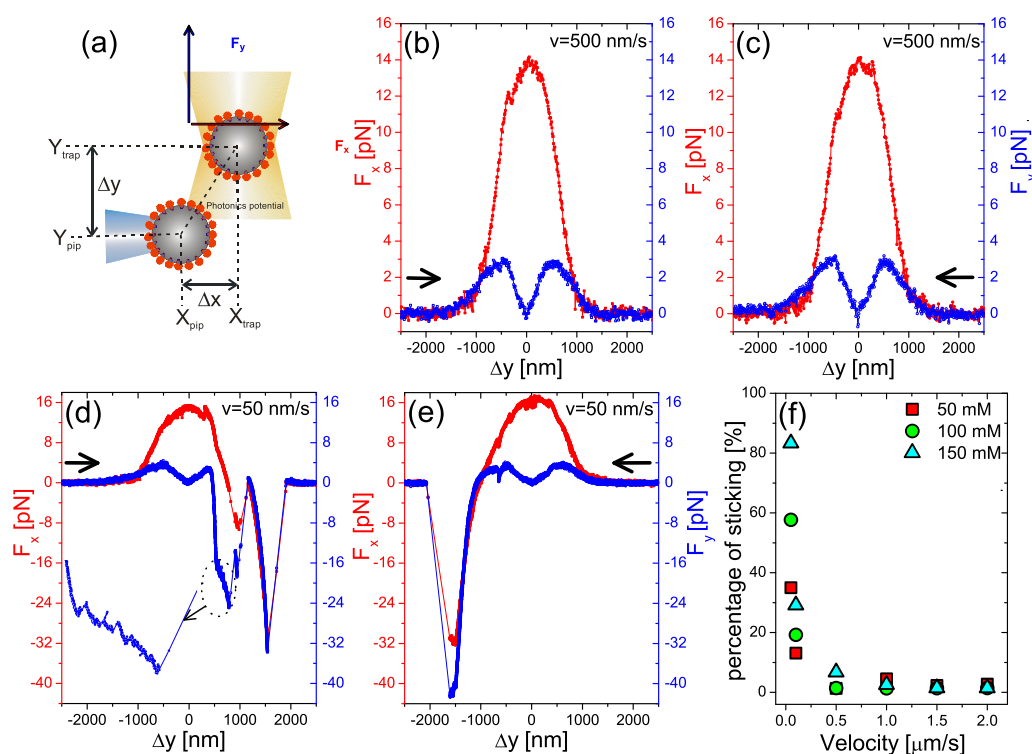


Figure 3.22: a) scheme of the geometric arrangement of the two colloids; one is fixed by a micropipet and moved in y -direction while the other is hold in the optical trap. The forces of interaction in x - and y -direction (F_x) and (F_y) are determined separately from the displacement of the latter out of the equilibrium position. All measurements are carried out within single pairs of DNA-grafted colloids immersed in 10 mM Tris buffered solution with different NaCl concentrations (50, 100 and 150 mM) at pH 8.5. (b, c) At high relative velocity (500 nm/s), the forces of interaction in x (F_x , filled red symbols) and y (F_y , open blue symbols)-directions, show sliding friction while at low velocity (50 nm/s), stick-slip friction takes place. The forces of interaction between the two colloids are 15 ± 5 pN. Arrows illustrate the forward and backward motion, respectively. (f) Percentage of sticking events versus relative velocity at different salt concentrations as indicated.

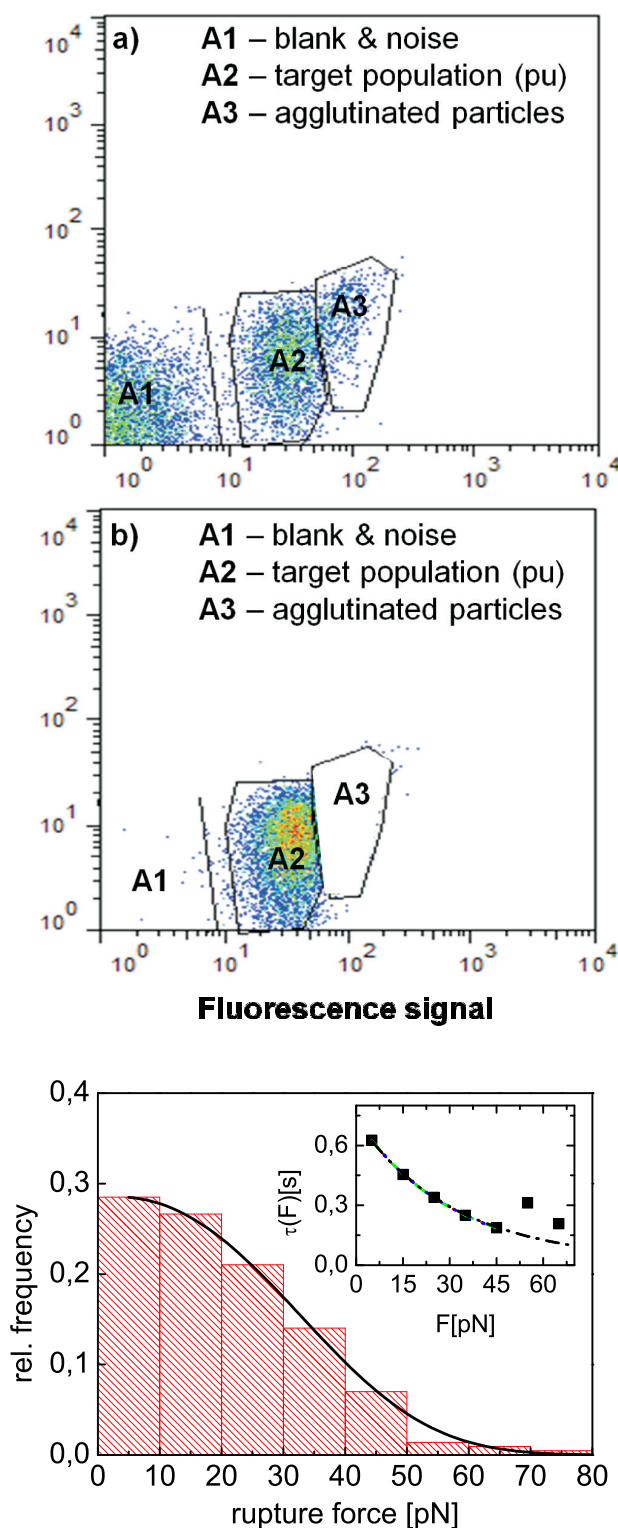


Figure 3.23: a) FACS-signal for MF-particle ($2\ \mu\text{m}$) before sorting. Three populations are visible: A1 contains blank colloids, A2 contains the fluorescence tagged particles and A3 contains agglutinated particles. b) FACS-signal for MF-particles ($2\ \mu\text{m}$) after sorting. Only population A2 remains. Population A1 and A3 are sorted out. c) Rupture force distribution for HPT 104 vs. fluorescent labeled tau-peptide. Fit (black line) corresponds to the theory of Dudko, Hummer and Szabo. The data fits to the model. Inset: The lifetime of the interaction between HPT-104 and the monophosphorylated peptide is shown in dependence on the force at a loading rate of $48\ \text{pN/s}$. The data are fitted globally to $\tau_0(F)$ from the DHS-model.

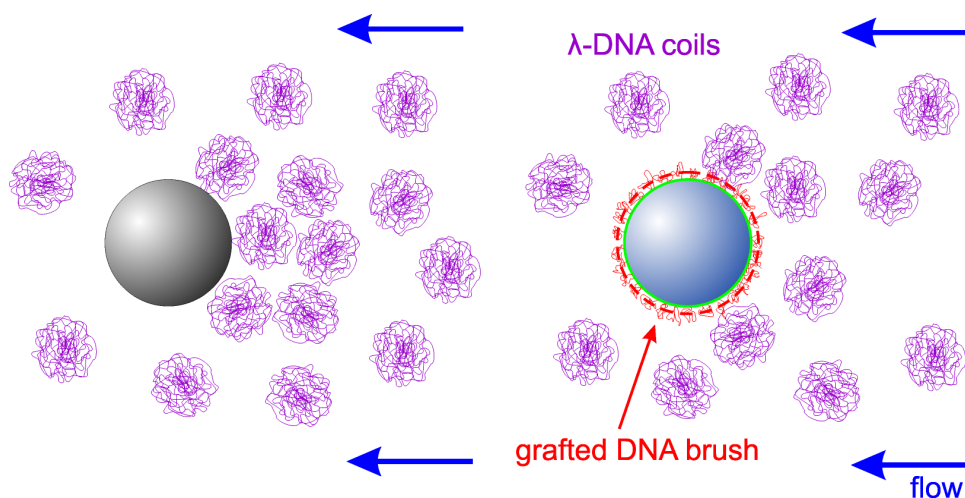


Figure 3.24: Schematic of the origin of the drag reduction effect. Left: The flow field around a hard sphere under no-slip condition leads to an accumulation of λ -DNA coils in front of and to the depletion of such behind the colloid. Right: The analogous scenario is shown for a grafted colloid (4000 bp DNA) with an effective hydrodynamic radius increased by 130 nm. While the minimum centre-centre distance for the grafted colloid and λ -DNA coils is the same as in the case of a blank colloid, the flow field vanishes now at an increased distance from the sphere surface. The radial component at the maximum-proximity distance of a λ -DNA coil is thus smaller (by approximately 44% in the depicted case), leading to a decrease of the extent of λ -DNA accumulation and depletion. As a result, the acting drag forces are equally decreased.

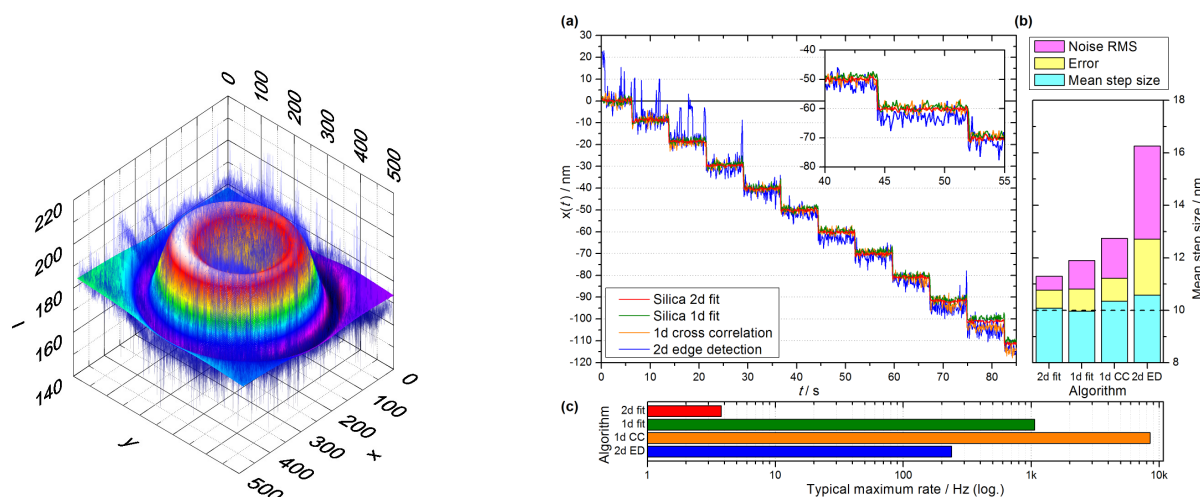


Figure 3.25: The new algorithm Silica 2d fit. Left: The intensity profile of silica microsphere (diameter of $4.71 \pm 0.47 \mu\text{m}$) is plotted (blue shaded noisy surface) and fitted to an empirical function (colour spectrum smooth surface). Right: Experimental investigation of the accuracy and precision of our two new and two established single silica algorithms. The experimentally acquired video microscopy images of a piezo stage position ramp are analyzed and plotted. The accuracy, the precision as well as the execution (i.e. computation) speed of these four algorithms are compared on the basis of this image analysis process.

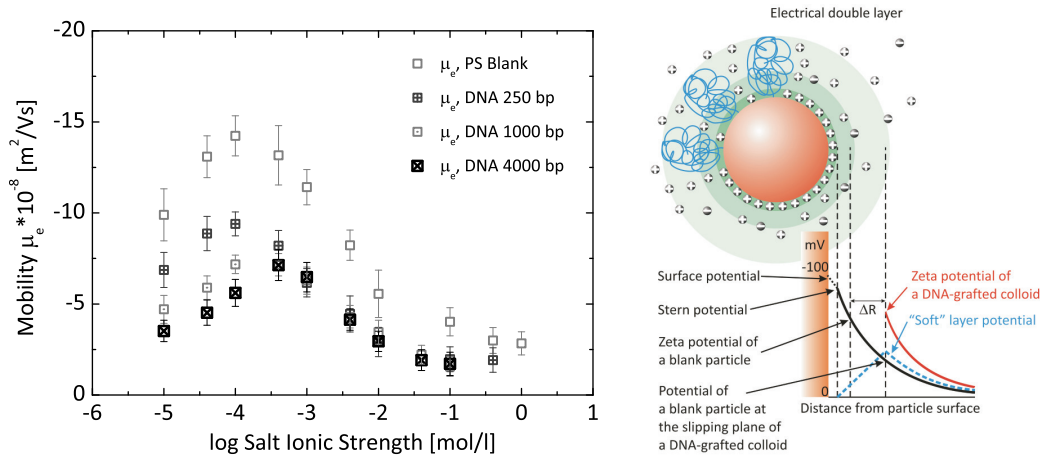


Figure 3.26: (left) the electrophoretic mobility vs. salt ionic strength of aqueous KCl solution for the negatively charged blank and ds-DNA-grafted colloids with varying DNA molecular weight (250, 1000 and 4000 base pairs) and grafting density 1250 chains per colloid. (right) Schematic diagram of the EDL (not to scale) at the negatively charged blank particle interface, depicting the probable electrostatic potential distribution above the blank particle's surface and possible shift of the shear plane due to DNA coating, where the Z_{eff}^{bare} is to be considered.

4

Physics of Interfaces

4.1 Introduction

The department of Physics of Interfaces (Grenzflächenphysik, GFP) is in a transition state since April 2009. From the 19 scientists employed in the Group in 2011, 18 were financed as PhD students or post-docs via third party funding and two received a grand as Heisenberg fellow of the DFG. Especially, the good situation in the third party funding allowed us to successfully contribute to research and teaching within the Institute of Experimental Physics I. Teaching obligations in several main courses of Experimental Physics were taken over by scientists and PhD students of the group. Prof. Dr. Grit Kalies left our group and started her new position as Professor for Thermodynamics at the Hochschule für Technik und Wirtschaft in Dresden.

Please find below the detailed descriptions of our research activities and project achievements in the field of molecules interacting with internal surfaces of micro- and mesoporous materials for 2011. If you are interested in our research, please do not hesitate to contact us.

Frank Stallmach

4.2 Diffusion of Fluids During Melting in Mesopores

D. Kondrashova, R. Valiullin

Nuclear magnetic resonance provides a variety of tools for structural characterization of porous solids. Among them, NMR cryodiffusometry has recently emerged as a novel, promising approach for probing interconnectivity of pore spaces [1–3]. This method is based on a simultaneous assessment of the phase state of intraporous liquids at low temperatures, using NMR-cryoporometry, and their transport properties, using NMR-diffusometry. Although its potentials to provide qualitative information has already been demonstrated using porous material with complex pore morphologies, in-depth studies aimed at more quantitative predictions are still lacking.

In our work, by choosing two model porous materials with ordered and disordered pore structures as host systems, we discuss both methodological and fundamental aspects related to NMR cryodiffusometry [4]. As an example, Fig. 4.1 shows an oscillating behavior of the effective, long-range diffusivity of nitrobenzene measured in

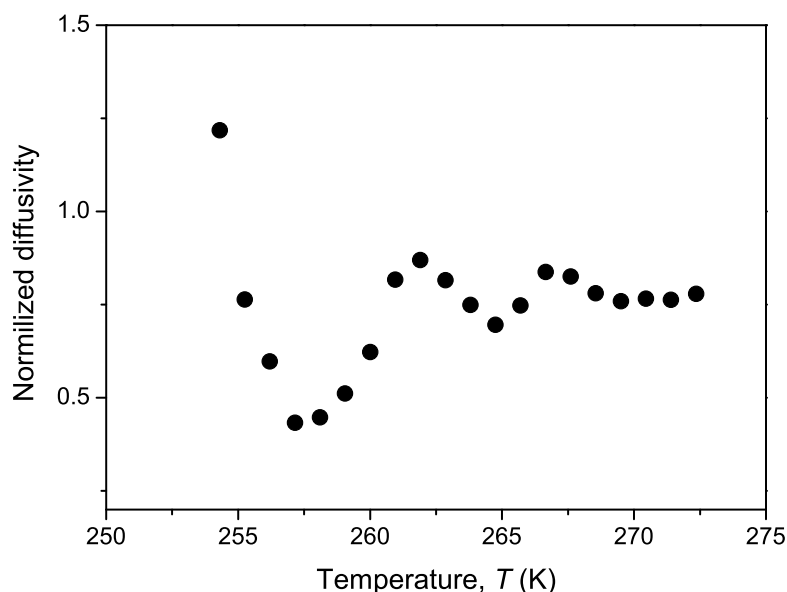


Figure 4.1: Normalized diffusivities of nitrobenzene in micro-structured mesoporous silicon sample as a function of temperature during warming.

mesoporous silicon sample with increasing temperature. The sample was fabricated to consist of alternating structural units with different pore sizes. The minima in the figure do correlate with melting of the frozen nitrobenzene in different units. Thus, with the use of an intentionally micro-structured mesoporous silicon we demonstrate how its structural features give rise to specific patterns in the effective molecular diffusivities measured upon progressive melting of a frozen liquid in the mesopores. We further establish a methodology how this type of experimental data may be converted to interconnectivity correlation map of a porous material.

- [1] A. V. Filippov and V. D. Skirda: *Colloid J.* **62**, 759 (2000)
- [2] M. Dvoyashkin et al.: *J. Chem. Phys.* **129**, 154702 (2008)
- [3] E. L. Perkins et al.: *Chem. Eng. Sci.* **65**, 611 (2010)
- [4] D. Kondrashova and R. Valiullin: *New J. Phys.* **13**, 015008 (2011)

4.3 Probing Fluid Distribution in Porous Materials

P. Zeigermann, R. Valiullin

The formation of adsorption hysteresis in mesoporous material with random pore structure may be interrelated with different distributions of the fluid density attained along different paths of the system preparation. Indeed, upon step-wise variation of the external gas pressure, the system gets trapped in quasi-equilibrium states with arrested liquid domain configurations. These states are kept from further equilibration by a very rugged landscape of the free-energy resulting from pore space disorder. Experimental

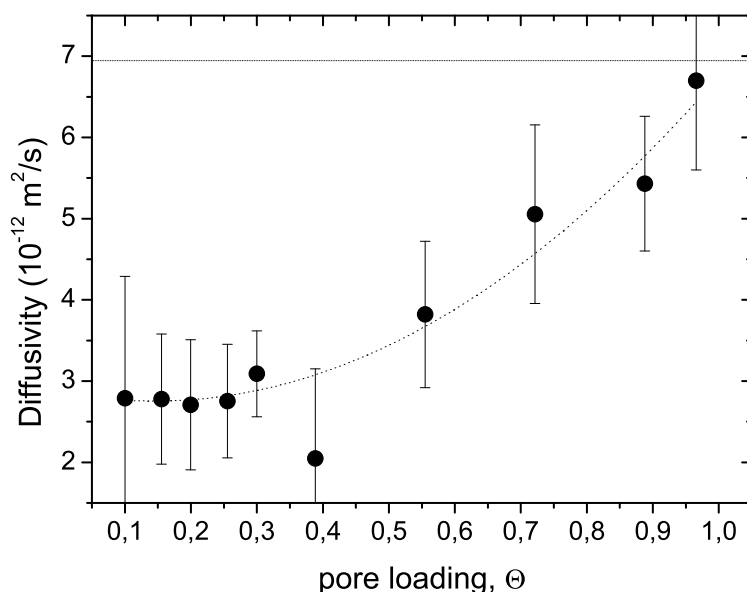


Figure 4.2: Diffusivities of probe molecules (TEHOS) as a function of the overall pore loading by the cyclohexane-TEHOS mixture.

assessment of such arrested states is far from trivial [1]. One of the main difficulties is determined by the fact that during their trajectories the molecules alternate between the liquid and gas phases. Thus, substantial part of information on structure contained in structure-interrelated diffusivities becomes averaged out.

In this work, to access microscopic details of these distributions we suggest an alternative approach [2]. In addition to the main sorptive liquid, distribution of which along the pore space was of interest, a small amount of a probe liquid has been added. The probe liquid was chosen to always reside in the liquid phase. Molecular diffusivities of both liquids then have been traced using pulsed field gradient NMR (diffusivities of probe species in Vycor porous glass are shown in Figure 4.2). The two molecular species explore different spaces occupied by the capillary-condensed (accessible for both species) and gaseous (accessible only for the molecules of the main sorptive) phases. Comparative analysis of the diffusion properties obtained at different states along the adsorption isotherm revealed further insight into character of the fluid distribution and mass transfer of binary fluids in pores.

[1] S. Naumov et al.: *Langmuir* **24**, 6429 (2008)

[2] P. Zeigermann et al.: *Adsorption* **17**, 69 (2011)

4.4 NMR Diffusion Studies Using Super-High Gradient Pulses

M. Gratz, M. Grossmann, S. Schlayer, F. Stallmach, P. Galvosas*,

*MacDiarmid Institute, Victoria University, Wellington, New Zealand

Nuclear magnetic resonance with pulsed magnetic field gradients (PFG NMR) has gained great importance for the non-invasive investigation of self-diffusion [1]. Current approaches are able to detect molecular displacements in the order of 100 nm. With the aim to extend the accessible length scale towards smaller displacements we developed a new probe (see Fig. 4.3), which is designed to generate bipolar gradients of up to 93 T/m. An adapted Maxwell coil arrangement was used in combination with commercially available gradient amplifiers providing currents as high as 100 A. Finite element simulations were conducted using COMSOL® yielding sufficient high linearity of the pulsed magnetic field within a cylindrical volume of 3 mm times 5 mm.

Initial calibration procedures [2] for the characterization of the new setup confirm the correct interplay between gradient amplifiers and gradient coil for gradients of up to 70 T/m. First PFG NMR experiments were conducted using samples with well-known properties while employing pulsed field gradients of up to 65 T/m. In particular we used the triblock copolymer P123 (BASF AG, Germany) being dissolved in 50 wt% D₂O, thus forming a hexagonal structure. We found diffusion coefficients as well as the expected diffusion anisotropy in agreement with previously published values [3].

Furthermore, the use of such super-high gradients allows to significantly shorten the observation time during the PFG NMR experiment, while still maintaining a reasonable spin echo attenuation. Thus, we were able to find root mean square displacements for short observation times (< 120 ms) that are in the order of a few 10 nm, which confirms the potentials of the presented setup for the extension of the accessible length scales towards smaller values.

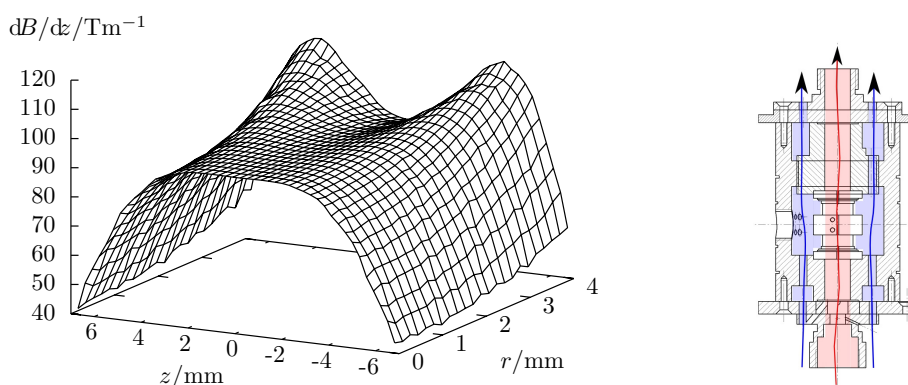


Figure 4.3: New probe design. The gradient profile at the sample region deviates only by 0.4 % (left). The scheme of the hardware (right) outlines gradient cooling (blue) and temperature control of the sample (red) by separated air streams.

- [1] F. Stallmach and P. Galvosas: *Annu. Rep. NMR Spectrosc.* **61**, 51 (2007)
- [2] A. C. Wright et al.: *J. Magn. Reson.* **186**, 17 (2007)
- [3] K. Ulrich et al.: *Phys. Rev. Lett.* **102**, 037801 (2009)

4.5 Magnetic Resonance Measurements of Iron Turn-Over Processes in Natural Sands

I. Mittreiter*, S.E. Oswald[†], F. Stallmach

*Department Hydrogeologie, UFZ - Helmholtz-Zentrum für Umweltforschung GmbH

[†]Institut für Erd- und Umweltwissenschaften, Universität Potsdam

Nuclear Magnetic Resonance (NMR) has been applied for non-destructive investigation of iron turn-over processes in natural sands [1, 2]. These processes play an important role in groundwater with varying redox and PH conditions. Iron (Fe^{3+}) dissolution and precipitation reactions were observed in water-saturated sand columns with high temporal and spatial resolution using the relaxation enhancement of water in the presence of paramagnetic ions as contrast mechanism [2, 3]. The dissolved Fe^{3+} concentrations were measured by the inversion recovery spin echo NMR pulse sequence with a read gradient in axial direction of the sand column. The results show the changes of local Fe^{3+} concentration after an sudden increase of PH in the top of the column (Fig. 4.4). They were analyzed by a reaction-diffusion model, demonstrating that Fe^{3+} transport through the sand column changes from diffusion-limited in the beginning to dissolution-limited at the end. Further information may be found in refs [1, 4].

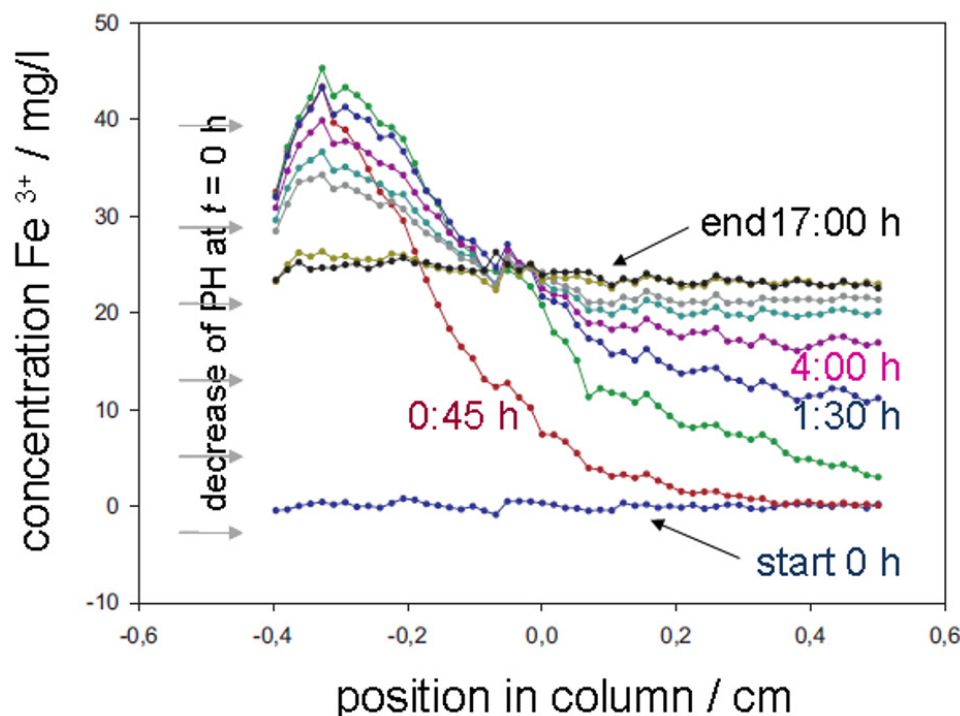


Figure 4.4: Time dependence of the Fe^{3+} concentration in a 1 cm long water-saturated sand column due to mineral dissolution after decrease of the PH by addition of hydrochloric acid on top of the sample [1, 4].

- [1] I. Mittreiter et al.: Grundwasser 16, 269 (2011), doi: 10.1007/s00767-011-0177-6;
 [2] I. Mittreiter et al.: Open Magn. Reson. 3, 46 (2010);

- [3] F. Furtado et al.: *Environ. Sci. Technol.* **45**, 8866 (2011), [dx.doi.org/10.1021/es2010946](https://doi.org/10.1021/es2010946);
 [4] I. Mittreiter: *NMR als Mittel zur Charakterisierung des biologischen Schadstoffabbaus im Porenraum*, phd Thesis, University Leipzig, 2010.

4.6 X Observe NMR Probe Design for Diffusion Studies with Li^+ and Cs^+ Cations and CO_2 in Porous Systems

St. Schlayer, C. Horch, A.-K. Pusch, St. Beckert, M. Peksa, F. Stallmach

An X observe NMR probe was equipped with a z-gradient coil to enable high-sensitivity pulsed field gradient NMR diffusion studies of non ^1H containing substances such as, e.g., metal cations in aqueous salt solutions and of adsorbed CO_2 or CO in porous systems. The necessary probe modifications, the coil support and the generated magnetic fields are shown in Fig. 4.5. The system yields pulsed field gradients of up to $\pm 16.2 \text{ Tm}^{-1}$. It was calibrated at ^2H resonance frequency and successfully applied for diffusion studies at ^7Li , ^{23}Na , ^{13}C and ^{133}Cs frequencies [1]. Significant reductions of the mobilities of the cations in LiCl_{ac} and CsCl_{ac} solution introduced into a porous mesocellular silica foams are observed. Single component self-diffusion of CO_2 and CH_4 (measured by ^1H NMR) as well as self-diffusion of the individual components in CO_2/CH_4 mixtures were studied in the MOF CuBTC and are currently further investigated in ZIF-8 [2]. The experimental results generally confirm high mobilities of the adsorbed gases in MOF's. [1–3].

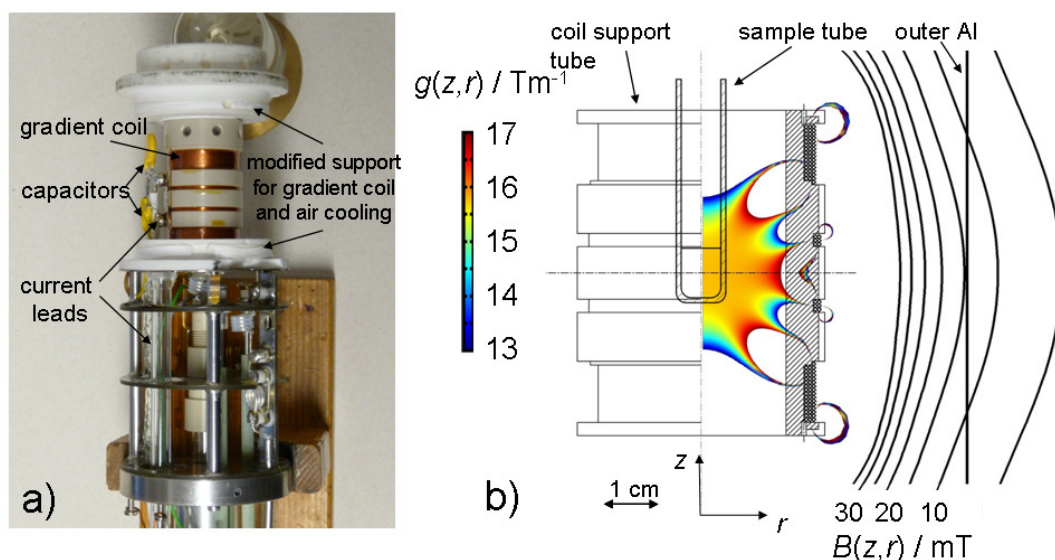


Figure 4.5: X observe NMR probe equipped with a z-gradient coil. (a) Photograph of the top part of the NMR probe with its metal cover removed. Added and modified components are indicated. (b) Drawing of the gradient coil support with the color plot of the calculated field gradient $g(z, r)$ at the NMR sample position and the contour plot of the stray field $B(z, r)$ of the gradient coil at the position of the metal tube (outer probe cover). The spatial dependence of the gradient and field values are plotted for the available gradient current of 100 A. [1]

- [1] A. Schlayer et al.: Materials **xx**, in press (2012);
 [2] E. Pantatosaki et al.: J. Chem. Phys. **116**, 201 (2011);
 [3] A.-K. Pusch et al.: PBAST-6 conference, submitted (2012);

4.7 Intra-Crystalline Diffusion Study of Light Hydrocarbons in Zeolite ZSM-58

T. Binder, F. Hibbe, J. Kärger, A. Martinez-Joaristi*, F. Kapteijn*, D. Ruthven†

*Delft University of Technology, Delft, The Netherlands

†University of Maine, Orono, USA

Recent investigations of the sorption behavior of small molecules in 8-ring zeolites reveal potential industrial applications of zeolite ZSM-58 (structure type DDR) for the separation of CO₂/CH₄ or propane/propylene [1]. With large and well-shaped crystals being available from different labs (Fig. 4.6 *left*), the single-crystal analysis by means of Interference Microscopy (IFM) [2] now allows a detailed study of the intra-crystalline diffusion of light hydrocarbons in the two-dimensional channel structure of ZSM-58.

Experimental data for adsorption and desorption of light hydrocarbons were obtained at room temperature yielding both, two-dimensional transient concentration profiles (Fig. 4.6 *right*) and single-crystal uptake curves which allow the immediate comparison with sorption kinetic studies of a powder sample, e.g. by Zero Length Column[3] or thermogravimetric uptake [4] experiments.

Furthermore, the wealth of intra-crystalline concentration profiles can be explored by analyzing e.g. the shape of concentration profiles, the centre line concentration or the profiles at short times, the latter approach leading to the concentration dependence of diffusivity using cylindrical symmetry and Fujita's diffusion solution [5].

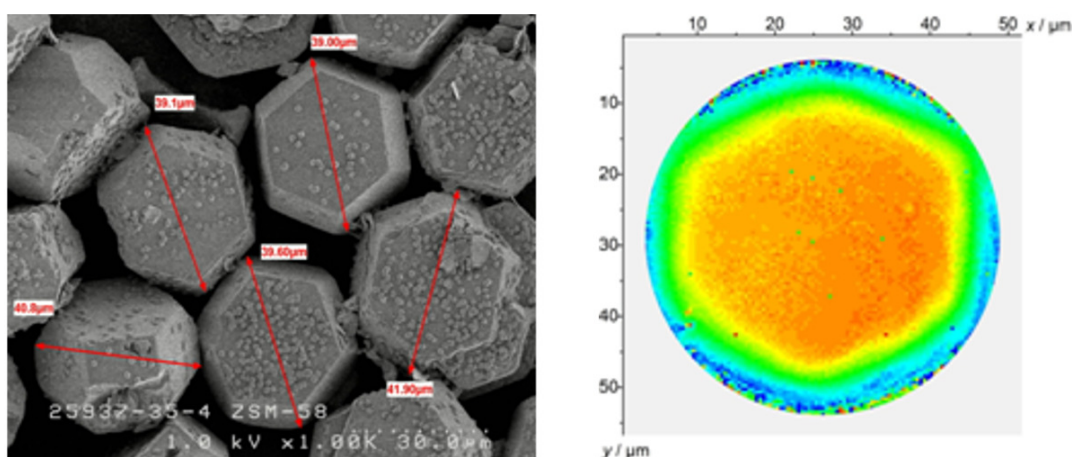


Figure 4.6: *left*: SEM picture of pure silica ZSM-58. The crystal's diameter is about 40 μm. *right*: Transient concentration profile of ethane adsorption (210 mbar) at $t = 30$ s. *green*: advance of the diffusion front, *orange*: not yet affected center part.

- [1] W. Zhu et al.: *Langmuir* **16**, 3322 (2000)
- [2] C. Chmelik et al.: *Chem. Ing. Tech.* **82**, 779 (2010)
- [3] A. Vidoni and D. Ruthven: *Ind. Eng. Chem. Res.* **51**, 1383 (2012)
- [4] D. Olson et al.: *Micropor. Mesopor. Mater.* **67**, 27 (2004)
- [5] J. Crank: *The Mathematics of Diffusion*, 1st Ed. (Oxford University Press, London 1956) p 167

4.8 Hinderling Effects in Diffusion of CO₂/CH₄ Mixtures in ZIF-8 Crystals

C. Chmelik, J. Kärger, H. Bux*, J. Caro*, J. M. vanBaten[†], R. Krishna[†],

*Leibniz Universität Hannover

[†]University of Amsterdam

Cage-type micro-porous materials such as LTA, CHA, SAPO-34, DDR, ERI, ZIF-7, and ZIF-8 have significant potential for use in membrane technologies for CO₂ capture. The permeation selectivities are governed by a combination of adsorption and diffusion selectivities, each of which can be separately manipulated. In this study we have investigated the characteristics of CO₂/CH₄ mixture diffusion in ZIF-8 by monitoring the uptake within crystals using infra-red microscopy (IRM) [1–3]. The uptake profiles were fitted to determine the "effective" Fick diffusivities of the individual components in the mixture. The diffusivity measurements, conducted for a range of loadings, clearly demonstrate that the preponderance of CO₂ at the window regions of ZIF-8 hinders the inter-cage transport of partner CH₄ molecules (Fig. 4.7). Such hindering effects serve to enhance the CO₂/CH₄ permeation selectivities across ZIF-8 membranes for high mixture loadings within the membrane above values anticipated on the basis of unary permeances.

- [1] C. Chmelik et al.: *J. Membr. Sci.* **397-398**, 87 (2011)
- [2] C. Chmelik et al.: *Chem. Soc. Rev.* **39**, 4864 (2010)
- [3] H. Bux et al.: *Adv. Mater.* **22**, 4741 (2010)

4.9 Funding

Advanced Materials as CO₂ Removers: A Computational Study of CO₂ Sorption Thermodynamics and Kinetics

PD Dr. F. Stallmach

EU project CP-FP 233502 AMCOS

Fundamental Host-Guest Interactions in Porous Metal Organic Frameworks. A Combined Experimental and Theoretical Approach.

PD Dr. F. Stallmach

DFG-Projekt STA 648/1-1 and STA 648/1-2, SPP 1362 MOFs

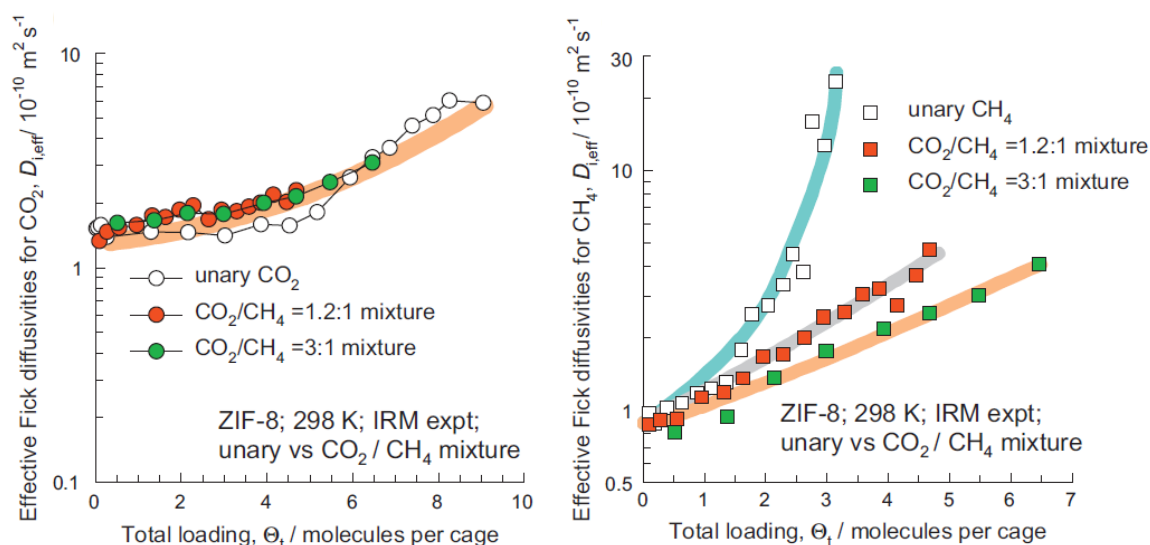


Figure 4.7: Effective Fickian diffusivities, $D_{i,\text{eff}}$, of individual components in mixtures of CO₂ and CH₄ in ZIF-8 crystal as a function of the total mixture loading, Θ_t [1].

International Research Training Group Diffusion in porous Materials

PD Dr. F. Stallmach, Prof. Dr. J. Kärger, Dr. R. Valiullin
DFG IRTG GK 1056/2

Thermodynamik und Vorausberechnung der Adsorption von Mischungen

Dr. G. Kalies
DFG KA 1560/3-2 und KA 1560/4-2

Assessing pore structure via diffusion measurements

Dr. R. Valiullin
DFG VA 463/4-1

Study of microscopic parameters of the translation of molecules in beds of nanoporous particles by PFG NMR and MC simulation

Prof. Dr. J. Kärger
DFG KA 953/19-2

Correlating diffusion processes in complementary pore spaces using NMR and theoretical modelling

Prof. Dr. J. Kärger, Prof. Dr. A. Bunde, Dr. R. Valiullin
DFG KA 953/30-1

Measuring Intracrystalline Profiles of Diffusion and Reactions in Zeolites by IR Microscopy

Dr. Ch. Chmelik
DFG KA 953/20-2

Knowledge-based development of supported ZIF membranes for liquid mixture separation by pervaporation

Dr. Ch. Chmelik, Prof. Dr. J. Kärger,
DFG KA 953/29-1 and CH 778/1-2, within SPP 1362 MOFs

Separating mixtures of chiral anesthetic gases by modified porous glasses

Dr. Ch. Chmelik

DFG CH 778/2-1, within SPP 1570

Studying Zeolitic Diffusion by Interference and IR Microscopy

Prof. Dr. J. Kärger,

DFG KA 953/18-3

Texturelle Charakterisierung von Sandsteinen (Bohrkernen) und kontaminierten Aktivkohlen

Dr. G. Kalies

Gaz de France

NMR Porosimetrie an Sedimentproben

Dr. F. Stallmach

GFZ Potsdam

4.10 Organizational Duties

Frank Stallmach

- Membership in Scientific Advisory Committee to the Bologna conference series "Magnetic Resonance in Porous Media"
- Faculty board member
- Referee: Micropor. Mesopor. Mat., Angewandte Chemie, J. Am. Chem. Soc., J. Magn. Res., J. Phys. Chem.
- Project Reviewer: Deutsche Forschungsgemeinschaft, National Science Foundation (USA)

Jörg Kärger

- Membership in the Programme Committee "Diffusion Fundamentals IV" (Troy, USA 2011), in the permanent DECHEMA committees Zeolites and Adsorption
- Editor: Diffusion Fundamentals; Membership in Editorial Boards: Adsorption
- Referee: Nature, Phys. Rev., Phys. Rev. Lett., Angew. Chem., Europhys. Lett., J. Chem. Phys., J. Phys. Chem., Langmuir, Micropor. Mesopor. Mat., Phys. Chem. Chem. Phys., J. Magn. Res.
- Project Reviewer: Deutsche Forschungsgemeinschaft

Rustem Valiullin

- Editorial Board Online Journal "Diffusion Fundamentals", Editorial Board "Dataset Papers in Physical Chemistry"
- Referee: J. Phys. Chem., J. Am. Chem. Soc., Adsorption, Micropor. Mesopor. Mat., Phys. Rev. B, Phys. Rev. E, Phys. Rev. Lett., Langmuir

Christian Chmelik

- Referee: J. Phys. Chem., Micropor. Mesopor. Mat.

4.11 External Cooperations

Academic

- Delft University, Inst.Chem. Tech., Delft, The Netherlands
Prof. Kapteijn
- Institut de Recherches sur la Catalyse, CNRS, Villeurbanne, France
Dr. Jobic
- GeoForschungsZentrum Potsdam (GFZ), Potsdam
H.-M. Schulz
- Helmholtz Zentrum für Umweltforschung UFZ Halle-Leipzig GmbH, Leipzig
S. Oswald
- Max Planck Institut für Kohlenforschung, Mülheim
Dr. Schmidt, Prof. Schüth
- TU München, Lehrstuhl Technische Chemie 2
Prof. Lercher, Dr. Jentys
- Universität Erlangen Nürnberg, Dept. Chem. Engn., Erlangen
Prof. Schwieger
- Universität Hannover, Dept. Phys. Chem., Hannover
Prof. Caro, Prof. Heitjans
- Universität Leipzig, Institut für Technische Chemie, Leipzig
Prof. Einicke, Prof. Gli $\frac{1}{2}$ ser, Prof. Enke
- Universität Leipzig, Institut für Anorganische Chemie, Leipzig
Prof. Krautscheid
- Universität Leipzig, Institut für Medizinische Physik und Biophysik, Leipzig
Prof. Huster
- TU Dresden, Inst. Biophysik, Dresden
Prof. Brunner
- Universität Stuttgart, Institut für Technische Chemie, Stuttgart
Prof. Klemm, Prof. Hunger
- University Athens, Dept Chem. Engn., Athens, Greece
Prof. Theodorou, Prof. Papadopoulos
- University of Amsterdam, Faculty of Science, The Netherlands
Prof. Krishna
- University of Maine, Dept. Chem. Eng., USA
Prof. Ruthven
- Cleveland University, Chem. and Biomed. Eng., USA
Prof. Shah
- University of Edinburgh, UK
Prof. Brandani

- Victoria University of Wellington, MacDiarmid Institute for Advanced Materials and Nanotechnology, School of Chemical and Physical Sciences, New Zealand
Dr. Galvosas, Prof. Callaghan
- LMU München, Dept. Chemistry and Biochemistry
Prof. Bräuchle, Dr. C. Jung
- University of Massachusetts, Dept. of Chemical Engineering, Amherst, USA
Prof. P.A. Monson
- Northwestern University, Dept. of Chem. Eng., Evanston, USA
Prof. Snurr
- Rutgers University, Dept. of Chem. & Chem. Biol., Piscataway, USA
Prof. Li, Prof. Olson
- University of Queensland, Division of Chem. Eng., Brisbane, Australia
Prof. Bhatia
- University of Alicante, Dept. of Inorg. Chem., Alicante, Spain
Prof. Rodriguez-Reinoso
- University of Anwerpen, Dept. of Chem., Wilrijk, Belgium
Prof. Cool, Prof. Vansant
- University of Florida, Dept. of Chem. Eng., Gainesville (FL), USA
Prof. Vasenkov
- Rensselaer Polytechnic Institute, Chem. & Biol. Eng., Troy, USA
Prof. Coppens
- Otto-von-Guericke-Universität Magdeburg, Institut für Verfahrenstechnik, Magdeburg
Prof. Seidel-Morgenstern

Industry

- BASF SE, Ludwigshafen, Germany
Dr. U. Müller
- DBI Gas- und Umwelttechnik GmbH, Leipzig, Germany
Dr. R. Rockmann
- Grace, Worms, Germany
Dr. McElhiney
- SINTEF, Oslo, Norway
Prof. Stöcker
- Südchemie, Berlin, Germany
Dr. Tissler, Dr. Tufar, Dr. Lutz
- Gaz de France, Production and Exploration GmbH Lingen, Germany
Dr.-Ing. W. Kleinitz
- Quantachrome Inc., USA
Dr. M. Thommes

4.12 Publications

Journals

- I. Mitreiter, S.E. Oswald, F. Stallmach: *Magnetic Resonance Measurements of Iron Turn-Over in Sands: Non-Invasive Characterization of Reaction Processes*, *Grundwasser* **16**, 269 (2011)
- S. Hertel, M. Wehring, S. Amirjalayer, M. Gratz, J. Lincke, H. Krautscheid, R. Schmid, F. Stallmach: *NMR Studies of Benzene Mobility in Metal-Organic Framework MOF-5*, *Eur. Phys J.–Appl. Phys.* **55**, 20702 (2011)
- F. Furtado, P. Gavosas, F. Stallmach, U. Roland, J. Karger, F.-D. Kopinke: *Paramagnetic Relaxation Enhancement (PRE) as a Tool for Probing Diffusion in Environmentally Relevant Porous Media*, *Envir. Sci. Techn.* **45**, 8866 (2011)
- M. Gratz, S. Hertel, M. Wehring, F. Stallmach, P. Galvosas: *Mixture Diffusion of Adsorbed Organic Compounds in Metal-Organic Frameworks as Studied by Magic-Angle Spinning Pulsed-Field Gradient Nuclear Magnetic Resonance*, *New J. Phys.*, **13**, 045016 (2011)
- M. Gratz, S. Hertel, M. Wehring, S. Schlayer, F. Stallmach, P. Galvosas: *MAS PFG NMR Studies of Mixtures in Porous Materials*, *AIP Conf. Proc.*, **1330**, 61 (2011)
- E. Pantatosaki, G. Megariotis, A.-K. Pusch, C. Chmelik, F. Stallmach, G. K. Papadopoulos: *On the Impact of Sorbent Mobility on the Sorbed Phase Equilibria and Dynamics: A Study of Methane and Carbon Dioxide within the Zeolite Imidazolate Framework-8*, *J. Phys. Chem* **116**, 201 (2011)
- F. Hibbe, J. M. van Baten, R. Krishna, C. Chmelik, J. Weitkamp, J. Kärger: *In-Depth Study of Mass Transfer in Nanoporous Materials by Micro-Imaging*, *Chem. Ing. Tech.* **83**, 2211 (2011)
- F. Hibbe, V. R. R. Marthala, C. Chmelik, J. Weitkamp, J. Kärger: *Micro-Imaging of Transient Guest Profiles in Nanochannels*, *J. Chem. Phys.* **135**, 184201 (2011)
- C. Chmelik, D. Enke, P. Galvosas, O. Gobin, A. Jentys, H. Jobic, J. Kärger, C. B. Krause, J. Kullmann, J. Lercher, S. Naumov, D. M. Ruthven, T. Titze: *Nanoporous Glass as a Model System for a Consistency Check of the Different Techniques of Diffusion Measurement*, *Chem. Phys. Chem.* **12**, 1130 (2011)
- C. Chmelik, J. Kärger *Unprecedented Wealth of Information on Guest Dynamics in Nanoporous Materials from Transient Concentration Profiles*, *Defect and Diffusion Forum Vols.* **309-310**, 177 (2011)
- C. Chmelik, D. Freude, H. Bux, J. Haase: *Ethene/Ethane Mixture Diffusion in the MOF Sieve ZIF-8 Studied by MAS PFG NMR Diffusometry*, *Micropor. Mesopor. Mater.* **147**, 135 (2011)
- V. R. R. Marthala, M. Hunger, F. Kettner, H. Krautscheid, C. Chmelik, J. Kärger, J. Weitkamp: *Solvothermal Synthesis and Characterization of Large-Crystal All-Silica, Aluminum-, and Boron-Containing Ferrierite Zeolites*, *Chem. Mater.* **23**, 2521 (2011)

- F. Hibbe, C. Chmelik, L. Heinke, S. Pramanik, J. Li, D. M. Ruthven, D. Tzoulaki, J. Kärger: *The Nature of Surface Barriers on Nanoporous Solids Explored by Microimaging of Transient Guest Distributions*, *J. Am. Chem. Soc.* **133**, 2804 (2011)
- H. Bux, C. Chmelik, R. Krishna, J. Caro: *Ethene/Ethane Separation by the MOF Membrane ZIF-8: Molecular Correlation of Permeation, Adsorption, Diffusion*, *J. Membr. Sci.* **369**, 284 (2011)
- C. Chmelik, H. Bux, H. Voß, J. Caro: *Adsorption and Diffusion - Basis for Molecular Understanding of Permeation through Molecular Sieve Membranes*, *Chem. Ing. Tech.* **83**, 104 (2011)
- T. Binder, Z. Adem, C. B. Krause, M. Krutyeva, A. Huang, J. Caro, J. Kärger: *Surface Permeability on Zeolite NaCaA Enhanced by Layer Deposition*, *Micropor. Mesopor. Mater.* **146**, 151 (2011)
- L. Heinke, J. Kärger: *Correlating Surface Permeability with Intracrystalline Diffusivity in Nanoporous Solids*, *Phys. Rev. Lett.* **106**, 074501 (2011)
- J. Lincke, D. Lässig, J. Moellmer, C. Reichenbach, A. Puls, A. Moeller, R. Gläser, G. Kalies, R. Staudt, H. Krautscheid: *A Novel Copper-based MOF Material: Synthesis, Characterization and Adsorption Studies*, *Micropor. and Mesopor Mater.* **142**, 62 (2011)
- C. Reichenbach, G. Kalies, J. Lincke, D. Lässig, J. Moellmer, H. Krautscheid, M. Thommes: *Unusual Adsorption Behavior of a Highly Flexible Copper-Based MOF*, *Micropor. Mesopor. Mater.* **142**, 592 (2011)
- D. Lässig, J. Lincke, J. Moellmer, C. Reichenbach, A. Moeller, G. Kalies, M. Thommes, R. Staudt, H. Krautscheid: *A Microporous Copper MOF with Exceptionally High H₂ and CO₂ Adsorption Capacity at Ambient Pressure*, *Angew. Chem. Int. Edit.* **50**, 10344 (2011)
- C. Reichenbach, G. Kalies, D. Enke, D. Klank: *Cavitation and Pore Blocking in Nanoporous Glasses*, *Langmuir* **27**, 10699 (2011)
- M. Bauer, R. Valiullin, G. Radons, J. Kärger: *How to Compare Diffusion Processes Assessed by Single-Particle Tracking and Pulsed Field Gradient Nuclear Magnetic Resonance*, *J. Chem. Phys.* **135**, 144118 (2011)
- M. Dvoyashkin, E. Romanova, W. D. Einicke, R. Gläser, J. Kärger, R. Valiullin: *Diffusion of Cyclohexane in Native and Surface-Modified Mesoporous Glasses*, *Adsorption* **17**, 93 (2011)
- F. Feil, S. Naumov, J. Michaelis, R. Valiullin, D. Enke, J. Kärger, C. Bräuchle: *Single-Particle and Ensemble Diffusivities - Test of Ergodicity*, *Angew. Chem. Int. Edit.* **51**, 1152 (2011)
- F. Furtado, P. Galvosas, M. Goncalves, F. D. Kopinke, S. Naumov, F. Rodriguez-Reinoso, U. Roland, R. Valiullin, J. Kärger: *The Evidence of NMR Diffusometry on Pore Space Heterogeneity in Activated Carbon*, *Micropor. Mesopor. Mater.* **141**, 184 (2011)

F. Furtado, P. Galvosas, M. Goncalves, F. D. Kopinke, S. Naumov, F. Rodriguez-Reinoso, U. Roland, R. Valiullin, J. Kärger: *Guest Diffusion in Interpenetrating Networks of Micro- and Mesopores*, J. Am. Chem. Soc. **133**, 2437 (2011)

M. Kohagen, M. Brehm, Y. Lingscheid, R. Giernoth, J. Sangoro, F. Kremer, S. Naumov, C. Iacob, J. Kärger, R. Valiullin, B. Kirchner: *How Hydrogen Bonds Influence the Mobility of Imidazolium-Based Ionic Liquids. A Combined Theoretical and Experimental Study of 1-n-Butyl-3-methylimidazolium Bromide*, J. Phys. Chem. B **115**, 15280 (2011)

D. Kondrashova, M. Dvoyashkin, R. Valiullin: *Structural Characterization of Porous Solids by Simultaneously Monitoring the Low-Temperature Phase Equilibria and Diffusion of Intrapore Fluids Using Nuclear Magnetic Resonance*, New J. Phys. **13**, 015008 (2011)

M. G. Mazza, M. Greschek, R. Valiullin, M. Schoen: *Role of Stringlike, Supramolecular Assemblies in Reentrant Supernematic Liquid Crystals*, Phys. Rev. E **83**, 051704 (2011)

R. Valiullin: *Phase State and Dynamics of Fluids in Mesoporous Solids*, AIP Conf. Proc. **1330**, 39 (2011)

R. Valiullin, J. Kärger: *The Impact of Mesopores on Mass Transfer in Nanoporous Materials: Evidence of Diffusion Measurement by NMR*, Chem. Ing. Tech. **83**, 166 (2011)

R. Valiullin, J. Kärger, K. Cho, M. Choi, R. Ryoo: *Dynamics of Water Diffusion in Mesoporous Zeolites*, Micropor. Mesopor. Mater. **142**, 236 (2011)

P. Zeigermann, M. Dvoyashkin, R. Gläser, R. Valiullin: *Diffusion NMR of Fluids Confined to Mesopores under High Pressures*, AIP Conf. Proc. **1330**, 97 (2011)

P. Zeigermann, M. Dvoyashkin, R. Valiullin: *Diffusion and Phase Equilibria of Binary Fluids in Mesopores*, Adsorption **17**, 69 (2011)

Books

C. Chmelik, D. M. Ruthven, J. Kärger: *Studying Diffusion and Mass Transfer at the Microscale*, in *Nanoporous Materials: Advanced Techniques for Characterization, Modeling, and Processing*, ed. by N. Kanellopoulos (Taylor & Francis Group, LLC, Boca Raton 2011), p 53

Talks

C. Chmelik: *New Insights into MOFs: Exploring the Fundamentals of Mass Transfer by Microscopic Techniques*, 9th International Symposium on the Characterisation of Porous Solids - COPS 9, Dresden, Germany, 05. – 08. June 2011

C. Reichenbach, D. Enke, G. Kalies: *Neuartige poröse Materialien - eine Herausforderung für die Charakterisierung mittels Gasadsorption*, Dechema Jahrestreffen der Fachgruppe Adsorption, Würzburg, Germany, 23. – 25. March 2011

G. Kalies, C. Reichenbach, P. Bräuer, D. Enke, R. Rockmann: *Verbesserte Voraussage der Adsorption mehrkomponentiger flüssiger Mischungen an Festkörpern*, Dechema Jahrestreffen der Fachgruppe Adsorption, Würzburg, Germany, 23. – 25. March 2011

P. Zeigermann, M. Dvoyashkin, R. Gläser, R. Valiullin: *Self-Diffusion in Mesoporous Solids at Sub- and Supercritical Conditions*, 44. Jahrestreffen Deutscher Katalytiker, Weimar, Germany, 16. – 18. March 2011

P. Zeigermann, R. Valiullin: *Diffusion of Fluids in Mesoporous Host Systems*, Diffusion Fundamentals IV, Troy, USA, 21. – 24. August 2011

F. Stallmach: *NMR Studies of Host-Guest Interaction in Porous Materials*, 14th IRTG Workshop, Twente, Netherlands, 1st November 2011

M. Gratz, S. Hertel, M. Wehring, M. Großmann, S. Schlayer, F. Stallmach, P. Galvosas: *Advanced Methods for NMR Diffusometry*, ICMRM 11, Beijing, China, 16th August 2011

M. Wehring, S. Amirjalayer, R. Schmid, F. Stallmach: *NMR Self-Diffusion Studies of Benzene in Metal Organic Frameworks*, 23. Deutche Zeolith-Tagung, Erlangen, Germany, 02. – 04. March 2011

Posters

C. Chmelik, D. Freude, H. Bux, J. Haase: *MAS PFG NMR Diffusometry and MAS NMR Spectroscopy of Paraffin-Olefin Mixtures Adsorbed in MOF ZIF-8*, 9th International Symposium on the Characterisation of Porous Solids - COPS 9, Dresden, Germany, 05. – 08. June 2011

T. Titze, C. Chmelik: *Configurational Entropy and Intersection Blocking Effects in Multi-Component Systems in MFI-Type Zeolites studied by IR Microscopy*, 23. Deutche Zeolith-Tagung, Erlangen, Germany, 02. – 04. March 2011

T. Binder, Z. Adem, J. Caro, J. Kärger: *Surface Permeability on Zeolite NaCaA Enhanced by Layer Deposition*, 23. Deutche Zeolith-Tagung, Erlangen, Germany, 02. – 04. March 2011

T. Binder, C. Chmelik, J. Kärger, W. Schmidt: *Microscopic Analysis of Phase Transition Effects during Benzene Sorption in MFI Type Zeolites*, Diffusion Fundamentals IV, Troy, NY, USA, 21. – 24. August 2011

F. Hibbe, C. Chmelik, V.R.R. Marthala, J. Kärger, J. Weitkamp: *Diffusion Studies on Large-Crystal Ferrierite Zeolites of Different Chemical Composition and Post-Synthesis Treatment*, 23. Deutche Zeolith-Tagung, Erlangen, Germany, 02. – 04. March 2011

F. Hibbe, C. Chmelik, V.R.R. Marthala, J. Kärger, J. Weitkamp: *Diffusion Studies on Large-Crystal Ferrierite Zeolites of Different Chemical Composition and Post-Synthesis Treatment*, Diffusion Fundamentals IV, Troy, NY, USA, 21. – 24. August 2011

F. Hibbe, L. Heinke, C. Chmelik, S. Pramanik, J. Li, D.M. Ruthven, D. Tzoulaki, J. Kärger: *The Nature of Surface Barriers on Nanoporous Solids Explored by Microimaging of Transient Guest Distributions and Monte Carlo Simulations*, Diffusion Fundamentals IV, Troy, NY, USA, 21. – 24. August 2011

C. Reichenbach, G. Kalies, D. Enke, D. Klank, M. Thommes. *Hysteresis Behaviour of Nitrogen and Argon in Novel Micro-Mesoporous Glasses*, 9th International Symposium on the Characterisation of Porous Solids - COPS 9, Dresden, Germany, 05. – 08 June 2011

G. Kalies, C. Reichenbach, J. Lincke, D. Lässig, H. Krautscheid, J. Moellmer, M. Thommes: *Which Information Can We Obtain from Gas Adsorption Isotherms on Highly Flexible Solids?*, 9th International Symposium on the Characterisation of Porous Solids - COPS 9, Dresden, Germany, 05. – 08 June 2011

D. Mehlhorn, R. Valiullin, J. Kärger, R. Ryoo: *Diffusion in Mesoporous Zeolites*, 23. Deutsche Zeolith-Tagung, Erlangen, Germany, 2. – 4. March 2011

C. Iacob, J. R. Sangoro, R. Valiullin, R. Gläser, J. Kärger, F. Kremer: *Charge Transport in Confined Ionic Liquids*, Diffusion Fundamentals IV, Troy, USA, 21. – 24. August 2011

D. Kondrashova, R. Valiullin: *Diffusion in Mesoporous Materials During Melting and Freezing*, Diffusion Fundamentals IV, Troy, USA, 21. – 24. August 2011

M. G. Mazza, M. Greschek, R. Valiullin, J. Kärger, M. Schoen: *Dynamics in Reentrant Nematics*, Diffusion Fundamentals IV, Troy, USA, 21. – 24. August 2011

D. Mehlhorn, R. Valiullin, J. Kärger, R. Ryoo: *Diffusion in Mesoporous Zeolites*, Diffusion Fundamentals IV, Troy, USA, 21. – 24. August 2011

P. Zeigermann, M. Dvoyashkin, R. Gläser, R. Valiullin: *Self-Diffusion in Mesoporous Solids at Sub- and Supercritical Conditions*, Diffusion Fundamentals IV, Troy, USA, 21. – 24. August 2011

S. Beckert, F. Stallmach, J. Kullmann, D. Enke: *Concentration Dependent Self-Diffusion Coefficients of Aqueous Electrolyte Solutions in Bulk Phase and Confined in Porous Glasses Measured by Pulsed Gradient NMR*, Diffusion Fundamentals IV, Troy, NY, USA, 21. – 24. August 2011

M. Gratz, M. Großmann, S. Schlayer, P. Galvosas: *NMR Diffusion Studies Using Super-High Gradient Pulses*, ICMRM 11, Beijing, China, 14.–18. August 2011

M. Gratz, S. Hertel, M. Wehring, F. Stallmach, P. Galvosas: *MAS PFG NMR Diffusion Measurements in Porous Coordination Polymers*, ICMRM 11, Beijing, China, 14.–18. August 2011

M. Wehring, S. Amirjalayer, R. Schmid, F. Stallmach: *Fundamental Host-Guest Interactions in Porous Metal Organic Frameworks. A Combined Experimental and Theoretical Approach.*, DFG priority program 1362, Dresden, Germany, October 2011

M. Wehring, S. Amirjalayer, R. Schmid, F. Stallmach: *Anisotropic Self-Diffusion of Guest Molecules in $Zn_2(bdc)_2dabco$* , Diffusion Fundamentals IV, Troy, NY, USA , 21. – 24. August 2011

A.-K. Pusch, S. Schlayer, F. Stallmach: ^{13}C NMR diffusion studies with CO_2 adsorbed at MOF CuBTC, 23. Deutsche Zeolith-Tagung, Erlangen, Germany, 02. – 04. March 2011

4.13 Graduations

Bachelor

- T. Splith
NMR-Diffusionsuntersuchungen von Methan in ZIF-8
Oktober 2011
- A. Maiwald
NMR-Untersuchungen von Alkanen im MOF CuBTC
November 2011
- D. Schneider
Analysis of the Adsorption Behavior in Conical Mesopores Using Different Computer Simulation Methods
September 2011
- O. Naumov
Gefrierverhalten von Nitrobenzol in ungeordneten Mesoporen
September 2011

4.14 Guests

- Prof. Rajesh Biniwale
NEERI Nagpur, India
April 1 - April 6, 2011
- Prof. George Papadopoulos
NTU Athens, Greece
April 3 - April 5, 2011
- Prof. Douglas M. Ruthven
University of Maine, USA
November 4 - December 18, 2011
- Dr. Petrik Galvosas
Victoria University of Wellington, New Zealand
December 16, 2011- January 7, 2012

5

Soft Matter Physics

5.1 Introduction

The Division of Soft Matter Physics strives to perform ground breaking research at the interdisciplinary forefront of Nanosciences, Biophysics as well as Medicine, and the group's work frequently has proven seminal for Polymer and Laser Physics, or provided new techniques for Biophysics and Materials Sciences. The group's research is aimed to understand the role of cell and molecular biomechanics in tumor progression, which is an important part of the emerging Physics of Cancer. In view of the fact that the group's work aims at the unique combination of Soft Matter Physics, Biophotonics and Medical Physics it has a redefining impact on medical diagnosis and therapy. It is one of the principles of the Division of Soft Matter Physics to be not solely outstanding in science, but also an inspiring place in teaching and mentoring. About 75% of the alumni decided to remain in science. Among those are professors that hold permanent appointments at the University of Cambridge, the Institute Curie, and Harvard University.

Josef A. Käs

5.2 Counterion-induced formation of regular actin bundle networks

F. Huber, D. Strehle, J.A. Käs,

Bottom-up approaches in conjunction with theoretical work led to the present understanding of actin networks in terms of rheology. While it is obvious that the network architecture largely determines its mechanical properties, little is known regarding the inherent ability of the actin machinery to dynamically regulate its structure. Aster-like structures have further been reported for actin-myosin systems upon fuel depletion partially translating active motors into inactive crosslinkers, as well as for high crosslinker densities. These examples overall display a rather random network architecture or no network structure at all. [1-3]

Positive multivalent ions were used to cross-link negatively charged actin filaments without a priory preferred mutual orientation due to the geometry of the crosslinker. This counter-ion condensation interaction is highly concentration-dependent and show

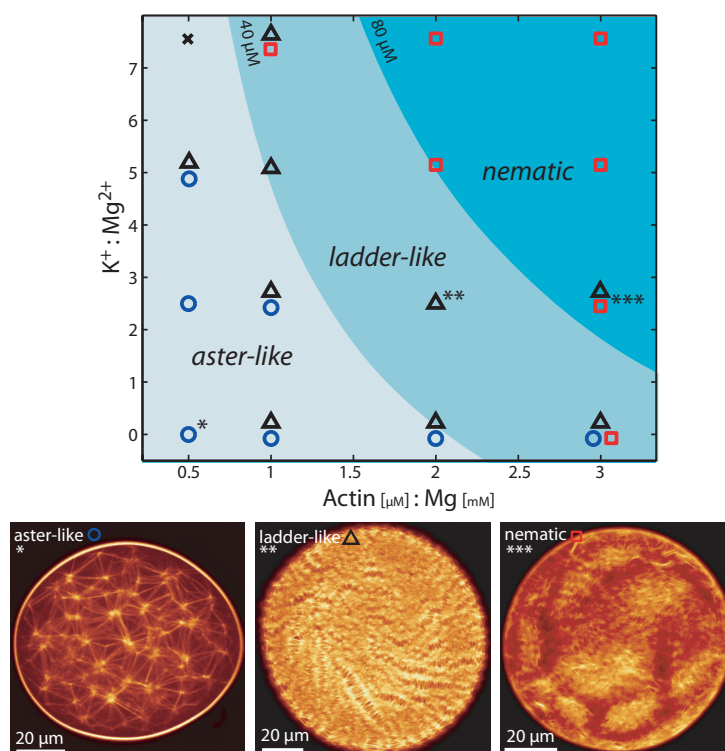


Figure 5.1: Observed network structures are marked by circles, triangles and squares with typical examples of aster-like, ladder-like and nematic structures, respectively, shown on the right. The shading boundaries in the diagram refer to actin concentrations of 40 and 80mM which correspond to the onset of partial and nematic alignment in F-actin solutions.

a sharp transition to bundling [4]. Observing the counterion-induced crosslinking transition within micrometer-sized confinements we found a novel state displaying regularly spaced networks of actin bundles connected by aster-like clusters. At high densities of long filaments liquid crystalline effects lead to further notable variations of these bundled networks such as ladder-like bundle structures of defined width. The observed regular networks reversibly formed within minutes and are not accounted for by current theoretical models.

We found the resulting patterns to be dependent on the concentration of actin at the bundling threshold. At actin concentrations below 40 μ M regularly-spaced aster-like centers connect to networks, at intermediate concentrations up to 80 μ M ladder-like stripes become increasingly prominent until at concentration above this long-range density fluctuations indicate microscopic phase separation of nematic and isotropic domains. Further experiments suggested that pre-orientation of filaments resulting from partial nematic alignment at intermediate concentration is the origin ladder-like stripes.

- [1] D. Smith et al.: *Biophys. J.*, **93**, 4445–4452 (2007).
- [2] F. Ziebert et al.: *New Journal of Physics* **9**, 421–421(2007).
- [3] Y. Ideses et al.: *PLoS ONE* **3**, e3297 (2008).
- [4] J. X. Tang et al.: *J. Biol. Chem.* **271**, 8556–8563 (1996).

5.3 Calcium imaging in the Optical Stretcher

M. Gyger, D. Rose, R. Stange, T. Kießling, M. Zink, B. Fabry*, J.A. Käs

*Friedrich-Alexander- University of Erlangen-Nürnberg

The Microfluidic Optical Stretcher (MOS) has previously been shown to be a versatile tool to measure mechanical properties of single suspended cells. In this study we combined optical stretching and fluorescent calcium imaging. Cells are held in place and manipulated by optically induced surface forces in the MOS while the Ca^{2+} signal is recorded with confocal laser scanning microscopy (CLSM). A cell line transfected with a heat sensitive cation channel was used as a model system to show the versatility of the setup. The cells were loaded with the Ca^{2+} dye Fluo-4 and imaged with confocal laser scanning microscopy while being stretched. During optical stretching heat is transferred to the cell causing a pronounced Ca^{2+} influx through the cation channel.

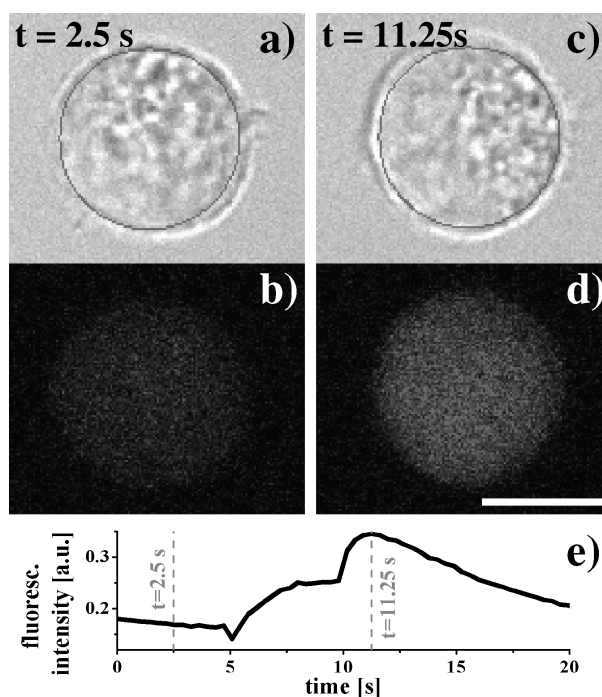


Figure 5.2: Fluorescent signal (b,d) and bright-field image (a,c) of a trapped cells. The signal of the cell's mid-plane was recorded with a confocal laser scanning microscope. The fluorescence was averaged over a disk lying well inside the cell indicated by the gray circle in a) and c) to avoid artifacts due to the deformation of the cell upon stretching. e) shows the time course of the averaged fluorescent signal.

The use of the CLSM allows for simultaneous observation of the trapped cells in bright-field images and recording of their fluorescence signals. This combination of optical trapping and CLSM opens a wide variety of functional tests using either the deformation or the heat developed in optical traps to induce a change in a fluorescent dye.

An interesting application of the presented setup might be measuring of the restructuring of fluorescent labeled actin or microtubuli upon cellular deformations involving

Ca^{2+} or other signaling messengers. This could help understanding the changes in the cytoskeleton during cancer development contributing to tumor formation and metastasis [1, 2].

In conclusion active cellular responses to heating or deformation mediated by Ca^{2+} signaling can strongly influence the mechanical properties of cells. Linear or passive biomechanical models [3–5] will thus not be able to explain the obtained data (see [6] for a recent review on active and passive cell rheology). Observation of signaling cascades might provide a key to understand these active responses of biological cells to external stimuli.

- [1] A. Fritsch et al.: *Nat Phys* **6**, 730 – 732 (2010).
- [2] C. Mierke et al.: *European Journal of Cell Biology* **87**, 669 – 676 (2008). FEBS Workshop: Invadopodia, Podosomes and Focal Adhesions in Tissue Invasion.
- [3] B. Fabry et al.: *Phys. Rev. Lett.* **87**, 148102 (2001).
- [4] F. Wottawah et al.: *Phys. Rev. Lett.* **94**, 098103 (2005).
- [5] R. Ananthakrishnan et al.: *Journal of Theoretical Biology* **242**, 502 – 516 (2006).
- [6] P. Kollmannsberger et al.: *Annual Review of Materials Research* **41**, 75–97 (2011).

5.4 The mechanics of cellular compartmentalization as a model for tumor spreading

A. Fritsch, S. Pawlizak, M. Zink, J.A. Käs, L.C. Horn*, M. Höckel†

*Institut für Pathologie, Universität Leipzig

†Klinik und Poliklinik für Frauenheilkunde

Based on a recently developed surgical method of M. Höckel [1], which makes use of cellular confinement to compartments in the human body, we study the mechanics of the process of cell segregation.

Compartmentalization is a fundamental process of cellular organization and occurs during embryonic development. A simple model system can demonstrate the process of compartmentalization: When two populations of suspended cells are mixed, this mixture will eventually segregate into two phases, whereas mixtures of the same cell type will not. In the 1960s, M. S. Steinberg [2] formulated the so-called differential adhesion hypothesis which explains the segregation in the model system and the process of compartmentalization by differences in surface tension and adhesiveness of the interacting cells. We are interested in to which extend the same physical principles affect tumor growth and spreading between compartments. For our studies, we use healthy and cancerous breast cell lines of different malignancy as well as primary cells from human cervix carcinoma. We apply a set of techniques to study their mechanical properties and interactions [3]. The Optical Stretcher is used for whole cell rheology, while cell-cell-adhesion forces are directly measured with a modified AFM. In combination with 3D segregation experiments in droplet cultures we try to clarify the role of surface tension in tumor spreading.

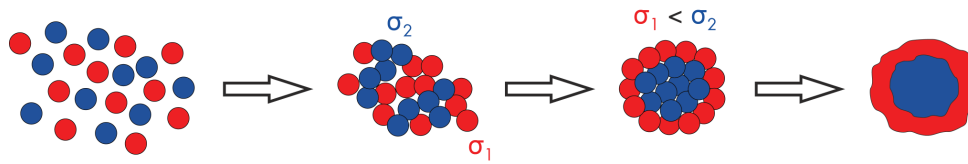


Figure 5.3: The Differential Adhesion Hypothesis by M. S. Steinberg gives a physical explanation for the phenomenon of compartmentalization. According to this, cell sorting and formation of cellular compartments result from different adhesiveness of the participating cells (molecular differences on the cell surface). The interplay of single cell biomechanics, cell adhesion and cell migration cause a surface tension σ . In the process of compartmentalization, the interfacial free energy is minimized and total cell-cell binding strength is maximized.

- [1] M. Höckel et al.: *The Lancet Oncology* **10**, 683 - 692 (2009).
- [2] R. A. Foty et al.: *Dev. Biol.* **278**, 255 - 263 (2005).
- [3] A. Fritsch et al.: *Nat. Phys.* **10**, 730 - 732 (2010).

5.5 Stochastic actin dynamics in lamellipodia reveal parameter space for cell type classification

M. Knorr, D. Koch*, T. Fuhs, U. Behn, J.A. Käs

*Georgetown University, Washington D.C.

The lamellipodium, a thin veil-like structure at the leading edge of crawling cells, is fundamental for cell migration and growth. Orchestrated activities of membrane components and an underlying biopolymer film result in a controlled movement of the whole system. Dynamics in two-dimensional cell motility are primarily driven by the actively moving protein film in the lamellipodium. Polymerization of actin filaments at the leading edge, back-transport of the actin network due to myosin motor activity, depolymerization in the back, and diffusive transport of actin monomers to the front control these dynamics. The same molecular prerequisites for lamellipodial motion are found in most eukaryotic cells and can function independently of the cell body. We investigated the stochastic lamellipodium dynamics within three different cell types and found that the dynamics differ strongly in different cell types according to their function. Path finding neuronal growth cones display strong stochastic fluctuations, wound healing fibroblasts that locally migrate in tissues exhibit reduced fluctuations while fish keratocytes move highly persistently. Experimental analysis and computer simulations showed that changes in the switching rates of 'On' and 'Off' actin polymerization and in the ratio of actin polymerization and retrograde transport velocity alone are sufficient for the cell to utilize the same, highly adaptive machinery to display this rich variety of behaviors.

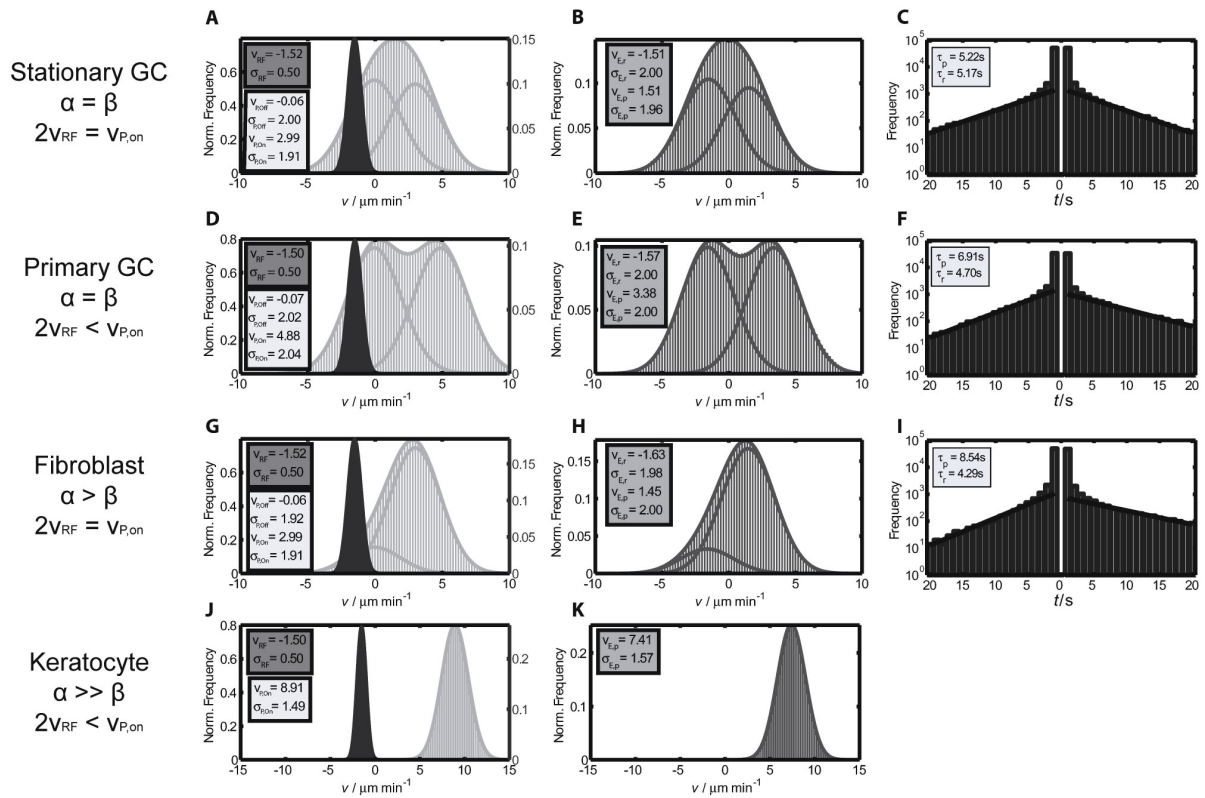


Figure 5.4: Outcome of computer simulation, where in each case only one parameter was changed. (A, D, G, and J) The appropriate results of retrograde flow and polymerization signal simulation. (B, E, H, and K) the particular edge velocity distributions and (C, F, and I) the residence time distributions (RTD). The first row shows the simulation outcome when the polymerization switching rates (between Off and On) are balanced and retrograde flow mean velocity was set twice as high as polymerization 'On' mean speed. This shows the behavior of NG108 stationary growth cones. In the simulations shown in the second row the same parameters like in the first simulation were used, but polymerization 'On' speed was set higher than two times the retrograde flow, simulating the behavior of primary growth cones. The simulation representing the dynamics of fibroblasts is shown in the third row. Here, polymerization 'On' velocity was set twice as high as retrograde flow, but the jumping rate of jumping into an 'On' state was set higher. Keratocyte movement was simulated by setting the polymerization switching rate of switching to an 'On' state much higher and additionally by increasing polymerization 'On' velocity.

5.6 Actin and microtubule networks contribute differently to cell response for small and large strain

K.D. Nnetu, T. Kießling, R. Stange, J.A. Käs

The interaction between the various cytoskeletal filaments within a cell provides it with mechanical stability and organizes the cytoplasm. These filaments include the actin and microtubule filaments. To understand the contribution of these filaments to a cell's response at small and large strain, MCF7 epithelial cells were analyzed systematically after treatment with cytoskeleton disrupting drugs. The cell's response was quantified

with the microfluidic optical stretcher (μ OS) by measuring the relative deformation and relaxation of the cells. In the small ($\leq 5\%$ of the relative deformation) and large ($> 5\%$ of the relative deformation) strain regimes, the cells deformed more after treatment with latrunculin A (LatA) which is an actin filament disrupting drug. Cells treated with the actin nucleating drug jasplakinolide (Jas) were found to be more deformable at small strains but showed no significant change at large strains. Additionally, cells treated with nocodazole (Noc), a microtubule disrupting drug, deformed more at large strains but Noc had no effect on the cells at small strains. Furthermore, cells treated with taxol (Tax), a microtubule stabilizing drug, showed no significant change in deformation at small strains. At large strains however, Tax had a concentration dependent impact on the cells. At low concentrations, Tax, made the cells more deformable while stiffening them at higher concentrations. This suggests that for suspended cells, the actin cortex is probed at small strains while at large strains, the whole cell is probed with a significant contribution from the microtubule. Moreover, with respect to all previous measurements on cell mechanics, a substantial amount of cells ($>10^4$) has been characterized and this exceeds previous statistics by more than a decade.

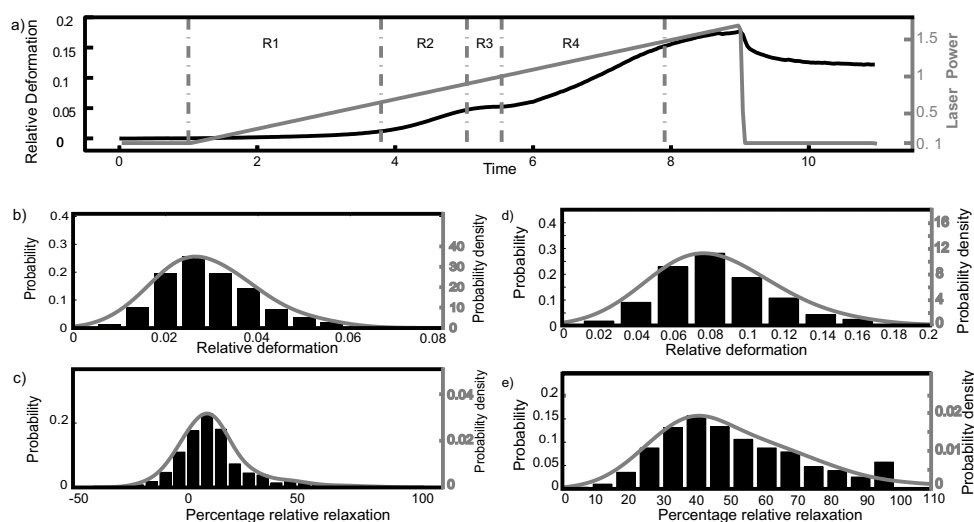


Figure 5.5: A plot of cells stretched with a ramp force and the distributions of the relative deformation and relaxation fitted with the probability density function. a) cells are stretched with increasing power from 100mW to 1700mW within 8 seconds. R1 is the threshold regime, R2 the linear regime, R3 the non-linear regime, and R4 the second linear regime. The cells in this work were stretched in the R2 region for small strains and R4 region for large strains. The gray bar is the laser power while the black line is the time dependent deformation of the cell. b) histograms of the relative deformation of cells at small strains and the probability density function. The distribution is not completely symmetric as expected for a normal distribution. c) a histogram showing the relative relaxation of cells at small strains. The distribution is symmetric as expected for a normal distribution. d) histograms of the relative deformation of cells at large strains which is broader and also non-symmetric. e) a histogram showing the relaxation of MCF7 cells at large strains that broader when compared to the small strain relaxation.

5.7 Directed persistent motion maintains sheet integrity during multi-cellular spreading and migration

K.D. Nnetu, M. Knorr, D. Strehle, M. Zink, J.A. Käs

Multi-cellular migration plays an important role in physiological processes such as embryogenesis, cancer metastasis and tissue repair. Collective cell migration involves specific single cell motility behavior that maintains the integrity of the monolayer and the fluid-like behavior of the sheet on long time scales. By studying the dynamics of MCF-10A, MDA-MB-231 epithelial cell monolayers and that of a NIH-3t3 fibroblast monolayer, we show that for the MCF-10A cells, in the case where cell-cell interactions are so weak that single cells can detach from the monolayer, a collective cell front can be maintained by the interplay between the directed persistent motion of the monolayer and the random motion of escaping single cells. The dynamics of the MCF-10A monolayer is contrasted with that of the MDA-MB-231 monolayer where single cells did not detach, non-interacting NIH-3t3 fibroblast cells which are always random walkers and that of a MCF-10A monolayer treated with a calcium chelating agent which reduces intercellular interactions.

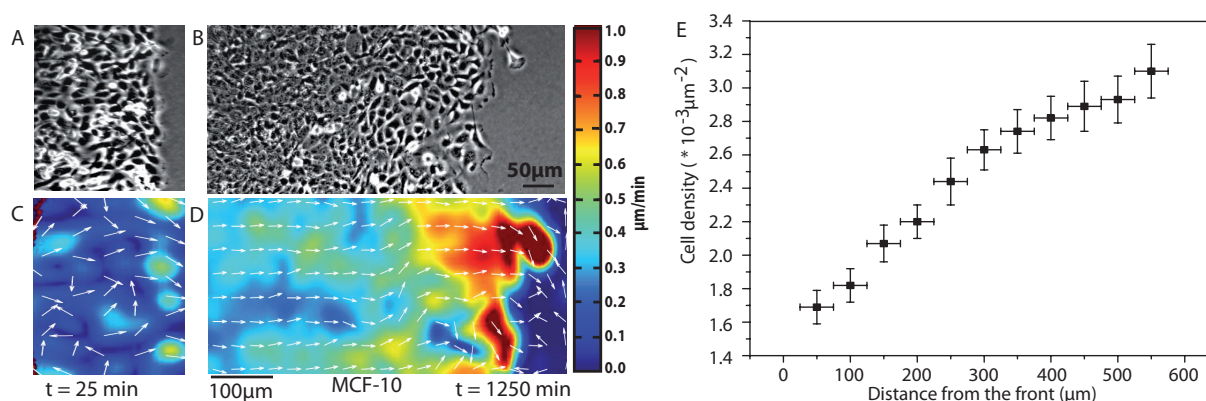


Figure 5.6: Phase contrast images, displacement fields and spatial velocity distribution of MCF-10A epithelial and NIH-3t3 fibroblast monolayers. (A) and (B) are phase contrast images showing MCF-10A epithelial cells after 25 and 1250 minutes of migrating respectively. (C) and (D) are the corresponding displacement fields. The displacement fields are random on short times (C) and mostly uni-directional on long times (D). Moreover, the velocity is generally spatially heterogeneous on both time scales with marginal cells having a higher velocity than submarginal cells. (E) is the spatial variation of the cell density (mean \pm standard deviation) from the front to the back of the monolayer. The cell density was obtained by automatically counting the number within an areas of $50 \times 50 \mu\text{m}^2$. This plot shows that the cell density increased from the front of the sheet to the back to the sheet thus establishing as density gradient as the monolayer migrates.

5.8 Nonlinear pattern formation in biomimetic lipid membranes

C. Händel, B. Käsemödel, J. Lippoldt, U. Dietrich, J.A. Käs

Plasma membranes are vital components of all living systems. They are highly complex organized and have functional and structural roles. They form closed compartments and play a key role in signal transduction processes. Many of these processes are regulated by nonlinear RD (reaction diffusion) systems. In this work a RD system should be studied in vitro to observe the interaction between the MARCKS (Myristoylated alanine rich C kinase substrate) protein and the membrane lipid PIP(2) (Phosphatidylinositol). It is well known that the periodic occurrence of this reaction at the cell membrane influences the signal transduction. The cyclic attachment/detachment of the protein at the membrane leads to the assumption of a periodic change of the lateral membrane organization depending on this cycle, like shown in figure 5.7.

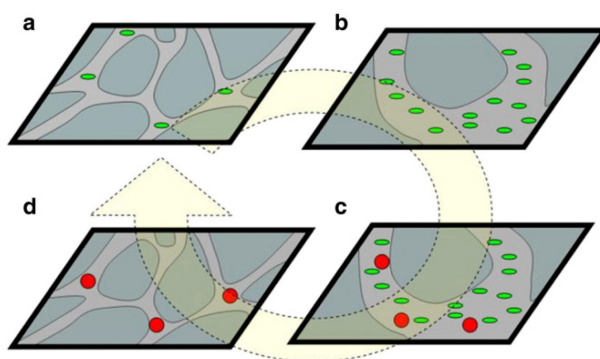


Figure 5.7: Example of the periodic changes of the lateral lipid organization in a biomimetic membrane (dark areas represent the condensed and the light areas the fluid phase). (a) initial state, (b) attachment of peptide, the channel size between the ordered domains increases, (c) attachment of PKC (red), (d) detachment of peptide, reduction of channel size, translocation of PKC [1].

Due to the complexity of biological membranes the use of artificial model membranes are essential to get an adequate experimental excess. One common model to build biomimetic membranes is the tBLM (tethered bilayer lipid membrane). A tBLM is a lipid bilayer linked via a spacer (polyethylene glycol) on a solid substrate (e.g. silicon or mica). The substrate with the mixed tBLM (DPPC/PIP(2)) is enclosed by a flow chamber wherein the composition of the ambient medium can be changed. With this model of a lipid membrane combined with micro fluidic devices we are able to realize an open dynamic RD system observable by fluorescence microscopy.

[1] S. Alonso et al.: *Biophys. J.* **100**, 939-947 (2011).

5.9 Structural Investigation on the Absorption of the MARCKS Peptide on Anionic Lipid Monolayers - Effects Beyond Electrostatic

U. Dietrich, P. Krüger*, J.A. Käs

*Fraunhofer Institute for Non-Destructive Testing, Dresden branch

The presence of charged lipids in the cell membrane constitutes the background for the interaction with numerous membrane proteins. As a result, the valence of the lipids plays an important role concerning their lateral organization in the membrane and therefore the very manner of this interaction. We have studied this aspect, particularly regarding to the interaction of the acidic membrane lipid DPPS with the highly basic charged effector domain of the MARCKS protein, examined in monolayer model systems. Film balance, fluorescence microscopy and x-ray reflection/diffraction measurements were used to study the behavior of DPPS in a mixture with DPPC for its dependence on the presence of MARCKS (151-175). The obtained results were compared with the interaction of MARCKS peptide with the polyvalent acidic PIP₂ in mixed monolayers. A sketch of the changes at the monolayer interface, derived from the experimental data, is depicted in figure 5.8. The primary protrusion of the PI(4,5) group of PIP₂ from the interface up to 15 Å [1] promotes the interaction with the charged peptide. This interaction has only an impact on the PI(4,5), as there was found no influence on the surrounding lipid matrix. This arrangement of polyvalent anionic lipid facing the aqueous phase consequently built the precondition for the electrostatic interaction of the MARCKS protein with the PIP₂ molecules. In this way, the PI(4,5) group forms a distinct electrostatic mark for association of the charged peptide. The presence of MARCKS (151-175) in the subphase, i.e. the clusters of its basic residues, produces locally positive electrostatic potentials. Thereby the PIP₂ molecules laterally diffuse within the membrane interface and form electrostatic complexes with the peptide [2]. Since the PIP₂ molecules are arranged in a uniform distribution in the disordered phase, the PIP₂/peptide complexes exist in the disordered phase as well. The enrichment of MARCKS peptide in the disordered phase facilitates potentially the diffusion of these complexes along the membrane interface. In contrast, the diffusion of the DPPS/peptide complexes is constricted due to their formation within the ordered crystalline phase [3]. That is caused by the smaller diffusion coefficient of the lipids in the ordered phase, compared to the lipids in the disordered phase [4]. Due to this hindered diffusion, the elevated concentration of PS caused by the interaction with MARCKS (151-175), accompanied with an elongation of the serine (up to 7 Å) and phosphodiester groups of the lipid fraction can induce a change in the curvature state of the monolayer and continuative of a bilayer. This could explain - on a molecular level - the increase of the vesicle endocytosis within the cell cycle due to lateral enrichment of PS [5].

[1] U. Dietrich et al.: *Biochim. Biophys. Acta* **1788**, 1474-1481 (2009).

[2] J. Wang et al.: *Biophys. J.* **86**, 1969-1986 (2004).

[3] U. Dietrich, P. Krüger, J. A. Käs: *Chem. Phys. Lipids* **164**, 266-275 (2011).

[4] A. Filippov et al.: *Biophys. J.* **86**, 891-896 (2004).

[5] E. Farge: *Biophys. J.* **69**, 2501-2506 (1995).

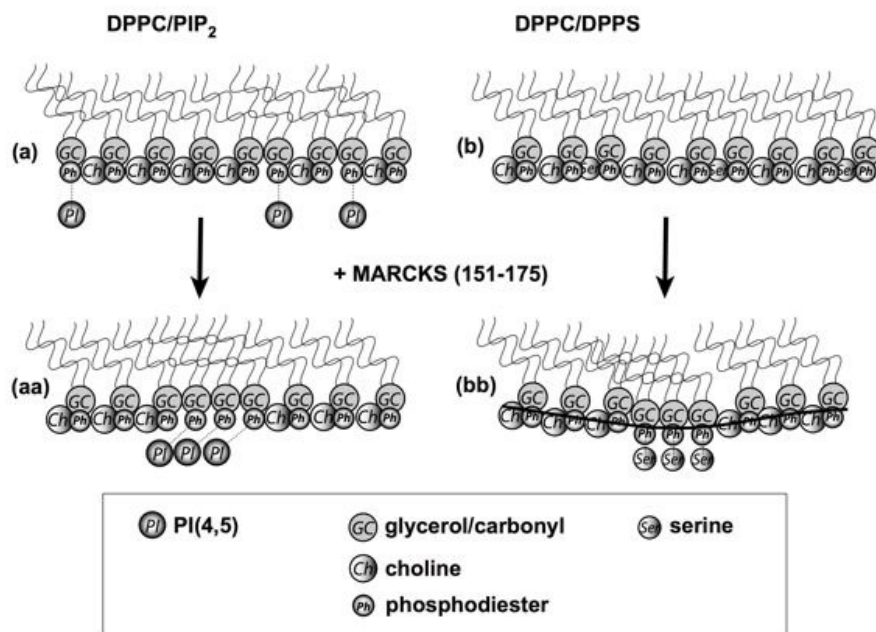


Figure 5.8: Sketch of the structure of the mixed monolayers. (a) DPPC/PIP₂, (aa) DPPC/PIP₂ with MARCKS (151-175) interaction, and (b) DPPC/DPPS, (bb) DPPC/DPPS with MARCKS (151-175) interaction; thereby are GC - glycerol/carbonyl fragment, Ch - choline group, Ph - phosphodiester group, PI - PI(4,5) group of PIP₂ and Ser - serine group of DPPS.

5.10 Actin Filament Elasticity and Retrograde Flow Shape the Force-Velocity Relation of Motile Cells

J. Zimmermann*, C. Brunner, M. Enculescu*, M. Goegler, A. Ehlicher, J.A. Käs, M. Falcke*

*Mathematical Cell Physiology, Max-Delbrück-Center for Molecular Medicine, Berlin

Cells migrate through a crowded environment during processes such as metastasis or wound healing, and must generate and withstand substantial forces. The cellular motility responses to environmental forces are represented by their force-velocity relation, which has been measured for fish keratocytes but remains unexplained. Even pN opposing forces slow down lamellipodium motion by three orders of magnitude. At larger opposing forces, the retrograde flow of the actin network accelerates until it compensates for polymerization, and cell motion stalls. Subsequently, the lamellipodium adapts to the stalled state. We present a mechanism quantitatively explaining the cell's force-velocity relation and its changes upon application of drugs that hinder actin polymerization or actomyosin-based contractility. Elastic properties of filaments, close to the lamellipodium leading edge, and retrograde flow shape the force-velocity relation. To our knowledge, our results shed new light on how these migratory responses are regulated, and on the mechanics and structure of the lamellipodium.

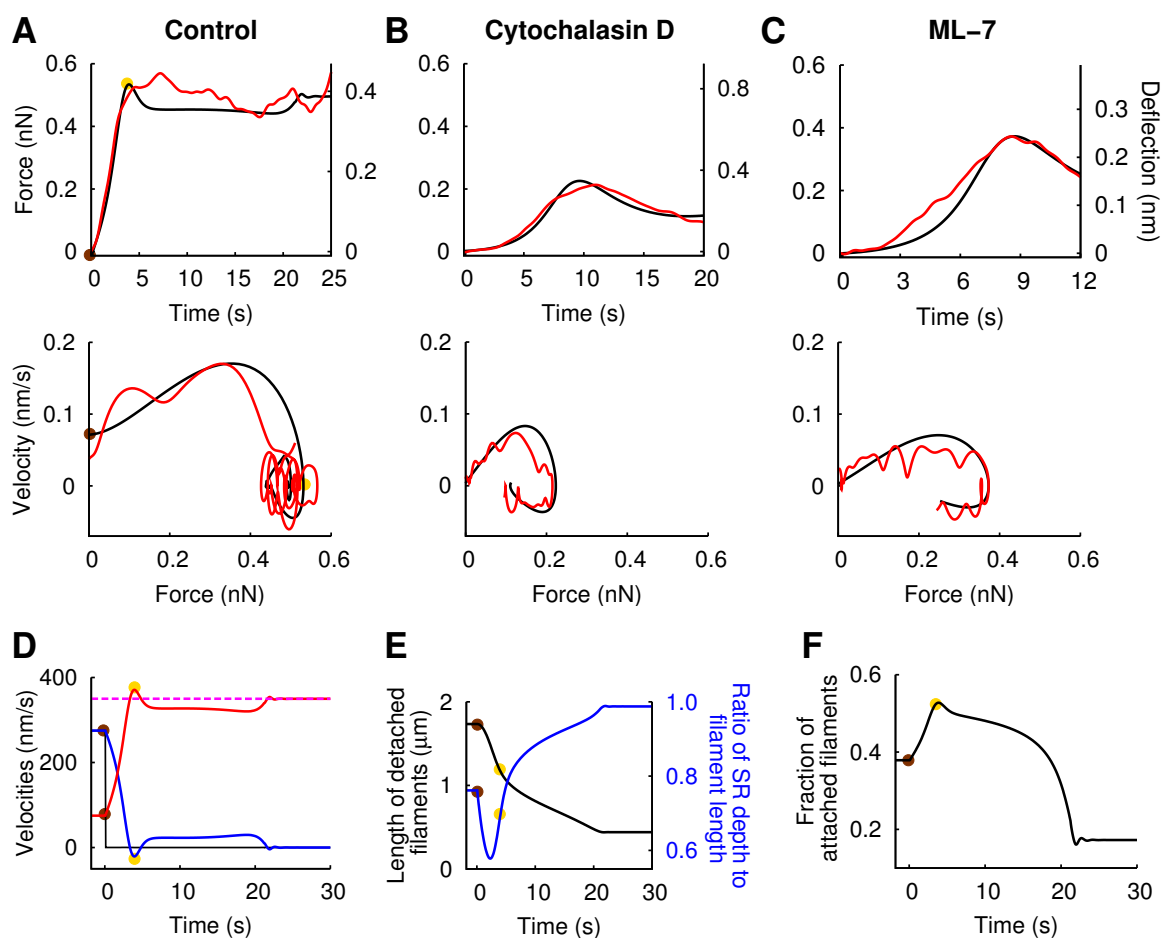


Figure 5.9: Cantilever deflections, force-velocity relations, and SR properties. (A–C) Comparison of simulations (black) and experiments (red) for (A) a control cell and cells influenced by the application of (B) cytochalasin D and (C) ML-7. (Upper row) Time course of the cantilever deflection due to the lamellipodium’s leading edge pushing against the bead on the cantilever; (lower row) force-velocity relation. (D–F) Simulated development of velocities and the semi-flexible region (SR) after cantilever contact for the control cell. (Brown dots) First cantilever contact; (yellow dots) time when motion stalls. (D) Development of the leading-edge velocity (black), the gel boundary velocity (blue), retrograde flow velocity (red), and the sum of the gel boundary and retrograde flow velocities (dashed magenta), which is essentially constant. (E) Time course of the ratio of SR depth to length of detached filaments (blue) and the filament length (black). The differential stiffness of the filaments is proportional to free filament length. (F) Time course of the fraction of filaments attached to the membrane.

5.11 Funding

Leipziger Schule der Naturwissenschaften - Bauen mit Molekülen und Nano-Objekten
 Prof. Dr. E. Hey-Hawkins, Prof. Dr. M. Grundmann and Prof. Dr. J. A. Käs
 BuildMoNa - Graduiertenschule

InterNeuro

Prof. Dr. J. A. Käs

DFG Graduiertenkolleg "InterNeuro" (GRK 1097), Leipzig, Projekte 5, 7

Optical Stretcher Methode zur Krebsdiagnose an Biopsien

Prof. Dr. J. A. Käs

EXPRIMAGE-Forschungsverbund

Inhärente zelluläre, physikalische und Materialeigenschaften zur molekular marker-freien Isolierung und Charakterisierung seltener Zelltypen

Prof. Dr. J. A. Käs, Prof. Dr. A. Robitzki et al.

-Theranostik- / SAB-Projekt

Zuverlässige Untersuchung und gezielte Modifikation der mechanischen Eigenschaften retinaler Zellen bei Netzhauterkrankungen und in Glianarben

Prof. Dr. J. Käs, Prof. Dr. A. Reichenbach et al.

Teilprojekt 2 / SAB-Projekt

Optische Messung zellulärer Materialeigenschaften für pharmakologische Hochdurchsatz-Technologie (Agescreen)

Prof. Dr. J. A. Käs

BMBF-Projekt

Von lokaler Beschränkung bis zu makroskopischem Transport - From local constraints to macroscopic transport

Prof. Dr. J. A. Käs, Dr. Stefan Diez et al.

DFG-Forschergruppe FOR 877, Teilprojekt 6 / DFG-Förderung

Light propagation through the retina: Vertebrate retinal optics

Prof. Dr. J. A. Käs, Prof. Dr. A. Reichenbach et al.

DFG-Förderung

5.12 Organizational Duties

Prof. Dr. J. A. Käs

- PWM Winterschool Spindlermühle CZ, February 2011
- 2nd Symposium "Physics of cancer", Coordinators: Prof. Dr. Josef Käs (University of Leipzig), Prof. Dr. Harald Herrmann (German Society for Cell Biology), Prof. Dr. Sarah Köster (Georg August University of Göttingen) October 13-15, 2011
- "BuildMoNa" Minisymposium "Hybrid Systems", November 10-11, 2011
- Journal review: Nature, Physical Review Letters, Physical Review E, Biophysical Journal, Biophysica and Biochemica Acta, Biochemistry, Proceedings of the National Academy of Science, European Biophysical Journal, Langmuir
- Grant review: National Science Foundation, Div. of Materials Research; National Science Foundation, Div. of Cellular Organization; National Science Foundation, Div. of Computational Biology; National Science Foundation, Div. of Physics, Special Programs; Deutsche Forschungsgemeinschaft, Alexander von Humboldt Foundation, Deutsche Studienstiftung, Centre National de Recherche

5.13 External Cooperations

Academic

- Institute Curie, Paris, France
Prof. Dr. J.-F. Joanny
- ESPCI, Paris, France
Prof. Dr. J. Prost
- University of Maryland, USA
Prof. Dr. W. Losert
- University of Maryland School of Medicine, USA
Prof. Dr. S. Martin
- Albert Einstein Institute of Medicine, U.S.A.
Prof. Dr. J. Condeelis
- Deutsche Gesellschaft für Zellbiologie (DGZ)
Prof. Dr. H. Herrmann
- Georg August University Göttingen
Prof. Dr. S. Köster
- Physikalisch-Technische Bundesanstalt
Prof. Dr. M. Bär
- Max-Delbrück-Zentrum für molekulare Medizin
Dr. M. Falcke
- Deutsches Krebsforschungszentrum
Prof. Dr. R. Eills
- Universität Leipzig, Klinik u. Poliklinik für Frauenheilkunde
Prof. Dr. M. Höckel
- Universität Leipzig, Institut für Pathologie
Prof. Dr. L.-C. Horn
- Universität Leipzig, Institut für Anorganische Chemie
Prof. Dr. E. Hey-Hawkins
- Universität Leipzig, Institut für Biochemie
Prof. Dr. A. Beck-Sickinger
- Universität Leipzig, Klinik u. Poliklinik f. Mund-, Kiefer- u. Plastische Gesichtschirurgie
Dr. T. Remmerbach
- Westfälische Wilhelms-Universität Münster
Dr. J. Schnekenburger

Industry

- Beiersdorf AG, Hamburg
Dr. C. Schulze

- JPK Instruments, Berlin
Dr. T. Müller
- Niendorf & Hamper, Hamburg
Prof. A. Niendorf
- ibidi GmbH, Martinsried
Dr. V. Kahl
- Inventages, London, GB
Prof. Dr. T. Bayerl

5.14 Publications

Journals

F. Huber, D. Strehle, J. A. Käs: *Counterion-induced formation of regular actin bundle networks*, *Soft Matter* **8**, Issue 4, 931-936 (2012)

S. Agte, S. Junek, S. Matthias, E. Ulbricht, I. Erdmann, A. Wurm, D. Schild, J. A. Käs, A. Reichenbach: *Müller glial cell-provided cellular light guidance through the vital guinea-pig retina*, *Biophysical Journal* **101**, Issue 11, 2611-2619 (2011)

O. Jonas, C. Mierke, J. A. Käs: *Invasive cancer cell lines exhibit biomechanical properties that are distinct from their noninvasive counterparts*, *Soft Matter* **7**, Issue 24, 11488-11495 (2011)

T. Betz, D. Koch, Y. Lu, K. Franze, J. A. Käs: *Growth cones as soft and weak force generators*, *PNAS* **108**, Issue 33, 13420-13425 (2011)

M. Gyger, D. Rose, R. Stange, T. Kießling, M. Zink, B. Fabry, J. A. Käs: *Calcium imaging in the optical stretcher*, *Optics Express* **19**, Issue 20, 19212-19222 (2011)

U. Dietrich, P. Krüger, J. A. Käs: *Structural investigation on the adsorption of the MARCKS peptide on anionic lipid monolayers - effects beyond electrostatic*, *Chemistry and Physics of Lipids* **164**, Issue 4, 266-275 (2011)

F. Wetzels, S. Röncke, K. Müller, M. Gyger, D. Rose, M. Zink, J. A. Käs: *Single cell viability and impact of heating by laser absorption*, *European Biophysics Journal* **40**, Issue 9, 1109-1114 (2011)

F. Huber, J. A. Käs: *Self-regulative organization of the cytoskeleton*, *Cytoskeleton* **68**, Issue 5, 259-265 (2011)

M. Knorr, D. Koch, T. Fuhs, U. Behn, J. A. Käs: *Stochastic Actin Dynamics in Lamellipodia Reveal Parameter Space for Cell Type Classification*, *Soft Matter* **7**, 3192-3203 (2011)

S. Alonso, U. Dietrich, C. Händel, J. A. Käs, M. Bär: *Oscillations in the Lateral Pressure of Lipid Monolayers Induced by Nonlinear Chemical Dynamics of the Second Messengers MARCKS and Protein Kinase C*, *Biophysical Journal* **100**, Issue 4, 939-947 (2011)

B. Stuhmann, F. Huber, J. A. Käs: *Robust organization principles of protrusive biopolymer networks in migrating living cells*, *PLoS ONE* **6**, Issue 1, e14471 (2011)

Y. Lu, I. Iandiev, M. Hollborn, N. Körber, E. Ulbricht, P. G. Hirrlinger, T. Pannicke, E. Wei, A. Bringmann, H. Wolburg, U. Wilhelmsson, M. Pekny, P. Wiedemann, A. Reichenbach, J. A. Käs: *Reactive glial cells: increased stiffness correlates with increased intermediate filament expression*, The FASEB Journal **25**, Issue 2, 624-631 (2011)

in press

L. Woiterski, D. W. Britt, J. A. Käs, C. Selle: *Oriented Confined Water Induced by Cationic Lipids*, Langmuir DOI:10.1021/la205043x (2012)

A. Leal-Egana, A. Fritsch, F. Heidebrecht, A. Diaz-Cuenca, M. Nowicki, A. Bader, J. A. Käs: *Tuning liver stiffness against tumors: An in vitro study using entrapped cells in tumor-like microcapsules*, J. Mech. Beh. Biomed. Mat. (2012)

Talks

Josef A. Käs

PWM Winter School, Spindler-Mühle, CZ

American Physical Society Meeting, Dallas, U.S.A., Feb. 27-March 03, 2011 (invited)

GOAL-Meeting 2011, University of Leipzig, "Physics meets Gynecologic Oncology" - "Änderungen in der Einzelbiomechanik als notwendige Bedingung für das Vordringen von Tumoren", March 09, 2011 (invited)

Spring meeting German Physics Society, Dresden, "Mechanics and Growth of Tissues: From Development to Cancer", March 13-18, 2011

Workshop "Mechanics and Growth of Tissues: From Development to Cancer" MPI for Complex Systems, Dresden, March 25, 2011 (invited)

Biozentrum, University of Basel, Switzerland, "Are biomechanical changes necessary for tumor progression?", May 17, 2011 (invited)

"Soft and Biological Matter" seminar "The Rudolf Peierls Centre for Theoretical Physics", Oxford University, GB, "Are biomechanical changes necessary for tumor progression?", May 31, 2011 (invited)

Einladung zum "Physikalischen Kolloquium", University of Magdeburg, "Are biomechanical changes necessary for tumor progression?", June 07, 2011 (invited)

EBSA - 8th European Biophysics Congress, Budapest, Hungary, "Are biomechanical changes necessary for tumor progression?", August 23-27, 2011 (invited)

12th International ICSB- Congress Heidelberg/ Mannheim, "Are biomechanical changes necessary for tumor progression?", August 28-30, 2011 (invited)

DYNACT11 - Workshop, Max Planck Institute for Physics of Complex Systems, Dresden, "Origin and spatial distribution of forces in motile fish keratocytes", August 29-September 01, 2011 (invited)

2nd Symposium “Physics of Cancer”, University of Leipzig, Georg August University of Göttingen, German Society for Cell Biology, Leipzig, Coordinator, October 13 -15, 2011

GRK “BuildMoNa” University of Leipzig: Minisymposium “Hybrid Systems”, Leipzig, PI - coordinator, November 10 -11, 2011

CeNTech Day 2011, Westfälische Wilhelms-Universität Münster, “Physics of Cancer - a new perspective”, November 28, 2011 (invited)

Mareike Zink

Spring meeting German Physics Society, Dresden, “Exploring the Impact of Cell Mechanics on Cancer Progression with the Microfluidic Optical Stretcher ”, March 13-18, 2011

Buchmesse Leipzig, “Die Physik von Krebszellen”, March 19, 2011 (invited)

2nd Symposium Physics of Cancer, “Exploring the Impact of Cell Mechanics on Cancer Progression with the Microfluidic Optical Stretcher”, Leipzig, October 13 -15, 2011 (invited)

Materials Research Society Fall Meeting, “Exploring the Impact of Cell Mechanics on Cancer Progression with the Microfluidic Optical Stretcher”, Boston, USA, December 2, 2011

Posters

Mareike Zink

Biophysical Society Meeting, Baltimore, U.S.A., “Are biomechanical changes necessary for tumor progression?”, March 2011

Biophysical Society Meeting, Baltimore, U.S.A., “Biocompatibility of ferromagnetic shape memory alloys for single cell actuation”, March 2011

MidTerm Review, Prag, Marie Curie Initial Training Eduglia (PITN- GA-2009-237956) funded by the EU, Seventh Framework Program (FP7), “Retinal Glia: Altered Biomechanics of Ocular Diseases” (with V. Dallacasagrande, S. G. Mayr, J. A. Käs and A. Reichenbach), August 2011

Materials Research Society Fall Meeting, Boston, U.S.A., “Biocompatibility of ferromagnetic shape memory alloys for single cell actuation”, December 2011

5.15 Graduations

Doctorate

- Claudia Brunner, Dipl.-Phys.
Origin and Spatial Distribution of Forces in Motile Cells
February 2011

- Christian Schulze, Dipl.-Phys.
Biomechanics of Human Skin Fibroblasts and its Implications for Skin Aging
March 2011
- Thomas Siegemund, Dipl.-Biochem.
Structure and properties of drug-loaded polymeric nanoparticles targeting β -amyloid
March 2011
- Undine Dietrich, Dipl.-Ing.
Structural and dynamic studies of MARCKS interaction with PIP_2 containing lipid membranes
October 2011

Diploma

- Steffen Grosser
Validity of the ray optics model for the passage of light through biological cells
May 2011
- Eva Rose
High Strain Behavior of Malignant Cells
August 2011
- Sebastian Koth
Dynamik des Zytoskeletts auf Mikrostrukturen
November 2011

Master

- Paul Heine
The mechanics of neuronal growth \exists Investigation via cytoskeletal dynamics
January 2011
- Lukas Hild
Developing a microfluidic based primary cell sorter
January 2011

Bachelor

- Lydia Reuter
Protrusion Forces Measurements of Migrating Cells
January 2011
- Rebecca Dennert
Mechanical Properties of Invasive Cells
July 2011
- Peter Palm
Studies in semiflexible biomechanics - Investigation of the persistence length of F-Actin
September 2011

- Sabrina Friebe
Generation of uniform cell morphologies for biomechanical measurements
October 2011
- Tom Kunschmann
Influence of substrate mechanical properties on neuronal growth cone edge fluctuations
November 2011
- Stefanie Puder
Neuronal growth mechanical sensitivity to different substrates
November 2011

5.16 Guests

- M. Sc. Valentina Dallacasagrande
EU-research assistant at the Paul-Flechsig-Institut for brain research and the Dept. Softmatter Physics, Universität Leipzig, March 2010 - approx. 2012
- Iris Vonderhaid
Technische Universität Wien, September 21, 2010 - October 30, 2011
- Anya Burkart
Creighton University, Omaha, U.S.A., September, 2011 - August 2012
- Federica Tavano
Laboratorio Nazionale TASC, Italy, September 15, 2011 - December 15, 2011

II

Institute for Experimental Physics II

6

Magnetic Resonance of Complex Quantum Solids

6.1 Introduction

The electronic properties of quantum-solids in which the electrons exhibit strong correlations with each other or with the lattice are particularly rich and will be of special importance in future functional materials. In addition, such solids are challenging for experiment, as well as theory, as the more than twenty-year history of high-temperature superconductivity shows: we still do not understand the electronic structure of these systems. One particular aspect of strongly correlated electronic materials is their tendency towards nano-scale electronic phase separation. Even in perfect lattices, electronic nano-structures can form. The investigation of such materials requires the use of methods that can give detailed information. Here, magnetic resonance, on nuclei and electrons, is of particular interest as they not only have atomic scale resolution, but also yield bulk information in contrast to surface techniques. We explore the properties of these materials with tailored new techniques of magnetic resonance.

Jürgen Haase

6.2 High-pressure spin shifts in the pseudogap regime of superconducting $\text{YBa}_2\text{Cu}_4\text{O}_8$ as revealed by ^{17}O NMR

T. Meissner, S.K. Goh ^{*}, J. Haase, G.V.M. Williams [†], P.B. Littlewood ^{*},

^{*}Department of Physics, Cavendish Laboratory, University of Cambridge, United Kingdom

[†]The MacDiarmid Institute and Industrial Research Limited, Wellington, New Zealand

A NMR anvil cell design is used for measuring the influence of high pressure on the electronic properties of the high-temperature superconductor $\text{YBa}_2\text{Cu}_4\text{O}_8$ above the superconducting transition temperature T_c . It is found that pressure increases the spin shift at all temperatures in such a way that the pseudogap feature has almost disappeared at 63 kbar. This change of the temperature-dependent spin susceptibility can be

explained by a pressure-induced proportional decrease (factor of 2) of a temperature-dependent component, and an increase (factor of 9) of a temperature-independent component, contrary to the effects of increasing doping. The results demonstrate that one can use anvil cell NMR to investigate the tuning of the electronic properties of correlated electronic materials with pressure.

6.3 NMR signal averaging in 62T pulsed fields

B. Meier, S. Greiser, J. Haase, T. Herrmannsdörfer *, F. Wolff-Fabris *, J. Wosnitza *,

*Dresden High Magnetic Field Laboratory, Forschungszentrum Dresden-Rossendorf

Nuclear Magnetic Resonance (NMR) experiments in pulsed high magnetic fields up to 62T at the Dresden High Magnetic Field Laboratory (Hochfeld-Magnetlabor Dresden) are reported. The time dependence of the magnetic field is investigated by observing various free induction decays (FIDs) in the vicinity of the maximum of the field pulse. By analyzing each FID's phase and its evolution with time the magnetic field's time dependence can be determined with high precision. Assuming a quadratic or cubic dependence on time near the field maximum its confidence is found to be better than 0.03ppm at low fields and 0.8ppm near 62T. In turn, the thus obtained time dependence of the field can be used to demodulate and phase-correct all FIDs so that they appear phase-locked to each other. As a consequence signal averaging is possible. The increase in signal-to-noise ratio is found to be close to that expected theoretically. This shows that the intrinsic time dependence of the pulsed fields can be removed so that the NMR signals appear to be taken at rather stable static field. This opens up the possibility of performing precise shift measurements and signal averaging also of unknown, weak signals if a reference signal is measured during the same field pulse with a double-resonance probe.

6.4 An Electron Spin Resonance Study of Nitroxide Radical Adsorption at Cupric Ions in the Metal-Organic Framework Compound $\text{Cu}_3(\text{Btc})_2$

B. Jee, K. Koch, L. Moschkowitz, D. Himsl *, M. Hartmann *, A. Pöppl

*Erlangen Catalysis Resource Center (ECRC), Friedrich-Alexander-University Erlangen-Nürnberg, Germany

The Cu(II) pairs in the paddle-wheel building blocks of the metal-organic framework compound $\text{Cu}_3(\text{Btc})_2$ give rise to an antiferromagnetic spin state with an electron spin resonance (ESR) silent $S=0$ ground state. However, the adsorption of di-tert-butyl nitroxide (DTBN) radicals leads to the formation of an unusual nitroxide ESR spectrum and later, upon thermal treatment of the samples, to distinct paramagnetic Cu(II) centers, whose ESR signals can be observed at temperatures below 70 K. HYSCORE spectroscopy reveals the presence of ^{14}N nuclei in the local environment of the formed paramagnetic Cu(II) species and thereby indicate that the DTBN radicals bind to the

Cu(II) pairs. Various scenarios for the suppression of the antiferromagnetic coupling of the Cu(II) ions in the paddle wheel units by the interaction with the nitroxide and the subsequent formation of these $S = 1/2$ copper centers are discussed.

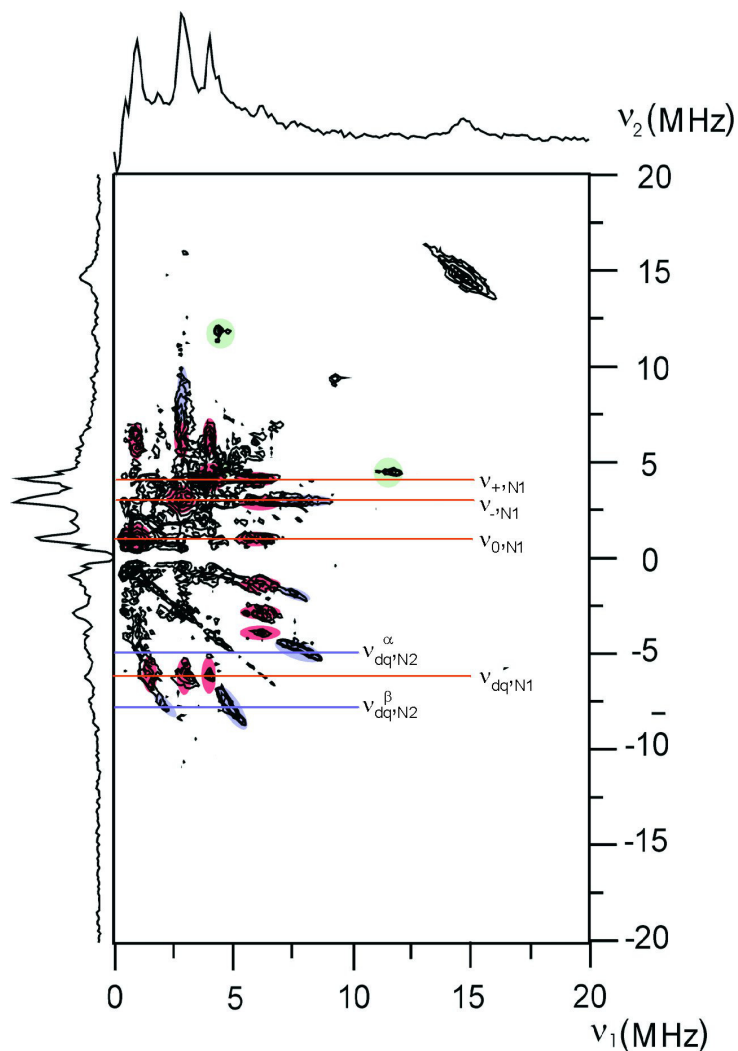


Figure 6.1: HYSCORE spectrum at 6 K of $\text{Cu}_3(\text{Btc})_2$ upon adsorption of DTBN and heating at 363 K for 16 h. Two spectra with pulse delays of $\tau = 104$ and 136 ns were recorded at 342.8 mT and the sum of the two spectra is displayed. Red and blue areas indicate cross peaks of nitrogen nuclei N1 and N2, respectively, green areas mark peaks of unknown origin.

6.5 Effects of varying water adsorption on a $\text{Cu}_3(\text{BTC})_2$ metal-organic framework (MOF) as studied by ^1H and ^{13}C solid-state NMR spectroscopy

F. Gul-E-Noor, B. Jee, A. Pöppel, M. Hartmann*, D. Himsl*, M. Bertmer

*Erlangen Catalysis Resource Center (ECRC), Friedrich-Alexander-University Erlangen-Nürnberg, Germany

The process of water adsorption on a dehydrated $\text{Cu}_3(\text{BTC})_2$ (copper (II) benzene 1,3,5-tricarboxylate) metal-organic framework (MOF) was studied with ^1H and ^{13}C solid-state NMR. Different relative amounts of water (0.5, 0.75, 1, 1.5, 2, and 5 mole equivalents with respect to copper) were adsorbed via the gas phase. ^1H and ^{13}C MAS NMR spectra of dehydrated and water-loaded $\text{Cu}_3(\text{BTC})_2$ samples gave evidence on the structural changes due to water adsorption within the MOF material as well as information on water dynamics. The analysis of ^1H spinning sideband intensities reveals differences in the ^1H $^{63/65}\text{Cu}$ hyperfine coupling between dehydrated and water-loaded samples. The investigation was continued for 60 days to follow the stability of the $\text{Cu}_3(\text{BTC})_2$ network under humid conditions. NMR data reveal that $\text{Cu}_3(\text{BTC})_2$ decomposes quite fast with the decomposition being different for different water contents.

6.6 Single Crystal to Single Crystal Topochemical Photoreactions: Measuring the Degree of Disorder in the [2 + 2] Photodimerization of *trans*-Cinnamic Acid Using Single-Crystal ^{13}C NMR Spectroscopy

R.C. Nieuwendaal*, S.J. Mattler[†], M. Bertmer, S.E. Hayes*

*Polymers Division, National Institute of Standards and Technology, Gaithersburg, MD

[†]Department of Chemistry, Washington University in St. Louis, St. Louis, MO

A single crystal of α -*trans*-cinnamic acid was synthesized with a ^{13}C -label at the β -carbon position and photoreacted to yield the [2 + 2] cycloaddition product, α -truxillic acid. $^{13}\text{C}^1\text{H}$ cross-polarization (CP) single-crystal NMR experiments were performed on the unreacted and sequentially photoreacted samples for different goniometer orientations, and the spectra were simulated using the SIMMOL and SIMPSON software packages. Atomic coordinates from single-crystal X-ray diffraction data were used as inputs in the simulations, which allowed the chemical shift tensor to be precisely measured and related to the unit cell (or molecular) reference frame of cinnamic acid. The line widths of the ^{13}C resonances observed at different goniometer rotations were utilized to estimate the orientational dispersion of the cinnamic acid species, which ultimately provides a measure of disorder in the single crystal. The photoreacted sample, a solid solution of cinnamic and truxillic acids, maintained its single-crystal nature, even up to 44% conversion to truxillic acid, keeping its $P2_1/n$ symmetry. Upon photoirradiation, however, a slight loss of order was observed in the cinnamic acid species as

evidenced by an increase in the ^{13}C NMR line widths, demonstrating that NMR can be used to monitor subtle orientational imperfections in single crystal to single crystal photoreactions.

6.7 Optimized NMR spectroscopic strategy to characterize water dynamics in soil samples

A. Jäger, G.E. Schaumann^{*}, M. Bertmer,

^{*}University of Koblenz-Landau, Institute for Environmental Sciences, Department of Environmental and Soil Chemistry, Landau

^1H wideline NMR spectra of soil samples offer the possibility to analyze soil material based on their proton mobility. Care has to be taken to remove unwanted signal contributions from the probe background. We demonstrate that unstructured wideline spectra can be analyzed quantitatively by a combination of a Gaussian line for rigid and a Lorentzian line for mobile protons. This is used to study effects of hydrogen-bonded water networks upon heat treatment for a series of different soil samples with varying water content as a contribution to study physical aging of soil organic matter (SOM). Results are combined with ^1H projections from ^{13}C 2D WISE (wideline separation) experiments representing solely the broad Gaussian line. Furthermore, for the first time applied to soils, ^1H structural information from soil samples is obtained from 2D PMLG phase modulated Lee-Goldburg measurements under magic angle spinning (MAS). Low water contents improve the resolution of main functional groups significantly.

6.8 Paramagnetic resonance study of nickel ions in hexagonal barium titanate

R. Böttcher, H.T. Langhammer^{*}, T. Müller[†],

^{*}Martin-Luther-Universität Halle-Wittenberg, Physikalisches Institut

[†]Martin-Luther-Universität Halle-Wittenberg, Chemisches Institut

X-ray diffraction patterns and electron paramagnetic resonance (EPR) powder spectra (9 and 34 GHz) of $\text{BaTiO}_3 + 0.04 \text{ BaO} + \chi \text{ NiO}$ ($0.001 \leq \chi \leq 0.02$) ceramics were studied to investigate the incorporation of Ni ions and their valence states as well as the development of the hexagonal phase (6H modification) of Ni-doped material with respect to doping level χ and sintering temperature T_s . The 6H modification begins to occur at a nominal Ni concentration of between $\chi = 0.005$ and 0.01 and its percentage increases with increasing sintering temperature. Ni-doped BaTiO_3 with $\chi = 0.02$ sintered at $T_s = 1400$ °C is completely hexagonal. In the 3C modification, present in as-sintered ceramics with low nominal Ni concentrations, only one type of Ni EPR spectrum was observed. By comparing its principal values of the g tensor with data of single-crystal measurements the clear assignment of this spectrum to Ni^+ ions is possible. Two different EPR spectra with orthorhombic g tensors are observed in the

as-sintered samples with hexagonal crystal structure. These spectra were assigned to Ni^{3+} ions with the electron spin $S = \frac{1}{2}$ (electron configuration $3d^7$, strong crystal field) substituted at Ti lattice sites corresponding to the different distorted octahedra of the hexagonal modification. Measurements of the concentration reveal that only 5 % of the doping material is in the state Ni^{3+} . No EPR spectra of Ni^{2+} ions have been detected in either 3C or 6H modification in as-sintered ceramics. Therefore, we suppose that the main part of nickel is substituted as Ni^{4+} ions on Ti^{4+} lattice sites. After heat treatment of the samples in H_2/Ar atmosphere a single-line spectrum with $g = 2.21 \pm 0.01$ at room temperature has been observed which is assigned to metallic Ni or antiferromagnetically coupled Ni^{2+} ions in secondary phases segregated at grain boundaries or triple points.

6.9 Funding

EuroMagNET, JRA NMR

Prof. J. Haase

EU, RII3CT-2004-506239.

Magnetic Ground State and Dynamics in High-Temperature Superconductors

Prof. J. Haase, Prof. O.P. Sushkov, Prof. B. Keimer

EU, DP0881336.

Nanocomposites, ferroelectric nanostructures

Prof. J. Haase, Prof. Dr. Cheng Tien

DAAD, 50750765.

MOF as carrier for nitric oxide delivery in biological systems, microscopic fundamentals of adsorption and controlled release studied by infrared and electron and nuclear spin spectroscopy

Prof. A. Pöppel

DFG, SPP1362.

Characterization of the [2+2] photodimerization of photo-active substances based on cinnamic acid incorporated in polymers and supramolecular structures with solid-state NMR

Dr. M. Bertmer

DFG BE 2434/2-3.

SOM-AGING II. Hydration-dehydration mechanisms at Biogeochemical Interfaces

Dr. M. Bertmer

within SPP 1315.

MOF as carrier for nitric oxide delivery in biological systems, microscopic fundamentals of adsorption and controlled release studied by infrared and electron and nuclear spin spectroscopy

Dr. M. Bertmer

DFG BE 2434/4-1 within SPP 1362.

Fabrication and physical properties of ferroelectrics confined in nanoporous materials

Prof. D. Michel, Prof. E. V. Charnaya

DFG Mi 390/25-1.

Microstructure and molecular mobility in aqueous solutions of organic molecules

Prof. D. Michel, Prof. V. I. Chizhik

DFG Mi 390/23-1.

6.10 Organizational Duties

J. Haase

- Dean of Faculty
- Vice Director of the Magnetic Resonance Center Leipzig (MRZ)
- Referee: Physical Review, GIF

A. Pöpl

- Referee: Journal of Magnetic Resonance, Journal of American Chemical Society, Physical Chemistry Chemical Physics, Chemical Physics Letters
- Project Reviewer: German-Israel-Foundation for Scientific Research and Development (GIF)

M. Bertmer

- Referee: Angewandte Chemie, Chemistry of Materials, Solid State Nuclear Magnetic Resonance

D. Michel

- Referee: Physical Review, Journal of Physics: Condensed Matter, Langmuir, Journal of Magnetic Resonance, Phys. Stat. Sol., Materials Chemistry and Physics, GIF

R. Böttcher

- Referee: Physical Review, Journal of Physics: Condensed Matter, Langmuir, Journal of Magnetic Resonance

6.11 External Cooperations

Academic

- Laboratoire National des Champs Magnétiques Pulsés Toulouse, France
Prof. Dr. Geert Rikken
- University of Illinois at Urbana-Champaign, Department of Physics, USA
Prof. Dr. Charles P. Slichter
- University of New South Wales Australia, School of Physics, Sydney, Australia
Prof. Dr. Oleg P. Sushkov
- University of Illinois at Urbana-Champaign, Department of Electrical and Computer Engineering, USA
Prof. Dr. Andrew G. Webb

- University of Minnesota, School of Physics and Astronomy, USA
Prof. Dr. Martin Greven
- The MacDiarmid Institute and Industrial Research Limited, New Zealand
Dr. Grant V. M. Williams
- Dresden High Magnetic Field Laboratory, Forschungszentrum Dresden-Rossendorf
Prof. Dr. Joachim Wosnitza
- Washington University, St. Louis, MO, USA, Department of Chemistry
Sophia E. Hayes
- Universität Koblenz-Landau, Koblenz, Abteilung Chemie
Gabriele E. Schaumann
- Martin-Luther-Universität Halle-Wittenberg, Physikalisches Institut
Dr. H. T. Langhammer
- Universität Augsburg, Advanced Materials Science, Institut für Physik
Prof. Dr. M. Hartmann
- NASU, Institute of Semiconductor Physics, Kiev, Ukraine
Prof. Dr. E. N. Kalabukhovaa
- Staatliche Universität Kazan, Tartastan, Russische Förderung
Prof. Dr. E. N. Kalabukhovaa
- Université du Maine, Faculté des Sciences, Laboratoire de Physique de l'Etat Condensé, Le Mans, France
Prof. Dr. A. Kassiba
- Walther-Meißner-Institute for Low Temperature Research, Bavarian Academy of Sciences and Humanities, Munich, Germany
Dr. A. Erb
- University of Vilnius, Faculty of Physics, Lithuania
Prof. Dr. J. Banys
- Technische Universität München, Anorganisch-chemisches Institut
Prof. Dr. K. Köhler

Industry

- NMR-Service, Erfurt
M. Braun
- Bruker BioSpin, Rheinstetten
F. Engelke

6.12 Publications

Journals

R. Böttcher, H. T. Langhammer, T. Müller: *Paramagnetic resonance study of nickel ions in hexagonal barium titanate*, J. Phys.: Condens. Matter **23** 115903 (9pp)(2011)

- N. Garnov, G. Thörmer, R. Trampel, W. Gründer, T. Kahn, M. Moche, H. Busse: *Suitability of miniature inductively coupled RF coils as MR-visible markers for clinical purposes*, *Med. Phys.* **38** 6327 (2011)
- B. Meier, J. Kohlrantz, J. Haase: *Eigenmodes in the long-time behavior of a coupled spin system measured with nuclear magnetic resonance*, arXiv: 1112.3626 (2011)
- J. Haase, D. Rybicki, C.P. Slichter, M. Greven, G. Yu, Y. Li, X. Zhao: *Two-component uniform spin susceptibility in superconducting $\text{HgBa}_2\text{CuO}_{4+\delta}$ single crystals determined with ^{63}Cu and ^{199}Hg NMR*, arXiv: 1110.6016 (2011)
- R. Ferra, K. Thiel, A. Winter, T. Klamroth, A. Pöppl, A. Kelling, U. Schilde, A. Taubert, P. Strauch: *Tetrahalidocuprates(II)-structure and EPR spectroscopy. Part 1: Tetrabromidocuprates(II)*, *New J. Chem.* **35** 2793-2803 (2011)
- A.A. Gabrienko, S.S. Arzumanov, A.V. Toktarev, D. Freude, J. Haase, A.G. Stepanov: *Hydrogen H/D Exchange and Activation of C1-n-C4 Alkanes on Ga-Modified Zeolite BEA Studied with ^1H MAS NMR In Situ*, *J. Phys. Chem. C* **115** 13877-13886 (2011)
- T. Meissner, S. K. Goh, J. Haase, G. V. M. Williams, P. B. Littlewood: *High-pressure spin shifts in the pseudogap regime of superconducting $\text{YBa}_2\text{Cu}_4\text{O}_8$ as revealed by ^{17}O NMR*, *Phys. Rev. B* **83** 220517 (R)(2011)
- F. Gul-E-Noor, B. Jee, A. Pöppl, M. Hartmann, D. Himsl, M. Bertmer: *Effects of varying water adsorption on a $\text{Cu}_3(\text{BTC})_2$ metal-organic framework (MOF) as studied by ^1H and ^{13}C solid-state NMR spectroscopy*, *Phys. Chem. Chem. Phys.* **13** 7783-7788 (2011)
- B. Jee, K. Koch, L. Moschkowitz, D. Himsl, M. Hartman, A. Pöppl: *Electron Spin Resonance Study of Nitroxide Radical Adsorption at Cupric Ions in the Metal-Organic Framework Compound $\text{Cu}_3(\text{BTC})_2$* , *J. Phys. Chem. Lett.* **2** 357-361 (2011)
- G. V. M. Williams, M. Jurkutat, D. Rybicki, J. Haase: *^{63}Cu nuclear magnetic resonance study of $\text{Pr}_{1.85}\text{Ce}_{0.15}\text{Cu}_{1-x}\text{Ni}_x\text{O}_4$: Ni-induced spin density oscillation and modification of the low energy spin fluctuations*, *J. Phys.: Condens. Matter* **23** 075701 (7pp) (2011)
- B. Meier, S. Greiser, J. Haase, T. Herrmannsdörfer, F. Wolff-Fabris, J. Wosnitza: *NMR Signal averaging in 62 T pulsed fields*, *Journal of Magnetic Resonance* **210** 1-6 (2011)
- A. Jäger, G. E. Schaumann, M. Bertmer: *Optimized NMR spectroscopic strategy to characterize water dynamics in soil samples*, *Organic Geochemistry* **42** 917-925 (2011)
- R. C. Nieuwendaal, S. J. Mattler, M. Bertmer, S. E. Hayes: *Single Crystal to Single Crystal Topochemical Photoreactions: Measuring the Degree of Disorder in the $[2 + 2]$ Photodimerization of trans-Cinnamic Acid Using Single-Crystal ^{13}C NMR Spectroscopy*, *J. Phys. Chem. B* **115** 5785-5793 (2011)
- D. V. Savchenko, E. N. Kalabukhova, A. Pöppl, E. N. Mokhov, B. D. Shanina: *EPR study of conduction electrons in heavily doped n-type 4H SiC*, *Phys. Status Solidi B* **248** 2950-2956 (2011)

in press

Jörg Lincke, Daniel Lässig, Karolin Stein, Jens Moellmer, Anusree Viswanath Kuttathayil, Christian Reichenbach, Andreas Moeller, Reiner Staudt, Grit Kalies, Marko Bertmer, Harald Krautscheid: *A novel Zn₄O-based triazolyl benzoate MOF: synthesis, crystal structure, adsorption properties and solid state ¹³C NMR investigations*, DOI: 10.1039/c1dt11431j

Talks

J. Haase: *NMR at the highest pressures and magnetic fields*, Colloquium St. Louis NMR Discussion Group, 19.01-20.01.2011, St. Louis MO, USA

J. Haase: *Cuprate High-Temperature Superconductors Shifts and High Pressure*, Fifth International Conference on Advanced Materials and Nanotechnology AMN-5, 07.02.-11.02.2011, Wellington, New Zealand

B. Jee: *Continuous wave (cw) and pulse EPR studies of metal organic framework (MOF) compounds*, 23. Deutsche Zeolith-Tagung, Erlangen, 2.03.-4.03.2011

T. Meissner, S.K. Goh, J. Haase, G.V.M. Williams: *Effects of High Pressure on YBa₂Cu₄O₈ probed by ¹⁷O NMR*, 13.03.-18.03.2011 DPG Spring Meeting, Dresden

J. Haase: *NMR of Cuprates: Shifts and High Pressure*, Intl. Workshop Unconventional Superconductivity, 21.04.-25.4.2011, Minneapolis MN, USA

J. Haase: *NMR in high-temperature superconducting cuprates*, 23.5.2011, Charles University Prague, Czech Republic

M. Bertmer: *Solid-State ¹H and ¹³C NMR of metal-organic frameworks (MOFs)*, 2nd SMARTER crystallography workshop, 23.05.-27.05.2011, Aveiro, Portugal

D. Rybicki: *Unconventional spin susceptibility behavior in HgBa₂CuO_{4+δ} single crystals - a ⁶³Cu and ¹⁹⁹Hg NMR study*, 23.5.2011, Charles University Prague, Czech Republic

D. Rybicki: *Two-component behavior of high-temperature superconductor HgBa₂CuO_{4+δ}*, 13.06.-15.06.2011, Estnisch-Deutscher Workshop, Cottbus,

M. Bertmer: *Structural Changes to Cu₃(BTC)₂ due to Incorporation of Small Molecules as Studied by ¹H and ¹³C solid-state NMR*, International Symposium on Metal-Organic Frameworks, 20.09.-21.09.2011, Dresden

A. Kuttathayil: *Solid state NMR studies on MOFs: Monitoring the changes induced by Metal Ligand Interactions*, 4th BuildMoNa Workshop for Doctoral Candidates, 26.09.-27.09.2011, Dresden

G. Thörmer, J. Otto, M. Reis-Zimmermann, M. Seiwerts, N. Garnov, M. Moche, T. Kahn, H. Busse: *Diagnostic value of ADC in patients with prostate cancer: influence of the choice of b-values*, Proc. of 19th ISMRM Annual Scientific Meeting, Montreal, 2011

G. Thörmer, M. Reis-Zimmermann, J. Otto, M. Moche, N. Garnov, T. Kahn, H. Busse: *Grundlagen zu einer endorektalen MR-Elastographie der Prostata*, Abstractband des 92. Deutschen Röntgenkongress, Hamburg 2011

G. Thörmer, J. Otto, M. Reis-Zimmermann, M. Seiwerts, N. Garnov, M. Moche, T. Kahn, H. Busse: *Diagnostischer Wert des ADCs bei Patienten mit Prostatakarzinom: Einfluss der Wahl verschiedener b-Werte*, Abstractband des 92. Deutschen Röntgenkongress, Hamburg 2011

G. Thörmer, J. Otto, M. Reis-Zimmermann, M. Seiwerts, N. Garnov, M. Moche, T. Kahn, H. Busse: *Diagnostic value of ADC in patients with prostate cancer: influence of the choice of b-values*, Proc. of ESMRMB Annual Scientific Meeting, Leipzig, 2011

J. Haase: *Kernspinresonanz bei höchsten Drücken und in den höchsten Magnetfeldern – Unerwartete Konsequenzen für normalste Metalle und Hochtemperatur-Supraleiter*, 22.11.2011 Otto-von-Guericke Universität Magdeburg

J. Haase: *Challenges in condensed matter physics: New insights from extreme NMR*, 06.12.2011 Leipzig

Posters

T. Meissner, S.K. Goh, J. Haase, G.V.M. Williams: *High Pressure Changes of the ^{17}O NMR Spin Shift Pseudogap of $\text{YBa}_2\text{Cu}_4\text{O}_8$* , Estnisch-Deutscher Workshop, 13.06.-15.06.2011, Cottbus,

A. Jäger, G. E. Schaumann, M. Bertmer: *Effects of Multivalent Cations on Soil Organic Matter*, Co-Evolution of soils and organic substances, 02.03.-04.03.2011, Landau/Pfalz, Germany

A. Jäger, G. E. Schaumann, M. Bertmer: *Long term DSC and ^1H NMR ageing experiments – setup and first results*, Co-Evolution of soils and organic substances, 02.03.-04.03.2011, Landau/Pfalz, Germany

M. Jurkutat, G. V. M. Williams, D. Rybicki, J. Haase: *^{63}Cu and ^{17}O NMR of electron-doped cuprates*, 13.03.-18.03.2011 DPG Spring Meeting, Dresden

A. Kuttatheyil: *^1H and ^{13}C Solid State NMR investigations of Cd and Zn/Co Heteronuclear Metal Organic Frameworks (MOFs)*, March 2011, 4th Scientific Symposium of the Graduate School of BuildMoNa, UFZ Leipzig

R. C. Nieuwendaal, S. J. Mattler, M. Bertmer, S. E. Hayes: *Photoreactions in the Solid State: a Study of Cinnamic Acid using Single Crystal NMR*, 52nd Experimental NMR Conference, 10.04.-15.04.2011, Pacific Grove, California, USA

M. Jurkutat, G. V. M. Williams, D. Rybicki, J. Haase: *^{63}Cu and ^{17}O NMR of electron-doped cuprates*, Estnisch-Deutscher Workshop, 13.06.-15.06.2011, Cottbus

B. Jee, D. Himsl, K. Koch, F. Gul-E-Noor, M. Bertmer, M. Hartmann, A. Pöppl: *Continuous wave (cw) and pulse ESR spectroscopy of metal organic framework (MOF) compounds and their adsorbate interactions*, EUROMAR Frankfurt a. Main, 21.08.-25.08.2011

A. V. Kuttatheyil, M. Bertmer, D. Lässig, J. Lincke, J. Haase, H. Krautscheid: *Solid State NMR Investigations of Zn/Co Heteronuclear MOFs*, EUROMAR Frankfurt a. Main, 21.08.-25.08.2011

F. Gul-E-Noor, M. Bertmer, B. Jee, A. Pöpl, M. Hartmann, D. Himsl: *Solid State NMR for Structural Analysis and Understanding of Adsorbate-Adsorbent Interaction of Metal Organic Frameworks*, EUROMAR Frankfurt a. Main, 21.08.-25.08.2011

M. Reis-Zimmermann, T. Kahn, G. Thörmer: *MR-Elastography of the prostate using an endorectal coil for actuation - a feasibility study*, Proc. of ECR 2011, Wien, 2011

G. Thörmer, J. Otto, C. Schröder, N. Garnov, M. Reis-Zimmermann, L.C. Horn, M. Do, M. Moche, T. Kahn, H. Busse: *Wertigkeit der diffusionsgewichteten und spektroskopischen MR-Bildgebung für eine Vorhersage der Tumoraggressivität beim Prostatakarzinom*, Book of Abstracts 10th Research Festival, Leipzig, 2011

G. Thörmer, H. Bertram, F. Dazinger, Raschpichler, E. Shang, M. Blüher, T. Kahn, H. Busse: *Software for fully automatic quantification of abdominal fat with manual correction option*, Proc. of ESMRMB Annual Scientific Meeting, Leipzig, 2011

6.13 Graduations

Diploma

- Daniel Blaschke
NMR-Charakterisierung der Festkörperphotodimerisierung von Zimtsäurederivaten im Hinblick auf molekulare optische Datenspeicher
January 2011
- Sebastian Sambale
Einkristall-NMR am Hochtemperatursupraleiter $YBa_2Cu_4O_8$
January 2011
- Sebastian Greiser
Homogenitätsmessungen in gepulsten Magneten für Höchstfeld-NMR
April 2011
- Matthias Mendt
Untersuchung des temperaturabhängigen strukturellen Phasenübergangs der metallorganischen Verbindung MIL-53 (Al/Cr) mit Elektronen Paramagnetischer Resonanz
August 2011
- Jonas Kohlrantz
Zeitentwicklung stark korrelierter Kernspinzustände
September 2011

Master

- Nataliya Georgieva
Characterization of multiferroic $\text{Eu}_x\text{Ba}_{1-x}\text{TiO}_3$
September 2011
- Katrin Lorenz
Nuclear Magnetic Resonance Imaging Using Arterial Blood-Nulling for Quantification of Human Cerebral Blood Volume
October 2011

Bachelor

- Andy Thäder
Aufbau eines Frequenzsynthesizers für die NMR
September 2011
- Christian Scheidler
NMR-Untersuchungen am Hochtemperatursupraleiter $\text{YBa}_2\text{Cu}_4\text{O}_8$
September 2011

6.14 Guests

- Alexey Donets, PhD
St. Petersburg State University, Institute of Physics, Petrodvorets, Russia
10.02.-10.03.2011
- Mikhail Andreevich Vovk
St. Petersburg State University, Institute of Physics, Petrodvorets, Russia
10.02.-10.03.2011
- Dmitry Yurievich Podorozhkin
St. Petersburg State University, Institute of Physics, Petrodvorets, Russia
26.04.-15.05.2011
- Petr V. Velikorussov
St. Petersburg State University, Institute of Physics, Petrodvorets, Russia
26.04.-15.05.2011
- O. P. Sushkov, Prof.
School of Physics, University of New South Wales, Sydney Australia
12.05.-15.05.2011
- Anna Orlova
Kazan Federal University, Republic of Tatarstan, Russian Federation
06.06.-05.09.2011
- Tankut Can
School of Physics, University of Chicago Department of Physics, Illinois USA
23.06.-03.08.2011
- Swee K. Goh, PhD
Trinity College, University of Cambridge Quantum Matter Group, Cavendish Laboratory, UK
27.06.-28.6.2011

- Boris Fine, PhD
Institute for Theoretical Physics, University of Heidelberg, Germany
31.07.-06.08.2011
- Mikhail Andreevich Vovk
St. Petersburg State University, Institute of Physics, Petrodvorets, Russia
07.09.-07.12.2011
- G.V.M Williams, PhD
School of Chemical and Physical Sciences, Viktoria University of Wellington, New Zealand
17.08.-14.09.2011
- Alexander Shengelaya, Prof.
Department of Physics, Tbilisi State University, Georgia
12.05.-15.05.2011
- Ralf Stanarius, Prof.
Institute of Experimental Physics, Faculty of Natural Sciences, Otto-von-Guericke University Magdeburg, Germany
24.11.2011
- Gunnar Jeschke, Prof.
Department of Physics, Swiss Federal Institute of Technology Zurich, Switzerland
24.11.2011
- Andreas Erb, PhD
Walther-Meissner-Institute for Low Temperature Research, Bavarian Academy of Sciences and Humanities, Munich, Germany
07.12.-08.12.2011
- Chahan Kropf
Institute for Theoretical Physics, University of Heidelberg, Germany
20.12.2011

7

Nuclear Solid State Physics

7.1 Introduction

The division of Nuclear Solid State Physics continued research in the field of material and life sciences. The working horse is the high-energy ion-nanoprobe LIPSION.

An important branch is ion beam analysis of solid objects, e.g. semiconductors or meteorites, as well as a broad range of biomedical samples from tissue sections down to single cells using Particle Induced X-Ray Emission (PIXE) and Rutherford Backscattering Spectrometry (RBS) with lateral resolutions down to about 300 nm, and Scanning Transmission Ion Microscopy (STIM) with lateral resolutions down to 100 nm. In order to increase the current density in the beam spot, thus enabling faster analysis, the ion-optical system was analysed and an octupole lens installed to correct for spherical aberrations as well as parasitic octupole contributions. Furthermore, a new RBS setup with an in-vacuum pre-amplifier was designed and installed with special emphasis on detection efficiency and energy resolution. In addition, a system for measuring the dead time of the detector electronics on a pixel by pixel basis was developed that allows quantitative elemental imaging in lateral strongly inhomogeneous samples like meteorites. In the field of tomography, STIM-T and PIXE-T were further developed.

The second important branch of research is materials modification, e.g. for the study of defect-related phenomena in solid state physics and Proton Beam Writing (PBW) and Sculpting. With protons, H_2^+ , and He-ions 3D-structures in a variety of photoresists and semiconductors can be created. For the first time, n-type ZnO was machined using PBW. Furthermore, greyscale PBW was successfully performed in p-type GaAs where the structure height could be controlled by the applied proton fluence.

The new fully digital TDPAC-spectrometer developed recently in our division proved its exceptional capabilities by a 5-fold gain in coincidence rate in the study of the NQI using a ^{180m}Hf probe compared to conventional spectrometers. The experience gained with this setup will be used for the development of a fully digital data acquisition system at LIPSION.

We gratefully acknowledge the financial support of our research by the European Commission, the Deutsche Forschungsgemeinschaft, and the Federal German Excellence Initiative and the cooperation with academic and industrial partners.

Daniel Spemann

7.2 Alignment tolerances and octupole aberration corrections in an ion nanoprobe

M. Rothermel, D. Spemann

Most reliable results can be achieved, if they are based on a vast number of measurements. This holds for every scientific area. Two examples we are working on are biological studies and tomography. The first mentioned principle holds for both areas in a different way. Biological studies need a high sample throughput to reduce effects of biodiversity, whereas tomography needs as many measurements from different angles as possible. In ion beam analysis studies, both areas can profit from a higher beam current. This is because the measurement time will be reduced by the same amount as the current is increased. Since the ion optical focusing system at LIPSION suffers from spherical and octupole aberrations, the maximum diameter of the object and aperture diaphragms is limited, if focus degradations shall be excluded. Whereas the spherical aberrations were tolerated during the system design to get a high symmetrical demagnification factor of 82.2 [1] (intentionally, in practice a demagnification factor of 130 was reached [2]), the octupole aberrations are parasitic due to inaccuracies in the magnetic quadrupole design. Jamieson et al. showed [3], that this can be overcome by inserting an octupole correction lens into the system. Thus, the Leipzig ion optical system was analyzed and an octupole correction lens was built, accompanied by simulations concerning alignment tolerances and their effect on the focus size and shape. The figures 7.1 and 7.2 show some results.

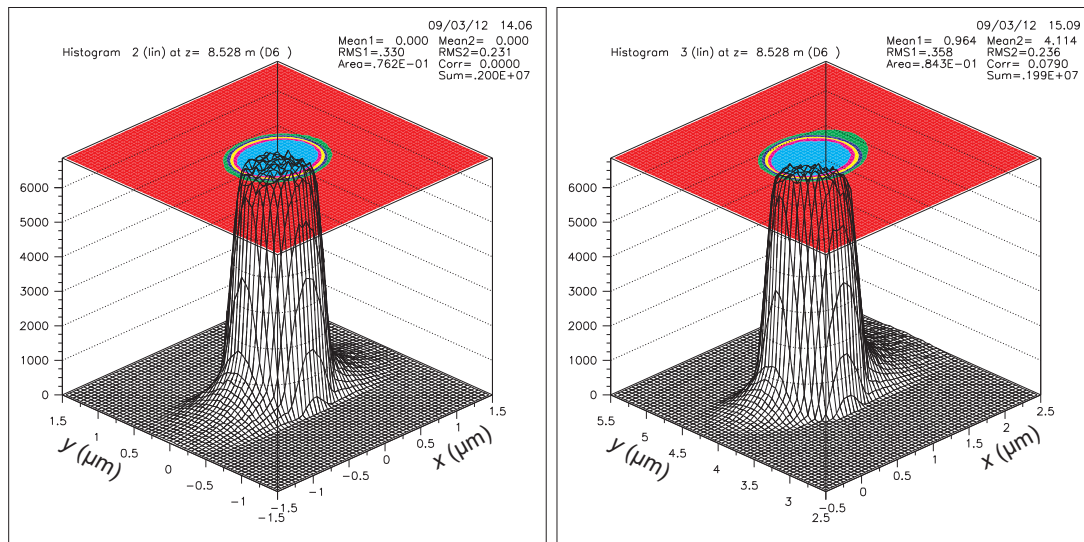


Figure 7.1: Simulated beam profiles of the Leipzig nanoprobe with (left) and without (right) a horizontal displacement of the first quadrupole block of 28.3 μm .

- [1] T. Butz, R.H. Flaggmeyer, J. Heitmann, D.N. Jamieson, G.J.F. Legge, D. Lehmann, U. Reibetanz, T. Reinert, A. Saint, D. Spemann, R. Szymanski, W. Tröger, J. Vogt, J. Zhu, Nucl. Instr. and Meth. B **160-163**, 323 (2000).

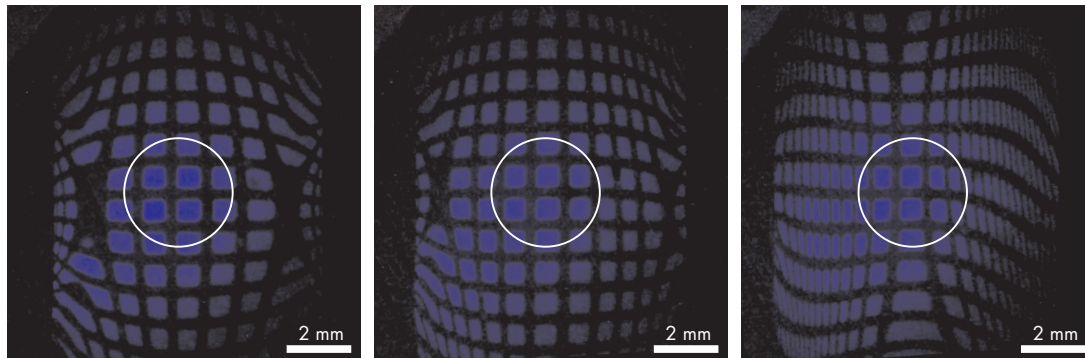


Figure 7.2: From left to right: Grid shadow patterns without and with octupole compensation and with an overcompensated octupole component. A 300 μm diameter aperture diaphragm, indicated by the circles, blocks particles from the outer regions with large aberrations.

[2] M. Rothermel, T. Butz, T. Reinert, Nucl. Instr. and Meth. B **267**, 2017 (2009).

[3] D.N. Jamieson, G.J.F. Legge, Nucl. Instr. and Meth. B **34**, 411 (1988).

7.3 Optimizing the Rutherford backscattering spectrometry setup at the LIPSION nanoprobe

N. Klingner, J. Vogt, D. Spemann

Rutherford Backscattering Spectrometry (RBS) is a non-destructive method that allows the quantification of film thicknesses and elemental concentrations in materials. For this purpose, a good mass separation and detection efficiency is needed. In nuclear microprobes with their relatively small beam currents a good detection efficiency requires a solid angle of the order of 100 msr. Since the energy of the backscattered ions depends on the scattering angle, they cover a certain energy range. This geometrical straggling cannot be neglected anymore for large solid angles.

In order to obtain the best mass separation under the experimental constraints of a nuclear microprobe, the kinematic factor, backscattering cross section and energy distribution due to geometrical straggling were calculated for circular RBS detectors at different positions, i.e. backscattering and solid angle (see fig. 7.3), for different projectile and target masses as well as projectile energies. Furthermore, a dedicated in-vacuum preamplifier based on an Amptek A250 was optimized with respect to energy resolution. The whole setup was designed in a single casing with small lateral dimensions and constructed using SMD-technology (see fig. 7.4).

The results show that annular detectors are the best way to do RBS with high mass resolution and good detection efficiency, especially for target elements with low atomic number. An energy resolution of around 14 keV for 2.25 MeV protons could be achieved for a 274 mm² annular PIPS detector mounted under 180° backscattering angle covering 84 msr. Under these conditions the geometrical straggling is negligible. The new system incorporates a secondary electron suppression and a system to measure the dead time of the detector setup. The sample chamber with the mounted RBS setup can be seen in fig. 7.5.

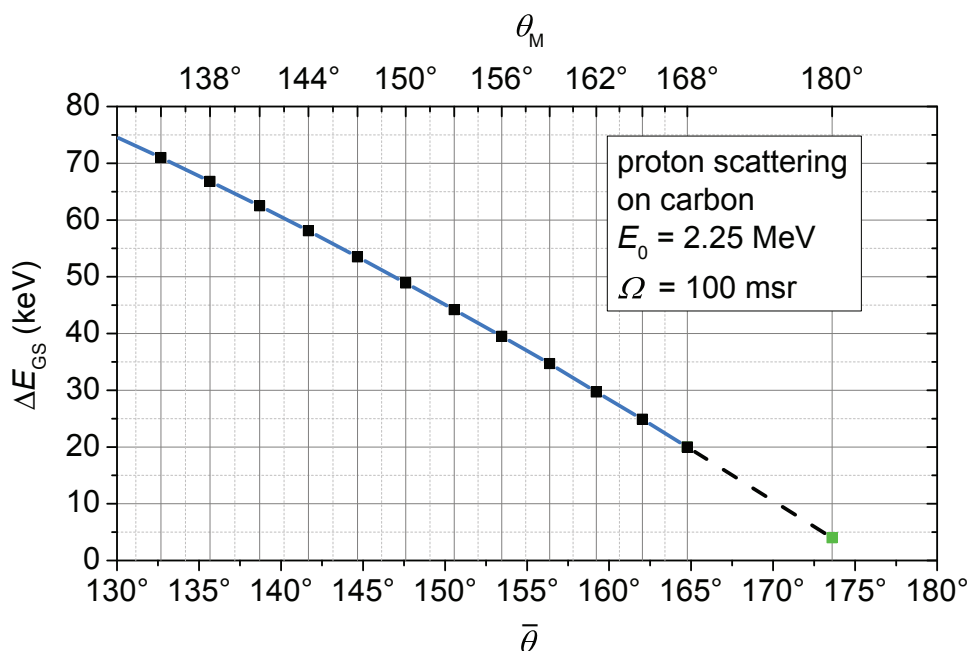


Figure 7.3: Angular dependence of the backscattering energy of 2.25 MeV protons on carbon due to geometrical straggling. The width of the energy distribution is shown versus θ_M , the angle under which the center of the detector is mounted as well as $\bar{\theta}$, the weighted backscattering angle. The value at $\theta_M = 180^\circ$ represents an annular detector.

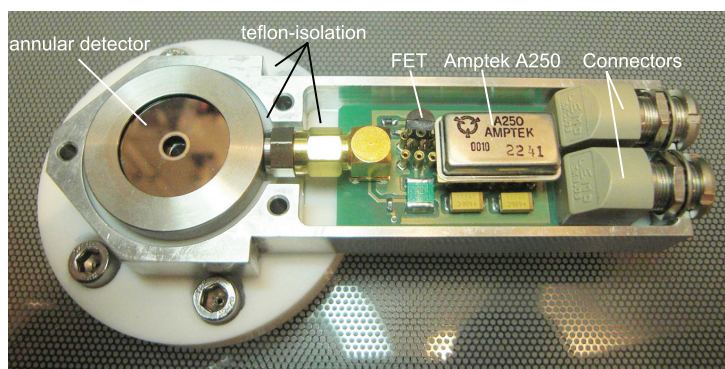


Figure 7.4: RBS detector system with open casing.

7.4 Quantitative microscopy of a macrodimensional specimen: high definition PIXE

N. Barapatre, M. Morawski*, T. Reinert†

*Paul-Flechsig-Institute of Brain Research, University of Leipzig

†Department of Physics, University of North Texas, Denton, USA

The combination of Particle Induced X-Ray Emission (PIXE) and Rutherford Backscattering Spectrometry (RBS) with sub-micron spatial resolution has manifold applications in biomedical research, where quantification of trace elements plays an important role.

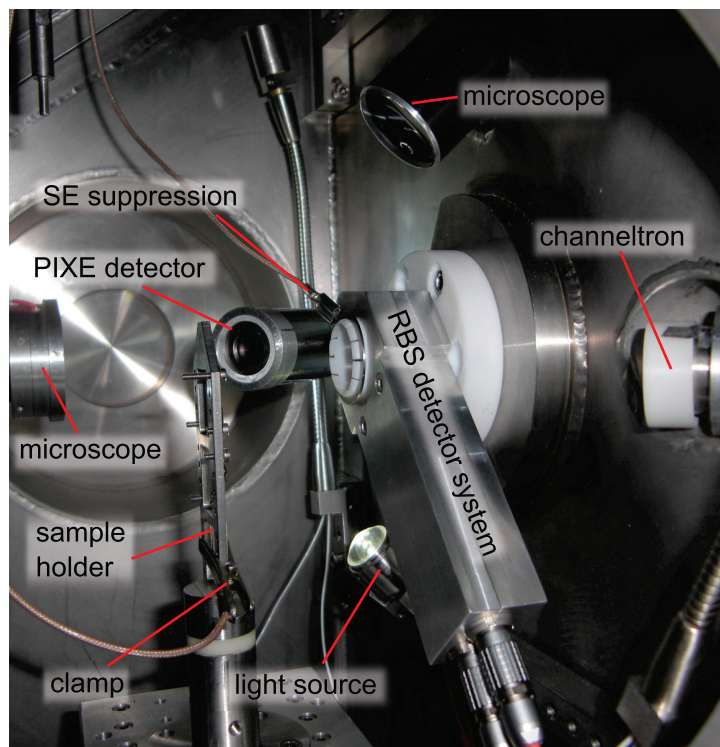


Figure 7.5: Sample chamber of LIPSION with mounted RBS setup.

Over the years we have improved and optimised our system for a number of studies in the field of biological and medical research. We have already shown the strength of this method in microanalytic studies of the Parkinson's disease [1] and *Drosophila melanogaster* [2], where the main focus was on sub-cellular resolution. However, the size of the specimen was always smaller than the largest possible scan size of the microbeam.

For large specimens, which can not be measured in a single scan, the measurements are performed segment-wise. The resulting PIXE maps are mosaiced together to generate a quantitative map of the whole specimen. In this way, a macro-dimensional specimen is measured quantitatively with a micrometer resolution. We measured a 6 μm thick coronal section of the mouse brain with dimensions of around 13 mm \times 10 mm. Figure 7.6 is a mosaic of 12 measurements. It shows the quantitative distribution of element nickel, which was used to stain the astroglia cells. The lateral resolution of around a micrometer is retained in the mosaic.

The ability to produce a quantitative element map of brain sections with micrometer resolution opens up the possibility of studying the relationship between whole brain areas/functions and their element content down to cellular level.

[1] N. Barapatre et al., Nucl. Instr. and Meth. B **268**, 2156 (2010).

[2] A. Reinert et al., Nucl. Instr. and Meth. B **269**, 2292 (2011).

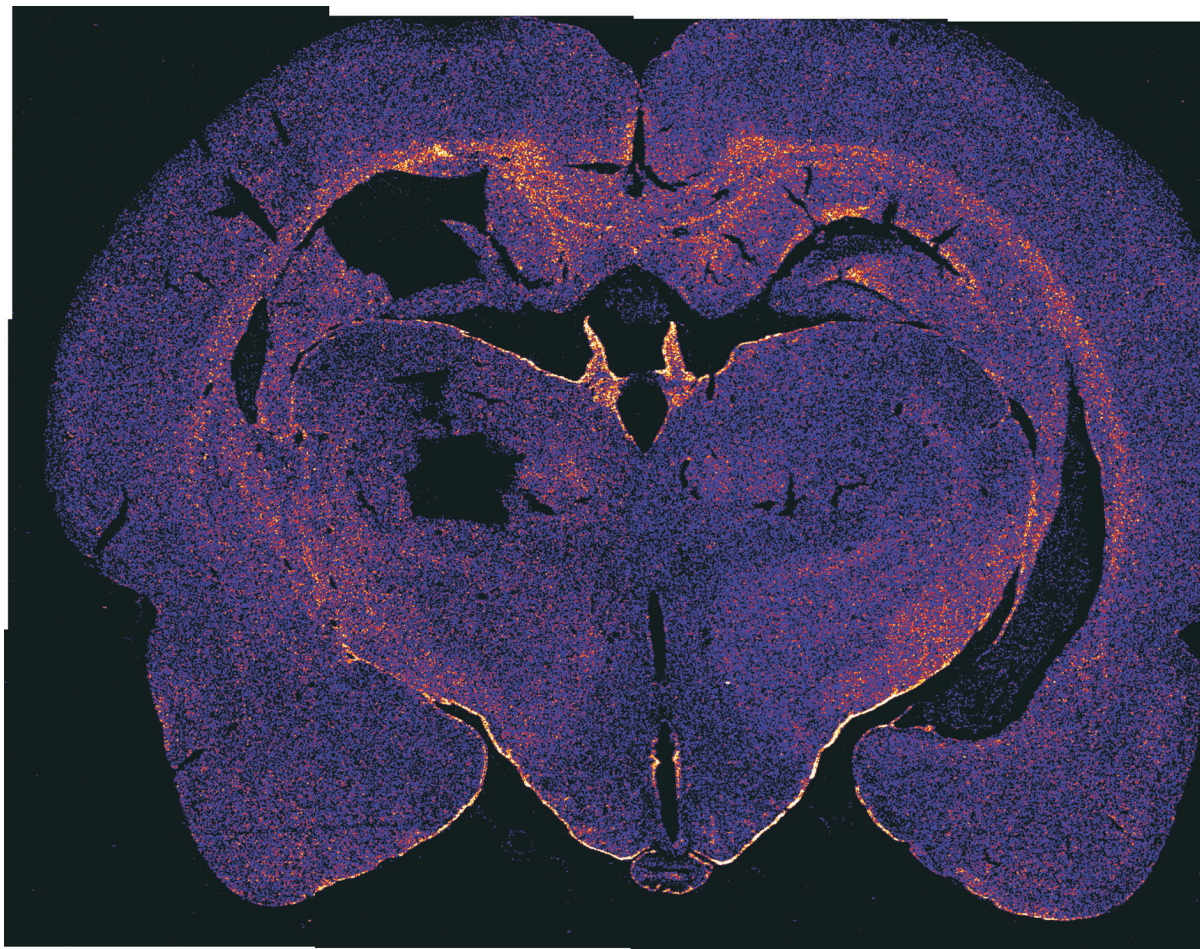


Figure 7.6: The image shows the distribution of astroglia cells stained with nickel. It has a size of around $13 \text{ mm} \times 10 \text{ mm}$, contains 10000×7874 pixels and provides a lateral resolution of around 1 micrometer.

7.5 3D analysis of an induced murine atherosclerotic lesion by PIXE stacking

A. Sickert, N. Barapatre, M. Rothermel, D. Teupser*, T. Butz

*Institut für Laboratoriumsmedizin, Klinische Chemie und Molekulare Diagnostik,
Universität Leipzig

Atherosclerosis is a progressive inflammatory disease of large and medium sized arteries. The lesions are characterized by accumulation of lipid-rich material and fibrous elements within the intimal layer of the artery wall [1, 2]. The atherosclerosis samples were received from a brachiocephalic artery of an LDL-Receptor deficient mouse raised on low fat, semi-synthetic diet with 0.02% cholesterol [3]. 52 serial sections of 10 micrometer thickness each were obtained.

In general, a lesion is spread a few hundreds of micrometers along the artery. Hence, a three-dimensional investigation is required. Since the artery in the present study is approximately a millimeter in diameter, it is not suitable for PIXE Tomography. Therefore, for the three-dimensional analysis a different method was proposed that uses the stack-

ing of two-dimensional PIXE maps. A program was written that allows the alignment of the individual sections by manual rotation and translation. Each section is aligned to the preceding section and the quality of the alignment is judged by eye. The aligned 2D element maps are exported as a three-dimensional data set which is then visualized by the iVolume routine of IDL (Interactive Data Language). The initial aim was to create a stack of all 52 artery sections leading to a stack height of 520 micrometers. However, there was a substantial alteration in the shape of many sections due to deficiencies in the cutting process. As a consequence, it was only possible to create four different stacks with up to seven slices per stack. Figure 7.7(a) shows the seven 2D sulphur maps of one of these stacks and the resulting 3D sulphur stack. The 3D nature of the

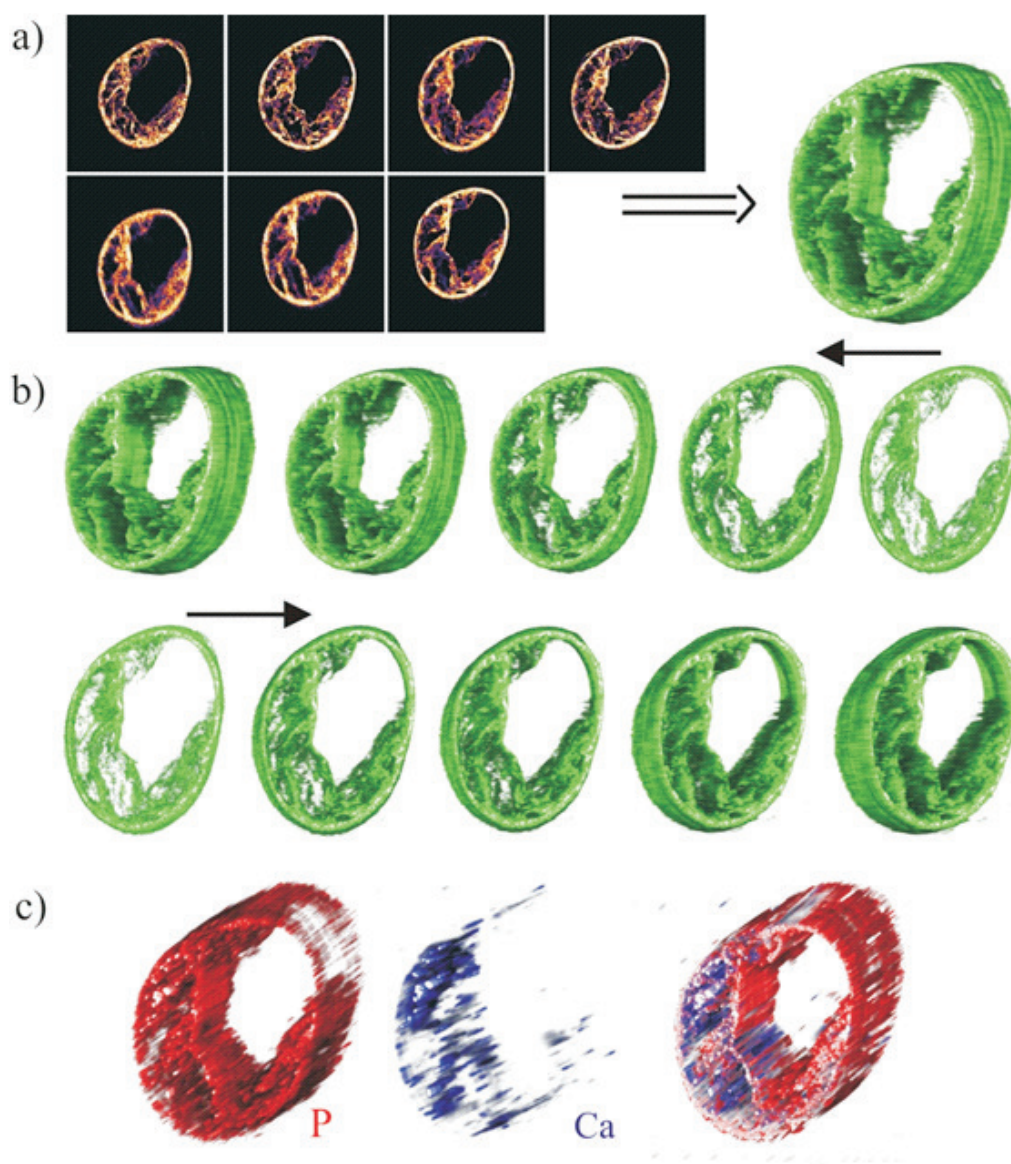


Figure 7.7: (a) Sulphur element maps of the seven artery slices that were chosen to create a stack. These arteries were aligned and subsequently stacked in this order to create a 3D volume. (b) 3D representation of the sulphur distribution viewed under different angles. (c) 3D visualization of P (red) and Ca (blue) as well as the composite volume of these two elements.

stack can also be recognized in figure 7.7(b), which shows the reconstructed volume from different perspectives. For the sake of visualization the slice thickness is inflated. It does not represent the true thickness of the section. Figure 7.7(c) shows individual and composite stacks of P and Ca. The new third dimension clearly shows calcification on the outer surface of the artery wall. This observation would not have easily been made in the 2D maps alone. In conclusion, this method of PIXE stacking provides a tool for the 3D analysis of samples which are otherwise not suitable for tomographic experiments.

[1] A.J. Lusic, *Nature* **407**, 233 (2000).

[2] R. Ross, *The New England Journal of Medicine* **340**, 115 (1999).

[3] D. Teupser et al., *Arterioscler. Thromb. Vasc. Biol.* **23**, 1907 (2003).

7.6 Iron and myelin in the human brain: Distribution and T_1 -contrast in gray matter

C. Stueber*, M. Morawski[†], K. Reimann*, N. Barapatre, S. Geyer*, R. Turner*

*Neurophysics, Max Planck Institute for Human Cognitive and Brain Sciences, Leipzig

[†]Paul-Flechsig-Institute of Brain Research, University of Leipzig

It has been shown recently that quantitative T_1 maps largely reflect the myeloarchitecture of the brain tissue, thus enabling in-vivo myeloarchitectonic cortical parcellation [1]. Furthermore it has been shown that distributions of iron and myelin overlap considerably in the cortex [2]. This raises the question whether spatial variations in T_1 are also correlated with iron concentration [3]. Unfortunately, the co-localization of myelin and iron in the cortex makes it difficult to determine the contribution of iron as an independent source of T_1 contrast. To disambiguate these sources of contrast, we used a state-of-the-art ion beam analysis, i.e. Proton Induced X-ray Emission (PIXE) [4] to determine quantitatively the elemental content and elemental distribution in a given sample. Using MRI scanning of highly myelinated and iron-rich blocks of human cadaver brain tissue, before histological processing, we could also study the role of iron in T_1 tissue contrast by scanning before and after the removal of iron.

Fig. 7.8(a,b,c) show the myelin, iron distribution and T_1 maps of the human somatosensory and motor cortex, respectively. The similarity of all images is obvious: cortical structures as well as the boundary between gray/white matter (GM/WM) are easily visible in all three images. Nevertheless the T_1 map reflects the intracortical iron distribution rather better than the myelin density, which might indicate that iron is responsible for the underlying MR tissue contrast of the gray matter. To verify these findings we extracted the iron from one block of the visual cortex, containing the Stria of Gennari (SoG) (Fig. 7.9). The disappearance of this myelin-rich cortical feature in the subsequent T_1 maps confirmed that iron does indeed play a significant role in brain tissue T_1 contrast.

Deeper understanding of the role that brain iron plays in different types of MRI contrast

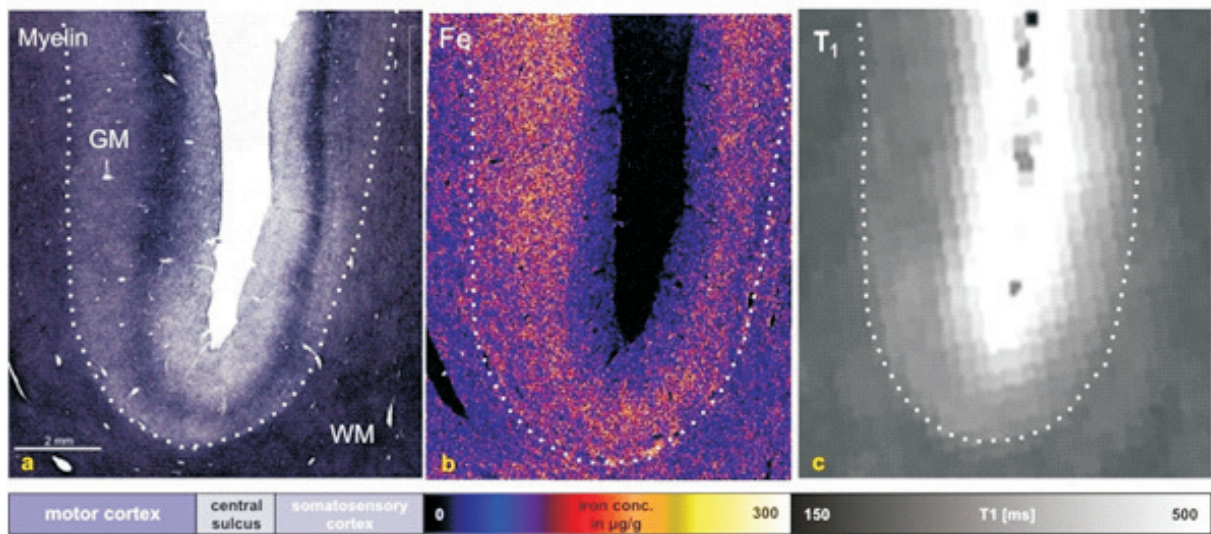


Figure 7.8: Motor-/somatosensory cortex (precentral/postcentral gyrus): (a) Myelin Basic Protein (immunohistochemistry); (b) iron map (ion beam analysis); (c) T_1 map (0.4 mm^3).

will assist in strategies for in-vivo cortical parcellation, and help to provide more quantitative assessment and staging of degenerative diseases in which iron concentration appears to be a biomarker, such as Parkinson’s disease.

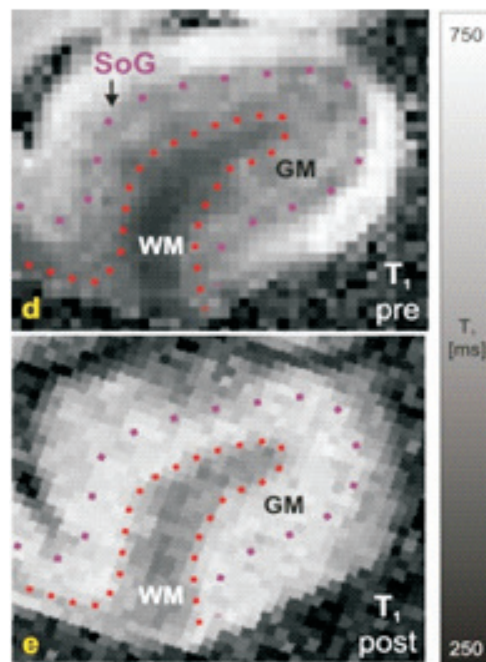


Figure 7.9: Visual cortex with Stria of Gennari: (d) T_1 map before iron extraction (0.25 mm^3); (e) T_1 map after iron extraction (0.25 mm^3).

[1] S. Geyer et al., *Front Hum Neurosci* **5**, 1 (2011).
 [2] C. Stueber et al., *ISMRM* **19**, # 2573 (2011).
 [3] R.J. Ogg et al., *Magn. Reson. Med.* **40**, 749 (1998).
 [4] T. Butz et al., *Nucl. Instrum. and Meth. B* **161**, 323 (2000).

7.7 Calibration and improvement of the single cell analysis setup at LIPSION

M. Dorn*, D. Spemann, J. Vogt, St. Jankuhn, I. Estrela-Lopis*, E. Donath*

*Institut für Medizinische Physik und Biophysik, Universität Leipzig

The Leipzig ion beam laboratory LIPSION is a powerful tool for analyzing elemental contents of biological specimens. A calibration of this system with 16 different certified elemental standards revealed an accuracy of $\pm 10\%$ for x-ray photons in the energy range between 2.0 and 16.5 keV. Additionally, the system was calibrated at four different x-ray detector positions. This allowed, in combination with an improved sample mounting method, to reduce the typical acquisition time in the single cell analysis by approximately a factor of two.

A549 cells were chosen as model system for the analysis of cellular elements (P, S, Cl, K, Ca, Fe, Zn) in single cells. The question was addressed whether the soluble ion concentration in cells can be determined with Ion Beam Microscopy (IBM) with sufficient accuracy. A strong dependence of the measured Cl, K, Ca contents in cells on the washing procedure was observed (Fig 7.10). Furthermore, washing with rubidium containing solutions, rubidium being a substitute for potassium, revealed a pronounced uptake of Rb. These data show that the intracellular concentration of soluble small ions cannot be determined by means of IBM, because of leakage from or ion permeation into the cells during sample preparation. On the other hand, structural elements like phosphorous and sulfur remained unaffected by the cell preparation protocol, qualifying them as internal elemental standards.

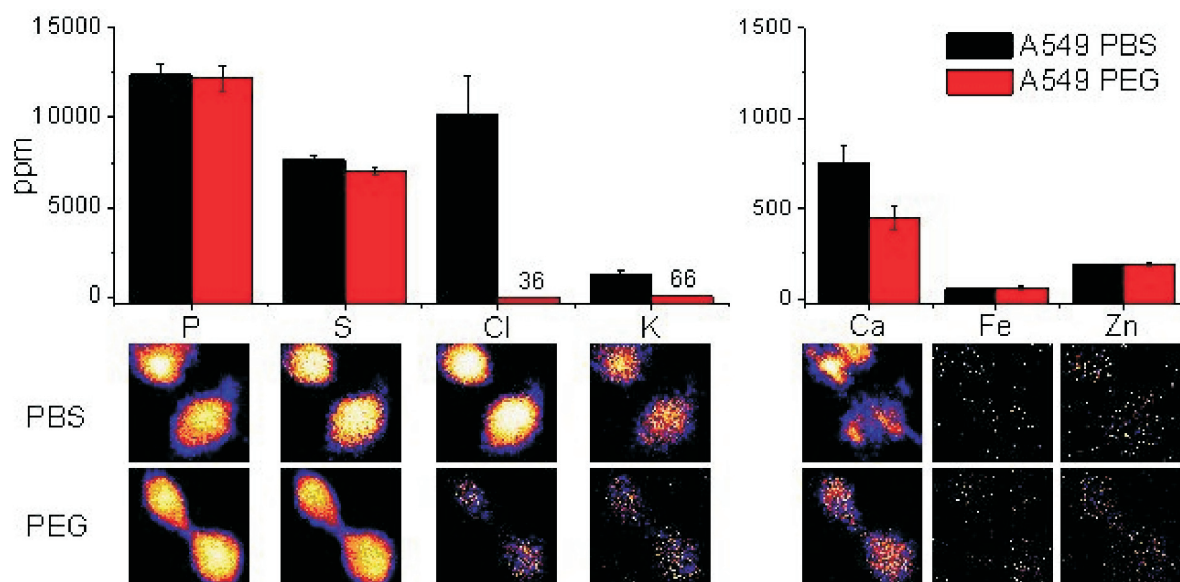


Figure 7.10: Cellular element content of A549 cells after treatment with different washing regimes. Prior to methanol fixation cells were washed five times with PBS (black) or PEG (red). All concentrations are given in $\mu\text{g/g}$ (ppm) dry weight.

7.8 Study of nanoparticle uptake and quantification in lung cells by ion beam microscopy

M. Dorn*, D. Spemann, J. Vogt, St. Jankuhn, J. Fleddermann*, I. Estrela-Lopis*, E. Donath*

*Institut für Medizinische Physik und Biophysik, Universität Leipzig

Understanding the mechanism of uptake and distribution of nanoparticles (NPs) in cells and organs are essential for assessing the risk of existing and appearing nanomaterials for human health and ecology [1, 2]. Due to their small size and changed physico-chemical properties NPs may influence physiological and biochemical processes in cells and tissues in a special way causing toxic effects. Moreover, since NPs may find applications as devices for diagnostic and therapeutic purposes studies on NP uptake and distributions are highly desirable [3, 4]. In this study alveolar type II cells (A459) were chosen as model system, because of their role as a major entrance barrier into the human body.

Ion Beam Microscopy (IBM) was applied to quantify the cellular uptake and distribution of NPs. IBM is a labelling-free technique and, therefore, can be applied for studying authentic NPs and nanomaterials. The Leipzig IBM lab LIPSION provides an excellent spatial resolution permitting to analyse single culture cells and tissues down to the cellular level. Data on uptake kinetics and localization of NPs can be obtained.

Particle Induced X-ray Emission (PIXE) and Rutherford Backscattering Spectrometry (RBS) were simultaneously applied. The accumulated charge, the area density of atoms (atoms/cm^2) and the elemental cell matrix composition were quantified using RBS and used as input for the subsequent quantitative analysis of the PIXE data. The concentrations of minor and trace elements (P, S, Cl, K, Ca, Fe, Zn, Ce and Ti) were calculated.

Cells were cultivated on thin polypropylene films and exposed to ZnO and CeO₂ NPs (3 – 30 $\mu\text{g}/\text{ml}$) over 24 to 72 hours. Subsequently, the cells were fixed with methanol and dried.

The study addresses the relationship between the applied dose of NPs and their genuine intracellular concentration. In parallel, intracellular dose dependent toxicity studies were conducted by means of Flow Cytometry. MTT tests complemented the IBM and Flow Cytometry investigations. This allowed for relating the observed toxicity effects to the intracellular or genuine dose. In this way, NP induced toxicity on culture cells can be compared regardless of different exposure scenarios.

The kinetics of NP uptake was studied for the case of CeO₂ NPs (Fig 7.11A). Intracellular processing of CeO₂ was responsible for cellular recovery from NP exposure. This study correlates with cell proliferation tests, where CeO₂ NPs - induced proliferation inhibition disappeared after 72 hours. Further studies addressed the question which NP properties can be correlated to the degree of uptake. The influence of the size of NPs and their surface modification by covering it with a protein layer (corona) on uptake were analysed. Both ZnO and CeO₂ NPs showed a significantly higher uptake without a protein corona. Figure 7.11B shows the NP uptake as function of size. A strong increase of uptake was observed for the NPs with a larger diameter.

NP internalization in cells was proved by means of RBS. For 80% of the cells exposed to CeO₂ NPs an energy loss of the backscattered protons from cerium atoms in comparison with the expected energy of protons backscattered from Ce atoms located at the surface

was observed (Fig 7.11C). Therefore, it was concluded that the CeO₂ NPs became internalized. Confocal Raman Microspectroscopy and Transmission Electron Microscopy supported this finding. On the contrary ZnO NP treated cells showed an absence of this RBS energy shift, indicating an association of ZnO NPs with the membrane from outside.

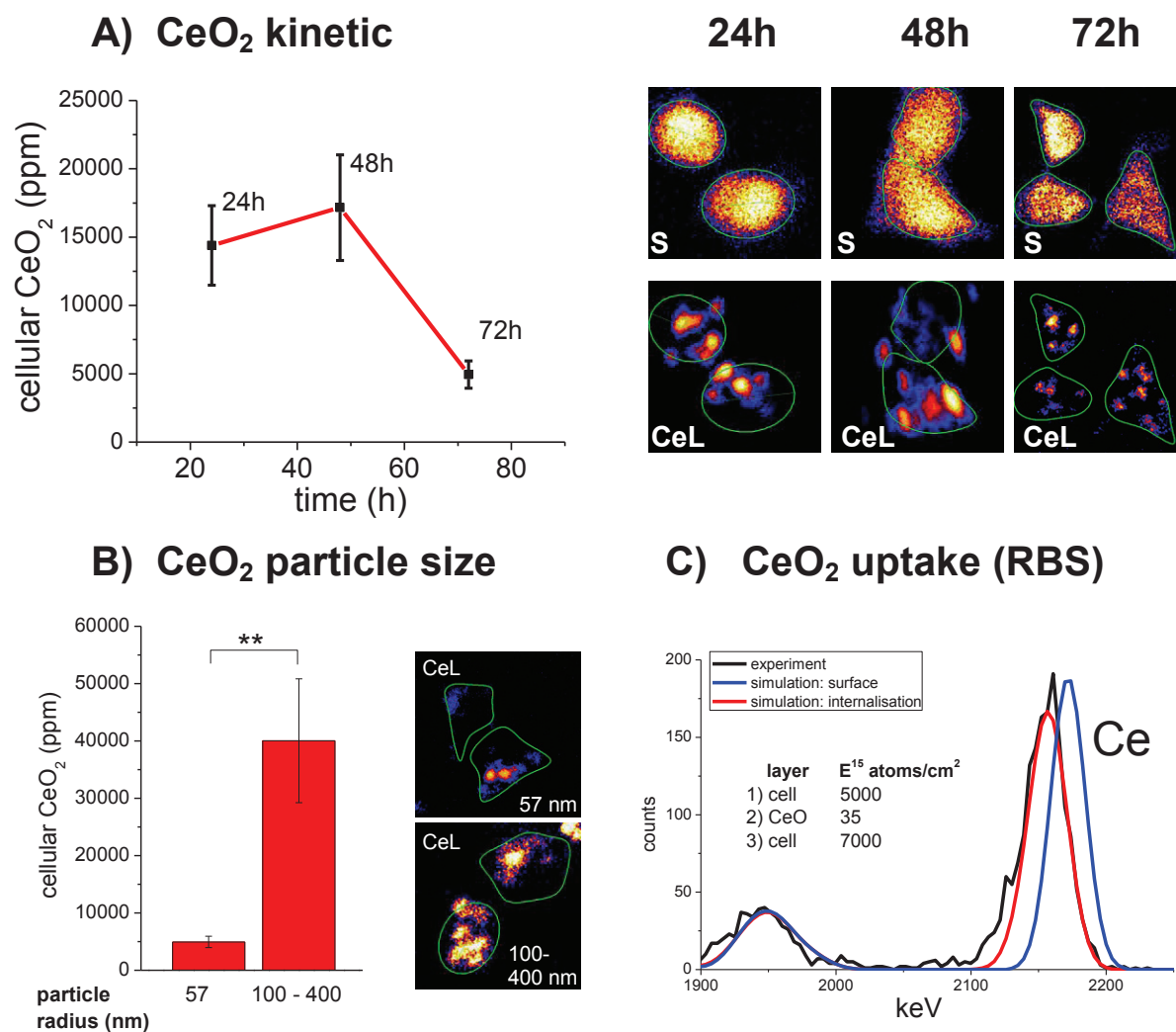


Figure 7.11: CeO₂ NP uptake (30 µg/ml) in A549 cells: A) Kinetic study of NP uptake at 24, 48 and 72h of incubation; B) Impact of NP size on intracellular CeO₂ concentration after 72 h; C) RBS signal of cellular CeO₂ in comparison to a separate experiment where the CeO₂-signal originated from the surface. Total scan area of images are 25 × 25 µm.

- [1] J. Lee, G.D. Lilly, R.C. Doty, P. Podsiadlo, N.A. Kotov, *Small* **5**, 1213 (2009).
- [2] J.M. Hillgeass, A. Shukla, S.A. Lathrop, M.B. MacPherson, N.K. Fukagawa, B.T. Mossman, *Wiley Interdiscip. Rev. Nanomed. Nanobiotechnol.* **2**, 219 (2010).
- [3] M.E. Davis, Z. Chen, D.M. Shin, *Nature Reviews Drug Discovery* **7**, 771 (2008).
- [4] A.G. Rockall, S.A. Sohaib, M.G. Harisinghani, S.A. Babar, N. Singh, A.R. Jeyarajah, D.H. Oram, I.J. Jacobs, J.H. Shepherd, R.H. Reznick, *J. Clinical Oncology* **23**, 2813 (2005).

7.9 Investigation of intracellular multilayer decomposition of layer-by-layer self-assembled particles by PIXE

U. Reibetanz*, St. Jankuhn

*Institute for Medical Physics and Biophysics, Universität Leipzig

Layer-by-layer coated micro- and nanocarriers represent a new concept of drug delivery systems which attract a high attention in medical applications. Due to the modular assembling of the oppositely charged biocompatible and biodegradable polyelectrolytes for building up a multilayer, multiple therapeutical, functional or sensoric molecules can be independently integrated in-between the layers or within the core [1, 2]. Multilayer material, surface modification but also the active agent's layer numbers and integration depth influence the transport and releasing capability of the carriers.

In order to release agents specifically into the cytoplasm, the carriers have to be endozytosed by cells, released into the cytoplasm and there processed by a subsequent multilayer decomposition [3]. Particularly, the determination of the cytoplasmic local and time-dependent releasing profile is of high interest regarding the design of specific and effective carrier systems. In our investigations, protamine sulphate and dextran sulphate were used as multilayer constituents coated on SiO₂ particles. Magnetite nanoparticles (Fe₃O₄, MNP) were integrated into the multilayer to be used as reporters for the multilayer decomposition. After time-dependent carrier application to HEK293T/17 cells, the spatial distribution of the MNPs within the cytoplasm was analyzed by proton-induced X-ray emission (PIXE). To ensure a direct localization of the carriers within cytoplasm, confocal laser scanning microscopic (CLSM) images [3] were correlated with the Fe maps. The investigations show that after 72 h of co-incubation of the functionalized microcarriers and cells, a release of the MNPs from the polyelectrolyte-coated silica cores occurs which is represented by an increasing distance between core and nanoparticles of up to several hundred nanometers [4].

- [1] L.J. De Cock et al., *Angew. Chem. Int. Edit.* **49**, 6954 (2010), [doi:10.1002/anie.200906266](https://doi.org/10.1002/anie.200906266)
- [2] A.L. Becker et al., *Small* **6**, 1836 (2010), [doi:10.1002/smll.201000379](https://doi.org/10.1002/smll.201000379)
- [3] U. Reibetanz et al., *Macromol. Biosci.* **6**, 153 (2006), [doi:10.1002/mabi.200500163](https://doi.org/10.1002/mabi.200500163)
- [4] U. Reibetanz et al., *Nucl. Instrum. and Meth. B* **269**, 2281 (2011), [doi:10.1016/j.nimb.2011.02.064](https://doi.org/10.1016/j.nimb.2011.02.064)

7.10 Methodical developments for quantitative high resolution ion beam analysis on lateral highly inhomogeneous meteorite samples

R. Wunderlich, J. Vogt, A. Bischoff*, D. Spemann, T. Butz

*Institut für Planetologie, Universität Münster

Extraterrestrial research is dominated by high-tech, like spacecrafts or telescopes and therefore highly cost-intensive. On the other side, meteorites provide a cheap source of information about the creation and development of our and other solar systems. Of particular interest is the concentration of trace elements in the rock building crystals of meteorites. The knowledge of the trace element concentration in certain crystals enables to reconstruct the geological history of minerals, like temperature and pressure conditions during growth and alteration. The investigated meteorite samples like the analyzed Acfer094 meteorite are the most unvaried and oldest rocks of our solar system. They are classified as chondrites, which are characterized by millimeter-sized globular silicate grains, called chondrules, that are embedded in a small grained matrix. These chondrules were melted and re-solidified independently of the meteorite mother body. Dependent on the melting conditions of the chondrule forming material the concentration of diffusing trace elements in the chondrules and the non-crystallized surrounding melt differs. These differences give an characteristic finger print of the geological history and enables to reconstruct processes of the formation of our solar system 4.5 billion years ago.

One of the main crystals of such chondrules is olivine $(\text{Mg, Mn, Fe})_2[\text{SiO}_4]$ and compatible with the element nickel. These crystals can often be found in close proximity to massive iron-nickel grains. These inhomogeneous samples are a challenge for ion beam analysis methods, like Particle Induced X-ray Emission (PIXE) or Rutherford Backscattering Spectrometry (RBS), due to the strongly varying dead time of detector electronics leading to incorrect concentration mapping on a local scale. To solve this problem, a noise triggered setup was developed, that generates defined pulses, that are fed into the preamplifier of the detector electronics and act as pseudo events in the data processing electronics. A comparison of the number of induced and processed pulses allows the computation of a dead time map, which enables the correction of the collected spectrum on a pixel by pixel basis (fig. 7.12).

The PIXE method has the advantage of less background due to bremsstrahlung compared to Electron induced X-ray Emission (EDX), which is a standard method in geoscience. Hence, PIXE provides a complementary technique especially for trace elements like nickel or calcium in a olivine crystal. Now, the new developed dead time mapping enables to record the correct spatial distribution of certain trace elements.

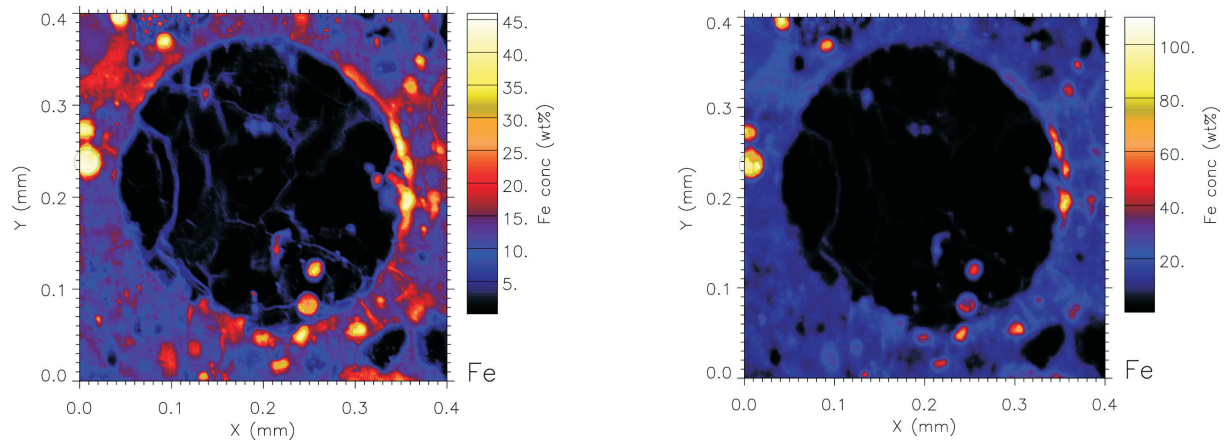


Figure 7.12: Iron distribution (computed by GeoPIXE 5.1b) without (left) and with (right) dead time correction, displayed using a false color scale. The corrected map seems to contain less structural information, but in fact now displays the correct concentration values.

7.11 3D imaging of cells using limited-angle STIM and PIXE tomography

T. Andrea, M. Rothermel, T. Butz

STIM (Scanning Transmission Ion Microscopy) tomography is a method which allows the three-dimensional characterization of samples in the micrometer range by measuring the energy loss of transmitted MeV ions from several directions. Mathematically, a set of projections covering an angular range of 180° contains sufficient information to reconstruct a sample. Yet for the analysis of cells fixated on a substrate only a limited angular range of ca. 120° can be realized experimentally. This makes it necessary to employ iterative reconstruction algorithms which compensate for the missing data. At the LIPSION accelerator laboratory a software based on the maximum entropy principle has been implemented which permits limited-angle reconstruction of fixated cells combining STIM and PIXE (particle induced X-ray emission) tomography. For the demonstration of the method a sample of HEK293 cells incubated with iron-coated silica microparticles ($3\ \mu\text{m}$ diameter) and fixated on a substrate was examined. The sample was mounted on a rotation axis and scanned with a beam of 2.25 MeV protons from various angles ranging 120° . Afterwards a series of elemental maps of the sample was obtained using PIXE under different rotation angles. In the three-dimensional reconstruction of the cell, density information obtained from STIM was superimposed with elemental information obtained from PIXE. The reconstruction showed that the microparticles were indeed incorporated by the cell and that the iron on their surface was visible (fig. 7.13).

7.12 Greyscale Proton Beam writing in p-type GaAs

D. Diering, D. Spemann, J. Lenzner

Proton Beam Writing (PBW) is a well known method for micromachining, e.g. of semi-

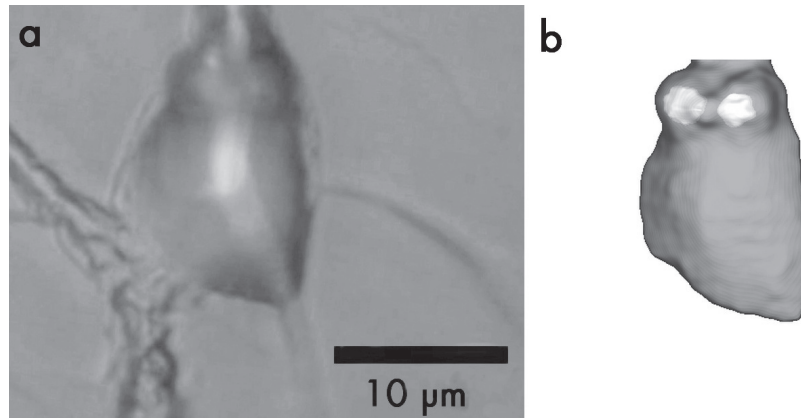


Figure 7.13: Optical micrograph (a) and tomographic reconstruction (b) of a cell containing silica microparticles. Density information was obtained using STIM tomography (depicted in gray). This information was superimposed with regions of high silicon concentration (white structures) obtained using PIXE tomography.

conductors. However, up to now, only few indication is given on how the resulting structure height in micromachined semiconductors can be controlled by means of fluence variation [1–3] which is a fast method and realized mainly by changing the irradiation time. This approach for 3D-microstructuring, called Greyscale PBW, was successfully demonstrated for negative photoresists [4]. Schulte-Borchers et al. used this approach to produce self-supporting structures in Gallium Arsenide (GaAs) by controlled undercutting [3].

In this study, (100) p-type GaAs was irradiated with 2.25 MeV protons and fluences in the range from $1.5 \times 10^{14} \text{ H}^+/\text{cm}^2$ to $2.4 \times 10^{17} \text{ H}^+/\text{cm}^2$ at the ion beam lab LIPSION and subsequently electrochemically etched with 10%-KOH in order to establish the dependency of structure height on ion fluence. In this way pyramid-like structures as well as concave-shaped structures could be created (see fig. 7.14). Furthermore, self-supporting structures were produced by undercutting. However, when comparing structures produced by simple undercutting and with those produced by using both protons and hydrogen molecule ions (H_2^+), the latter show far better structure definition due to the smaller lateral end-of-range straggling for H_2^+ .

GaAs showed a laterally anisotropic etch behaviour during the development step. Further measurements with Atomic Force Microscopy and Scanning Capacitance Microscopy are under way to obtain laterally resolved information on surface roughness and electronic properties in the structured areas.

- [1] M.B.H. Breese, F.J.T. Champeaux, E.J. Teo, A.A. Bettiol, D.J. Blackwood, *Phys. Rev. B* **73** 035428 (2006).
- [2] E.J. Teo, E.P. Tavernier, M.B.H. Breese, A.A. Bettiol, F. Watt, M.H. Liu, D.J. Blackwood, *Nucl. Instr. and Meth. B* **222**, 513 (2004).
- [3] M. Schulte-Borchers, U. Vetter, T. Koppe, H. Hofsäss, *J. Micromech. and Microeng.* **22**, 025011 (2012).
- [4] F. Menzel, D. Spemann, T. Koal, T. Butz, *Nucl. Instr. and Meth. B* **269**, 2427 (2011).

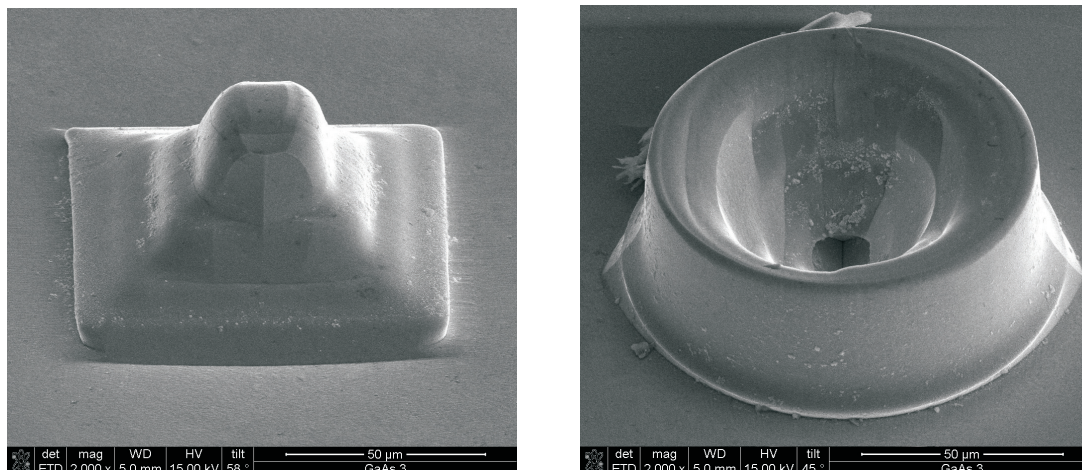


Figure 7.14: Pyramid-like (left) and concave-shaped structure (right) produced in p-type GaAs using Greyscale PBW.

7.13 Development of a fully digital user-friendly TDPAC-spectrometer

M. Jäger, T. Butz

Conventional time differential perturbed angular correlation (TDPAC) spectrometers use nuclear electronics such as preamplifiers, spectroscopy amplifiers, and single channel analyzers for energy discrimination in the so-called slow-circuit and constant fraction discriminators in the so-called fast circuit. Both are combined via delays in the fast circuit in fast-slow coincidences and routers as well as time-to-amplitude converters and amplitude-to-digital converters. The delayed coincidence counts are stored in a multichannel analyzer for different detector combinations.

To avoid adjustment complications and to increase setup reliability a fully digital TDPAC-spectrometer with user-friendly handling was developed. The 6-detector setup can be used with 38 mm diameter \times 38 mm height LaBr₃(Ce) scintillators mounted on XP2020URQ photomultipliers or 44.5 mm diameter \times 44.5 mm height (conically capped [1]) BaF₂ scintillators on XP2020Q photomultipliers and is now used at ISOLDE/CERN for TDPAC measurements. Figure 7.15 shows the current complete spectrometer set-up.

The detector anode signals are directly fed in modern high speed digitizer with field programmable gate array (FPGA) based digital signal processing units. 3 digitizers of type Agilent U1080A (also known as Acqiris AC240) outside of a measurement PC are used for the present digital TDPAC spectrometer. While common digitizers consist of an analogue-to-digital converter (ADC), a sampling data storage unit, and a digital bus to transfer sampling data to a PC, the digitizers used for this project have the FPGA as an additional needed feature. Each U1080A digitizer includes 2 ADC channels with 1 GS/s, 8-bit and a Virtex-II Pro FPGA from the company Xilinx.

The developed digital TDPAC-spectrometer exploits the massive parallel processing performance of the digitizer FPGAs. Already inside the FPGAs the energy selection and the time stamp calculation is done in hard real time by digital circuits contrary to other types of digital TDPAC-spectrometers [2], [3]. The transferred data to the measurement

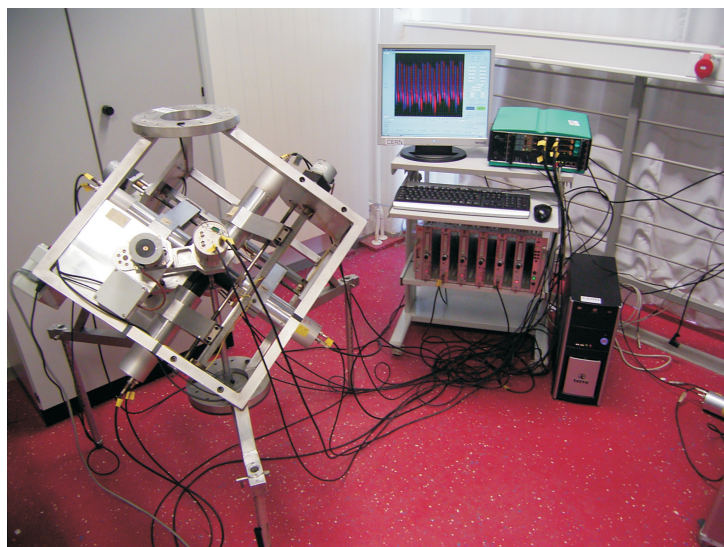


Figure 7.15: Photograph of the complete spectrometer set-up: detector cube (left), digitizers (green box), high voltage supplies and measurement PC (right).

PC is only 8 byte per detector event independent of the scintillators type. Because of the FPGA pre-processing the digital TDPAC-spectrometer in this work only needs one measurement PC with low performance or storage requirements. The coincidence extraction of the detector time stamp datasets is done in real time and immediately viewed in time spectra by the spectrometer software.

Since for TDPAC time resolution is critical we decided to implement some time stamp calculation approaches inside the FPGA. These are the centroid, the constant fraction of amplitude (CFA) [4], and the true constant fraction trigger (CFT) algorithms as proposed by [5]. Concerning the time resolution CFA and CFT reaches the same results. For instance 247 ps with BaF₂ for (1330, 1170) keV (⁶⁰Co), 344 ps with LaBr₃(Ce) for 511 keV (⁴⁴Ti), and 291 ps with LaBr₃(Ce) for (1275, 511) keV (²²Na). The gap between hardware CFTs and digital CFTs is now almost closed.

It is planned to use the experience about FPGA digitizers, digital energy resolution techniques, and digital time resolution techniques to build a fully digital data acquisition and analysis system for the LIPSION nanoprobe.

- [1] T. Butz, S. Saibene, T. Fraenzke, M. Weber, Nucl. Instr. and Meth. A **284**, 417 (1989).
- [2] M. Nagl, U. Vetter, M. Uhrmacher, H. Hofsäss, Rev. Sci. Instrum. **81**, 073501 (2010).
- [3] J. Röder, C. Herden, J.A. Gardner, K.D. Becker, M. Uhrmacher, H. Hofsäss, Hyperfine Interact. **181**, 131 (2008).
- [4] L. Bardelli, G. Poggi, M. Bini, G. Pasquali, N. Taccetti, Nucl. Instr. and Meth. A **521**, 480 (2004).
- [5] A. Fallu-Labruyere, H. Tan, W. Henning, W.K. Warburton, Nucl. Instr. and Meth. A **579**, 247 (2007).

7.14 FPGA implementation of digital constant fraction algorithm with fractional delay for optimal time resolution

M. Jäger, T. Butz

In a recent development of a fully digital spectrometer for time differential perturbed angular correlations a true constant fraction trigger (CFT) algorithm was implemented that, however, allowed for integer delays, i.e. integer multiples of the sampling interval, only. With a sampling rate of 1 GS/s and BaF₂ scintillators this turned out to be insufficient. Therefore, we designed an extension of the algorithm to fractional delays implemented in field programmable gate arrays (FPGAs). Furthermore, we derive a criterion for the delay for optimum timing based on the steepest slope of the CFT signal. Experimental data are given for LaBr₃(Ce) scintillators and 511 keV – 511 keV prompt coincidences that corroborate the theoretical result.

7.15 Perturbed Angular Correlation of the stretched cascade in the decay of ^{180m}Hf using a digital spectrometer

M. Jäger, T. Butz

We performed a measurement of the nuclear quadrupole interaction (NQI) at Hf sites using the nuclear probe ^{180m}Hf in HfF₄ · HF · 2H₂O at 300 K by exploiting all possible start quanta in the stretched cascade with a digital Time Differential Perturbed Angular Correlation (TDPAC) spectrometer. With conventional spectrometers, multiple prompt start signals would paralyze the router. The gain in coincidence rate is about a factor of 5 compared to a conventional spectrometer using a single start only. With multiple starts ^{180m}Hf is a promising new isomeric nuclear probe in TDPAC experiments. As an additional feature to the existing fully digital TDPAC-spectrometer at ISOLDE/CERN we implemented the possibility to measure up to four cascades simultaneously in order to save data collection time or to measure isobaric contaminations like ^{111m}Cd and ¹¹¹In as frequently encountered with the General Purpose Separator.

7.16 Funding

Leipzig School of Natural Sciences - Building with Molecules and Nano-objects (Build-Mona)

Prof. Dr. T. Butz

GSC 185/1

DFG Graduiertenkolleg Interdisciplinary Approaches in Cellular Neurosciences (InterNeuro)

Prof. Dr. T. Butz
GRK 1097

Non-Targeted Effects of ionising Radiation – NOTE

Prof. Dr. T. Butz

EU Integrated Project FI6R-036465

7.17 Organizational Duties

T. Butz

- Vertrauensdozent der Studienstiftung des deutschen Volkes
- Sprecher der Ortsgruppe Leipzig des deutschen Hochschulverbandes
- Co-tutor for students of Tautenburg (astrophysics), DESY/Zeuthen (particle physics)
- Reviewer: DFG, Studienstiftung des deutschen Volkes
- Referee: BMBF, Radiochimica Acta, University of Copenhagen (recruitment), University of Aveiro, Portugal (PhD defense)

F. Menzel

- Referee: Nucl. Instrum. Meth. B

M. Rothermel

- Referee: Nucl. Instrum. Meth. B
- Doktorandensprecher der Graduiertenschule “Leipzig School of Natural Sciences - Building with Molecules and Nano-objects” (BuildMoNa)
- Doktorandensprecher des Graduiertenzentrums Mathematik/Informatik und Naturwissenschaften der “Research Academy Leipzig”

D. Spemann

- Referee: Nucl. Instrum. Meth. B, J. Micromech. Microeng.

J. Vogt

- Referee: Nucl. Instrum. Meth. B

7.18 External Cooperations

Academic

- Université de Bordeaux I
CENBG, Prof. Ph. Moretto
- CERN, Genf
ISOLDE Collaboration
- Institute of Physics, Kraków
Dr. Z. Stachura
- IOM Leipzig
Dr. K. Zimmer

- KVL, Kopenhagen
Dr. L. Hemmingsen
- University of Amsterdam, Cognitive Science Centre, Netherlands
Dr. B. Forstmann
- MPI für Demografische Forschung, Rostock
A. Fabig
- National University of Singapore
Center for Ion Beam Applications, Prof. F. Watt, Dr. T. Osipowicz
- Universität Leipzig, Medizinische Fakultät
Paul-Flechsig-Institut, Prof. T. Arendt, Dr. M. Morawski
- Universität Leipzig, Medizinische Fakultät
Institut für Rechtsmedizin, Dr. M. Weber, S. Wernecke
- Universität Leipzig, Medizinische Fakultät
Institut für Laboratoriumsmedizin, Kl. Chemie und Mol. Diagnostik, Prof. J. Thiery,
Dr. D. Teupser
- Universität Leipzig, Medizinische Fakultät
Institut für Medizinische Physik und Biophysik, Prof. E. Donath, Dr. U. Reibetanz,
Dr. I. Estrela-Lopis, DBc. M. Dorn
- MPI für Kognitions- und Neurowissenschaften, Leipzig
Prof. R. Turner
- Universität Leipzig, Fakultät für Mathematik und Informatik
Prof. M. Bogdan
- Helmholtz-Zentrum für Umweltforschung – UFZ, Leipzig
Dr. M. Kraus
- The University of Melbourne
Microanalytical Research Centre, Prof. D. Jamieson
- TU Wien
Prof. K. Schwarz, Prof. P. Blaha
- Universität Hannover
Arbeitskreis Prof. P. Behrens
- Universität Hannover
Arbeitskreis Prof. C. Vogt
- Universität Rostock
Prof. Dr. G. Hildebrandt
- Martin-Luther-University Halle-Wittenberg
Dr. A. Guittoum, Prof. R. Krause-Rehberg
- MPI of Microstructure Physics, Halle (Saale)
Dr. O. Moutanabbir
- TU Bergakademie Freiberg, Freiberg
Prof. J. Heitmann
- University of North Texas, Denton, TX, USA
Assoc. Prof. T. Reinert

Industry

- Dechema
Dr. E. Zschau, Self-employed expert in materials research

7.19 Publications

Journals

M. Jäger, K. Iwig, T. Butz: *A user-friendly fully digital TDPAC-spectrometer*, *Hyperfine Interactions* **198**, 167 (2011)
[doi:10.1007/s10751-010-0201-8](https://doi.org/10.1007/s10751-010-0201-8)

M. Jäger, K. Iwig, T. Butz: *A compact digital time differential perturbed angular correlation-spectrometer using field programmable gate arrays and various timestamp algorithms*, *Review of Scientific Instruments* **82**, 065105 (2011)
[doi:10.1063/1.3599417](https://doi.org/10.1063/1.3599417)

T. Butz, S.-b. Ryu, St. Jankuhn, S.K. Das, S. Ghoshal: *TiO₂ Nanomaterials Studies by ⁴⁴Ti(EC)⁴⁴Sc Time Differential Perturbed Angular Correlations: Volume and Surface Properties*, *Defect and Diffusion Forum* **311**, 137 (2011)
[doi:10.4028/www.scientific.net/DDF.311.137](https://doi.org/10.4028/www.scientific.net/DDF.311.137)

K. Bechstein, J. Michels, J. Vogt, G. C. Schwartz, C. Vogt: *Position-resolved determination of trace elements in mandibular gnathobases of the Antarctic copepod *Calanoides acutus* using a multimethod approach*, *Anal. Bioanal. Chem.* **399**, 501-508 (2011)
[doi:10.1007/s00216-010-4373-5](https://doi.org/10.1007/s00216-010-4373-5)

T. Andrea, M. Rothermel, T. Reinert, T. Koal, T. Butz: *Creation of 3D microsculptures in PMMA by multiple angle proton irradiation*, *Nucl. Instr. and Meth. B* **269**, 2431 (2011)
[doi:10.1016/j.nimb.2011.02.038](https://doi.org/10.1016/j.nimb.2011.02.038)

W. Larisch, T. Koal, R. Werner, M. Hohlweg, T. Reinert, T. Butz: *Proton Beam Writing of microstructures in Agar gel for patterned cell growth*, *Nucl. Instr. and Meth. B* **269**, 2444 (2011)
[doi:10.1016/j.nimb.2011.02.041](https://doi.org/10.1016/j.nimb.2011.02.041)

R. Feder, F. Menzel, T. Butz: *Micro-fluidic target chamber machined by proton beam writing for the in-situ analysis of gas absorption in synthetic crystals*, *Nucl. Instr. and Meth. B* **269**, 2439 (2011)
[doi:10.1016/j.nimb.2011.02.048](https://doi.org/10.1016/j.nimb.2011.02.048)

D. Spemann, T. Reinert, J. Vogt, T. Andrea, N. Barapatre, R. Feder, A.M. Jakob, N. Liebing, Ch. Meinecke, F. Menzel, M. Rothermel, T. Butz: *Materials Analysis and Modification at LIPSION – Present State and Future Developments*, *Nucl. Instr. and Meth. B* **269**, 2175 (2011)
[doi:10.1016/j.nimb.2011.02.054](https://doi.org/10.1016/j.nimb.2011.02.054)

F. Menzel, D. Spemann, T. Koal, T. Butz: *3D-structures with Arbitrary Shapes Created in Negative Resists by Grayscale Proton Beam Writing*, Nucl. Instr. and Meth. B **269**, 2427 (2011)

doi:10.1016/j.nimb.2011.02.060

F. Menzel, D. Spemann, T. Butz: *High-aspect Ratio Microstructures in p-type GaAs and InP Created by Proton Beam Writing*, Nucl. Instr. and Meth. B **269**, 2457 (2011)

doi:10.1016/j.nimb.2011.02.061

A.M. Jakob, D. Spemann, R. Thies, J. Vogt, T. Butz: *A Characterisation of Electronic Properties of Alkaline-texturized Polycrystalline Silicon Solar Cells Using IBIC*, Nucl. Instr. and Meth. B **269**, 2345 (2011)

doi:10.1016/j.nimb.2011.02.040

T. Reinert, N. Barapatre, A. Reinert, D. Spemann, T. Andrea, W. Larisch, Ch. Meinecke, T. Koal, R. Werner, M. Hohlweg, J. Vogt, T. Butz: *Biomedical Research at LIPSION – Present State and Future Developments*, Nucl. Instr. and Meth. B **269**, 2254 (2011)

doi:10.1016/j.nimb.2011.02.071

U. Reibetanz, St. Jankuhn: *Magnetite nanoparticles as reporters for microcarrier processing in cytoplasm*, Nucl. Instr. and Meth. B **269**, 2281 (2011)

doi:10.1016/j.nimb.2011.02.064

U. Scholz, F. Menzel, M. Pluta, W. Grill, T. Butz: *Acoustic mode converters micromachined in silicon by proton beam writing*, Nucl. Instr. and Meth. B **269**, 2452 (2011)

doi:10.1016/j.nimb.2011.02.065

A. Reinert, N. Barapatre, S. Sachse, T. Reinert: *μ PIXE for a μ Brain: The Vinegar Fly's Brain, Antenna, Sensilla Hairs and Eye Ion Concentrations*, Nucl. Instr. and Meth. B **269**, 2292 (2011)

doi:10.1016/j.nimb.2011.02.066

D. Banerjee, S.K. Das, P. Das, S.V. Thakare, T. Butz: *Zr-doped rutile TiO₂: a nuclear quadrupole interaction study*, Hyperfine Interact. **197**, 193 (2011)

doi:10.1007/s10751-010-0210-7

C.C. Dey, S. Dey, S.C. Bedi, S.K. Das, M. Lorenz, M. Grundmann, J. Vogt, T. Butz: *Hafnium oxide thin films studied by time differential perturbed angular correlations*, J. Appl. Phys. **109**, 113918 (2011)

doi:10.1063/1.3592245

M. Khalid, P. Esquinazi, D. Spemann, W. Anwand, G. Brauer: *Hydrogen-mediated ferromagnetism in ZnO single crystals*, New J. Phys. **13**, 063017 (2011)

Matthias Brandt, Michael Bonholzer, Marko Stölzel, Gabriele Benndorf, Daniel Spemann, Michael Lorenz, Marius Grundmann: *Electrical transport in strained Mg_xZn_{1-x}O:P thin films grown by pulsed laser deposition on ZnO(000-1)*, phys. stat. sol. B **249**, 82 (2012)

doi:10.1002/pssb.201147212

Markus Jäger, Tilman Butz: *FPGA implementation of digital constant fraction algorithm with fractional delay for optimal time resolution*, Nucl. Instr. and Meth. A **674**, 24 (2012) doi:10.1016/j.nima.2012.01.022

Books

T. Butz: *Fouriertransformation für Fußgänger*, 7. Aufl.(Vieweg+Teubner, Wiesbaden 2012), ISBN: 978-3-8348-0946-9

Talks

N. Barapatre, A. Sickert, M. Morawski, T. Reinert, D. Teupser, T. Butz
Quantitative microscopy with trace element sensitivity: application in biomedical field
Colloquium Analytische Atomspektroskopie, 13.–16.03.11, Leipzig

U. Reibetanz, M. Schönberg, M. Göse, S. Rathmann, V. Strehlow, S. Jankuhn, J. Leßig
Colloidal Microcarriers as Drug Delivery Systems
16. Leipziger Workshop Cytomics in LIFE, 14.–16.04.11, Leipzig

M. Jäger, T. Butz
DIGIPAC - a real time digital Perturbed Angular Correlation spectrometer
CERN, 24.06.11, Genf

D. Spemann, T. Andrea, N. Barapatre, R. Feder, N. Klingner, J. Lehnert, F. Menzel, A. Reinert, M. Rothermel, J. Vogt, T. Butz
Materials Analysis and Modification Using High-energy Ions at LIPSION
International Conference on Materials for Advanced Technologies, 26.06.–01.07.11, Singapur

T. Butz
Was wir unseren Kindern über Kernenergie sagen sollten
XV. Theodor-Litt Symposium, 27.–28.10.11, Leipzig

M. Jäger, T. Reinert
Digital Signal Processing with High-speed Digitizers for Spectrometry
Physics Colloquium, 22.11.11, University of North Texas, Denton, USA

N. Barapatre, A. Sickert, M. Morawski, T. Reinert, D. Teupser, T. Butz
Quantitative microscopy with trace element sensitivity: application in biomedical field
7th Int. Symposium on Bio-PIXE, 30.10.–04.11.11, Sendai, Japan

Posters

T. Andrea, M. Rothermel, T. Butz
3D imaging of cells and creation of microsculptures using MeV proton tomography
Fourth Scientific Symposium of the Graduate School BuildMoNa, 21.03.11, Leipzig

R. Feder
Defect production by ions traversing multi graphene
Fourth Scientific Symposium of the Graduate School BuildMoNa, 21.03.11, Leipzig

A. Sickert, N. Barapatre, M. Rothermel, D. Teupser, T. Reinert
3D Analysis of an Induced Murine Atherosclerotic Lesion by PIXE Stacking
7th Int. Symposium on Bio-PIXE, 30.10.–04.11.11, Sendai, Japan

M. Dorn, D. Spemann, J. Vogt, J. Fleddermann, I. Estrela-Lopis, E. Donath
Study of nanoparticle uptake and quantification in lung cells by ion beam microscopy
Leipzig Research Festival for Life Sciences 2011, 16.12.2011, Leipzig

7.20 Graduations

Diploma

- Julia Trützscher
Untersuchung zu Magnetismus und Fehlordnung in Titandioxid-Dünnschichten
Septembre 2011

Bachelor

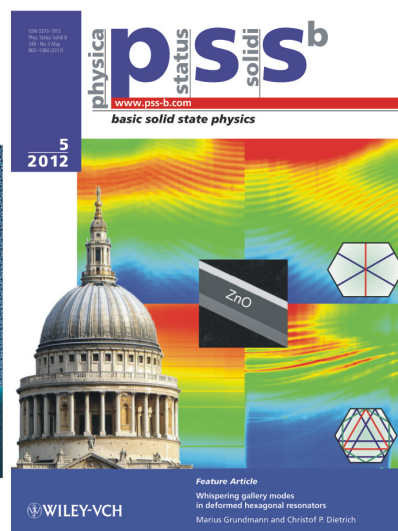
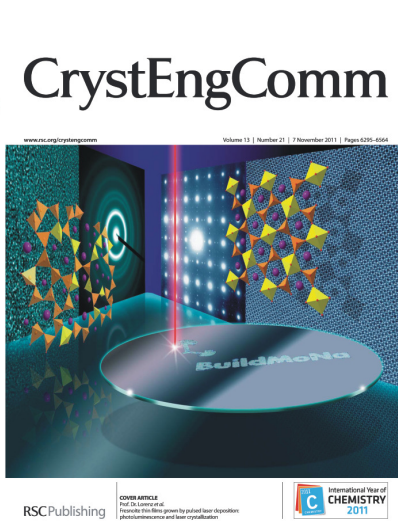
- Jan Lehnert
Bestimmung der Prozessparameter für die Herstellung von Mikrostrukturen in Zinkoxid mittels Protonenstrahlschreiben
Septembre 2011

8

Semiconductor Physics

8.1 Introduction

In 2011 we have solved a problem that has been worked on intensively worldwide for more than a decade - a reproducible and stable oxide pn-diode. Using the ZnCo_2O_4 spinel in amorphous state, deposited at room temperature, a suitable p-type material for an oxide heterostructure pn-diode has been realized by us. Rectification is several orders of magnitude better than any oxide diode before. These diodes have also allowed us to fabricate the first oxide junction field-effect transistor (JFET). We found also other spinel oxides such as ZnFe_2O_4 to have interesting and tunable properties such as conductivity and magnetization. We have made further progress in our research on transparent electronics: Our PdO_x/ZnO Schottky diodes on ZnO thin films are comparable or better than the best contacts on ZnO single crystals. Tungsten trioxide turns out to be a high- κ dielectric for ZnO-based MISFETs with low gate leakage and small sub-threshold voltage swing $SS=80\text{mV/decade}$ close to the thermodynamic limit. Using (Mg,Zn)O layers of various Mg-content we have demonstrated transparent narrowband UV-photodetectors. Prof. Marius Grundmann has won the the Leipziger Wissenschaftspreis 2011 of the Stadt Leipzig, Universität Leipzig and the Sächsische Akademie der Wissenschaften zu Leipzig for his work on transparent electronics.



In our all-oxide microcavities with ZnO bulk active medium we have achieved a Bose-Einstein condensate of exciton-polaritons up to 250 K and have observed its ballistic propagation. For his work on optical modes in ZnO nano- and microwires with various symmetries Christof Peter Dietrich has won a BuildMoNa award 2011 for distinguished research achievement. Please go through the following short articles to learn about this and other research work we have performed in 2011.

Privatdozent Dr. Rainer Pickenhain has retired in August 2011. He has established our work on deep level transient spectroscopy and we wish him well in his future activities. In recognition of his outstanding research achievements and his commitment to teaching, Privatdozent Dr. Michael Lorenz has been appointed as apl. Prof., officially effective March 2011, and has in the meantime received all professorial rights. We are very grateful to our funding agencies in particular Deutsche Forschungsgemeinschaft (DFG) and European Social Fund (ESF). We are grateful for the continued funding of Sonderforschungsbereich SFB 762 "Functionality of Oxide Interfaces" (2012–2015) and our project in the newly established Forschergruppe FOR 1616 "Nanowire Optoelectronics" (2012–2014). The work of our students and researchers together with our academic and industrial partners near and far (in particular France, Portugal, South Africa and New Zealand) was fruitful and enjoyable and thus it is with pleasure that the semiconductor physics group presents their progress report.

Marius Grundmann

8.2 Structural and electrical properties of CoFe_2O_4 and NiFe_2O_4 thin films grown by pulsed-laser deposition

K. Brachwitz, M. Lorenz, M. Grundmann

Ferrites constitute a class of materials that has been recognized to have significant potential in applications ranging from millimeter wave integrated circuitry to magnetic recording [1]. For instance zinc ferrite (ZnFe_2O_4) thin films can be considered as magnetic semiconductor [2]. Cobalt ferrite (CoFe_2O_4) and nickel ferrite (NiFe_2O_4) are also promising candidates for the application as electrodes in magnetic tunnel junctions. In this respect we have investigated CoFe_2O_4 and NiFe_2O_4 thin films grown by pulsed-laser deposition (PLD). These thin films crystallize in cubic spinel structure. The studies include the dependence of structural properties as well as electrical characteristics on the growth parameters.

Stoichiometric PLD targets were mixed, pressed and sintered from high-purity NiO- (or CoO-) and Fe_2O_3 -powders. In this study we have varied the growth temperature (T_S) by controlling the heater power (P_H) in a range from 400 °C ($P_H = 150$ W) to 730 °C ($P_H = 700$ W). The ferrite thin films were grown on (100)-oriented strontium titanate (SrTiO_3) single crystals at $p(\text{O}_2) = 5 \times 10^{-5}$ mbar. The preferential (100) out-of-plane orientation of the films and the lattice constant a were obtained by X-ray diffraction (XRD) and temperature dependent resistivity measurements have been conducted at a Hall effect setup.

Figure 8.1 (a) shows $2\theta - \omega$ scans of CoFe_2O_4 and NiFe_2O_4 thin films for different growth temperatures. A decreasing 2θ -angle of the (400) reflex and thus an increasing

out-of-plane lattice constant was obtained with decreasing heater power. Figure 8.1 (b) depicts the out-of-plane lattice constant of ZnFe_2O_4 , NiFe_2O_4 and CoFe_2O_4 films as function of P_H . The thin film thickness and the large lattice mismatch between ferrite film and SrTiO_3 substrate leads to strain relaxation and Stranski-Krastanov growth.

Table 8.1: Bulk lattice constant a_{bulk} , lattice mismatch of bulk ferrite to SrTiO_3 substrate, and activation energies of thermally activated electrical conduction mechanism of the respective ferrite material.

material	a_{bulk} (Å)	$\Delta a_{\text{bulk}}/a_{\text{SrTiO}_3}$ (%)	E_{A1} (meV)	E_{A2} (meV)
ZnFe_2O_4	8.441	8.1	70-120	52 ± 4
CoFe_2O_4	8.392	7.5	90-100	50 ± 4
NiFe_2O_4	8.338	6.8	105-120	60 ± 2

The resistivity of the investigated thin films can be tuned by different substrate temperatures during growth. Figure 8.2 (a) shows the correlation of the resistivity with the applied heater power. Similar dependencies were observed for n-type ZnFe_2O_4 thin films [2, 3]. The conduction mechanism is probably not only affected by electron hopping between Fe^{2+} and Fe^{3+} but also structural disorders like grain boundaries and oxygen vacancies have great influence. This is confirmed by the larger FWHM of the NiFe_2O_4 Bragg peaks for 700 W (see Fig. 8.1(a)), which results in lower resistivity. The temperature dependence of the electrical conductivity of CoFe_2O_4 and NiFe_2O_4 (Figure 8.2 (b)) is similar to that of ZnFe_2O_4 [2]. The conductivity is thermally activated and a model with two activation energies fits the temperature dependent conductivity best (see Table 8.1).

- [1] Y. Suzuki, Annu. Rev. Mater. Res. **31**, 265 (2001)
- [2] M. Lorenz *et al.*, Phys. Status Solidi Rapid Res. Lett. **5**, 438, (2011)
- [3] A. Marcu *et al.*, J. Appl. Phys. **102**, 023713 (2007)
- [4] C. E. Rodríguez Torres *et al.*, Phys. Rev. B **84**, 064404 (2011)

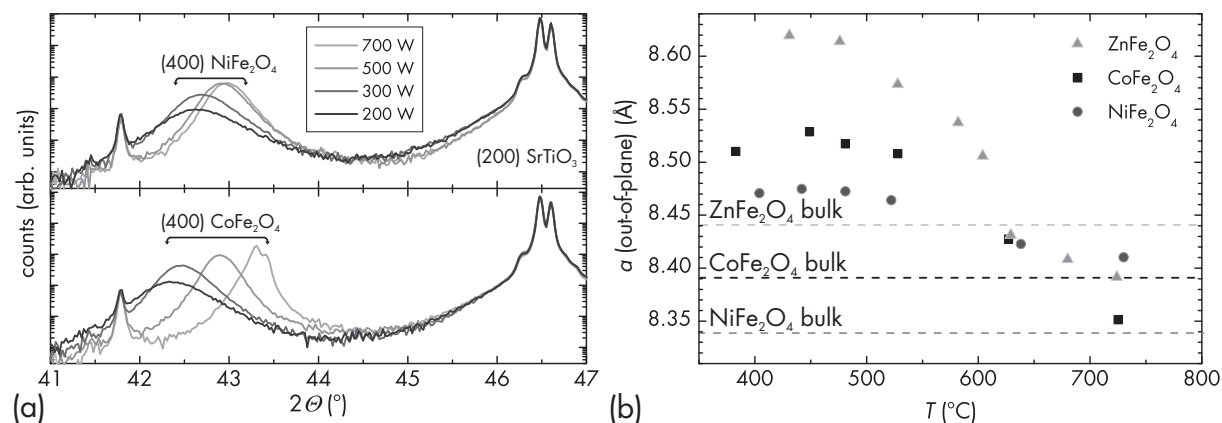


Figure 8.1: (a) XRD $2\theta - \omega$ scans ($\text{Cu K}\alpha$) of the CoFe_2O_4 and NiFe_2O_4 thin films for different heater power as indicated for $p(\text{O}_2) = 5 \times 10^{-5}$ mbar. (b) Dependence of the out-of-plane a -lattice constant on the growth temperature. The dashed lines show the respective bulk lattice-constants (see Table 8.1).

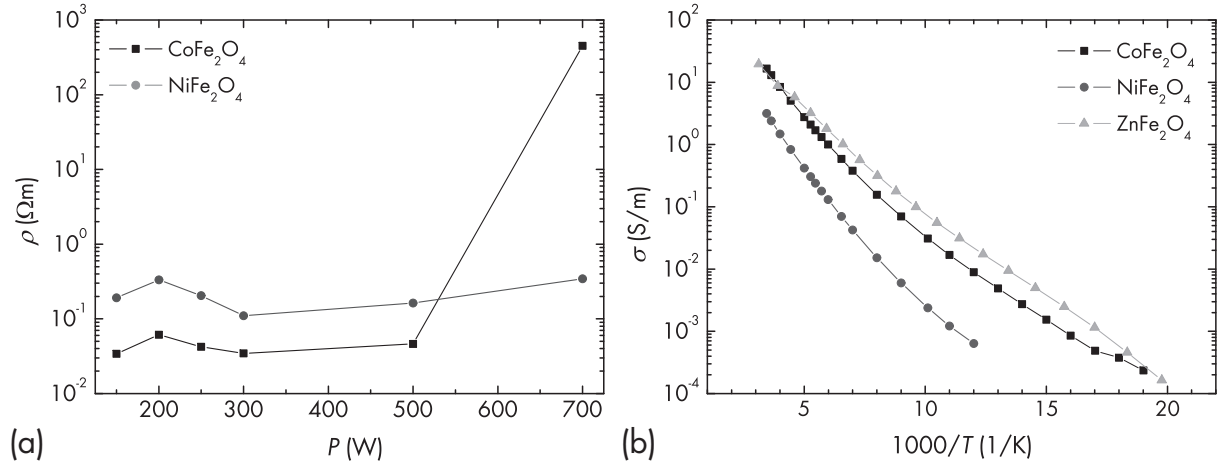


Figure 8.2: (a) Electrical resistivity as function of heater power for CoFe_2O_4 and NiFe_2O_4 thin films on SrTiO_3 . (b) Temperature dependent electrical conductivity for thin films grown at $p(\text{O}_2) = 5 \times 10^{-5}$ mbar and $P_H = 200$ W on SrTiO_3 substrate.

8.3 ZnO-based *n*-channel junction field-effect transistor with room-temperature fabricated amorphous *p*-type ZnCo_2O_4 gate

F.-L. Schein, H. von Wenckstern, H. Frenzel, M. Grundmann

Field-effect transistors (FETs) based on transparent semiconducting oxides (TSOs) are the key element for future ultrahigh-definition transparent displays. Most of the TSO-based FETs use a metal-insulator-semiconductor (MIS) structure for the transistor gate, but also metal-semiconductor (MES) structures have been successfully realized [1]. In comparison to MIS- and MESFETs, a junction FET (JFET) can have enhanced bias-stress stability due to the absence of an insulating layer which often represents a charge carrier trap, or improved temperature stability due to the absence of MES degradation effects. Here we present the first oxide-based JFET [5] using *n*-ZnO and amorphous *p*- ZnCo_2O_4 in a top-gate approach as shown in Fig. 8.3c.

The oxides were grown by pulsed-laser deposition on an *a*-plane sapphire substrate. A standard photolithography and lift-off process was used for device patterning. First, a 40 nm thin ZnO film was deposited at $p(\text{O}_2) = 0.02$ mbar and $T_{\text{growth}} = 685$ °C. Afterwards mesa-shaped transistor channels were formed by wet etching with diluted phosphoric acid. Next, the source and drain contacts were dc-sputtered from a metallic Gold target at 0.02 mbar in Ar atmosphere. Finally a 43 nm thin ZnCo_2O_4 layer for the top gate was grown at 0.05 mbar and room temperature followed by deposition of a dc-sputtered Au capping layer. This ZnCo_2O_4 layer is X-ray amorphous and *p*-type conducting as confirmed by X-ray diffraction and Seebeck-effect measurements.

In Fig. 8.3a the transfer characteristic of a JFET at a source-drain voltage of 2 V is shown. The amount of drain current can be controlled over 7 decades by applying gate voltages in the range of $-3.9 \text{ V} < V_{\text{GS}} \leq 0 \text{ V}$. The threshold voltage V_T was determined by the linear extrapolation of a $I_{\text{DS}}^{1/2}$ versus V_{GS} plot to $I_{\text{DS}}^{1/2} = 0$ and found to be $V_T = -2.92$ V. The steepness of the transfer characteristic is represented by the

subthreshold slope of $S = 91$ mV/decade which is close to the thermodynamical limit of about 60 mV/decade. Only a small hysteresis ($\Delta V < 0.1$ V) with the tendency of higher currents for the 'backward' measuring direction is detected. The gate-source diode shows a clear rectifying behavior and reaches a current on/off ratio of 1.2×10^8 as known from separate measurements. This far exceeds rectification ratios of similar, but all amorphous p - n junctions using p -ZnRh₂O₄/ n -InGaZnO₄ [2] and p -ZnCo₂O₄/ n -InGaZnO [3] having on/off = 1×10^3 at ± 5 V and 1×10^2 at ± 7 V.

A clear saturation and pinch-off behavior can be seen in the output characteristics in Fig. 8.3b. From this plot a channel mobility of $\mu_{\text{ch}} = 8.4$ cm²/Vs was determined. Presumably due to scattering effects at the ZnO/ZnCo₂O₄ interface this is about half of the Hall mobility $\mu_{\text{Hall}} = 17.6$ cm²/Vs.

The JFET performance (μ_{ch} , $I_{\text{on/off}}$, S) is among the best well-established oxide-based FETs since other TSO-based MISFETs with $I_{\text{on/off}} > 1 \times 10^7$ exhibit mobilities from $\mu_{\text{ch}} = 1.9$ cm²/Vs up to $\mu_{\text{ch}} = 45$ cm²/Vs but typically in the region of 5–15 cm²/Vs [1]. The subthreshold slope is only outperformed by MESFETs (81 mV/dec [1]) and MISFETs [4] with tungsten oxide as gate dielectric (80 mV/dec).

A shift of the threshold voltage V_T due to gate-bias stress is a common and serious problem for oxide-based MISFETs. The JFET was stressed for 25 000 s (≈ 7 h) with gate voltages of 1 V or -5 V before (Fig. 8.3d(i)) and 109 days after (Fig. 8.3d(ii)) temperature dependent measurements and a V_T -shift of less than 0.18 V was observed. Compared to oxide MISFETs at similar gate-bias stress conditions having δV_T of 0.03 V, 1.0 V, 1.7 V and 22.0 V, this shift is very small.

In the middle part of Fig. 8.3d V_T and I_{off} are shown for elevated temperatures up to 150 °C and 3 min or 9 h after temperature stress (two points right from *dashed line*), respectively. The reversible increase of V_T may be explained by acceptor-like trap states at the gate/channel interface or by a change in carrier trap density with temperature. The off-current increases irreversibly with temperature but recovers later to values in the range of 4×10^{-11} A. With that I_{off} is less than one order of magnitude larger than it was before the heating.

In conclusion, the first oxide-based JFET exhibits competitive device performance which changed slightly from $\mu_{\text{ch}} = 8.4$ cm²/Vs, $I_{\text{on/off}} = 1.3 \times 10^7$ and $S = 91$ mV/decade to $\mu_{\text{ch}} = 6.8$ cm²/Vs, $I_{\text{on/off}} = 3.3 \times 10^6$ and $S = 128$ mV/decade after all bias-stress and temperature cycles. The device is bias-stress stable and its functionality remains up to 150 °C.

- [1] M. Grundmann, H. Frenzel, A. Lajn, M. Lorenz, F. Schein, H. von Wenckstern, *Physica Status Solidi A*. **207**, 1437 (2010)
- [2] S. Narushima, H. Mizoguchi, K. Shimizu, K. Ueda, H. Ohta, M. Hirano, T. Kamiya, H. Hosono, *Adv. Mater.* **15**, 1409 (2003)
- [3] S. Kim, J. A. Cianfrone, P. Sadik, K.-W. Kim, M. Ivill, D. P. Norton, *J. Appl. Phys.* **107**, 103538 (2010)
- [4] M. Lorenz, H. von Wenckstern, M. Grundmann, *Adv. Mater.* **23**, 5383 (2011)
- [5] F.-L. Schein, H. von Wenckstern, H. Frenzel, M. Grundmann, *IEEE Electron Device Letters* **33**, xx (2012)

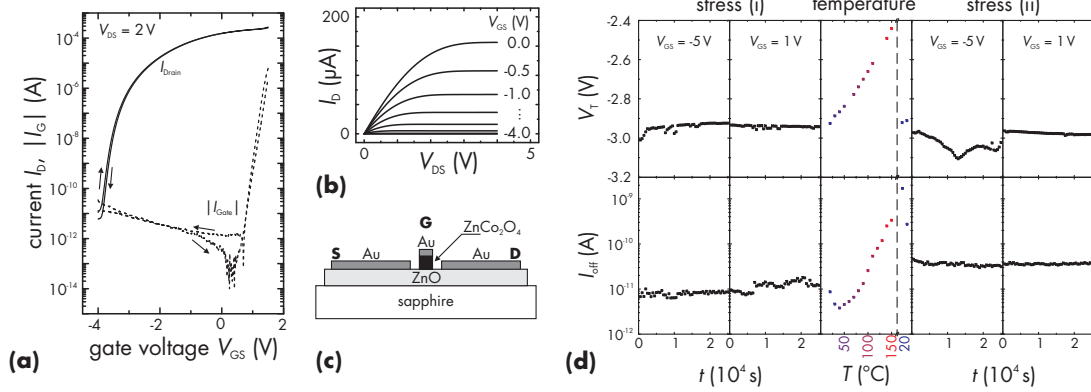


Figure 8.3: (a) Double-sweep transfer characteristic (*solid line*) of the JFET. The *dashed line* shows the absolute gate current. (b) Output characteristics of the JFET. (c) Schematic of the device structure. The gate width-to-length-ratio is $W/L = 430 \mu\text{m}/40 \mu\text{m}$. (d) Threshold voltage V_T and drain off-current I_{off} as function of gate stress duration t or temperature T .

8.4 Double-sided (Mg,Zn)O narrow bandwidth metal-semiconductor-metal photodetectors

Z. P. Zhang, H. von Wenckstern, M. Schmidt, M. Grundmann

The ternary semiconductor (Mg,Zn)O system in wurtzite modification is well suited for realization of visible-blind photodetectors (PDs). The band gap E_g increases with increasing Mg-content and can be tuned between 3.3-4.8 eV for wurtzite modification hence the corresponding cut-off wavelength can be adjusted from 380 to 260 nm. We reported on narrow bandwidth metal-semiconductor-metal (MSM) PDs based on $\text{Mg}_y\text{Zn}_{1-y}\text{O}/\text{Mg}_x\text{Zn}_{1-x}\text{O}$ -heterostructures ($0 \leq y < x \leq 0.5$), allowing to design wavelength-selective detectors (FWHM ≈ 7 nm) [1]. Within this construction, the $\text{Mg}_x\text{Zn}_{1-x}\text{O}$ acts as an integrated optical edge filter blocking high energy radiation. Subsequently, the active $\text{Mg}_y\text{Zn}_{1-y}\text{O}$ layer of the devices was deposited on the filter layer (see FIG. 1 of [1]).

The interdiffusion at interface of the heterostructure and the diffusion length of carriers from filter to active layer can affect the space-charge region of the Schottky contacts and limit the minimum FWHM of the PDs. In order to minimize these impacts, we attempt to separate the filter and active layer. Thereby, the filter $\text{Mg}_x\text{Zn}_{1-x}\text{O}$ layer about 300 nm was primarily grown on a double-side polished a-plane sapphire substrate by pulsed-laser deposition (PLD). Subsequently, the active $\text{Mg}_y\text{Zn}_{1-y}\text{O}$ layer about 500 nm was deposited on the other side of the substrate (see the schematic device layout in Fig. 8.4(a)).

Ideally only light in a defined photon energy of $E_g^y < E_{\text{ph}} < E_g^x$ contributes to the photon response under backside illumination. The spectral bandwidth is given by the band gap difference ΔE_g of the two (Mg,Zn)O layers and the spectral center of photo response can be tuned by different $y : x$ -combinations [1]. The different Mg-content in the two layers was realized with a PLD-target but two different oxygen partial pressures p_{O_2} . Note, the Mg-incorporation decreases with increasing p_{O_2} . The Schottky contacts of the 300 μm -long interdigital MSM-electrodes (inset of Fig. 8.5(a)) with width and spacing of 5 μm (Fig. 8.4(a)) were fabricated by photolithography and reactive dc-

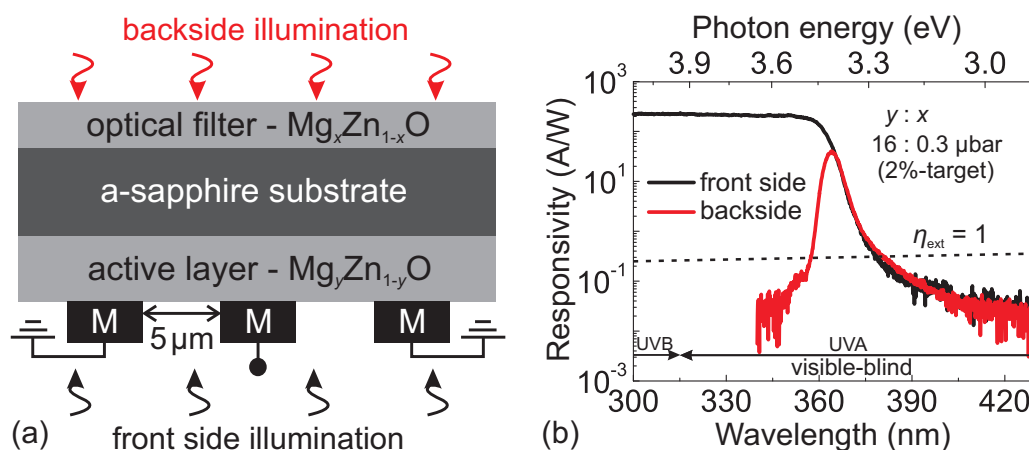


Figure 8.4: (a) Schematic layout of $\text{Mg}_y\text{Zn}_{1-y}\text{O}/\text{a-sapphire}/\text{Mg}_x\text{Zn}_{1-x}\text{O}$ -structure with different Mg-content ($y < x$) under illumination; (b) spectral responsivity of a visible-blind MSM-PD measured at 4 V bias with a $y : x$ -combination of 2%-target at 0.016 and 0.0003 mbar.

sputtering of palladium (Pd) in an Ar/O_2 -atmosphere [2] with a metallic Pd-capping layer, which was subsequently deposited in pure Ar [3].

Fig. 8.4(b) shows the spectral responsivity of a MSM-PD for an $y : x$ -combination, which was realized with a 2%-PLD-target but two different p_{O_2} of 0.016 and 0.0003 mbar, respectively. The black line is photo response under front side illumination. Within this configuration, the optical filter layer is inactive and the photo response extends to deep ultraviolet (UV) range by keeping a constant responsivity with a long-wavelength cut-off at 360 nm ($E_g = 3.45$ eV). The red line depicts the photo response under backside illumination with a maximum responsivity at 364 nm and the short-wavelength cut-off is due to absorption in the optical edge filter. It indicates that narrow bandwidths with very small FWHM of only 5 nm ($\Delta E_g = 48$ meV) in the present case can be achieved. The signal-to-ratio of the PD under front- and back-side are more than four and three orders of magnitude, respectively.

As obvious from Fig. 8.4(b), the responsivity of the sample exceeds the theoretical limit, depicted as dotted line of external quantum efficiency $\eta_{\text{ext}} = 1$ in the absorption regime and shows that an internal gain mechanism exists within the PD. Hence, the current-voltage (IV) characteristics of corresponding Schottky electrode for the MSM-PD in dark and under backside UV-illumination at the wavelength of maximum photo response were measured and are shown in Fig. 8.5(b). Upon 364 nm illumination, the reverse and forward current density increases by about a factor of three and one magnitude compared with that in dark, respectively. A decrease of the effective Schottky barrier height ($\Delta\Phi_{\text{Bn}} = 0.14$ V) is observed and it can be explained by minority carrier (holes) trapping [4] at $\text{PdO}_z/(\text{Mg,Zn})\text{O}$ -interface and causes the Schottky barrier height lowering under UV-illumination [1].

- [1] Z. P. Zhang, H. von Wenckstern, M. Schmidt and M. Grundmann: Appl. Phys. Lett. **99**, 083502 (2011), doi: 10.1063/1.3628338
- [2] A. Lajn, H. von Wenckstern, Z. Zhang, C. Czekalla, G. Biehne, J. Lenzner, H. Hochmuth, M. Lorenz, M. Grundmann, S. Wickert, C. Vogt, and R. Denecke: J. Vac. Sci. Technol. B. **27**, 1769 (2009), doi: 10.1116/1.3086718

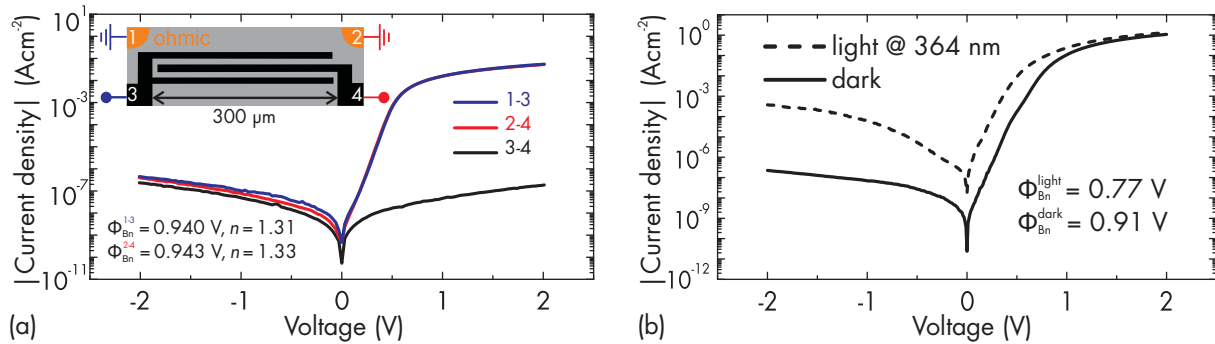


Figure 8.5: (a) A similar IV-characteristic of both high-quality Schottky electrodes of a MSM-PD (inset: top view of the MSM-structure with ohmic edge contact (orange color)) (b) IV-measurements of corresponding Schottky electrodes for the MSM-PD in dark and under back-side 364 nm-illumination.

- [3] H. von Wenckstern, Z. P. Zhang, M. Lorenz, C. Czekalla, H. Frenzel, A. Lajn, and M. Grundmann: Mater. Res. Soc. Symp. Proc. Vol. 1201, H04-02 (2010)
- [4] O. Katz, G. Bahir, and J. Salzman: Appl. Phys. Lett. **79**, 1417 (2001), doi: 10.1063/1.1394717

8.5 Tungsten trioxide as high- κ gate dielectric for highly transparent and temperature-stable zinc-oxide-based thin-film transistors

M. Lorenz, H. von Wenckstern, M. Grundmann,

Transparent electronics has become a key-word in today's research and development on electronic devices. Thin-film transistors (TFTs) are a fundamental switching element in electronic circuits and are constantly improved to higher switching speed, yet at lower feature size. High- κ gate dielectrics like HfO_2 or Al_2O_3 have a relative permittivity ϵ_r larger than that of silicon dioxide (SiO_2 , $\epsilon_r = 3.9$), which was commonly used in highly integrated circuits. The ongoing process of miniaturization demands smaller and smaller thickness of the gate dielectric, by which tunneling currents are inherently introduced, leakage currents increased and heat dissipation reached non-feasible limits. With the introduction of high- κ gate dielectrics the thickness of the insulator could be increased yet maintaining an equivalent oxide thickness similar to SiO_2 [1]. Transparent oxide semiconductors like zinc oxide (ZnO) are crucial for the overall performance of the device because of their higher values of the electron mobility compared to commonly used amorphous silicon. ZnO-based metal-insulator-semiconductor field-effect transistors (MISFETs) [2] and metal-semiconductor field-effect transistors [3] with excellent device characteristics have been reported. Tungsten oxide is currently used as part of electrochromic devices [4] and in pH-sensing ion-sensitive field-effect transistors [5]. But its potential as high- κ gate dielectric grown by pulsed-laser deposition (PLD) at room temperature for ZnO-based MISFETs [6] has not been reported, yet.

Tungsten oxide was deposited by PLD from a WO_3 target at different oxygen pressures p to tune the optical and electrical characteristics. Fig.8.6(a) depicts the specific resistance ρ vs. p . For $p < 0.03$ mbar highly conductive metallic WO_x ($x < 3$) with $\rho < 10^{-3} \Omega \text{ cm}$ is obtained. By increasing the growth pressure x increases towards $x = 3$ but the resulting layers are still non-stoichiometric and semiconducting, which was confirmed by temperature dependent Hall-effect measurements [6]. For $p \geq 0.1$ mbar highly insulating WO_3 with $\rho > 10^8 \Omega \text{ cm}$ is grown. It can be seen from the dashed line in Fig.8.6(a), that the average transmittance in the visible spectral range follows a similar trend: For pressures below 0.03 mbar very low values of transmittance are obtained. By increasing p the avg. transmittance increases before it saturates for $p > 0.07$ mbar to a value of about 88%. The quartz glass substrates used for the measurements has an avg. transmittance of 92.5%, thus absorption in the visible spectral range of WO_3 thin-films is negligible.

20 nm ZnO on Corning 1737 glass substrates were grown by PLD at 710°C and an oxygen pressure of $p = 3 \times 10^{-4}$ mbar. The Hall-effect mobility of these thin-films is typically about $5 \text{ cm}^2/\text{Vs}$ and the electron concentration $n_e \approx 6 \times 10^{18} \text{ cm}^{-3}$. By using standard photolithography and wet chemical etching, mesas were defined in order to inhibit cross talk between adjacent devices on the sample chip. Following this step the source and drain contacts consisting of gold were dc-sputtered in an Ar atmosphere using an Au target and subsequently patterned using lift-off technique. In the final step the gate was formed. Using PLD at room temperature and a pressure of $p = 0.2$ mbar about 150 nm WO_3 gate dielectric was grown followed by ZnO: 3% Al_2O_3 wt. being the gate electrode. Although the gate layer stack consists of the glass substrate, ZnO-channel, gate dielectric and the gate electrode the average transmittance in the visible spectral range is 86%. Fig. 8.6(b) depicts its transfer characteristics. Due to the 20 nm thick ZnO-channel and $n_e > 10^{18} \text{ cm}^{-3}$ the device is normally-on with a turn-on voltage $V_{\text{on}} = -1.4 \text{ V}$. The on/off-current ration of the drain-current is larger than 8 orders of magnitude with the off- and gate leakage current I_G being less than 1 pA. The subthreshold swing SS with a value of $SS = 80 \text{ mV/decade}$ is close to the thermodynamic limit of 60 mV/decade. The field-effect mobility $\mu_{\text{FE}} = 4.9 \text{ cm}^2/\text{Vs}$ is close the Hall-effect mobility. Both facts indicate a low defect density at the semiconductor-insulator interface. From quasi-static capacitance-voltage (QSCV) measurements the relative permittivity was calculated to be about 70. This gives rise to gate sweep voltages of only $\Delta V_{\text{SG}} \approx 2 \text{ V}$ necessary to turn the transistor from the on-state ($V_{\text{SG}} = 0.5 \text{ V}$) into the off-state ($V_{\text{SG}} = -1.5 \text{ V}$). Fig.8.6(c) depicts the transfer characteristics at elevated temperatures in order to test the temperature stability of the device. As can be seen from the figure the device remains fully operational up to temperatures of at least $T = 423^\circ\text{C}$, which marks the limit of the employed set-up. The lowering of the hysteresis is due to faster charging/discharging of defects at elevated temperatures. The inset depicts the subthreshold slope SS . For temperatures below 353 K (80°C) it remains constant at $SS = 80 \text{ mV/decade}$. For $T > 353 \text{ K}$ SS increases linearly as predicted by theory (solid line).

[1] G.D. Wilk, R.M. Wallace, J.M. Anthony: J. Appl. Phys. **89**, 5243 (2001)

[2] E. Fortunato, A. Pimentel, L. Pereira, A. Gonçalves, G. Lavareda, H. Águas, I. Ferreira, C.N. Carvalho, R. Martins: J. Non-cryst. Solids **338**, 806 (2004)

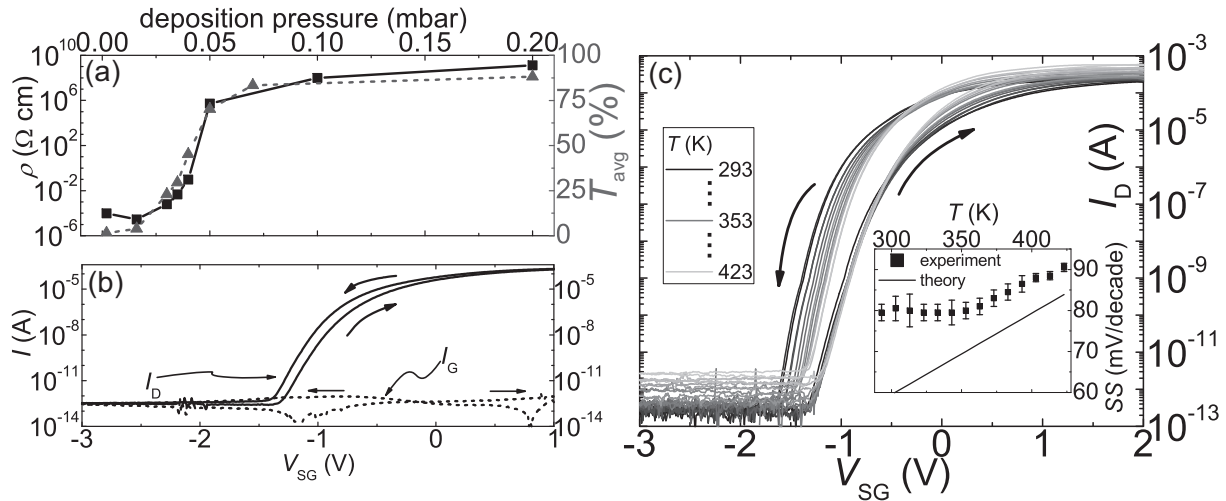


Figure 8.6: (a) Specific resistance ρ (solid - squared) and average transmittance in the visible spectral range (dashed - triangled) of tungsten oxide thin-films on quartz glass substrate vs. the deposition during PLD. (b) Transfer characteristic I_D and gate leakage current I_G of a ZnO-based MISFET with WO_3 gate dielectric on Corning 1737 glass substrate. The arrows indicate the sweeping direction starting at $V_{SG} = 2$ V. (c) Transfer characteristics at elevated temperatures from 293 K up to 423 K. The inset depicts the subthreshold slope SS vs. the temperature derived from the transfer curve.

- [3] M. Lorenz, A. Lajn, H. Frenzel, H. von Wenckstern, M. Grundmann, P. Barquínha, R. Martins, E. Fortunato: *Appl. Phys. Lett.* **97**, 243506 (2010)
- [4] G.A. Niklasson, C.G. Granqvist: *J. Mater. Chem.* **17**, 127 (2006)
- [5] J-C. Chou, J-L. Chiang, *Sensors and Actuators B* **62**, 81 (2000)
- [6] M. Lorenz, H. v. Wenckstern, M. Grundmann: *Adv. Mater.* **23**, 5383 (2011)

8.6 ZnO-based active multielectrode arrays for cells on chip measurements

F.J. Klüpfel, A. Lajn, S. Schmidt*, J.A. Käs*, H. von Wenckstern, M. Grundmann

*Soft Matter Physics Group

Multi-electrode arrays are a tool routinely used for the examination of signals in nerve cell networks. Besides the commercially available passive devices, the fabrication of silicon-based chips has been reported, which improve the lateral measurement resolution by far. However, the optical characterization of the cell network is restrained by the opacity of silicon [1]. Furthermore, the signal-to-noise ratio is rather bad, compared to the passive devices. We would like to apply oxide-based electronics in both active and transparent multi-electrode arrays. The wide range of materials and techniques reported in this field offers a multitude of possible approaches, which might also lead to an optimization of the signal-to-noise ratio of the devices.

We fabricated chips based on metal-semiconductor field-effect transistors with ZnO as channel material. A chip with the current layout can be seen in figure 8.7. We

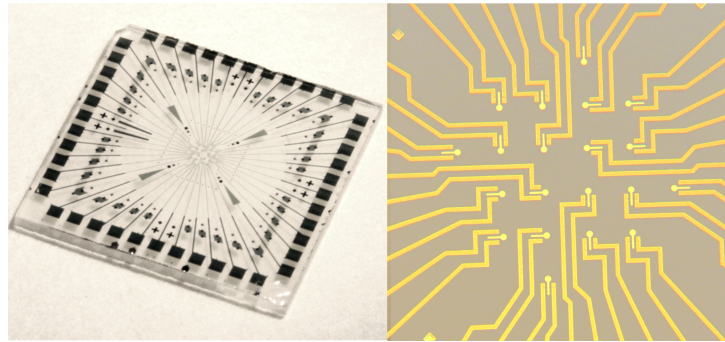


Figure 8.7: Photograph of a MEA chip (left side) and microscope image of the central area of the chip (right side). The chip is 10 mm x 10 mm large, the spacing between the electrodes is 200 μm .

evaluated the switching speed of these devices (see fig. 8.8) and paid special attention to the passivation layer of the chip. This layer insulates the electronics electrically and chemically from the electrolytic cell medium, in which the neurons are cultivated. However, the passivation can also influence the performance of the transistors by reacting with surface states of the channel material. The epoxy-based photo resist SU-8 is at the moment our best candidate for this layer, providing good insulation and even improving the transistor properties.

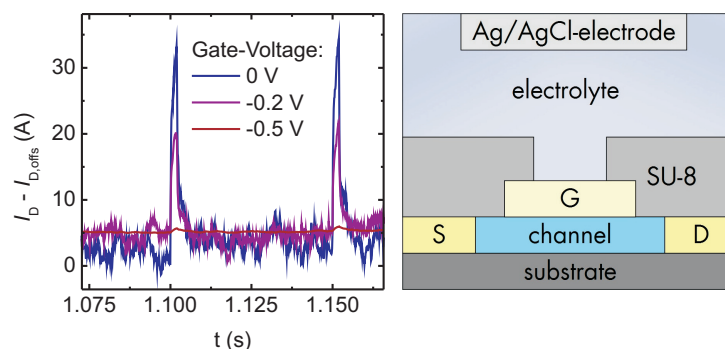


Figure 8.8: Test measurement of a MEA chip. Rectangular voltage pulses with a width of 2 ms and height of 8 mV were applied at the Ag/AgCl-electrode in an electrolyte (physiologic salt solution, see schematic drawing on the right side) and the modulation of the source-drain-current was measured.

Experiments proved so far, that the transistors can be switched by an Ag/AgCl-electrode in the electrolyte, and that pulses of few millivolts at the electrolyte modulate the source-drain-current (see figure 8.8). This provides the basis for the next important step namely the measurement of the action potential of actual neuronal cells.

[1] Fromherz et al., Solid-State Electronics, 52, 1364 (2008)

[2] Klüpfel et al., Journal of Applied Physics, 109, 074515 (2011)

8.7 Temperature-dependent investigations of high quality PdO_x/ZnO Schottky contacts on ZnO thin films

S. Müller, H. von Wenckstern, M. Grundmann

In the past decade zinc oxide (ZnO) as semiconductor was investigated with a renewed interest. The band gap of about 3.4 eV at room temperature makes ZnO a prime candidate for next generation UV-opto- and transparent microelectronics. Especially, in the scope of ZnO-based metal-semiconductor field effect transistors great advances were recently attained [1]. Therefore, Schottky contacts (SC) as key element of such unipolar devices were investigated with particular interest.

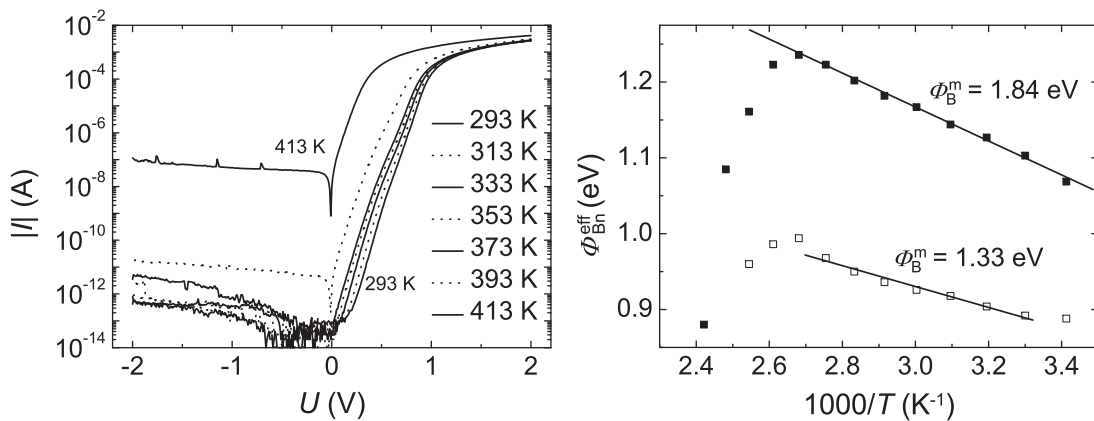


Figure 8.9: (a) Temperature-dependent Current-voltage characteristics of a high barrier height PdO_x/ZnO diode. (b) Effective barrier height of the low and high barrier region of the Schottky contact in dependence of $1000/T$.

Here, we present high quality SCs on ZnO thin films grown by pulsed laser deposition on *a* - plane sapphire substrates. The ZnO thin film consists of two different layer. First, a highly aluminum doped layer with a thickness of about 200 nm is deposited. This layer is used as ohmic back contact [2]. Afterward a nominally undoped ZnO thin film with a thickness of about 1 μm is grown. Both layers were deposited at a growth temperature of 650 °C and an oxygen partial pressure of 0.016 mbar. Circular SCs were defined by photolithography. The SCs were prepared by reactive DC-sputtering. We investigated various metal for the SCs, e.g. Au, Pd or Pt.

Figure 8.9 (a) shows the temperature-dependent current-voltage (I - V) characteristics of a selected PdO_x/ZnO SC. The I - V characteristics measured at temperatures between 293 K and 393 K exhibits two different slopes in forward direction. These slopes are caused by region exhibiting different barrier height. At low forward voltages the current transport is primarily through a small region with comparatively low barrier height. The low barrier regions are caused by incorporation of aluminum oxide particles in the thin film during the grown of the ohmic back contact layer or due to an inhomogeneous oxidation of the sputtered SC [4]. At backward voltages the measured current is near the noise level of the setup used. However, a current flow through small

shunts is visible in the I - V characteristics at temperatures below 383 K and reverse voltages higher than 0.5 V. At temperatures above 383 K the backward characteristic is only dominated by thermionic emission, which is indicated by the nearly voltage independent reverse current. The extracted characteristic contact parameters of the 293 K I - V characteristic impressively show the high quality of our SCs. With an effective barrier height of 1.07 eV, an ideality factor of 1.4 and an on/off ratio ($|I(2\text{ V})/I(-2\text{ V})|$) of 1.7×10^{10} . The properties of our SCs are similar or better than the best published SCs on ZnO single crystals and represent the best SCs on ZnO thin films.

The effective barrier height of the low and high barrier region is depicted in Fig. 8.9 (b) in dependence on the inverse temperature. The linear dependence of the effective barrier height on the inverse temperature indicates barrier height inhomogeneities with a lateral expansion in the range of several nm. The largest effective barrier height was determined at a temperature of 383 K to be 1.24 eV. At higher temperatures the effective barrier height decreases. This decrease is caused by a thermal degradation of the SC, which becomes irreversible if the diode is subjected to a temperature of 420 K or higher. A linear fit for the low and high barrier region yields a mean barrier height of 1.33 eV and 1.84 eV, respectively.

- [1] M. Grundmann, H. Frenzel, A. Lajn, F. Schein, and H. von Wenckstern, *Phys. Status Solidi A* **207**, 1437 (2010), doi:0.1002/pssa.200983771
- [2] H. von Wenckstern, G. Biehne, R. Abdel Rahman, H. Hochmuth, M. Lorenz, and M. Grundmann, *Appl. Phys. Lett.* **88**, 092102 (2006), doi:10.1063/1.1638898
- [3] M. W. Allen, X. Weng, J. M. Redwing, K. Sarpatwari, S. E. Mohney, H. von Wenckstern, M. Grundmann, and S. M. Durbin, *IEEE Transaction on Electron Devices*, **56**, 2160 (2009) doi:10.1109/TED.2009.2026393
- [4] S. Müller, H. von Wenckstern, O. Breitenstein, J. Lenzner, and M. Grundmann, *IEEE Transaction on Electron Devices*, **59**, 536 (2012), doi:10.1109/TED.2011.2177984

8.8 On the T2 deep-level in zinc oxide thin films

M. Schmidt, M. Ellguth, R. Karsthof, H. von Wenckstern, R. Pickenhain, M. Grundmann, G. Brauer*, F.C.C. Ling[†]

*Helmholtz-Zentrum Dresden-Rossendorf, Institut für Ionenstrahlphysik

[†]The University of Hong Kong, Department of Physics, People's Republic of China

Electronic defect states in the wide bandgap semiconductor zinc oxide (ZnO) are under investigation since the late 1940s. A set of deep-levels several hundred meV below the conduction band edge have been detected by space charge spectroscopic methods, e.g. deep-level transient spectroscopy (DLTS). In such experiments the temperature-dependence of the rate e_n^{th} with that charge carriers trapped by a deep-level are thermally emitted into the conduction band is measured. An Arrhenius representation of $e_n^{\text{th}}(T)$ is usually regarded as a fingerprint of a deep-level. From a linear fit of the data the thermal activation energy E_a (slope) and the high-temperature limit of the electron capture cross-section σ_n^{th} (offset) can be obtained. In fig. 8.10(a) $e_n^{\text{th}}(T)$ literature data of different deep-levels is plotted in Arrhenius representation. For the levels E3 and

E4 the plots look very systematic. In the upper right of the diagram the fingerprints of a set of differently labelled levels (L1, Cu_{Zn}, E2b, E280, Ecd1) is found (red lines) with no systematics on first glance. However, plotting E_a vs. σ_n^{th} of these levels reveals an exponential relation between these quanta fig. 8.10(c). This finding provoke the questions: Could the levels L1, Cu_{Zn}, E2b, E280 and Ecd1 be electronic states of one defect T2 with ambiguous $e_n^{\text{th}}(T)$ fingerprint? And if so, on which parameters do E_a and σ_n^{th} of T2 deep-level depend?

In this study we investigated a set of pulsed-laser deposited ZnO thin films on *a*-sapphire substrates which underwent different post-growth treatments by space charge spectroscopic methods. We demonstrated that T2 is generated by the implantation of zinc ions and subsequent thermal treatment of the sample [1]. Furthermore it was found that the T2 concentration in the ZnO thin films increased when the samples were annealed at temperatures above 950 K under lowered oxygen partial pressure [2]. Therefore, we draw the conclusion that T2 favourably forms under zinc-rich conditions. The T2 concentration in the samples was determined spatially resolved using the double DLTS technique or optical capacitance-voltage spectroscopy. In the differently treated samples the temperature dependence of e_n^{th} was measured by DLTS and E_a and σ_n^{th} , respectively, were obtained from an Arrhenius evaluation. We found that these quanta decrease with increasing T2 concentration in the sample, fig. 8.10(b). Please note that E_a drops by roughly 100 meV and σ_n^{th} by almost four orders of magnitude! E_a vs. σ_n^{th} obey an exponential relation similar to the one obtained for the literature data, in fig. 8.10(c). This strongly supports our hypothesis that L1, Cu_{Zn}, E2b, E280 and Ecd1 are identical to T2.

How can these results be explained? At first sight these experimental results suggest T2 to be an extended defect since the effect occurs for T2 concentrations where the mean space between these centres is roughly 60 nm such that an overlap of their electronic orbitals can be excluded for point defects. However, no relation between the net doping density of the sample and E_a and σ_n^{th} , respectively, was found. A more detailed look at its electronic properties also suggests T2 rather to be a point defect than an extended one. By optical DLTS the T2 photo-ionisation cross-section spectrum was measured [3]. Fitting the Chantre-Vincent-Bois model [4] to this data, the photon-energy for the photo-ionisation threshold was determined to $h\nu \approx 700$ meV and the extent of the electron wave function to 0.35 nm. In other words: the lattice in the vicinity of T2 is strongly distorted and the electron is tightly bound. This is further supported by the observed increase of e_n^{th} with increasing electric field strength which is typical for phonon-assisted tunnel-emission of electrons trapped by point defects.

Based on these experimental results we suggest the T2 defect to be a donor-acceptor pair where the donor is fixed and the acceptor is mobile along the ZnO *c*-axis, fig. 8.10(d). It is known that the presence of an acceptor in the vicinity of a donor lowers its binding energy. In contrast to the well-known donor-acceptor pair model, the mean donor-acceptor distance can not become arbitrarily small since the acceptor is immobile in crystal directions other than the *c*-axes. With increasing acceptor concentration, the mean donor-acceptor distance becomes smaller which explains qualitatively the observed dependence of E_a on the self-concentration of the defect.

[1] M. Schmidt, M. Ellguth, C. Czekalla, H. von Wenckstern, R. Pickenhain, M. Grund-

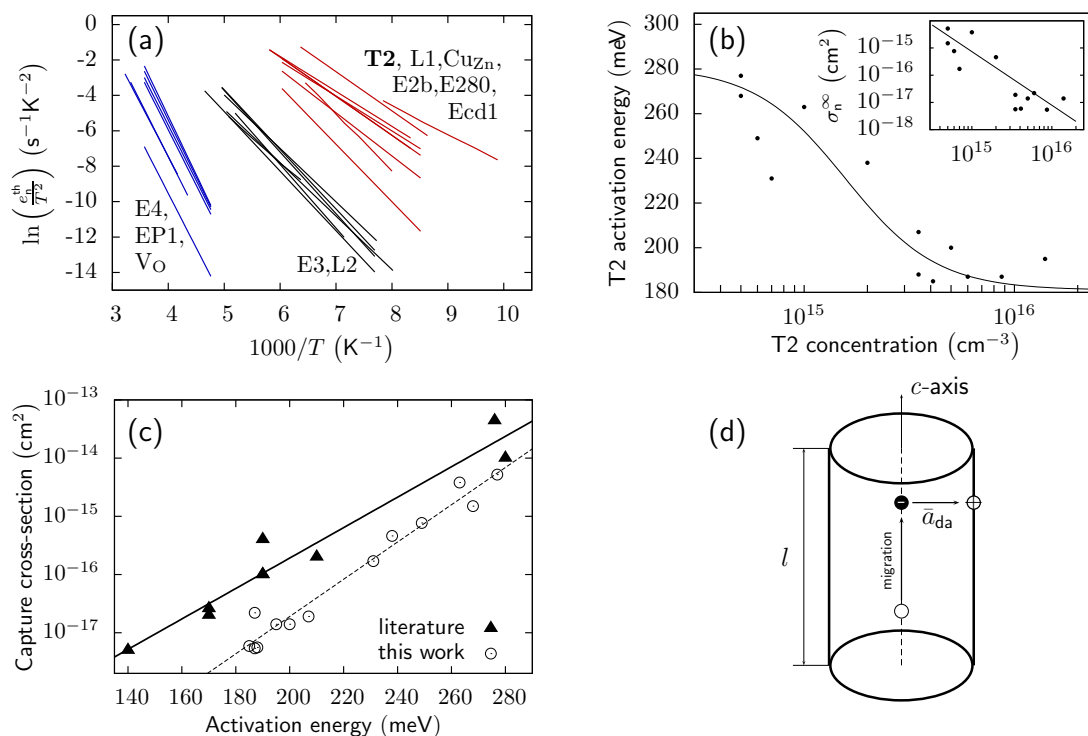


Figure 8.10: The T2 deep-level in ZnO thin films. (a) Literature data of $e_n^{\text{th}}(T)$ of different deep-levels in ZnO in Arrhenius representation. (b) Dependence of the thermal activation energy for the T2 ionisation in dependence of the T2 concentration in the sample. (c) Relation between E_a and σ_n^{th} . (d) Donor-acceptor pair model for T2. The acceptor is mobile in along the ZnO c -axis.

- mann, G. Brauer, W. Skorupa, M. Helm, Q. Gu, F.C.C. Ling, *J. Vac. Sci. Technol. B* **27** 1597-1560 (2009), doi: 10.1116/1.3086659
- [2] M. Schmidt, M. Ellguth, R. Karsthof, H. von Wenckstern, R. Pickenhain, M. Grundmann, G. Brauer, F.C.C. Ling, *Phys. Stat. Sol.(B)* **249** 588-595 (2012), doi: 10.1002/pssb.201147271
- [3] M. Ellguth, M. Schmidt, R. Pickenhain, H. von Wenckstern, M. Grundmann, *Phys. Stat. Sol.(B)* **248** 941-949 (2011), doi: 10.1002/pssb.201046244
- [4] A. Chantre, G. Vincent, D. Bois, *Phys. Rev. B* **23** 5335-5359 (1981), doi: 10.1103/PhysRevB.23.5335

8.9 Defect-studies on nickel-doped ZnO thin films

F. Schmidt, H. von Wenckstern, M. Schmidt, M. Grundmann

Zinc oxide has versatile properties for applications in electronics, optoelectronics, photovoltaics, and sensors. Doping of ZnO with various elements (e.g. Bi, Sb, Co, Mn, Ni, Cr) is a key requirement for enhancing and controlling its electrical and optical properties. Rare earth or transition metal cations are known to introduce electronic states in the band gap of semiconductors. Nickel in ZnO was investigated via optical methods like luminescence or optical absorption and reflection [1], but only few reports on

nickel related electronic defect states and the diffusion of nickel ions in the ZnO matrix exist [2].

The incorporation of nickel introduces an electron trap labelled TN1 and lying approximately 540 meV below the ZnO conduction band edge. This level was tentatively attributed to nickel on zinc lattice site [3]. We studied Ni-related carrier traps in pulsed laser-deposition (PLD) grown ZnO thin films and correlated the concentration of such defects with the concentration gradient of ZnO:Ni realized by diffusion.

ZnO thin films were grown on a 2"-wafer of *a*-plane sapphire by PLD at 650° C in an oxygen ambient of 0.016 mbar. An Al-doped ZnO layer served as highly conducting ohmic back-contact [7]. A thin film of nickel was thermally evaporated onto the surface and subsequent annealed under oxygen atmosphere. Schottky contacts with different distances to the edge of the evaporated nickel were realized by reactive direct-current sputtering of palladium followed by a metallic capping (sputtered palladium in pure argon) [5].

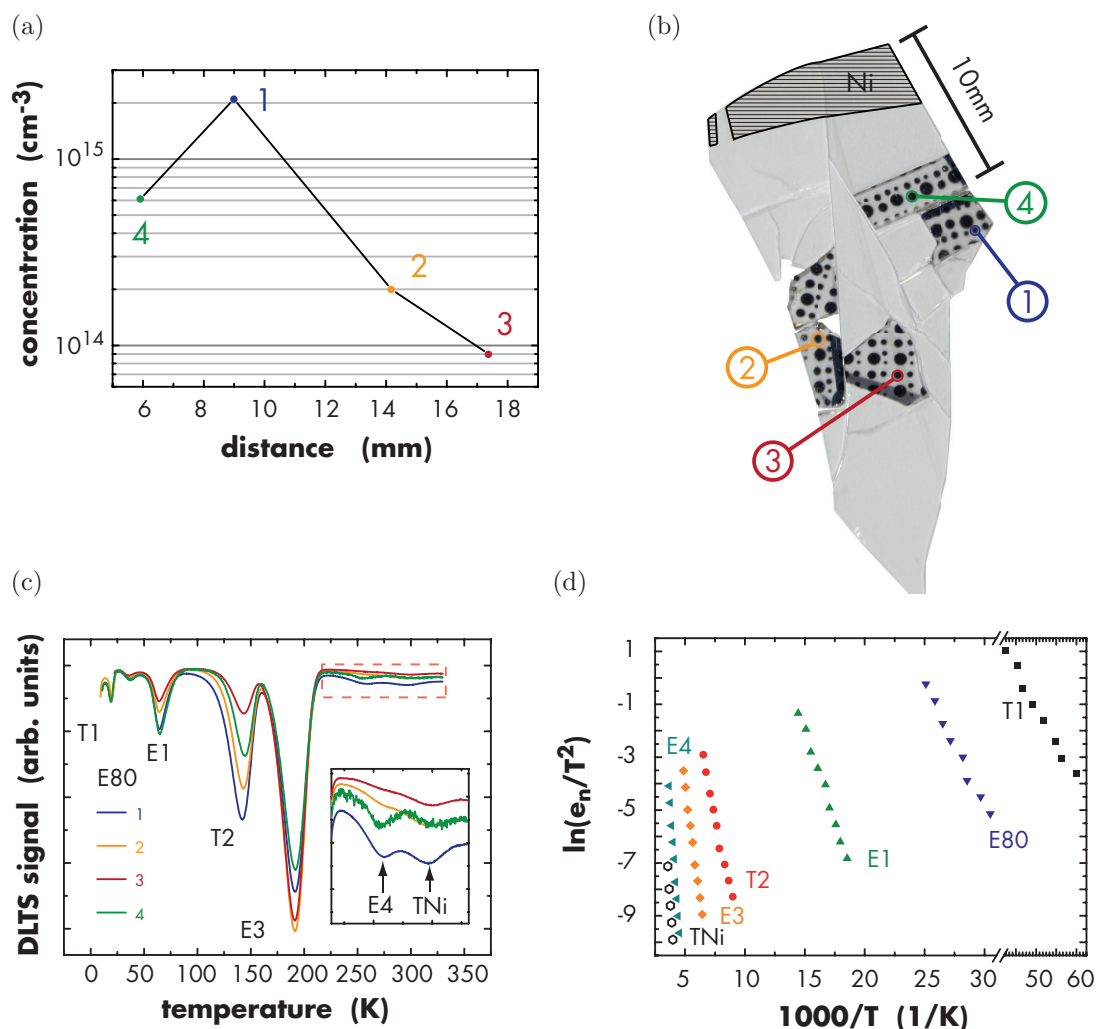


Figure 8.11: (a) Concentration of the defect level TNi over diffusion distance. (b) ZnO thin film sample, nickel was evaporated on the top edge of the sample. (c) DLTS scan for a ratewindow of $rw = 200$ Hz. The inset shows the DLTS peaks of E4 and the nickel trap TNi, respectively. (d) Arrhenius evaluation for all defect levels found in the sample.

Fig. 8.11 (a) shows the deep level transient spectroscopy (DLTS) measurement of all samples and therefore different nickel-concentrations. A rate window of $rw = 200$ Hz was used. The trap parameter were determined by an arrhenius evaluatuion, the arrhenius plot is shown in fig. 8.11 (d). The defect concentration was obtained from the peak height of the DLTS signal and are shown in fig. 8.11 (a).

The diffusion of nickel causes a lateral spread of the defect concentrations within the thin film (sample 1-3). In the vicinity of the edge of the evaporated Ni layer (sample 4, fig. 8.11 (b)) the incorporation of structural defects is the dominant influence. Furthermore the DLTS measurements revealed the electronic defect states T1 [6], T2 [7], E1 [8], E3 [8], E4 [8], an electron trap with a thermal activation energy of 80 meV (labeled E80) and the the nickel-related level TNi [3].

- [1] U. G. Kaufmann *et al.*, J. Phys. C 7, 791-806 (1974).
- [2] B. J. Wuesch *et al.*, J. Phys. Chem. Solids Vol. 55, 10:975-984 (1994).
- [3] M. Schmidt *et al.*, Phys. Status Solidi B 248, 1949-1955 (2011).
- [7] H. von Wenckstern *et al.*, Appl. Phys. Lett. 88 (9), 092102 (2006).
- [5] A. Lajn *et al.*, J. Vac. Sci. Technol. B 27 (3), 1769 (2009).
- [6] D. C. Look *et al.*, Phys. Rev. Lett. 82, 2552-2555 (1999).
- [7] M. Schmidt *et al.*, Phys. Status Solidi B 249, No. 3, 588-595 (2012).
- [8] F. D. Auret *et al.*, Appl. Phys. Lett. 80, 1340-1342 (2002).

8.10 Defect studies on 1.6 MeV proton-bombarded ZnO thin-films

F. Schmidt, H. von Wenckstern, M. Schmidt, M. Grundmann, P. J. Janse van Rensburg*, F. D. Auret*

*Physics Department, University of Pretoria, Lynnwood Road, Pretoria 0002, South Africa

Zinc oxide (ZnO) with its direct bandgap of $E_g = 3.37$ eV is a potential material for optoelectronic devices emitting in the near UV [1]. Radiation hardness makes ZnO a suitable material for sensor applications in outer space, hence a key requirement is the operation in a wide temperature range. ZnO withstands high energy particle radiation because of defect annealing at low temperatures. Reports on the generation of lattice defects at room temperature due to proton [2–4] and electron bombardment exist. In these studies mostly irradiations were performed at room-temperature, which in principle does not allow to study primary defects.

In one particular study it was shown that the deep-level defect E4 is introduced by proton bombardment [4] and is stable up to room-temperature. The defect was also found in ZnO thin films [5], a relation of E4 to the oxygen-vacancy was proposed [6] but studies on the generation of E4 in ZnO thin film samples are scarce. We studied the introduction of primary lattice-defects in ZnO thin-films by low-temperature ($T = 30$ K) proton bombardement and their annealing.

The thin films were grown on *a*-plane sapphire by pulsed laser deposition at 730°C in an oxygen ambient of 0.04 mbar. Highly conducting ohmic back-contacts were realised by a 200 nm thick Al-doped ZnO layer [7]. ZnO layers itself have a thickness of 1 μ m.

Evaporated palladium formed the Schottky contacts. Successive proton irradiations with doses between $1.2 \times 10^{12} \text{ cm}^2$ and $8.0 \times 10^{15} \text{ cm}^2$ were carried out at a van-de-Graff accelerator at the University of Pretoria.

The irradiation was carried out at $T = 30 \text{ K}$. During cool-down we measured the temperature-dependence of the capacitance, which is a measure for the net-doping density $N_d - N_a$ (curve 1 in fig. 8.12 (a)). There is no significant change in the net-doping density upon cooling. In contrast at 30 K a strong decrease of the net-doping density occurs after irradiation, which is due to the introduction of primary of defects leading to a higher degree of compensation (dashed line in fig. 8.12 (a)).

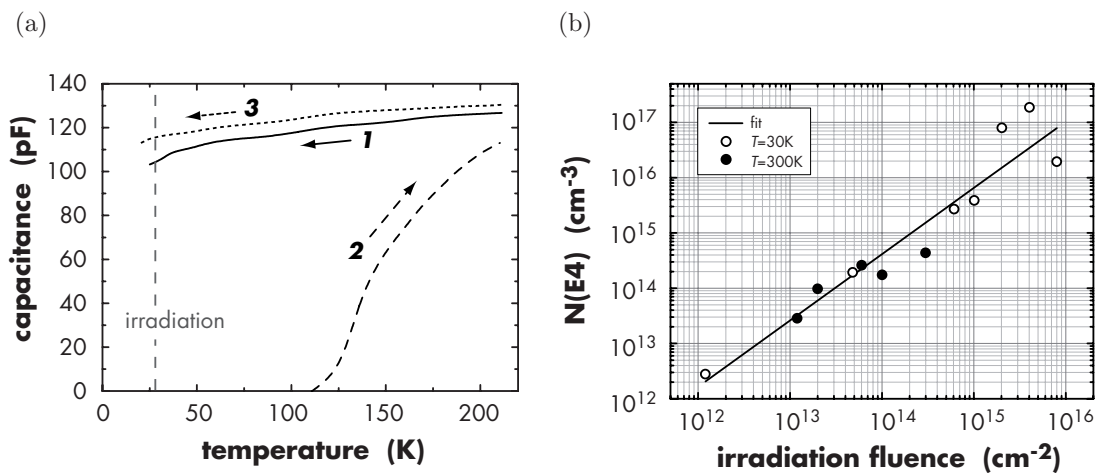


Figure 8.12: (a) Temperature-dependence of the capacitance (1) prior to irradiation starting from room-temperature, (2) after irradiation starting from 30 K, and (3) after irradiation downward ramping from room-temperature. (b) Concentration of the E4 defect versus proton irradiation dose. The full and empty circles represent data of samples irradiated at room-temperature and at $T = 30 \text{ K}$, respectively.

The following heat-up to room-temperature leads to an increase of the net-doping density again, indicating the anneal-out of a significant amount of the introduced defects (curve 2 in fig. 8.12 (a)). More precisely until approx. $T = 110 \text{ K}$ the sample is highly resistive, which is due to the high compensation and the resultant low carrier-concentration. Above 110 K the capacitance signal of the sample is due to the annealing process measurable again: the electron-concentration (capacitance) increases while the degree of compensation decreases.

A subsequent (second) downward ramping to 30 K has only minor influence on the net doping density (curve 3 in fig. 8.12 (a)) compared to reference sample (curve 1 in fig. 8.12 (a)).

Deep level transient spectroscopy (DLTS) was conducted using different rate windows in the range of $rw = 5 \text{ Hz}$ and 2000 Hz . The steady state reverse bias voltage was fixed at $V_r = -2.5 \text{ V}$ and a pulse voltage of $V_p = 3.0 \text{ V}$ was applied for $t_p = 1 \text{ ms}$ in order to inject majority carriers. We investigated the influence of low-temperature annealing on the concentrate of the E4 defect. Therefore we irradiated the sample at a temperature of 30 K and also at room temperature with doses between $1.2 \times 10^{12} \text{ cm}^2$ and $8.0 \times 10^{15} \text{ cm}^2$. Figure 8.12 (b) shows the concentration of E4 over the applied irradiation fluence for irradiations conducted at 30 K (solid circles) and room-temperature (empty circles). Both, the low-temperature irradiation as well as the room-temperature

irradiation yield almost the same introduction rate of the E4 defect of approximately 1 cm^{-1} . Hence, the generation of the E4 defect is similar for the investigated implantation temperatures and the defect is not annealed at low temperatures.

- [1] Ü. Özgür *et al.*, J. Appl. Phys. **98**, 041301 (2005).
- [2] A. Y. Polyakov *et al.*, J. Appl. Phys. **94**, 2895-2900 (2003).
- [3] T. Frank *et al.*, Appl. Phys. A **88**, 141 (2007).
- [4] F. D. Auret *et al.*, Appl. Phys. Lett. **79**, 3074-3076 (2001).
- [5] M. Ellguth *et al.*, Phys. Status Solidi B **248**, No. 4, 941-949 (2011).
- [6] C. G. Van de Walle *et al.*, Physica B, Condens. Matter **308-310**, 899-903 (2001).
- [7] H. von Wenckstern *et al.*, Applied Physics Letters **88** (9), 092102 (2006).

8.11 Extraction of the effective Richardson constant from Pd/ZnO Schottky contacts on ZnO thin film

S. Müller, H. von Wenckstern, M. Grundmann

The effective Richardson constant is a fundamental parameter that characterizes the current transport through Schottky contacts (SC) by thermionic emission. In the past several publications reported Richardson constants for zinc oxide (ZnO) [1, 2] which are significantly smaller than the expected theoretical value of $32 \text{ Acm}^{-2}\text{K}^{-2}$. Recently, Allen *et al.* reported a Richardson constant of $10 \text{ Acm}^{-2}\text{K}^{-2}$ [3], determined for silver oxide Schottky contacts on Zn-polar hydrothermal bulk ZnO being close to the theoretical value. This investigations were performed at nearly ideal Schottky contacts (ideality factor ≈ 1.1) with large effective barrier height of about 1.2 eV. This report exposed the necessity of a thermionic emission transport process over a homogeneous single Schottky barrier for an adequate determination of the effective Richardson constant. For zinc oxide thin films no reported value of the Richardson constant is close to the theoretical value so far.

For this study we used ZnO thin films grown on a ZnO:Al buffer on $10 \times 10 \text{ mm}^2$

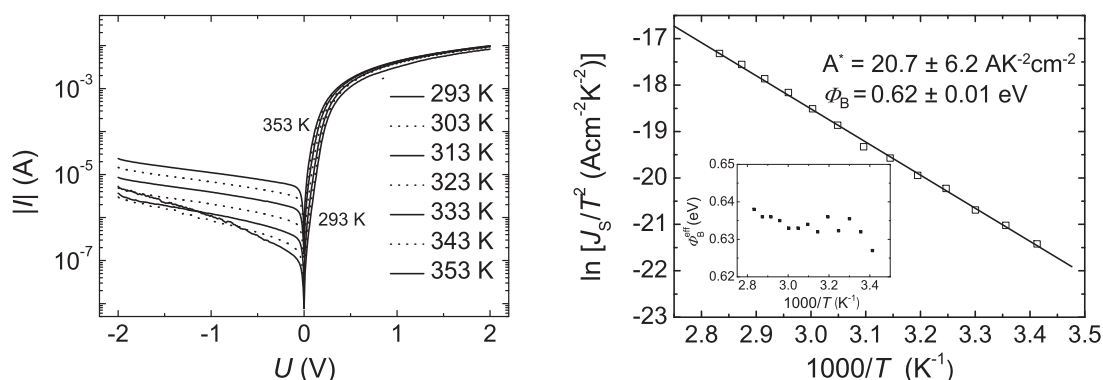


Figure 8.13: (a) Temperature-dependent current-voltage characteristics of a Pd/ZnO diode. (b) Richardson plot of $\ln(J_S/T^2)$ vs $1000/T$. The solid line indicates a linear fit, which yields the Richardson constant of the semiconductor and the mean barrier height of the Schottky contact. The inset depicts the effective barrier height of the Schottky contact in dependence of $1000/T$.

a-plane sapphire wafer by pulsed-laser deposition. On the nominally undoped ZnO layer Schottky contacts were fabricated by thermal evaporation of Pd on the as-grown surface. In Fig. 8.13 (a) the current-voltage (IV)-characteristics of a selected Pd/ZnO Schottky contact in a temperature range between 293 K and 353 K are depicted. The characteristics show a homogeneous increase of the forward and backward current, respectively, which is explainable by thermionic emission theory. The extracted ideality factors of 1.1 ± 0.01 are nearly temperature independent within the deployed temperature range. Due to the high crystalline quality of the ZnO thin film and the in principle laterally homogeneous Schottky barrier potential the ideality factor is close to the limit of 1.03 determined by image force lowering. The temperature dependence of the effective barrier height vs the inverse temperature is depicted in the inset of Fig. 8.13 (b). The nearly temperature independent behavior clarifies the homogeneous barrier height distribution, as well. The Richardson plot of $\ln(J_s/T^2)$ vs $1000/T$ in Fig. 1b was constructed by using the saturation current density obtained from fitting the forward current in the regions of the exponential thermionic emission regime at small forward voltages. A linear fit of the Richardson plot provides a Richardson constant of $(20.7 \pm 6.2) \text{ A cm}^{-2} \text{ K}^{-2}$ and a mean barrier height of $(0.62 \pm 0.01) \text{ eV}$. The extracted Richardson constant is up to now the closest to the theoretical value for ZnO thin films and the mean barrier height coincides very well with determined effective barrier height substantiating the high homogeneities of the Schottky barrier.

- [1] H. Sheng, S. Muthukumar, N. W. Emanetoglu, and Y. Lu, *Appl. Phys. Lett.* **80**, 2132 (2002), doi:10.1063/1.1463700
- [2] H. von Wenckstern, G. Biehne, R. Abdel Rahman, H. Hochmuth, M. Lorenz, and M. Grundmann, *Appl. Phys. Lett.* **88**, 092102 (2006), doi:10.1063/1.1638898
- [3] M. W. Allen, X. Weng, J. M. Redwing, K. Sarpatwari, S. E. Mohny, H. von Wenckstern, M. Grundmann, and S. M. Durbin, *IEEE Transaction on Electron Devices*, **56** 2160 (2009), doi:10.1109/TED.2009.2026393

8.12 Exciton-Polaritons in ZnO-based microcavities – macroscopic quantum states and pseudo-spin polarization

R. Schmidt-Grund, H. Franke, S. Linke, C. Sturm, S. Richter, and M. Grundmann

Exciton-polaritons are quasi-particles with bosonic character arising from the strong coupling of excitons with photons in a microcavity (MC). As composite quasi-particles, they combine properties of both constituents. On the one hand, long-range interaction is mediated by the photonic component, allowing, along with the low mass of these particles, wavefunction synchronisation, quantum mechanical entanglement, and condensation in a quantum mechanical coherent state, a so called dynamic Bose-Einstein condensate (BEC), at very low particle densities and high temperature - for ZnO predicted above room temperature. Such BECs in MC can go along with interesting phenomena like lasing or superfluidity, providing the possibility for information transport. On the other hand, the excitonic part provides properties of electronic systems like

magnetic moments or in general spin, allowing information storage or manipulation. So, combining all of these properties, exciton-polariton systems in MC can be used for quantum information technology as well as for low-power sources of coherent or entangled light. We report on the observation of BEC of exciton-polaritons in a ZnO-based MC, discuss its propagation properties (sec. 8.12.1), and show interesting results concerning their so called pseudo-spin properties (sec. 8.12.2).

The MCs under investigation consist of a ZnO bulk cavity as active medium, with an optical thickness of about half a medium wavelength, that is sandwiched between two all-oxide Bragg reflectors (BR). Yttria stabilised zirconia and Al_2O_3 are used as BR materials. The samples are grown by means of pulsed laser deposition (PLD) typically at temperatures of (150–650) °C and an oxygen background pressure of (0.02–0.002) mbar on *c*-sapphire substrates. The cavity layer is wedge-shaped, enabling to change the photonic mode properties simply by varying the position on the sample. More information on the general properties of the samples and the experimental techniques used can be found elsewhere [1–4].

8.12.1 Propagating Bose-Einstein condensates

We have observed macroscopically coherent states of exciton-polaritons up to 250K [5]. Excitation power dependent photoluminescence investigations reveal the typical threshold behaviour of polariton condensation for negative detunings, as shown in figures 8.14a and b for the temperature $T = 130$ K and a detuning of $\Delta \approx -40$ meV. Below a threshold power density of $P_0 \approx 37$ W/cm² the dispersion of the lower polariton branch (LPB) is observed, which is characteristic for the strong coupling regime. The emission of the upper polariton branch is self-absorbed in the ZnO-cavity layer [1, 6]. Above threshold, a non-linear increase of the emission intensity is observed. The FWHM of the emission decreases more than one order of magnitude at threshold and then slightly increases as a function of pump power. Also the expected blue-shift in energy is observed (figure 8.14c).

For positive detunings no condensation occurred but the emission from an electron-hole plasma was detected, which is the standard gain mechanism for lasing in ZnO [7]. The observed dispersionless lines can be explained by 3D photonic confinement, where the grains in the cavity layer provide additional confinement.

The most striking feature in all of our Fourier images - showing a condensate - is, that at threshold the condensate energy exhibits an exceptionally large blue-shift of several ten meV with respect to the dispersion minimum of the LPB. This indicates the presence of large repulsive interaction potentials in our MC. At low temperatures, where the propagation length is long enough (up to several μm) - this leads to a ballistic propagation of the condensate. Therefore, these MC are promising candidates for applications based on polariton transport like polariton neurons [8].

8.12.2 Pseudo-spin polarization

The pseudo-spin of exciton-polaritons directly corresponds to the polarization of the photons emitted out of the MC by their radiative decay [9]. Therefore, the Stokes vector

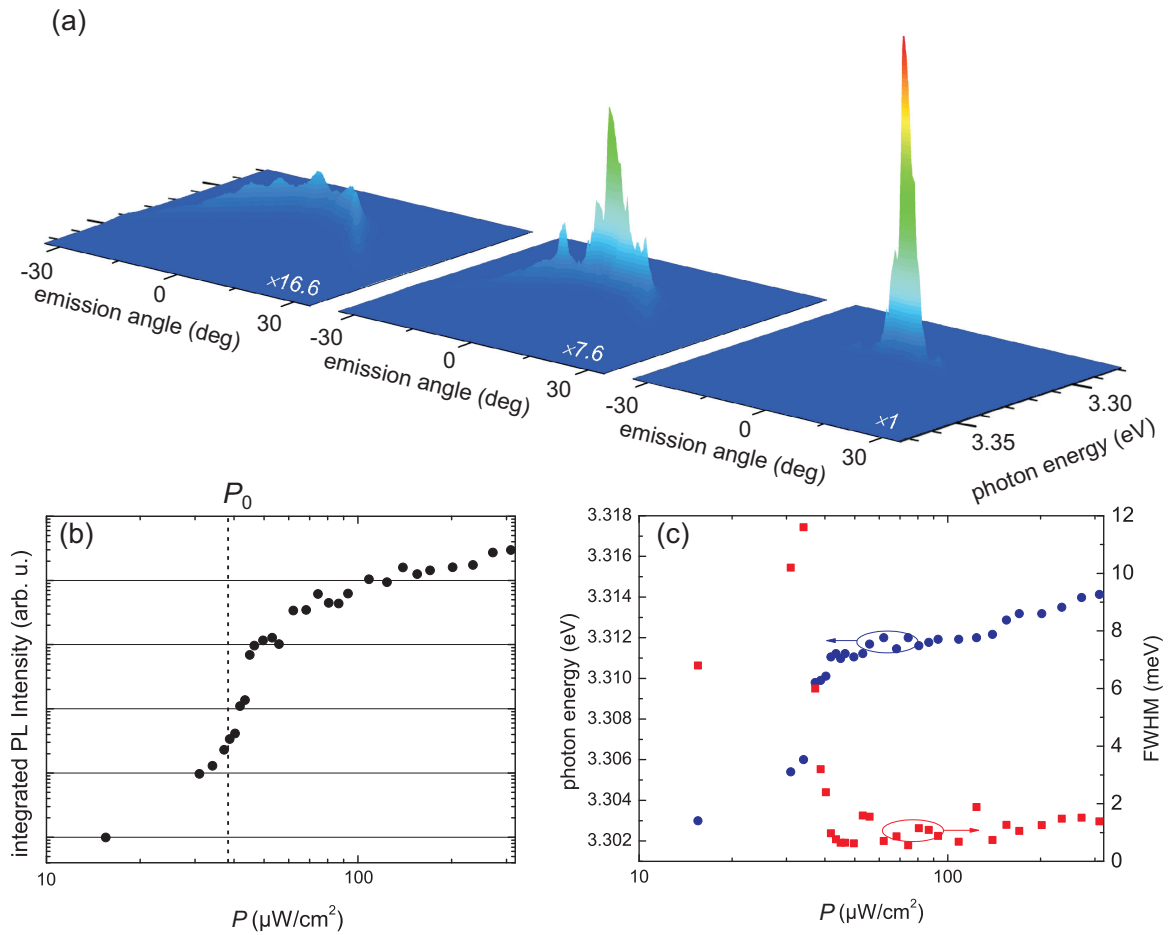


Figure 8.14: (a) From left to right: Fourier images in a linear color scale below ($P = 0.4P_0$), slightly ($P = 1.1P_0$) and clearly ($P = 1.25P_0$) above threshold for $T = 130$ K and a detuning of $\Delta \approx -40$ meV with $P_0 = 37$ W/cm² showing the strong increase in photoluminescence intensity and the peak narrowing of the condensate emission. The scaling factors are indicated in the figures. (b) Integrated intensity of the condensate and (c) corresponding blueshift of the emission energy and FWHM of the emission. The cavity mode energy is $E_{\text{Cav}}(k_{\parallel} = 0) = 3.325$ eV and the exciton energy is $E_X = 3.365$ eV.

of the emitted photons contains all information of the respective polariton pseudo-spin orientation. The Stokes vector components related to the linear polarization under non-resonant excitation and the occupation of the two orthogonal linear polarized eigenmodes (transversal electric - TE and transversal magnetic - TM) of the LPB with exciton-polaritons has already been investigated previously [2, 4]. Here we present the complete Stokes vector for certain temperatures between 10 K and 290 K, with focus on the components related to the circular polarization.

For determination of the Stokes vector components or rather the polarization state of the emission from the two (TE-polarized and TM-polarized) exciton-polariton modes, we developed a measurement procedure using different angular positions of a compensator and analyzer. The developed data analysis method takes care of incoherent contributions of the TE- and TM-modes and yield precise results even for a low degree of the circular polarization.

The dispersion behaviour of the LPB for $\Delta \approx -90$ meV at $T = 10$ K is shown in Fig. 8.15a. We observe a large TE-TM splitting of about 10 meV between both polariton modes. With increasing Δ towards less negative values this splitting gets smaller due to the decreasing photonic fraction of the LPB (Fig. 8.15b). Figure 8.15d shows the circular polarization degree (expressed by S_3/S_0) of the LPB at the energetic position of the TE-mode. A clear increase of the degree of circular polarization for increasing emission angle is obvious, similarly to the behaviour of the TE-TM splitting. The angle corresponding to the maximum degree of polarization is also similar to that of the maximum TE-TM splitting. For the TM-mode, a similar behaviour was observed but with opposite sign of the circular polarization. With increasing Δ and increasing temperature the degree of circular polarization gets smaller and almost vanishes at room temperature.

For an explanation of the observations we propose the following hypothesis: One has to consider that the TE-TM splitting causes an effective in-plane magnetic field [10], which can be understood like an inversion of the Zeeman effect. Further, the TE- and TM-polarization can be interpreted as a superposition of left and right circular polarization, differing only in a phase term that results in different pseudo-spin orientations. Connecting the circular polarized components to the up and down pseudo-spin components of the polaritons, two processes can be considered to cause the observed excess circular polarization. As the pseudo-spin expresses real excitonic angular momenta, the effective magnetic field can cause its precession. This would cause a change of the polarization of the emitted light and so break the balance between the left and right circular components of the linear polarized TE and TM states, yielding an excess of circular polarization. On the other hand, one can conclude that in presence of the effective magnetic field, analogue to the Zeeman effect, the energy levels split. Hence, the pairs of Zeeman-like energy levels should be occupied (or partially occupied, influenced by the polariton mode dispersion) with excess spin-up and spin-down polaritons, also yielding a finite and opposite degree of circular polarization of the emission from the two polariton eigenmodes. As the effective magnetic field scales with the amount of the TE-TM splitting and as this is solely determined by the properties of the photonic mode, the observed temperature and detuning evolution can be understood considering one or both of these processes.

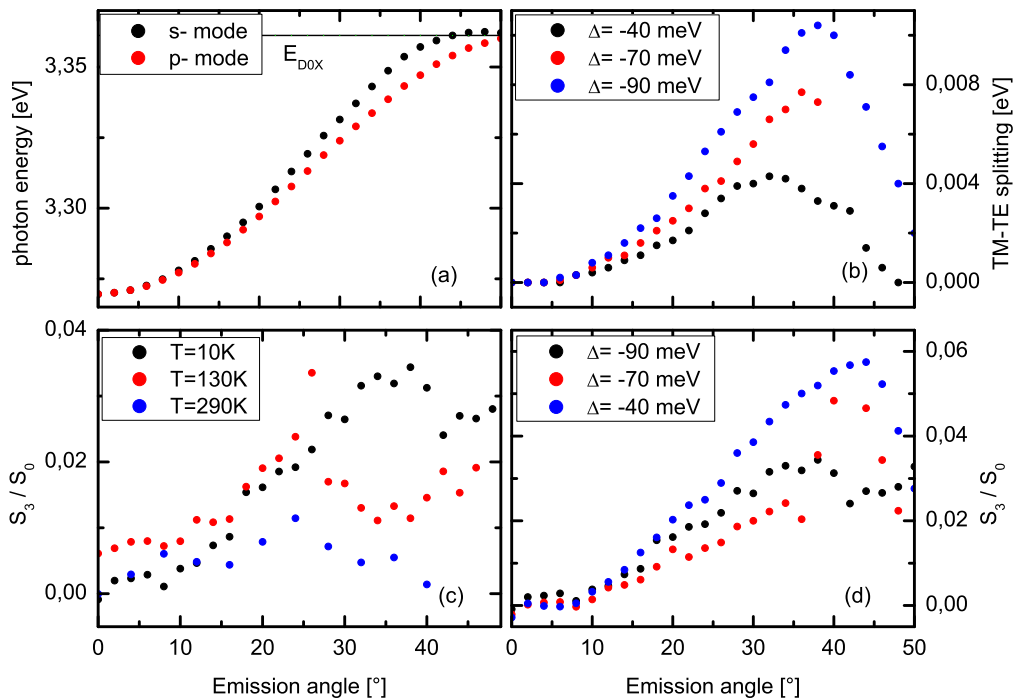


Figure 8.15: (a) Dispersion of the LPB at $T = 10$ K and $\Delta = -90$ meV for the s and p polarization. (b) TE-TM splitting for different Δ . (c) Degree of circular polarization with $\Delta = -40$ meV at different temperatures. (d) Degree of circular polarization at $T = 10$ K for different detuning Δ . All in dependence on the emission angle

(2009).

- [2] C. Sturm, H. Hilmer, R. Schmidt-Grund, and M. Grundmann, *New J. Phys.* **13**, 033014, (2011).
- [3] C. Sturm, H. Hilmer, B. Rheinländer, R. Schmidt-Grund and M. Grundmann, *Phys. Rev. B* **83**, 205301 (2011).
- [4] C. Sturm, H. Hilmer, B. Rheinländer, R. Schmidt-Grund and M. Grundmann, in *The Physics Institutes of Universität Leipzig, Report 2010*, M. Grundmann (Ed.), pp. 179, Leipzig, 2011.
- [5] H. Franke, C. Sturm, R. Schmidt-Grund and M. Grundmann, *New J. Phys.* **14**, 013037 (2012).
- [6] S. Faure, T. Guillet, P. Lefebvre, T. Bretagnon and B. Gil, *Phys. Rev. B* **78**, 235323 (2008).
- [7] C. Klingshirn, *phys. stat. sol. b* **244**, 3027 (2007).
- [8] T.C.H. Liew, I.A. Shelykh and G. Malpuech, *Physica E* **43**, 1543 (2011).
- [9] R. I. Dzhioev, H. M. Gibbs, E. L. Ivchenko, G. Khitrova, V. L. Korenev, M. N. Tkachuk, and B. P. Zakharchenya, *Phys. Rev. B* **56**, 13405 (1997).
- [10] A. Kavokin, G. Malpuech, and M. Glazov, *Phys. Rev. Lett.* **95**, 136601 (2005).

8.13 Whispering gallery modes in irregular and inhomogeneous hexagonal resonators

C.P. Dietrich, M. Lange, C. Sturm, M. Stölzel, R. Schmidt-Grund, M. Grundmann

The investigation of light emitters has become one of the most prominent fields of research in the last two decades due to the increasing demand for photonic and optoelectronic devices. Small optical resonators are the centerpiece of these technical applications whose efficient operation requires low lasing thresholds of the resonator eigenmodes. The presence of distinct cavity signatures is thereby strongly correlated to the resonator morphology. In the following, we will focus on dielectric resonators with hexagonal cross section to illustrate the effects that occur when the resonator shape changes from a regular polygon to irregular or inhomogeneous polygons.

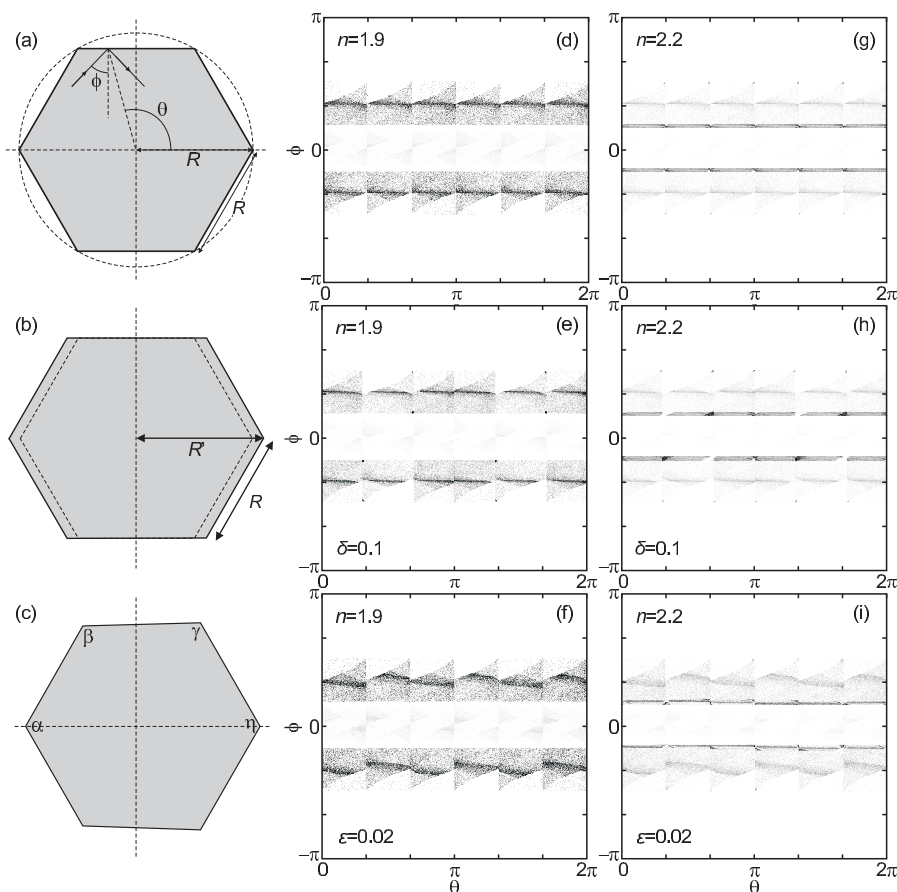


Figure 8.16: (a-c) Cross sections of regular (a), elongated (b) and deformed (c) hexagonal resonators. (d-i) Poincaré SOS of a regular resonator (d,g), an elongated resonator with $R' = R(1+\delta)$ and $\delta = 0.1$ (e,h), and a deformed resonator with $\epsilon = 0.02$ (f,i). The refractive index is $n = 1.9$ in (d-f) and 2.2 in (g-i).

Experimentally, it has been shown that ZnO microwires naturally embody dielectric hexagonal resonators by exhibiting whispering gallery mode (WGM) signatures in luminescence spectra[1]. Besides, we were able to demonstrate that ZnO microwires even maintain their cavity properties when their cross section (i) is deformed by bending[2],

(ii) is elongated[3] (see section 8.13.1) or (iii) has a varying dielectric landscape by the incorporation of heterointerfaces[4] (see section 8.13.2). Subsequently, regular, deformed and elongated hexagons have been theoretically examined in terms of their capability to exhibit WGM. Therefore, Poincaré section of surfaces (SOS) were calculated and can be seen in Fig.8.16. The deformation is parameterized by the strain ε (see Fig.8.16g), the elongation by δ with $R' = R(1 + \delta)$ (see Fig.8.17d). The effect of inhomogeneity is elaborated by the change of the refractive index n .

The Poincaré SOS for $n = 1.9$ in (d-f) show intensity maxima at $\pm 2\pi/3$ that can be attributed to WGM with hexagonal optical pathway. The intensity of these modes is lowered in (e) indicating an absence of WGM in elongated hexagons (compare with section 8.13.1). Further, the signature of hexagonal WGM is broadened but clearly visible in an deformed hexagon. This is surprising since deformed hexagons theoretically do not provide closed loops for hexagonal modes[5]. Increasing the refractive index to $n = 2.2$ additionally visualizes cavity modes with angle of incidence $\phi = \pm\pi/3$. These modes are triangular WGM and are absent for $n = 1.9$ due to a limiting angle for total internal reflection above $\pi/3$ in that case. However, triangular WGM are most clearly detectable in the regular hexagon but loose intensity in elongated and deformed hexagons.

8.13.1 The elongated hexagon: one- and two-dimensional cavity modes in ZnO microwires

ZnO microwires were grown by carbothermal vapor-phase transport[6]. We show that the change of the resonator cross section from regular hexagonal to elongated hexagonal leads to a transition from two-dimensional WGM to one-dimensional Fabry-Pérot modes (FPM)[2].

Fig.8.16 shows SEM pictures of ZnO microwires that either exhibit a regular hexagonal (a) or irregular (elongated) hexagonal (b) cross section. We propose, that the irregular elongated cross section occurs due to inhomogeneous material supply during the highly random growth process. Angular-resolved, TE polarized PL scans of an irregular (top row) and a regular (bottom row) ZnO microwire can be seen in Fig.8.16e and show spectral modulations that can be assigned to cavity modes inside the microwires. The cavity modes blueshift with increasing emission angle due to photonic dispersions that indicate spatial confinement in the direction of measurement. Since cavity modes in the elongated microwire show dispersion curves in both directions - parallel and perpendicular to the wire axis - they are of one-dimensional character, i.e. FPM. In contrast to that, cavity modes in a regular hexagon only show a dispersion parallel to the wire axis, thus propagate in the cross section plane and are of two-dimensional character, i.e. WGM.

The absence of WGM in an elongated hexagon can be explained by the loss of the hexagonal symmetry in this case. However, the absence of FPM in a regular microwire such as Fig.8.16a is not directly correlated to the morphology but more to the microwire diameter which is only $2.6 \mu\text{m}$ for the bottom scan but $12.2 \mu\text{m}$ for the top scan. FPM experience large optical losses with every reflection in contrast to WGM that are totally reflected. Increasing the wire diameter reduces the number of reflections in a given time period but also reduces the optical losses and subsequently increases the probability to observe FPM.

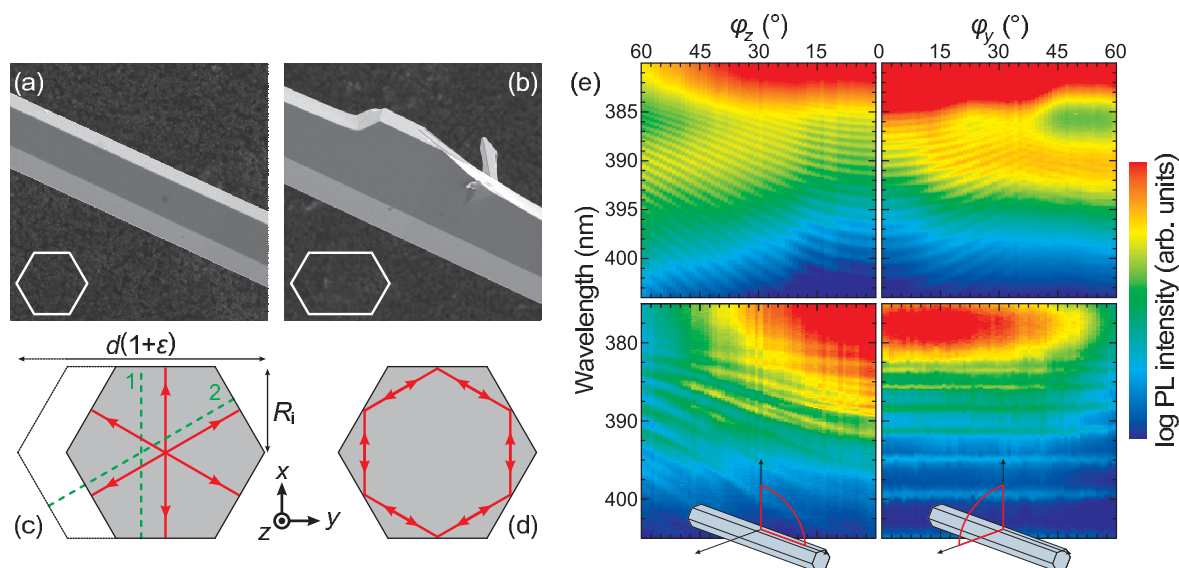


Figure 8.17: (a,b) SEM pictures of ZnO microwires with (a) $d = 8.9\mu\text{m}$ and (b) $16.1\mu\text{m}$. (c,d) Optical pathways of (c) FPM and (d) WGM inside a regular (gray) hexagon. Hexagons are parametrized by their diameter $d(1+\epsilon)$ and inner radius R_i , where $\epsilon \neq 0$ represents an elongated hexagon and $\epsilon = 0$ represents a regular hexagon. 1 and 2 denote possible FPM pathways in an elongated hexagon. (e) Angular-resolved, TE-polarized PL spectra at room temperature for the angles ϕ_z (left) and ϕ_y (right) of a tapered ZnO microwire. Spectra were recorded at positions with $d = 12.2\mu\text{m}$, $\delta = 0.37$ (top) and $2.6\mu\text{m}$ (bottom).

8.13.2 The inhomogeneous hexagon: microwire quantum well heterostructures

The majority of modern semiconductor technologies is grounded on the successful integration of heterointerfaces and the subsequent miniaturization of the building blocks. Also recent concepts such as exciton-polariton lasers that provide the possibility to emit light under ultra-low lasing thresholds require the implementation of quantum wells (QW) or quantum dots into the laser structure and are most likely fabricated in pillar-like structures[7].

However, most material systems (e.g. GaAs) suffer from the fact that excitons are absent at room temperature due to insufficient exciton stability. This can be overcome by using ZnO-based heterostructures that exhibit stable excitons up to temperatures above 1000°C . According to that, we present the first successful fabrication of radial ZnO microwire quantum well heterostructures that offer the unique opportunity to couple spatially and spectrally confined whispering gallery modes (WGM) with QW excitons on the pathway towards possible polariton lasing. Thereby, heterostructures were obtained that either emit above or below the ZnO bandgap by using ZnO or (Zn,Cd)O QWs in (Mg,Zn)O barriers, respectively.

Pure microwires were transferred onto the edges of sapphire substrates in a fashion that their main part protrudes over the substrate edge while their bottom part was attached to the substrate (see Fig.8.17b) in order to ensure an optimal heat transfer from substrate to wire during the coating which has been carried out by pulsed-laser deposition. Subsequently, the upper part of the microwire is freestanding and can

homogeneously be deposited on all side facets - exemplarily shown in Fig.8.17a. CL spectra of coated ZnO microwires can be seen in Fig.8.17c for (Mg,Zn)O/ZnO and Fig.8.17d for ZnO/(Zn,Cd)O heterostructures. All heterostructures were grown along non-polar crystal directions that inhibits possible effects due to internal electrical fields.

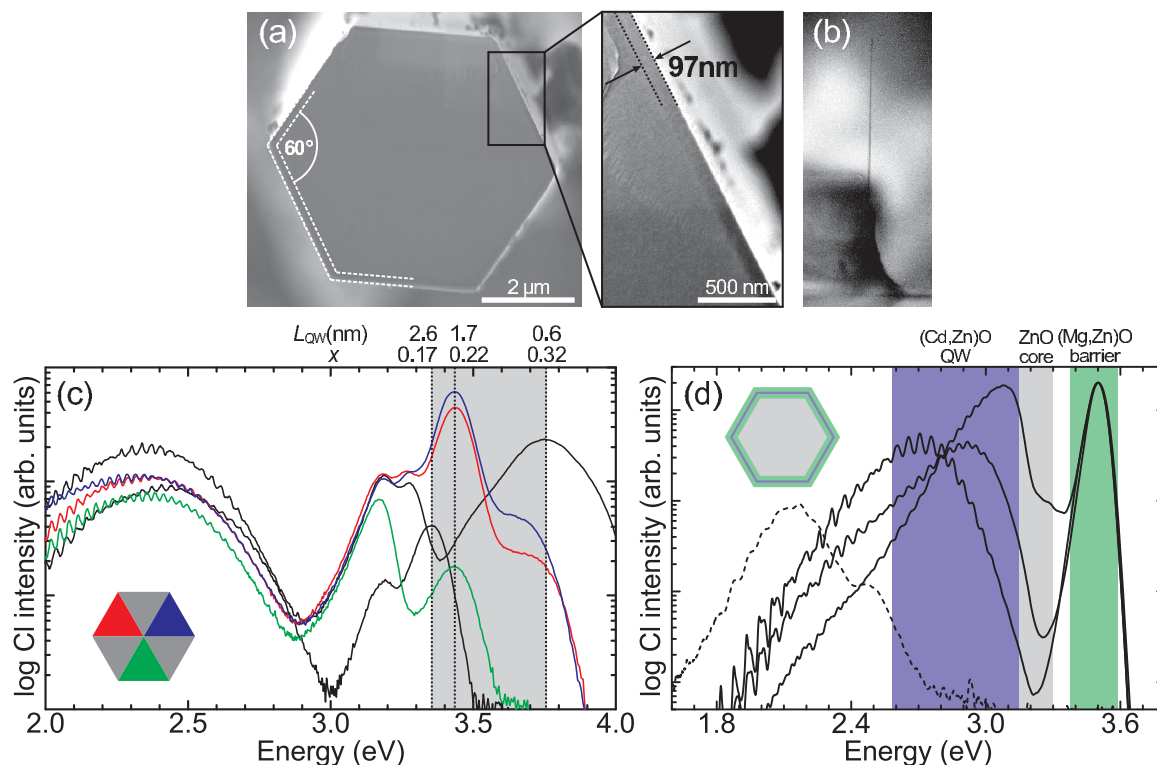


Figure 8.18: (a) SEM pictures in cross-sectional view of a ZnO microwire coated with a $\text{Mg}_{0.17}\text{Zn}_{0.83}\text{O}/\text{ZnO}/\text{Mg}_{0.17}\text{Zn}_{0.83}\text{O}$ shell. The overall shell thickness is 97 nm. (b) Optical image of a coated ZnO microwire stuck with its bottom part to the substrate edge. (c) RT-CL spectra of a coated ZnO microwire recorded at three different wire facets as indicated in the sketch, together with spectra from microwires with maximum and minimum QW energy. Respective well thicknesses L_{QW} and barrier compositions x are given above. The shadowed area highlights the possible QW emission energy range for our (Mg,Zn)O/ZnO heterostructures. (d) RT-CL spectra of ZnO microwires surrounded by either a multi-layer system containing $\text{Zn}_{0.76}\text{Cd}_{0.24}\text{O}$ QWs with different thicknesses (ranging from 0.8 to 2.1 nm) in $\text{Mg}_{0.15}\text{Zn}_{0.85}\text{O}$ barriers (solid lines) or by a single layer $\text{Zn}_{0.75}\text{Cd}_{0.25}\text{O}$ (dashed line). (Mg,Zn)O barriers, ZnO core and (Cd,Zn)O QWs are highlighted by colored areas.

CL spectra of (Mg,Zn)O/ZnO quantum well heterostructures show luminescence from the ZnO core at 2.5 eV (deep defect centers) and 3.25 eV (free excitons), the quantum well and the (Mg,Zn)O barriers (in spectral order). Quantum confinement in this case is proven by the size-dependent (QW thickness $L_{\text{QW}} = 0.6 - 2.6$ nm) blueshift of the QW emission which is obvious in Fig.8.17c. However, spectra of the same microwire but recorded at different facets all show similar luminescence bands proving the homogeneous deposition and constant QW thickness around the wire. In addition to that, all CL spectra are modulated by narrow peaks. This is most clearly visible for the ZnO green band. These peaks can be assigned to WGM propagating through the whole wire heterostructure. The presence of cavity modes is an indication for the interface quality

since WGM only constructively interfere by total internal reflection at smooth facets.

Luminescence of the (Zn,Cd)O QW is shown in Fig. 8.17d. Emissions from the (Zn,Cd)O QWs and the (Mg,Zn)O barriers are clearly visible. Again, quantum confinement is proven by the size-dependent ($L_{\text{QW}} = 0.8 - 2.1$ nm) shift of the QW emission. Another reference is given by a spectrum of a single coated microwire (with $\text{Zn}_{0.75}\text{Cd}_{0.25}\text{O}$) emitting at 2.5 eV which is below the QW emission [8]. Apart from this, all spectra are again modulated by WGM, but in this case QW excitons and WGM spatially and spectrally overlap which is the main prerequisite for the formation of polaritons in these structures.

- [1] T. Nobis *et al.*, Phys. Rev. Lett. **93**, 103903 (2004).
- [2] C.P. Dietrich *et al.*, Appl. Phys. Lett. **98**, 031105 (2011).
- [3] C.P. Dietrich *et al.*, New J. Phys. **13**, 103021 (2011).
- [4] C.P. Dietrich *et al.*, Appl. Phys. Lett. **100**, 031110 (2012).
- [5] M. Grundmann and C.P. Dietrich, phys. stat. sol. b, in press (2012).
- [6] C.P. Dietrich *et al.*, J. Appl. Phys. **109**, 013712 (2011).
- [7] S.I. Tsintzos *et al.*, Nature **453**, 372 (2008).
- [8] M. Lange *et al.*, phys. stat. sol. RRL **6**, 31 (2012).

8.14 Visible emission from ZnCdO/ZnO multiple quantum well structures

M. Lange, C.P. Dietrich, K. Brachwitz, M. Stölzel, M. Lorenz, M. Grundmann

Due to the large demand for optoelectronic devices covering a wide spectral range from green to ultraviolet, extensive research was triggered into wide-bandgap semiconductors. In particular GaN- and ZnO-based devices have been studied so far. The efficiency of the devices is often based on the usage of semiconductor heterostructures, e.g. quantum wells (QWs). However, for pulsed-laser deposition (PLD)-grown QW samples the lowest reported QW-emission energy is as high as 2.76 eV [1]. This is caused by the low solubility of Cd in ZnO resulting in difficulties to obtain large Cd-contents in the QWs.

In this work, $\text{Zn}_{0.75}\text{Cd}_{0.25}\text{O}/\text{ZnO}$ -multiple QW structures (MQWS), emitting in the visible spectral range, were grown by using PLD [2]. A large Cd-content of 0.25 and abrupt interfaces were achieved by applying a low growth temperature of ≈ 300 °C.

A precise knowledge of the thicknesses of the ZnO and $\text{Zn}_{0.75}\text{Cd}_{0.25}\text{O}$ layers is important for the design of efficient heterostructures. In this regard, high resolution X-ray diffraction $2\theta - \omega$ scans were performed. The $\text{Zn}_{0.75}\text{Cd}_{0.25}\text{O}/\text{ZnO}$ -(00.2) Bragg reflex is obviously modulated by superlattice satellites (see Fig. 8.19 (a)), as result of the periodicity of the MQWS. The thickness of the $\text{Zn}_{0.75}\text{Cd}_{0.25}\text{O}/\text{ZnO}$ -stacks was deduced from a linear fit of the angular positions of the satellites as function of the peak order. QW-thicknesses between 0.7 nm - 3.5 nm were calculated from the periodicity, considering the growth rates of the ZnO and $\text{Zn}_{0.75}\text{Cd}_{0.25}\text{O}$.

Time-resolved and time-integrated photoluminescence (PL) measurements were performed at $T = 2$ K to characterize the emission of the QWs. Besides the luminescence

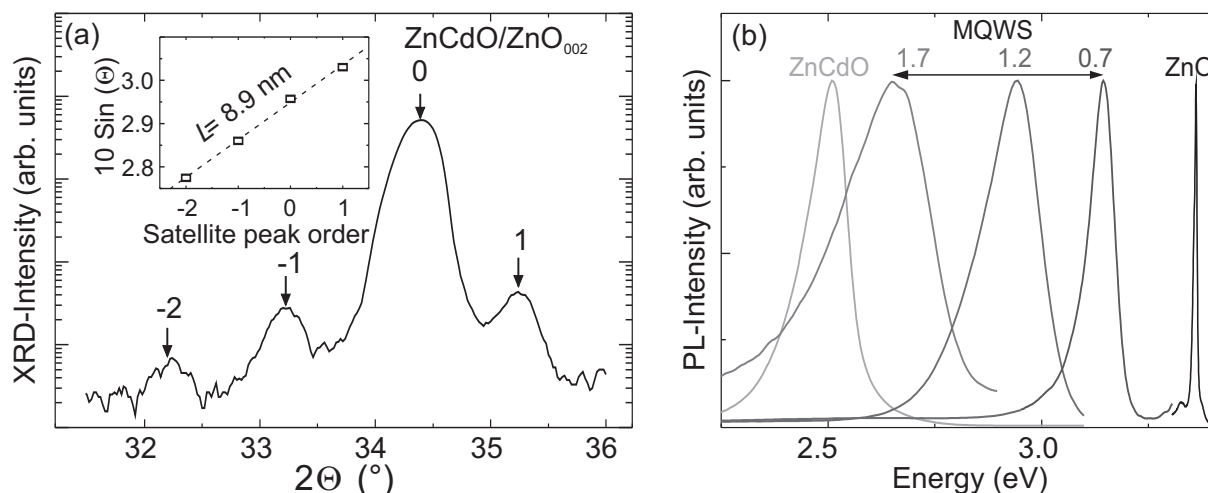


Figure 8.19: (a) HR-XRD $2\theta - \omega$ diffractogram around the $\text{Zn}_{0.75}\text{Cd}_{0.25}\text{O}/\text{ZnO}$ -(00.2)-reflex exhibiting superlattice satellites. The superlattice period is calculated by plotting the sine of θ over the satellite peak order (see inset). The dashed line shows a fit with a periodicity of the superlattice of 8.9 nm for a QW-thickness of 1.0 nm. (b) PL-spectra of samples with different QW-thicknesses in comparison to ZnO- and $\text{Zn}_{0.75}\text{Cd}_{0.25}\text{O}$ -thin films.

of the ZnO-barriers an intense luminescence is observed that is assigned to the MQW. The spectral position of the MQW-luminescence band was tuned from green to violet (2.5 eV to 3.1 eV) by reducing the QW-thickness (see Fig. 8.19 (b)).

In the luminescence measurements several phenomena occur that are explained with the Quantum-Confined Stark Effect (QCSE). The presence of the QCSE is expected in polar oriented ZnO-based MQWs with a high interface quality [3] and therefore also in the studied samples. The phenomena are: (i) In excitation intensity dependent measurements a blue-shift of the MQW-emission with increasing intensity is observed. (ii) Already for a QW-thickness of 3.5 nm the MQW related maximum is observed at the energy of the thin film. (iii) A significant increase of the average decay time with increasing QW-thickness is deduced from TR-PL measurements. For the determination of the average decay time PL-transients were fitted with stretched exponential decay functions. The increase of the average decay time is larger than three orders of magnitude although the largest QW-thickness was as small as 1.7 nm. This is expected to result from the large internal electric field that is present along the c -direction in the QWs.

The negative influence of the electron-hole separation in c -direction on the oscillator strength and the resulting decrease in the luminescence intensity due to the QCSE, is expected to be reduced by non-polar growth that should be promoted in future. With the presented $\text{Zn}_{0.75}\text{Cd}_{0.25}\text{O}/\text{ZnO}$ -MQWS, a wide spectral range between 2.5 eV and 3.1 eV was made accessible with PLD-grown QWs, which is much larger in comparison to previously reported results. Energies above 3.2 eV were already obtained in structures with ZnO-quantum wells embedded between MgZnO-barriers.

- [1] H. Matsui, T. Osone und H. Tabata: J. Appl. Phys. **107**, 093523 (2010). doi:10.1063/1.3359720
- [2] M. Lange, C. P. Dietrich, K. Brachwitz, M. Stölzel, M. Lorenz, und M. Grundmann: phys. status solidi (RRL) **6**, 31 (2012). doi:10.1002/pssr.201105489

- [3] M. Brandt, M. Lange, M. Stölzel, A. Müller, G. Benndorf, J. Zippel, J. Lenzner, M. Lorenz, and M. Grundmann: Appl. Phys. Lett. **97**, 052101 (2010). doi:10.1063/1.3475402

8.15 Radiative decay times in ZnO/(Mg,Zn)O quantum wells with and without the quantum-confined Stark effect

M. Stölzel, A. Müller, G. Benndorf, M. Brandt, M. Lorenz, and M. Grundmann

We performed temperature dependent time-integrated and time-resolved photoluminescence measurements on ZnO/(Mg,Zn)O quantum wells (QWs) grown by pulsed laser deposition (PLD) on a-sapphire substrates ($T = 650^\circ\text{C}$, $p_{\text{O}_2} = 0.004$ mbar). The energy density during the PLD process has been varied between 1.8 and 2.4 J/cm² to prepare QWs exhibiting excitonic transitions with and without the quantum-confined Stark effect (QCSE)[1].

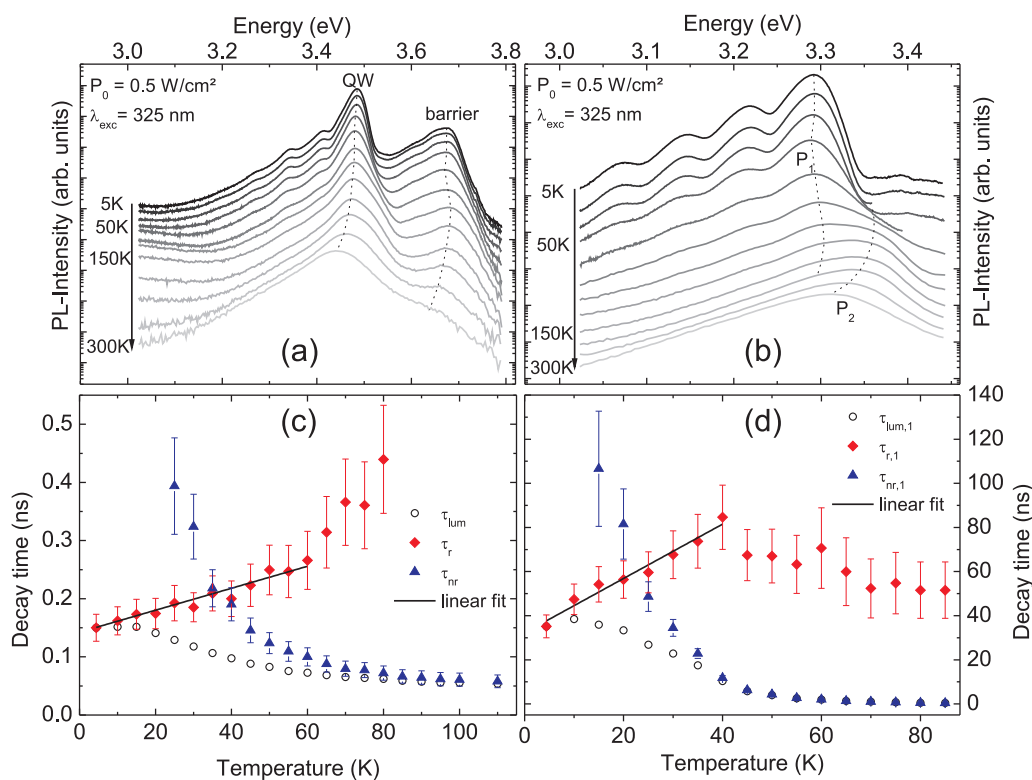


Figure 8.20: Temperature dependent PL spectra and calculated radiative and non-radiative decay times together with the measured luminescence decay time of a QW sample exhibiting excitons (a,c) without and (b,d) with a distinct QCSE. The dotted lines in (a,b) indicate the dependence of the PL peaks. The black lines in (c,d) are linear fits to the radiative lifetime with a slope of (a) (1.9 ± 0.3) ps/K and (b) (1.2 ± 0.1) ns/K.

In Fig. 8.20 (a,b) PL spectra of a QW structure (a) without and (b) with the QCSE are shown. Without an internal electric field, the energetic position of the QW luminescence decreases monotonically with temperature following the bandgap of the well material. In the presence of an internal electric field, the luminescence of the QW ground state (P1) dominates the spectrum at low temperatures. Above 75 K a second peak (P2) arises on the high energy side, dominating the spectrum above 150 K. This peak is mainly determined by states nearly fully screened, leading to a behavior similar to QWs without the QCSE. The pronounced S-shape shift of the zero-phonon line of the barrier luminescence can be explained in terms of the freeze-out-effect for alloy semiconductors[2].

Additionally, we performed time-resolved measurements to determine the luminescence decay time and to investigate the carrier dynamics. We calculated the radiative τ_r and non-radiative τ_{nr} decay times assuming that the luminescence intensity is proportional to the internal quantum efficiency $\eta = \tau_{nr}/(\tau_r + \tau_{nr})$. With $\tau_{lum}^{-1} = \tau_r^{-1} + \tau_{nr}^{-1}$ and the assumption that $\eta = 1$ for $T = 0$ K we obtain a lower limit for the radiative decay time $\tau_r = \tau_{lum}/\eta$ as shown in Fig. 8.20 (c,d). For both types of QWs, the radiative decay time of the QW luminescence increases linearly at low temperatures, indicating free exciton recombination as the major recombination process. This indicates a vanished influence of defect related emission which dominates PL spectra at low temperatures in bulk material.

[1] M. Brandt et al.: Appl. Phys. Lett. **97**, 052101 (2010), doi:10.1063/1.3475402

[2] A. Müller et al.: Sol. Stat. Comm. **148**, 570 (2008),doi:10.1016/j.ssc.2008.09.045

8.16 Tunneling dynamics of excitons in random semiconductor alloys

A. Müller, M. Grundmann

At low temperatures, excitons localized within random alloy potential fluctuations often show an asymmetric photoluminescence (PL) lineshape as well as a time-dependent shift of the luminescence maximum to lower energies. This can be understood by the distribution of local potential minima, into which the excitons relax within a few picoseconds. From these, the excitons can reach energetically lower states only by tunnelling as the localized states are separated by potential barriers.

During relaxation, an exciton can, in average, reach a number of $N(t)$ different states increasing with time. Due to the low thermal energy, it will most probably be transferred into the lowest of these. Assuming that the localized states are Gaussian distributed in energy and show a random spatial distribution within the alloy, the resulting distribution of the occupied states was found to follow the minima distribution of Gaussian distributed random numbers:

$$i_N(E) = \frac{N}{\sqrt{2\pi}(1 - \exp(-N))} \exp\left(-\frac{N}{2} \operatorname{erf}\left(\frac{E - E_0}{\sqrt{2}\sigma}\right) - \frac{1}{2} - \frac{(E - E_0)^2}{2\sigma^2}\right). \quad (8.1)$$

Using this model, we were able to reproduce the line shape of the individual time-delayed PL spectra of an $\text{Mg}_{0.18}\text{Zn}_{0.82}\text{O}$ thin film over three orders of magnitude with a total dynamic range of six orders of magnitude. The modeled spectra are shown in Fig. 8.21 (a), where additionally the donor-bound exciton recombination (for $t < 5$ ns) and the contribution of the first longitudinal optical phonon replica were taken into account.

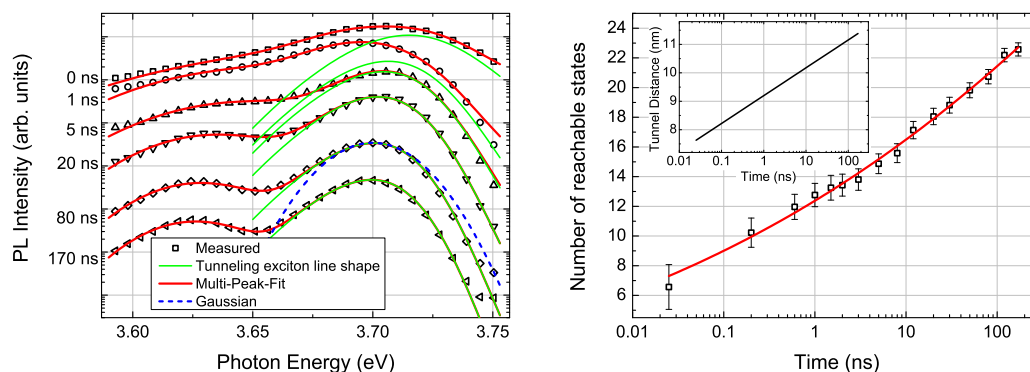


Figure 8.21: (a) Modeled delayed spectra of an $\text{Mg}_{0.18}\text{Zn}_{0.82}\text{O}$ thin film grown on a-sapphire. To illustrate the asymmetry of the spectra, a Gaussian lineshape is shown for comparison. (b) Number of reachable states as a function of time. The inset depicts the tunnelling range.

The average number N of reachable states for a single exciton, which were determined from the model parameters of the spectra, are shown in Fig. 8.21 (b). From these, the tunneling range could be estimated as a function of time. The time-dependence indicates a tunnel length of $l_t \approx 0.5$ nm, in agreement with the wave function attenuation within the barrier.

8.17 Overestimation of the Stokes shift due to self absorption in MgZnO

A. Müller, G. Benndorf, M. Grundmann

Temperature-dependent photoluminescence (PL) and transmission measurements [1] have been performed on an $\text{Mg}_{0.18}\text{Zn}_{0.82}\text{O}$ thin film grown on a-sapphire substrate. In Fig. 8.22 (a), the mean exciton energy determined from the transmission spectra as well as the PL maximum are plotted as a function of temperature (open symbols). For increasing temperatures, the mean exciton transition energy shows a monotonic red shift according to a Bose-Einstein-Model [2]. The S-shaped shift of the PL maximum typical for alloys can be explained by the thermalization of the excitons [3]. According to the model, for increasing temperature the excitons are expected to reach energetically excited states, approaching the mean exciton transition energy. This would lead to a decrease of the Stokes shift according to the thermalization energy $\Delta E = \sigma^2/kT$.

However, the observed energy difference between emission and absorption maximum increases for temperatures above 200 K. We explain this by the self absorption of the luminescence within the thin film. Depending on the emission depth z and the absorption coefficient $\alpha(h\nu)$, only a fraction of the photons can reach the surface and

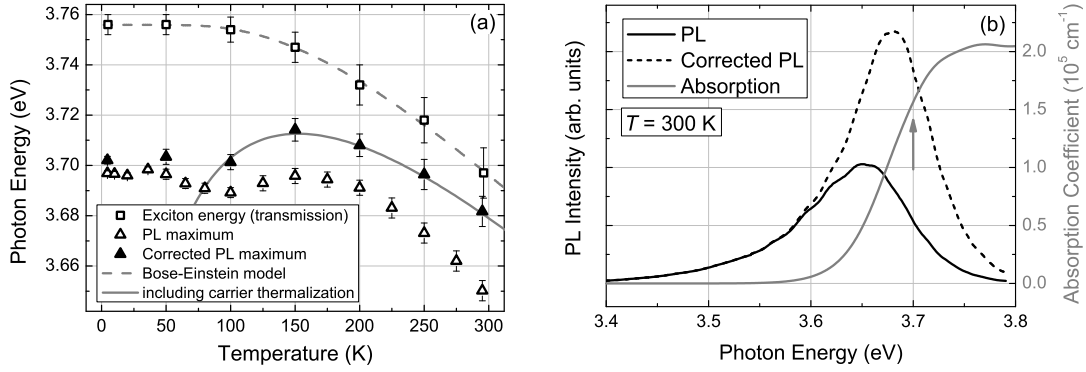


Figure 8.22: (a) Exciton energy in comparison to measured and corrected PL maximum energy of an $\text{Mg}_{0.18}\text{Zn}_{0.82}\text{O}$ sample as a function of temperature. (b) Measured and corrected PL spectrum of the sample for $T = 300\text{ K}$ compared to the absorption spectrum. The mean exciton energy is marked by an arrow.

can be detected as PL signal. Assuming a homogeneous excitation of the film (thickness $d = 200\text{ nm}$), this is given by

$$p(h\nu) = \frac{1}{d} \int_0^d \exp(-\alpha(h\nu)z) dz = \frac{1 - \exp(-\alpha(h\nu)d)}{\alpha(h\nu)d}. \quad (8.2)$$

The measured PL spectra were corrected by dividing the intensity by eq. (8.2). For 300 K, the self absorption accounts for an additional red shift of 30 meV (see Fig. 8.22 (b)). The corrected PL maxima are plotted as a function of temperature (closed symbols) in Fig. 8.22 (a). As expected, the corrected Stokes shift decreases with increasing temperature, in agreement with the thermalization energy.

- [1] A. Müller, G. Benndorf, S. Heitsch, Ch. Sturm, and M. Grundmann: Solid State Comm. **148**, 570 (2008)
- [2] S. Logothetidis, L. Viña, and M. Cardona: Phys. Rev. B **31**, 947 (1985)
- [3] A. Bell, S. Srinivasan, C. Plumlee, H. Omiya, F. A. Ponce, J. Christen, S. Tanaka, A. Fujioka, and Y. Nakagawa: J. Appl. Phys. **95**, 4670 (2004)

8.18 Persistent layer by layer growth in Pulse Laser Homoepitaxy of (0001) ZnO thin films

J. Zippel, M. Lorenz, M. Grundmann

ZnO is a brilliant emitter and therefore a candidate for making short-wavelength LEDs and diode lasers. However, in addition, the large exciton binding energy, i.e. as large as 60 meV and can be increased to over 100 meV in superlattices [1], provides opportunities for making highly efficient lasers operable at roomtemperature. [2]

If ZnO is ever used to produce robust and stable devices, the quality of epitaxial layers has to be improved as it is done for other compound semiconductors [3].

Here we present a way to establish a persistent layer by layer growth mode for homoepitaxially grown (0001) oriented ZnO thin films, giving the opportunity to *in-situ* control the growth process by reflection high-energy electron diffraction (RHEED).

The problem of pulsed laser deposition (PLD) is a limited interlayer mass transport results in nucleation on top of 2D islands before completion of a unit cell layer. This leads to a roughening of the surface with increasing film thickness.

As proposed by G. Koster et al. [4] for SrTiO₃ an interval PLD approach can be used to overcome this problem. A small number (at least one) of unit cell layers is deposited in a very short-time interval, followed by a much longer interval during which the deposited material can rearrange. Only small islands will be formed due to the high supersaturation typical for PLD.

As shown in Figure 8.23 (a), in each interval, between two to four RHEED oscillations (indicated by arrow) are observable, showing the growth of respective unit cell layers. After interruption of the growth procedure, the RHEED intensity increases as a consequence of the rearrangement of the surface layer. Such transient RHEED signals can be observed over the whole ablation process as exemplarily shown in the inset of Figure 8.23 (a), where the 25, 26 and 27th interval are shown. As depicted in Figure 8.23 (b), the surface remains smooth and the vicinal structure of the surface is still visible. Step heights of $c/2$ or c are shown without any observable hillocks.

In Figure 8.23 (c), the photoluminescence (PL) spectrum of the (0001) ZnO thin film grown by interval PLD is shown. It is remarkable, that the FWHM of the recombination lines is very small as shown exemplarily for the I₆ line, where the FWHM value is 0.7 meV. The notation follows the publication of B. K. Meyer et al. [5]. The sharp lines are an indication of the high quality of the thin film.

In summary, we present a growth method for (0001)-oriented ZnO thin films homoepitaxially on (0001) ZnO substrates. The film grow in a persistent layer by layer mode being proofed by RHEED oscillations showing the two dimensional character of the growth. The thin films reveal sharp PL lines indicating a high quality of the thin film.

- [1] Chia, C. H. et al., Appl. Phys. Lett. 82, 1848-1850 (2003).
- [2] Bagnall, D. M. et al., Appl. Phys. Lett. 70, 2230-2232 (1997).
- [3] Haase, M. A. et al., Appl. Phys. Lett. 59, 1272-1274 (1991).
- [4] Koster, G. et al., Appl. Phys. Lett. 71, 3729-3731 (1999).
- [5] Meyer, B. K. et al., phys. stat. sol. (b) 241, 231-260 (2004).

8.19 Model for 1LO Raman scattering mechanisms in wurtzite crystals excited above the band gap

C. Kranert, R. Schmidt-Grund, M. Grundmann

The Raman spectrum of wurtzitic semiconductors typically shows a series of lines assigned to the multiple scattering from longitudinal optical (LO) phonons. The appearance of emission lines from such high order processes is generally explained by means of a cascade model. This, in its simplest form, describes the mechanism as

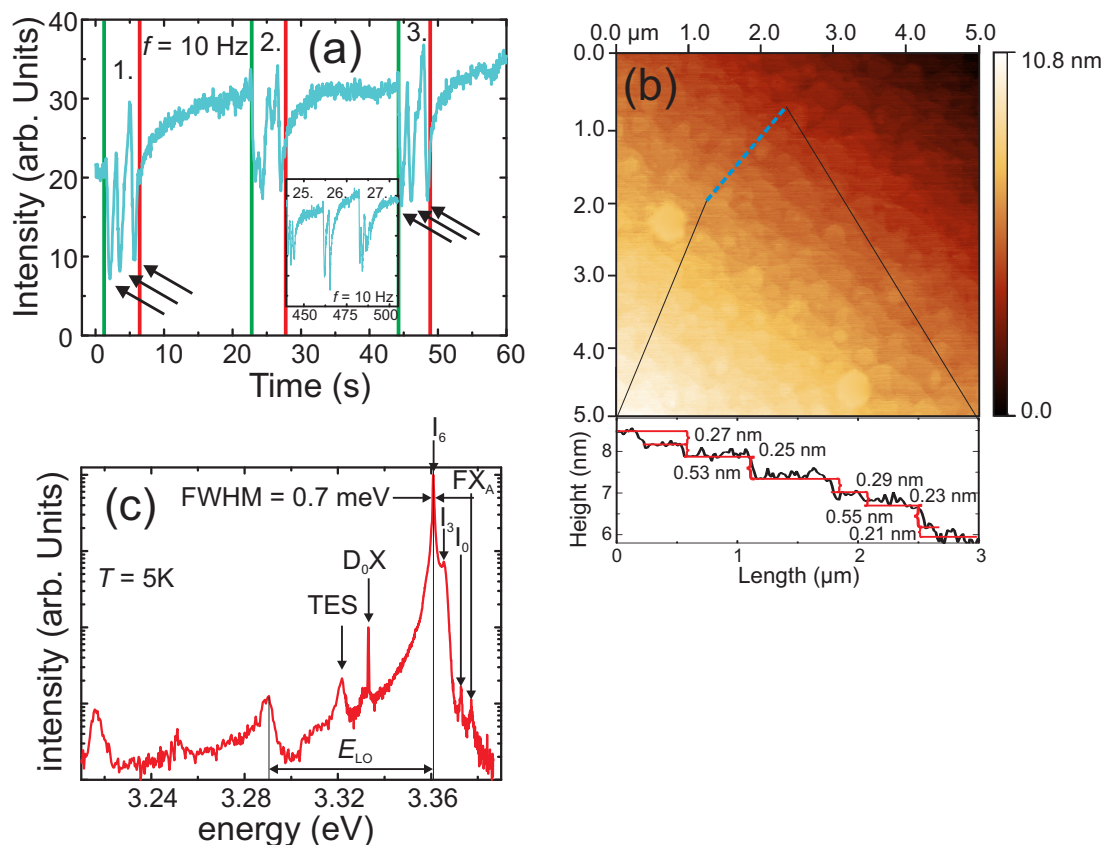


Figure 8.23: (a) RHEED signal of a homoepitaxially (0001)-oriented ZnO thin film grown by interval PLD. The green line marks the start, the red one the end of an interval. Black arrows indicate the oscillations observed. The inset shows the 25, 26 and 27th interval. (b) AFM surface image of the ZnO thin film of (a). (c) Photoluminescence spectrum of the ZnO thin film. The notation follows the publication of B.K. Meyer [5].

follows: The photon generates a correlated electron hole pair which scatters into the bound exciton state by emission of an LO phonon. The exciton is strongly coupled to these kind of phonons and can therefore scatter by several further of them. Finally, it can recombine by emission of one final LO phonon before having been fully relaxed. The involvement of the excitonic intermediate states in the scattering process causes the strong enhancement of the n LO lines. However, this model is only valid for $n \geq 2$ because of the need for one LO phonon each to scatter into and out of the excitonic state. The description of the enhancement of the 1LO line requires this model to be extended by one inelastic scattering process at an impurity substituting one of the LO phonon scattering processes.

The resonance profile of the 1LO emission and the influence of defects on them has been treated theoretically and experimentally [1–3] for cubic semiconductors. However, there are no thorough discussions on spectral position, line shape and polarisation dependence of this line yet, especially for the case of wurtzitic crystals. On the basis of own measurements and data available from the literature we propose a model differentiating between two types of defects: the inherently present surface at the excitation spot and point like defects caused by impurities.

The surface can be considered as onedimensionally confined and thus scattering from it leads to a violation of exciton wave vector conservation in only one direction, particularly the one normal to the surface. Therefore only LO phonons with a wave vector perpendicular to the surface contribute to the 1LO line in this scattering process. Contrarily, LO phonons from all directions of the Brillouin zone are involved for the inelastic scattering occurring at point defects. We further postulate that surface related scattering conserves the linear polarisation of the incident light while impurity related scattering leads to a (partially) depolarised line. This shows up to be consistent with several experimental observations.

Experimentally the surface scattering process described above is supposed to occur in any crystal caused by the inherently present surface. It is manifested by a dependence of the spectral position of the 1LO line on the surface which the excitation is carried out on [4–6]. This dependence was previously thought to be caused by the direction of the incident and scattered light wave propagation [4, 6]. However, we have shown by Raman measurements on ZnO and GaN with varying incidence angles that this is not the case.

Because of the contribution of phonons from all directions of the Brillouin zone, the spectral position of the according 1LO line is inbetween those determined by the surface scattering if excited on a surface parallel respective perpendicular to the c -axis. If it is spectrally close to the surface related line, it superimposes the latter and leads to an increased overall 1LO intensity in impure crystals (see Fig. 8.24).

The different polarisation dependence of the lines originating from the two scattering mechanisms leads to the fact that in rather pure crystals only a small 1LO peak occurs in the crosspolarised spectra which is shifted to higher energies with respect to the parallelpolarised one [7, 8]. In doped samples the parallelpolarised peak shifts towards crosspolarised one, and the intensity ratio between both decreases (see Fig. 8.24).

- [1] A. Gogolin and E. Rashba: Solid State Commun. **19**, 1177-1179 (1976)
doi:10.1016/0038-1098(76)90813-9

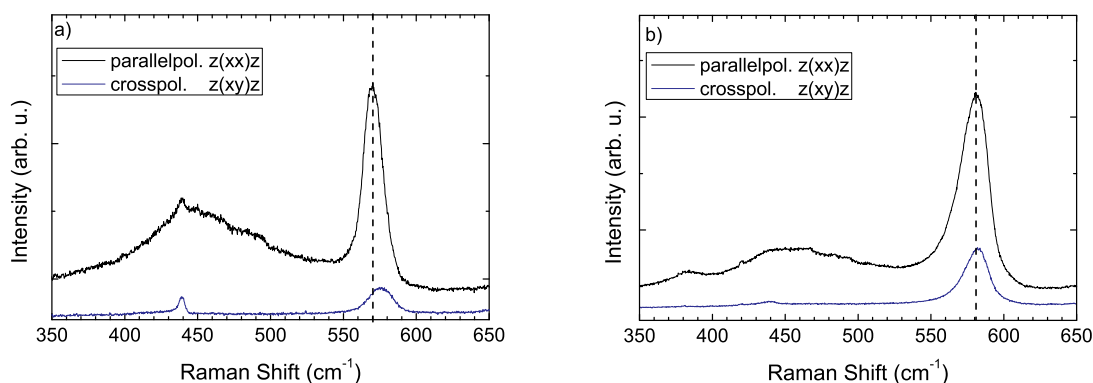


Figure 8.24: Polarised UV Raman spectra ($\lambda_{\text{exc}} = 325 \text{ nm}$, $T = 10 \text{ K}$) of (a) undoped c-oriented ZnO and (b) Al-doped c-oriented ZnO at $T = 10 \text{ K}$. The dashed line indicates the respective intensity maximum of the 1LO peak in the parallelpolarised spectrum. The range of the y -axis of (b) is increased by a factor of 3 compared to (a).

- [2] J. Menéndez and M. Cardona: Phys. Rev. B **31**, 2696-3704 doi:10.1103/PhysRevB.31.3696
- [3] C. Trallero-Giner et al.: Phys. Rev. B **45**, 6601-6613 (1992) doi:10.1103/PhysRevB.45.6601
- [4] E. Alarcón-Lladó et al.: J. Raman Spectrosc. **42** 153-159 doi:10.1002/jrs.2664
- [5] L. Bergmann et al.: J. Appl. Phys. **98** 093507 (2005) doi:10.1063/1.2126784
- [6] V. Y. Davydov et al.: Phys. Rev. B **80**, 081204 (2009) doi:10.1103/PhysRevB.80.081204
- [7] V. Y. Davydov et al.: Appl. Phys. Lett. **75**, 3297-3299 (1999) doi:10.1063/1.125330
- [8] A. Kasic et al.: Phys. Rev. B **65**, 115206 (2002) doi:10.1103/PhysRevB.65.115206

8.20 Magneto-optical ellipsometry

T. Böntgen, T. Herzig, R. Schmidt-Grund, M. Grundmann

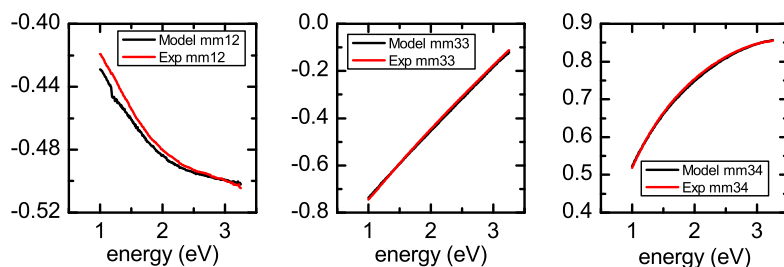


Figure 8.25: Selected MM elements. The fit curve resembles the tabulated values.

We have investigated room temperature magneto-optical properties of Co thin films deposited on glass substrates. The measurements were carried out using spectroscopic ellipsometry. The magnetic field was applied using two permanent magnets with the opposite poles facing each other. A thin Co film was then inserted in the resulting

homogenous field between the two magnets. This setup allows a high flexibility at a very low cost. As is well known Co exhibits a Kerr-Effect when placed in a magnetic field. This results in a rotation of the polarization of the incident light.

In general the optical properties of any sample can be described by the dielectric function tensor ϵ . In the special case of isotrop samples ϵ has only diagonal elements. If the sample exhibits a Kerr-Effect the off-diagonal elements of ϵ become non zero. The strength of the Kerr-Effect dose also depend on the exact ϵ -tensor. To determine

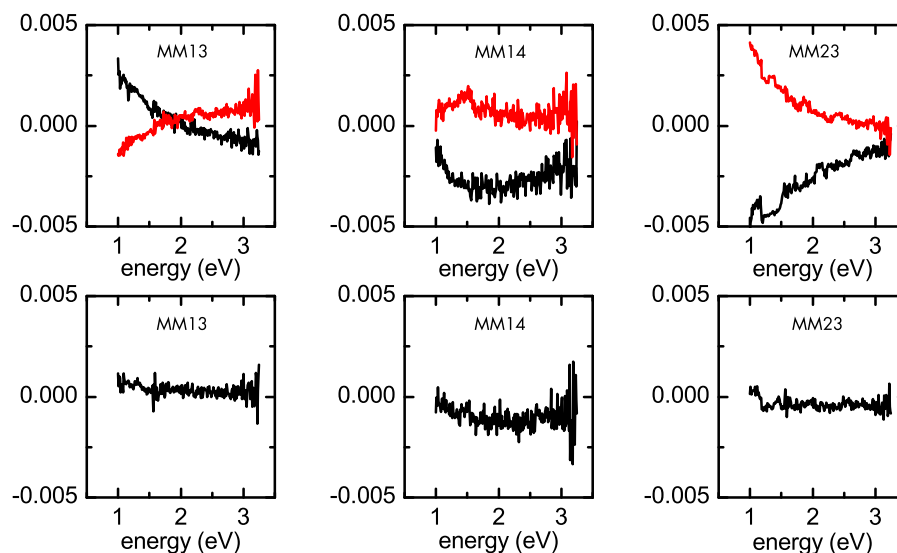


Figure 8.26: Selected off diagonal MM elements. The fit curve resembles the tabulated values.

the influence of the samples magnetization we employed a two step process. First the sample was measured with standard Müller-Matrix (MM) ellipsometry yielding the optical properties of the sample. Then a magnetic field was applied and the sample was measured again. The measured Müller-Matrix now includes the magnetic effects. The first measurement was then analyzed using a layer-stack model consisting of a layer for the glass substrate and a layer for the thin Co film. The dielectric function of the substrate has been previously measured. For the Co layer tabulated values were used. The tabulated Co values were then fitted to the measured data using a point-by-point routine. The measured off diagonal Müller-Matrix elements are all zero if no magnetic field is applied. This proves, that the Cobalt sample is not magnetized nor anisotropic in its virgin state. The diagonal MM elements show a reasonable agreement with the tabulated data prior to the point-by-point fit. The second measurement with magnetic field was then analyzed using the previously determined model. To account for the Kerr-Effect a magneto-optical layer that contains only off-diagonal elements for ϵ was added to the Co layer. The magneto-optical measurements were also carried out with an inverted magnetic field. The off-diagonal MM elements now clearly deviate from zero. Additionally when comparing measurements with inverse field directions the MM elements change sign. This demonstrates, that the non zero elements are indeed caused by the magnetization. Furthermore when comparing opposite MM elements (e.g. MM23 and MM32) a slight asymmetry is observed. This suggests, that the magnetization is not pointing completely out of the sample plain but is slightly tilted. With the magnetization direction and the magneto-optical coupling constant as free parameters

the measured spectra can be fitted over a large spectral range. The model yields a tilt of the magnetization of 80° and a Kerr-Rotation of 0.3° .

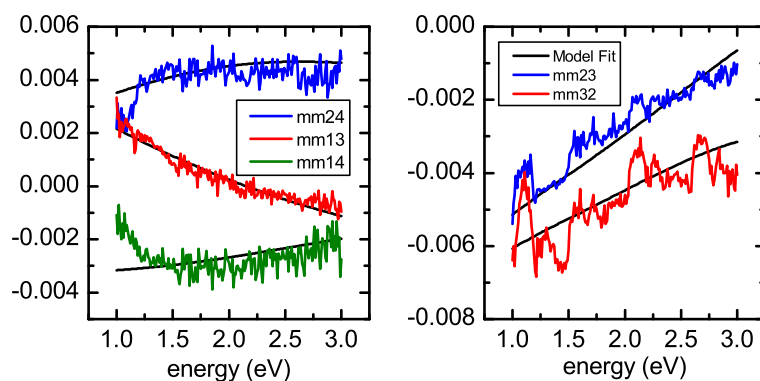


Figure 8.27: Off-diagonal MM elements and the corresponding best fit.

8.21 Plasmons on structured substrates

T. Böntgen, J. Lorbeer*, R. Schmidt-Grund, M. Grundmann

*Leibniz-Institut für Oberflächenmodifizierung e.V., Leipzig, Germany

We have investigated the anisotropic optical properties of structured SiO_2 surfaces. Flat SiO_2 substrates have been patterned using ion beam erosion under high angles of incidence. This causes the formation of a wave like or rippled surface.[1][2] The periodicity of the ripples is usually 40nm-80nm. An anisotropic optical response is found for wavelength on the same length scale as the periodicity of the pattern. However exploiting plasmon resonances the structural anisotropy can be transferred to an optical anisotropy for wavelength much longer than the pattern periodicity. Thus we have deposited a thin gold layer onto the structured substrate. The gold does not form a closed layer but rather small particles. These particles can accommodate plasmons with resonance frequency in the visible spectral range. The exact position of the resonance mainly depends on the particle size and shape and the dielectric constant of the surrounding medium. As is clearly seen from the AFM measurements the size of the gold particles varies. However there is no clear anisotropy in the shape of the particles. The optical properties of the samples have been investigated using spectroscopic ellipsometry. The pseudo dielectric

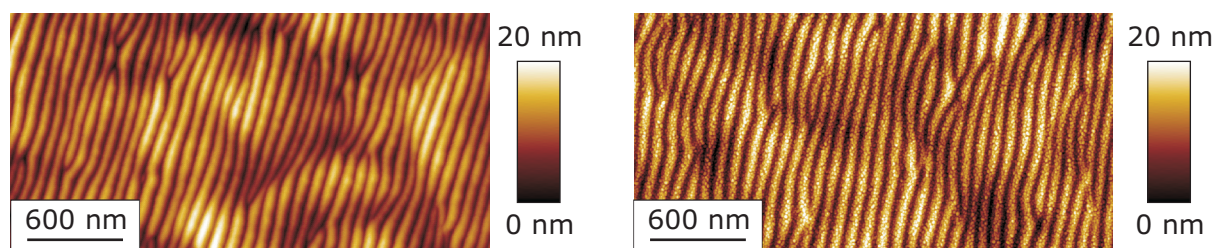


Figure 8.28: AFM images of the patterned substrate (left) and the substrate with a thin gold layer (right). The gold forms individual particles instead of a closed film.

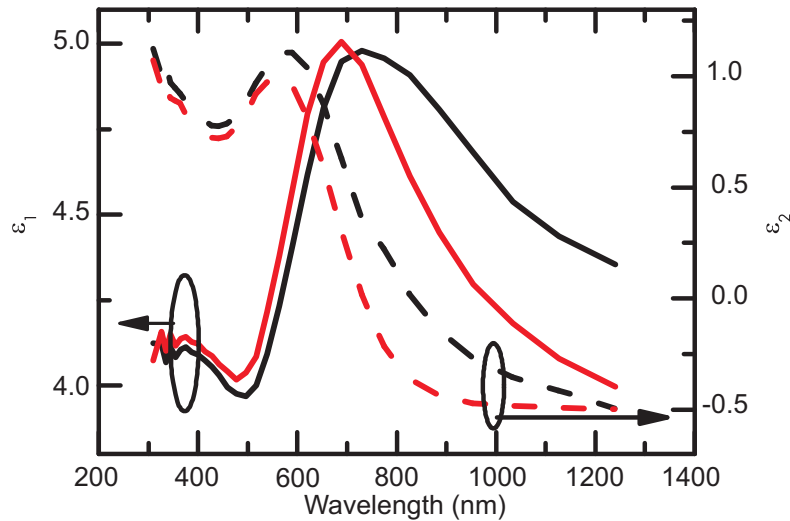


Figure 8.29: Pseudo dielectric function of the structured substrate with gold layer. The peak belongs to the particle plasmon resonance. The two curves are for 0° deg (along the ripples, black lines) and 90° (perpendicular to the ripples, red lines).

function shows a distinct peak at ≈ 680 nm that originates from the particle plasmon. Measurements along and perpendicular to the structure reveal a pronounced change in the dielectric function close to the plasmon resonance. This demonstrates that the plasmon is effected by the structural anisotropy of the substrate and thus maps this anisotropy into the visible spectral range.

- [1] D. Flamm et al., Appl. Surf. Sci. 96 (179), 2001
- [2] J. Völlner et al., J. Appl. Phys. 043501 (109), 2011

8.22 Funding

Leipzig School of Natural Sciences - Building with Molecules and Nano-objects (Build-MoNa)

Prof. Dr. M. Grundmann

DFG GS 185/1

Polarisationswechselwirkung in Laser-MBE Wurtzit-Perowskit-Heterostrukturen

Prof. Dr. M. Lorenz

SFB 762/1-2008, TP A2 within SFB 762 *Funktionalität Oxidischer Grenzflächen*

Optische Untersuchungen zur dielektrischen Funktion und Ihrer Dynamik an oxidischen Heterostrukturen

Prof. Dr. M. Grundmann, Prof. Dr. H. Gräner (Martin-Luther-Universität Halle-Wittenberg)

SFB 762/1-2008, TP B03 within SFB 762 *Funktionalität Oxidischer Grenzflächen*

Lateraler Transport in oxidischen Feldeffekt-Strukturen

Prof. Dr. M. Grundmann, Prof. Dr. J. Christen (Otto-von-Guericke-Universität Magdeburg)

SFB 762/1-2008, TP B04 within SFB 762 *Funktionalität Oxidischer Grenzflächen*

Spinabhängiges Tunneln in oxidischen Heterostrukturen

Prof. Dr. M. Grundmann, Prof. Dr. I. Mertig (Martin-Luther-Universität Halle-Wittenberg)

SFB 762/1-2008, TP B06 within SFB 762 *Funktionalität Oxidischer Grenzflächen*

Bose-Einstein-Kondensation von Exziton-Polaritonen bei Raumtemperatur

Prof. Dr. M. Grundmann, Dr. R. Schmidt-Grund

DFG GR 1011/20-1

Herstellung und Charakterisierung von UV-Mikrokavitäten

Dipl.-Phys. H. Franke

Landesinnovationsstipendium des Freistaates Sachsen im Rahmen des Europäischen Sozialfonds

Herstellung und Charakterisierung von transparenten Feldeffekttransistoren

Dipl.-Phys. A. Lajn

Landesinnovationsstipendium des Freistaates Sachsen im Rahmen des Europäischen Sozialfonds

Herstellung und Charakterisierung von Quantendraht-Heterostrukturen

Dipl.-Phys. M. Lange

Landesinnovationsstipendium des Freistaates Sachsen im Rahmen des Europäischen Sozialfonds

Magnetische Tunnelkontakte

Dipl.-Phys. J. Zippel

Landesinnovationsstipendium des Freistaates Sachsen im Rahmen des Europäischen Sozialfonds

Funktionalisierte Nanosäulen

Prof. Dr. M. Grundmann, Dr. H. von Wenckstern

ESF-Nachwuchsforschergruppe *Funktionale multiskalige Strukturen* des Freistaates Sachsen im Rahmen des Europäischen Sozialfonds*Elektron-Phonon-Wechselwirkung in Mikro- und Nanonadeln*

Dipl.-Phys. Christian Kranert

Landesinnovationspromotionsstipendium des Freistaates Sachsen im Rahmen des Europäischen Sozialfonds

Magnetotunnel-Widerstände mit oxidischen Kontakten

Michael Bonholzer, M.Sc.

Landesinnovationspromotionsstipendium des Freistaates Sachsen im Rahmen des Europäischen Sozialfonds

Internationale Zusammenarbeit in Bildung und Forschung mit Neuseeland: Grundlegende Eigenschaften und Anwendungen von MgZnO/ZnO Heterostrukturen

Dr. H. von Wenckstern

NZL 10/010, Deutsches Zentrum für Luft- und Raumfahrt e. V., Internationales Büro des BMBF

Internationale Zusammenarbeit in Bildung und Forschung mit Südafrika: Elektrische Charakterisierung von bei tiefen Temperaturen in ZnO Volumenmaterial und ZnO Nanostrukturen eingebrachten Defekten

Dr. H. von Wenckstern

SUA 09/037, Deutsches Zentrum für Luft- und Raumfahrt e. V., Internationales Büro des BMBF

Diluted magnetic oxides on the basis of TM doped

Prof. Dr. M. Grundmann, Prof. Dr. N. Sobolev (Universidade de Aveiro, Portugal)

DAAD, 50111259

8.23 Organizational Duties

M. Grundmann

- Direktor des Instituts für Experimentelle Physik II
- Coordinator of the European Network of Excellence on "Self-Assembled semiconductor Nanostructures for new Devices in Photonics and Electronics" (SANDiE, <http://www.sandie.org>)
- Stellvertretender Sprecher der Graduiertenschule "Leipzig School of Natural Sciences - Building with Molecules and Nano-objects" (BuildMoNa), <http://www.buildmona.de>
- Stellvertretender Sprecher des Sonderforschungsbereiches 762 "Funktionalität Oxidischer Grenzflächen", <http://www.physik.uni-halle.de/sfb762>
- Sprecher der Fächerübergreifenden Arbeitsgemeinschaft Halbleiterforschung Leipzig (FAHL), <http://www.uni-leipzig.de/~fahl>

- Project Reviewer: Deutsche Forschungsgemeinschaft (DFG), Alexander von Humboldt-Stiftung (AvH), Schweizerischer Nationalfonds zur Förderung der wissenschaftlichen Forschung (FNSNF), Fonds zur Förderung der Wissenschaften (FWF), EU
- Referee: Advanced Materials, Appl. Phys. Lett., Electr. Lett., J. Appl. Phys., Nanotechnology, Nature, Physica E, Phys. Rev. B., Phys. Rev. Lett., Phys. Stat. Sol. Science, Semiconductor Science and Technology, Thin Solid Films

M. Lorenz

- Project Reviewer: Deutsche Forschungsgemeinschaft (DFG)
- Referee: Advanced Functional Materials, Applied Physics Letters, Applied Surface Science, Crystal Growth and Design, European Physics Journal, IEEE Transactions on Nuclear Science, Journal of Physical Chemistry, Journal of Physics D: Applied Physics, Japanese Journal of Applied Physics, Materials Science and Engineering, Nanotechnology, Physica Status Solidi (a) and RRL, Thin Solid Films

H. von Wenckstern

- Referee: Appl. Phys. Lett., J. Appl. Phys., Thin Solid Films, Solid State Electron., Phys. Stat. Sol., Superlatt. Microstruct., J. Electron. Mater., Turk. J. Phys., J. Mater. Sci., Mater. Electron., J. Vac. Sci. Technol., Mater. Sci. Eng. B, J. Nanosci. Nanotechnol., Microelectron. Eng., J. Phys. D, J. Cryst. Growth, Surf. Sci.

R. Schmidt-Grund

- President of the Arbeitskreis Ellipsometrie – Paul Drude e.V. (AKE PD e.V.) – German working group ellipsometry
- Project Reviewer: Deutsche Forschungsgemeinschaft (DFG), US Department of Energy, Basic Energy Science
- Referee: Thin Solid Films, Current Applied Physics, Phys. Stat. Sol. C, Nature Communications, Appl. Phys. Lett., Optics Express, Journal of Electromagnetic Waves and Applications, Opt. Materials, ACS Applied Materials & Interfaces

8.24 External Cooperations

Academic

- Leibniz-Institut für Oberflächenmodifizierung e. V., Leipzig, Germany
Prof. Dr. B. Rauschenbach, Prof. Dr. S. Mayr, Dr. J. Gerlach, Dr. K. Bundesmann
- Universität Leipzig, Fakultät für Chemie und Mineralogie, Germany
Prof. Dr. H. Krautscheid, Prof. Dr. R. Denecke
- Universität Halle-Wittenberg, Germany
Prof. Dr. I. Mertig, Prof. Dr. W. Widdra
- Max-Planck-Institut für Mikrostrukturphysik, Halle/Saale, Germany
Dr. O. Breitenstein, Dr. A. Ernst, Dr. P. Werner, Prof. Dr. D. Hesse
- Forschungszentrum Dresden-Rossendorf, Germany
Prof. Dr. M. Helm, Dr. K. Potzger, Dr. H. Schmidt
- Technische Universität Berlin, Germany
Prof. Dr. D. Bimberg, Prof. Dr. A. Hoffmann

- University of Aveiro, Portugal
Prof. N. A. Sobolev
- Universität Gießen, Germany
Prof. Dr. B. Meyer
- Universität Magdeburg, Germany
Prof. Dr. A. Krost, Dr. J. Bläsing, Prof. Dr. J. Christen
- Universität Jena, Germany
Prof. Dr. C. Ronning
- Göteborg University, Sweden
Prof. Dr. M. Willander
- NCSR "Demokritos", Institute of Materials Science, Greece
Prof. Dr. A. Travlos
- Université Joseph Fourier, Grenoble, France
Prof. Dr. D. Le Si Dang
- University of Pretoria, South Africa
Prof. F. D. Auret
- University of Canterbury, Christchurch, New Zealand
Prof. Dr. M. Allen
- University of Nebraska, Lincoln, USA
Prof. Dr. M. Schubert
- Centre de Recherche sur l' Hétéro-Epitaxie et ses Applications (CNRS-CRHEA),
Valbonn, France
Dr. J. Zúñiga-Pérez
- University at Buffalo
Prof. Dr. S.M. Durbin

Industry

- Solarion AG, Leipzig Germany
Dr. Alexander Braun, Dr. Andreas Rahm
- Freiburger Compound Materials GmbH, Freiberg, Germany
Dr. G. Leibiger
- Q-Cells SE, Thalheim, Germany
Dr. K. Petter

8.25 Publications

Journals

T. Böntgen, S. Schöche, R. Schmidt-Grund, C. Sturm, M. Brandt, H. Hochmuth, M. Lorenz, M. Grundmann: *Optical properties of BaTiO₃/ZnO heterostructures under the effect of an applied bias*, Thin Solid Films **519**, 2933-2935 (2011)

M. Brandt, H. von Wenckstern, M. Stölzel, H. Hochmuth, M. Lorenz, M. Grundmann: *Semiconducting oxide heterostructures*, Semic. Sci. Technol. **26**, 014040 (2011)

C.C. Dey, S. Dey, S.C. Bedi, S.K. Das, M. Lorenz, M. Grundmann, J. Vogt, T. Butz: *Hafnium Oxide Thin Films Studied by Time Differential Perturbed Angular Correlations*, J. Appl. Phys. **109**, 113918 (6 pages) (2011)

C.P. Dietrich, M. Lange, C. Sturm, R. Schmidt-Grund, M. Grundmann: *One- and two-dimensional cavity modes in ZnO microwires*, New J. Phys. **13**, 103021 (9 pages) (2011)

C.P. Dietrich, M. Grundmann: *Comment on "Exciton-polariton microphotoluminescence and lasing from ZnO whispering-gallery mode microcavities" [Appl. Phys. Lett. 98, 161110 (2011)]*, Appl. Phys. Lett. **99**, 136101 (2011)

C.P. Dietrich, M. Lange, F.J. Klüpfel, H. von Wenckstern, R. Schmidt-Grund, M. Grundmann: *Strain distribution in bent ZnO microwires*, Appl. Phys. Lett. **98**(3), 031105 (3 pages) (2011)

C.P. Dietrich, M. Brandt, M. Lange, J. Kupper, T. Böntgen, H. von Wenckstern, M. Grundmann: *Defect properties of ZnO and ZnO:P microwires*, J. Appl. Phys. **109**, 013712 (5 pages) (2011)

M. Ellguth, M. Schmidt, R. Pickenhain, M. Grundmann: *Characterization of point defects in ZnO thin films by Optical Deep Level Transient Spectroscopy*, phys. stat. sol. (b) **248**(4), 941-949 (2011)

H. Frenzel, M. Lorenz, F.-L. Schein, A. Lajn, F.J. Klüpfel, T. Diez, H. von Wenckstern, M. Grundmann: *Metal-semiconductor field-effect transistors and integrated circuits based on ZnO and related oxides*, Handbook of Zinc Oxide and Related Materials, Vol. 2 Devices and Nano-Engineering, Z.C. Feng, ed. (Taylor and Francis/CRC Press, Florida, USA, 2011), ISBN 978-1439855744

M. Grundmann: *Formation of Epitaxial Domains: Unified Theory and Survey of Experimental Results*, phys. stat. sol. (b) **248**(4), 805-824 (2011)

F.J. Klüpfel, A. Lajn, H. Frenzel, H. von Wenckstern, M. Grundmann: *Gate- and drain-lag effects in (Mg,Zn)O-based metal-semiconductor field-effect transistors*, J. Appl. Phys. **109**, 074515 (4 pages) (2011)

A. Lajn, T. Diez, F. Schein, H. Frenzel, H. von Wenckstern, M. Grundmann: *Light and temperature stability of fully transparent ZnO-based inverter circuits*, IEEE Electron Device Letters **32**(4), 515-517 (2011)

A. Lajn, M. Schmidt, H. von Wenckstern, M. Grundmann: *Erratum to: Transparent rectifying contacts for visible-blind ultraviolet photo diodes based on ZnO*, J. Electr. Mat. **40**, 477 (1 page) (2011)

A. Lajn, M. Schmidt, H. von Wenckstern, M. Grundmann: *Transparent rectifying contacts for visible-blind ultraviolet photo diodes based on ZnO*, J. Electr. Mat. **40**, 473-476 (2011)

- M. Lange, C.P. Dietrich, G. Benndorf, M. Lorenz, J. Zúñiga-Pérez, M. Grundmann: *Thermal stability of ZnO/ZnCdO/ZnO double heterostructures grown by pulsed laser deposition*, J. Cryst. Growth **328**(1), 13-17 (2011)
- M. Lange, C.P. Dietrich, J. Zúñiga-Pérez, H. von Wenckstern, M. Lorenz, M. Grundmann: *MgZnO/ZnO quantum well nanowire heterostructures with large confinement energies*, J. Vac. Sci. Technol. A **29**, 03A104 (5 pages) (2011)
- M. Lorenz, H. von Wenckstern, M. Grundmann: *Tungsten oxide as gate dielectric for highly transparent and temperature-stable zincoxide-based thin-film transistors*, Adv. Mater. **23**, 5383-5386 (2011)
- M. Lorenz, M. Brandt, K. Mexner, K. Brachwitz, M. Ziese, P. Esquinazi, H. Hochmuth, M. Grundmann: *Ferrimagnetic ZnFe₂O₄ thin films on SrTiO₃ single crystals with highly tunable electrical conductivity*, phys. stat. sol. RRL **5**(12), 438-440 (2011)
- M. Lorenz, H. Hochmuth, C. Grüner, H. Hilmer, A. Lajn, D. Spemann, M. Brandt, J. Zippel, R. Schmidt-Grund, H. von Wenckstern, M. Grundmann: *Oxide thin film heterostructures on large area, with flexible doping, low dislocation density and abrupt interfaces - grown by Pulsed Laser Deposition*, Laser Chemistry 2011, **140976** (27 pages) (2011) (Hindawi, New York, 2011)
- A. Müller, M. Lorenz, K. Brachwitz, J. Lenzner, K. Mittwoch, W. Skorupa, M. Grundmann, T. Höche: *Fresnoite Thin Films grown by Pulsed Laser Deposition: Photoluminescence and Laser Crystallization*, CrystEngComm **13**, 6377-6385 (2011)
- M. Schmidt, K. Brachwitz, F. Schmidt, M. Ellguth, H. von Wenckstern, R. Pickenhain, M. Grundmann, G. Brauer, W. Skorupa: *Nickel-related defects in ZnO - A deep-level transient spectroscopy and photo-capacitance study*, phys. stat. sol. (b) **248**(8), 1949-1955 (2011)
- R. Schmidt-Grund, P. Kühne, C. Czekalla, D. Schumacher, C. Sturm, M. Grundmann: *Determination of the refractive index of single crystal bulk samples and micro-structures*, Thin Solid Films **519**, 2777-2781 (2011)
- C. Sturm, H. Hilmer, R. Schmidt-Grund, M. Grundmann: *Occupation behaviour of the lower exciton-polariton branch in ZnO-based microresonators*, AIP Conf. Proc., **1399**, 447 (2011)
- C. Sturm, H. Hilmer, R. Schmidt-Grund, M. Grundmann: *Exciton-polaritons in a ZnO-based microcavity: polarization dependence and non-linear occupation*, New J. Phys. **13**, 033014 (17 pages) (2011)
- C. Sturm, H. Hilmer, B. Rheinländer, R. Schmidt-Grund, M. Grundmann: *Cavity-photon dispersion in one-dimensional confined microresonators with an optically anisotropic cavity material*, Phys. Rev. B **83**(20), 205301 (12 pages) (2011)
- H. von Wenckstern, R. Schmidt-Grund, C. Bundesmann, A. Müller, C.P. Dietrich, M. Stölzel, M. Lange, M. Grundmann: *The (Mg,Zn)O Alloy*, Handbook of Zinc Oxide and Related Materials, Vol. 1 Materials, Z.C. Feng, ed. (Taylor and Francis/CRC Press, Florida, USA, 2011), ISBN 978-1439855706

J. Zippel, M. Lorenz, J. Lenzner, M. Grundmann, T. Hammer, A. Jacquot, H. Böttner: *Electrical transport and optical emission of $Mn_xZr_{1-x}O_2$ ($0 < x < 0.5$) thin films*, J. Appl. Phys. **110**, 043706 (6 pages) (2011)

Zh. Zhang, H. von Wenckstern, M. Schmidt, M. Grundmann: *Wavelength selective metal-semiconductor-metal photodetectors based on (Mg,Zn)O-heterostructures*, Appl. Phys. Lett. **99**(8), 083502 (3 pages) (2011)

Patents

H. Frenzel, A. Lajn, H. von Wenckstern, M. Grundmann: *Transparente gleichrichtende Metall-Metalloxid-Halbleiterkontaktstruktur und Verfahren zu seiner Herstellung und Verwendung*, DE 10 2009 030 045 B3 (Deutsches Patent- und Markenamt, München, 2011)

Talks

S. Acharya, S. Chouthe, T. Böntgen, R. Schmidt-Grund, M. Grundmann, G. Seifert: *Ultrafast Dynamics of ZnO and ZnO-BaTiO₃ thin films*, 75th DPG Spring Meeting, Dresden, Germany, March 2011

T. Böntgen, J. Zippel, R. Schmidt-Grund, M. Lorenz, M. Grundmann: *Refractive Index matching of BaTiO₃/SrTiO₃ Heterostructures*, 75th DPG Spring Meeting, Dresden, Germany, March 2011

T. Böntgen, J. Zippel, R. Schmidt-Grund, M. Lorenz, M. Grundmann: *Refractive index tuning in BaTiO₃/SrTiO₃ heterostructures*, 6th workshop ellipsometry, Berlin, Germany, February 2011

C.P. Dietrich, M. Lange, F.J. Klüpfel, R. Schmidt-Grund, H. von Wenckstern, M. Grundmann: *Strain distribution in ZnO microwires*, 75th DPG Spring Meeting, Dresden, Germany, March 2011

C.P. Dietrich, M. Lange, F.J. Klüpfel, R. Schmidt-Grund, H. von Wenckstern, M. Grundmann: *Strain distribution in ZnO microwires*, E-MRS Spring Meeting 2011, Nice, France, May 2011

C.P. Dietrich, M. Lange, M. Stölzel, H. Franke, and M. Grundmann: *ZnO microwire quantum well heterostructures*, MRS Fall Meeting 2011, Boston, MA, USA, November/December 2011

H. Franke, C. Sturm, R. Schmidt-Grund, M. Grundmann: *Nonequilibrium exciton-polariton condensates in a ZnO-based microcavity*, Optics of Excitons in Confined Systems (OECS), Paris, France, September 2011

M. Grundmann: *Transparent Electronics using Oxide Materials*, 75th DPG Spring Meeting, Dresden, Germany, March 2011, invited

M. Grundmann: *Polaritons in ZnO based planar and rod-like structures*, 11th Int. Conf. on Physics of Light-Matter Coupling in Nanostructures (PLMCN-11), Berlin, Germany, April 2011, invited

M. Grundmann: *ZnO with conformal oxide heterostructures*, E-MRS Spring Meeting 2011, Nice, France, May 2011, invited

M. Grundmann: *Metalloxide - Mehr als Rost*, Festvortrag anlässlich der Verleihung des Leipziger Wissenschaftspreises 2011, Leipzig, Germany, April 2011

H. Hilmer, C. Sturm, R. Schmidt-Grund, M. Grundmann: *ZnO mesa-structures in planar microcavities*, 75th DPG Spring Meeting, Dresden, Germany, March 2011

H. Hilmer, C. Sturm, R. Schmidt-Grund, M. Grundmann: *Trapped polariton condensates in a ZnO-based microcavity*, Physics of Light-Matter Coupling in Nanostructures (PLMCN), Berlin, Germany, April 2011

T. Jakubczyk, W. Pacuski, A. Golnik, C. Kruse, D. Hommel, H. Hilmer, R. Schmidt-Grund, J.A. Gaj: *Control over CdTe QDs emission using ZnTe-based micropillar cavities*, 40th "Jaszowiec" International School & Conference on the Physics of Semiconductors, Krynica-Zdrój, Poland, June 2011

F.J. Klüpfel, A. Lajn, H. Frenzel, H. von Wenckstern, M. Grundmann: *Dynamic Properties of (Mg,Zn)O-based MESFETs*, 75th DPG Spring Meeting, Dresden, Germany, March 2011

M. Lange, C.P. Dietrich, K. Brachwitz, M. Stölzel, M. Lorenz, M. Grundmann: *ZnCdO thin films and ZnCdO/ZnO multiple quantum well structures grown by pulsed-laser deposition*, MRS 2011 Fall Meeting, Boston, MA, USA, November/December 2011

M. Lange, C.P. Dietrich, H. von Wenckstern, K. Brachwitz, M. Stölzel, M. Lorenz, M. Grundmann: *ZnCdO thin films and heterostructures grown by pulsed-laser deposition*, 75th DPG Spring Meeting, Dresden, Germany, March 2011

M. Lorenz, *Elektrische Eigenschaften transparenter amorpher Oxide*, Transparent Conductive Oxide Workshop, Dresden, Germany, May 2011, invited

M. Lorenz, A. Lajn, H. Frenzel, H. von Wenckstern, M. Grundmann, P. Barquinha, E. Fortunato, R. Martins: *Low-temperature processed Schottky-gated field-effect transistors based on gallium-indium-zinc-oxide channels*, Electronic Materials Conference, Santa Barbara, USA, July 2011

M. Lorenz: *Physics and technology of ZnO*, International School on Oxide Electronics (ISOE 2011), Corsica, France, October 2011

M. Lorenz, A. Müller, K. Brachwitz, J. Lenzner, K. Mittwoch, W. Skorupa, M. Grundmann, T. Höche: *Local enhancement of luminescence intensity in fresnoite scintillator films by direct laser writing*, International Topical Workshop on Subsecond Thermal Processing of Advanced Materials 2011subtherm-2011, Dresden, Germany, October 2011

M. Lorenz: *Methoden zur Züchtung und Analyse von Dünnschichten und Oberflächen*, Transfermeeting Neue Materialien, Universität Leipzig and IHK Leipzig, Germany, November 2011

S. Müller, H. v Wenckstern, O. Breitenstein, J. Lenzner, M. Grundmann: *Investigation of multibarrier Schottky contacts*, 75th DPG Spring Meeting, Dresden, Germany, March 2011

S. Müller, H. v Wenckstern, O. Breitenstein, J. Lenzner, M. Grundmann: *Investigation of Multi-Barrier ZnO-Schottky Contacts*, Electronic Materials Conference, Santa Barbara, USA, July 2011

F.-L. Schein, T. Böntgen, M. Winter, H. von Wenckstern, H. Frenzel, M. Grundmann: *ZnCo₂O₄ - A p-type semiconducting oxide - Thin films and devices*, MRS 2011 Fall Meeting, Boston, MA, USA, November/December 2011

F. Schmidt, H. von Wenckstern, M. Schmidt, M. Stölzel, G. Benndorf, M. Grundmann: *Strain-related defects in MgZnO thin films*, 75th DPG Spring Meeting, Dresden, Germany, March 2011

D. Schumacher, R. Schmidt-Grund, H. Hilmer, C. Sturm, H. Hochmuth, M. Lorenz, M. Grundmann: *ZnO mesa-structures in planar microcavities*, 75th DPG Spring Meeting, Dresden, Germany, March 2011

M. Stölzel, M. Brandt, A. Müller, G. Benndorf, M. Lorenz, M. Grundmann: *Luminescence redshift of polar (Mg,Zn)O/ZnO quantum wells: Separating the role of Stokes shift and quantum-confined Stark effect*, 15th International Conference on II-VI Compounds, Mayan Riviera, Mexico, August 2011

M. Stölzel, M. Brandt, A. Müller, J. Kupper, G. Benndorf, M. Lorenz, M. Grundmann: *Optical and electrical properties of polar (Mg,Zn)O/ZnO quantum wells*, 4th BuildMoNa Workshop for Doctoral Candidates, Dresden, Germany, September 2011

C. Sturm, H. Hilmer, S. Linke, R. Schmidt-Grund, M. Grundmann: *Polarization properties of the exciton-polariton occupation in ZnO-based microresonators*, 75th DPG Spring Meeting, Dresden, Germany, March 2011

H. von Wenckstern, S. Müller, J. Lenzner, O. Breitenstein, M. Grundmann: *Schottky contacts on ZnO*, South African Conferene on Photonic Materials, Kariega, RSA, May 2011

H. von Wenckstern: *Electric and electronic properties of defects in semiconductors: Case studies of mc-Si and single-crystalline ZnO*, Universität Bremen, Bremen, Germany, June 2011, invited

H. von Wenckstern: *ZnO-based Schottky Diodes and Their Utilization in Transparent Electronics*, 58th Annual Meeting of the American Vacuum Society, Nashville, USA, October 2011, invited

H. von Wenckstern: *ZnO-based Schottky Diodes and Their Utilization in Transparent Electronics*, MRS Fall Meeting, Boston, USA, November/December 2011, invited

Posters

T. Böntgen, T. Herzig, R. Schmidt-Grund, M. Lorenz, M. Grundmann: *Magneto-Optical Ellipsometry on Ferromagnetic Co thin films*, 6th workshop ellipsometry, Berlin, Germany, February 2011

K. Brachwitz, T. Böntgen, J. Lenzner, K. Ghosh, M. Lorenz, M. Grundmann: *Structural and magnetic properties of $Zn_{1-x}Fe_xO_z$ thin films grown by pulsed-laser deposition*, 75th DPG Spring Meeting, Dresden, Germany, March 2011

F. Daume, C. Scheit, S. Puttnins, A. Rahm, M. Grundmann: *Series resistance mapping of $Cu(In,Ga)Se_2$ solar cells by voltage dependent electroluminescence*, 75th DPG Spring Meeting, Dresden, Germany, March 2011

F. Daume, S. Puttnins, C. Scheit, H. Zachmann, A. Rahm, A. Braun, M. Grundmann: *Damp heat treatment of $Cu(In,Ga)Se_2$ solar cells with different sodium content*, E-MRS 2011 Spring Meeting, Nice, France, May 2011

F. Daume, C. Scheit, S. Puttnins, A. Rahm, M. Grundmann: *Application of series resistance imaging techniques to $Cu(In,Ga)Se_2$ solar cells*, EU-PVSEC, Hamburg, Germany, 2011

C.P. Dietrich, M. Lange, C. Sturm, H. Hilmer, R. Schmidt-Grund, M. Grundmann: *One- and two-dimensional optical eigenmodes in ZnO microwires*, 4th Scientific Symposium of the Graduate School BuildMoNa, Leipzig, Germany, March 2011

C.P. Dietrich, M. Lange, J. Zippel, J. Lenzner, M. Lorenz, M. Grundmann: *Growth and characterization of ZnO- and ZnO:P-microwires*, 11th International Conference on Physics of Light Matter Coupling in Nanostructures, Berlin, Germany, April 2011

T. Herzig, T. Böntgen, R. Schmidt-Grund, M. Lorenz, M. Grundmann: *Magneto-Optical Ellipsometry of Ferromagnetic Thin Films*, 75th DPG Spring Meeting, Dresden, Germany, March 2011

H. Hilmer, T. Michalsky, C. Sturm, R. Schmidt-Grund, J. Zúñiga-Pérez, R. Fechner, F. Frost, M. Grundmann: *Combinatorial growth of ZnO resonators*, 75th DPG Spring Meeting, Dresden, Germany, March 2011

H. Hilmer, C. Sturm, R. Schmidt-Grund, J. Zúñiga-Pérez, M. Lange, A. Meißner, J. Lenzner, G. Zimmermann, M. Cornejo, R. Fechner, F. Frost, H. Hochmuth, M. Lorenz, M. Grundmann: *PLD growth of ZnO-based planar and cylindrical microresonators*, Physics of Light-Matter Coupling in Nanostructures (PLMCN), Berlin, Germany, April 2011

C. Kranert, T. Böntgen, R. Schmidt-Grund, M. Lorenz, M. Grundmann: *Growth induced structural defects in $BaTiO_3$ -ZnO-heterostructures*, 75th DPG Spring Meeting, Dresden, Germany, March 2011

A. Lajn, H. Frenzel, T. Diez, F. Schein, H. von Wenckstern, M. Grundmann: *Transparent rectifying contacts: A novel approach in transparent electronics*, 7th International Thin-Film Transistor Conference, Cambridge, UK, March 2011

M. Lange, A. Reinhardt, C.P. Dietrich, G. Benndorf, M. Lorenz, M. Grundmann: *Thermal stability of ZnO/ZnCdO/ZnO double heterostructures*, 75th DPG Spring Meeting, Dresden, Germany, March 2011

M. Lange, C.P. Dietrich, K. Brachwitz, M. Stölzel, H. von Wenckstern, M. Lorenz, M. Grundmann: *ZnCdO thin films and heterostructures grown by pulsed laser deposition*, E-MRS 2011 Spring Meeting, Nice, France, May 2011

J. Lorbeer, T. Böntgen, J. Zippel, R. Schmidt-Grund, M. Lorenz, M. Grundmann: *Spectroscopic ellipsometry for process control in PLD growth*, 75th DPG Spring Meeting, Dresden, Germany, March 2011

M. Lorenz, A. Lajn, H. Frenzel, H. von Wenckstern, M. Grundmann, P. Barquinha, E. Fortunato, R. Martins: *Low-temperature processed Schottky-gated field-effect transistors based on gallium-indium-zinc-oxide channels*, 7th International Transistors Conference, Cambridge, United Kingdom, January 2011

M. Lorenz, A. Lajn, H. Frenzel, H. von Wenckstern, M. Grundmann, P. Barquinha, E. Fortunato, R. Martins: *Low-temperature processed Schottky-gated field-effect transistors based on amorphous oxide channel material*, 75th DPG Spring Meeting, Dresden, Germany, March 2011

M. Lorenz: *Polarisationswechselwirkung in Wurtzit-Perowskit-Spinell-Heterostrukturen*, Verteidigungskolloquium des SFB 762, Halle, Germany, September 2011

A. Müller, M. Stölzel, G. Benndorf, M. Grundmann: *Particle Wave Functions in Alloys*, 75th DPG Spring Meeting, Dresden, Germany, March 2011

S. Müller, H. v Wenckstern, O. Breitenstein, J. Lenzner, M. Grundmann: *Microscopic identification of hot spots in multi-barrier Schottky contacts on pulsed laser deposition grown zinc oxide thin films*, FAHL Academia 2011 workshop, Leipzig, Germany, September 2011

F.-L. Schein, T. Böntgen, H. von Wenckstern, M. Lorenz, M. Grundmann: *Structural and electrical properties of p-type conducting $ZnCo_2O_4$ thin films*, 75th DPG Spring Meeting, Dresden, Germany, March 2011

F. Schmidt, H. von Wenckstern, M. Schmidt, M. Grundmann: *Defect-studies on nickel-doped ZnO thin films*, FAHL Academia 2011 workshop, Leipzig, Germany, September 2011

D. Schumacher, R. Schmidt-Grund, P. Kühne, H. Hilmer, C. Sturm, H. Hochmuth, M. Lorenz, M. Grundmann: *Low-temperature dielectric tensor of MgZnO thin films and ZnO single crystals*, 6th Workshop Ellipsometry, Berlin, Germany, February 2011

M. Stölzel, A. Müller, S. Müller, G. Benndorf, M. Lorenz, H. von Wenckstern, M. Grundmann: *Donor-acceptor pair recombination in ZnO*, 75th DPG Spring Meeting, Dresden, Germany, March 2011

M. Stölzel, A. Müller, S. Müller, G. Benndorf, M. Lorenz, H. von Wenckstern, M. Grundmann: *Donor-acceptor pair recombination in ZnO*, 4th Scientific Symposium of the Graduate School BuildMoNa, Leipzig, Germany, March 2011

C. Sturm, H. Hilmer, S. Linke, R. Schmidt-Grund, M. Grundmann: *Pseudo-ellipsometry on ZnO-based microresonators in the strong coupling regime*, 6th workshop ellipsometry, Berlin, Germany, February 2011

C. Sturm, H. Hilmer, R. Schmidt-Grund, M. Grundmann: *Cavity-photon mode dispersion in 1D confined optically anisotropic microresonators*, 75th DPG Spring Meeting, Dresden, Germany, March 2011

C. Sturm, H. Hilmer, R. Schmidt-Grund, M. Grundmann: *Cavity-photon dispersion in 1D confined anisotropic microcavities*, 11th International Conference on Physics of Light-Matter Coupling in Nanostructures (PLMCN11), Berlin, Germany, April 2011

C. Sturm, H. Hilmer, R. Schmidt-Grund, M. Grundmann: *Exciton-polariton occupation in a ZnO-based microcavity: polarization and non-linear effects*, 11th International Conference on Physics of Light-Matter Coupling in Nanostructures (PLMCN11), Berlin, Germany, April 2011

C. Sturm, H. Franke, S. Linke, R. Schmidt-Grund, M. Grundmann: *Stokes-vector analysis of the exciton-polariton emission from a ZnO-based microcavity*, OECS 12, Paris, France, September 2011

Z.P. Zhang, H. von Wenckstern, J. Lenzner, M. Lorenz, H. Hochmuth, M. Grundmann: *Back-illuminated visible-blind and wavelength selective metal-semiconductor-metal photodetectors based on MgZnO-heterostructures*, 75th DPG Spring Meeting, Dresden, Germany, March 2011

Z.P. Zhang, H. von Wenckstern, M. Schmidt, M. Grundmann: *Wavelength selective metal-semiconductor-metal UV-photodetectors based on (Mg,Zn)O-heterostructures*, 2011 MRS Fall Meeting, Boston, USA, November/December 2011

8.26 Graduations

Doctorate

- Claudia Kaufß
Untersuchungen der Oberflächenanisotropie von dotierten und undotierten A-III/B-V-Halbleitern bei der Abscheidung mittels MOVPE
April 2011
- Chris Sturm
Exciton-Polaritons in ZnO-based Microresonators: Dispersion and Occupation
October 2011

Master

- Michael Bonholzer
Magnetische Tunnelkontakte auf der Basis von Zinkferrit und Cobalt
September 2011
- Julia Benke
Characterization of thin $\text{Ge}_2\text{Sb}_2\text{Te}_5$ films produced via ultra-short pulsed laser deposition
December 2011

Bachelor

- Tom Michalsky
Mikroresonatoren mit MgZnO-ZnO Quantengraben
February 2011
- Agnes Holtz
Optimierung des Prozessgases Argon/Wasserstoff im STRING RIBBONTM - Verfahren zur Waferherstellung
September 2011
- Tobias Herzig
Aufbau und Test eines Messplatzes für Magnetooptische Ellipsometrie
September 2011
- Daniel Splith
Passivierung von ZnO-MESFETs
September 2011
- Alexander Schneider
Drain- und Gatelag-Effekte von Silber-dotierten ZnO-Feldeffekttransistoren
September 2011
- Markus Purfürst
Photolumineszenzuntersuchungen an (Mg,Zn)O/ZnO Quantengrabenstrukturen
October 2011

8.27 Guests

- Prof. Dr. Francois Daniel Auret
University of Pretoria, Pretoria, South Africa
18. September – 23. September 2011
- Robert Heinhold
University of Canterbury, Christchurch, New Zealand
28. March – 21. July 2011
- Dr. Walter Ernst Meyer
University of Pretoria, Pretoria, South Africa
18. September – 24. September 2011

9

Superconductivity and Magnetism

9.1 Introduction

The research of the Division of Superconductivity and Magnetism is focused on the study of magnetic ordering and superconductivity in a range of materials, especially carbon-based systems and magnetic oxides.

Prof. Pablo Esquinazi

9.2 A spin-calorics device based on $\text{La}_{0.7}\text{Sr}_{0.3}\text{MnO}_3/\text{SrRuO}_3$ superlattices

M. Ziese

High quality $\text{La}_{0.7}\text{Sr}_{0.3}\text{MnO}_3/\text{SrRuO}_3$ superlattices with ultra-thin individual layers were studied by magnetometry and magnetoresistance measurements. Depending on layer thickness and structural quality, exchange biasing could be observed both in magnetization and magnetotransport. In this regime the superlattice magnetization forms an exchange spring that leads to a reversible field dependence of the magnetoresistance and the magnetic work. It is shown that the magnetic work and the magnetocaloric effect can be tuned by the SrRuO_3 layer thickness, see Fig. 9.1. This opens up the possibility of fabricating spin-caloric devices from wedge-shaped superlattices with self-sustaining Seebeck effect.

9.3 Exchange coupling and exchange bias in $\text{La}_{0.7}\text{Sr}_{0.3}\text{MnO}_3$ - SrRuO_3 superlattices

M. Ziese, E. Pippel*, E. Nikulina*, M. Arredondo*, I. Vrejoiu*

*Max Planck Institute of Microstructure Physics, 06120 Halle, Germany

$\text{La}_{0.7}\text{Sr}_{0.3}\text{MnO}_3$ - SrRuO_3 superlattices with and without nanometrically thin SrTiO_3 , BaTiO_3 and $\text{Ba}_{0.7}\text{Sr}_{0.3}\text{TiO}_3$ interlayers were grown by pulsed laser deposition. Transmission electron microscopy studies showed coherent growth of $\text{La}_{0.7}\text{Sr}_{0.3}\text{MnO}_3$, SrRuO_3

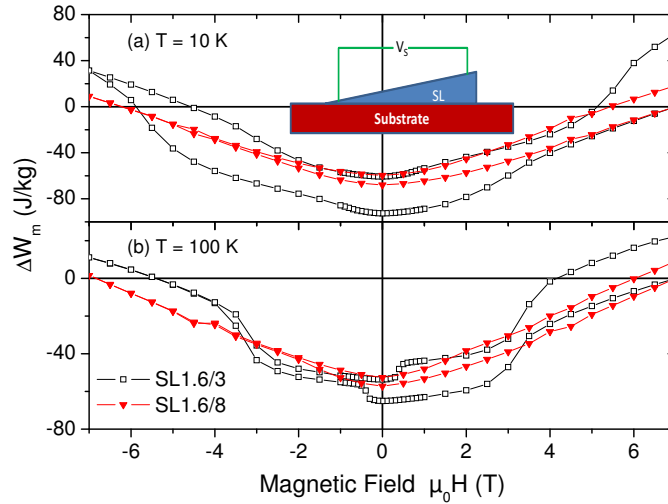


Figure 9.1: Magnetic work done on superlattices SL1.6/3 and SL1.6/8 at (a) 10 K and (b) 100 K. The superlattices had 1.6 nm thick $\text{La}_{0.7}\text{Sr}_{0.3}\text{MnO}_3$ and 5 (8) nm thick SrRuO_3 layers. Hysteresis loops started at 7 T in a state close to magnetic saturation. Note that the shape of the hysteresis loop as well as the magnetic work difference after completing the sweep strongly depend on the SrRuO_3 layer thickness. The inset shows the schematics of a Seebeck wedge.

and SrTiO_3 layers with atomically sharp interfaces, even if individual layers were as thin as one or two unit cells. In contrast, misfit dislocations and unit cell high interfacial steps were observed at the interfaces between BaTiO_3 and one of the ferromagnetic layers. The presence of the interlayers as well as these extended defects had a significant influence on the magnetic properties of the superlattices, especially on the antiferromagnetic interlayer exchange coupling between the $\text{La}_{0.7}\text{Sr}_{0.3}\text{MnO}_3$ and SrRuO_3 layers and the exchange biasing. Surprisingly, exchange biasing was found to increase with decreasing strength of the antiferromagnetic interlayer exchange coupling. This is illustrated in Fig. 9.2: whereas the exchange bias field in strongly coupled superlattices vanishes, it is finite in the superlattice containing BaTiO_3 interlayers. This was explained by different magnetization reversal mechanisms acting in the regimes of strong and weak interlayer exchange coupling.

9.4 Hall effect of orthorhombic and tetragonal SrRuO_3 layers

M. Ziese, I. Vrejoiu*

*Max Planck Institute of Microstructure Physics, 06120 Halle, Germany

High quality $\text{Pr}_{0.7}\text{Ca}_{0.3}\text{MnO}_3/\text{SrRuO}_3$ superlattices were fabricated by pulsed laser deposition. The SrRuO_3 layers grew either in orthorhombic or tetragonal symmetry depending on the thickness of the $\text{Pr}_{0.7}\text{Ca}_{0.3}\text{MnO}_3$ layers. Since the $\text{Pr}_{0.7}\text{Ca}_{0.3}\text{MnO}_3$ layers were insulating at low temperatures, this for the first time allowed for the measurement of the anomalous and ordinary Hall effect of tetragonal SrRuO_3 layers. The carrier concentration was 1.5 and 1.25 electrons per formula unit in the orthorhombic and tetragonal phase, respectively. The anomalous Hall constant is positive in tetragonal

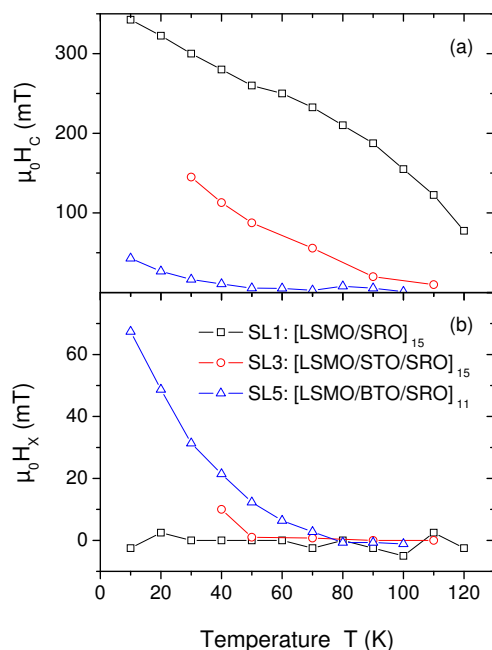


Figure 9.2: (a) Coercive field H_C and (b) exchange bias field H_X of samples SL1 (a direct $\text{La}_{0.7}\text{Sr}_{0.3}\text{MnO}_3$ - SrRuO_3 superlattice), SL3 (with SrTiO_3 interlayers) and SL5 (with BaTiO_3 interlayers). The coercive field decreases, whereas the exchange-bias field increases with the degree of magnetic coupling.

SrRuO_3 in contrast to the negative values seen at low temperatures in the orthorhombic phase. This is illustrated in Fig. 9.3.

9.5 Angular dependence of the magnetoelectric effect in orthorhombic HoMnO_3 films

M. Ziese, A. Setzer, R. Wunderlich, C. Zandalazini, P. Esquinazi

Epitaxial orthorhombic HoMnO_3 films were grown on Nb-doped SrTiO_3 (001) single-crystal substrates. X-ray diffractometry showed a uniform crystallographic orientation with the c-axis along the substrate normal and an anisotropic compressive stress along the b-axis of the Pbnm structure. The rotational anisotropy of the magnetoelectric effect was measured. Whereas magnetic field rotation in the $(110)_o$ and $(110)_o$ planes showed a twofold pattern with the smallest magnetoelectric effect observed in magnetic fields along the c-axis, in-plane $(001)_o$ magnetic field rotations revealed an intricate rotational symmetry, see Fig. 9.4. A magnetic-field-induced crossover was observed from a low-field region with fourfold rotation patterns to a high-field region with rotation patterns up to the 12th order. This complex rotational symmetry arises from spin-orbit coupling of the Ho^{3+} moments that induces a modulation of the magnetoconductance as well as a magnetoelectric effect through the Maxwell-Wagner mechanism.

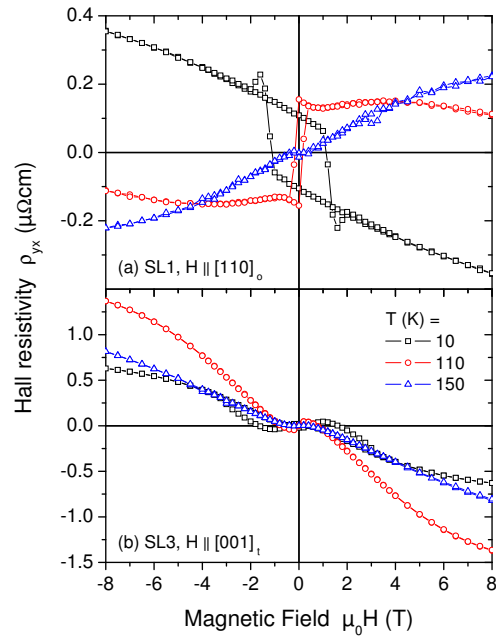


Figure 9.3: Hall resistivity ρ_{yx} of (a) the orthorhombic superlattice SL1 and (b) the tetragonal superlattice SL3 as a function of applied field for various temperatures. The high field slope is negative indicating electron conduction. In case of the tetragonal sample the low field slope is positive yielding a positive anomalous Hall constant. In orthorhombic SrRuO_3 the anomalous Hall effect changes its sign from negative at low temperatures to positive above about 100 K.

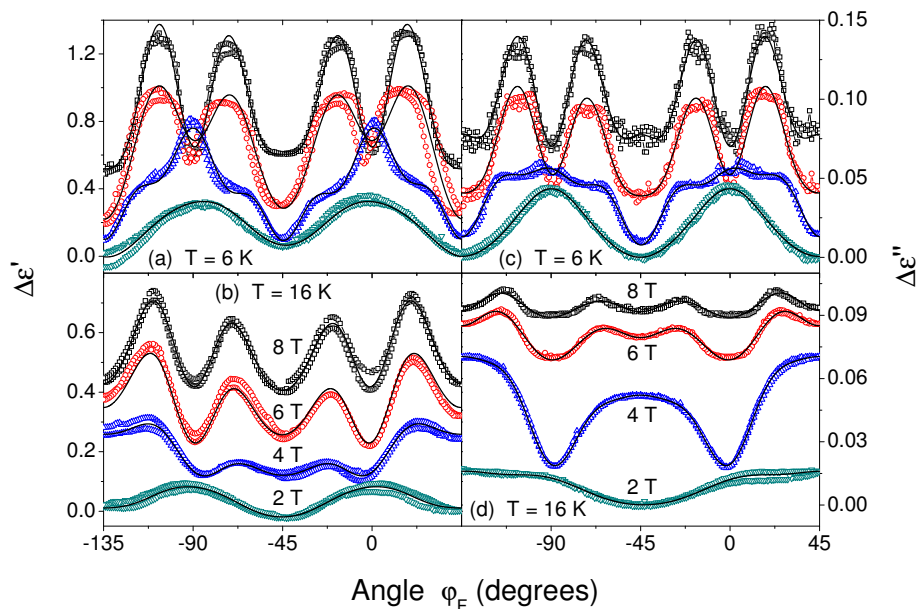


Figure 9.4: Angular dependence of the [(a),(b)] real and [(c),(d)] imaginary part of the dielectric permittivity of a HoMnO_3 film for field rotations in the $(001)_o$ plane at [(a),(c)] 6 K and [(b),(d)] 16 K. The solid lines are fits of a model based on symmetry considerations to the data.

9.6 Enhancement of the ferromagnetic order of graphite after sulphuric acid treatment

J. Barzola-Quiquia, W. Böhlmann, P. Esquinazi, A. Schadewitz, A. Ballestar, S. Dusari, L. Schultze-Nobre* B. Kersting[†]

*Helmholtz Centre for Environmental Research-UFZ, Permoserstrasse 15, D-04318 Leipzig, Germany

[†]Institut für Anorganische Chemie, Universität Leipzig, Johannisallee 29, D-04103 Leipzig, Germany

We have studied the changes in the ferromagnetic behavior of graphite powder and graphite flakes after treatment with diluted sulphuric acid. We show that this kind of acid treatment enhances substantially the ferromagnetic magnetization of virgin graphite micrometer size powder as well as in graphite flakes. The anisotropic magnetoresistance amplitude at 300 K measured in a micrometer size thin graphite flake after acid treatment reaches values comparable to polycrystalline cobalt.

9.7 Andreev Reflection and Granular Superconductivity Features Observed in Mesoscopic Samples Using Amorphous Tungsten Carbide Superconductors

J. Barzola-Quiquia, S. Dusari, C. Chilotte,* P. Esquinazi

*Departamento de Física, FCEyN, Universidad de Buenos Aires, Pabellon 1, Ciudad Universitaria, Buenos Aires, Argentina

Point-contact Andreev reflection and magnetoresistance measurements were done using amorphous tungsten carbide (WC_x) superconductors. Superconducting tips as well as microwires were grown directly under a focused Ga^+ -ion beam (FIB) on pre-patterned samples. Using ebeam lithography, the electrical contacts were prepared later using a special geometry. Current-voltage measurements as a function of temperature and magnetic field clearly showed the signatures of Andreev reflection. We observed anomalies in the differential conductivity at voltages above the energy gap values. These anomalies can be well understood as due to a weak-link formation with narrow band properties contributing in parallel at the interfaces of the contacts. We also observed Andreev oscillations as a function of magnetic field similar to those found recently in specially prepared normal-superconducting-normal nanostructures and multigraphene samples. In some of the structures, we were able to produce interfaces in which clear granular behavior in a certain temperature region was observed, such as, for example, an anomalous field hysteresis loop compatible with the existence of granular superconductivity, similar to that found also in thin mesoscopic graphite samples

9.8 Spin transport in a thin graphite flake

J. Barzola-Quiquia, P. Esquinazi

We have studied the spin transport on a 30 nm thick and several micrometer long oriented graphite flake using a spin-valve configuration with four ferromagnetic Co electrodes of different widths and several μm separation. A 5-nm thin Pt layer has been introduced in between the ferromagnetic Co injector/detector and the graphite surface. In spite of the conductivity mismatch problem, efficient electrical spin injection and detection in graphite has been achieved. The magnetoresistance in the local and half-local electrodes shows clear maxima with symmetry around zero field. The spin transport can be detected up to 150 K.

9.9 Funding

Study of intrinsic and extrinsic phenomena in the electrical transport properties of multi-graphene

Prof. P. Esquinazi
DFG ES 86/16-1

Defect-induced Magnetism in Oxides

Prof. P. Esquinazi and Dr. M. Ziese
DFG SFB762 B1

Spin-dependent Transport and Exchange-Biasing in multiferroic Heterostructures

Dr. M. Ziese and Prof. P. Esquinazi
DFG SFB 762 B5

Study of the anisotropy ratio of the conductivities of graphite

Prof. P. Esquinazi
DAAD

Transport properties of oxide and carbon nanostructures

Prof. P. Esquinazi
Buildmona

Transport properties of carbon nanotubes

DFG

9.10 Organizational Duties

P. Esquinazi

- Dean of Studies
- Project Reviewer: Deutsche Forschungsgemeinschaft (DFG), National Science Foundation (USA), German-Israeli Foundation (GIF), Israel Science Foundation, Department of Energy (Washington), DAAD
- Referee: Phys. Rev. Lett, Phys. Rev. B., Appl. Phys. Lett., Chem. Phys. Lett., Nature Physics, Nature Materials, Physica C, Phys. Lett. A, phys. stat. sol., J. Low Temp. Phys., Carbon, J. Chem. Phys., Eur. J. Phys. B, J. Magn. Mater.

M. Ziese

- Head of the Undergraduate Physics Laboratory
- Member of the study commission
- Project Reviewer: German-Israeli Foundation (GIF)
- Referee: Phys. Rev. Lett., Phys. Rev. B., Appl. Phys. Lett., J. Appl. Phys., New J. Physics, J. Phys. D: Appl. Phys., pss Rapid Research Letters, phys. stat. sol., J. Magn. Magn. Mater., Europhysics Lett., Thin Solid Films, Vacuum, JVST A, J. of Inorganic Materials, J. of the European Ceramic Society, Materials Science and Engineering B

W. Böhlmann

- Referee: J. Physical Chemistry, J. of American Chemical Society, Microporous and Mesoporous Materials

9.11 External Cooperations

Academic

- State University of Campinas, Campinas, Brazil
Prof. Dr. Yakov Kopelevich
- Max-Planck Institute of Microstructure Physics, Halle, Germany
Dr. Ionela Vrejoiu
- Max-Planck Institute of Microstructure Physics, Halle, Germany
Prof. Dietrich Hesse
- Max-Planck Institute of Microstructure Physics, Halle, Germany
Dr. Marin Alexe
- Max-Planck Institute of Microstructure Physics, Halle, Germany
Dr. Arthur Ernst
- Martin-Luther Universität Halle-Wittenberg, Halle, Germany
Prof. Ingrid Mertig
- Martin-Luther Universität Halle-Wittenberg, Halle, Germany
Prof. Wolfram Hergert
- Martin-Luther Universität Halle-Wittenberg, Halle, Germany
Dr. Angelika Chassé
- Martin-Luther Universität Halle-Wittenberg, Halle, Germany
Dr. Manfred Dubiel
- Stanford Synchrotron Radiation Laboratory, USA
Dr. Hendrik Ohldag
- Max-Planck-Institut für Metallforschung, Stuttgart, Germany
Dr. Eberhard Goering
- Laboratorio de Física de Sistemas Pequeños y Nanotecnología, Consejo Superior de Investigaciones Científicas, Madrid, Spain
Prof. N. García (Madrid)

- Forschungszentrum Dresden-Rossendorf e.V., Institut für Ionenstrahlphysik und Materialforschung, Germany
Dr. W. Anwand
- Forschungszentrum Dresden-Rossendorf e.V., Institut für Ionenstrahlphysik und Materialforschung, Germany
Dr. G. Brauer
- Tucuman University, Argentina
Prof. S. P. de Heluani
- University of La Plata, Argentina
Dr. C. E. Rodriguez Torres
- Universidad Autónoma de Madrid, Spain
Prof. Dr. Miguel Angel Ramos
- University of Ioannina, Greece, Ioannina, Greece
Prof. I. Panagiotopoulos

9.12 Publications

Journals

- J. Barzola-Quiquia, S. Dusari, C. Chilotte and P. Esquinazi:
Andreev Reflection and Granular Superconductivity Features Observed in Mesoscopic Samples Using Amorphous Tungsten Carbide Superconductors
J. Supercond. Nov. Magn. **24**, 463 (2011)
- S. Dusari, J. Barzola-Quiquia and P. Esquinazi:
Superconducting Behavior of Interfaces in Graphite: Transport Measurements of Microconstrictions
J. Supercond. Nov. Magn. **24**, 401 (2011)
- A. Ballestar, A. Setzer, P. Esquinazi and N. García:
Absence of field anisotropy in the intrinsic ferromagnetic signals of highly oriented pyrolytic graphite
J. Magn. Magn. Mater. **323**, 758 (2011)
- J. Barzola-Quiquia and P. Esquinazi:
Spin transport in a thin graphite flake
J. Mater. Science **46**, 4614 (2011)
- A. M. Jakob, D. Spemann, R. Thies, J. Barzola-Quiquia, J. Vogt and T. Butz:
A characterization of electronic properties of alkaline texturized polycrystalline silicon solar cells using IBIC
Phys. Res. B **269**, 2345 (2011)
- S. Dusari, J. Barzola-Quiquia, P. Esquinazi and N. García:
Ballistic transport at room temperature in micrometer-size graphite flakes
Phys. Rev. B **83**, 125402 (2011)

J. Barzola-Quiquia, W. Böhlmann, P. Esquinazi, A. Schadewitz, A. Ballestar, S. Dusari, L. Schultze-Nobre and B. Kersting:

Enhancement of the ferromagnetic order of graphite after sulphuric acid treatment
Appl. Phys. Lett. **98**, 192511 (2011)

M. Khalid, P. Esquinazi, D. Spemann, W. Anwand and G. Brauer:

Hydrogen-mediated ferromagnetism in ZnO single crystals
New J. Phys. **13**, 063017 (2011)

C. Zandalazini, P. Esquinazi, G. Bridoux, J. Barzola-Quiquia, H. Ohldag and E. Arenholz:

Uncompensated magnetization and exchange-bias field in $\text{La}_{0.7}\text{Sr}_{0.3}\text{MnO}_3/\text{YMnO}_3$ bilayers: The influence of the ferromagnetic layer

J. Magn. Magn. Mater. **323**, 2892 (2011)

C. Zapata, M. Khalid, G. Simonelli, M. Villafuerte, S. P. Heluani and P. Esquinazi:

Magnetic field influence on the transient photoresistivity of defect-induced magnetic ZnO films

Appl. Phys. Lett. **99**, 112503 (2011)

J. Haug, A. Chaasé, M. Dubiel, Ch. Eisenschmidt, M. Khalid and P. Esquinazi:

Characterization of lattice defects by x-ray absorption spectroscopy at the Zn K-edge in ferromagnetic pure ZnO films

J. Appl. Phys. **110**, 063507 (2011)

J. Barzola-Quiquia, A. Ballestar, S. Dusari and P. Esquinazi:

Experimental Study of the Intrinsic and Extrinsic Transport Properties of Graphite and Multigraphene Samples

Chapter 8 in "Graphene", Intech Open Publishers, pp. 115-140 (2011)

M. Ziese, I. Vrejoiu, E. Pippel, A. Hähnel, E. Nikulina and D. Hesse:

Orthorhombic-to-tetragonal transition of SrRuO_3 layers in $\text{Pr}_{0.7}\text{Ca}_{0.3}\text{MnO}_3/\text{SrRuO}_3$ superlattices

J. Phys. D: Appl. Phys. **44**, 345001 (2011)

M. Ziese, E. Pippel, E. Nikulina, M. Arredondo and I. Vrejoiu:

Exchange coupling and exchange bias in $\text{La}_{0.7}\text{Sr}_{0.3}\text{MnO}_3\text{-SrRuO}_3$ superlattices

Nanotechnology **22**, 254025 (2011)

M. Ziese, I. Vrejoiu, E. Pippel, E. Nikulina, and D. Hesse:

Magnetic properties of $\text{Pr}_{0.7}\text{Ca}_{0.3}\text{MnO}_3/\text{SrRuO}_3$ superlattices

Appl. Phys. Lett. **98**, 132504 (2011)

M. Ziese:

Comment on "Fourfold symmetric anisotropic magnetoresistance based on magnetocrystalline anisotropy and antiphase boundaries in reactive sputtered epitaxial Fe_3O_4 films" [*Appl. Phys. Lett.* **96**, 092502 (2010)]

Appl. Phys. Lett. **98**, 146101 (2011)

C. E. Rodríguez Torres, F. Golmar, M. Ziese, P. Esquinazi and S. P. Heluani:
Evidence of defect-induced ferromagnetism in ZnFe_2O_4 thin films
Phys. Rev. B **84**, 064404 (2011)

M. Ziese and I. Vrejoiu:
Anomalous and planar Hall effect of orthorhombic and tetragonal SrRuO_3 layers
Phys. Rev. B **84**, 104413 (2011)

M. Ziese, A. Setzer, R. Wunderlich, C. Zandalazini, and P. Esquinazi:
Angular dependence of the magnetoelectric effect in orthorhombic HoMnO_3 films
Phys. Rev. B **84**, 214424 (2011)

M. Ziese:
A spin-calorics device based on $\text{La}_{0.7}\text{Sr}_{0.3}\text{MnO}_3/\text{SrRuO}_3$ superlattices
Phys. Status Solidi RRL **5**, 444 (2011)

M. Lorenz, M. Brandt, K. Mexner, K. Brachwitz, M. Ziese, P. Esquinazi, H. Hochmuth
and M. Grundmann:
Ferrimagnetic ZnFe_2O_4 thin films on SrTiO_3 single crystals with highly tunable electrical
conductivity
Phys. Status Solidi RRL **5**, 438 (2011)

in press

R. Wunderlich, C. Chilotte, G. Bridoux, T. Maity, Ö. Kocabiyik, A. Setzer, M. Ziese and
P. Esquinazi:
Structural, magnetic and electric properties of HoMnO_3 films on SrTiO_3 (001)
J. Magn. Magn. Mater. **324**, 460 (2012)

Talks

M. Ziese, Orthorhombic-to-tetragonal transition of SrRuO_3 layers in $\text{Pr}_{0.7}\text{Ca}_{0.3}\text{MnO}_3/\text{SrRuO}_3$
superlattices, Invited Talk, DPG Tagung Dresden 2011

9.13 Guests

- Xun Li
Chinese Academy of Sciences Nanjing, China
05.04.2011 - 18.04.2011
- Ivan Landa
Prague University of Sciences, Czech Republic
01.06.2011 - 12.07.2011
- Worapon Boonkerd
IAESTE Student, Thailand
01.06.2011 - 31.07.2011

- Harriet Mijimah
IAESTE Student, Ghana
01.07.2011 - 31.08.2011
- Prof. Yakov Kopelevich
State University of Campinas, Campinas, Brazil
07.10.2011 - 15.10.2011

III

Institute for Theoretical Physics

10

Computational Quantum Field Theory

10.1 Introduction

The Computational Physics Group performs basic research into classical and quantum statistical physics with special emphasis on phase transitions and critical phenomena. In the centre of interest are the physics of spin glasses, diluted magnets and other materials with quenched, random disorder, soft condensed matter physics with focus on fluctuating paths and interfaces, biologically motivated problems such as protein folding, aggregation and adsorption as well as related properties of homopolymers, and the intriguing physics of low-dimensional quantum spin systems. Our investigations of a geometrical approach to the statistical physics of topological defects with applications to superconductors and superfluids and research into fluctuating geometries with applications to quantum gravity, e.g., dynamical triangulations, build on the recently concluded European Research Training Network (RTN) "ENRAGE": *Random Geometry and Random Matrices: From Quantum Gravity to Econophysics*, a collaboration of 13 teams throughout Europe. Moreover, within a bi-national Institute Partnership initiated by a research grant of the Alexander von Humboldt Foundation the statistical mechanics of complex networks is studied in collaboration with our partner university in Krakow, Poland.

The methodology is a combination of analytical and numerical techniques. The numerical tools are currently mainly Monte Carlo computer simulations and high-temperature series expansions. The computational approach to theoretical physics is expected to gain more and more importance with the future advances of computer technology, and is likely to become the third cornerstone of physics besides experiment and analytical theory as sketched in Fig. 10.1. Already now it can help to bridge the gap between experiments and the often necessarily approximate calculations of analytical work.

To achieve the desired high efficiency of the numerical studies we develop new algorithms, and to guarantee the flexibility required by basic research all computer codes are implemented by ourselves. The technical tools are Fortran, C, and C++ programs running under Unix or Linux operating systems and computer algebra using Maple or Mathematica. The software is developed and tested at the Institute on a cluster of PCs and workstations, where also most of the numerical analyses are performed.

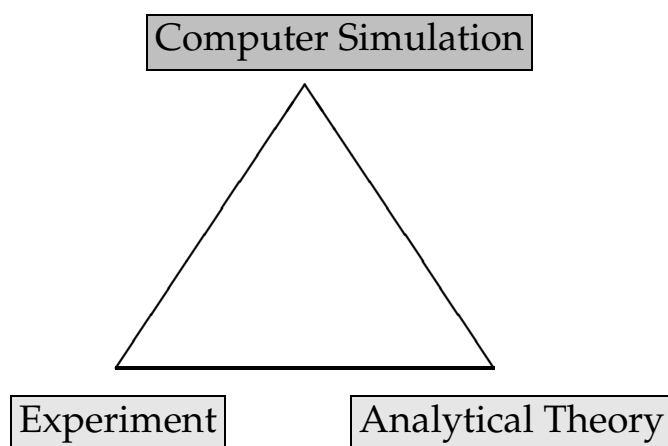


Figure 10.1: Sketch of the relationship between theory, experiment and computer simulation.

Currently we are also exploring the possibilities of the rapidly developing graphics card computing, that is computer simulations on graphics processing units (GPUs) with many cores. Large-scale simulations requiring vast amounts of computer time are carried out at the Institute on quite powerful compute servers, at the parallel computers of the University computing center, and, upon successful grant application at the national supercomputing centres in Jülich, Stuttgart and München on parallel supercomputers. This hierarchy of various platforms gives good training opportunities for the students and offers promising job perspectives in many different fields for their future career.

Within the University, our research activities are closely integrated into the Graduate School “BuildMoNa”: Leipzig School of Natural Sciences – *Building with Molecules and Nano-objects* funded by the German Research Foundation (DFG) within the German Excellence Initiative and the international DFH-UFA Graduate School *Statistical Physics of Complex Systems* with Nancy Université, France, supported by the Deutsch-Französische Hochschule. For the latter we submitted in 2010 a successful extension proposal, securing enhanced funding for the period 2011–2013 and now incorporating also Coventry University in England as an associated partner. The two Graduate Schools are both “Classes” of the Research Academy Leipzig (RALeipzig), providing the organizational frame for hosting visiting students and senior scientists, offering language courses, organizing childcare and for many other practical matters. At the post-graduate level our research projects are embedded into the “Sächsische DFG-Forschergruppe” FOR877 *From Local Constraints to Macroscopic Transport*, which also has been successfully extended in 2010 for the period 2011–2014, the Sonderforschungsbereich/Transregio SFB/TRR 102 *Polymers under Multiple Constraints: Restricted and Controlled Molecular Order and Mobility* together with Halle University, which started operation in July 2011, and the International Max Planck Research School (IMPRS) *Mathematics in the Sciences*. Our group also actively contributes to two of the top level research areas (“Profilbildende Forschungsbereiche (PbF)”) and the Centre for Theoretical Sciences (NTZ) of the University. Beside “BuildMoNa” the latter structures are particularly instrumental for our cooperations with research groups in experimental physics and biochemistry on the one hand and with mathematics and computer

science on the other.

On an international scale, our research projects are carried out in a wide net of collaborations funded by the German Academic Exchange Service (DAAD) and the Alexander von Humboldt Foundation through the Institute Partnership with the Jagiellonian University in Krakow, Poland, as well as their Fellowship Programmes, and in part initiated by the European Research Training Network "ENRAGE". Since June 2011 our group is hosting Professor Handan Arkin-Olgar from Ankara University in Turkey who was awarded an Alexander von Humboldt Fellowship for Experienced Researchers. Further close contacts and collaborations are established with research groups in Armenia, Austria, China, France, Great Britain, Israel, Italy, Japan, Poland, Russia, Spain, Sweden, Taiwan, Turkey, Ukraine, and the United States. These contacts are refreshed and furthered through topical Workshops and Tutorials and our International Workshop series *CompPhys: New Developments in Computational Physics*, taking annually place at the end of November just before the first advent weekend.

Wolfhard Janke

10.2 How Grafting of a Single Polymer Influences its Statistical Properties near an Attractive Substrate

M. Möddel, M. Bachmann*, W. Janke

*Center for Simulational Physics, The University of Georgia, Athens, USA

There is a significant difference in the conformational behaviour of a polymer grafted, i.e. firmly attached at one end, to an attractive substrate compared to one that can move freely within a certain distance to that substrate [1]. Especially at the adsorption transition, we expected such differences after a microcanonical analysis of the nongrafted polymer revealed first-order like signals for short extended conformations that get more pronounced with increasing translational entropy of desorbed conformations [2, 3]. To systematically compare the two cases, a combined canonical and microcanonical analysis was performed for a wide range of surface attraction strengths ϵ_s and temperature T [4]. This way not only the adsorption transition, but also the collapse and the freezing transition of an individual self-interacting polymer in solution were covered.

The model is a simple bead-stick model with 12-6 Lennard-Jones (LJ) interaction between nonbonded monomers, a weak bending stiffness and an attraction to a flat substrate that is proportional to a parameter ϵ_s . This surface attraction is a 9-3 LJ potential obtained by integrating the 12-6 LJ potential over a half space and, e.g., $\epsilon_s = 5$ roughly gives a surface attraction that exceeds the monomer-monomer attraction by a factor of five. This model is once considered in a box within which it can move freely and once with one end grafted to the substrate. All simulations were performed with the parallel tempering Monte Carlo method that allowed to highly parallelize the simulation and obtain good statistics over the whole energy range.

It turned out, that qualitative differences really only occur at the adsorption transition. Here, however, four cases need to be differentiated for finite chains: (1) the adsorption of extended nongrafted polymers, (2) the adsorption of extended grafted

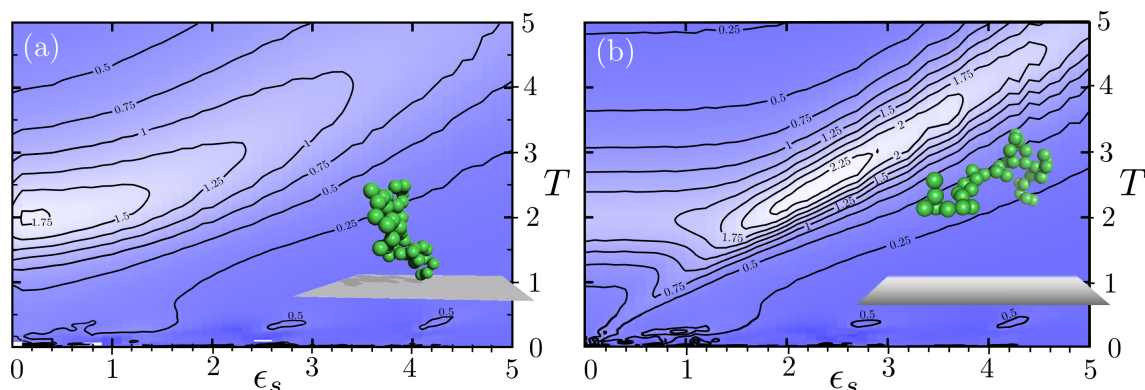


Figure 10.2: Fluctuation of the tensor component of the radius of gyration perpendicular to the substrate $d\langle R_{\text{gyr},\perp}^2\rangle/dT$ for (a) the grafted and (b) the free polymer as a contour plot versus surface attraction strength ϵ_s and temperature T .

polymers, (3) the adsorption of globular nongrafted polymers and (4) the adsorption of globular grafted polymers. Only in the first case, the microcanonical entropy, which is proportional to the logarithm of the density of states, gets convex such that the adsorption transition is first-order-like here with a dynamic phase coexistence. In the cases (2) and (3) a continuous adsorption is observed already for short chains, while in case (4) the adsorption signals get reduced significantly and only the weaker wetting transition is left.

How this is for example reflected in the temperature derivative of the canonical expectation value of the tensor component of the radius of gyration perpendicular to the substrate is visualized in Fig. 10.2. While for the nongrafted polymer a maximum over the whole diagonal $T_{\text{ads}} \propto \epsilon_s$ is visible, this signal is strongly weakened for extended grafted conformations ($\epsilon_s \gtrsim 1.9$, $T \gtrsim 2$) and even disappears for globular grafted conformations ($\epsilon_s \lesssim 1.9$, $T \lesssim 2$). For grafted chains, in this observable only the collapse transition at $T \approx 2$ is signaled for low ϵ_s values.

It is among others this necessary distinction between the adsorption of globular and extended conformations that demonstrates that it is not just the difference in translational, but also in conformational entropy that gives rise to the differences. This has been carefully described and explained in Ref. [4].

[1] M. Möddel et al.: J. Phys. Chem. B **113**, 3314 (2009)

[2] M. Möddel et al.: Phys. Chem. Chem. Phys. **12**, 11548 (2010)

[3] M. Möddel et al.: Comput. Phys. Commun. **182**, 1961 (2011)

[4] M. Möddel et al.: Macromolecules **44**, 9013 (2011)

10.3 Thermodynamics of Polymer Adsorption to a Flexible Membrane

S. Karalus*, M. Bachmann†, W. Janke

*Institut für Theoretische Physik, Universität zu Köln, Germany

†Center for Simulational Physics, The University of Georgia, Athens, USA

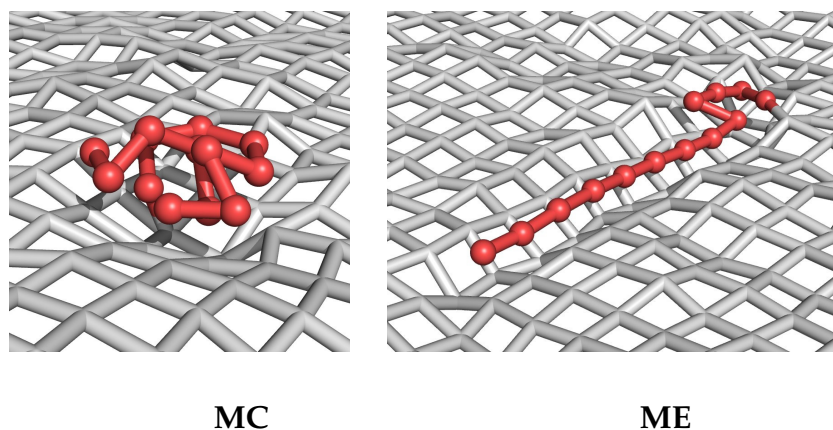


Figure 10.3: Embedded compact (MC) and expanded (ME) conformations exhibited by a polymer grafted to a flexible membrane at low temperatures and strong polymer-membrane attraction.

The interaction of macromolecules with cell membranes is essential for almost all biological processes. Membrane proteins like glycoproteins and transmembrane proteins govern the exchange of signals, small molecules, and ions between the intra- and extra-cellular solvent. Membrane embedded receptors are specific for the binding of ligands. The conformational changes caused by the binding process can, e.g., trigger cellular motion, drug delivery, or enzymatic catalysis.

It is therefore an important problem to investigate the conformational behaviour of a polymer interacting with a *flexible, fluctuating* substrate such as a membrane under thermal conditions. So far much work has been dedicated to the identification of structural transitions polymers and peptides experience when adsorbing to *solid* substrates [1–4]. In this project we extend these studies by considering a simple coarse-grained off-lattice model system consisting of a polymer grafted to a fluctuating substrate and performing extensive generalized-ensemble Monte Carlo computer simulations [5]. Adjacent monomers of the polymer are tied together by a finitely extensible nonlinear elastic (FENE) potential and all monomers interact pairwise via a standard 12–6 Lennard-Jones (LJ) potential. The fluctuating substrate is modeled by a tethered membrane with the individual building segments (nodes) again tied together by a FENE potential to form a 2D surface with $L_x \times L_y$ nodes in total. Finally, the interaction between the polymer, which is anchored at the membrane center, and the membrane is modeled by another LJ potential between all pairs of monomers and membrane nodes.

By means of extensive parallel tempering Monte Carlo simulations we have shown that the system exhibits a rich phase behaviour ranging from highly ordered, compact to extended random coil structures and from desorbed to completely adsorbed or even partially incorporated conformations, cf. Fig. 10.3. These findings are summarized in the pseudophase diagram shown in Fig. 10.4 indicating the predominant class of conformations as a function of the external parameters polymer-membrane interaction strength and temperature. By comparison with adsorption to a stiff membrane surface it is shown that the flexibility of the membrane gives rise to qualitatively new behaviour. At low temperatures, we found the membrane adapting its structure such that it partially incorporates the polymer. This leads to the “embedded compact” (MC), oblate shaped and the “embedded expanded” (ME), almost linearly stretched conformations

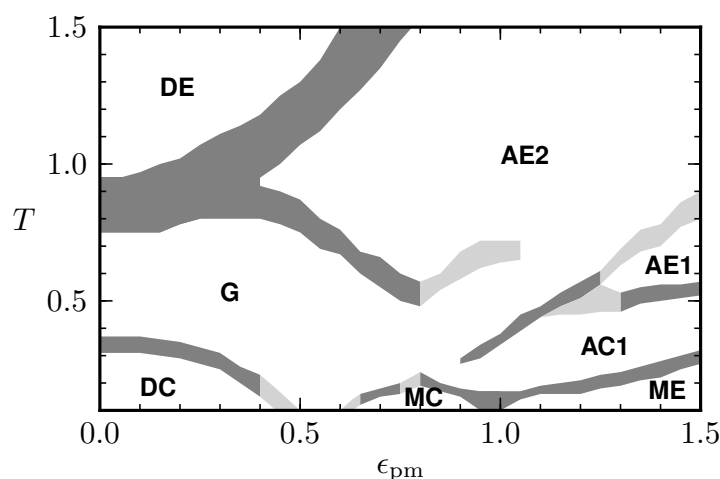


Figure 10.4: Phase diagram of a polymer grafted to a fluctuating membrane parametrized by polymer-membrane attraction strength ϵ_{pm} and temperature T . The letter code stands for DE = desorbed expanded, G = globular, DC = desorbed compact, AE = adsorbed expanded, and AC = adsorbed compact. Representative conformations of the embedded compact (MC) and expanded (ME) phases are shown in Fig. 10.3.

shown in Fig. 10.3, which both most clearly reflect the influence of the back-reaction between polymer and membrane fluctuations.

- [1] M. Bachmann, W. Janke: Phys. Rev. Lett. **95**, 058102 (2005); Phys. Rev. E **73**, 041802 (2006); Phys. Rev. E **73**, 020901(R) (2006); Phys. Part. Nucl. Lett. **5**, 243 (2008)
- [2] M. Möddel et al.: J. Phys. Chem. B **113**, 3314 (2009)
- [3] M. Möddel et al.: Phys. Chem. Chem. Phys. **12**, 11548 (2010); Comput. Phys. Commun. **182**, 1961 (2011)
- [4] M. Möddel et al.: Macromolecules **44**, 9013 (2011)
- [5] S. Karalus et al.: Phys. Rev. E **84**, 031803 (2011)

10.4 Polymer Adsorption to a Fractal Substrate

V. Blavatska*, W. Janke

*Institute for Condensed Matter Physics, National Academy of Sciences of Ukraine,
Lviv, Ukraine

The conformational statistics of polymers interacting with substrates is a subject of growing interest in polymer science. It plays an important role both in technology (adhesion, stabilization of colloidal dispersions) and biological physics (proteins adsorption on membranes) [1]. Particularly interesting is the case of an attractive substrate, where below a critical temperature T_A a second-order phase transition into an adsorbed state takes place. As order parameter one considers the fraction of the average number of monomers N_s adsorbed to the surface and the total length N of the polymer chain, obeying for long chains the scaling law $\langle N_s \rangle / N \sim N^{\phi_s - 1}$ where ϕ_s is the surface

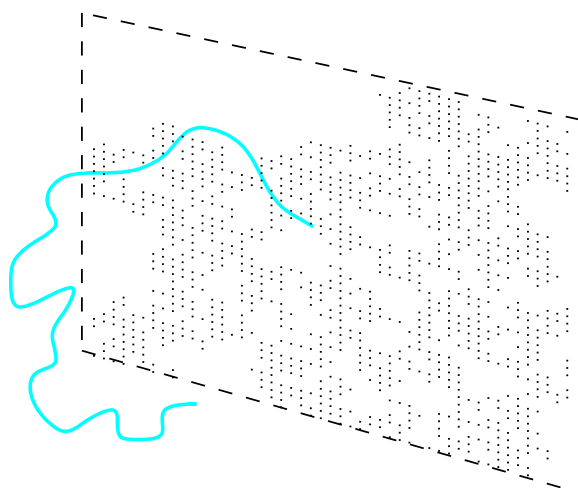


Figure 10.5: Sketch of a polymer chain grafted to an attractive “sieve” formed by a percolation cluster.

crossover exponent [2]. Most naturally occurring substrates are rough and energetically (or structurally) inhomogeneous, and, in fact, are often of fractal nature. In the language of lattice models, where polymers can be represented by self-avoiding random walks (SAWs) [3], such surfaces can be modeled as a two-dimensional regular lattice with different types of randomly distributed defects. Fractal properties emerge at the percolation threshold where a spanning percolation cluster of attractive sites with fractal dimension $d_s^{p_c} = 91/49 \approx 1.89 < 2$ appears [4], cf. Fig. 10.5.

We have studied this problem with the help of the pruned-enriched Rosenbluth method (PERM) [5] for simulating the polymer chains. We examined the behaviour of the components of the radius of gyration $\langle R_{g\parallel}^2 \rangle$, $\langle R_{g\perp}^2 \rangle$ in directions parallel and perpendicular to the surface, and found that the critical exponent governing the scaling of the size of the polymer chain adsorbed on a fractal substrate formed by a percolation cluster is larger than that for a homogeneously attractive surface. A value $\nu_2^{p_c} = 0.772 \pm 0.006$ is obtained [6], to be compared with the compatible result $\nu_2^{p_c} = 0.782 \pm 0.003$ for the average size of a polymer strictly confined onto a two-dimensional percolating cluster [7] and $\nu_2 = 0.742 \pm 0.006 \approx 3/4$ for a plain surface [6]. Examining the peak structure of the heat capacity, we find an estimate for the surface crossover exponent $\phi_s^{p_c} = 0.425 \pm 0.009$, compared to $\phi_s = 0.509 \pm 0.009$ for the plain surface [6]. As expected, the adsorption is diminished, when the fractal dimension of the surface is smaller than that of the plain Euclidean surface due to the smaller number of contacts of monomers with attractive sites.

- [1] A.F. Xie, S. Granick: *Nature Materials* **1**, 129 (2002)
- [2] E. Eisenriegler et al.: *J. Chem. Phys.* **77**, 6296 (1982)
- [3] C. Vanderzande: *Lattice Models of Polymers* (Cambridge University Press, Cambridge (England) 1998)
- [4] S. Havlin, D. Ben Abraham: *Adv. Phys.* **36**, 155 (1987)
- [5] P. Grassberger: *Phys. Rev. E* **56**, 3682 (1997)
- [6] V. Blavatska, W. Janke: *J. Chem. Phys.* **136**, 104907 (2012)
- [7] V. Blavatska, W. Janke: *Europhys. Lett.* **82**, 66006 (2008); *J. Phys. A* **42**, 015001 (2009)

10.5 Polymer Chain Inside an Attractive Sphere Potential

H. Arkin^{*}, W. Janke

^{*}On leave from Department of Physics Engineering, Faculty of Engineering,
Ankara University, Tandogan, 06100 Ankara, Turkey

A most important class of molecules in living cells consists of various types of proteins. Their importance to biological systems cannot be overstated [1]: they catalyze and regulate the cell's activities when acting as enzymes. As is well known, proteins with globular structure fold into compact configurations in which they are biologically active. The cellular environment in which a protein folds and performs its functions is crowded with several biological molecules including lipids, carbohydrates and other proteins. An important issue is understanding the mechanism by which proteins attain their folded structure, factors that contribute to the folding and the environmental conditions that make the folding transition possible [2, 3]. Such understanding is important not only as a scientific issue but also due to debilitating diseases such as Alzheimer's and Parkinson's that are believed to be the result of accumulation of toxic protein aggregates [4]. Although the three-dimensional structure of native proteins is controlled mostly by their amino acid sequence, their transport properties and the kinetics of their folding depend on the local environment. But, whereas protein folding in dilute solutions under bulk conditions is relatively well understood, because most of experimental, theoretical and computational studies on protein folding have relied on studying proteins in the infinitely dilute limit, the more important problem of protein folding in a confined environment is not. The understanding of protein folding in confined or crowded media is one of the most challenging objectives in biologically motivated research. It is crucial to understand for a given protein what are the thermally accessible conformations, the folding pathways and controlling parameters from the environment, of which some of them have been explored in detail in Refs. [5, 6]. Also adsorption phenomena near flat surfaces within lattice and off-lattice formulations have been investigated [7, 8].

In this study [9], we performed multicanonical Monte Carlo simulations in order to determine the thermodynamic and structural properties of a polymer chain inside an attractive, unstructured sphere. The main objective of this study is to analyze the influence of the attracting sphere in terms of thermodynamical quantities when varying the attraction strength ϵ of the sphere and temperature T . All these canonical expectation values of energetic and structural quantities and their thermal fluctuations are summarized in the pseudophase diagram in the $\epsilon - T$ plane shown in Fig. 10.6.

- [1] C. Branden, J. Tooze: *Introduction to Protein Structure* (Garland Publishing, New York 1998)
- [2] C.B. Anfinsen: *Science* **181**, 223 (1973)
- [3] D.K. Klimov, D. Thirumalai: *Phys. Rev. Lett.* **76**, 4070 (1996); L. Mirny, E. Shakhnovich: *Annu. Rev. Biophys. Biomol. Struct.* **30**, 361 (2001)
- [4] M. Hayer-Hartl, A.P. Minton: *Biochemistry* **45**, 13356 (2006); D.A. Kirschner et al.: *Proc. Natl. Acad. Sci. (USA)* **83**, 503 (1986); E.H. Koo et al.: *ibid.* **96**, 9989 (1999); K.A. Conway et al.: *ibid.* **97**, 571 (2000); D.G. Lynn, S.C. Meredith: *J. Struct. Biol.* **130**, 153 (2000)

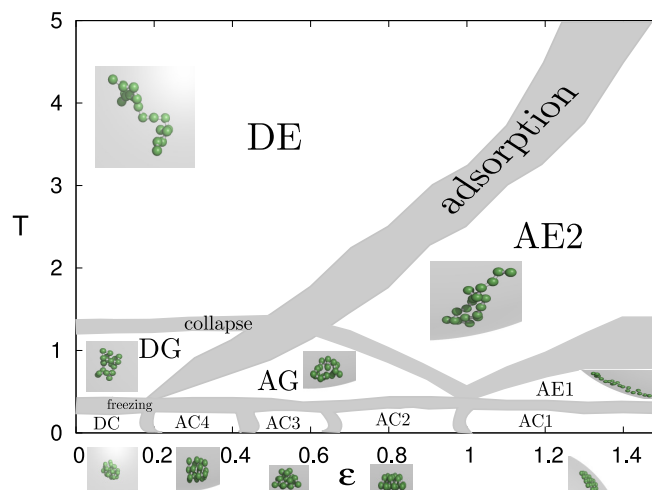


Figure 10.6: The phase diagram of the homopolymer-attractive sphere system as obtained in extensive computer simulations. The boundaries in the phase diagram separate the individual conformational phases. The band width shows the variation of the corresponding peaks of the temperature derivatives of different structural observables which are analyzed simultaneously. DE, DG, and DC denote the desorbed phases of expanded, globular and compact/crystalline conformations, respectively. AE1 stands for completely adsorbed expanded structures and AE2 for partially adsorbed expanded structures. AG reflects the adsorbed globular regime and the compact/crystalline structures occur with different topologies. These have different number of layers: AC4 – adsorbed spherically symmetric, AC3 – adsorbed three-layer structures, AC2 – adsorbed two-layer structures, and finally AC1 – adsorbed mono-layer structures.

- [5] S. Schnabel et al.: Phys. Rev. Lett. **98**, 048103 (2007); J. Chem. Phys. **126**, 105102 (2007)
- [6] H. Arkin: Phys. Rev. E **78**, 041914 (2008)
- [7] M. Bachmann, W. Janke: Phys. Rev. Lett. **95**, 058102 (2005); Phys. Rev. E **73**, 041802 (2006); Phys. Rev. E **73**, 020901(R) (2006)
- [8] C. Junghans et al.: Phys. Rev. Lett. **97**, 218103 (2006); J. Chem. Phys. **128**, 085103 (2008); M. Möddel et al.: J. Phys. Chem. B **113**, 3314 (2009); Phys. Chem. Chem. Phys. **12**, 11548 (2010); Comput. Phys. Commun. **182**, 1961 (2011); Macromolecules **44**, 9013 (2011)
- [9] H. Arkin, W. Janke: Phys. Rev. E **85**, 051802 (2012)

10.6 Thermodynamics of a Model Protein in Spherical Confinement

M. Bilsel ^{*}, B. Taşdizen ^{*}, H. Arkin [†], W. Janke

^{*}Department of Physics Engineering, Faculty of Engineering,
Ankara University, Tandogan, 06100 Ankara, Turkey

[†]On leave from Department of Physics Engineering, Faculty of Engineering,
Ankara University, Tandogan, 06100 Ankara, Turkey

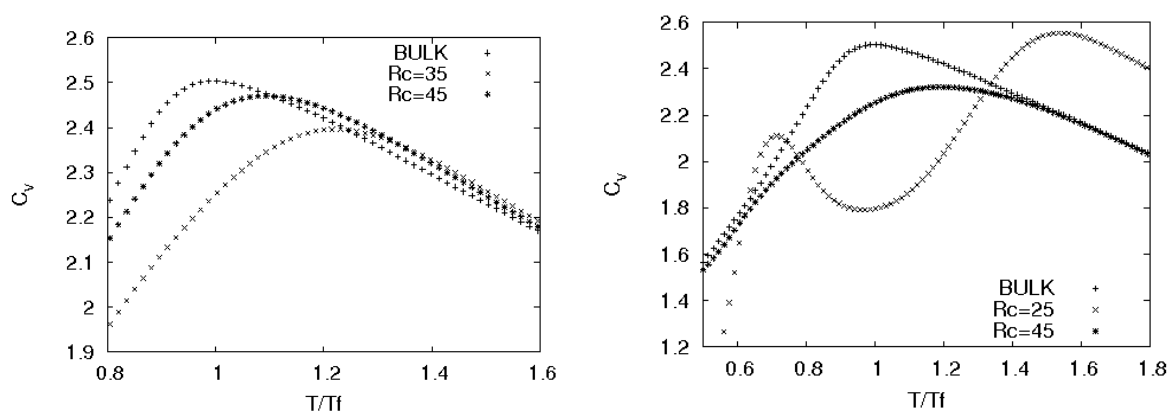


Figure 10.7: Specific heat as a function of temperature for the AB model protein $BA_6BA_4BA_2BA_2B_2$ in a spherical confinement with sphere radius R_c . The temperature T is given in units of the folding temperature T_f in the bulk. *Left:* Purely repulsive potential. *Right:* Attractive potential.

We have performed Monte Carlo computer simulations in generalized ensembles of a model protein confined in a spherical cage to investigate the dynamics of the folding mechanism [1]. The problem of whether proteins are misfolded or aggregated or, on the contrary, fold properly more promptly in spatial confinement has recently attracted much interest [2, 3]. A detailed understanding of this subject would play a key role for finding treatments to diseases caused by misfolding of proteins. Our goal is thus to analyze the thermodynamics of the folding mechanism and to investigate whether the folding mechanism is controlled or not in a confining environment. To do so we have employed exhaustive multicanonical Monte Carlo simulations by using a minimalistic AB model where hydrophobic residues are labeled by A and the polar or hydrophilic ones by B [4, 5]. Adjacent residues or monomers are connected by rigid covalent bonds. Thus, their distance is kept fixed and set to unity. The contact interaction is replaced by a distance- and residue-dependent 12 – 6 Lennard-Jones potential accounting for short-range excluded volume repulsion and long-range interaction. An additional interaction accounts for the bending energy of any pair of successive bonds. In this study, we focused on the folding of a model protein with 20 residues arranged in the sequence $BA_6BA_4BA_2BA_2B_2$.

The model protein is enclosed by a sphere of radius R_c . Apart from the steric hindrance effect, we assumed two different types of wall interactions, one with a purely repulsive wall potential and another that exhibits an attractive part close to the inner sphere wall. By monitoring the specific heat as a function of temperature, we observe in the first, purely repulsive case merely a monotonic finite-size scaling shift of the folding temperature, cf. Fig. 10.7 (left). The second case with attractive wall interaction is much more interesting since here, for small enough sphere radius R_c , the protein is first adsorbed to the (inner) surface of the sphere and in a second step the folding takes place. This is indicated by the two peaks of the specific heat for $R_c = 25$ in Fig. 10.7 (right) [6].

[1] J.A. Hubbell: *Curr. Opin. Biotechnol.* **10**, 123 (1999); S. Santosa et al.: *Nano Lett.* **2**,

- 687 (2002); S. Vauthey et al.: Proc. Natl. Acad. Sci. USA **99**, 5355 (2002)
- [2] F. Takagi et al.: Proc. Natl. Acad. Sci. USA **100**, 11367 (2003); N. Rathore et al.: Biophys. J. **90**, 1767 (2006); D. Lu et al.: Biophys. J. **90**, 3224 (2006)
- [3] S. Kumar, M.S. Li: Phys. Rep. **486**, 1 (2010)
- [4] F.H. Stillinger, T. Head-Gordon: Phys. Rev. E **52**, 2872 (1995); A. Irback et al.: Phys. Rev. E **58**, R5249 (1998)
- [5] M. Bachmann et al.: Phys. Rev. E **71**, 031906 (2005)
- [6] M. Bilsel et al.: *Effects of confinement on the thermodynamics of a model protein*, Ankara/Leipzig preprint (2011)

10.7 Shapes of Θ -Polymers in Crowded Media under Stretching Force

V. Blavatska*, W. Janke

*Institute for Condensed Matter Physics, National Academy of Sciences of Ukraine,
Lviv, Ukraine

Long flexible polymers in a good solvent form crumpled coil conformations which are perfectly described by self-avoiding random walks (SAW) on a regular lattice [1]. This regime holds at temperatures T well above the so-called Θ -point. When lowering the temperature, the effect of monomer-monomer attraction grows and the polymer radius shrinks. At $T = T_\Theta$, a crossover occurs from high-temperature SAW behaviour to the Θ -statistics. At this particular temperature, polymers in $d = 3$ dimensions behave effectively as simple random walks (RW). Below the Θ -temperature, the entropic effects, which make the polymer chain swell, are overcome by interaction energy and a collapse to the globule regime occurs. The coil-globule transition is considered to be of second order [1], in the sense that the density of an infinite globule is zero at $T = T_\Theta$ and increases continuously when further lowering the temperature.

The coil-globule transition is of interest in various respects, being deeply connected with problems like protein folding and DNA condensation. The properties of polymers in the vicinity of the Θ -point can be successfully studied on the basis of self-attracting self-avoiding walks (SASAW), where a nearest-neighbor interaction is included: an attractive energy $-\epsilon$ between two neighbour sites is introduced. When studying the folding dynamics and transport properties of proteins, an important role is played by global shape properties of a typical polymer conformation. The asymmetry of polymer shape can be characterized, e.g., by the invariant asphericity [2]

$$A_d = \frac{1}{d(d-1)} \sum_{i=1}^d \frac{(\lambda_i - \bar{\lambda})^2}{\bar{\lambda}^2} = \frac{d}{d-1} \frac{\text{Tr } \hat{\mathbf{Q}}^2}{(\text{Tr } \mathbf{Q})^2}, \quad (10.1)$$

with λ_i being the eigenvalues of the gyration tensor $Q_{ij} = \frac{1}{N} \sum_{n=1}^N (x_n^i - x_{\text{CM}}^i)(x_n^j - x_{\text{CM}}^j)$, $i, j = 1, \dots, d$, where x_n^j is the j th coordinate of the position vector of the n th monomer of a polymer chain ($n = 1, \dots, N$), and $x_{\text{CM}}^j = \sum_{n=1}^N x_n^j / N$ is the coordinate of the center-of-mass position vector, $\bar{\lambda} \equiv \text{Tr } \mathbf{Q} / d$, and $\hat{\mathbf{Q}} \equiv \mathbf{Q} - \bar{\lambda} \mathbf{I}$ with \mathbf{I} denoting the

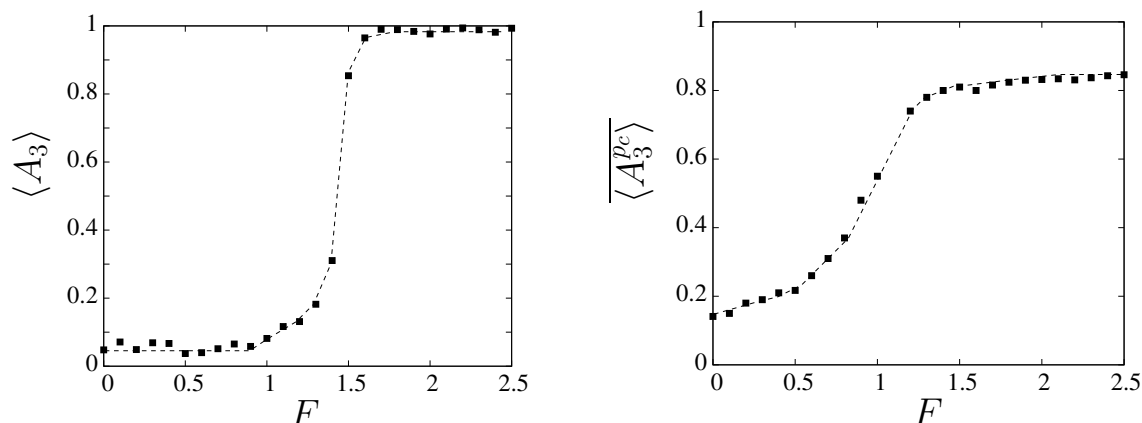


Figure 10.8: Averaged asphericity of an $N = 90$ -step SASAW as function of applied force F in $d = 3$ below the Θ -point. *Left:* Pure lattice ($T = 1.8$). *Right:* Backbone of percolation cluster ($T = 0.2$). Lines are guides to the eyes.

unity matrix. This universal quantity equals zero for a spherical conformation, where all the eigenvalues are equal, and takes a maximum value of one in the case of a rod-like conformation, where all the eigenvalues equal zero except of one. Thus, the inequality $0 \leq A_d \leq 1$ holds. It was realized experimentally [3] that the majority of globular proteins are characterized by $\langle A_d \rangle \approx 0.1$, thus being almost spherical.

A subject of great importance in polymer physics is the understanding of the behaviour of macromolecules in the presence of structural disorder [4]. Biological cells, for instance, can be described as a very crowded environment built of biochemical species that occupy a large fraction of the total volume. In lattice models, such a crowded environment can be described by assigning obstacles to a certain fraction of randomly chosen sites [5]. In this situation one is often interested in the response of polymers to applied tension and stress. Of special interest in biophysics is the stretching of globular polymers below the Θ -point. Applied force not only influences the structural properties of polymers, but also may introduce a new completely stretched state which is otherwise not accessible [6].

Figure 10.8 shows the averaged asphericity of SASAWs, giving information about the internal structure of the polymer conformation under applied force, at a temperature well below the Θ -point for the cases of a pure lattice and the backbone of a percolation cluster modeling the crowded medium [7]. Note that in the absence of force, $\langle A_3 \rangle$ for SASAWs on a pure lattice is very close to zero, whereas in the disordered case, due to the complicated structure of the underlying percolative lattice, globular conformations are more elongated with larger $\langle A_3^{pc} \rangle$ values. At small F , a polymer chain is still in the compact folded state and is just slightly oriented along the force direction. Under increasing force, the polymer chain takes on a conformation similar to the extended (swollen) structure. Note, that completely stretched states, corresponding to $\langle A_d \rangle \approx 1$, can be obtained only in the pure case. In contrast, they are not accessible on the percolative lattices due to the complicated fractal structure of the underlying percolation cluster.

[1] A.Y. Grosberg, A.R. Khokhlov: *Statistical Physics of Macromolecules* (American

- Institute of Physics, New York 1994); C. Vanderzande: *Lattice Models of Polymers* (Cambridge University Press, Cambridge (England) 1998)
- [2] V. Blavatska, W. Janke: *J. Chem. Phys.* **133**, 184903 (2010)
- [3] R.I. Dima, D. Thirumalai: *J. Phys. Chem. B* **108**, 6564 (2004); C. Hyeon et al.: *J. Chem. Phys.* **125**, 194905 (2006); N. Rawat, P. Biswas: *J. Chem. Phys.* **131**, 165104 (2009)
- [4] S. Kumar, M.S. Li: *Phys. Rep.* **486**, 1 (2010)
- [5] V. Blavatska, W. Janke: *Europhys. Lett.* **82**, 66006 (2008); *Phys. Rev. Lett.* **101**, 125701 (2008); *J. Phys. A* **42**, 015001 (2009)
- [6] V. Blavatska, W. Janke: *Phys. Rev. E* **80**, 051805 (2009); in: *Computer Simulations in Condensed Matter Physics XXII*, ed. by D.P. Landau et al., *Physics Procedia* **3**, 1431 (2010)
- [7] V. Blavatska, W. Janke: *Comput. Phys. Commun.* **182**, 1966 (2011)

10.8 Scale-Free Enumeration of Self-Avoiding Walks on Critical Percolation Clusters

N. Fricke, W. Janke

Self-avoiding walks on randomly diluted lattices have attracted much interest over the last decades. They are a basic model for polymers in disordered media and feature universal scaling behaviour with non-trivial exponents [1]. The scaling of the end-to-end distance R and the number of chain conformations Z with the number of steps N is described by the universal exponents ν and γ :

$$\left[\sqrt{\langle R^2 \rangle} \right] \sim N^\nu, \quad [Z] \sim \mu^N N^{\gamma-1}. \quad (10.2)$$

Here μ is the (non-universal) connectivity constant, and the square brackets denote quenched averages over all disorder configurations.

Most interesting is the case at the critical percolation threshold where the fractal dimension of the substrate changes and the disorder covers all length scales. To investigate this problem, researchers have used Monte Carlo simulations, field-theoretical renormalization techniques, as well as exact enumeration. The last method has the benefit of yielding exact results (for single disorder configurations) but is normally limited to very small systems ($N \approx 45$ in 2D [2]) as the computational effort increases exponentially with N .

We found, however, that this exponential complexity can be circumvented through the use of physical ideas: At the percolation threshold, a cluster of occupied sites that spans the whole system is self-similar and just barely connected. It can therefore be decomposed into a hierarchy of nested “blobs”, each of which has only a small number of “children” and few connecting sites to its “parent” (see Fig. 10.9). To determine the different self-avoiding walk conformations through a blob, we only need to enumerate the paths that lie outside of its children and connect them with the paths through the children, which can be counted separately. Starting with the smallest blobs, this procedure can be applied recursively. That way it is possible to enumerate walks of $N = 1000$ steps in a couple of minutes (which otherwise would take over 10^{150} years).

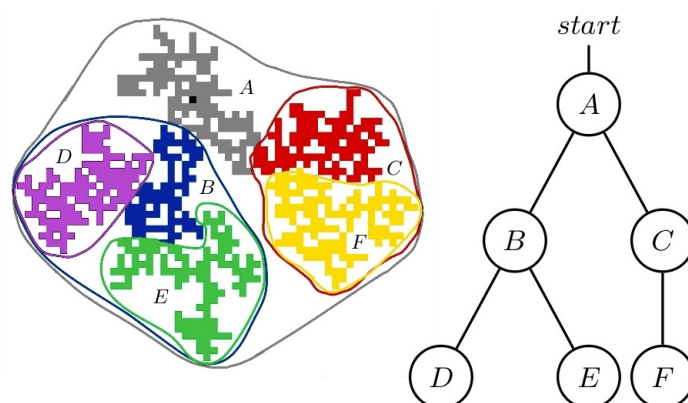


Figure 10.9: Decomposition of a critical percolation cluster and corresponding tree hierarchy. The starting position of the walker is marked in black (in blob A).

Thus we were able to enumerate all self-avoiding walks of 1000 steps on 2×10^5 clusters, allowing us to estimate the scaling exponents with unprecedented accuracy [3]. So far we have implemented the method only in 2D, but the adaptation to three and more dimensions is in progress.

- [1] B. Barat, B.K. Chakrabarti: *Phys. Rep.* **258**, 377 (1995)
- [2] A.R. Singh et al.: *J. Chem. Phys.* **131**, 065103 (2009)
- [3] N. Fricke, W. Janke: *Scale-free enumeration of self-avoiding walks on critical percolation clusters*, Leipzig preprint (2011), submitted to *Europhys. Lett.*

10.9 Two-Dimensional Pinned Flexible Polymers in Hard-Disk Disorder

S. Schöbl, J. Zierenberg, W. Janke

The upcoming interest of physicists in biological systems during the last twenty years has strongly reinforced the interest in polymeric systems. Especially the interest in polymers exposed to disorder has gained great importance as interaction of polymers with their natural environment is a common situation in vivo. This study is concerned with a systematic investigation of pinned polymers located in two-dimensional hard-disk disorder.

The flexible polymer is modeled as a freely jointed chain, consisting of N non-interacting monomers. It can be considered as a random walk with $N - 1$ steps. We investigated this model with the intention to include bending energy between neighboring bonds later on, which describes semiflexible polymers. The disorder is modeled as hard disks that occupy the sites of a square lattice with a certain probability p . The interaction between polymer and disorder is steric, i.e., the monomers are not allowed to sit on the disks. We chose this arrangement in order to be able to control arising subtle structures such as cavities and channels [1]. Exemplary polymer conformations can be seen in Fig.10.10(a).

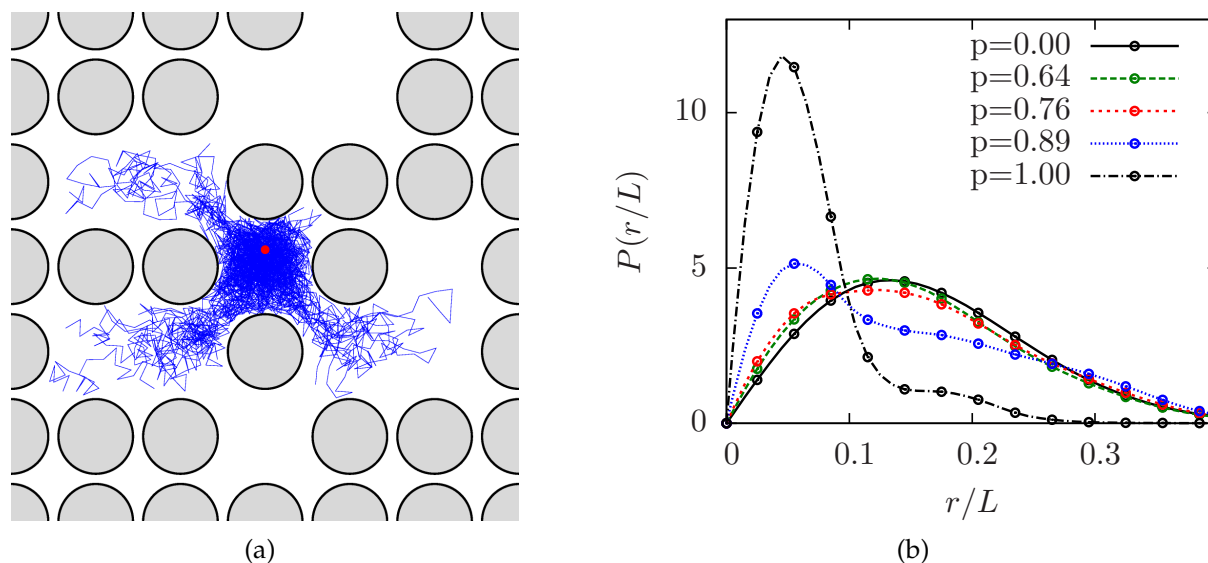


Figure 10.10: (a) Exemplary disorder configuration and typical polymer conformations. (b) The end-to-end distribution function of a flexible polymer with $N = 30$ monomers and bond length b , exposed to hard-disk disorder with different occupation probabilities on a square lattice. The diameter of the disks $\sigma = 4.5b$ is slightly smaller than the lattice constant $a = 5b$.

In a first step, we applied two conceptually different algorithms to the problem addressed here. For one thing, we used an off-lattice chain growth algorithm [2], for another thing we applied the multicanonical Monte Carlo method to the problem.

We considered quenched disorder averages at different occupation probabilities p and were able to show that both algorithms yield the same results within the chosen parameter range (see, e.g., Fig. 10.10(b)). We could clearly approve results from literature [3], namely that high densities strongly influence the extension of flexible polymers, causing a shift in the end-to-end distribution to shorter end-to-end distances. Beyond that, we investigated in detail the effect of small structures such as narrow channels and cavities on the statistical properties of the polymer [1].

[1] S. Schöbl et al.: Phys. Rev. E **84**, 051805 (2011)

[2] T. Garel, H. Orland: J. Phys. A **23**, L621 (1990)

[3] A. Baumgärtner, M. Muthukumar: J. Chem. Phys. **87**, 3082 (1987)

10.10 Development of a Framework Allowing fast Programming of Monte Carlo Simulation of Polymers

M. Marenz, J. Zierenberg, W. Janke

We have started to create an environment for writing fast and efficient Monte Carlo (MC) simulations for arbitrary polymer models. Simulations of such systems yield a better understanding of the behaviour of polymers in specific circumstances [1], or may provide a good initial guess for creating new ones with specific properties [2]. There are a lot of different Molecular Dynamics (MD) programs available, which are capable

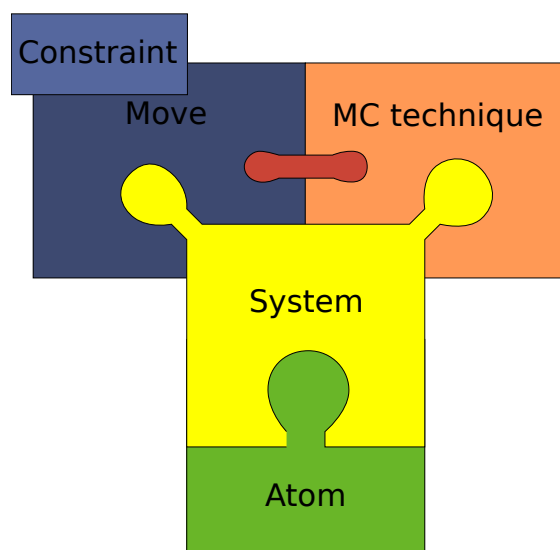


Figure 10.11: The five basic building blocks of the MC simulations framework.

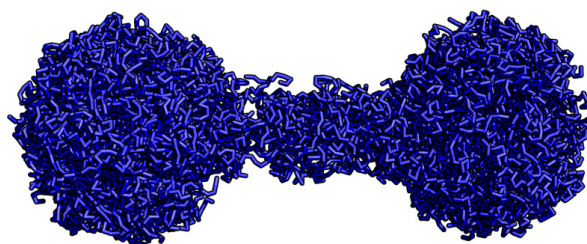


Figure 10.12: Overlay of 1000 steps of one MC simulation of a polymer in a barbell confinement.

of simulating biological or synthetic polymers. However, their abilities to perform MC simulations are rather limited because sophisticated update algorithms are, if at all, implemented only rudimentary. Although MC techniques, in contrast to MD, cannot investigate dynamical properties, they are very convenient for investigating phase transitions and the general character of phase space of arbitrary models in a very efficient manner. The efficiency comes from the broad range of improved MC techniques and the possibility to design a suitable propagation of the system as a Markov process freely.

Unfortunately there exists no widely-used program for MC simulations of polymers. To write a single program which implements all these techniques and possibilities at the same time and still remains efficient is nearly impossible. The alternative, writing a new program from scratch for every demand could be very annoying. That is one reason, why we developed a framework for MC simulations of polymers. The aim of this framework is to provide an environment in the C++ programming language, allowing to perform MC simulations for specific problems in a short time. Another goal of the framework is the expandability. Thus, one can add new methods, potentials, systems and update methods, without adjusting all other parts of the framework. To achieve this goal we divided the problem into single parts, which fit into each other. One can imagine every part as a brick, which can be combined in order to construct a simulation.

There are five basic building blocks: The smallest building blocks are the atoms. The next block is the system, which combines all needed atoms and defines the Hamiltonian of the physical system. On top of the system are the last two main building blocks, the update move and the MC technique. Moves define single updates of the system, propagating from the current state to the next one. Additionally a constraint can be added to every move, in order to simulate a polymer in confinement. An organogram of the simulation framework is sketched in Fig. 10.11.

Until now, we have implemented several MC techniques such as parallel tempering [3], multicanonical [4], Wang-Landau [5] and of course Metropolis Monte Carlo [6]. As

system there are all kinds of linear polymers available, such as simple bead-spring or bead-stick models, with Lennard-Jones, spring, FENE and bending potentials. Adding further pair or bending potentials is extremely simple. We have also implemented confinement constraints such as steric walls, a sphere or a barbell.

As first examples, we are looking at the behaviour of a homopolymer in two different confinements, a polymer inside a sphere and inside a barbell (cf. Fig. 10.12). One important question here is to what extent the confinement modifies the phase transition properties compared to those of a free polymer.

- [1] M. Möddel et al.: Phys. Chem. Chem. Phys. **12**, 11548 (2010); Macromolecules **44**, 9013 (2011)
- [2] M. Bachmann et al.: Angew. Chem. Int. Ed. **49**, 9530 (2010) [Angew. Chem. **122**, 9721 (2010)]
- [3] K. Hukushima, K. Nemoto: J. Phys. Soc. Japan **65**, 1604 (1996)
- [4] B.A. Berg, T. Neuhaus: Phys. Lett. B **267**, 249 (1991); Phys. Rev. Lett. **68**, 9 (1992)
- [5] F. Wang, D. P. Landau: Phys. Rev. Lett. **86**, 2050 (2001); Phys. Rev. E **64**, 056101 (2001)
- [6] W. Janke: Lect. Notes Phys. **739** (Springer, Berlin 2008), pp. 79-140; *Monte Carlo simulations in statistical physics – From basic principles to advanced applications*, Leipzig preprint, invited lecture notes, to appear in: *Order, Disorder and Criticality: Advanced Problems of Phase Transition Theory*, Vol. 3, edited by Y. Holovatch (World Scientific, Singapore 2012), in print

10.11 Stochastic Description of a Binary Frustrated Unit

A. Garai^{*}, B. Waćław[†], H. Nagel, W. Janke, H. Meyer-Ortmanns^{*}

^{*}Jacobs University Bremen, School of Engineering and Science

[†]School of Physics and Astronomy, University of Edinburgh, UK

Oscillations are an essential feature of processes in biological systems. Biological oscillators can be found in vivo in a multitude of different realizations such as the regulatory glycolytic oscillator, circadian clocks or regulatory genetic circuits. In the description of biological oscillators, two elements are identified to be essential: an inhibitory feedback loop and a source of delay in that loop allowing the oscillating variables to overshoot a steady state [1].

We considered a biological oscillator realized as a simple genetic regulatory circuit [Figs. 10.13(a), (b)] with two populations of proteins A and B, where higher concentration of A *activates* production of A and B while higher concentration of B *inhibits* production of A which, in turn, leads to frustration effects. Oscillations manifest themselves as limit cycles in a Hopf bifurcation with the activated protein production rate α acting as the principal bifurcation parameter [2].

We employed both analytical and numerical methods to analyze the dynamic properties: Treatment of the non-linear master equation using a linear noise approximation, simulation of the stochastic process using a continuous time Monte Carlo method [3]. With those methods we were able to reproduce the limit of the continuous system to check the validity of our extended models. We then focused on the new aspects of the stochastically implemented model, especially for very small systems ($N_{A,B} < 100$):

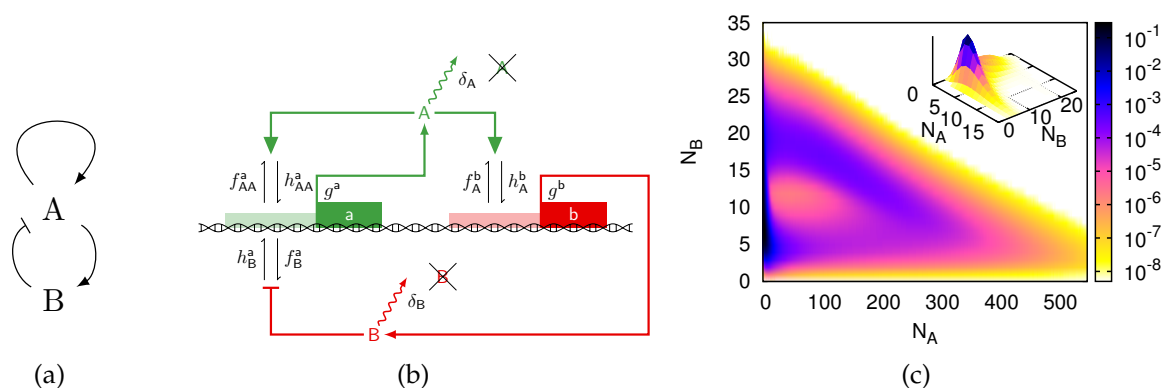


Figure 10.13: (a) Basic motif of the oscillatory genetic circuit. (b) Implementation of the basic motif in a more detailed model with protein production rates controlled by gene states. These in turn are switched through binding of the activator/inhibitor protein to the respective genes promoter regions. (c) Probability density plot from the fixed point regime ($\alpha = 15$, bifurcation points: $\alpha_1 \approx 31.10$, $\alpha_2 \approx 98.93$), highlighting the shape of oscillatory trajectories.

- 1) Occurrence of oscillations deep in the fixed point regimes [Fig. 10.13(c)]. Fluctuations drive the system away from the fixed point followed by a large excursion along the trajectory of the limit cycle-regime.
- 2) Stabilization of the oscillatory behaviour against parameter changes (i.e. external influences) [4].

- [1] W.O. Friesen, G.D. Block: *Am. J. Physiol.* **246**, R847 (1984)
 [2] P. Kaluza, H. Meyer-Ortmanns: *Chaos* **20**, 043111 (2010)
 [3] D.T. Gillespie: *J. Phys. Chem.* **81**, 2340 (1977)
 [4] A. Garai et al.: *J. Stat. Mech.* P01009 (2012)

10.12 Mass Condensation in Stochastic Transport Models

E. Ehrenpreis, H. Nagel, W. Janke

Generic examples for stochastic mass transport processes are traffic flow, force propagation in granular media, aggregation and fragmentation of clusters, and many others [1]. The transport is classically modeled by probabilities for hopping events from one site to another. Since such processes are usually out-of-equilibrium, it is in general difficult to predict possible stationary states. Still, in some cases it is possible to identify a transition between a liquid-like phase and a phase with a condensate (e.g., a “traffic jam”) that are associated with different stationary states. One speaks of a condensate when a finite fraction M' of constituent particles condenses onto a finite extension W in space, sometimes even onto a single site. This can be observed in the thermodynamic limit where the number of particles M along with the volume N is sent to infinity, with the density $\rho = M/N$ hold fixed. The formation of a condensate is an example for spontaneous symmetry breaking which here, in contrast to equilibrium systems, can happen even in a one-dimensional system.

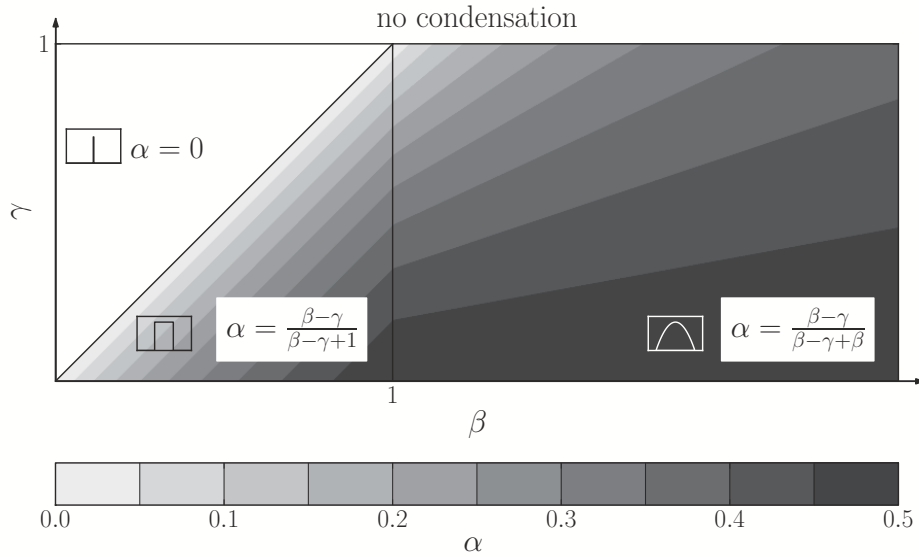


Figure 10.14: Theoretically predicted phase diagram for $K(x) \sim e^{-x^\beta}$ and $p(m) \sim e^{-m^\gamma}$, exhibiting condensed phases with point-like, rectangular and parabolic shapes (from left to right). The predicted value of the exponent α in the scaling law for the condensate extension W with the number M' of condensed particles, $W \simeq M'^\alpha$, is indicated by the gray code.

In previous analytical work [2–4] we concentrated on a class of models with steady states that factorize over the links of arbitrary connected graphs, so-called pair-factorized steady states (PFSS). This property enables at least partially an analytic treatment of the transport properties. In one dimension we could predict the critical mass density at the condensation transition and in particular the condensate shape and its scaling with the system size. The shape of the condensate turned out to be not universal. Rather it can be tuned from “extended” to “point-like” via the competition of local (K) and ultralocal (p) interactions that are implemented in the hopping rates of the stochastic transport process [5]. The resulting phase diagram for the choice $K(x) \propto \exp(-x^\beta)$ and $p(m) \propto \exp(-m^\gamma)$ and the predicted exponent α in the scaling law for the condensate extension, $W \sim M'^\alpha$, are shown in Fig. 10.14.

Since the analytical treatment is based on several approximations, we have performed extensive computer simulations of the hopping events [6]. As a result we find a very nice qualitative agreement of the numerically determined phase diagram with the theoretical prediction given in Fig. 10.14. This is demonstrated in Fig. 10.15 where the measured condensate shapes are displayed in the β - γ plane. By performing the power-law fits of the obtained condensate widths W against the number of constituent particles M' , we also find very good agreement with the predicted values of the exponent α : In most parts of the β - γ plane the agreement is better than 1%.

- [1] M.R. Evans et al.: Phys. Rev. Lett. **97**, 010602 (2006)
- [2] B. Waław et al.: J. Phys. A: Math. Theor. **42**, 315003 (2009)
- [3] B. Waław et al.: Phys. Rev. Lett. **103**, 080602 (2009)
- [4] B. Waław et al.: J. Stat. Mech. P10021 (2009)

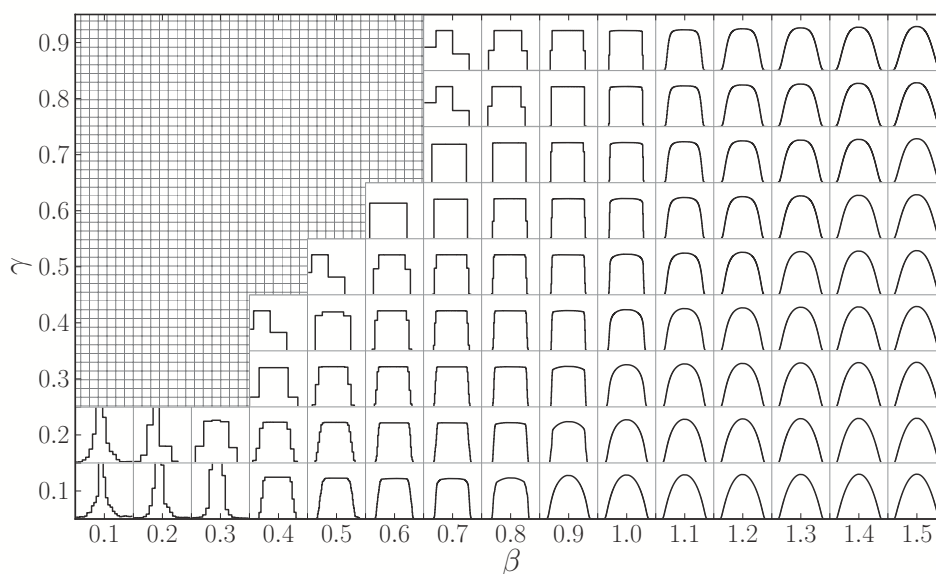


Figure 10.15: Numerically determined characteristic condensate shapes for systems of various β and γ at a condensate volume of about 10^5 masses. The shapes are derived from averages over many measured condensate states. The point-like shapes in the upper left region of the parameter space have not been identified with the present techniques.

[5] B. Waćlaw et al.: J. Phys.: Conf. Ser. **246**, 012011 (2010)

[6] E. Ehrenpreis et al.: Leipzig preprint in preparation

10.13 Mixed Heisenberg Spin Chains: Theory and Quantum Monte Carlo Simulations

R. Bischof, W. Janke

The original Heisenberg model (developed by Heisenberg during his time in Leipzig) and its variants are the basis for understanding quantum magnetism. For instance high-temperature superconducting cuprates can be successfully described as 1D and 2D quantum antiferromagnets at low doping. Depending on the size of the spins and types of coupling mechanisms, the model exhibits a rich variety of zero-temperature quantum critical phenomena. It is well known that uniform chains of half-odd integer spins have no energy gap between the ground state and first excited states (i.e., they are quantum critical), whereas chains with integer spins do show an excitation gap [1]. Moreover by tuning appropriate parameters (such as bond alternation, exchange anisotropy, next-nearest-neighbour interaction, spin-phonon coupling, etc.), spin chains can be driven to or away from criticality.

In this project we consider mixed anisotropic Heisenberg (XXZ) spin chains with bond alternation for which much less is known than for uniform chains. Specifically, our focus is on two different mixed quantum XXZ chains consisting of two different

kinds of spins, $S_a = 1/2$ and $S_b = 1$ or $3/2$, that appear alternately in pairs [2]. In order to investigate their quantum critical properties we employ self-implemented versions of the continuous time loop algorithm [3] and Lanczos exact diagonalization. By successful generalization of recently proposed quantum reweighting methods [4] to improved estimators of the loop algorithm, we have been able to determine the phase diagram in the XY-like region to high precision and could establish a line of continuously varying critical exponents. This strongly suggests that mixed spin chains are in the Gaussian universality class characterized by a central charge of $c = 1$. Furthermore, we could show the presence of logarithmic corrections in the mixed spin models at the SU(2) symmetric isotropic point. These logarithmic corrections influence the scaling and finite-size scaling behaviour on all length scales, which makes the extraction of critical exponents particularly difficult. It is well known that the homogeneous spin chains of $S = 1$ do exhibit such types of corrections [5].

By invoking conformal field theory, we have identified several scaling dimensions that can all be parametrized in terms of one fundamental parameter, a typical sign of the Gaussian universality class. To this end we proposed novel string-like order parameters as a generalization of the disorder parameters of the quantum Ashkin-Teller model. For the $S = 1$ chain our generalization corresponds to the order parameter of the dimerized phase in contrast to the usual string order parameter of the Haldane phase. These new order parameters offer access to scaling dimensions that differ from those of spin operators. As a consequence, the validity of scaling relations can be tested with higher accuracy [7].

Another exotic order parameter is the twist order parameter [6] that is particularly well suited to signal quantum phase transitions between different valence-bond configurations in 1D chains. Despite its potential to accurately locate pseudo-critical points in quantum Monte Carlo simulations, its scaling behaviour has not yet been studied. Our attempts to identify scaling behaviour seem to fail due to the inherently non-local nature of the twist order parameter [7], even though according to [6] a scaling dimension can be assigned.

- [1] F.D.M. Haldane: Phys. Rev. Lett. **50**, 1153 (1983)
- [2] K. Takano: Phys. Rev. Lett. **82**, 5124 (1999); Phys. Rev. B **61**, 8863 (2000); Z. Xu et al.: Phys. Rev. B **67**, 214426 (2003)
- [3] B.B. Beard, U.J. Wiese: Phys. Rev. Lett. **77**, 5130 (1996); H.G. Evertz: Adv. Phys. **52**, 1 (2003)
- [4] M. Troyer et al.: Braz. J. Phys. **34**, 377 (2004)
- [5] C.J. Hamer et al.: Phys. Rev. Lett. **68**, 214408 (2003); T. Papenbrock et al.: Phys. Rev. B **68**, 024416 (2003)
- [6] M. Nakamura, S. Todo: Phys. Rev. Lett. **89**, 077204 (2002)
- [7] R. Bischof, W. Janke: To be published

10.14 Directional Ordering in the Three-Dimensional Compass Model

M.H. Gerlach, W. Janke

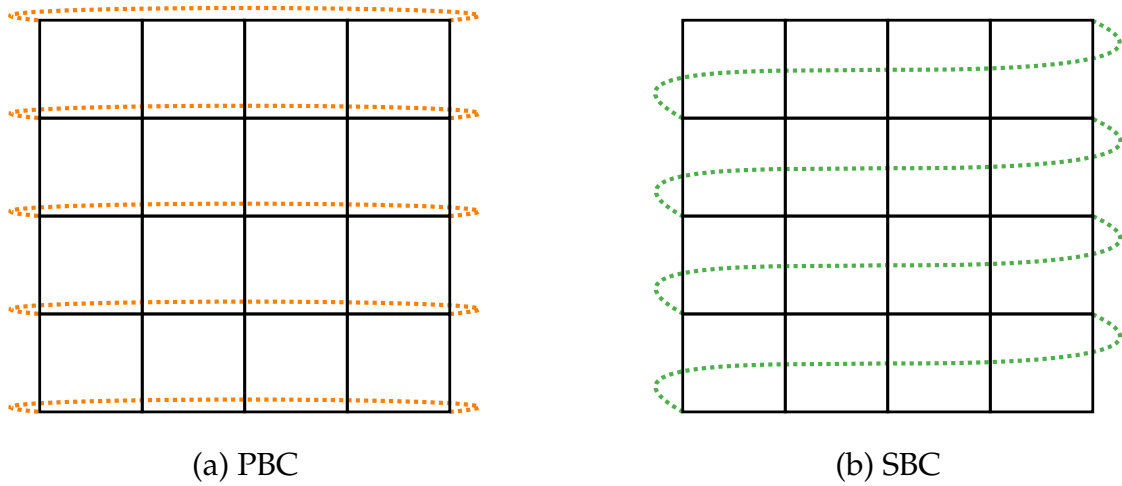


Figure 10.16: Sketch of periodic (PBC) and screw-periodic boundary conditions (SBC) along the x -axis of a two-dimensional lattice. In the SBC picture the link between the lower right and the upper left corner is not shown. Equivalent boundary conditions are applied to the y -direction. Here a screw parameter of $S = 1$ is used.

Both the classical and the quantum version of the compass model have recently attracted much interest in the literature. The reason is its connection to interesting quantum phenomena ranging from orbital order in transition metal compounds to topologically protected qubits [1–3]. In three dimensions the classical model is defined by the Hamiltonian

$$\mathcal{H} = J \sum_{i=1}^N \left(\sigma_i^x \sigma_{i+e_x}^x + \sigma_i^y \sigma_{i+e_y}^y + \sigma_i^z \sigma_{i+e_z}^z \right), \quad (10.3)$$

where $\sigma = (\sigma^x, \sigma^y, \sigma^z)$ are three-dimensional unit spin vectors, e_x , e_y , and e_z are unit vectors in x , y , and z direction, and J is a coupling constant. Although simple looking at first sight, surprisingly little is known about this model in three dimensions. Most studies so far focused on the two-dimensional analogue which still turned out to be rather hard to study numerically. It was shown to possess rich physics ranging from highly degenerate ground states to quantum phase transitions to an exciting thermal phase transition [4, 5].

In recent analyses of high-temperature series expansions of the three-dimensional quantum model (where the classical spins are replaced by Pauli matrices) it was claimed that this model does not exhibit a phase transition at any finite temperature [6]. This motivated us to consider first the three-dimensional classical model and to investigate whether this model exhibits a phase transition [7]. To this end we employed state-of-the-art Monte Carlo computer simulations using Metropolis, cluster, and parallel tempering (PT) techniques. From our previous studies in two dimensions [5] we knew that employing so-called screw-periodic boundary conditions [8] sketched in Fig. 10.16 considerably improves the finite-size scaling behaviour of this model. As a result we obtained convincing numerical evidence for a phase transition of first-order at the temperature $T_0 = 0.098328 \pm 0.000003$. This value is in good agreement with a brief remark in Ref. [9]. The nature of the phase transition can be read off from the histograms

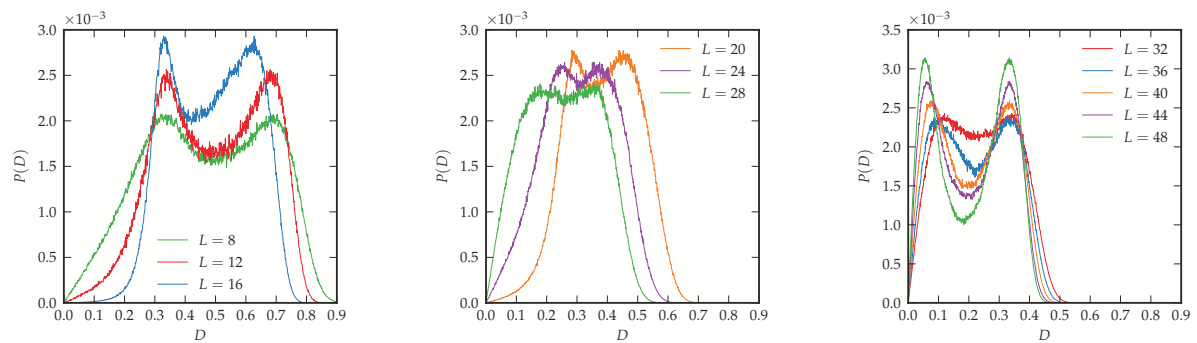


Figure 10.17: Histograms of the directional order parameter D in the three-dimensional compass model with screw-periodic boundary conditions for various lattice sizes L .

of the directional order parameter D of the model in Fig. 10.17 which exhibit for large lattice sizes L a characteristic double-peak structure. Note the nonmonotonic behaviour as function of lattice size: Initially, the double peak becomes *less* pronounced until $L \approx 28 - 32$, and only from then on it becomes more pronounced with further increasing L . By analyzing the ratio of peak maximum to peak minimum, we arrive at a definitely nonzero, albeit small value for associated interface tension, $\sigma_{od} \approx 3 \times 10^{-4}$.

- [1] K.I. Kugel, D.I. Khomskii: Sov. Phys. Usp. **25**, 231 (1982)
- [2] B. Douçot et al.: Phys. Rev. B **71**, 024505 (2005)
- [3] A. Kitaev: Ann. Phys. **321**, 2 (2006)
- [4] S. Wenzel, W. Janke: Phys. Rev. B **78**, 064402 (2008); see also “Publisher’s Note” in Phys. Rev. B **78**, 099902(E) (2008) [Fig. 1 selected for Phys. Rev. B “Kaleidoscope” August 2008]
- [5] S. Wenzel et al.: Phys. Rev. E **81**, 066702 (2010) [arXiv:1002.3508]
- [6] J. Oitmaa, C.J. Hamer: Phys. Rev. B **83**, 094437 (2011)
- [7] M.H. Gerlach, W. Janke: Leipzig preprint in preparation
- [8] E. Bittner et al.: Nucl. Phys. B **820**, 694 (2009)
- [9] S. Wenzel, A.M. Läuchli: Phys. Rev. Lett. **106**, 197201 (2011)

10.15 Multicanonical Analysis of the Gonihedric Ising Model and its Dual

W. Janke, D.A. Johnston*, M. Müller

*Department of Mathematics and the Maxwell Institute for Mathematical Sciences,
Heriot-Watt University, Edinburgh, UK

Fluctuating random surfaces are of great interest in condensed matter and high energy physics – and appear in interdisciplinary research on complex networks of membranes and other biological systems, too [1]. One special case is the Gonihedric Ising model that originates from a discrete bosonic string theory. It describes a surface swept out by the string world-sheet as it moves through space-time. The basic properties of such a

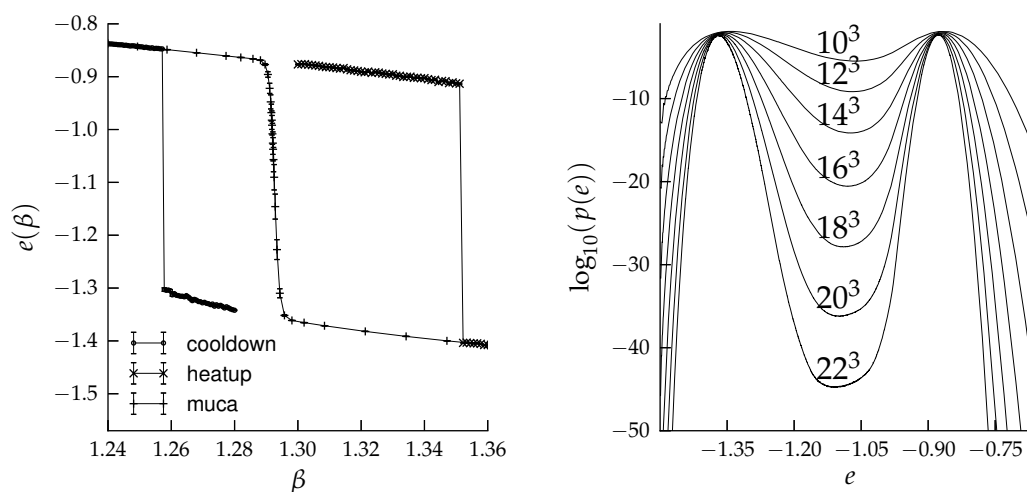


Figure 10.18: *Left:* Hysteresis loop of the dual model and the energy over inverse temperature $\beta = 1/k_B T$ obtained by a multicanonical simulation of the same lattice. The latter is located within the hysteresis loop and should therefore improve any estimates on the transition temperature. *Right:* Energy probability density of the dual model near the phase transition temperature for various lattice sizes. The rare states between the peaks are strongly suppressed but sufficiently sampled by the multicanonical algorithm allowing to extract the interface tension.

surface have been translated into a Hamiltonian of classical Ising spins interacting on a (hyper-)cubic lattice in the 1990s [2, 3]. A $(d - 1)$ -dimensional discretised surface is spanned by plaquettes in the dual lattice that separate spins of opposite sign.

The representation of the surface by classical spins allows the three-dimensional model to be examined by various methods such as mean-field calculations, cluster-variation-Padé-approximation, low-temperature series expansion, the transfer-matrix method and canonical Monte Carlo simulations. All these methods revealed interesting behaviour depending on a control parameter that determines the strength of self-avoidance of the surface. Continuous and discontinuous phase transitions have been found, but the details of the phases are still to be discovered.

In the special case of surfaces that do not suffer an energy penalty upon self-intersection, a first-order phase transition is observed, as well as interesting glassy dynamics upon cooling in simulations [4]. Recently the phase transition has been analysed again using canonical Monte Carlo simulations on dual representations of the model [5–7]. However, the transition temperatures in these studies did not coincide with the original formulation.

We investigated the discontinuous phase transition in the original model and its dual representation with multicanonical simulations that are tailored to overcome slow dynamics in first-order transitions [8]. The transition temperature found by finite-size scaling of the specific heat and Binder’s energy cumulant suggests that the discrepancy in the literature was introduced due to a strong hysteresis effect. The interface tension energetically separating the phases is quite strong and has been measured for both the original model and the dual representation (cf. Fig. 10.18) for the first time.

[1] R. Lipowsky: Nature **349**, 475 (1991)

[2] A. Cappi et al.: Nucl. Phys. B **370**, 659 (1992)

- [3] R.V. Ambartzumian et al.: Phys. Lett. B **275**, 99 (1992)
- [4] D.A. Johnston et al.: in *Rugged Free Energy Landscapes*, ed. W. Janke, *Lecture Notes in Physics*, Vol. **736** (Springer-Verlag, Berlin 2008), pp. 173–199
- [5] D.A. Johnston, R.P.K.C.M. Ranasinghe: J. Phys. A: Math. Theor. **44**, 295004 (2011)
- [6] D.A. Johnston, R.P.K.C.M. Ranasinghe: arXiv:1106.0325 (2011)
- [7] D.A. Johnston, R.P.K.C.M. Ranasinghe: arXiv:1106.4664 (2011)
- [8] M. Müller et al.: Leipzig preprint in preparation

10.16 GPU Computing: Parallel Tempering Simulations of Polymer Statistics

J. Gross^{*}, M. Bachmann[†], W. Janke

^{*}IFF-2 and IAS-2, Forschungszentrum Jülich, Germany

[†]Center for Simulational Physics, The University of Georgia, Athens, USA

Graphics processing units (GPUs) have become a very powerful computer platform, in recent years, driven by the professional computer gaming industry. GPUs possess a massively parallel architecture. With the latest release of NVIDIA's convenient programming language CUDA, GPUs have become popular in scientific computing. GPU computing finds its application in many fields, such as astronomy, medicine, time series analysis for financial markets, molecular dynamics simulations, Monte Carlo studies of spin systems, and Quantum Monte Carlo applications [1–3].

We are mainly interested in employing GPU computing for studying the thermodynamical properties of polymer models, both on lattice and off-lattice. The purpose of this project was to investigate whether GPU simulations can be efficiently performed for off-lattice polymer models – without any need of highly sophisticated tricks of implementation. For a straightforward implementation of parallel tempering Monte Carlo simulations [4] of an off-lattice model for elastic polymers we investigated the possible speedup factors on three different GPUs. We tested the two GT200-based GPUs Tesla C1060 (GPU1) and GTX285 (GPU2) with 240 cores and NVIDIA's new generation Fermi-based GTX480 card (GPU3) with 480 cores. As reference CPU system one core of a quadcore Xeon E5620 processor was considered [5, 6].

With the most naive implementation of distributing the replica of the parallel tempering algorithm over the cores, only moderate speed-up factors of about 6 to 9 could be achieved. Having observed that, an improved version was implemented with a parallel calculation of the energy function. This implementation is much faster than the CPU version, when more than 2 replica are simulated. The maximum speed-up factor for the Tesla C1060 card (GPU1) is 68, for the GTX285 card (GPU2) it is 78 and for the Fermi-based GTX480 card (GPU3) even 130, cf. Fig. 10.19. Furthermore it is possible to access multiple graphics cards in a single workstation from one and the same program with no extra effort. Also nodes of established cluster computers can be equipped with GPUs, a combination of the traditional message passing interface (MPI) and CUDA is used in such a scenario. Thus GPUs promise great gains in productivity as well as energy efficiency and are already now on their way to enter the architecture of the next-generation supercomputers [7, 8].

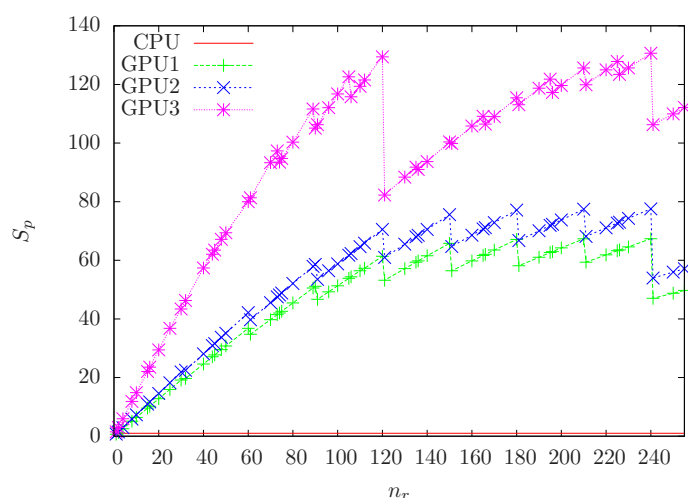


Figure 10.19: Speed-up factor S_p vs number of parallel-tempering replicas n_r for the GPU version with parallelized energy calculation. Drawn lines are only guides to the eye.

- [1] T. Preis et al.: J. Comput. Phys. **228**, 4468 (2009)
- [2] M. Weigel: Comput. Phys. Commun. **182**, 1833 (2011); Phys. Rev. E **84**, 036709 (2011); J. Comput. Phys. **231**, 3064 (2012)
- [3] M. Weigel, T. Yavorskii: Physics Procedia **15**, 92 (2011)
- [4] K. Hukushima, K. Nemoto: J. Phys. Soc. Japan **65**, 1604 (1996)
- [5] J. Gross et al.: Comput. Phys. Commun. **182**, 1638 (2011)
- [6] J. Gross et al.: Physics Procedia **15**, 29 (2011)
- [7] The Top500 List: The 500 most powerful commercially available computer systems, <http://www.top500.org>
- [8] The Green500 List: Environmentally responsible supercomputing, <http://www.green500.org>

10.17 Funding

Graduate School “BuildMoNa”: Leipzig School of Natural Sciences – Building with Molecules and Nano-objects

W. Janke (Principal Investigator)

Deutsche Forschungsgemeinschaft (DFG), Excellence Initiative

Graduate School *Statistical Physics of Complex Systems*

W. Janke (with B. Berche, Nancy)

Deutsch-Französische Hochschule, “Deutsch-Französisches Doktorandenkollegium (DFDK)” with “Co-tutelle de Thèse”, jointly with Nancy Université, France, and Coventry University, UK, as associated partner, Grant No. CDFA-02-07

International Max Planck Research School (IMPRS) *Mathematics in the Sciences*

W. Janke (Scientific Member)

Max Planck Society and Klaus Tschira Foundation

Sonderforschungsbereich/Transregio SFB/TRR 102 *Polymers under Multiple Constraints*:

Restricted and Controlled Molecular Order and Mobility

W. Janke (Principal Investigator, project B04)

Deutsche Forschungsgemeinschaft (DFG)

Forschergruppe 877 From Local Constraints to Macroscopic Transport

W. Janke (Principal Investigator, project P9 in collaboration with K. Kroy)

Deutsche Forschungsgemeinschaft (DFG), Grant No. JA 483/29-1

Host of Prof. Dr. Handan Arkin-Olgar (Ankara University, Turkey), Fellowship for Experienced Researchers

W. Janke

Alexander von Humboldt Foundation

Host of Buket Taşdizen (Ankara University, Turkey), ERASMUS Fellowship

W. Janke

ERASMUS Programme

Dynamik und Statik von Spingläsern

W. Janke

Deutsche Forschungsgemeinschaft (DFG), Grant No. JA 483/22-1

Molecular Conformation Mechanics of Proteins and Polymers

W. Janke

Deutsche Forschungsgemeinschaft (DFG), Grant No. JA 483/24-3

Mass Transport Models on Networks

W. Janke (twin project with H. Meyer-Ortmanns, Jacobs University Bremen)

Deutsche Forschungsgemeinschaft (DFG), Grant No. JA 483/27-1

Grafted and Non-Grafted Polymer Adsorption to (Patterned) Substrates

W. Janke and M. Möddel

NIC Jülich (computer time grant for "JUROPA"), Grant No. hlz17

10.18 Organizational Duties

Wolfhard Janke

- Director, Institute for Theoretical Physics (ITP), Universität Leipzig
- Director, Naturwissenschaftlich-Theoretisches Zentrum (NTZ), Universität Leipzig
- Member of Department Council ("Fakultätsrat"), Faculty for Physics and Earth Sciences, Universität Leipzig
- Member Priority Research Area PbF1 *Molecules and Nano-objects*
- Member Priority Research Area PbF2 *Mathematical Sciences*
- Member of the Steering Committee ("Direktorium") of the Graduate Centre *Mathematics/Computer Science and Natural Sciences*, Research Academy Leipzig
- Spokesperson of the German-French Graduate College *Statistical Physics of Complex Systems*
- Spokesperson of the German-Ukrainian Institute Partnership Leipzig-Lviv of the Alexander von Humboldt Foundation

- Chairperson of the Programme Committee “Scientific Computing” of Forschungszentrum Jülich
- Member of the Scientific-Technical-Council of the Supervisory Board (“Aufsichtsrat”) of the Forschungszentrum Jülich GmbH
- External Member of the Jagiellonian University Graduate School *International Ph.D. Studies in Physics of Complex Systems*, Krakow, Poland
- Specialist Editor, *Computer Physics Communications (CPC)*, Elsevier, Amsterdam, The Netherlands
- Editor “Computational Sciences”, *Lecture Notes of Physics*, Springer, Berlin, Heidelberg, Germany
- Editor “Computational Physics”, *Central European Journal of Physics*, Krakow, Poland
- Member of Editorial Board, *Condens. Matter Phys.*, Lviv, Ukraine
- Permanent Member of the “International Advisory Board”, *Conference of the Middle European Cooperation in Statistical Physics (MECO)*
- Member of the Programme Committee for the *European Conference on Complex Systems 2011 (ECCS’11)*, Vienna, Austria, 12.–16. September 2011
- Member of the Programme Committee for the 4th Conference on *Statistical Physics: Modern Trends and Applications*, Lviv, Ukraine, 03.–06. July 2012
- Co-organizer of the “BuildMoNa” Theory Module *Structure and Mechanics of Foams and Cellular Matter* (with K. Kroy), Universität Leipzig, 22.–23. September 2011
- Organizer of the Workshop *CompPhys11 – 12th International NTZ Workshop on New Developments in Computational Physics*, ITP, Universität Leipzig, 24.–26. November 2011
- Organizer of the Workshop *CompPhys12 – 13th International NTZ Workshop on New Developments in Computational Physics*, ITP, Universität Leipzig, 29. November – 01. December 2012
- External Reviewer for Humboldt-Stiftung (AvH); Deutsche Forschungsgemeinschaft (DFG); Studienstiftung des deutschen Volkes; the Jeffress Memorial Trust, Bank of America, Virginia, USA; “Fond zur Förderung der wissenschaftlichen Forschung (FWF)”, Österreich; “The Royal Society”, Great Britain; The “Engineering and Physical Sciences Research Council (EPSRC)”, Great Britain; The University of Warwick, England, Great Britain; Coventry University, England, Great Britain; CECAM, Lyon, France; National Science Foundation (NSF), USA; Natural Sciences and Engineering Research Council of Canada (NSERC), Canada; Israel Science Foundation, Israel
- Referee for *Physical Review Letters*, *Physical Review B*, *Physical Review E*, *Journal of Chemical Physics*, *Europhysics Letters*, *Physics Letters A*, *Physics Letters B*, *The European Physical Journal B*, *Physica A*, *Proceedings of the Royal Physical Society*, *Journal of Physics A*, *Computer Physics Communications*, *JSTAT*, *New Journal of Physics*, *International Journal of Modern Physics C*

10.19 External Cooperations

Academic

- Institut für Festkörperforschung (IFF-2) and Institute for Advanced Simulation (IAS-

- 2), Forschungszentrum Jülich, Germany
Dr. Michael Bachmann, Jonathan Gross, Dr. Thomas Vogel
- Institute of Physics, Jagiellonian University, Kraków, Poland
Prof. Dr. Piotr Białas, Dr. Leszek Bogacz, Prof. Dr. Zdzisław Burda
 - CEA/Saclay, Service de Physique Théorique, France
Dr. Alain Billoire
 - Institut für Physik, Universität Mainz, Germany
Prof. Dr. Kurt Binder, Dr. Hsiao-Ping Hsu, Andreas Nußbaumer, Prof. Dr. Friderike Schmid, Dr. Martin Weigel
 - Institut für Theoretische Physik, Universität Heidelberg, Germany
Dr. Elmar Bittner
 - Laboratoire de Physique des Matériaux (UMR CNRS No 7556), Nancy Université, France
Prof. Dr. Bertrand Berche, Dr. Christophe Chatelain, Dr. Olivier Collet, Prof. Dr. Malte Henkel, Dr. Dragi Karevski
 - Groupe de Physique des Matériaux (UMR CNRS No 6634), Université de Rouen, France
Dr. Pierre-Emmanuel Berche
 - SUPA, School of Physics and Astronomy, University of Edinburgh, Scotland, UK
Dr. Richard A. Blythe, Prof. Dr. Martin R. Evans, Dr. Bartłomiej Waćław
 - Istituto Nazionale di Fisica Nucleare, Sezione di Milano-Bicocca, Milano, Italy
Prof. Dr. Pablo Butera
 - Jülich Supercomputing Centre (JSC), Forschungszentrum Jülich, Germany
Prof. Dr. Peter Grassberger, PD Dr. Thomas Neuhaus
 - IAC-1, Universität Stuttgart
Prof. Dr. Rudolf Hilfer, Anjan Prasad Gantapara
 - Complex Systems Division, Department of Theoretical Physics, Lunds Universitet, Lund, Sweden
Prof. Dr. Anders Irbäck, Simon Mitternacht
 - Department of Mathematics and the Maxwell Institute for Mathematical Sciences, Heriot-Watt University, Edinburgh, Scotland, UK
Prof. Dr. Desmond A. Johnston
 - Applied Mathematics Research Centre, Coventry University, England, UK
Dr. Ralph Kenna, PD Dr. Christian von Ferber, Dr. Martin Weigel
 - Inst. für Theoretische Physik, FU Berlin, Germany
Prof. Dr. Hagen Kleinert
 - Max-Planck Institut für Physik komplexer Systeme, Dresden, Germany
Dr. Andreas Läuchli
 - Atominstitut, TU Wien, Austria
Prof. Dr. Harald Markum, Dr. Rainer Pullirsch
 - Jacobs Universität Bremen, Germany
Dr. Ashok Garai, Prof. Dr. Hildegard Meyer-Ortmanns

- Applied Mathematics, Universitat Pompeu Fabra, Barcelona, Spain
Dr. Ramon Villanova
- EPF Lausanne, Switzerland
Dr. Sandro Wenzel
- Department of Engineering of Physics, Ankara University, Turkey
Prof. Dr. Handan Arkın (Olgar), Mustafa Bilsel, Buket Taşdizen
- Dept. of Physics, Hacettepe University, Ankara, Turkey
Prof. Dr. Tarik Çelik, Gökhan Gököğlü
- Institute for Condensed Matter Physics, National Academy of Sciences, Lviv, Ukraine
Dr. Viktoria Blavatska, Prof. Dr. Yuriy Holovatch
- Yerevan Physics Institute, Yerevan, Armenia
Prof. Dr. David B. Saakian
- Landau Institute for Theoretical Physics, Chernogolovka, Russia
Prof. Dr. Lev N. Shchur
- Banaras Hindu University, Varanasi, India
Prof. Dr. Sanjay Kumar
- Dept. of Physics, Florida State University, Tallahassee, USA
Prof. Dr. Bernd A. Berg
- Dept. of Physics, Michigan Technological University, Houghton, USA
Prof. Dr. Ulrich H.E. Hansmann
- Center for Simulational Physics, The University of Georgia, Athens, USA
Prof. Dr. Michael Bachmann, Jonathan Gross, Prof. Dr. David P. Landau, Dr. Stefan Schnabel, Dr. Thomas Vogel
- Physics Department, Carnegie Mellon University, Pittsburgh, USA
Prof. Dr. Robert H. Swendsen
- Dept. of Physics, Virginia Tech, Blacksburg, USA
Prof. Dr. Michel Pleimling, Prof. Dr. Beate Schmittmann, Prof. Dr. Royce K.P. Zia
- The University of Tokyo, Japan
Prof. Dr. Nobuyasu Ito
- Nagoya University, Japan
Tetsuro Nagai, Prof. Dr. Yuko Okamoto
- Laboratory of Statistical and Computational Physics, Institute of Physics, Academia Sinica, Nankang, Taipei, Taiwan
Prof. Dr. Chin-Kun Hu
- Zhejiang Institute of Modern Physics, Zhejiang University, Hangzhou, P.R. China
Prof. Dr. He-Ping Ying, Prof. Dr. Bo Zheng

10.20 Publications

Journals

E. Bittner, W. Janke: *Parallel-Tempering Cluster Algorithm for Computer Simulations of Critical Phenomena*, Phys. Rev. E **84**, 036701-1–4 (2011)

V. Blavatska, W. Janke: *Θ -Polymers in Crowded Media under Stretching Force*, Comput. Phys. Commun. **182**, 1966–1969 (2011)

J. Gross, W. Janke, M. Bachmann: *Massively Parallelized Replica-Exchange Simulations of Polymers on GPUs*, Comput. Phys. Commun. **182**, 1638–1644 (2011)

J. Gross, W. Janke, M. Bachmann: *A GPU Approach to Parallel Replica-Exchange Polymer Simulations*, in *Computer Simulation Studies in Condensed-Matter Physics XXIV*, eds. D.P. Landau, S.P. Lewis, H.-B. Schüttler, Physics Procedia **15**, 29–32 (2011)

W. Janke, T. Neuhaus, A.M.J. Schakel: *Worms Exploring Geometrical Features of Phase Transitions*, in *Computer Simulation Studies in Condensed-Matter Physics XXIV*, eds. D.P. Landau, S.P. Lewis, H.-B. Schüttler, Physics Procedia **15**, 54–58 (2011)

C. Junghans, W. Janke, M. Bachmann: *Hierarchies in Nucleation Transitions*, Comput. Phys. Commun. **182**, 1937–1940 (2011)

S. Karalus, W. Janke, M. Bachmann: *Thermodynamics of Polymer Adsorption to a Flexible Membrane*, Phys. Rev. E **84**, 031803-1–12 (2011)

M. Möddel, W. Janke, M. Bachmann: *Adsorption of Finite Polymers in Different Thermodynamical Ensembles*, Comput. Phys. Commun. **182**, 1961–1965 (2011)

M. Möddel, W. Janke, M. Bachmann: *Comparison of the Adsorption Transition for Grafted and Non-Grafted Polymers*, Macromolecules **44**, 9013–9019 (2011)

S. Schnabel, W. Janke, M. Bachmann: *Advanced Multicanonical Monte Carlo Methods for Efficient Simulations of Nucleation Processes of Polymers*, J. Comput. Phys. **230**, 4454–4465 (2011)

S. Schöbl, J. Zierenberg, W. Janke: *Simulating Flexible Polymers in a Potential of Randomly Distributed Hard Disks*, Phys. Rev. E **84**, 051805-1–8 (2011)

Books

in press

H. Arkin, W. Janke: *Structural Behavior of a Polymer Chain Inside an Attractive Sphere*, Phys. Rev. E **85**, 051802-1–9 (2012)

M. Bilsel, B. Taşdizen, H. Arkin, W. Janke: *Effects of Confinement on the Thermodynamics of a Model Protein*, to appear in Proceedings of the NIC Workshop *From Computational Biophysics to Systems Biology 2011*, Jülich, 20–22 July 2011, John von Neumann Institute for Computing, Forschungszentrum Jülich, IAS Series, in print (2012)

V. Blavatska, W. Janke: *Polymer Adsorption on a Fractal Substrate: Numerical Study*, J. Chem. Phys. **136**, 104907-1–8 (2012)

V. Blavatska, W. Janke: *Conformational Properties of Polymers Near a Fractal Surface*, in *Computer Simulation Studies in Condensed-Matter Physics XXV*, eds. D.P. Landau, S.P. Lewis, H.-B. Schüttler, to appear in Physics Procedia (2012), in print

N. Fricke, W. Janke: *Exact Enumeration of Self-Avoiding Walks on Percolation Clusters*, in *Computer Simulation Studies in Condensed-Matter Physics XXV*, eds. D.P. Landau, S.P. Lewis, H.-B. Schüttler, to appear in Physics Procedia (2012), in print

A. Garai, B. Waclaw, H. Nagel, H. Meyer-Ortmanns: *Stochastic Description of a Bistable Frustrated Unit*, J. Stat. Mech. P01009 (2012)

W. Janke: *Monte Carlo Simulations in Statistical Physics – From Basic Principles to Advanced Applications*, invited lecture notes, to appear in *Order, Disorder and Criticality: Advanced Problems of Phase Transition Theory*, Vol. 3, ed. Y. Holovatch (World Scientific, Singapore 2012), in print

M. Möddel, M. Bachmann, W. Janke: *Grafted versus Non-Grafted Polymer Adsorption*, in *NIC Symposium 2012, Proceedings*, eds. K. Binder, G. Münster, M. Kremer, John von Neumann Institute for Computing, Forschungszentrum Jülich, NIC Series, Vol. **45** (2012), pp. 277–284

Talks

H. Arkin: *Simulations of Biological Molecules*, SFG FOR877 Kick-Off Meeting, Universität Leipzig, 24. June 2011

N. Fricke: *A Numerical Study of Self-Avoiding Walks (SAWs) on Disordered Two-Dimensional Lattices*, Spring Meeting of the German Physical Society, Dresden, 18. March 2011

N. Fricke: *Numerical Treatment of Self-Avoiding Walks on Disordered Lattices*, Seminar of the cdfa-dfdk, Nancy, France, 14. June 2011

N. Fricke: *Exact Enumeration of Self-Avoiding Walks on Percolation Clusters*, Applied Mathematics Seminar, Coventry University, UK, 26. October 2011

N. Fricke: *Scale-Free Enumeration of Self-Avoiding Walks on Critical Percolation Clusters*, Seminar of the cdfa-dfdk, Leipzig, 15. December 2011

W. Janke: *The Ising Model in Statistical Physics II*, IMPRS Ringvorlesung “Discrete Structures in Physics”, International Max Planck Research School, Max-Planck-Institut für Mathematik in den Naturwissenschaften, Leipzig, 04. January 2011

W. Janke: *The Ising Model in Statistical Physics III*, IMPRS Ringvorlesung “Discrete Structures in Physics”, International Max Planck Research School, Max-Planck-Institut für Mathematik in den Naturwissenschaften, Leipzig, 11. January 2011

W. Janke: *Worms Exploring Geometrical Features of Phase Transitions*, 24th CSP Workshop on Recent Developments in Computer Simulation Studies in Condensed Matter Physics, The University of Georgia, Athens, USA, 21.–25. February 2011

W. Janke: *Monte Carlo Simulations in Multicanonical Ensembles*, invited talk, 2nd Stellenbosch Workshop on Statistical Physics, NITheP, Stellenbosch, South Africa, 07.–18. March 2011

W. Janke: *Thermodynamics of Polymer Statistics: Perspectives from Three Statistical Ensembles*, invited talk, 2nd Stellenbosch Workshop on Statistical Physics, NITheP, Stellenbosch, South Africa, 07.–18. March 2011

W. Janke: *Worms Exploring Geometrical Features of Phase Transitions*, 36th Conference of the Middle European Cooperation in Statistical Physics MECO36, Institute for Condensed Matter Physics, Lviv, Ukraine, 05.–07. April 2011

M. Marenz: *Worm Algorithm – Simulating Spin Systems via Path Representation*, Seminar of the cdfa-dfdk, Nancy, France, 18. October 2011

M. Möddel: *Effects of Polymer Grafting on the Thermodynamic Equilibrium Behavior of Single Polymer Adsorption*, Spring Meeting of the German Physical Society, Dresden, 16. March 2011

M. Möddel: *Some Aspects of the Thermodynamic Equilibrium Behaviour of a Finite Single Polymer Near an Attractive Substrate*, research seminar, Applied Mathematics Research Centre, Coventry University, Coventry, England, 23. May 2011

H. Nagel: *Stochastic Description of a Bistable Frustrated Unit*, Seminar of the Applied Mathematics Research Centre, Coventry University, 12. October 2011

J. Zierenberg: *Simulating Semiflexible Polymers in Hard Disc Background Potentials*, Seminar of the cdfa-dfdk, Nancy, France, 25. October 2011

Posters

M. Bilsel, B. Taşdizen, H. Arkın, W. Janke: *Effects of Confinement on the Thermodynamics of a Model Protein*, Conference From Computational Biophysics to System Biology 2011, NIC, Forschungszentrum Jülich, 20.–22. July 2011

R. Bischof, W. Janke: *Gaußsche Universalitätsklasse in gemischten Quantenspinketten*, RAL-Evaluation, Universität Leipzig, 10.–19. October 2011

R. Bischof, W. Janke: *Gaussian Universality Class in Mixed Quantum Spin Chains*, 12th International NTZ-Workshop on New Developments in Computational Physics – CompPhys11, Universität Leipzig, 24.–26. November 2011

N. Fricke, W. Janke: *How to count 10^{100} Self-Avoiding Walks on a Critical Percolation Cluster*, Spring Meeting of the German Physical Society, Dresden, 13.–18. March 2011

N. Fricke, W. Janke: *A new Technique for Complete Enumeration of Self-Avoiding Walks on Percolation Clusters*, 36th Conference of the Middle European Cooperation in Statistical Physics *MECO36*, Institute for Condensed Matter Physics, Lviv, Ukraine, 05.–07. April 2011

N. Fricke, W. Janke: *Scale-Free Enumeration of Self-Avoiding Walks on Critical Percolation Clusters*, 12th International NTZ-Workshop on New Developments in Computational Physics – *CompPhys11*, Universität Leipzig, 24.–26. November 2011

M. Marenz, W. Janke: *Worm Algorithm in Ordered and Disordered Media*, Spring Meeting of the German Physical Society, Dresden, 13.–18. March 2011

M. Marenz, W. Janke: *Worm Algorithm in Ordered and Disordered Media*, Mainz Materials Simulation Days, Universität Mainz, 25.–27. May 2011

M. Marenz, W. Janke: *Worm Algorithm in Ordered and Disordered Media*, CECAM Jülich Summer School, Forschungszentrum Jülich, 12.–16. September 2011

M. Möddel, M. Bachmann, W. Janke: *Comparison of Grafted and Non-Grafted Polymer Adsorption in Different Ensembles*, 4th Scientific Symposium of the Graduate School *BuildMoNa*, Universität Leipzig, 21. March 2011

M. Möddel, M. Bachmann, W. Janke: *Comparison of Grafted and Non-Grafted Polymer Adsorption in Different Ensembles*, 12th International NTZ-Workshop on New Developments in Computational Physics – *CompPhys11*, Universität Leipzig, 24.–26. November 2011

H. Nagel, B. Waclaw, W. Janke: *Time Scale of Mass Condensation in Stochastic Transport with Pair Factorized Steady States*, Spring Meeting of the German Physical Society, Dresden, 13.–18. March 2011

S. Schöbl, K. Kroy, W. Janke: *Broadscale Examination of the Influence of Disorder on Semiflexible Polymers*, 4th Scientific Symposium of the Graduate School *BuildMoNa*, Universität Leipzig, 21. March 2011

J. Zierenberg, B.A. Berg, W. Janke: *Structure of the Tip4p Water Model in the Ice I_h Phase*, Spring Meeting of the German Physical Society, Dresden, 13.–18. March 2011

J. Zierenberg, B.A. Berg, W. Janke: *Structure of the Tip4p Water Model in the Ice I_h Phase*, Mainz Materials Simulation Days, Universität Mainz, 25.–27. May 2011

J. Zierenberg, B.A. Berg, W. Janke: *All-Atom Simulations of Tip4p Water on Graphics Cards using OpenGL*, International Symposium *Computer Simulations on GPU*, Universität Mainz, 30. May – 01. June 2011

J. Zierenberg, B.A. Berg, W. Janke: *Structure of the Tip4p Water Model in the Ice I_h Phase*, CECAM Jülich Summer School, Forschungszentrum Jülich, 12.–16. September 2011

10.21 Graduations

Diploma

- Marco Müller
Multicanonical Analysis of the Gonihedric Ising Model and its Dual
01. November 2011

10.22 Guests

- Dr. Stefan Schnabel
University of Georgia, Athens, USA
01.–10. January 2011
- Dr. Bartłomiej Waclaw
University of Edinburgh, UK
NTZ Colloquium/FOR877 Seminar
A Dynamical Phase Transition in a Model for Evolution with Migration
26.–28. January 2011
- Prof. Dr. Yuko Okamoto
Nagoya University, Japan
NTZ Colloquium
Biomolecular Simulations by Efficient Conformational Sampling Techniques
04.–06. May 2011
- Prof. Dr. Royce P.K. Zia
Virginia Tech, Blacksburg, USA
NTZ Colloquium/FOR877 Seminar
Modeling Translation by Totally Asymmetric Simple Exclusion Processes (TASEP)
07. July 2011
- Dr. Christoph Junghans
MPI für Polymerforschung, Mainz, Germany
DFH-UFA Seminar
Locality Analysis via Adaptive Resolution Simulations
11.–13. July 2011
- Dr. Ashok Garai
Jacobs University, Bremen, Germany
DFH-UFA Seminar
Stochastic Simulations of a Bistable Frustrated Unit
12.–14. July 2011
- Jeremi Ochab
Jagiellonian University, Krakow, Poland
Epidemics on Networks
01. August – 31. October 2011
- Dr. Viktoria Blavatska
Institute for Condensed Matter Physics, Lviv, Ukraine

Humboldt Fellow/FOR877 guest
NTZ Colloquium/FOR877 Seminar
Numerical Study of Polymer Adsorption on Fractal Substrates
01. October – 30. November 2011

- Prof. Dr. Robert H. Swendsen
Carnegie Mellon University, Pittsburgh, USA
NTZ Colloquium/DFH-UFA Seminar
The Entropy Wars
23.–29. October 2011
- Prof. Dr. Robert H. Swendsen
Carnegie Mellon University, Pittsburgh, USA
NTZ Colloquium
How the Maximum Step Size in Monte Carlo Simulations Should be Adjusted
20.–26. November 2011
- Pádraig Mac Carron
Applied Mathematics Research Centre, Coventry University, UK
Mythological Networks
22.–28. November 2011
- Prof. Dr. Alexander Hartmann
Universität Oldenburg, Germany
Random-Field Ising Magnet with Correlated Disorder
23.–25. November 2011
- Prof. Dr. Heiko Rieger
Saarland University, Saarbrücken, Germany
Strong Roughening of Spontaneous Imbibition Fronts
23.–25. November 2011
- Prof. Dr. Antun Balaz
Scientific Computing Laboratory, Institute of Physics, University of Belgrade, Serbia
Numerical Simulations of Faraday Waves in Binary Bose-Einstein Condensates
23.–26. November 2011
- Hsiao-Ping Hsu
Universität Mainz, Germany
Structure and Scaling Analysis of Stretched Semiflexible Polymer Chains
23.–26. November 2011
- Prof. Dr. Malte Henkel
Nancy Université, France
Logarithmic Extensions of Local Scale Invariance
23.–27. November 2011
- Prof. Dr. Ferenc Iglói
Institute of Theoretical Physics, Research Institute for Solid State Physics and Optics,
Budapest, Hungary
Quantum Relaxation After a Quench in Systems with Boundaries
23.–27. November 2011

- Prof. Dr. Desmond A. Johnston
Heriot-Watt University, Edinburgh, UK
Gonihedric Ising Models: Order Parameter(s) and Dual(s)
23.–27. November 2011
- Tetsuro Nagai
Nagoya University, Japan
Application of Two-Dimensional Simulated Tempering (ST) to the Two-Dimensional Ising Model
23.–27. November 2011
- Jeremi Ochab
Jagiellonian University, Krakow, Poland
Pair-Factorised Steady State Model Exhibits a Condensate's Growth on Monolayers
23.–27. November 2011
- Prof. Dr. Yuko Okamoto
Nagoya University, Japan
Generalized-Ensemble Simulations of Spin Models and Biomolecular Systems
23.–27. November 2011
- Dr. Sergio Perez-Gaviro
Institute for Biocomputation and Physics of Complex Systems (BIFI), University of Zaragoza, Spain
Anisotropy Impact in the 3D Heisenberg Spin-Glass Model
23.–27. November 2011
- Prof. Dr. Mark Taylor
Hiram College, Hiram, OH, USA
Partition Function Zeros and Phase Transitions of a Polymer Chain
23.–27. November 2011
- Karol Trojanowski
Jagiellonian University, Krakow, Poland
Resonance and Pattern Formation in the Kuramoto Model with Manhattan Delay
23.–27. November 2011
- Marcin Zagórski
Jagiellonian University, Krakow, Poland
Motifs Emerge from Function in Model Gene Regulatory Networks
23.–27. November 2011
- PD Dr. Thomas Neuhaus
Jülich Supercomputing Centre, Forschungszentrum Jülich, Germany
NTZ Colloquium/DFH-UFA Seminar
Numerical Study of Quantum Annealing for the Hardest Case of 2SAT and 3SAT
23. November – 03. December 2011
- Dr. Elmar Bittner
Universität Heidelberg, Germany
Parallel-Tempering Cluster Algorithm for Computer Simulations of Critical Phenomena
24.–28. November 2011

- PD Dr. Thomas Neuhaus
Jülich Supercomputing Centre, Forschungszentrum Jülich, Germany
Precision Calculation of Spin-Spin Correlators in the Ising Model via Worm Updates
25. November 2011
- Buket Taşdizen
Ankara University, Turkey
01. December 2011 – 29. February 2012

11

Molecular Dynamics / Computer Simulation

11.1 Introduction

The central aim of our group is the investigation of classical many-particle systems using methods of statistical physics and computer simulations.

Particularly we are examining the behavior of guest molecules within pores and at the surfaces of porous solids.

For about 30 years a basic motivation of our work has always been to build up a bridge between theoretical and experimental physics exchanging challenges and stimuli in both directions.

By means of analytical theories of statistical physics and computer simulations (Molecular dynamics, Monte Carlo procedures, Transition State Theory, Virial expansion) using modern workstations and supercomputers we examine subjects for which high interest exists in basic research and industry as well. The examinations involve adsorption and transport properties (diffusion of guest molecules) in zeolites and the new exciting class of porous Metal-Organic-Frameworks (so called MOF's).

Especially we are interested to understand

- the diffusion behaviour of guest molecules in porous crystals in dependence on thermodynamic parameters, steric conditions, intermolecular potentials and the concentration of the guest molecules,
- structure and phase equilibria of adsorbed species in e.g. pores or model membranes in exchange with free gas systems in dependence on geometric and thermodynamic conditions,

in microscopic detail and to compare the results with experimental data.

The use of a network of PC's and workstations (Unix, Linux, Windows), the preparation and application of programs (Fortran, C, C++), and the interesting objects (zeolites, MOF's, membranes) give excellent possibilities for future careers of undergraduates, graduate students and postdocs. Our research is part of several national and international programs (DFG - Schwerpunktprogramm SPP1362, including a joint research project DFG/TRF-Thailand, and, an International Research Graduate Training program (IRTG 1056) and includes a close collaboration with the Institute of Experimental

Physics I (Physics of Interfaces and Biomembranes) of Leipzig University and many institutions in Germany and other countries. Details are given in the list of external cooperations.

S. Fritzsche

11.2 Analytical Treatment and Computer Simulations of the influence of the crystal surface on the exchange of guest molecules between zeolite nanocrystals and the surrounding gas phase

S. Fritzsche^{*}, O. Saengsawang[†], T. Nanok[‡], S. Vasenkov[§]

^{*}Abteilung MDC

[†]Chulalongkorn University, Bangkok, Thailand

[‡]Kasetsart University, Bangkok

[§]University of Florida, Gainesville, USA

Our research in the framework of the DFG priority program SPP 1155 about the surface effects influencing the dynamics of adsorption and diffusion of guest molecules into porous crystals was continued and finished.

Some new results about the interplay between diffusion within zeolite crystals, along its surface and through mesopores surrounding these crystals together with earlier results have been gathered together in a final publication [1].

It turned out that a remarkable part of the diffusing molecules enter the crystals in spite of the free space around them and that this has large influence on the transport of gas through powders which are more easily to produce and cheaper than membranes.

[1] O. Saengsawang, T. Nanok, S. Vasenkov and S. Fritzsche, *Soft Materials* **10** (2012) 202-215

11.3 Diffusion and Rotation of Water in the Zeolite Chabazite

S. Fritzsche^{*}, R. Channajaree^{*}, P. A. Bopp[†], J. Kärger[‡],

^{*}Abteilung MDC

[†]University Bordeaux, France

[‡]Institut für Experimentelle Physik I, Abteilung GFP

Basing on earlier own work [1] rotation and diffusion of water in the zeolite chabazite was re-investigated in a project in the framework of the International Research Training Group (IRTG) "Diffusion in Porous Materials". New theoretical methods like boost potential MD and more powerful computational tools led to considerable improvements of the earlier results.

The agreement with experimental results could be improved and an explanation for the need to correct an analytical ansatz used in the literature for jump probabilities could be found and published [2].

- [1] S. Jost, P. Biswas, A. Schüring, J. Kärger, P. A. Bopp, R. Haberlandt, Siegfried Fritzsche, *J. Phys. Chem. C*, **111**, 14707 (2007)
- [2] R. Chanajaree, Ph. A. Bopp, J. Kärger and S. Fritzsche, *Microporous and Mesoporous Materials* **146** (2011) 106–118

11.4 Influence of the shape of the potential landscape on diffusion

S. Fritzsche*, S. Yashonath[†], C. Krishna[†], A. Schüring*, J. Kärger[‡],

*Abteilung MDC

[†]University Bangalore, India

[‡]Institut für Experimentelle Physik I, Abteilung GFP

The strong influence of variations of interaction parameters on the transport mechanism of methane in Linde type A zeolite has been proven and investigated in Molecular Dynamics computer simulations using jump models, free energy profiles and potential landscapes [1].

It could be shown that the concentration dependence of the self diffusion coefficient can be even reversed by relatively small changes in the diameter of the window connecting adjacent pores in the zeolite.

- [1] C. A. Krishna, S. Yashonath, A. Schüring, S. Fritzsche and J. Kärger, *Adsorption Science and Technology* **29** (2011) 553-567

11.5 Lattice Flexibility and Diffusion of Guest Molecules in the Metal Organic Framework Zntbip

S. Fritzsche*, K. Seehamart*, S. Hannongbua[†], T. Remsungnen[‡], J. Kärger[§], C. Chmelik[§], R. Krishna[¶], J. M. van Baten[¶]

*Abteilung MDC

[†]Chulalongkorn University, Bangkok, Thailand

[‡]Khon Khaen University, Khon Khaen, Thailand

[§]Institut für Experimentelle Physik I, Abteilung GFP

[¶]Van't Hoff Institute for Molecular Sciences, University of Amsterdam, The Netherlands

Within the framework of the SPP1362 in a common DFG project with experimental groups (Prof. Kärger, Leipzig, Prof. Caro, Hannover, Dr. Wiebcke, Hannover) and NRCT (Thailand, Prof. Hannongbua) and theoretical physicists from Amsterdam the investigation of the surprisingly strong influence of the lattice flexibility on diffusion

of guest molecules within the promising new material Zntbip, published in [1] was continued.

After some subsequent papers, during the last years, with the recent one [2] the investigations were extended to the behavior of mixtures of guest molecules. It turned out that the influence of the lattice flexibility exists also for other substances but, is most drastical for ethane which we investigated first in [1].

Knowledge about the importance of the lattice flexibility is particularly important because most simulations about Metal Organic Frameworks (MOF's) are still being done by simplifying the system by use of a rigid framework.

- [1] K. Seehamart, T. Nanok, R. Krishna, J.M. van Baten, T. Remsungnen, S. Fritzsche, *Microporous and Mesoporous Materials*, **125**(2009)97–100
 [2] K. Seehamart and C. Chmelik and R. Krishna and S. Fritzsche, *Microporous and Mesoporous Materials* **143** (2011) 125–131

11.6 Simulation and Experiments of Membrane Diffusion of guest molecules in the Metal Organic Framework ZIF-8

S. Fritzsche^{*}, M. Knauth^{*}, C. Chmelik[†], J. Caro[‡], H. Bux[‡], S. Hannongbua[§], T. Remsungnen[¶],

^{*}Abteilung MDC

[†]Institut für Experimentelle Physik I, Abteilung GFP

[‡]Institut für Anorganische Chemie, Leibniz Universität Hannover, Callinstraße 9, 30167 Hannover, Germany

[§]Chulalongkorn University, Bangkok, Thailand

[¶]Khon Kaen University, Khon Khaen, Thailand

Within the framework of a consortium formed by 4 groups in Germany (2 in Leipzig, 2 in Hannover) in cooperation with colleagues from the Chulalongkorn university, Bangkok and the University of Khon Kaen (both Thailand) the experimental findings from Leipzig and Hannover could be examined by simulation.

The simulations have been performed with flexible lattice although the effort is considerable. To define all of the bonds, angles and torsions within the MOF crystal about 10000 lines in the input file to the simulation package DL_POLY are necessary and the computer time needed for such simulations is large and requires modern supercomputers.

Therefore, most simulations reported in the literature are done with rigid lattice.

ZIF-8 is a stable MOF that is very promising for industrial applications. It was investigated in our group in [1]–[5] for various guest molecules.

In the literature it was stated that methane with a kinetic diameter of about 3.6 Å is too large to pass the windows connecting adjacent cavities in the MOF ZIF-8. Hence, Sholl et al. [6] reported from their simulations with rigid lattice a separation factor of 10^7 between H₂ and CH₄.

In contrast to [6] the membrane selectivity, which is the product of the adsorption selectivity and the diffusion selectivity according to

$$\alpha_{ij}^{\text{membrane}} = \alpha_{ij}^{\text{diff}} \cdot \alpha_{ij}^{\text{adsorp}} \quad (11.1)$$

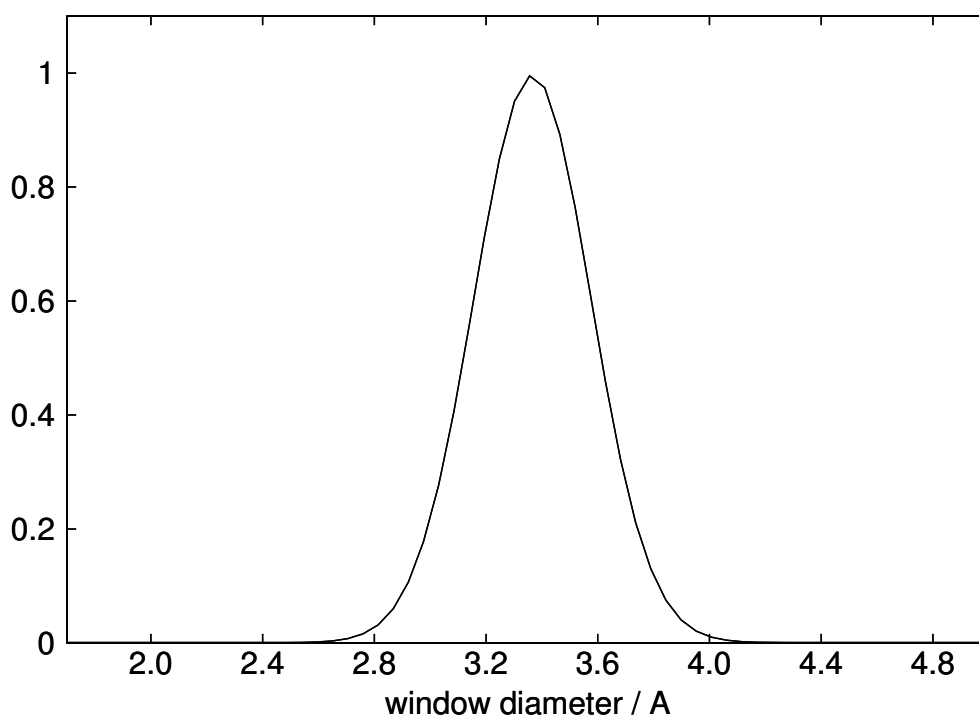


Figure 11.1: The distribution of window diameters in ZIF-8.

has been found from our simulations [1] to be 13.2 in good agreement with the experimental value of 16. The remaining difference can be explained by the fact that in the simulations in which the diffusion selectivity was obtained an equimolar mixture has been assumed. But, due to the adsorption selectivity a H_2 to CH_4 ratio of 1:12 should appear in the membrane.

Using instead of an equimolar mixture a diffusion selectivity based on single-component diffusivities we find a forecasted membrane selectivity of 17.3, which is even closer to the measured value of 16.

In any case these results are far from the forecasted value 10^7 as obtained from simulations with rigid lattice in [6].

The reason can be understood as follows.

A histogram of diameters of the windows (apertures connecting adjacent cavities) as observed during the simulation can be seen in Figure 11.1. The maximum probability corresponds to a diameter of the window of about 3.4 Å which is also the value of this diameter in a rigid ZIF-8 and would be too small to allow diffusion of methane. It can be seen that window diameters larger than 3.6 Å appear during the simulation with flexible window often enough to allow diffusion.

This justifies the huge effort to take into account lattice flexibility in the MD the simulations.

- [1] L. Hertäg, J. Caro, H. Bux, C. Chmelik, T. Remsungnen, M. Knauth, S. Fritzsche, *Journal of Membrane Science* **377** (2011) 36–41
- [2] L. Hertäg, Diplomarbeit, University Leipzig, 2010
- [3] K. Kirchner, Diplomarbeit, University Leipzig, 2010
- [4] S. Reimann, Bachelor-Thesis, University Leipzig, 2011

- [5] M. Stiller, Bachelor–Thesis, University Leipzig, 2011
[6] E. Haldoupis, S. Nair and D. S. Sholl, JACS **132** (2010) 7528–7539

11.7 Funding

Analytical Treatment and Computer Simulations of the influence of the crystal surface on the exchange of guest molecules between zeolite nanocrystals and the surrounding gas phase

S. Fritzsche, S. Vasenkov

DFG SPP 1155, project code FR 1486/2-3

Diffusion and Rotation of Water in the Zeolite Chabazite

S. Fritzsche, R. Channajaree

International Research Training Group, DFG IRTG 1056

Lattice Flexibility and Diffusion of Guest Molecules in the Metal Organic Framework Zntbip

S. Fritzsche

DFG SPP 1362, project code FR 1486/5-1

Simulation and Experiments of Membrane Diffusion of guest molecules in the Metal Organic Framework ZIF-8

S. Fritzsche, M. Knauth, U. Arsawang

DFG SPP 1362, project code FR 1486/5-1

11.8 Organizational Duties

S. Fritzsche

- Project leader of one project in the International Research Training Group, IRTG 1056
- Project leader of one project in the SPP1155, DFG-code FR1486/2-3, (finishing)
- Project leader of one project in the SPP1362, DFG-code FR1486/5-1
- Referee for journals (Journal of Physical Chemistry, Microporous and Mesoporous Materials, JACS, Adsorption Science and Technology, Journal of Molecular Modeling, International Journal of Heat and Mass Transfer, Langmuir)

11.9 External Cooperations

Academic

- Chulalongkorn University, Bangkok, Thailand
Prof. S. Hannongbua (Dean of the faculty of science), Dr. O. Saensawang, Dr. R. Channajaree
- Khon Kaen University, Khon Khaen, Thailand
Prof. T. Remsungnen, Dr. P. Puphasuk, Dr. K. Seehamart

- University of Bordeaux, France
Prof. P. A. Bopp
- University of Bangalore, India
Prof. S. Yashonath
- University of Gainesville, USA
Prof. S. Vasenkov
- University of Hannover
Prof. J. Caro, Prof. M. Wiebcke
- University of Leipzig, Ins. of Experimental Physics I
Prof. J. Kärger, Dr. C. Chmelik

11.10 Publications

Journals

L. Hertäg, J. Caro, H. Bux, C. Chmelik, T. Reimsungnen, M. Knauth, S. Fritzsche, *Journal of Membrane Science* **377** (2011) 36–41

K. Seehamart and C. Chmelik and R. Krishna and S. Fritzsche, *Microporous and Mesoporous Materials* **143** (2011) 125–131

C. A. Krishna, S. Yashonath, A. Schüring, S. Fritzsche and J. Kärger, *Adsorption Science and Technology* **29** (2011) 553–567

O. Saengsawang, T. Nanok, S. Vasenkov and S. Fritzsche, *Soft Materials* **10** (2012) 202–215

R. Chanajaree, Ph. A. Bopp, J. Kärger and S. Fritzsche, *Microporous and Mesoporous Materials* **146** (2011) 106–118

Talks

S. Fritzsche, *Importance of Lattice Flexibility in MOF - Computer Simulations*, Talk March 9th 2011 at the Chulalongkorn University, Bangkok, Thailand

S. Fritzsche, *Treatment of Rare Events in Computer Simulations* Talk August 11th 2011 at the Chulalongkorn University, Bangkok, Thailand

S. Fritzsche, *MD Simulations - An Introduction into a Valuable Mathematical Tool in Chemistry and Molecular Physics*, Talk August 29th 2011 at the University of Kon Khaen, Dept. of Mathematics, Kon Khaen, Thailand

Posters

Guest-Induced Window Size in ZIF-8 Studied by Molecular Dynamics,
T. Chokbunpiam, O. Saengsawang, R. Channajaree, S. Fritzsche and S. Hannongbua,
Poster on the International Symposium on Metal-Organic Frameworks, Dresden, 20th–21st September 2011

11.11 Graduations

Doctorate

- R. Chanajaree
The Motions of Guest Water Molecules and Cations in Chabazite
University of Leipzig, April 2011
- K. Seehamart
Investigation of the diffusion mechanisms of several hydrocarbons in the Metal-Organic-Framework Zn(tbip)
University of Leipzig, April 2011

Bachelor

- S. Reimann
Studies of the lattice dynamics of the metal-organic framework ZIF-8
University of Leipzig, June 2011
- M. Stiller
Diffusion of Ethylene through a Metal-Organic Framework
University of Leipzig, October 2011

11.12 Guests

- Prof. Dr. S. Hannongbua
Dean of the faculty of science, Chulalongkorn University, Bangkok, Thailand
3 October - 7 October 2011
- Prof. Dr. T. Reimsungnen
University of Kon Khaen, Thailand
2 May - 30 June 2011
- Dr. Pikul Puphasuk
University of Kon Khaen, Thailand
15 May - 30 June 2011
- Dr. O. Saengsawang
Chulalongkorn University, Bangkok, Thailand
2 May - 31 May 2011

12

Quantum Field Theory and Gravity

12.1 Temperature Dependence of the Casimir Force

M. Bordag,

The vacuum of quantum fields shows a response to changes in external conditions with measurable consequences. The most prominent manifestation is the Casimir effect. It belongs to the few number of macroscopic quantum effects and it is of big importance in nanometer sizes systems. At present, the problem of the dependence of the Casimir forces on temperature is in the focus of actual interest. There are two reasons for, the possibility to measure these forces due to improved experimental techniques and the more theoretical question on the violation of the third law of thermodynamics observed in a certain model.

Actual research was on the temperature dependent Casimir force between a sphere and a plane and on media with temporal dispersion, [1, 2].

- [1] M. Bordag and I. G. Pirozhenko. On the Casimir entropy for a ball in front of a plane. *Phys. Rev. D*, 82:125016, 2010.
- [2] M. Bordag, B. Geyer, G. L. Klimchitskaya, and V. M. Mostepanenko. On the definition of dielectric permittivity for media with temporal dispersion in the presence of free charge carriers. *J. Phys.*, A43:015402, 2010.

12.2 Higher order correlation corrections to color ferromagnetic vacuum state at finite temperature

M. Bordag, V. Skalozub*,

*U Dnepropetrovsk

Topic of the investigation is the stability of the ground state of QCD with temperature and color magnetic background field by means of the calculation of the polarization tensor of the gluon field. Special attention was devoted to the investigation of the polarization tensor for the color charged gluons at finite temperature. A new technique for a parametric representation was found which allowed for an explicit separation of

the Debye and the magnetic masses and, for instance, for an easy calculation of the Debye mass's field and temperature dependence [1].

Another line of research in this collaboration was on long range magnetic fields.

- [1] M. Bordag, V. Demchik, and V. Skalozub. Characteristics of gluon plasma in chromomagnetic field at high temperature. In K.A. Milton and M. Bordag, editors, *Proceedings of the 9th Conference on Quantum Field Theory Under the Influence of External Conditions (QFEXT09)*. World Scientific, Singapore, 2010.

12.3 Structure of the gauge orbit space and study of gauge theoretical models

G. Rudolph, Sz. Charzynski*, E. Fuchs H. Grundling[†], A. Hertsch, J. Huebschmann[‡] P. Jarvis[§], J. Kijowski*, M. Schmidt,

*U Warsaw

[†]U Sydney

[‡]U Lille

[§]U Hobart

The investigation of gauge theories in the Hamiltonian approach on finite lattices with emphasis on the role of nongeneric strata was continued. Based on [1], the work on the stratified Kähler quantization for gauge groups SU(2) and SU(3) was continued [2] and extended to arbitrary compact gauge groups [3]. Aspects of the classical dynamics of these models were investigated [4].

Based on [5], in collaboration with P. Jarvis and H. Grundling, the investigations of the structure of the algebra of observables and its representations for specific models of quantum lattice gauge theory in terms of gauge invariant quantities were continued [6].

In collaboration with A. Hertsch, the work on the classification of the orbit types of the action of the group of local gauge transformations on the space of connections for arbitrary compact gauge group was developed [7].

- [1] J. Huebschmann, G. Rudolph, M. Schmidt, *Commun. Math. Phys.* **286**, Nr. 2 (2009) 459–494
- [2] F. Fürstenberg: Charakterisierung der Strata eines SU(2)-Gitterreichmodells durch geometrische Invariantentheorie, Master thesis, University of Leipzig, 2011
- [3] M. Hofmann: On the costratified Hilbert space structure of a lattice gauge model with semisimple gauge group, Master thesis, University of Leipzig, 2011
- [4] E. Fuchs: Durch Hamiltonsche Flüsse induzierte Polarisierungen auf Kotangentialbündeln analytischer Mannigfaltigkeiten, Master thesis, University of Leipzig, 2011
- [5] J. Kijowski, G. Rudolph, C. Śliwa, *Annales H. Poincaré* **4** (2003) 1137
J. Kijowski, G. Rudolph, *J. Math. Phys.* **46** (2005) 032303; *Rep. Math. Phys.* **55** (2005) 199
- P. Jarvis, J. Kijowski, G. Rudolph, *J. Phys. A* **38** (2005) 5359

- [6] J. Phys. A **44** (2011) 235205
 [7] Ann. H. Poincaré **12**, nr. 2 (2011) 351

12.4 Quantum field theory on non-commutative geometries, quantum field theory and cosmology, generally covariant quantum field theory

R. Verch, M. Borris, T. Ludwig, M. Gransee F. Lindner, A. Knospe, B. Eltzner, J. Zschoche

One of the questions of recent interest is if there is a general framework for quantum field theory on non-commutative spacetimes. This question is analysed in collaboration with M. Borris. On one hand, an approach to Lorentzian non-commutative geometry in the spirit of spectral geometry is being established. On the other hand, the quantization of such structures is shown to lead to simple examples of quantum field theories on non-commutative spacetimes for concrete non-commutative spacetime models. The research on these topics is in progress. The relation between the Euclidean and Lorentzian approach to non-commutative quantum field theory is investigated with T. Ludwig, in collaboration with H. Grosse and G. Lechner.

In collaboration with C.J. Fewster it is investigated how to specify that quantum field theories are the same on all spacetimes, which is an extension of the framework of generally covariant quantum field theory.

The definition and analysis of states which can be viewed as local thermal equilibrium states in quantum field theory will be extended to quantum fields in curved spacetime, with a view on application in cosmological situations. Current research work with J. Schlemmer analyzes the question of existence of thermal equilibrium states. Further work with F. Lindner investigates the stability of local thermal equilibrium with respect to variations of the spacetime metric. Solutions to the semiclassical Friedman equations in local thermal equilibrium states are studied with M. Gransee and A. Knospe, the results indicate that quantum corrections lead to an increase in temperature in scenarios of early cosmology compared to the classical results. The role of the renormalization ambiguity in cosmic temperature evolution is investigated in collaboration with K. Fredenhagen and T.-P. Hack.

12.5 Funding

Spectral Zeta Functions and Heat Kernel Technique in Quantum Field Theory with Nonstandard Boundary Condition

Priv.-Doz. Dr. M. Bordag

Heisenberg-Landau programme

New Trends and Applications of the Casimir Effect (CASIMIR)

Research Networking Program der ESF (European Research Foundation)

Priv.-Doz. Dr. M. Bordag, member of the Steering Committee

Non-commutative quantum field theory

M. Borris, T. Ludwig
IMPRS fellowship

Local thermodynamic equilibrium in cosmological spacetimes

B. Eltzner, M. Gransee, J. Zschoche
IMPRS fellowship

Quantum Theory of Lattice Gauge models

E. Fuchs
IMPRS fellowship

Workshop "Mathematics and Quantum Theory", ITP, University of Leipzig, April 13, 2010

RALeipzig, PbF2

27th LQP Workshop "Foundations and Constructive Aspects of QFT", ITP, University of Leipzig, Nov. 19-20, 2010

Ev. Studienwerk Villigst, RALeipzig, PbF2

12.6 Organizational Duties

Priv.-Doz. Dr. Michael Bordag

- Referee: J. Phys. A, Phys. Rev. D, J. Math. Phys.
- Chair of the International Organizing Committee
Conference on Quantum Field Theory under the Influence of External Conditions (QFEXT11), Benasque (Spain), 18-24.9.2011
Member of the Steering Committee of the ESF Research Networking Program *New Trends and Applications of the Casimir Effect (CASIMIR)*

Prof. Dr. G. Rudolph

- Referee: Class. Quant. Grav., J. Math. Phys., J. Geom. Phys., J. Phys. A, Rep. Math. Phys., Commun. Math. Phys.
- Referee for the German Research Council (DFG) and the Alexander von Humboldt Foundation

Dr. Matthias Schmidt

- Referee: J. Phys. A, Int. J. Mod. Phys. A, Class. Quant. Grav.

Prof. Dr. Rainer Verch

- Speaker, Profilbildender Forschungsbereich 2 (since Nov. 2010)
- Director of the Institute for Theoretical Physics, University of Leipzig
- Chairman of Examining Board, Physics and Meteorology
- Head of Quality Assurance Committee, Faculty of Physics and Earth Sciences
- Associate Editor, Journal of General Relativity and Gravitation
- Book Series Editor, Fundamental Theories of Physics (Springer)
- IMPRS Board Member
- Referee for the Alexander von Humboldt Foundation

- Referee for Studienstiftung des Deutschen Volkes
- Referee: Commun. Math. Phys., J. Math. Phys., JHEP, Rev. Math. Phys., Class. Quantum Grav., Gen. Rel. Grav.

12.7 External Cooperations

Academic

- II. Inst. f. Theoretische Physik, Universität Hamburg
Prof. Dr. K. Fredenhagen
- Mathematisches Institut, Universität Göttingen
Prof. Dr. D. Bahns
- Mathematisches Institut, Universität Münster
Prof. Dr. R. Wolkenhaar
- Institut für Mathematik, Universität Paderborn
Dr. Ch. Fleischhack
- Department of Mathematics, University of York, England
Dr. C.J. Fewster
- School of Mathematics, Cardiff University, Wales
Prof. Dr. S. Hollands
- Dipartimento di Science, Università di Trento, Italy
Prof. Dr. V. Moretti
- Dipartimento di Matematica, Università di Genova, Italy
Prof. Dr. N. Pinamonti
- Université des Sciences et Technologies de Lille
Prof. Dr. J. Huebschmann
- Polish Academy of Sciences, Center for Theoretical Physics, Warsaw
Prof. Dr. J. Kijowski
Dr. Sz. Charzynski
- National University, Dnepropetrovsk
Prof. V. Skalozub
- St. Petersburg University
Prof. Yu.V. Novozhilov
- VIK Dubna
Dr. V. Nesterenko, Dr. I. Pirozhenko
- University of Tasmania, Hobart
Prof. Dr. P. Jarvis
- University of New South Wales, Sydney
Prof. H. Grundling

12.8 Publications

Journals

A. Hertsch, G. Rudolph, M. Schmidt
Gauge orbit types for theories with gauge group $O(n)$, $SO(n)$ or $Sp(n)$
Ann. H. Poincaré **12**, nr. 2 (2011) 351

P.D. Jarvis, G. Rudolph, L.A. Yates
A class of quadratic deformations of Lie superalgebras
J. Phys. A **44** (2011) 235205

Master

- Florian Fürstenberg
Charakterisierung der Strata eines $SU(2)$ -Gittereichmodells durch geometrische Invariantentheorie
January 3, 2011
- Martin Hofmann
On the costratified Hilbert space structure of a lattice gauge model with semisimple gauge group
January 3, 2011
- Erik Fuchs
Durch Hamiltonsche Flüsse induzierte Polarisierungen auf Kotangentialbündeln analytischer Mannigfaltigkeiten
January 3, 2011

Bachelor

- Benjamin Knorr
Geometric Fundamentals of Loop Quantum Gravity
July 08, 2011
- Johannes Zähle
Das Noether-Theorem in der Theorie Hamiltonscher Systeme
November 18, 2011

12.9 Guests

- N. Khusnutdinov
University of Kazan
June 14–25, 2011
- Prof. Dr. Jerzy Kijowski
September 01–30, 2011
- G. Klimchitskaya
North-West Polytechnical University, St. Petersburg
October 01–December 29, 2011

- V.M. Mostepanenko
Noncommercial Partnership “Scientific Instruments” of the Ministry of Industry,
Sciences and Technologies, Moscow
October 01–December 29, 2011
- V. Skalozub
National University, Dnepropetrovsk
December 01–December 13, 2011

13

Statistical Physics

13.1 Introduction

The focus of research in the SPT group is on low-dimensional and mesoscopic interacting systems. These systems are fascinating because on the one hand they allow to study fundamental questions of quantum statistical mechanics, and on the other hand they have a great potential for technological applications. The interplay of a reduced dimensionality with enhanced interaction effects, non-equilibrium physics, and possibly disorder allows the observation of many interesting phenomena, which pose a stimulating challenge for theoretical analysis. The mathematical language used for the description of these systems is quantum field theory, including techniques like functional integrals, renormalization group, instanton calculus, the Keldysh technique for non-equilibrium situations, and the replica method for disordered systems. These analytical tools are supplemented by the use of computer algebra (Mathematica) and numerical calculations (Matlab, Perl, C++). We try to combine the analysis of theoretically interesting problems with relevance to experiments on nanostructures.

Fractional quantum Hall (QH) systems display perhaps the richest and most beautiful physics of all condensed matter systems. They are a prime example for the idea that the whole is more than the sum of its parts, as low lying excitations of a fractional QH fluid carry only a fraction of the electron charge and are thus qualitatively different from the system constituents. Recently, interest in fractional QH physics has been reinvigorated by the prospect that quasiparticles (QPs) of the fractional QH state at filling fraction $5/2$ may be non-abelian anyons, i.e. their braiding may not only gives rise to a multiplication of the wave function with a complex phase, but in addition corresponds to a unitary transformation of the highly degenerate ground state. Due to the topological nature of braiding, these unitary transformations are robust against local perturbations and guarantee a high degree of stability of the quantum weave of braids, lending it to the construction of topological quantum bits. Future research in this field will concentrate on both the analysis of qualitative properties of topologically ordered systems and the description of experimentally relevant consequences in nanostructured systems.

Similarly to the edge states of QH systems, in single channel nanowires interactions strongly modify the dynamics of electrons. In the presence of strong spin-orbit coupling and in proximity to a superconductor, nanowires can support a topologically ordered state suitable for the formation of topological quantum bits. In multimode nanowires,

a quantum phase transition between superconductor and diffusive metal can occur, which is tuned by an external magnetic field and is experimentally realized in niobium and molybdenum-germanium systems. Comparatively small changes in the external magnetic field can give rise to a large change in conductivity. Quantum mechanical fluctuations of the superconducting phase can restore part of the the density of states, which is reduced due to scattering of electrons off the superconducting order parameter.

B. Rosenow

13.2 Topological superconductivity in the doped Kitaev-Heisenberg model

T. Hyart, A.R. Wright, G. Khaliullin, B. Rosenow

The concept of topological order, originally introduced in the context of quantum Hall systems, has recently been extended to topological band insulators and topological superconductors [2]. One of the exciting properties of these systems is the prospect of observing non-abelian quasiparticles. A prototype model for non-abelian quasiparticles is the Kitaev honeycomb model with a topological spin liquid phase [2].

It has been theoretically proposed that the Kitaev model with an admixture of antiferromagnetic Heisenberg exchange

$$H = -J_K \sum_{\langle ij \rangle} S_i^\gamma S_j^\gamma + J_H \sum_{\langle ij \rangle} \vec{S}_i \cdot \vec{S}_j. \quad (13.1)$$

can be realized in honeycomb iridates Li_2IrO_3 and Na_2IrO_3 [3]. The first term in the Hamiltonian (13.1) is called the Kitaev interaction, and it describes an Ising-like coupling between the γ components of spins $S_i^\gamma = \frac{1}{2} f_{i,\alpha}^\dagger \sigma_{\alpha\beta}^\gamma f_{i,\beta}$ at each bond in the γ -direction. The second term describes an isotropic Heisenberg interaction with interaction strength J_H . The recent experiments indicate that in the honeycomb iridates the Kitaev interaction strength J_K is not strong enough to induce the topological spin liquid phase, and therefore these materials are Mott insulators with magnetically ordered ground states at the half-filling [4].

Fortunately, there might be another way to obtain interesting topological properties in these materials. It is known that a Mott insulator with an antiferromagnetic ground state can become a high- T_c superconductor upon doping. Hence one may expect superconductivity in the doped Kitaev-Heisenberg model, and can ask how the superconducting order parameter depends on the relative strengths of antiferromagnetic Heisenberg exchange and the Kitaev interaction. We have addressed these questions in our recent paper [5] by solving the phase-diagram for the doped Kitaev-Heisenberg model. Our results are summarized in Fig. 13.1. The Heisenberg interaction supports a time-reversal violating d-wave singlet superconductivity. On the other hand, the Kitaev interaction favors a time-reversal invariant p-wave superconductivity, similar to the B phase in superfluid ^3He . By calculating the topological Z_2 invariant, we find topologically nontrivial superconductivity when the doping level is larger than one quarter, whereas trivial superconductivity appears at the smaller doping. The topological phase

transition appears due to a change of the topology of the Fermi surface from hole pockets around the two inequivalent K points to a particle like Fermi surface around the Γ point. In the topologically nontrivial phase, we find a pair of counter-propagating helical Majorana modes at the edges of the sample and one pair of Majorana zero modes at the vortices. Importantly, we find also that the p-wave superconducting phase is considerably more robust to adding a Heisenberg exchange than the spin liquid phase itself at zero doping, and the p-wave superconductivity is not sensitive to the details of the band structure. Thus, we think that it maybe possible to observe this type of topological superconductivity in the doped iridates, and the physics discussed in our paper might be representative for a class of materials with strong spin-orbit coupling.

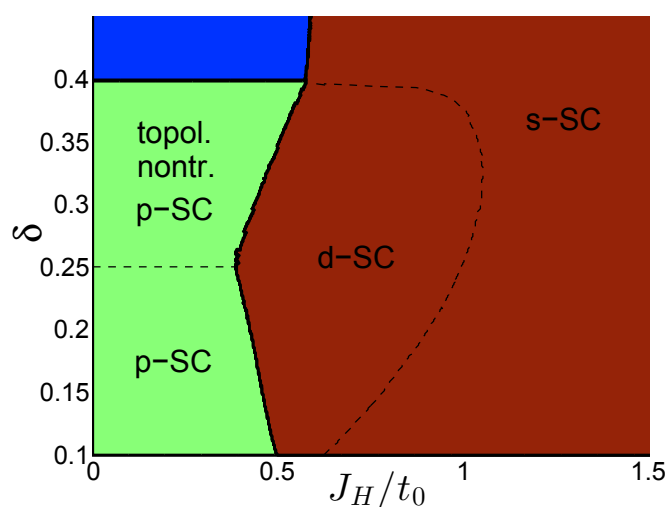


Figure 13.1: (a) Phase diagram for the doped Kitaev-Heisenberg model.

- [2] M.Z. Hasan and C.L. Kane, *Rev. Mod. Phys.* **82**, 3045 (2010); X.-L. Qi and S.-C. Zhang, *Rev. Mod. Phys.* **83**, 1057 (2011).
- [2] A. Kitaev, *Ann. Phys.* **321**, 2 (2006).
- [3] J. Chaloupka, G. Jackeli, and G. Khaliullin, *Phys. Rev. Lett.* **105**, 027204 (2010).
- [4] Y. Singh, S. Manni, J. Reuther, T. Berlijn, R. Thomale, W. Ku, S. Trebst, and P. Gegenwart, *Phys. Rev. Lett.* **108**, 127203 (2012).
- [5] T. Hyart, A. R. Wright, G. Khaliullin, B. Rosenow, accepted for publication in *Physical Review B Rapid Communications*; Eprint: arXiv:1109.6681v2.

13.3 Robust one-dimensional wires in lattice mismatched bilayer graphene

A.R. Wright, T. Hyart

Two of the most prominent topological phases of matter in condensed matter physics occur in the quantum Hall systems [1] and in topological insulators [2]. The former

does not require any symmetries while the latter relies on the retention of time reversal symmetry. The topological insulator state was first predicted in graphene [3], but later it was found that the spin-orbit coupling is too weak that this effect could actually be observed in this material. On the other hand, marginal topological properties can still emerge at the domain walls and edges of gapped graphene and bilayer graphene. Although, in principle these states are not protected against coupling of the two valleys of the graphene, in practice they have been found to be very robust against the disorder [4].

In our recent paper [5], we have shown that this type of domain walls in lattice mismatched bilayer graphene can realize robust one-dimensional wires. By considering a single domain wall, where the masses of the Dirac electrons change their sign, we established a general projection principle, which determines how the existence of topological zero-energy domain wall states depends on the direction of the domain wall and locations of the massive Dirac cones inside the bulk Brillouin zone. Moreover, we generalized this idea for arbitrary patterns of domain walls, and found that the topologically protected states exist only in the presence of an odd number of topological domain walls.

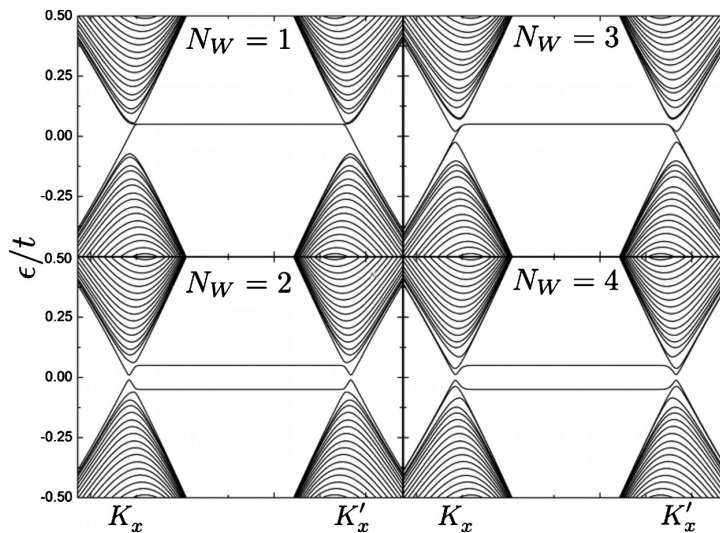


Figure 13.2: Explicit band structure calculation demonstrating the even-odd effect in a typical zigzag graphene nanoribbon with different number of domain walls N_W . The system is gapless only if N_W is odd.

- [1] D. J. Thouless, M. Kohmoto, M. P. Nightingale, and M. den Nijs, *Phys. Rev. Lett.* **49**, 405 (1982).
- [2] M.Z. Hasan and C.L. Kane, *Rev. Mod. Phys.* **82**, 3045 (2010); X.-L. Qi and S.-C. Zhang, *Rev. Mod. Phys.* **83**, 1057 (2011).
- [3] C. L. Kane and E. J. Mele, *Phys. Rev. Lett.* **95**, 226801 (2005).
- [4] J. Li, I. Martin, M. Buettiker, and A. F. Morpugo, *Nat. Phys.* **7**, 38 (2011).
- [5] A. R. Wright and T. Hyart, *Appl. Phys. Lett.* **98**, 251902 (2011).

13.4 Gapless Excitations in Strongly Fluctuating Superconducting Wires

D. Meidan*, B. Rosenow, Y. Oreg† G. Refael‡

*Dahlem Center for Complex Quantum Systems and Institut f'ur Theoretische Physik, Freie Universit'at Berlin, 14195 Berlin, Germany

†Department of Condensed Matter Physics, Weizmann Institute of Science, Rehovot, 76100, Israel

‡Department of Physics, California Institute of Technology, Pasadena, California 91125, USA

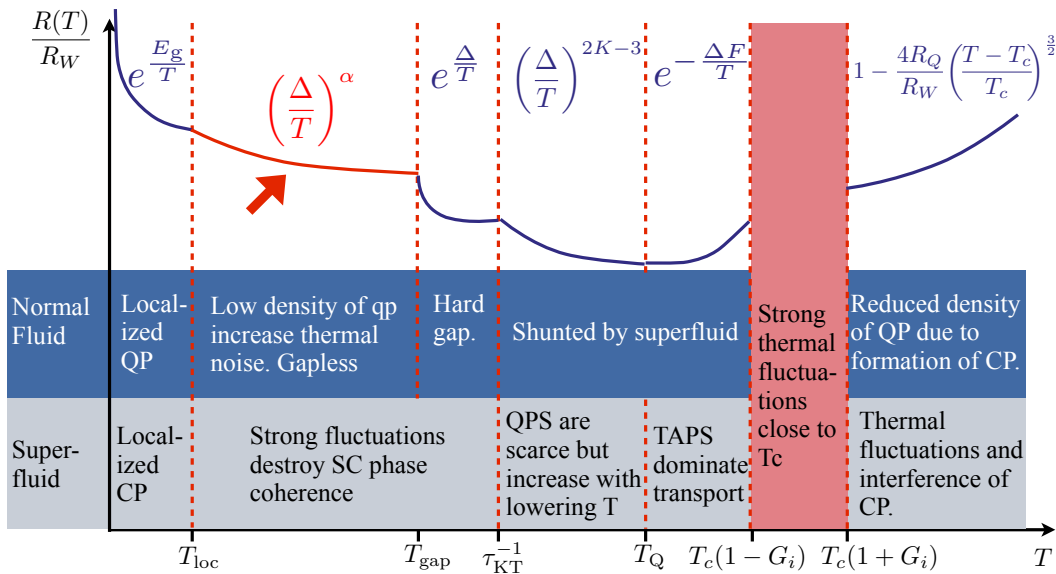


Figure 13.3: A qualitative phase diagram of a fluctuating wire, whose normal resistance is R_W , as a function of temperature. Here T_c is the mean field transition temperature and T_Q is the temperature at which quantum phase slips (QPS) dominate the response of the system. At τ_{KT}^{-1} QPS proliferate, blocking the conductance of the superfluid channel. Gapless excitations appear at $T < T_{gap}$, where the resistance scales as a power law of the temperature, marked by an arrow. At T_{loc} QP and CP are localized, and conductance is controlled by their thermally activated hopping with a typical gap E_g . For large R_ξ the gap regime disappears. Here K is the Luttinger parameter, and G_i is the Ginzburg Levanyuk number. The figure is not true to scale.

Phase fluctuations of superconductors are responsible for a broad range of fascinating phenomena. Their effect is particularly dramatic in narrow wires, where the proliferation of phase slips induces a putative superconductor-insulator transition. Experiments probing this transition, however, challenge our understanding of the insulating phase, as they exhibit a low-temperature metallic behavior in thin wires where phase-slips proliferate. Ref. [1] discussed the phase-slip induced breakdown of superconductivity in a wire, speculating that a metallic phase arises. Could the strong phase fluctuations induce a finite quasi-particle (QP) density of states that maintains a finite conductivity?

In [2], we study the low-temperature tunneling density-of-states (tDOS) of the phase-slip proliferated regime. We argue that the scarcity of normal excitations and

the blocking of the Cooper pair conduction channel give rise to strong dephasing, through electromagnetic field fluctuations. This, in turn, should lead to pair breaking. From a self-consistent study of the tDOS, we find that at a broad temperature regime (roughly $T < 0.1T_c$), no hard spectral gap exists. Furthermore, because the conductivity is dominated by quasi-particles, it vanishes at most linearly in temperature, as opposed to an exponentially-suppressed conductivity characteristic of a gapped phase. Eventually, at very low temperatures, the QP are localized and the metallic phase ceases to be valid. These effects should be manifest in tunneling measurements of wires with an increasing resistance upon cooling.

Our argument follows from the dependence of dephasing on the dissipative response of diffusive electron systems. For this purpose, it is insightful to interpret the response of the wires we consider in terms of coexisting normal quasi-particles and condensed Cooper pairs. In the phase-slip proliferated regime, where the normal resistance of a coherence-length segment obeys $R_\xi \gtrsim R_Q = h/4e^2 \approx 6.4k\Omega$, the conductivity is dominated by the normal QPs, as long as they remain diffusive. Similarly to normal diffusive systems, electron-electron interactions lead to the suppression of quantum interference of these diffusive QP after a typical dephasing time τ_ϕ . Using the fluctuation-dissipation theorem the dephasing is dictated by the electrical response of the system, $\sigma(T)$ [3]:

$$\tau_\phi(T) = \left(\frac{\sigma(T)A}{e^2T\sqrt{2D}} \right)^{2/3} = \tau_\phi^N \left(\frac{\sigma(T)}{\sigma_N} \right)^{2/3}, \quad (13.2)$$

where σ_N is the conductivity in the normal state, A is the cross-section area of the wire, and D is the diffusion constant. When the Cooper-pairs are formed but not condensed due to quantum phase slips proliferation, QP are expected to be scarce, and therefore $\sigma(T) < \sigma_N$. This increases voltage fluctuations and the dephasing rate.

- [1] A. D. Zaikin, D. S. Golubev, A. van Otterlo, and G. T. Zimanyi, Phys. Rev. Lett. **78**, 1552 (1997).
- [2] D. Meidan, B. Rosenow, Y. Oreg and G. Refael, Phys. Rev. Lett. **107**, 227004 (2011).
- [3] B. L. Altshuler, A. G. Aronov, and D. E. Khmelnsky, J. Phys. C **15**, 7367 (1982).

13.5 Signatures of non-Abelian statistics in non-linear coulomb blockaded transport

R. Ilan*, B. Rosenow, A. Stern*

*Department of Condensed Matter Physics, Weizmann Institute of Science, Rehovot 76100, Israel

Anyons obeying Non-Abelian statistics were predicted to exist in quantum Hall (QH) systems almost twenty years ago [1, 2]. This prediction has raised an extensive interest, both due to the unique properties of non-Abelian states of matter and due to their possible uses for topological quantum computation. Although many efforts have been made to suggest and perform experiments to test that hypothesis[3], there is still no clear-cut proof for it. This work proposes an experimental setup along with

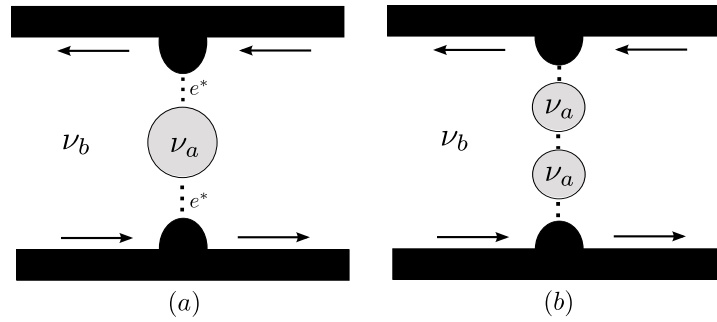


Figure 13.4: Antidots in a Hall bar geometry. The bulk filling fraction ν_b determines the tunneling excitation, and the antidot's filling fraction is ν_a . (a) A single antidot. (b) Double antidot geometry, discussed towards the end of the paper.

a set of measurements designed to unravel signatures of such statistics in the putative non-Abelian QH state at $\nu = 5/2$. In particular, we show that the current-voltage characteristics of a Coulomb blockaded system in the non-linear regime may detect the neutral Majorana edge mode which is an essential property of the proposed non-Abelian state. Moreover, it allows us to study the spectrum of this mode, and explore the effect of the presence of quasiparticles (QPs) on that spectrum.

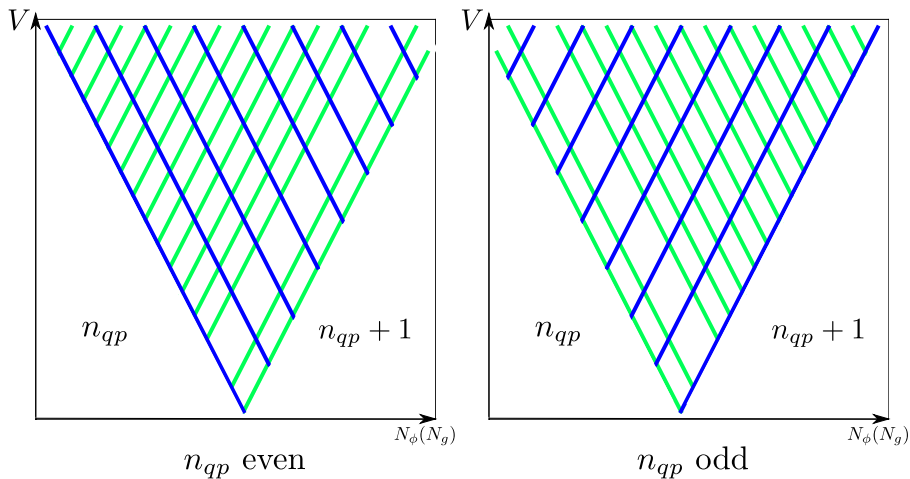


Figure 13.5: Coulomb blockade diamond shapes in dI/dV for a transition between n_{qp} and $n_{qp} + 1$ quasi-particles on the dot. White region represent a stable state of a dot with n_{qp} or $n_{qp} + 1$ quasiparticles (Coulomb blockaded regions). Green lines are separated by half the distance separating blue lines.

Here [4] we analyze dI/dV in a CB measurement as a function of source-drain voltage and magnetic field. In contrast with linear CB, current-voltage characteristics in the non-linear regime of the CB hold information of the many particle excitation spectrum of the system. A peak in the differential conductance dI/dV will appear whenever a proper resonance condition between the source-drain voltage and the excitations of the dot is met. We show that the "diamond structure" that characterizes the CB out of the linear response regime could serve to identify the nature of the $\nu = 5/2$ state. We consider a Hall bar or a Corbino disk in which a quantum anti-dot, a puddle of filling fraction ν_a , is embedded in a bulk of filling factor ν_b (see Fig. 13.4). The puddle is surrounded by a gapless region. Since this region is compact, its spectrum is quantized. Transport

from one edge of the sample to the other is facilitated by tunneling of charge carriers (whose precise nature is discussed below) through the anti-dot, and is characterized by resonances corresponding to the internal states of the gapless region around the antidot. The edges are connected to reservoirs and their spectrum is continuous. We assume that the anti-dot is weakly and symmetrically coupled to the nearby edges, and that tunneling through the anti-dot can be treated in the sequential tunneling approximation.

- [1] G. Moore, N. Read, Nucl. Phys. B **360**, 362 (1991).
- [2] C. Nayak, F. Wilczek, Nucl. Phys. B, **479**, 529 (1996).
- [3] C. Nayak, S.H. Simon, A. Stern, M. Reedman, S. Das Sarma, Rev. Mod. Phys., **80**, 1083 (2008).
- [4] R. Ilan, B. Rosenow, A. Stern, Phys. Rev. Lett. **106**, 136801 (2011).

13.6 Neutral mode heat transport and fractional quantum Hall shot noise

S. Takei*, B. Rosenow

*Condensed Matter Theory Center, Department of Physics, The University of Maryland
College Park, MD 20742

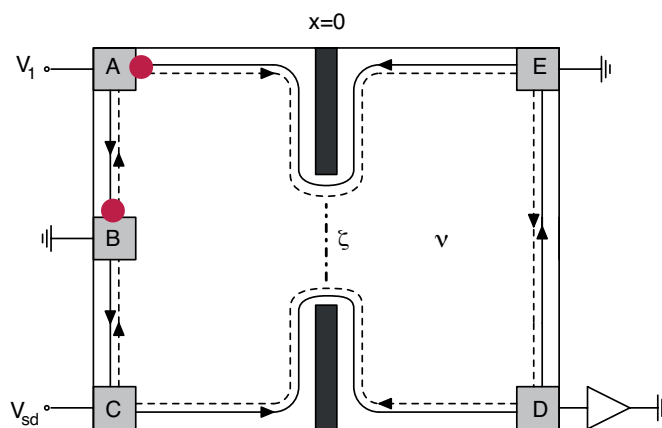


Figure 13.6: Schematic diagram of the considered setup. The magnetic field is oriented so that charge transport along the edge (solid black lines) occurs with the counterclockwise chirality. There is one or several neutral modes (dashed lines) propagating clockwise, and the dash-dotted line denotes backscattering at the constriction. Hot spots caused by a finite V_1 are indicated by red dots.

Many of the peculiar properties of quantum Hall (QH) systems can be attributed to the existence of quasi-one-dimensional electronic states along the perimeter of the sample, the so-called edge states. In the integer quantum Hall regime edge states can be modeled by non-interacting electrons, while in the fractional QH regime interactions play an essential role, and edge states must be described as Luttinger liquids, in some cases with excitations propagating both with and against the orientation imposed by

the magnetic field. For instance, in the case of filling fraction $\nu = 2/3$ two counter-propagating edge modes are predicted, which would give rise to non-universal Hall and two-terminal conductances. Experimentally, however, conductances are quantized and a counter-propagating charge mode was not observed. This problem is resolved by taking into account that in the presence of random edge scattering the $\nu = 2/3$ edge undergoes reconstruction into a disorder-dominated phase with a single downstream-propagating charge mode and a single upstream-propagating neutral mode [1].

Interest in neutral quantum Hall edge modes was revived because one or several neutral Majorana edge modes are expected to encode the non-abelian statistics of the QH state at filling fraction $\nu = 5/2$. Neutral quantum Hall modes are notoriously difficult to observe as they do not participate in charge transport. Recently, experimental evidence for neutral modes was presented by demonstrating that injection of a DC current can influence the low frequency noise generated at a quantum point contact (QPC) located *upstream* of the contact where the current is injected [2]. Partitioning of a DC current by a QPC and the influence of downstream heat transport on a second QPC was studied both experimentally and theoretically.

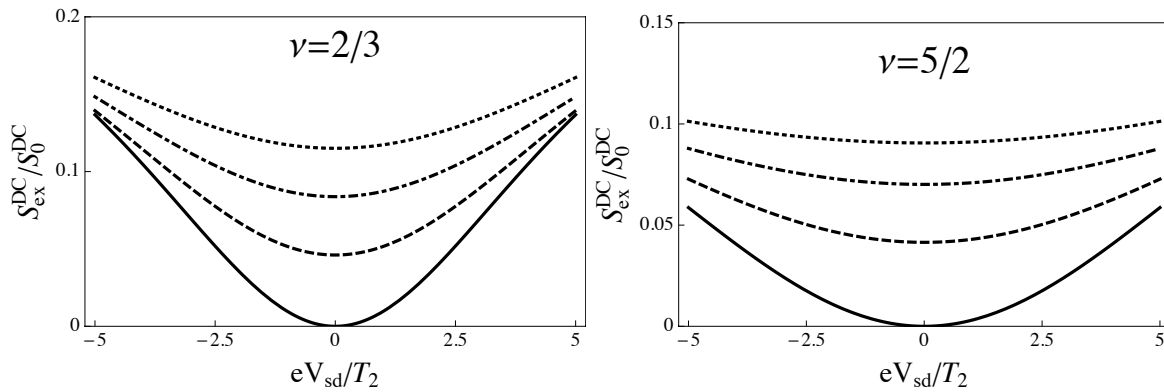


Figure 13.7: Excess noise for the random $\nu = 2/3$ edge (upper panel) and the random $\nu = 5/2$ anti-Pfaffian edge (lower panel) as a function of the source-drain voltage. We consider top edge temperatures $T_1 = T_2$ (Solid); $T_1 = 1.5T_2$ (Dashed); $T_1 = 2T_2$ (Dot-dashed); and $T_1 = 2.5T_2$ (Dotted) locally at the tunneling site. The noise is in units of $ge^2 T_2 / 2\pi$, where g is the scaling dimension of the local edge creation operator of QPs (see text). Tunneling amplitudes have been chosen so that the QPC has a transmission of 0.9 at $T_1 = T_2$. For $\nu = 2/3$, we have taken $\zeta_1^2 = \zeta_2^2 = \zeta_3^2$.

In [3], we theoretically analyze a setup akin to that of Ref. [2] and find that a current injected into a quantum Hall mode downstream of a QPC indeed enhances the charge noise due to scattering at the QPC. We consider the limit of a strong inelastic coupling between charge and neutral edge modes, such that the longitudinal conductance is quantized [1] on scales much shorter than the distance between contact A and the QPC. Then, the injected current causes a hot spot in contact A , and in the presence of one or several neutral modes propagating in the direction opposite to that imposed by the magnetic field for charge pulses, heat is conducted from contact A to the QPC and gives rise to excess noise in the current scattered across the QPC. When the model is generalized to the non-abelian $\nu = 5/2$ quantum Hall state the enhancement of the charge noise, also observed in this state [2], limits the possible descriptions of the state to those that support counter-propagating neutral modes, namely, the anti-Pfaffian and

an edge-reconstructed Pfaffian state.

- [1] C.L. Kane, M.P.A. Fisher and J. Polchinski, Phys. Rev. Lett. **72**, 4129 (1994).
- [2] A. Bid, N. Ofek, H. Inoue, M. Heiblum, C.L. Kane, V. Umansky, and D. Mahalu, Nature **466**, 585 (2010)).
- [3] S. Takei and B. Rosenow Phys. Rev. B **84**, 235316 (2011)

13.7 Theory of the Fabry-Perot quantum Hall interferometer

B.I. Halperin^{*}, A. Stern[†], I. Neder, B. Rosenow

^{*}Physics Department, Harvard University, Cambridge MA 02138, USA

[†]Department of Condensed Matter Physics, Weizmann Institute of Science, Rehovot 76100, Israel

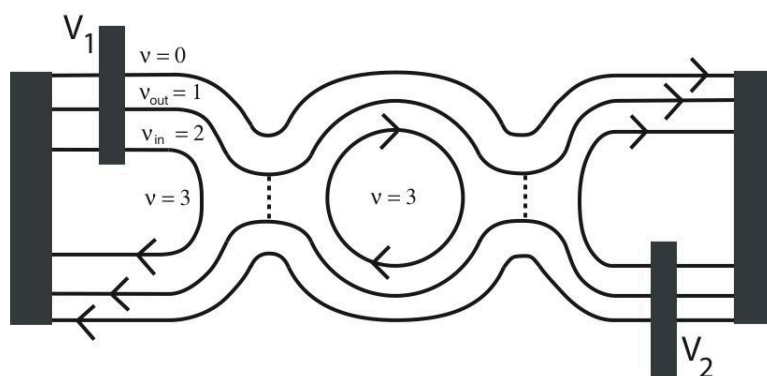


Figure 13.8: Fabry-Perot interferometer in integer QHE regime, with $f_T = 1$ totally transmitted edge mode. The partially transmitted edge mode separates quantized Hall regions with nominal filling $\nu_{\text{out}} = 1$ and $\nu_{\text{in}} = 2$. A third edge mode is totally reflected before entering the constrictions, because the electron density in the constriction is smaller than in center of the interferometer. Dotted lines in each constriction show the locations of scattering between the two edges, indicated here as weak backscattering.

In the last few years there has been a surge of interest in electronic interference phenomena in the regime of the quantum Hall effect. This interest, both theoretical and experimental, results in large part from the hope of utilizing interference to probe unconventional statistics in various fractional quantum Hall states. Interestingly, interferometer experiments have led to puzzling results even in the integer regime, which have posed a challenge to our theoretical understanding. Arguably the simplest realization of a quantum Hall interferometer is an analog to the optical Fabry-Perot device. It is constructed of a Hall bar perturbed by two constrictions, each of which introduces an amplitude for inter-edge scattering. The backscattering probability of a wave packet that goes through the constrictions is then determined by an interference of trajectories. In the limit of weak inter-edge scattering, two trajectories interfere, corresponding to

scattering across each of the two constrictions. As the scattering amplitudes get larger, multiple reflections play a more significant role.

Typically, experiments measure the “diagonal resistance” R_D [1], which is essentially the two-terminal Hall resistance of the interferometer region. We find that R_D has an oscillatory part δR , which is a periodic function of B and δV_G . In the limit of weak backscattering it may be written as

$$\delta R = \text{Re} \left(\sum_{m=-\infty}^{\infty} R_m e^{2\pi i(m\phi + \alpha_m \delta V_G)} \right), \quad \text{where } \phi \equiv B\bar{A}/\Phi_0, \quad (13.3)$$

and the coefficients R_m , α_m are real and only slowly varying functions of B , V_G . The voltage V_G affects the phases $e^{2\pi i(m\phi + \alpha_m \delta V_G)}$ in (13.3) in two ways. First, it affects the flux ϕ through its effect on the area \bar{A} . Second, it affects the density in the bulk of the interferometer, indirectly affecting the interference through interactions of the edge with the bulk. The coefficients α_m quantify the latter effect.

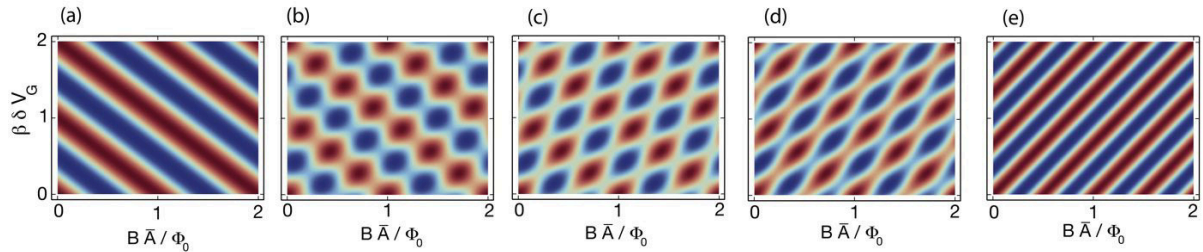


Figure 13.9: $\langle \delta R \rangle = \text{Re} \left(R_1 e^{2\pi i \phi} + R_{-f_T} e^{-2\pi i f_T \phi} \right)$ as a color map in the plane of B and V_G , for $f_T = 2$, with the parameter γ chosen equal to 3.5β . Panels (a), (b), (c), (d), and (e), have, respectively $|R_{-2}/R_1| = 0, 0.5, 1, 2, \text{ and } \infty$, corresponding to the AB, mixed and CD regimes. All Fourier components other than $m = 1$ and $m = -f_T$ are neglected. Alternating red and blue regions represent positive and negative values, respectively, while white signifies a value close to zero.

Electron-electron interactions lead to two important differences between the quantum Hall interferometer and a naive Aharonov-Bohm interference experiment. First, as mentioned above, the area A_I of the interference loop is not rigidly constrained a priori, but can fluctuate slightly. Thus, the area of the interference loop varies with magnetic field and the flux within the loop is generally not a simple linear function of the magnetic field. The position of the edge is related to the charge it encloses, and its variation in our model is a consequence of considerations of energy. Second, we model the region enclosed by the interference loop as one in which there are localized states close to the chemical potential. The number N_L of electrons (in the IQHE regime) or quasi-particles (in the FQHE regime) that are localized in the bulk is an integer, and varies discretely. Due to considerations of energy, an abrupt change of occupation of a localized state as the magnetic field is varied affects also the position of the interfering edge, and hence induces an abrupt change in the flux enclosed by the interference loop. More detailed can be found in [2]

[1] C.W.J. Beenakker and H. van Houten in: H. Ehrenreich and D. Turnbull, Editors, *Solid State Physics* **44**, Academic Press, New York (1992), p. 1.

[2] B. I. Halperin, A. Stern, I. Neder, and B. Rosenow, Phys. Rev. B **83**, 155440 (2011).

13.8 Charge fractionalization on quantum Hall edges

M. Horsdal, M. Rypestøl*, H. Hansson†, J.M. Leinaas*

*University of Oslo

†Stockholm University

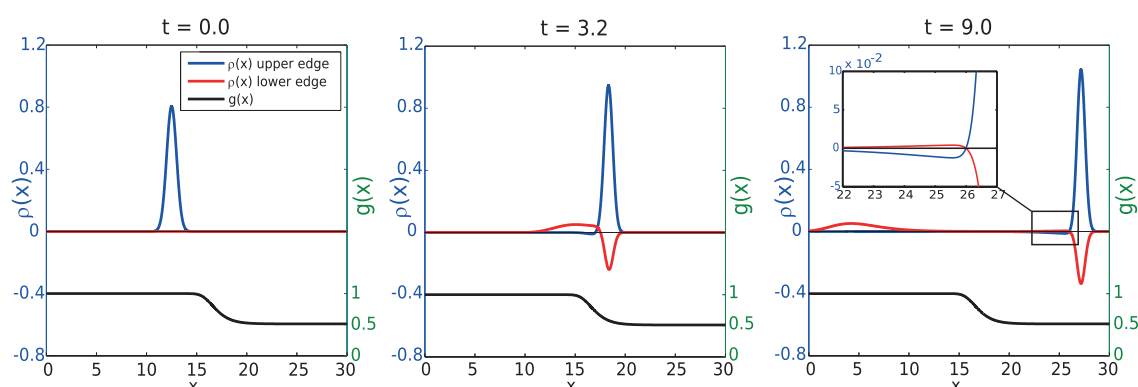


Figure 13.10: The time evolution of an initial pulse at three different timesteps. Notice how a contribution builds up on the lower edge as the pulse enters the interacting region, $g \neq 1$ (black line). In the last timestep we can clearly see that the front pulse has retained its shape, while the long tail depends on the details of the transition region.

Charge fractionalization, the appearance of quasiparticles, which carry a fraction of the charge unit, is a remarkable effect that is found in certain quantum many-body systems with unusual properties. Well-studied examples are the two dimensional electron fluids of the quantum Hall effect. More recently, it has been suggested that excitations with fractional charge may appear in one-dimensional systems described by Luttinger liquid theory [1, 2]. Here, the fractionalization is linked to chiral separation of charges that are introduced in the system, so that fractions of a unit charge move to the right and the left, respectively [3, 4].

The fractionalization can be seen as a polarization effect between the two chiralities [5]. Here we use that idea and study the propagation and fractionalization of localized charges on the edges of quantum Hall bars of variable widths, see Fig 13.10. The interaction between the edges will therefore give rise to a variable Luttinger parameter g . When the edge-edge separation varies smoothly the initial pulse will be separated into a sharply defined front pulse and a broader tail [6]. We particularly focus on the front pulse, which retain its shape through the transition and acquires the charge \sqrt{g} times the electric charge, while the shape of the tail is determined by the specific details of the transition region. The presence of the sharp front pulse can in principle be detected in measurements of the noise in the current created by electrons tunneling into the system.

- [1] M.P.A. Fisher and L.I. Glazman, in Mesoscopic Electron Transport, NATO Advanced Study Institute, Series E: Applied Sciences, edited by L. Kouwenhoven, G. Schoen, and L. Sohn (Kluwer, Dordrecht, 1997), Vol 345.
- [2] K.-V. Pham, M. Gabay, and P. Lederer, Phys. Rev. B **61**, 16 (2000).
- [3] I. Safi and H.J. Schulz, Phys. Rev. B **52**, R17040 (1995).
- [4] I. Safi, Ann. Phys. Fr. **22**, 463 (1997).
- [5] J.M. Leinaas, M. Horsdal, and T.H. Hansson, Phys. Rev. B **80**, 115327 (2009).
- [6] M. Horsdal, M. Rypestøl, T.H. Hansson and J.M. Leinaas, Phys. Rev. B **84**, 115313 (2011).

13.9 Photonic Josephson effect, phase transitions, and chaos in optomechanical systems

J. Larson*, M. Horsdal

*Stockholm University

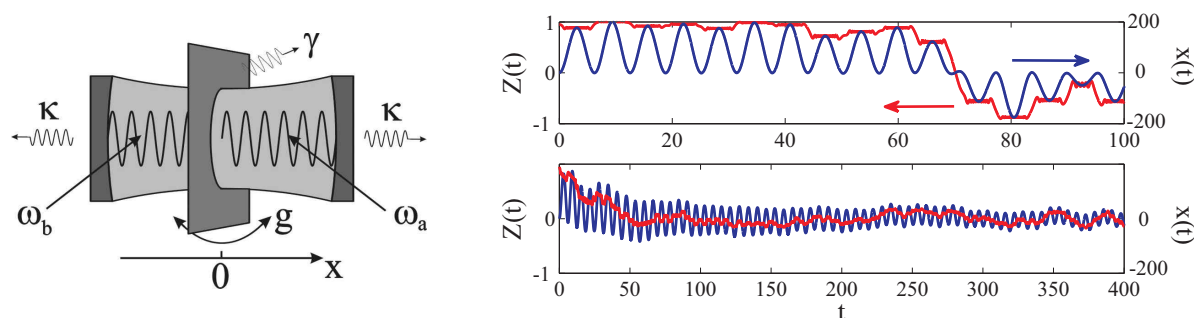


Figure 13.11: Left panel: The system consisting of a cavity divided in two by a semitransparent membrane. The coupling between the membrane and the photon pressure gives rise to chaotic effects. Right panel: Time evolution of the mean field photon inversion (red) and the membrane position (blue). In the upper plot the system is closed and there are no photon losses or damping of the membrane, while the lower plot shows a system with both photon and phonon losses at finite temperature.

The Josephson effect describes macroscopic tunneling made possible by inherent coherence of the underlying quantum many-body state. The resulting Josephson oscillations, first discussed for weakly coupled superconductors, have turned out to be relevant for a wide range of physical systems like Bose-Einstein condensates in double well traps, spinor condensates, liquid helium, graphene and Hall systems, and nonlinear optics. Lately, the possibility of observing the Josephson effect for photons in systems of coupled high-Q optical cavities has been discussed. Together with related schemes containing arrays of coupled cavities or single cavities filled with a Kerr medium, these proposals pave the way for genuine quantum many-body models to be studied by means of photons.

Here we study a photonic analog of the Josephson effect in a system formed by a partly transparent mechanical membrane dividing an optical cavity in two halves [1]. The photonic pressure exerts a force on the membrane which in turn shifts the resonance frequency of the cavity. The coupling of the photonic and mechanical degrees induces a nonlinearity, which results in a rich dynamical structure. For example, contrary to standard bosonic Josephson systems, we encounter chaos. By means of a mean-field approach, we identify the various regimes given by the loss of photons and the loss of vibrational quanta of the membrane. In the case of an isolated system (no losses) chaos manifests itself in sudden jumps of the photon inversion (the difference in photon numbers between the two cavity modes), see Fig 13.11. This chaos is also manifest at short timescales for a dissipative system, while for longer timescales the behaviour depends on the losses of the system. Fig 13.11 also shows an example where the chaos persist due to the final temperature of the system.

[1] J. Larson and M. Horsdal, Phys. Rev. A **84**, 021804(R) (2011).

13.10 Funding

Untersuchungen zum topologischen Quanten-Computing

B. Rosenow together with J. Smet (MPI FKF) and W. Dietsche (MPI FKF)
BMBF 01BM0900

13.11 Organizational Duties

B. Rosenow

- Member of the Studienkommission of the Faculty of Physics and Earth Science
- Referee for Science, Phys. Rev. Lett., Phys. Rev. B, Europhys. Lett., Adv. Cond. Matter, JSTAT, Physica A, NSF, Studienstiftung des Deutschen Volkes

13.12 External Cooperations

Academic

- MPI für Festkörperforschung Stuttgart
Prof. W. Dietsche, Dr. J. Smet, Prof. K. von Klitzing
- Harvard University
Prof. B.I. Halperin, Prof. C.M. Marcus, Prof. S. Sachdev
- Weizmann Institute for Science
Prof. Y. Gefen, Prof. A. Stern, Prof. Y. Oreg
- Oxford University
Prof. S. Simon
- California Institute of Technology
Prof. G. Refael

- Universität zu Köln
Prof. A. Altland
- Missouri University of Science and Technology
Prof. T. Vojta
- Universidade de Sao Paulo
Prof. J.A. Hoyos
- UBC Vancouver
Dr. A. Del Maestro
- The University of Maryland College Park
Dr. S. Takei
- FU Berlin
Dr. D. Meidan
- University of Oslo
Jon Magne Leinaas, Marianne Rypestøl
- Stockholm University
Hans Hansson, Jonas Larson

13.13 Publications

Journals

- D. Meidan, B. Rosenow, Y. Oreg and G. Refael, *Gapless excitations in strongly fluctuating superconducting wires*, Phys. Rev. Lett. **107**, 227004 (2011).
- A. R. Wright and T. Hyart, *Robust one-dimensional wires in lattice mismatched bilayer graphene*, App. Phys. Lett. **98**, 251902 (2011).
- M. Horsdal, M. Rypestøl, H. Hansson and J. M. Leinaas, *Charge fractionalization on quantum Hall edges*, Phys. Rev. B **84**, 115313 (2011).
- T. Hyart and B. Rosenow, *Quantitative description of Josephson-like tunneling in $\nu_T = 1$ quantum Hall bilayers*, Phys. Rev. B **83**, 155315 (2011).
- B.I. Halperin, A. Stern, I. Neder, and B. Rosenow, *Theory of the Fabry-Perot Quantum Hall Interferometer*, Phys. Rev. B **83**, 155440 (2011).
- J. Larson and M. Horsdal, *Photonic Josephson effect, phase transitions, and chaos in optomechanical systems*, Phys. Rev. A **84**, 021804(R) (2011).
- R. Ilan, B. Rosenow, and A. Stern, *Signatures of non-Abelian statistics in non-linear coulomb blockaded transport*, Phys. Rev. Lett. **106**, 136801 (2011).
- S. Takei and B. Rosenow, *Neutral mode heat transport and fractional quantum Hall shot noise*, Phys. Rev. B **84**, 235316 (2011).
- J. Nuebler, B. Friess, V. Umansky, B. Rosenow, M. Heiblum, K. v. Klitzing and J. Smet, *A Quantized $\nu = 5/2$ State in a Two-Subband Quantum Hall System*, Phys. Rev. Lett. **108**, 046804 (2012)

in press

T. Hyart, A.R. Wright, G. Khaliullin, and B. Rosenow, *Competition between d-wave and topological p-wave superconductivity in the doped Kitaev-Heisenberg model*, Phys. Rev. B (Rapid Communications), in press (2012).

A. Altland, Y. Gefen, and B. Rosenow, *Incoherent scatterer in a Luttinger liquid: a new paradigmatic limit*, Phys. Rev. Lett. (Editor's Suggestion, highlighted in *Physics*), in press (2012).

Talks

T. Hyart, *Josephson-like tunneling and Shapiro steps in quantum Hall exciton condensates*, Ringberg meeting of the von Klitzing department, 18.-21.9.2011.

T. Hyart, *Josephson-like tunneling and Shapiro steps in quantum Hall exciton condensates*, Wegscheider group of Advanced Semiconductor Quantum Materials, ETH Zurich, 9.11.2011.

B. Rosenow: *Mesoskopische Systeme, eine Einführung & topologisches Quantencomputing*, TheoWorkshop JDPG 2011 in Böhlen.

B. Rosenow: *Theory of the pairbreaking superconductor-metal transition in nanowires*, Theoretical Physics Seminar, Max-Planck Institute for Complex Systems Dresden, Februar 2011.

B. Rosenow: *Fabry-Perot interference and non-linear Coulomb blockaded transport in the quantum Hall regime*, Theoretical Physics Seminar, California Institute of Technology, Juni 2011.

B. Rosenow: *Majorana Fermions in Condensed Matter Physics*, Physics Colloquium, LMU München, November 2011.

B. Rosenow: *Observing the topological phase transition in Semiconductor-Superconductor Nanowires*, Workshop Quantum Information and Condensed Matter Physics, NUI Maynooth, September 2011.

T. Wright: *Some interesting things about Graphene*, TheoWorkshop JDPG 2011 in Böhlen.

T. Wright: *Graphene: Nobel Prize 2010*, Colloquium at University Queensland, February 2011.

T. Wright: *Theory of Topological Insulators*, Physics Seminar at University Queensland, February 2011.

T. Wright: *Topological Insulators : Do they really exist?*, Seminar at University of New South Wales, March 2011.

13.14 Guests

- Dr. Paul Eastham
Trinity College Dublin
March 15-17 and June 9-10
- Dr. Benoit Hackens
Université catholique de Louvain
April 27-29
- Dr. Andreas Schnyder
MPI FKF Stuttgart
June 22-24
- Prof. Klaus von Klitzing
MPI FKF Stuttgart
July 12-13
- Dr. So Takei
University of Maryland
September 18-25
- Prof. Yuval Gefen
Weizmann Institute of Science
October 6-9
- Dr. Dganit Meidan
FU Berlin
October 13
- Prof. Ady Stern
Weizmann Institute of Science
November 1-2
- Prof. Dirk Morr
University of Illinois at Chigago
November 7-11

14

Theory of Condensed Matter

14.1 Introduction

Major research topics in our group include nonequilibrium phenomena and pattern formation in systems of various nature, e.g. in soft condensed matter and in biological systems. Modern analytic methods of statistical physics and computer simulations complement and stimulate each other. Cooperations with mathematicians, theoretical and experimental physicists, biologists and medical researchers in Germany, Europe and around the world are well established. Specifically we are interested in the following problems.

Noise induced phenomena (Behn). Noise induced non-equilibrium phase transitions and non-equilibrium fluctuation theorems are studied in coupled arrays of stochastically driven nonlinear systems.

Mathematical modeling of the immune system (Behn). Using methods of nonlinear dynamics and statistical physics, we study the architecture and the random evolution of the idiotypic network of the B-cell subsystem. We describe the regulation of balance between T-cell subsystems, its relation to allergy and the hyposensitization therapy (cooperation with G. Metzner, Clinical Immunology) and the differentiation and plasticity of peripheral CD4⁺ cells.

Non-equilibrium dynamics in soft-condensed-matter systems (Kroy). The systems under investigation range from desert dunes spontaneously developing as a generic consequence of aeolian sand transport, through non-equilibrium gels of adhesive colloids and proteins, the viscoelastic mechanics of the cytoskeleton, to the non-equilibrium dynamics of single DNA molecules under strong external fields. (Related experimental work is currently in progress at EXP1: PWM, PAF.) A common feature is the presence of strong fluctuations and stochastic dynamics on the micro-scale. The emergence of macroscopic structure and (non-linear) deterministic macroscopic dynamics is to be understood. The applied methods range from analytical studies of stochastic integro-differential equations through liquid-state theories, mode-coupling theory, effective hydrodynamic equations, phenomenological modeling, to numerical simulations.

14.2 Stochastic Phenomena in Systems with Many Degrees of Freedom

U. Behn, M. Höll, N. Kühn, R. Kürsten

Arrays of coupled nonlinear dynamical systems subject to multiplicative or additive noise show close analogies to phase transitions in equilibrium [1]. Concepts such as ergodicity breaking, order parameter, critical behaviour, critical exponents etc. developed to describe equilibrium phase transitions can be transferred to noise induced nonequilibrium phase transitions. In the limit of strong coupling there is a clear separation of time scales: The fast degrees of freedom of the relative coordinates r_i are enslaved by the slow center of mass coordinate R which exhibits a critical behaviour.

For multiplicative noise, essential characteristics of phase transitions can be found already in finite arrays. In the limit of strong coupling, analytical results for probability distribution and expectation value of the center of mass coordinate agree with simulations [2].

For large, but finite coupling we developed self-consistent mean field theories to determine the probability distributions of both center of mass and relative coordinates, where the mean value $\langle R \rangle$ and the variance $\langle r_i^2 \rangle$ serve as order parameters. Applications include systems with additive [3] and multiplicative noise [4] where the inverse coupling strength and the inverse system size are considered as small parameters. New numerical methods to simulate Langevin equations with rarely visited regions of state space are developed and successfully applied [3], cf. Fig. 14.1.

For arrays of coupled Stratonovich models where the control parameter is changed according to different protocols we investigated, using both analytical and numerical methods, the validity of various nonequilibrium fluctuation theorems, including the detailed and integral fluctuation theorems and the work-free energy relation [5].

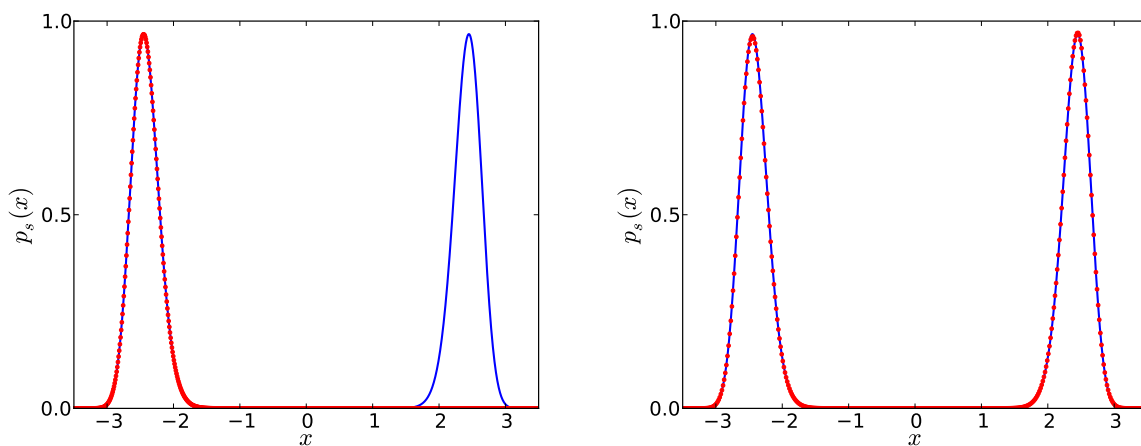


Figure 14.1: Stationary probability density of the simple test system $\dot{x} = ax - x^3 + \sigma \cdot \xi$ for $a = 6$, $\sigma = 1$, $\xi(t)$ is a Gaussian white noise. The analytical result (solid blue line) is compared with simulations (red symbols) using $8.4 \cdot 10^9$ time steps. **Left:** Conventional method. **Right:** Interval method [3]. With the same computational costs the interval method covers the whole state space.

- [1] F. Sagués, J. García-Ojalvo, J.M. Sancho, *Rev. Mod. Phys.* **79**, 829 (2007)
- [2] F. Senf et al.: *New J. Phys.* **11**, 063010 (2009)
- [3] R. Kürsten: Masterarbeit, Universität Leipzig, 2012
- [4] M. Höll: Diplomarbeit, Universität Leipzig, 2012
- [5] N. Kühn: Diplomarbeit, Universität Leipzig, 2011

14.3 Randomly Evolving Idiotypic Networks

U. Behn, A. Kühn, H. Schmidtchen, H. Sachsenweger, R. Schulz, S. Willner

The paradigm of idiotypic networks developed few decades ago by Jerne [1] finds today a renewed interest mainly from the side of system biology and from clinical research. A review with focus on modeling is given in [2], biological concepts and clinical applications are discussed in [3].

B-cells express receptors (antibodies) of a given idiootype. Crosslinking these receptors by complementary structures (antigen or antibodies) stimulates the lymphocyte to proliferate; unstimulated B-cells die. Thus a macroscopically large, though finite, functional network of lymphocytes, the idiotypic network emerges. The dynamics is driven by the influx of new idiotypes randomly produced in the bone marrow and by the population dynamics of the lymphocytes themselves.

In our minimalistic model [4] idiotypes are represented by bitstrings. The model network evolves towards a highly organized architecture where groups of nodes which share statistical characteristics can be identified. We can analytically compute size and connectivity of these groups [5] and calculate in a modular mean field theory mean occupation, cf. Fig. 14.3 and mean life time of the nodes [6].

We extended the mean field theory considering correlations based on the notion of conditional independence for the 12-group architecture. The agreement with simulations is improved by an order of magnitude [8].

To describe biological features we allowed for weighted links and included antigens. For a range of parameters a bistable situation was found where the antigen induces an internal image which persists after the antigen is defeated. In a second exposition to the antigen the network responds faster and more efficient [7, 9]. Further, in the presence of a long lasting self-antigen the architecture of the network organizes such that the idiotypes complementary to self are only weakly occupied. This is a first hint that our model can describe self-tolerance [7].

A new method to describe a broad class of patterns in the network based on the algebraic properties of Cayley graphs was proposed in [9]. We automatized the real time pattern identification based on the center of mass coordinate and optimized the code which allows now simulation of networks with about 2^{20} nodes (Sachsenweger).

- [1] N.K. Jerne: *Ann. Inst. Pasteur Immunol.* **125C**, 373 (1974)
- [2] U. Behn: *Immunol. Rev.* **216** 142 (2007)
- [3] U. Behn: *Idiotype Network*, in: *Encyclopedia of Life Sciences*, John Wiley & Sons, Ltd, Chichester, doi:10.1002/9780470015902.a0000954.pub2 (2011)
- [4] M. Brede, U. Behn: *Phys. Rev. E* **67**, 031920 (2003)

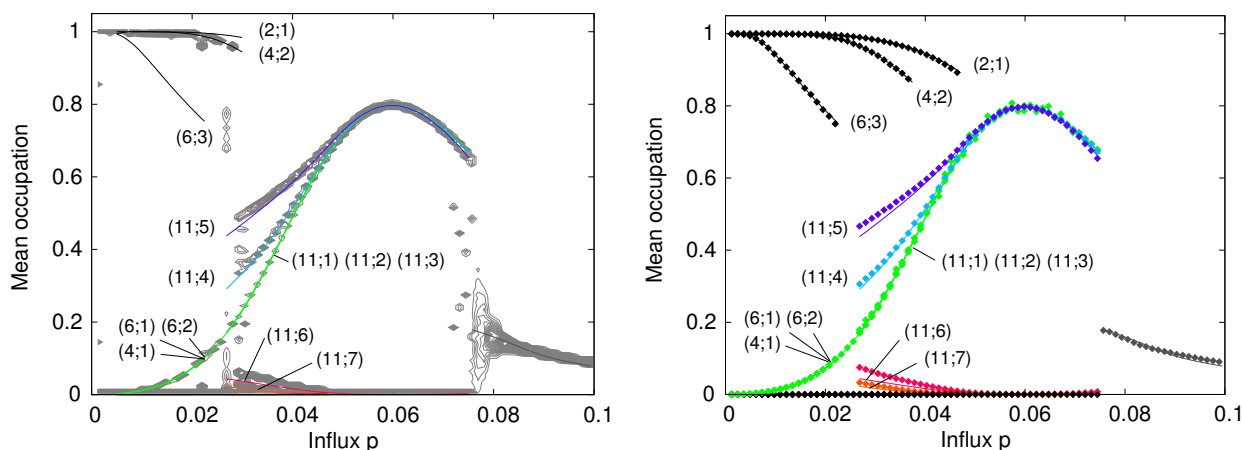


Figure 14.2: Mean occupation of nodes vs influx probability p of new idiotypes obtained in simulations and in mean field theory (solid lines) for a network of 2^{12} nodes. Different patterns occur, which can be labeled by the dimension of their elementary pattern module d_M , consisting of $d_M + 1$ groups of nodes which share statistical properties. The lettering indicates $(d_M, \text{group index})$. **Left:** Simulations starting from scratch (isolines of histograms). **Right:** Simulations starting from prepared patterns (symbols). From [6].

- [5] H. Schmidtchen, M. Thüne, U. Behn, *Randomly Evolving Idiotypic Networks: Structural Properties and Architecture*, arXiv:1201.3618, under review
- [6] H. Schmidtchen, U. Behn, *Randomly Evolving Idiotypic Networks: Modular Mean Field Theory*, arXiv:1201.3530, under review
- [7] B. Werner: Diplomarbeit, Universität Leipzig, 2010
- [8] A. Kühn: Diplomarbeit, Universität Leipzig, 2011
- [9] S. Willner: Diplomarbeit, Universität Leipzig, 2011

14.4 T Cell Regulation, Differentiation, and Plasticity

U. Behn, F. Groß*, D. Kröber, G. Metzner†

*European School of Molecular Medicine, Milan

†Institute of Clinical Immunology, University Leipzig

T-helper lymphocytes have subtypes which differ in their spectrum of secreted cytokines. These cytokines have autocrine effects on the own subtype and cross-suppressive effects on the other subtype and regulate the type of immunoglobulines secreted by B-lymphocytes. In allergy, the balance of Th1- and Th2-cells is perturbed: the response to allergen is Th2-dominated. Recent clinical studies show that during specific immunotherapy the concentration of Tregs is increasing [3, 4].

We extended our previous model [1] to include these regulatory T-cells [5]. If successful, the periodic injections of allergen in the maintenance phase of the therapy drive the system towards a stable fixed point where a high population of Tregs dominates both Th2- and Th1-cells, similar to experimental findings. We used the stable manifold of the unstable fixed point of a stroboscopic map to determine the boundary between the basins of attraction of the stable fixed points [5].

To include the novel Th-subtype Th17 which plays a role, e.g., in allergic asthma we developed a minimalistic model of the differentiation and plasticity of peripheral CD4⁺ T cells. The dynamics induced by the network of cytokines and transcription factors [6] is analyzed using Boolean cellular automata [7], cf. Fig. 14.3. The model reproduces, for example, the higher plasticity of Treg and Th17 cells compared to Th1 and Th2 cells.

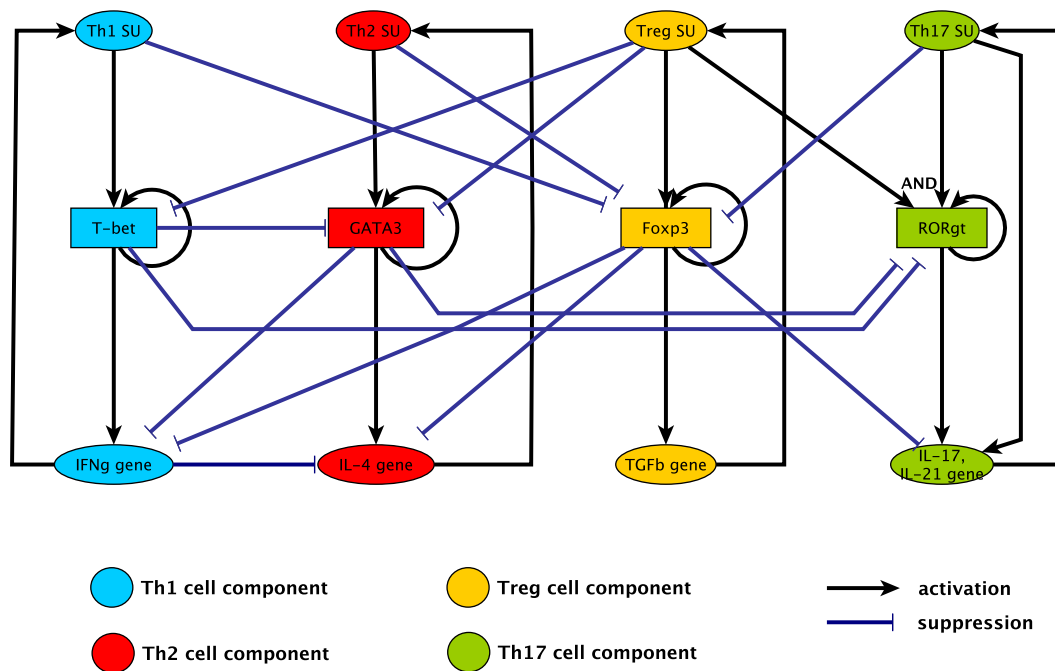


Figure 14.3: Simplified network of regulation mechanisms of CD4⁺ T cells which are taken into account in the Boolean cellular automaton to describe differentiation and plasticity between Th1, Th2, Treg, and Th17 lineage commitment [7].

- [1] J. Richter et al.: *J. Theor. Med.* **4**, 119 (2002)
- [2] R. Vogel, U. Behn: in *Mathematical Modeling of Biological Systems*, Volume II. ed. by A. Deutsch et al. (Birkhäuser, Boston 2008) p145
- [3] M. Larché et al.: *Nature Reviews Immunology* **6**, 761 (2006)
- [4] E. Mamessier et al.: *Clin. Exp. Allergy* **36**, 704 (2006)
- [5] F. Groß et al.: *J. Theor. Biol.* **269**, 70-78 (2011), doi:10.1016/j.jtbi.2010.10.013
- [6] J. Zhu, W.E. Paul: *Immunol. Rev.* **238**, 247-262 (2010)
- [7] D. Kröber: Masterarbeit, Universität Leipzig, 2011

14.5 Generalized Stokes–Einstein relation for hot Brownian motion

D. Chakraborty, M.V. Gnann*, D. Rings, J. Glaser, F. Otto*, F. Cichos[†], K. Kroy

*Max Planck Institute for Mathematics in the Sciences, Leipzig

[†]Molecular Nanophotonics, Institute for Experimental Physics I

Hot Brownian motion is the Brownian motion of nanoscopic colloidal particles that have an elevated temperature compared to their solvent [1]. It is described by a recently developed effective Markov theory [2, 3] based on fluctuating hydrodynamics the predictions of which were scrutinized over a wide temperature range using large-scale GPU-powered molecular dynamics simulations of a hot nanoparticle in a Lennard-Jones fluid [3]. The particle positions and momenta were found to be Boltzmann distributed according to distinct effective temperatures T_{HBM} and T_{k} , cf. Fig. 14.4. For T_{HBM} we derived a formally exact theoretical prediction and established a generalized Einstein relation that links it to directly measurable quantities. This provides unique insights into the physics of hot Brownian motion and an excellent starting point for further experimental tests and applications involving laser-heated nanobeads, nanorods and Janus particles.

- [1] D. Rings et al.: Phys. Rev. Lett. **105**, 090604 (2010), [doi:10.1103/PhysRevLett.105.090604](https://doi.org/10.1103/PhysRevLett.105.090604)
- [2] D. Rings et al.: Soft Matter **7**, 3441 (2011), [doi:10.1039/C0SM00854K](https://doi.org/10.1039/C0SM00854K)
- [3] D. Chakraborty et al.: EPL **96**, 60009 (2011), [doi:10.1209/0295-5075/96/60009](https://doi.org/10.1209/0295-5075/96/60009)

14.6 Inelastic mechanics of biopolymer networks and cells

L. Wolff, K. Kroy

Mechanical cues are an important determinant for the behavior of living cells, with influences reaching much farther than only the cell's own mechanical state. Many physiologically important processes, from the cell's spreading behavior and motility to stem cell differentiation, depend on cell mechanics.

We study cell mechanics using a model for biopolymer networks. Biopolymer networks constitute the major load-bearing structure of the cell, the cytoskeleton. Our model, the inelastic glassy wormlike chain (inelastic GWLC), is rooted in the standard wormlike chain model for isolated semiflexible polymers, but additionally takes into account weak bonds to a background network in a mean-field spirit.

The model is capable of rationalizing recently discovered cell-mechanical phenomena such as fluidization and viscoelastic shake down. Further, by using analytical approximations, we use perturbation analysis to derive formulas characterizing the weakly nonlinear response of a transiently crosslinked biopolymer network. We demonstrate how the weakly nonlinear response can easily be mistaken as a linear response in standard experiments, and how the nonlinear coupling introduces nontrivial nonmonotonic terms in the apparently linear rheological spectrum (Fig. 14.5).

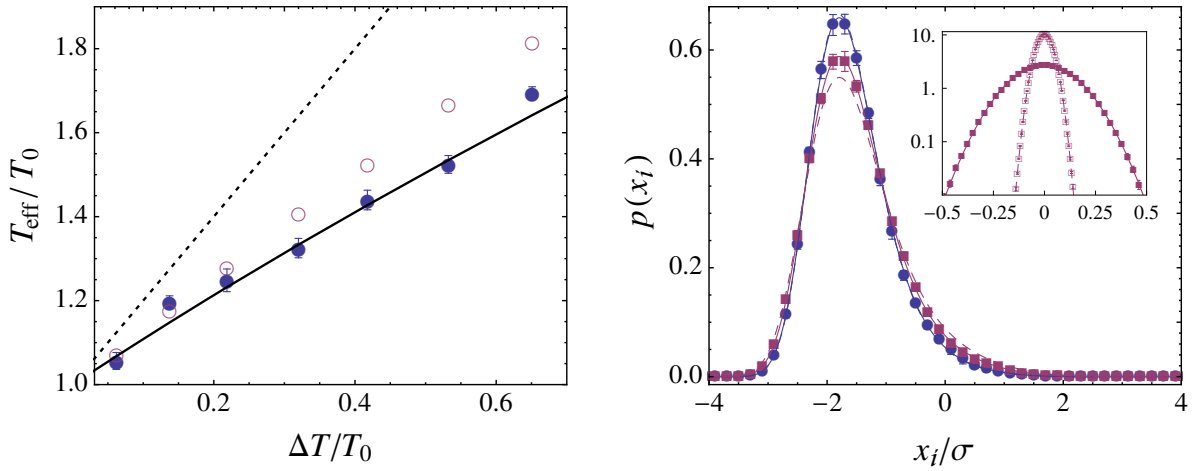


Figure 14.4: **Left:** Effective temperatures of translational hot Brownian motion. The simulation results for T_{HBM} (●) were deduced from ζ_{HBM} and D_{HBM} using the generalized Einstein relation. The theoretical prediction (solid line) was evaluated within the idealized theory for an incompressible fluid using the radial viscosity profile $\eta(r)$ determined in the MD simulation. We find that the kinetic degrees of freedom are governed by a different temperature T_{k} (○), and both differ from the fluid temperature at the surface of the nanoparticle (dotted line). **Right:** The main figure depicts the measured distribution of the configurational degrees of freedom of a hot Brownian particle in an anharmonic and asymmetric potential U , for temperatures of the nanoparticle of $T_{\text{p}} = 1.00 \epsilon/k_{\text{B}}$ (●) and $2.25 \epsilon/k_{\text{B}}$ (■). The solid and the dashed lines are the plots of the Boltzmann distribution $e^{-\beta U - \beta \mathcal{F}}$, with $\beta^{-1} = k_{\text{B}} T_{\text{HBM}}$ and $\beta^{-1} = k_{\text{B}} T_{\text{k}}$, respectively. *Inset:* The measured distribution of the configurational (■) and kinetic (□) degrees of freedom of a hot Brownian particle in a harmonic potential with a stiffness $K = 50$. The corresponding Boltzmann distribution for configurational (solid line) and kinetic (dashed line) degrees of freedom are also shown [3].

[1] L. Wolff et al.: *New J. Phys.* **12**, 5 (2010), doi:10.1088/1367-2630/12/5/053024

14.7 Tube-width fluctuations in entangled stiff polymers

J. Glaser, K. Kroy

The tubelike cages of stiff polymers in entangled solutions have been shown to exhibit characteristic spatial heterogeneities (Fig. 14.6). We explain these observations by a systematic theory generalizing previous work by Morse [1]. With a local version of the binary collision approximation, the distribution of confinement strengths is calculated, and the magnitude and the distribution function of tube radius fluctuations are predicted. Our main result is a unique scaling function for the tube radius distribution, in good agreement with experimental and simulation data.

[1] D.C. Morse: *Phys. Rev. E* **63**, 0131502 (2001), doi:10.1103/PhysRevE.63.0131502

[2] J. Glaser, K. Kroy: *Phys. Rev. E* **84**, 051801 (2011), doi:10.1103/PhysRevE.84.051801

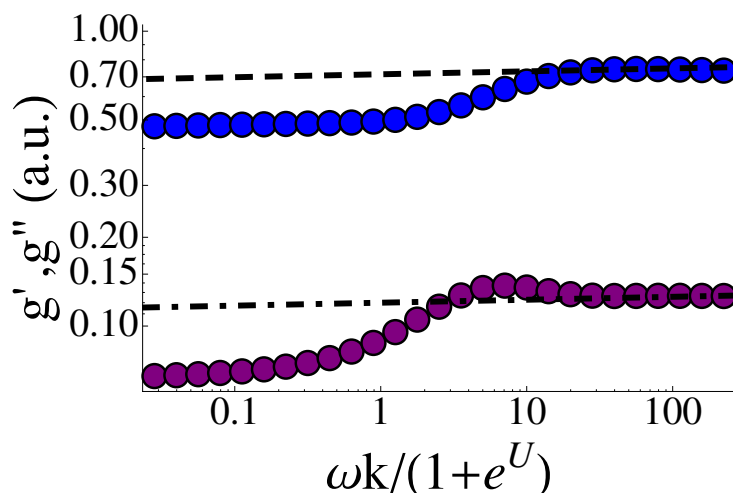


Figure 14.5: Nonlinear (symbols) and linearized (lines) moduli for the inelastic model. Due to transient bond breaking, a shoulder develops in the in-phase response (blue), and a peak is observed in the out-of-phase response (purple).

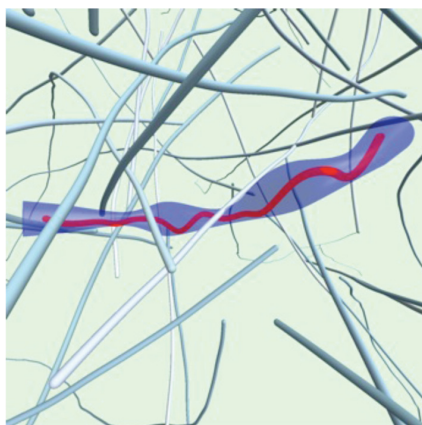


Figure 14.6: Test polymer in a background solution, confined into a tube of spatially varying radius

14.8 WLC monomer dynamics

J.T. Bullerjahn, S. Sturm, L. Wolff, K. Kroy

In contrast to their synthetic counterparts, biopolymers are stiff or semiflexible, resulting in an anisotropic response to external perturbations. The *wormlike chain* (WLC) model provides a minimal description of such semiflexible polymers in terms of an inextensible elastic beam, and has successfully been used to interpret experimental data on polymer fluctuations and their force response. However, the experimental manipulation of biopolymers often relies strongly on localized force probes or actuators, such as chemically attached tracer particles, thus motivating an effective single particle description. Starting from the WLC model, we derive a generalized Langevin equation for the tracer's motion in an externally controlled potential (cf. Fig. 14.7), as well as the associated power spectrum and mean square displacement [1]. Deformations of the attached polymer induce a frequency-dependent noise and memory friction, rendering

the tracer's motion subdiffusive. Our analytical results provide the basis for an exact theoretical treatment of various single-molecule experiments.

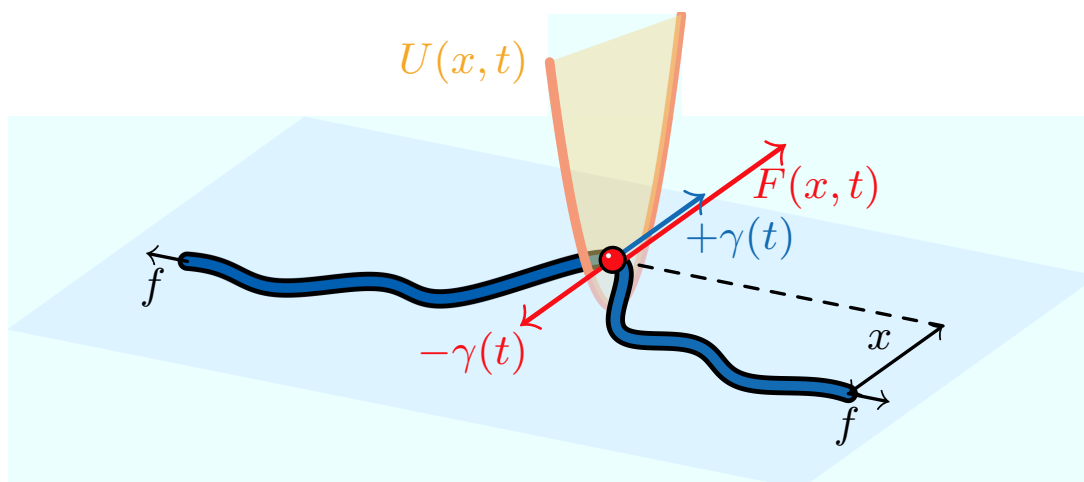


Figure 14.7: Force diagram for the combined system of a tracer (red) and an attached WLC (blue). The tracer is displaced by the external force $F(x, t) = -U(x, t)$, which has to overcome the effective polymeric drag $-\gamma(t)$ [1].

[1] J.T. Bullerjahn et al.: EPL **96**, 48005 (2011), doi:10.1209/0295-5075/96/48005

14.9 Wind driven sand transport. A two-species continuum model of aeolian sand transport.

M. Lämmel, D. Rings, K. Kroy, L. Kimme

Wind-driven sand transport is the dominant process shaping the morphology of arid regions on Earth, Mars and elsewhere. It is responsible for the spontaneous creation of a whole hierarchy of self-organized dynamic structures from ripples over isolated dunes to devastating fields of shifting sands. It also contributes considerably to dust proliferation, which is a major determinant of our global climate.

Predicting aeolian sand fluxes by mathematical models is very much complicated by the complex turbulent nature of the driving medium (e.g. streaming air) and the erratic grain hopping it excites [1]. Yet, it is by now well understood that this hopping of grains accelerated by the wind has some characteristic structure [2]. Highly energetic “saltating” grains make a dominant contribution to the overall mass transport. When impacting on the sand bed, they dissipate some of their energy in a complex process called splash, ejecting a cloud of “reptating” grains. This coarse-grained picture is sketched in Fig. 14.8.

We are developing a mathematical description of the sand transport process beyond popular mean-field models, such as the Sauermann model [3], but without sacrificing their computational efficiency. The mobile grains are represented by two sub-populations, instead of one, the so-called saltating and reptating grains. By this

conceptual improvement, we can overcome certain shortcomings of the one-species mean-field models, yet keep their concise mathematical structure. The predicted stationary sand transport rate is in excellent agreement with wind tunnel experiments simulating wind conditions ranging from the onset of saltation to storms. Our closed set of equations thus provides an analytically tractable, numerically precise, and computationally efficient starting point for applications addressing a wealth of phenomena from dune formation to dust emission.

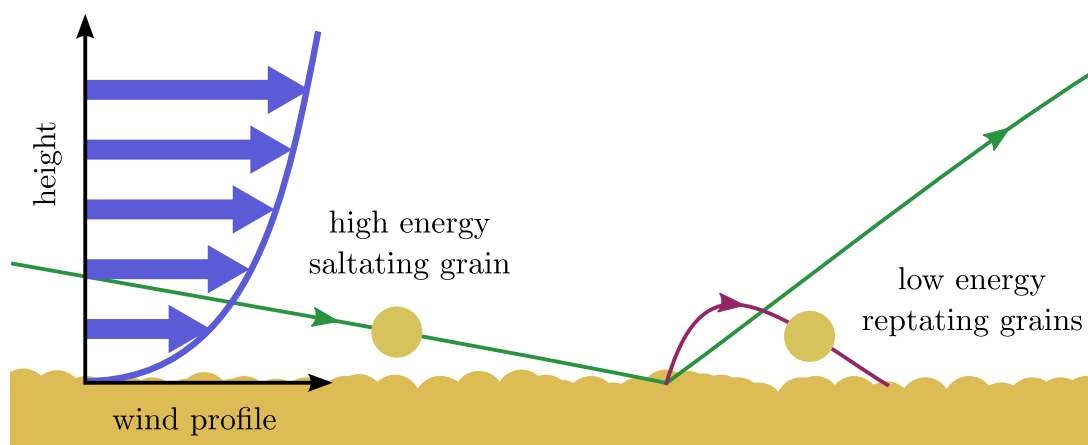


Figure 14.8: The two-species picture of aeolian sand transport: Driven by the wind (blue arrows represent the wind speed profile), high energy grains rebound upon impact and eject a certain number of low energy grains. In our model, we map the whole ensemble of trajectories onto one for the rebounded “saltating” grains (green line) and a second one for all the ejected “reptating” grains (purple line).

- [1] R.A. Bagnold: *The physics of blown sand and desert dunes* (Dover Publications, New York 1941)
- [2] R.S. Anderson et al.: *Acta Mechanica Supplement* **1**, 1 (1991)
- [3] G. Sauermaun et al.: *Phys. Rev. E* **64**, 031305 (2001), [doi:10.1103/PhysRevE.64.031305](https://doi.org/10.1103/PhysRevE.64.031305)

14.10 Time-symmetric quantum mechanics

A. Kramer, K. Kroy

Although quantum mechanics is able to explain the experimental results perfectly, its interpretation appears questionable. One way to avoid several interpretational problems is assuming a standpoint outside time, as proposed by Price [1], and therewith permitting forward and backward causation. The idea that the future affects the present may seem strange at first sight. But given the time symmetry on the microscopic level, there seems to be no obvious reason for treating past and future differently.

Indeed, there already exist some approaches to time-symmetric quantum mechanics, which turned out to be quite different from each other. The reason for this may be the fact that the meaning of the wavefunction is still unexplained, so that there

is a priori no prescription for the construction of a reasonable time-symmetric wavefunction. Consequently, we first formulated mechanics, especially the Hamilton–Jacobi formalism, with time-symmetric boundary conditions and then passed over to quantum mechanics. The resulting formalism is in accordance with one of the existing ones, the two-state vector formalism [2].

The state in the time between two standard quantum measurements can be accessed using the concept of weak measurements first developed by Aharonov et al. [3]. Weak measurements are currently of great interest to experimentalists and have been voted as the top breakthrough of 2011 by Physics World.

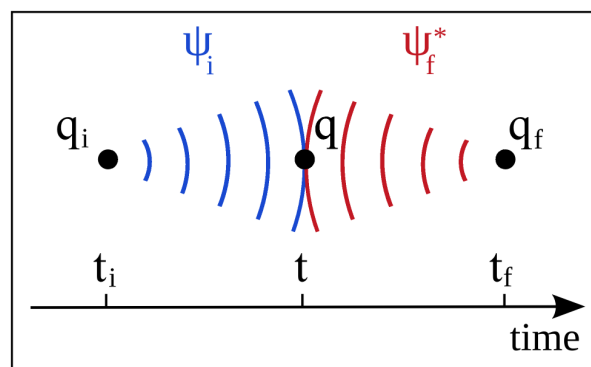


Figure 14.9: The quantum state at any intermediate time t is assumed to be jointly determined by a forward-evolving wavefunction ψ_i depending on the past, and by a backward-evolving wavefunction ψ_f^* depending on the future.

- [1] H. Price: *Time's Arrow and Archimedes' Point*. New Directions for the Physics of Time (Oxford University Press, New York 1996)
- [2] Y. Aharonov, L. Vaidman: *J. Phys A: Math. Gen.* **24**, 2315 (1991), doi:10.1088/0305-4470/24/10/018
- [3] Y. Aharonov, L. Vaidman: *Phys. Rev. A* **41**, 11 (1990), doi:10.1103/PhysRevA.41.11

14.11 Funding

Leipzig School of Natural Sciences – Building with Molecules and Nano-objects (Build-MoNa)

Prof. Dr. K. Kroy (Principal Investigator)
DFG GS 185/1

DFG FOR 877 "From Local Constraints to Macroscopic Transport"

Prof. Dr. K. Kroy (Principal Investigator)
KR 3381/2-2 and KR 3381/3-1

Humboldt Fellowship

Dr. D. Chakraborty (together with Prof. Dr. F. Cichos)

Landesinnovationsstipendium des Freistaates Sachsen im Rahmen des Europäischen Sozialfonds

Dipl.-Phys. J.T. Bullerjahn, Dipl.-Phys. M. Lämmel, Dipl.-Phys. S. Sturm

14.12 Organizational Duties

U. Behn

- Speaker of the Condensed Matter Theory Group
- Vertrauensdozent für die Nobelpreisträgertagungen in Lindau
- Bibliotheksbeauftragter of the Faculty
- Member of PbF2
- Scientific Member of the International Max Planck Research School "Mathematics in the Sciences"
- Referee: J. Theor. Biol.
- Reviewer: Stony Brook Univ., Univ. Of Illinois at Urbana-Champaign, Boston University, University of Manchester

K. Kroy

- Vice Director of the Institute for Theoretical Physics
- Member of the graduation committee
- Member of the committee for information & communication technology
- Study counselor for physics
- Member of PbF1 and PbF2
- PI in DFG FOR 877 and Leipzig School of Natural Sciences – Building with Molecules and Nano-objects (BuildMoNa)
- Scientific Member of the International Max Planck Research School "Mathematics in the Sciences"
- Organization of the Minerva Gentner Symposium on Aeolian Processes, Eilat, Israel, 23–28 October 2011
- Organization of the symposium "Hot Nanoparticles and Nanostructures", Leipzig, 10–11 October 2011
- Referee: Proc. Nat. Acad. Sci. (USA), Phys. Rev. Lett., Phys. Rev. E, Soft Matter, PLoS ONE, Eur. Phys. J. E., etc.
- Reviewer: DFG, NSF

A. Kramer

- Coordinator of the DFG Research Unit "From Local Constraints to Macroscopic Transport"
- Member of the BuildMoNa Office

14.13 External Cooperations

Academic

- University of Cambridge
Dr. U. Keyser, O. Otto
- FZ Jülich
Prof. R. Merkel, Dr. M. Degawa, Dr. I. Lauter
- Max Planck Institute for Mathematics in the Sciences, Leipzig
Prof. F. Otto, M.V. Gnann

- Molecular Nanophotonics, Institute for Experimental Physics I
Prof. F. Cichos
- Otto-von-Guericke-Universität Magdeburg
Prof. Dr. J. Richter
- Joint Institute for Nuclear Research, Dubna, Russia
Prof. Dr. N.M. Plakida
- Ernst-Moritz-Arndt-Universität Greifswald
Prof. Dr. H. Fehske
- Philipps-Universität Marburg
Prof. Dr. G. Germano, Dr. E. Martin
- Institut für Klinische Immunologie
Prof. Dr. G. Metzner
- European School of Molecular Medicine, Milan, Italy
Dipl.-Phys. F. Groß
- Physik Weicher Materie, Institut für Experimentalphysik I
Prof. Dr. A. Käs, Dipl.-Math. M. Knorr

14.14 Publications

Journals

- J.T. Bullerjahn, S. Sturm, L. Wolff, K. Kroy: *Monomer dynamics of a wormlike chain*, EPL **96**, 48005 (2011)
- D. Chakraborty, M.V. Gnann, D. Rings, J. Glaser, F. Otto, F. Cichos, K. Kroy: *Generalised Einstein relation for hot Brownian motion*, EPL **96**, 60009 (2011)
- D. Chakraborty: *Velocity autocorrelation function of a Brownian particle*, Euro. Phys. J. B **83**, 375–380 (2011)
- J. Glaser, K. Kroy: *Tube-width fluctuations of entangled stiff polymers*, Phys. Rev. E **84**, 051801 (2011)
- F. Gross, G. Metzner, U. Behn: *Mathematical Modelling of Allergy and Specific Immunotherapy: Th1-Th2-Treg Interactions*, J. Theor. Biol. **269**, 70-78 (2011)
- M. Härtel, J. Richter, D. Ihle: *Thermodynamics of the frustrated one-dimensional spin-1/2 Heisenberg ferromagnet in a magnetic field*, Phys. Rev. B **83**, 214412 (2011)
- M. Härtel, J. Richter, D. Ihle, J. Schnack, S.-L. Drechsler: *Thermodynamics of the one-dimensional frustrated Heisenberg ferromagnet with arbitrary spin*, Phys. Rev. B **84**, 104411 (2011)
- E. Martin, U. Behn, G. Germano: *First-passage and first-exit times of a Bessel-like stochastic process*, Phys. Rev. E **83**, 051115 (2011)

M. Knorr, D. Koch, T. Fuhs, U. Behn, J.A. Käs: *Stochastic Actin Dynamics in Lamellipodia Reveal Parameter Space for Cell Type Classification*, *Soft Matter* **7**, 3192-3203 (2011), DOI: 10.1039/C0SM01028F

D. Rings, M. Selmke, F. Cichos, K. Kroy: *Theory of hot Brownian motion*, *Soft Matter* **7**, 3441–3452 (2011)

A. A. Vladimirov, D. Ihle, N. M. Plakida: *Dynamic spin susceptibility of superconducting cuprates: A microscopic theory of the magnetic resonance mode*, *Phys. Rev. B* **83**, 024411 (2011)

B. Zenker, D. Ihle, F. X. Bronold, H. Fehske: *Slave-boson field fluctuation approach to the extended Falicov-Kimball model: Charge, orbital, and excitonic susceptibilities*, *Phys. Rev. B* **83**, 235123 (2011)

Books

U. Behn, *Idiotypic Networks*, in: *Encyclopedia of Life Sciences*, John Wiley & Sons, Ltd, Chichester, doi:10.1002/9780470015902.a0000954.pub2 (Online posting date: 15th April 2011).

Talks

D. Chakraborty: *Brownian motion of a heated colloid*, Group Seminar “Theory of Condensed Matter”, Max Planck Institute for Metals Research, Stuttgart, 5 July 2011

D. Chakraborty: *Hot Brownian motion*, Symposium “Hot Nanoparticles and Nanostructures”, Leipzig, 10–11 October 2011

J. Glaser: *From stiff polymers to cell mechanics*, North Dakota State University, Fargo, 9 February 2011

K. Kroy: *Brownian motion: from stiff polymers to heated nanoparticles*, Group Seminar, MPI MIS, Leipzig, 12 January 2011

K. Kroy: *Brownian motion: from stiff polymers to heated nanoparticles*, Lecture Series, MPI MIS, Leipzig, January 2011

K. Kroy: *Hot Brownian motion*, Section Seminar, Institute for Building Materials, ETH Zürich, 3 February 2011, invited

K. Kroy: *Hot Brownian motion*, Colloquium, MPI PKS, Dresden, 21 February 2011, invited

K. Kroy: *Nonlinear mechanics of biopolymer networks*, Workshop “Nonlinear Response of Soft Matter”, Konstanz, 28 February–2 March 2011, invited

K. Kroy: *Hot Brownian motion*, Université de Fribourg, Switzerland, 11 March 2011, invited

K. Kroy: *Inelastic mechanics of biopolymer networks*, 75th Annual Meeting of the German Physical Society, Dresden, 13–18 March 2011, invited

K. Kroy: *Inelastic mechanics of biopolymer networks*, NORDITA, Stockholm, Sweden, 15 March 2011, invited

K. Kroy: *Hot Brownian motion: when big beads beat bittie beads*, Workshop on Dynamics in Viscous Liquids, Rom, Italy, 30 March–2 April 2011, invited

K. Kroy: *How a polymer breaks a bond*, CECAM Workshop "Multiscale Computational Biomechanics", ETH Zürich, Switzerland, 12–15 April 2011, invited

K. Kroy: *Nonlinear mechanics of biopolymer networks*, SFB Kolloquium, Universität Göttingen, 17 May 2011, invited

K. Kroy: *Structure and dynamics of soft matter*, Invited Lecture Series, Graduate Days, Universität Heidelberg, 4–8 October 2011

K. Kroy: *Physicists playing in the sandpit*, Minerva Gentner Symposium on Aeolian Processes, Eilat, Israel, 23–28 October 2011, invited

K. Kroy: *Hot Brownian motion*, ZiF-Conference "Stochastic Dynamics in Mathematics, Physics and Engineering", Bielefeld, 2–4 November 2011, invited

M. Lämmel: *A two-species continuum model of aeolian sand transport*, Minerva Gentner Symposium on Aeolian Processes, Eilat, Israel, 23–28 October 2011

D. Rings: *Hot Brownian motion*, Group seminar "Theory of condensed matter", Max Planck Institute for Metals Research, Stuttgart, 27 January 2011

D. Rings: *Effective temperatures in hot Brownian motion*, 75th Annual Meeting of the German Physical Society, Dresden, 13–18 March 2011

D. Rings: *Sand-induced dust emission*, Minerva Gentner Symposium on Aeolian Processes, Eilat, Israel, 23–28 October 2011

S. Sturm: *Effective diffusion of biopolymers in transversal binding potentials*, Scientific Symposium of Sächsische Forschergruppe FOR 877, Chemnitz, 24 February 2011

Posters

J.T. Bullerjahn: *How a polymer breaks a bond*, Workshop "Multiscale Computational Biomechanics", Zürich, Switzerland, 12–15 April 2011

J.T. Bullerjahn: *Hot biopolymers*, Symposium "Hot Nanoparticles and Nanostructures", Leipzig, 10–11 October 2011

D. Chakraborty, D. Rings, F. Cichos, K. Kroy: *Molecular dynamics simulation of hot Brownian motion*, 75th Annual Meeting of the German Physical Society, Dresden, 13–18 March 2011

D. Chakraborty, D. Rings, F. Cichos, K. Kroy: *Brownian motion of a heated colloid*, International Symposium "Computer Simulations on GPU", Mainz, 30 May–1 June 2011

J. Glaser: Tube width fluctuations in F-actin solutions, Discussion Meeting "Challenges in and Potential of Polymer Physics", Schluchsee, 4–6 May 2011

M. Lämmel: *The tube model for semiflexible biopolymer networks*, 4th European Cell Mechanics Meeting, Amsterdam, Netherlands, 17–19 October 2011

D. Rings, D. Chakraborty, F. Cichos, K. Kroy: *Rotational hot Brownian motion*, Symposium "Hot Nanoparticles and Nanostructures", Leipzig, 10–11 October 2011

S. Sturm: *Subdiffusive polymer dynamics and bond kinetics*, Scientific Symposium of the Graduate School BuildMoNa, Leipzig, 21 March 2011

14.15 Graduations

Doctorate

- Jens Glaser
Semiflexible polymer networks
May 2011
- Lars Wolff
Inelastic mechanics of biopolymer networks and cells
October 2011

Diploma

- Jakob Tómas Bullerjahn
Ein Bindungsmodell für Netzwerke semiflexibler Polymere
February 2011
- Andrea Kramer
Time-symmetric quantum mechanics
August 2011
- Andreas Kühn
Idiotypische Netzwerke: Mean-Field-Theorie mit Korrelationen
January 2011
- Norma Kühn
Fluctuation Theorems in Systems of Globally Coupled Stratonovich Models
April 2011
- Marc Lämmel
Aeolian sand transport
April 2011
- Sven Willner
Patterns in the Bitstring Model of Idiotypic Networks
February 2011

Master

- Damaris Kröber
Modelling CD4+ T Cell Differentiation and Plasticity using Boolean Cellular Automata
August 2011

14.16 Guests

- Dr. Pablo Fernández
TU München
04–05 April 2011
- Prof. Dr. Sean Sun
Johns Hopkins University, Baltimore, USA
29 April 2011
- Dr. Nuno Araujo
ETH Zürich, Switzerland
03 May 2011
- Dr. Ralf Eichhorn
NORDITA, Stockholm, Sweden
10–11 May 2011
- Prof. Dr. Roberto Piazza
Politecnico di Milano, Italy
17–19 May 2011
- Sandeep Patil
Heidelberg Institute for Theoretical Studies
23–27 May 2011
- Dr. Manlio Tassieri
University of Glasgow, School of Engineering, UK
10–11 July 2011
- Hugo Brandao
McGill University, Montreal, Kanada
13 June–20 August 2011
- Michael Lindon
University of Warwick, UK
04 July–09 September 2011

15

Theory of Elementary Particles

15.1 Introduction

The Particle Physics Group performs basic research in the quantum field theoretic description of elementary particles and in phenomenology. Topics of current interest are conformal symmetry and its breaking in the context of supersymmetric theories, the formulation of models which realize noncommutative geometry, renormalization problems, electroweak matter at finite temperature, the lattice formulation of gauge theories, the derivation of Regge behaviour of scattering amplitudes from Quantum Chromodynamics and the related study of integrable models with and without supersymmetry. Perturbative and non-perturbative methods are applied to answer the respective questions. In perturbation theory the work is essentially analytic using computers only as a helpful tool. Lattice Monte Carlo calculations as one important non-perturbative approach however are based on computers as an indispensable instrument. Correspondingly the respective working groups are organized: in analytical work usually very few people collaborate, in the lattice community rather big collaborations are the rule. Our group is involved in many cooperations on the national and international level (DESY, Munich, Regensburg; UK, France, Russia, Armenia, USA, Japan).

Klaus Sibold

15.2 Propagators and Wilson loops in numerical stochastic perturbation theory

H. Perlt, A. Schiller

In collaboration with authors from different locations we have continued our research programme using numerical stochastic perturbation theory (NSPT). It is well known that lattice perturbation theory (LPT) is much more involved compared to its continuum QCD counterpart. The complexity of diagrammatic approaches increases rapidly beyond the one-loop approximation. By now only a limited number of results up to two-loop accuracy have been obtained.

Applying the standard Langevin dynamics [1, 2] to the problem of weak coupling expansions for lattice QCD, a powerful numerical approach for higher loop calculations – called numerical stochastic perturbation theory (NSPT) – has been proposed in [3].

In collaboration with the Parma and Berlin group we applied that technique to find higher loop contributions to ghost and gluon propagators in SU(3) Lattice Gauge Theory. Our final aim was to eventually compare with results from lattice simulations in order to enlight the genuinely non-perturbative content of the latter. In a first paper [4] we have computed the ghost propagator in Landau gauge up to three loops. We presented results in the infinite volume and $a \rightarrow 0$ limits, based on a general strategy that we have discussed in detail.

In a second paper [5] the gluon propagator has been computed: results range from two up to four loops, depending on the different lattice sizes. The non-logarithmic constants for one, two and three loops have been extrapolated to the lattice spacing $a \rightarrow 0$ continuum and infinite volume $V \rightarrow \infty$ limits.

Finally in cooperation with the Berlin group we have compared those results with detailed Monte Carlo studies of the Landau gauge gluon and ghost propagators of SU(3) gauge theory, employing the logarithmic definition for the lattice gluon fields and implementing the corresponding form of the Faddeev-Popov matrix. At weak coupling and large momentum, the bare propagators and the ghost-gluon coupling are seen to be approached by those of higher-order NSPT [6].

With colleagues from the QCDSF collaboration we have continued our research on higher order expansion of Wilson loops in NSPT and have calculated perturbative Wilson loops of various sizes up to loop order $n = 20$ at different lattice sizes for pure plaquette and tree-level improved Symanzik gauge theories using the technique of Numerical Stochastic Perturbation Theory [7]. This allows us to investigate the behavior of the perturbative series at high orders. We have observed differences in the behavior of perturbative coefficients as a function of the loop order. Up to $n = 20$ we do not see evidence for the often assumed factorial growth of the coefficients. Based on the observed behavior we sum this series in a model with hypergeometric functions. Alternatively we have estimated the series in boosted perturbation theory. Subtracting the estimated perturbative series for the average plaquette from the non-perturbative Monte Carlo result we estimated the gluon condensate. A detailed report is in preparation.

- [1] G. Parisi and Y. s. Wu,
Sci. Sin. **24** (1981) 483.
- [2] G. G. Batrouni, G. R. Katz, A. S. Kronfeld, G. P. Lepage, B. Svetitsky and K. G. Wilson,
Phys. Rev. D **32** (1985) 2736.
- [3] F. Di Renzo, E. Onofri, G. Marchesini and P. Marenzoni,
Nucl. Phys. B **426** (1994) 675
[arXiv:hep-lat/9405019].
- [4] F. Di Renzo, E. -M. Ilgenfritz, H. Perlt, A. Schiller and C. Torrero,
"The ghost propagator in Landau gauge,"
Nucl. Phys. B **831** (2010) 262
[arXiv:0912.4152 [hep-lat]].
- [5] F. Di Renzo, E. -M. Ilgenfritz, H. Perlt, A. Schiller and C. Torrero,
Nucl. Phys. B **842** (2011) 122
[arXiv:1008.2617 [hep-lat]].
- [6] E. -M. Ilgenfritz, C. Menz, M. Muller-Preussker, A. Schiller and A. Sternbeck,
Phys. Rev. D **83** (2011) 054506

- [arXiv:1010.5120 [hep-lat]].
- [7] R. Horsley, G. Hotzel, E. -M. Ilgenfritz, Y. Nakamura, H. Perlt, P. E. L. Rakow, G. Schierholz and A. Schiller, PoS LATTICE **2010** (2010) 264 [arXiv:1010.4674 [hep-lat]].

15.3 Symmetries and integrability in gauge field theories

R. Kirschner

Integrable quantum systems are applied successfully to the study of the high-energy asymptotics and of the renormalization of composite operators in gauge theories [1–4]. These application stimulated the development of the methods of integrable quantum systems. Relying on solutions of the Yang-Baxter relations we have constructed Baxter operators for quantum spin chains. The case of undeformed $sl(2)$ symmetry has been studied in detail [5] and also the cases of trigonometrically and elliptically deformed symmetry have been considered. The relation of several types of Baxter operators has been established and the path from generic to integer or half-integer spin representations has been indicated. In particular our work answers questions raised in recent publications [6] and provides a more powerful method.

- [1] L.N. Lipatov, *High-energy asymptotics of QCD and exactly solvable lattice models* Padova preprint DFPD-93-TH-70B; and JETP Lett. B342 (1994)596.
- [2] L. D. Faddeev and G. P. Korchemsky, ‘High-energy QCD as a completely integrable model,’ Phys. Lett. B **342** (1995) 311 [arXiv:hep-th/9404173].
- [3] V. M. Braun, S. E. Derkachov and A. N. Manashov, ‘Integrability of three-particle evolution equations in QCD,’ Phys. Rev. Lett. **81** (1998) 2020 [arXiv:hep-ph/9805225].
- [4] N. Beisert, Phys. Rept. **407** (2004) 1.
- [5] D. Chicherin, S. Derkachov, D. Karakhanyan and R. Kirschner, ‘Baxter operators for arbitrary spin,’ parts I and II, Nucl. Phys. B **854** (2012) 393 and 433 [arXiv:1106.4991 [hep-th]] and [arXiv:1107.0643 [hep-th]].
- [6] V. V. Bazhanov, T. Lukowski, C. Meneghelli and M. Staudacher, ‘A Shortcut to the Q-Operator,’ J. Stat. Mech. **1011** (2010) P11002 [arXiv:1005.3261 [hep-th]].

15.4 Funding

Propagators and Wilson loops in numerical stochastic perturbation theory
Supported by DFG under contract SCHI 422/8-1

Symmetry and integrability in gauge field theories
Supported by DFG (GZ KI-623/8-1)

15.5 Organizational Duties

A. Schiller

- Referee: Phys. Rev. D

R. Kirschner

- Referee: Phys. Rev. D, Phys. Letters B
- Member of the PhD commission of the faculty

15.6 External Cooperations

Academic

- St. Petersburg, Nuclear Physics Institute
Prof. L.N. Lipatov
- St. Petersburg, St. Petersburg branch of Steklov Mathematical Institute
Dr. S.E. Derkachov
- Yerevan Physics Institute, Theory Dept.
Prof. Ara Sedrakyan
- Soltan Institut of Nucl. Studies, Warsaw
Dr. Lech Szymanowski
- Sobolev Institut of Mathematics, Novosibirsk
Dr. Dmitri Yu. Ivanov
- Univ. Hamburg, Inst. f. Theor. Physik/ DESY
Prof. J. Bartels
- Universität Regensburg, Inst.f. Theor. Physik
Prof. A. Schäfer, Prof. V. Braun, Dr. M. Göckeler, Prof. G. Bali, Dr. A. Sternbeck
- Humboldt- Universität zu Berlin
Prof. M. Müller-Preussker
- VIK Dubna, Russland
Dr. E.-M. Ilgenfritz
- Ecole Polytechnique, Paris-Palaiseau
Prof. B. Pire
- DESY, Hamburg
Prof. G. Schierholz

- Edinburgh University, UK
Dr. R. Horsley
- Department of Mathematics, Liverpool University, UK
- Parma University
Prof. F. Di Renzo

15.7 Publications

Journals - Citations

F. Di Renzo, E. -M. Ilgenfritz, H. Perlt, A. Schiller and C. Torrero: *Two-point functions of quenched lattice QCD in Numerical Stochastic Perturbation Theory. (II) The Gluon propagator in Landau gauge*, Nucl. Phys. B **842** (2011) 122

E.-M. Ilgenfritz, C. Menz, M. Muller-Preussker, A. Schiller and A. Sternbeck: *SU(3) Landau gauge gluon and ghost propagators using the logarithmic lattice gluon field definition*, Phys. Rev. D **83** (2011) 054506

W. Bietenholz, V. Boryakov, M. Gockeler, R. Horsley, W. G. Lockhart, Y. Nakamura, H. Perlt and D. Pleiter et al.: *Flavour blindness and patterns of flavour symmetry breaking in lattice simulations of up, down and strange quarks*, Phys. Rev. D **84** (2011) 054509

D. Chicherin, S. Derkachov, D. Karakhanyan and R. Kirschner: *Baxter operators for arbitrary spin*, Nucl. Phys. B **854** (2012) 393

D. Chicherin, S. Derkachov, D. Karakhanyan and R. Kirschner: *Baxter operators for arbitrary spin II*, Nucl. Phys. B **854** (2012) 433

S. E. Derkachov and A. N. Manashov: *Noncompact $sl(N)$ spin chains: BGG-resolution, Q -operators and alternating sum representation for finite dimensional transfer matrices*, Lett. Math. Phys. **97** (2011) 185

D. Karakhanyan and S. Khachatryan: *New solutions to the $sl_q(2)$ -invariant Yang-Baxter equations at roots of unity*, Nucl. Phys. B **850** (2011) 522

Proceedings

F. Di Renzo, E. -M. Ilgenfritz, H. Perlt, A. Schiller and C. Torrero: *Two-point functions of quenched lattice QCD in Numerical Stochastic Perturbation Theory*, AIP Conf. Proc. **1343** (2011) 236

15.8 Graduations

Bachelor

- Ecaterina Bodnariuc
The plaquette of two dimensional lattice SU(2) in Numerical Stochastic Perturbation Theory
July 20, 2011

Author Index

A

Amecke, N. 45
 Andrea, T. 153
 Anton, M. 67
 Arkin, H. 240, 241
 Arredondo, M. 219

B

Bachmann, M. 235, 236, 257
 Ballestar, A. 223
 Barapatre, N. 142, 144, 146
 Barzola-Quiquia, J. 223
 Beckert, St. 90
 Behn, U. 107, 307, 308
 Benndorf, G. 195, 197
 Bertmer, M. 128, 129
 Bilsel, M. 241
 Binder, T. 91
 Bischof, R. 252
 Bischoff, A. 152
 Blavatska, V. 238, 243
 Brachwitz, K. 166, 193
 Brandt, M. 195
 Brauer, G. 177
 Braun, M. 39, 41, 43
 Bregulla, A. 38
 Brunner, C. 113
 Bubar, V. 38
 Bujdoso, R. 72
 Bullerjahn, J.T. 312
 Butz, T. 144, 152, 153, 155, 157
 Bux, H. 92

Böhlmann, W. 223
 Böntgen, T. 202, 204
 Böttcher, R. 129

C

Caro, J. 92
 Chakraborty, D. 310
 Chilotte, C. 223
 Chmelik, C. 92
 Cichos, F. 38, 39, 41–43, 45, 310

D

Diering, D. 153
 Dietrich, C.P. 189, 193
 Dietrich, U. 111, 112
 Donath, E. 148, 149
 Dorn, M. 148, 149
 Dusari, S. 223

E

Ehlicher, A. 113
 Ehrenpreis, E. 250
 Ellguth, M. 177
 Elmahdy, M.M. 72, 75
 Enculescu, M. 113
 Ene, R. 64, 67
 Esquinazi, P. 221, 223
 Estrela-Lopis, I. 148, 149

F

Fabry, B. 105

- Falcke, M. 113
 Fleddermann, J. 149
 Franke, H. 184
 Frenzel, H. 168
 Fricke, N. 245
 Fritsch, A. 106
 Fuhs, T. 107
- G**
-
- Galvosas, P. 87
 Garai, A. 249
 Gerlach, M.H. 253
 Geyer, S. 146
 Glaser, J. 310, 311
 Gnann, M.V. 310
 Goegler, M. 113
 Goh, S.K. 125
 Gratz, M. 87
 Greiser, S. 126
 Groß, F. 308
 Gross, J. 257
 Grossmann, M. 87
 Grundmann, M. ... 166, 168, 170, 174, 176,
 177, 179, 181, 183, 184, 189, 193,
 195–199, 202, 204
 Gul-E-Noor, F. 128
 Gutsche, C. 67, 68, 70, 72–75
 Gyger, M. 105
- H**
-
- Haase, J. 125, 126
 Halperin, B.I. 296
 Hansson, H. 298
 Hartmann, M. 126, 128
 Hayes, S.E. 128
 Heber, A. 43
 Heerklotz, L. 42
 Herrmannsdörfer, T. 126
 Herzig, T. 202
 Hibbe, F. 91
 Himsl, D. 126, 128
 Hoffmann, R. 68, 73
 Horch, C. 90
 Horn, L.C. 106
 Horsdal, M. 298, 299
- Huber, F. 103
 Hyart, T. 288, 289
 Händel, C. 111
 Höckel, M. 106
- I**
-
- Iacob, C. 59, 61–64
 Ilan, R. 292
- J**
-
- Janke, W. 235, 236, 238, 240, 241, 243,
 245–247, 249, 250, 252, 253, 255,
 257
 Jankuhn, St. 148, 149, 151
 Jasiurkowska, M. 64
 Jee, B. 126, 128
 Johnston, D.A. 255
 Jäger, A. 129
- K**
-
- Kapteijn, F. 91
 Karalus, S. 236
 Karsthof, R. 177
 Kersting, B. 223
 Keyser, U.F. 72
 Khaliullin, G. 288
 Kießling, T. 105, 108
 Kimme, L. 313
 Kipnusu, W. 58, 64
 Kipnusu, W.K. 59, 61
 Kirschner, R. 325
 Klüpfel, F.J. 174
 Knorr, M. 107, 110
 Koch, D. 107
 Koch, K. 126
 Kondrashova, D. 85
 Kortenbruck, N. 42
 Kossack, W. 64–67
 Kramer, A. 314
 Kranert, C. 199
 Kremer, F. 53, 54, 56–59, 61–68, 70, 72–75
 Krishna, R. 92
 Kroy, K. 41, 310–314
 Kröber, D. 308
 Krüger, P. 112

Käsemödel, B. 111
 Kärger, J. 91, 92
 Käs, J.A. 103, 105–108, 110–113, 174
 Kühn, A. 307
 Kühne, K. 73

L

Lajn, A. 174
 Lange, M. 189, 193
 Langhammer, H.T. 129
 Larson, J. 299
 Leinaas, J.M. 298
 Lenzner, J. 153
 Ling, F.C.C. 177
 Linke, S. 184
 Lippoldt, J. 111
 Littlewood, P.B. 125
 Loebel, S. 43
 Lorbeer, J. 204
 Lorenz, M. 166, 193, 195, 198
 Lämmel, M. 313

M

Mapesa, E.U. 53, 54, 56–58
 Marenz, M. 247
 Martinez-Joaristi, A. 91
 Mattler, S.J. 128
 Meier, B. 126
 Meissner, T. 125
 Metzner, G. 308
 Meyer-Ortmanns, H. 249
 Mittreiter, I. 89
 Morawski, M. 142, 146
 Moschkowitz, L. 126
 Möddel, M. 235
 Müller, A. 195–197
 Müller, M. 255
 Müller, S. 176, 183
 Müller, T. 129

N

Nagel, H. 249, 250
 Neder, I. 296
 Nieuwendaal, R.C. 128
 Nikulina, E. 219

Nnetu, K.D. 108, 110

O

Oswald, S.E. 89
 Otto, F. 310
 Otto, O. 72

P

Papadopoulos, P. 64–67
 Parkinson, M. 65
 Pawlizak, S. 106
 Peksa, M. 90
 Perlt, H. 323
 Pickenhain, R. 177
 Pippel, E. 219
 Plotzki, D. 45
 Prades, F. 65
 Pumpa, M. 43
 Pusch, A.-K. 90
 Pöpl, A. 126, 128

R

Reibetanz, U. 151
 Reimann, K. 146
 Reinert, T. 142
 Richter, S. 184
 Rings, D. 41, 310, 313
 Rose, D. 105
 Rosenow, B. 288, 292, 294, 296
 Rothermel, M. 140, 144, 153
 RumeSangoro, J. 64
 Ruthven, D. 91
 Rypestol, M. 298

S

Sachsenweger, H. 307
 Sangoro, J.R. 59, 61–63
 Schachoff, R. 41
 Schadewitz, A. 223
 Schaumann, G.E. 129
 Schein, F.-L. 168
 Schiller, A. 323
 Schlayer, S. 87

- Schlayer, St. 90
 Schmidt, F. 179, 181
 Schmidt, M. 170, 177, 179, 181
 Schmidt, S. 174
 Schmidt-Grund, R. . 184, 189, 199, 202, 204
 Schmidtchen, H. 307
 Schultze-Nobre, L. 223
 Schulz, R. 307
 Schöbl, S. 246
 Selmke, M. 39, 41, 43
 Semenov, I. 75
 Setzer, A. 221
 Sickert, A. 144
 Singer, D. 68, 73
 Spemann, D. 140, 148, 149, 152, 153
 Stallmach, F. 87, 89, 90
 Stange, R. 105, 108
 Stangner, T. 68, 70, 72–74
 Stern, A. 292, 296
 Strehle, D. 103, 110
 Stueber, C. 146
 Sturm, C. 184, 189
 Sturm, S. 312
 Stölzel, M. 189, 193, 195

T

- Takei, S. 294
 Tacdizen, B. 241
 Teupser, D. 144
 Treß, M. 53, 54, 56–58
 Turner, R. 146

U

- Ueberschär, O. 68, 70, 72–75

V

- Valiullin, R. 85, 86
 Vogt, J. 148, 149, 152
 von Wenckstern, H. 168, 170, 174, 176,
 177, 179, 181, 183
 Vrejoiu, I. 219, 220

W

- Waclaw, B. 249

- Wagner, C. 68, 70, 72–74
 Wagner, R. 42
 Williams, G.V.M. 125
 Willner, S. 307
 Wolff, L. 310, 312
 Wolff-Fabris, F. 126
 Wosnitza, J. 126
 Wright, A.R. 288, 289
 Wunderlich, R. 152, 221

Z

- Zandalazini, C. 221
 Zeigermann, P. 86
 Zhang, Z. P. 170
 Zierenberg, J. 246, 247
 Ziese, M. 219–221
 Zimmermann, J. 113
 Zink, M. 105, 106, 110
 Zippel, J. 198

Minisymposium

UNIVERSITÄT LEIPZIG

Quantum Coherence in Nanostructures



Quantum coherence in systems with restricted geometry or topology can lead to novel quantum phases and offers exciting new perspectives for the applications of low energy and soft modes in hard condensed matter.

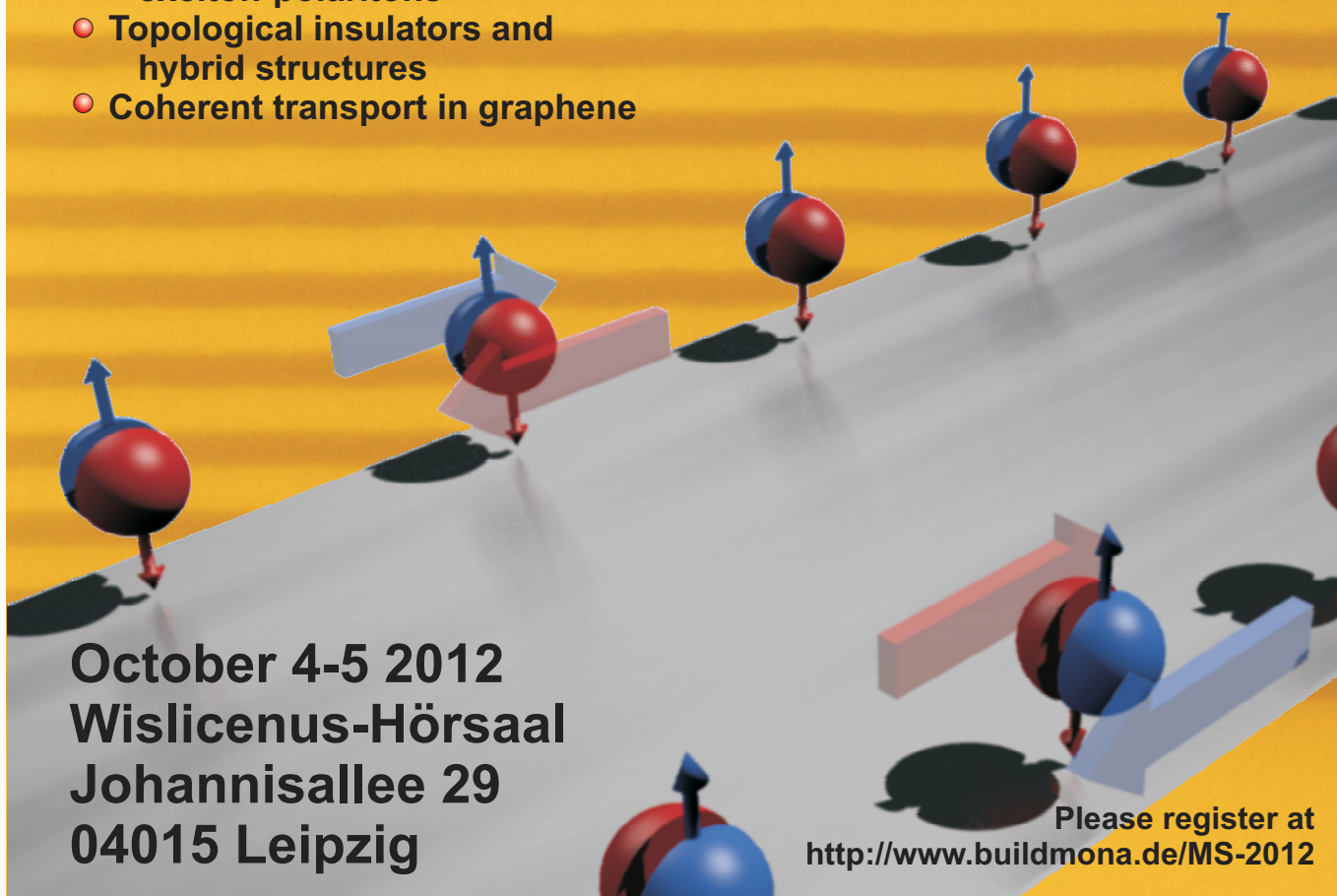
The BuildMoNa module A3, held 2012 as minisymposium focuses on three topics:

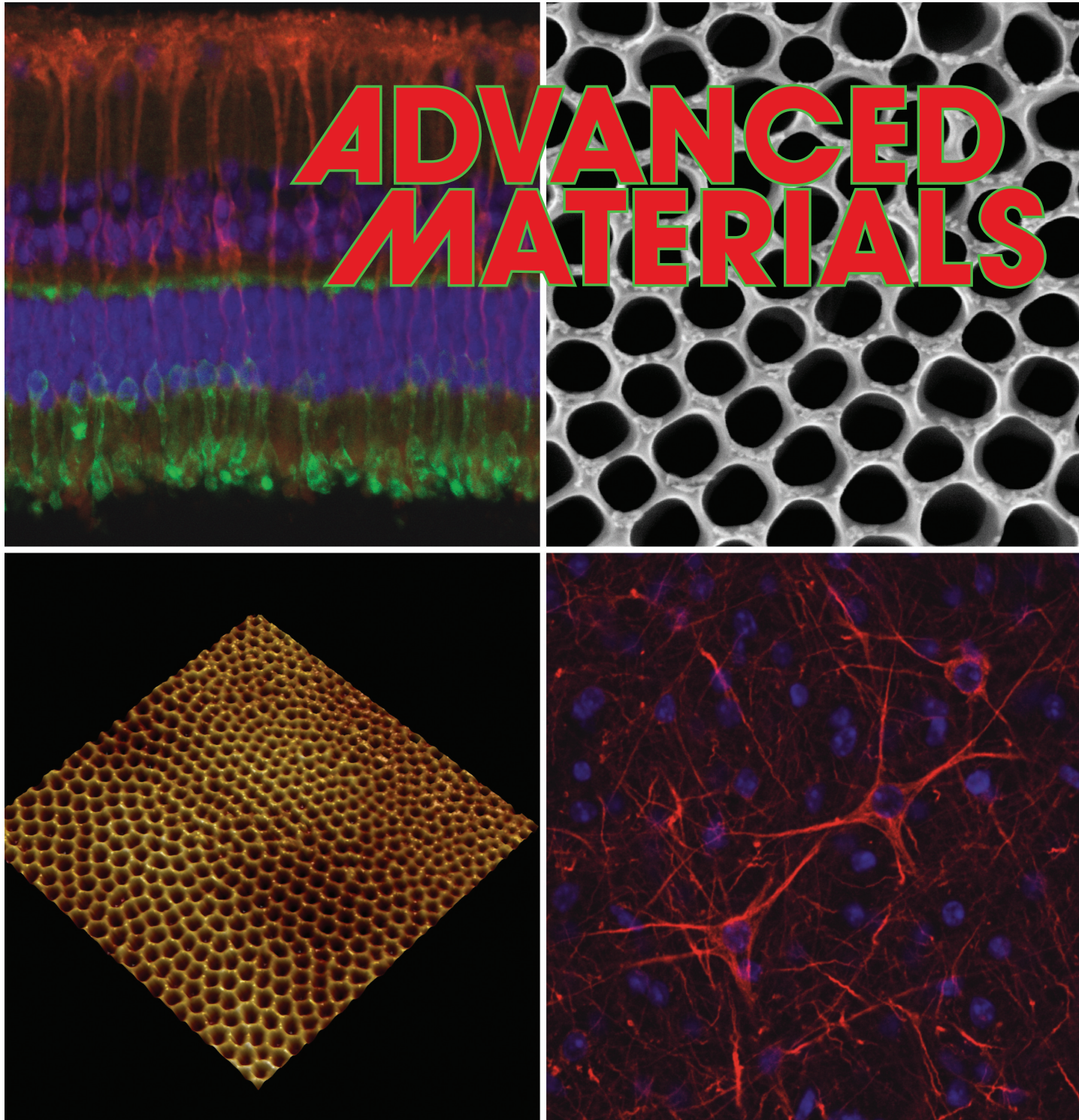
- Bose-Einstein condensation of exciton-polaritons
- Topological insulators and hybrid structures
- Coherent transport in graphene

Jacqueline Bloch CNRS LPN, Paris
Hartmut Buhmann
Universität Würzburg
Paul Eastham Trinity College, Dublin
Klaus Ensslin ETH Zürich
Nicolas Grandjean EPF Lausanne
Charles M. Marcus
Niels Bohr Institute, Copenhagen
Gil Refael Caltech, Pasadena
Jürgen Smet
MPI f. Festkörperforschung, Stuttgart
Björn Trauzettel, Würzburg
Universität Würzburg

October 4-5 2012
Wislicenus-Hörsaal
Johannisallee 29
04015 Leipzig

Please register at
<http://www.buildmona.de/MS-2012>





ADVANCED MATERIALS

TISSUE ENGINEERING

Organotypic culture of adult neuronal tissue over several weeks is an unresolved challenge due to rapid distortion and cell death. M. Zink, S. G. Mayr, and co-workers demonstrate for the first time on page 2399 that superhydrophilic nanostructured substrates with tunable surface morphologies offer ideal conditions for culturing adult retinal explants (upper right) and adult brain slices (lower left). Even after two weeks, the neuronal tissue structures are maintained without signs of degeneration, which paves the way for in-vitro retina and brain tissue regeneration.